frontiers | Research Topics

Light-mediated regulation of plant physiology

Edited by
Andres Romanowski, Carlos Esteban Hernando, Jordi Moreno-Romero, Elena Monte, John Christie, Gabriela Toledo-Ortiz and Karen Halliday

Published in
Frontiers in Plant Science

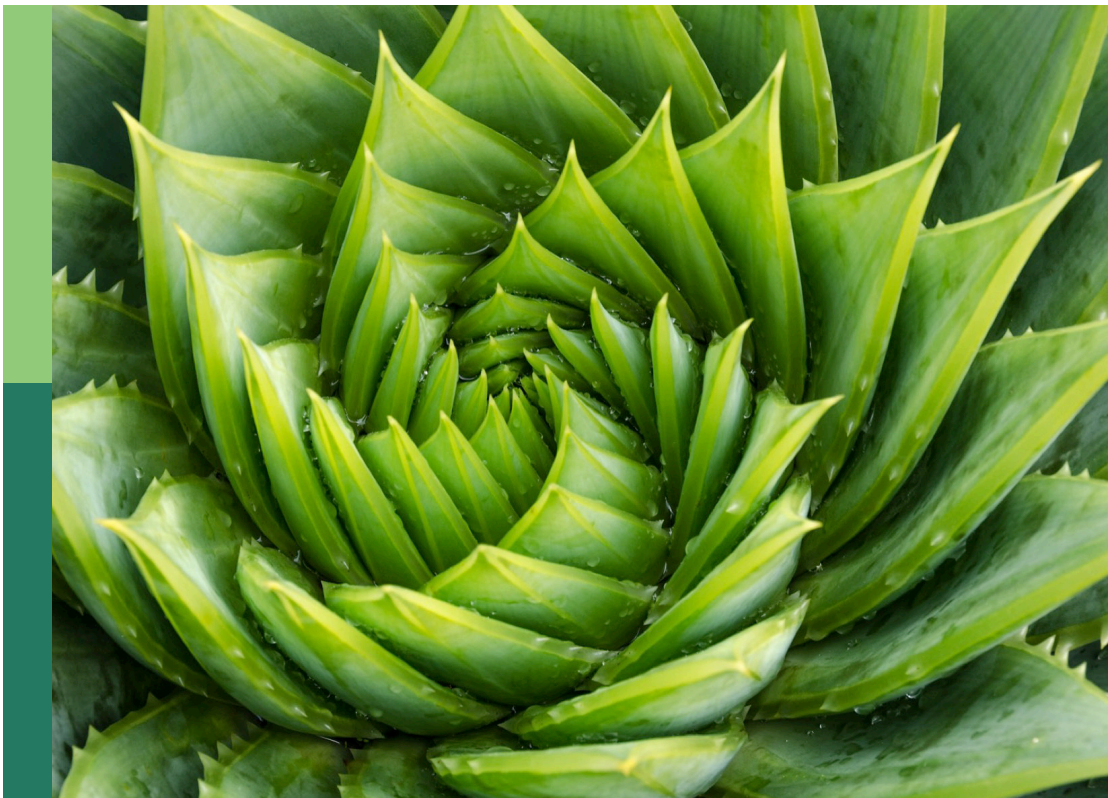

ISSN 1664-8714
ISBN 978-2-8325-5900-0
DOI 10.3389/978-2-8325-5900-0

About Frontiers

Frontiers is more than just an open access publisher of scholarly articles: it is a pioneering approach to the world of academia, radically improving the way scholarly research is managed. The grand vision of Frontiers is a world where all people have an equal opportunity to seek, share and generate knowledge. Frontiers provides immediate and permanent online open access to all its publications, but this alone is not enough to realize our grand goals.

Frontiers journal series

The Frontiers journal series is a multi-tier and interdisciplinary set of open-access, online journals, promising a paradigm shift from the current review, selection and dissemination processes in academic publishing. All Frontiers journals are driven by researchers for researchers; therefore, they constitute a service to the scholarly community. At the same time, the *Frontiers journal series* operates on a revolutionary invention, the tiered publishing system, initially addressing specific communities of scholars, and gradually climbing up to broader public understanding, thus serving the interests of the lay society, too.

Dedication to quality

Each Frontiers article is a landmark of the highest quality, thanks to genuinely collaborative interactions between authors and review editors, who include some of the world's best academicians. Research must be certified by peers before entering a stream of knowledge that may eventually reach the public - and shape society; therefore, Frontiers only applies the most rigorous and unbiased reviews. Frontiers revolutionizes research publishing by freely delivering the most outstanding research, evaluated with no bias from both the academic and social point of view. By applying the most advanced information technologies, Frontiers is catapulting scholarly publishing into a new generation.

What are Frontiers Research Topics?

Frontiers Research Topics are very popular trademarks of the *Frontiers journals series*: they are collections of at least ten articles, all centered on a particular subject. With their unique mix of varied contributions from Original Research to Review Articles, Frontiers Research Topics unify the most influential researchers, the latest key findings and historical advances in a hot research area.

Find out more on how to host your own Frontiers Research Topic or contribute to one as an author by contacting the Frontiers editorial office: frontiersin.org/about/contact

Light-mediated regulation of plant physiology

Topic editors

Andres Romanowski — Wageningen University and Research, Netherlands
Carlos Esteban Hernando — IIBBA-CONICET Leloir Institute Foundation, Argentina
Jordi Moreno-Romero — Autonomous University of Barcelona, Spain
Elena Monte — Centre for Research in Agricultural Genomics, Spanish National Research Council (CSIC), Spain
John Christie — University of Glasgow, United Kingdom
Gabriela Toledo-Ortiz — The James Hutton Institute, United Kingdom
Karen Halliday — University of Edinburgh, United Kingdom

Citation

Romanowski, A., Hernando, C. E., Moreno-Romero, J., Monte, E., Christie, J., Toledo-Ortiz, G., Halliday, K., eds. (2025). *Light-mediated regulation of plant physiology*. Lausanne: Frontiers Media SA. doi: 10.3389/978-2-8325-5900-0

Table of contents

frontiers | Frontiers in Plant Science

TYPE Editorial
PUBLISHED 03 January 2025
DOI 10.3389/fpls.2024.1531410

OPEN ACCESS

EDITED AND REVIEWED BY
Anna N Stepanova,
North Carolina State University, United States

*CORRESPONDENCE
Andres Romanowski
andres.romanowski@wur.nl
Jordi Moreno-Romero
jordi.moreno.romero@uab.cat

RECEIVED 20 November 2024
ACCEPTED 09 December 2024
PUBLISHED 03 January 2025

CITATION
Romanowski A, Monte E, Hernando CE, Toledo-Ortiz G, Christie JM, Moreno-Romero J and Halliday KJ (2025) Editorial: Light-mediated regulation of plant physiology.
Front. Plant Sci. 15:1531410.
doi: 10.3389/fpls.2024.1531410

Editorial: Light-mediated regulation of plant physiology

Andres Romanowski[1]*, Elena Monte[2], Carlos Esteban Hernando[3], Gabriela Toledo-Ortiz[1], John M. Christie[4], Jordi Moreno-Romero[5]* and Karen J. Halliday[6]

[1]Laboratory of Molecular Biology, Wageningen University and Research, Wageningen, Netherlands, [2]Centre for Research in Agricultural Genomics (CRAG), CSIC-IRTA-UAB-UB, Cerdanyola del Vallès, Barcelona, Spain, [3]Instituto de Investigaciones Bioquimicas de Buenos Aires (IIBBA) - Consejo Nacional de Investigaciones Científicas y Técnicas (CONICET), Ciudad Autonoma de Buenos Aires, Argentina, [4]School of Molecular Biosciences, College of Medical, Veterinary and Life Sciences, Bower Building, University of Glasgow, Glasgow, United Kingdom, [5]Departament de Bioquimica i Biologia Molecular, Universitat Autonoma de Barcelona (UAB), Bellaterra, Barcelona, Spain, [6]Institute of Molecular Plant Sciences, School of Biological Sciences, University of Edinburgh, Edinburgh, United Kingdom

KEYWORDS

photomorphogenesis, phytochrome, miRNA, pigment biosynthesis, splicing, translation, circadian clock, light signalling

Editorial on the Research Topic
Light-mediated regulation of plant physiology

The field of plant photobiology has evolved rapidly over the past decade, expanding our understanding of how light influences every aspect of plant life, from gene expression to ecosystem interactions. This Research Topic aims to update the current knowledge on the intricate mechanisms underlying light-driven growth and metabolic/environmental adaptation processes, offering insights into the cellular complexity that underpins plant adaptability to varying light conditions.

Here, we highlight the primary contributions of these studies, grouped into four major themes that encompass a broad perspective on light-mediated regulation in plants.

Regulatory layers in photomorphogenesis: phytochromes, microRNAs, and pigment biosynthesis

Photomorphogenesis, the developmental transition from dark to light conditions, involves multiple regulatory layers, including (but not limited to) light perception, signalling and changes in gene expression and translation. Cota-Ruiz et al. explored the interplay between

phytochromes and zinc finger proteins (ZFPs) in Arabidopsis, revealing that phytochrome-dependent regulation of hypocotyl elongation can be modulated through ZFPs. This study provides insights into how phytochromes orchestrate complex molecular mechanisms that control light-mediated development. Lakatos et al. delved into the role of RNA-induced silencing complex (RISC)-loaded microRNAs in Arabidopsis de-etiolation, showing that while RISC loading impacts active miRNA formation in organ-specific pools, it has a limited role in global miRNA regulation during photomorphogenesis, as total levels and the RISC-loaded miRNAome show minimal changes. However, there is one notable exception: while miR163 is present at low levels in the dark, it sharply increases in abundance and RISC loading efficiency when seedlings are shifted to light. Furthermore, increased miR163 expression is required for normal photomorphogenesis. This study demonstrated the existence of specialized miRNA regulatory mechanisms for fine-tuning specific responses. Xie et al. employed transcriptomic and metabolomic analyses to identify key genes and transcription factors involved in light-regulated anthocyanin biosynthesis in *Perilla frutescens*. These findings have implications for medicinal and ornamental applications. Together, these studies emphasise the importance of multiple molecular layers in mediating photomorphogenesis.

The influence of light quality and quantity on plant development

Light quality, encompassing different wavelengths, plays diverse roles in the regulation of distinct developmental and physiological processes in plants. Tang et al. demonstrated how specific wavelengths, such as red and blue light, impact both the transcriptome and metabolome of *Mesona chinensis*, with red light markedly boosting growth-related traits. This study highlights the importance of combining transcriptomic and metabolomic data to determine the regulatory effects of light on plant development. Zioutopoulou et al. revealed that Ultraviolet radiation B (UV-B) radiation could trigger photoperiodic flowering in Arabidopsis via the UV-B resistance 8 (UVR8) pathway, underscoring its role in modulating the vegetative to reproductive transition. Sheridan et al. further examined UV-B exposure, showing its specific influence on primary root elongation by directly affecting meristematic cell proliferation in Arabidopsis, an indication of light's spatial specificity in plant tissues. Berardi et al. demonstrated the existence of a novel signalling pathway involving increased production of singlet oxygen in response to low red-to-far-red ratios, contributing to a greater understanding of the complexity behind shade avoidance strategies in Arabidopsis. Beyond quality, the intensity or quantity of light also plays a role. Serrano-Pérez et al. investigated the molecular mechanisms underlying high light resistance in the charophyte alga *Klebsormidium nitens*, uncovering ancient photoprotective mechanisms that may have been crucial for plant terrestrialisation. Together, these studies have revealed the complex and multifaceted roles of both light quality and quantity in shaping plant growth and metabolism.

Light-mediated mechanisms of regulation of gene expression: splicing and mRNA translation

In plants, light exerts control over gene expression at the post-transcriptional level through splicing and mRNA translation. Ma et al. explored the impact of light on alternative splicing in *Artemisia annua*, showing that light-induced intron retention could regulate sesquiterpenoid biosynthesis. Schwenk et al. identified a novel cytoplasmic function of phytochrome A in mediating far-red light-induced disassembly of processing bodies in Arabidopsis, leading to the release of translationally halted mRNA. Together, these studies enrich the understudied field of post-transcriptional and translational regulation of gene expression, shedding light on the nuanced control mechanisms employed by plants to modulate gene activity.

Interplay of circadian rhythm with light and stress in plants

Circadian rhythms enable plants to anticipate daily environmental changes. Light is a key modulator of this internal clock. Rhodes et al. uncovered the dual role of Far-Red Elongated Hypocotyls 3 (FHY3) in light input to the circadian clock, revealing a red-light-specific disruption of rhythmicity in *fhy3* mutants and suggesting an integrative role for FHY3 in the red/blue light ratio in clock regulation. Jurca et al. demonstrated that the blue light receptor ZEITLUPE (ZTL) modulates Abscisic acid (ABA)-induced stomatal closure, a critical adaptation under drought stress. These studies illustrate the intricate linkages between light signalling, circadian rhythm, and stress responses, highlighting the adaptive advantages conferred by these interconnected systems.

Closing remarks

Light has a pervasive function in plant biological processes. This is evidenced in the research presented in this Research Topic, which reveals light's intricate and versatile roles in plant development, physiology, and stress response across various species, including the model plant *Arabidopsis*. By employing different techniques, including transcriptomic, metabolomic, and physiological approaches, these studies provide valuable insights into the molecular frameworks underlying light-mediated plant responses, revealing the interconnected nature of light signalling pathways across different biological levels. This Research Topic advances our fundamental understanding and opens new avenues for applied research, with implications for agriculture and plant-based industries.

Author contributions

AR: Conceptualization, Writing – original draft, Writing – review & editing. EM: Writing – review & editing. CH: Writing – review &

editing. GT-O: Writing – review & editing. JC: Writing – review & editing. JM-R: Writing – original draft, Writing – review & editing. KH: Writing – review & editing.

Acknowledgments

We thank the contributing authors for their outstanding research and the reviewers for their invaluable feedback on enhancing the quality of this Research Topic. We hope that the insights presented here will inspire further exploration of light-mediated regulation in plants to address critical challenges in plant science and beyond.

Conflict of interest

The authors declare that the research was conducted in the absence of any commercial or financial relationships that could be construed as a potential conflict of interest.

Publisher's note

frontiers in Plant Science

ORIGINAL RESEARCH
published: 29 September 2021
doi: 10.3389/fpls.2021.733505

Genome-Wide Analysis of Light-Regulated Alternative Splicing in *Artemisia annua* L.

Tingyu Ma[1,2†], Han Gao[1,3†], Dong Zhang[1,4,5†], Wei Sun[1], Qinggang Yin[1], Lan Wu[1], Tianyuan Zhang[6], Zhichao Xu[2], Jianhe Wei[7], Yanyan Su[8], Yuhua Shi[1], Dandan Ding[1], Ling Yuan[9], Gangqiang Dong[8], Liang Leng[1], Li Xiang[1,9]* and Shilin Chen[1]**

[1] Key Laboratory of Beijing for Identification and Safety Evaluation of Chinese Medicine, Institute of Chinese Materia Medica, China Academy of Chinese Medical Sciences, Beijing, China, [2] Key Lab of Chinese Medicine Resources Conservation, State Administration of Traditional Chinese Medicine of the People's Republic of China, Institute of Medicinal Plant Development, Chinese Academy of Medical Sciences and Peking Union Medical College, Beijing, China, [3] School of Life Sciences, Central China Normal University, Wuhan, China, [4] College of Agriculture, South China Agricultural University, Guangzhou, China, [5] Guangdong Laboratory for Lingnan Modern Agriculture, Guangzhou, China, [6] State Key Laboratory of Agricultural Microbiology, Huazhong Agricultural University, Wuhan, China, [7] Hainan Provincial Key Laboratory of Resources Conservation and Development of Southern Medicine, Hainan Branch of the Institute of Medicinal Plant Development, Chinese Academy of Medical Sciences and Peking Union Medical College, Haikou, China, [8] Amway (China) Botanical R&D Center, Wuxi, China, [9] Department of Plant and Soil Sciences, Kentucky Tobacco Research and Development Center, University of Kentucky, Lexington, KY, United States

OPEN ACCESS

Edited by:
Carlos Esteban Hernando, IIBBA-CONICET Leloir Institute Foundation, Argentina

Reviewed by:
Rohini Garg, Shiv Nadar University, India
Maximiliano Estravis-Barcala, Umeå University, Sweden

***Correspondence:**
Liang Leng
lleng@icmm.ac.cn
Li Xiang
lxiang@icmm.ac.cn
Shilin Chen
slchen@icmm.ac.cn

[†] These authors have contributed equally to this work

Specialty section:
This article was submitted to Plant Physiology, a section of the journal Frontiers in Plant Science

Received: 06 July 2021
Accepted: 03 September 2021
Published: 29 September 2021

Citation:
Ma T, Gao H, Zhang D, Sun W, Yin Q, Wu L, Zhang T, Xu Z, Wei J, Su Y, Shi Y, Ding D, Yuan L, Dong G, Leng L, Xiang L and Chen S (2021) Genome-Wide Analysis of Light-Regulated Alternative Splicing in Artemisia annua L. Front. Plant Sci. 12:733505. doi: 10.3389/fpls.2021.733505

Artemisinin is currently the most effective ingredient in the treatment of malaria, which is thus of great significance to study the genetic regulation of *Artemisia annua*. Alternative splicing (AS) is a regulatory process that increases the complexity of transcriptome and proteome. The most common mechanism of alternative splicing (AS) in plant is intron retention (IR). However, little is known about whether the IR isoforms produced by light play roles in regulating biosynthetic pathways. In this work we would explore how the level of AS in *A. annua* responds to light regulation. We obtained a new dataset of AS by analyzing full-length transcripts using both Illumina- and single molecule real-time (SMRT)-based RNA-seq as well as analyzing AS on various tissues. A total of 5,854 IR isoforms were identified, with IR accounting for the highest proportion (48.48%), affirming that IR is the most common mechanism of AS. We found that the number of up-regulated IR isoforms (1534/1378, blue and red light, respectively) was more than twice that of down-regulated (636/682) after treatment of blue or red light. In the artemisinin biosynthetic pathway, 10 genes produced 16 differentially expressed IR isoforms. This work demonstrated that the differential expression of IR isoforms induced by light has the potential to regulate sesquiterpenoid biosynthesis. This study also provides high accuracy full-length transcripts, which can be a valuable genetic resource for further research of *A. annua*, including areas of development, breeding, and biosynthesis of active compounds.

Keywords: *Artemisia annua*, single molecule real-time (SMRT) sequencing, alternative splicing, intron retention, light-regulated, artemisinin

INTRODUCTION

The main natural source of Artemisinin, a sesquiterpene lactone with peroxide bridge, is the medicinal herb *Artemisia annua* (Miller and Su, 2011; Tu, 2011). Artemisinin is famous for its role in artemisinin combination therapies (ACT), the most effective malaria treatment currently available (Czechowski et al., 2016). Development of new uses of artemisinin and its derivatives, e.g., dihydroartemisinin in the treatment of systemic lupus erythematosus, is still ongoing. These efforts show some potential in anti-tumor, anti-parasitic, anti-fibrosis, and anti-arrhythmic effects (Bin and Hong, 2010). As a result, the demand for artemisinin and its derivatives will increase significantly (Peplow, 2013). Although biosynthesis and chemical synthesis of Artemisinin have seen significant progress in recent years[5,6], the final steps in the conversion of dihydroartemisinic acid (DHAA) to artemisinin are still non-enzymatic and require extracellular treatments (Graham et al., 2010; Czechowski et al., 2016). For example, *in vitro* biosynthesis of artemisinin is still not possible because yeast cannot provide the special oil oxidization environment required for the synthesis of artemisinin (Paddon et al., 2013; Paddon and Keasling, 2014). Thus, the market supply of artemisinin is currently relied on extraction from *A. annua* (Paddon et al., 2013; Ma et al., 2018; Triemer et al., 2018). Great efforts, particularly in molecular analysis, are needed to understand the biology of *A. annua* in order to improve artemisinin content of the plant and to reduce production cost.

Transcriptional regulation of genes, such as terpenoid synthase, is central to artemisinin biosynthesis (Nagegowda et al., 2008; Nagegowda, 2010; Tan et al., 2015). Thus, research efforts have focused on the *A. annua* transcriptome. Alternative splicing (AS) plays a fundamental role in eukaryote gene regulation (Nilsen and Graveley, 2010; Reddy et al., 2013; Staiger and Brown, 2013). During the process of precursor mRNA maturation, AS produces multiple mature mRNA from the same gene, which then results in the production of different proteins. The alternative splicing of precursor RNA with multiple exons increases the diversity of proteins encoded by organisms and the complexity of regulating gene expression (Brett et al., 2002; Matlin et al., 2005; Keren et al., 2010; Nilsen and Graveley, 2010). In human, nearly all multi-exon genes are alternatively spliced (Pan et al., 2008; Wang et al., 2008), while in plants the corresponding proportion is over 60% (Reddy et al., 2013). AS can occur through different mechanisms, e.g., exon skipping, alternative 3′/5′ splice sites, or intron retention (IR) (Reddy et al., 2013). In contrast to human, in which exon skipping accounts for the largest proportion of alternative splicing products, plants tend to use IR as the main mechanism of AS (Kim and Yin, 2005; Keren et al., 2010; Reddy et al., 2013). For example, the IR rates in Arabidopsis and rice are as high as 64.1 and 55%, respectively (Zhang et al., 2016). AS also participates in the process of antibiotic stress response (Staiger and Brown, 2013; Filichkin et al., 2015). Plants produce secondary metabolites to defend against biological or abiotic stress, e.g., light, plant hormones, temperature, saline and drought stresses (Li et al., 2007; Yu Z. X. et al., 2012; Shen et al., 2016; Vashisth et al., 2018; Lopes et al., 2019). Specifically, the expression of isoforms produced by IR splicing can be regulated depending on source of stress (Filichkin et al., 2010; Abdel-Ghany et al., 2016). For example, light is an important environmental factor that regulates plant physiological adaptation and influences the synthesis of plant secondary metabolites in plant. Light regulation has been demonstrated to promote the accumulation of artemisinin, anthocyanins, ginsenoside and charantin (Cuong et al., 2017; Kochan et al., 2019; Lopes et al., 2019; Sun et al., 2020). Light exposure immediately induced IR, with many alternatively spliced transcripts expressed from genes with functions related to light signaling, suggesting a potential impact on pre-mRNA splicing and photomorphogenic gene regulation in response to light (Petrillo et al., 2014a,b; Godoy Herz et al., 2019).

In recent years high-throughput sequencing technology has proven to be a powerful strategy to study medicinal plant genome, full-length transcriptomes and AS (Wang et al., 2009; Martins et al., 2011; Ozsolak and Milos, 2011; Song et al., 2018; Liu et al., 2021). The main advantage of the most popular high throughput sequencing technology used for transcriptomics, i.e., Next Generation Sequencing, is the ability to study all expressed genes simultaneously. However, current NGS technology suffers from insufficient read length (100–300 bp currently), and the inability to accurately construct full-length splice variants (Pan et al., 2008; Au et al., 2013). The third generation sequencing (TGS) technology, e.g., SMRT sequencing from the PacBio platform (Pacific Biosciences of California, Inc., [1]), produces a long sequence with much longer read length >8 kb (Au et al., 2010; Mason and Elemento, 2012; Rhoads and Au, 2015). A major drawback of TGS technology, compared with NGS technology, is the high error rate (Au et al., 2010; Koren et al., 2012; Jiao et al., 2013). Two alternatives may be helpful to overcome this problem. First, the length of raw pacbio read is several times longer than the length of most genes; thus, the circular consensus sequence (CCS) mode of pacbio technology could enable a single transcript (cDNA) to be sequenced by multiple passes, and sequencing error of the raw TGS read could be corrected since they were randomly generated (Sharon et al., 2013; Rhoads and Au, 2015). Second, hybrid sequencing, i.e., integrating of NGS sequencing and TGS sequencing technology, could also be applied to the correct the error of PacBio reads (Au et al., 2010, 2013). TGS sequencing technology is widely used in plant AS studies, e.g., *Salvia miltiorrhiza* (Xu et al., 2015), *Zea mays* (Thatcher et al., 2014), *Fragaria ananassa* (Li et al., 2018), *Scutellaria baicalensis* (Gao T. et al., 2019) and *Andrographis paniculata* (Gao H. et al., 2019).

Considering the importance of *Artemisia annua* biology and recent progress in TGS sequencing, we sequenced multiple tissues of *Artemisia annua* to investigate its alternative splicing landscape. Together with current genome assembly and annotation (Shen et al., 2018), in this work we aimed to supply a useful resource to the *Artemisia annua* community with a new genome wide isoform set. Previous studies have shown that different light conditions can affect artemisinin synthesis and accumulation. However, the mechanism by which light regulates artemisinin synthesis is unclear. Many transcription factors have

[1] http://www.pacificbiosciences.com/

previously been found to regulate artemisinin synthesis at the transcriptional regulatory level, but it is not clear whether AS can affect artemisinin synthesis. Herein, the classification and gene-expression of AS isoforms under different light conditions could provide novel insights in the molecular mechanism of light's influence on artemisinin synthesis.

MATERIALS AND METHODS

Plant Materials Preparation

The variety of *A. annua* used in this study is a wild type variety originally collected in Hainan (19°56′44″N, 110°13′23″W, 2015) and cultured in Guangxi "Seed cultivation and planting base of ecological of *A. annua*" (25°13′2″N, 109°24′39″W). The seeds were then transplanted to Beijing (40°20′17.8″N, 116°33′40″W) in March 2018 from Guangxi and preserved in the Artemisinin Research Center, China Academy of Chinese Medical Sciences. The seeds were cultured in white light at 25°C for 4 weeks. The light intensity of white light was 50 ± 5 μmol/m^2s, and the photoperiod was 16/8 h (day/night). Then, the seedlings were transferred to four continuous light treatments for 2 days. After different light treatments, we collected the aboveground parts of 10 seedlings randomly as a sample. The light intensity was 50 ± 5 μmol/m^2s in all the treatments, including light-emitting diode (LED) red light (wavelength 670 nm), LED blue light (wavelength 470 nm), and LED far-red light (wavelength 735 nm) (Zhang et al., 2017). For the purposes of full-length transcriptome and Illumina short reads analysis, samples of *A. annua* were obtained from four different organs of plant: young leaf, stem, open flower, and root. Each plant organs collected three biological samples for Illumina short reads analysis.

mRNA-seq Library Preparation and Sequencing

The total RNA from each sample for RNA-seq were extracted from seedlings using RNAprep Pure Plant Kit (Tiangen, Beijing, China) following the manufacturer's instructions (Zhang et al., 2017). Total RNA in this paper was used for Illumina Hi-seq 2500 platform. We prepared total RNA to construct the sequencing libraries using NEBNext® Ultra™ RNA Library Prep Kit for Illumina® (NEB, MA, United States) with 28S/18S RNA ratio ≥ 1.8, and a minimum integrity number (RIN) value of 8.5 and 250–300 bp insertion element. The integrity of RNA was assessed using the Agilent 2100 Bioanalyzer (Agilent Technologies, CA, United States). Detection of RNA samples, including 1% agarose electrophoresis, was performed to detect degradation and genomic DNA contamination; Nanodrop detects the purity of the RNA (OD260/280 ratio); Qubit quantifies RNA precisely.

In the reaction of synthesizing cDNA, the SMART primers of 3′ terminal oligo (dG) were added beforehand, and reverse transcribed from the RNA3′ terminal with oligo dT as primer. Touching the "hat structure" (methylated G) of eukaryote mRNA at the 5′ end of mRNA adds several (dC) to the end of cDNA. The oligo (dG) of the SMART primer is paired with several C protruding at the end of the synthesized cDNA to form an extension template of the cDNA. The reverse transcriptase automatically converts the template, and the SMART primer continues to extend the cDNA single strand until the end of the primer. In this way, the cDNA contains the starting primer (oligo dT) and SMART primers, which can be amplified by universal primer sequence. The full-length cDNA from pooled poly (A) RNA samples was normalized and subjected to SMRT sequencing using the PacBio RS platform (Novogene, Beijing, China). The full-length cDNA from polymerized (A) RNA samples was normalized and SMRT sequenced by PacBio RS platform (Beijing, China).

Preprocessing of Single Molecule Real-Time Long Reads

Three steps were conducted to obtain the final SMRT long reads for subsequent analysis. Firstly, circular consensus sequence (CCS) reads were generated from raw subreads using the Pacific Biosciences SMRT-Analysis pipeline version 2.2.0 (Berlin et al., 2015; Ardui et al., 2018). Secondly, full-length reads were identified from the CCS reads by running hmmer_wrapper.py. To define full-length reads, hmmer_wrapper.py requires both 5′ and 3′ primer sequences, as well as a poly (A) tail. The primer sequences and poly (A) tail sequence were then trimmed off prior to further analysis.[2]; finally, PE150 short reads, generated using an Illumina HiSeq 2500, were used to correct full-length reads (PBcR) (Koren et al., 2012). Since this correction step was resource-consuming, we randomly down-sampled illumina short RNA-seq reads to about 12 Gb per tissue for correction. The quality of final full-length reads was assessed by mapping reads to the reference genome using STAR version 2.5.2a (Dobin et al., 2013).

Isoform Detection and Prediction and Alternative Splicing Type Identification

The SpliceMap-isoform detection and prediction (IDP) pipeline (Au et al., 2013) was used to detect and predict isoforms in four tissues, separately. We initially used SpliceMap to detect the junctions of Illumina short reads obtained from stem, leaf, flower and root samples, and then used IDP to detect and predict isoforms by integrating both Illumina short reads and SMRT long reads. These Illumina RNA-seq reads were all used for SpliceMap analysis, and both full-length reads and corrected full-length reads were merged for IDP. The IDP results indicate the sites where isoforms are located on the genome. We followed our previous work to identify alternative splicing events (Gao H. et al., 2019). Briefly, we used the original annotated genes as reference isoform (hereinafter ref isoform). Original annotation files were downloaded from https://www.ncbi.nlm.nih.gov/genome/?term=Artemisia+annua (Shen et al., 2018). If a gene already has more than one transcript or isoform, we defined the longest isoform as the ref isoform and other isoforms as AS isoforms. We then compared the location information of ref isoforms and AS isoforms to identify the type of AS that might occur in a gene.

[2]https://github.com/Magdoll/PacBio-generic/blob/master/hmmer_wrapper.py

Isoform Quantification and Analysis of Differentially Expressed Isoforms

All ref and AS isoform sequences were combined into a new fasta-format file and quantified using Kallisto version 0.43 (Bray et al., 2016; Jin et al., 2017). A previously published light-treated RNA-seq data were re-calculated with this new *A. annua* isoform set (Zhang et al., 2018). Briefly, plant seedlings were treated with different lights, i.e., FR/far red, R/red, B/blue, WL/white and D/Dark. Each treatment comprised three biological replicates (including 10 seedlings per replicate). In total, 45 RNA-seq libraries were analyzed based on the new *A. annua* isoform set. We also conducted differentially expressed (DE) analysis on FR vs. WL, R vs. WL, B vs. WL as well as WL vs. D, FR vs. D, R vs. D and B vs. D. DE analysis was conducted using R package DEseq2 (Love et al., 2014; Maza, 2016). Genes with adjusted *p*-value being less than 0.05 were kept as differentially expressed ones.

Analysis of the Intron Retention Isoform Expression Levels of Genes Related to the Artemisinin Biosynthesis Pathway

According to the identified isoforms and their expression, genes involved in artemisinin biosynthesis were manually curated and alternatively spliced isoforms of these genes were selected (Graham et al., 2010; Czechowski et al., 2016, 2018; Ma et al., 2018; Shen et al., 2018). Pheatmap package was used to generate heat maps of isoforms of these genes and the expression patterns of the ref and IR isoforms were analyzed (Kolde, 2015). Enrichment analysis of gene ontology (GO) terms was conducted on differentially expressed IR isoforms using the clusterProfiler package (Yu G. et al., 2012). Functional categories of GO terms with adjusted *p*-value smaller than 0.05 were considered as significantly enriched.

RESULTS

Summary of Single Molecule Real-Time Sequencing

To identify AS events in *A. annua*, we applied both Illumina and SMRT RNA-sequencing and analyzed these data in four tissues separately, i.e., leaf, flower, stem and root. We generated ∼15 Gb NGS data and more than 10 Gb TGS data for each tissue (**Table 1**). For TGS RNA-sequencing data, 7–10 million raw subreads were obtained in each tissue, with median lengths of raw subreads are 1,898 bp, 1,451 bp, 1,093 bp and 1,794 bp in leaf, flower, stem and root, respectively (**Table 1**). We further generated full length reads from raw subreads (**Table 1** and **Supplementary Table 1**). The number of full-length reads ranges from 341,083 in flower to 412,999 in root, while the median lengths changed to 1,973, 1,956, 2,185, and 1,962 bp in leaf, flower, stem and root, respectively (**Table 1** and **Supplementary Table 1**). We mapped the full length reads to the reference genome and accessed the quality (**Supplementary Table 2**). Overall, the quality of the reads is high; mapped fractions range from 97.4 to 99.4%, while match rates are around 98 percent. By examining unmapped or deficiently mapped reads manually, we found that a large fraction of these sequences have poly A/G/C/T structure and are therefore difficult to map. We thus corrected these full reads with Illumina short reads. After correction, the number of corrected full-length read ranges from 338,27 in flower to 411,076 in root (**Table 1** and **Supplementary Table 1**). While mapped fraction and mismatch rates only improved by a small proportion, deletion/insertion rate, which may be the result of inaccurate poly-A/G/C/T, decreased (**Supplementary Table 2**).

The New *Artemisia annua* Isoform Annotation Set

The *A. annua* genome was assembled and annotated previously (Shen et al., 2018). This version of annotation has 63,226 genes, of which 3,062 genes comprise more than one isoform (**Table 2**). However, only 159 AS genes involve intron retention (IR), which contrasts with previous observation showing that ∼30% of all AS events are IR (Keren et al., 2010). Thus, we made use of our newly generated full-length reads to update the current *A. annua* genome annotation and to generate a new *A. annua* isoform annotation set. We identified 13,328 AS events, 11,832 AS isoforms and 7,210 AS genes. Together with the previously published annotation set, here we generated a new *A. annua* annotation set, which consists of 63,226 genes and 75,058 transcripts in total.

We mined out all possible AS events separately from the four tissues, then combined newly identified events and AS events annotated in the current gene annotation to form a final isoform annotation set (**Table 2** and **Supplementary Table 3**). Our sequencing in the four tissues jointly identified 5,155 genes which comprise at least one AS isoform. Together with the current gene annotation, the new *A. annua* isoform set comprises 7,210 AS genes (**Figure 1A** and **Table 2**). Among the 7,210 AS genes, 11,832 AS isoforms were identified (**Supplementary Table 3**). More than half of all AS genes have only two isoforms, i.e., a reference isoform and a AS isoform. The largest number of isoforms a gene comprises of is 12 (**Figure 1B**). We further classified all AS events into five types: AA, alternative 3′ splice site; AD, alternative 5′ splice site; ES, exon skipping; IR, intron retention; others. We found a total of 13,328 AS events from 11,832 AS isoforms, while 5,854 AS isoforms involve IR events (**Supplementary Tables 3, 4** and **Figure 1C**). We defined IR genes as genes which bring at least one IR event. Some AS isoforms could consist of multiple AS events or types (**Figure 1D**); for example, 317 AS isoforms consist of both IR and AA events. Some AS isoforms were independently found in more than one tissue (**Figure 1E**). For example, 270 AS isoforms were found in all four tissues. The final isoform set consists of 7,210 AS genes, of which 3,895 are IR genes (**Table 2**).

Differential Expression of Intron Retention Isoforms Under Light Treatments

In the following part we focused on IR genes and isoform expression under light treatments and of artemisinin synthesis pathway related genes. Five light treatments were conducted, each with three biological replicates (**Supplementary Table 4**). TPM being 1 was chosen as the cutoff to determine whether

TABLE 1 | Summary of the sequencing libraries statistics of next generation sequencing (NGS) and third generation transcriptome sequencing (TGS) data in leaf, flowers, stem and root in *A. annua*.

Tissue	Illumina read		SMRT raw read			Full length read		Corrected full length read	
	Total base	Used for correction	Num. of reads	Total base	Median length	Num. of reads	Median length	Num. of reads	Median length
Leaf	∼14G	∼12G	10,171,843	∼20G	1,898	370,515	1,973	369,984	1,963
Flower	∼16G	∼12G	7,532,512	∼12G	1,451	341,083	1,956	338,277	1,923
Stem	∼15G	∼12G	7,075,767	∼10G	1,093	366,742	2,185	352,311	2,013
Root	∼17G	∼12G	7,217,207	∼13G	1,794	412,999	1,962	411,076	1,934

TABLE 2 | Number of AS and IR gene.

	Num. of AS gene	Num. of IR gene
Leaf	1,613	961
Flower	1,925	1,188
Stem	2,792	2,186
Root	1,940	1,123
All new identified	5,155	3,789
Previously published	3,062	159
Final set	7,210	3,895

a gene is expressed or not. The median TPM of expressed IR isoforms ranges from 2.91 under white light treatment to 3.37 under far-red light treatment (**Figure 2A**), while that of expressed non-AS genes (which has one isoform per gene) ranges from 6.55 under blue to 6.96 under far red (**Figure 2B**). The fraction of expressed IR isoforms ranges from 30.2% (1,771) under dark to 34.4% (2,013) under red, while that of non-AS gene ranges from 34.7% (19,425) under dark to 39.3% (22,008) in red (**Figures 2C,D** and **Supplementary Table 5**).

We further performed differential expression analysis on seven combinations of light treatment: far red vs. white (FR-WL), red vs. white (R-WL), blue vs. white (B-WL), white vs. dark (WL-D), far red vs. dark (FR-D), red vs. dark (R-D), and blue with dark (B-D). In these comparisons, we observed more up-regulated isoforms than down-regulated ones, and this pattern is largely consistent between IR isoforms and non-AS genes apart from WL-D (**Figures 3A,B**). Moreover, the proportion of IR isoforms which were differentially expressed under different light treatments is higher than that of non-AS genes (**Figure 3C** and **Supplementary Table 6**). For instance, 37% of IR isoforms is differentially expressed between the B-D comparison, while the corresponding fraction of non-AS genes is 28% (p-value $< 2.2e^{-16}$, Chi-squared test, **Figure 3C**).

Gene Ontology Enrichment Analysis of Differentially Expressed Alternative Splicing and Intron Retention Isoforms

Since AS isoforms are more likely to be differentially expressed under light treatment, we used GO enrichment analysis to investigate gene function of differentially expressed AS (**Supplementary Table 7**) genes, especially IR genes (**Table 3** and **Supplementary Table 8**). For all AS genes, the functional enrichment analysis revealed that transcription regulator activity usually enriches in differentially expressed AS genes since adjusted p-values of this GO term (GO: 0140110) are significant in six comparisons, i.e., B-D, B-WL, FR-WL, R-WL and WL-D. Besides, lipid binding (GO: 0008289) is also enriched in four comparisons, i.e., B-D, B-WL, R-D and R-WL. For IR genes, among seven comparisons we found a total of 23 enriched GO terms in six comparisons, belonging to 11 GO annotations (**Table 3**). No enrichment was found in the FR-D comparison due to the limited number of differentially expressed IR isoforms (**Supplementary Table 6**). Five GO annotations were enriched in more than one comparison, i.e., nucleotide binding (GO: 0000166) in R-D and R-WL, RNA-binding (GO: 0003723) in R-D and B-WL, lipid metabolic process (GO: 0006629) in B-D, WL-D and B-WL, cellular protein modification (GO: 0006464) in B-D, R-D, B-WL and R-WL, membrane (GO: 0016020) in B-D, R-D, WL-D, B-WL, FR-W and R-WL. These functional enrichments suggest the evolution of IR genes with specific functions in response to light conditions. For instance, we found that three overlapping genes (CTI12_AA107750, CTI12_AA262950 and CTI12_AA419320) regulating sugar transporters have responses to blue, red and far-red light (**Supplementary Table 9**). The ref isoform of the CTI12_AA107750 gene was down-regulated in blue, red and far-red treatment in contrast to dark treatment (green label). However, the IR isoform of the corresponding gene was up-regulated in blue, red and far red treatment (red label). The ref isoform and IR isoforms of the CTI12_AA262950 gene have a similar regulatory mechanism in blue and red-light treatments in contrast to dark. Similarly, the ref isoform and IR isoforms of the CTI12_AA419320 gene was down-regulated and up-regulated in far-red light treatment compared with dark.

Analysis of Intron Retention Genes Related to Artemisinin Synthesis Pathway

We compared the AS genes we identified with genes predicted to be involved in the biosynthesis pathway for the general sesquiterpenes precursor FPP and artemisinin synthesis. Among 24 genes related to artemisinin synthesis pathway and its upstream MVA and MEP pathways (**Supplementary Figure 3**), fifteen genes with AS behaviors were identified. Nine AS genes in the MEP pathway were identified, belonging to the 1-Deoxy-D-xylulose 5-phosphate synthase (DXS), 1-deoxy-D-xylulose- 5-phosphate reductoisomerase (DXR), 4-(Cytidine 5-diphospho)-2-C-methyl-D-erythritol kinase (CMK), 2-C-methyl-D-erythritol-4-(cytidyl-5-diphosphate) transferase

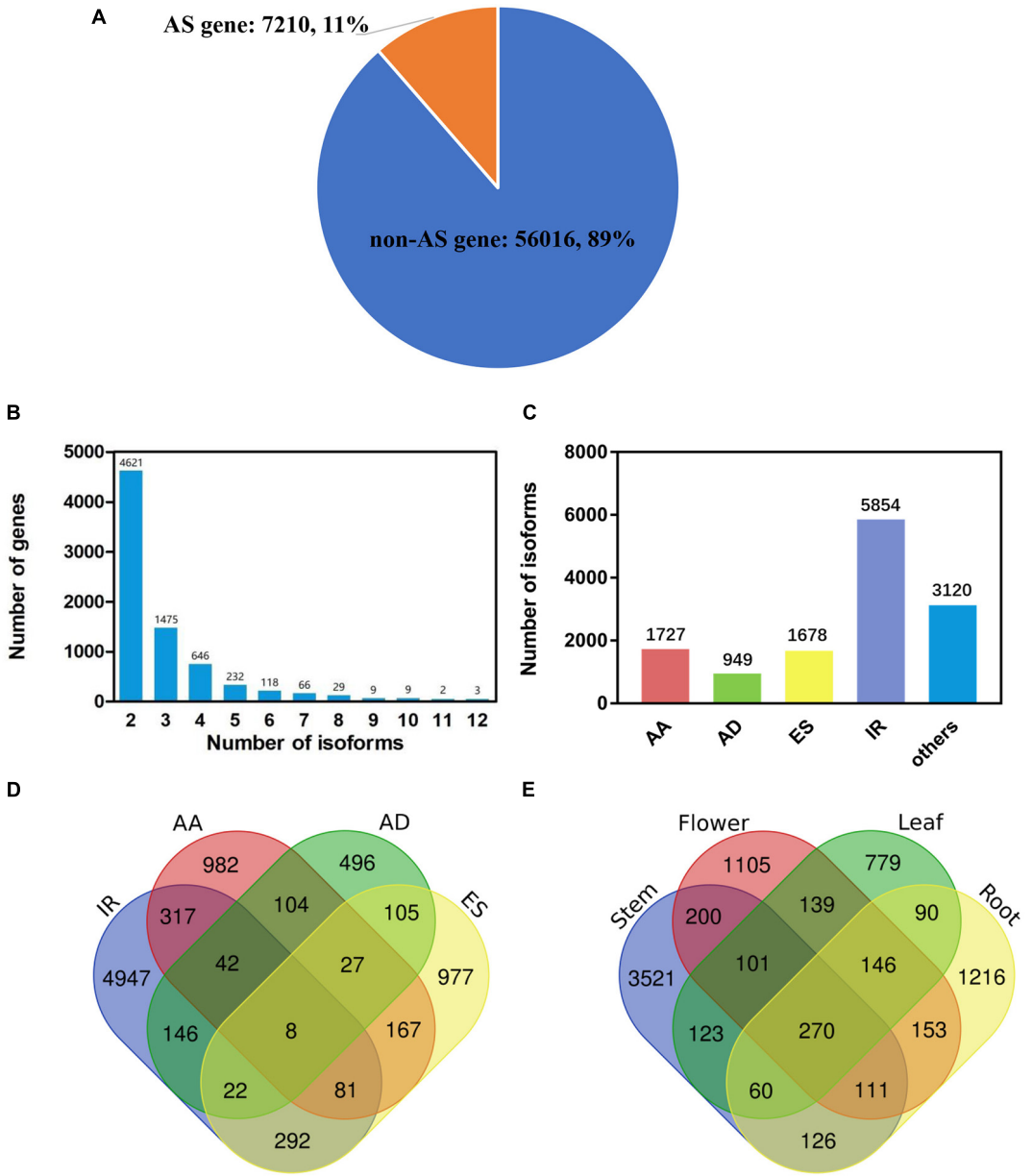

FIGURE 1 | Identification and classification of gene isoforms in *Artemisia annua* L. **(A)** The number and proportion of AS and non-AS gene. **(B)** The number distribution of alternatively spliced isoforms per gene. **(C)** Types of alternatively spliced isoforms: AA, alternative 3′ splice site; AD, alternative 5′ splice site; ES, exon skipping; IR, intron retention. **(D)** The number of isoforms produced by one or more splicing mechanisms. Venn diagram shows the combination of the four types of isoforms. **(E)** The number of new isoforms found in leaf, flower, stem and root. Venn diagram shows the common and specific isoforms in different tissues.

(MCT), 2-C-methyl-D-erythritol-2,4-cyclodiphosphate synthase (MCS), and R-linalool synthase (LS) gene families (**Supplementary Table 10**). Five genes in the MVA pathway were identified, belonging to the acetoacetyl-CoA thiolase (AACT), mevalonate kinase (MVK), and farnesyl diphosphate synthase (FDS) gene families (**Supplementary Tables 10, 11**). One gene in the artemisinin synthesis pathway, belonging to the cytochrome P450 reductase (CPR) gene family, was identified. These genes produced a total of 39 isoforms, including 16 IR isoforms. The CPR gene was most highly expressed is an AS isoform, and the remaining genes have highest expression of the ref isoform (**Figure 4**).

Ten genes were identified that produce IR type isoforms in the artemisinin pathway (**Figure 4**). The expression of ref isoforms produced by CTI12_AA095890 (DXS), CTI12_AA182630 (DXS), CTI12_AA123070 (DXS), CTI12_AA422860 (DXR), CTI12_AA094970 (LS), CTI12_AA348050 (MCT), CTI12_AA584370 (AACT), CTI12_AA079320 (MVK), CTI12_AA174930 (FDS), and CTI12_AA484860 (CPR) genes, were up-regulated (red label), compared with dark

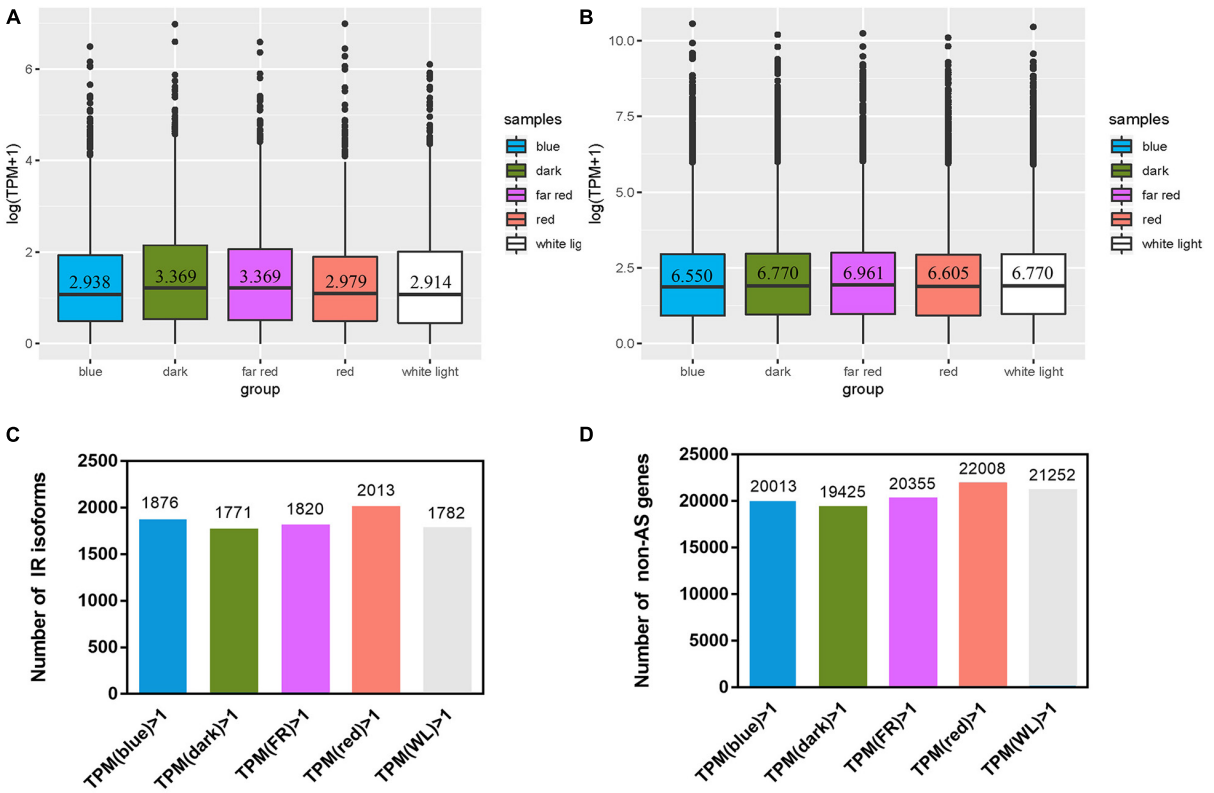

FIGURE 2 | Expression of intron retention (IR) isoforms and non-alternatively spliced (non-AS) genes after light treatment. Isoforms with a TPM > 1 were defined as expressed ones. **(A,B)** Box-plots using log (TPM + 1) as the ordinate show TPM distribution of expressed IR isoforms and non-AS genes under five treatments, respectively. **(C,D)** the number of expressed IR isoforms and non-AS genes, respectively.

treatment (**Supplementary Table 10**). Several IR isoforms were alternatively expressed under different light treatments. For example, under white light treatment, expression of the IR isoforms produced by CTI12_AA095890 (DXS) and CTI12_AA094970.6 (LS) genes were up-regulated, while the expression of the IR isoforms produced by CTI12_AA422860 (DXS), CTI12_AA182630 (DXR) and CTI12_AA484860 (CPR) genes were down-regulated. In addition, more IR isoforms are up-regulated in blue light, such as CTI12_AA348050 (MCT), CTI12_AA463490 (MVK), CTI12_AA422860 (DXS), CTI12_AA484860 (CPR) and CTI12_AA123070 (LS), compared with white light (**Supplementary Table 10**).

Interestingly, the ref isoform of the CPR gene was up-regulated and the IR isoform down-regulated in all light treatments when compared with dark (**Supplementary Tables 10, 11**). However, the expression of IR isoform produced by CPR gene was up-regulated when contrasted with white light (**Supplementary Table 10**). CPR has been hypothesized to serve as a redox partner for CYP71AV1, which catalyzes the conversion of amorphadiene to more oxygenated products in *A. annua* (Paddon et al., 2013). Moreover, if a gene has multiple isoforms, i.e., more than one IR isoform, these IR isoforms may contribute in the same or opposite ways under different light conditions as in the CPR or LS cases (**Supplementary Table 10**). In the artemisinin pathway, we observed genes that produced IR isoforms, e.g., nine genes in the MEP pathway, five genes in the MEP pathway and one gene in the artemisinin synthesis pathway. More IR isoforms are produced in the upstream biosynthesis pathway of artemisinin. Compared with dark, we found the IR isoforms of all 10 genes are up-regulated under light treatment. More IR isoforms were up-regulated under blue and red-light treatments. However, only blue light treatment has more IR expression up-regulated when we compared with white light. One main consequence of IR is the occurrence of premature stop codon (PTC) in retained intron (**Supplementary Figures 1, 2**). We checked whether PTC exists in IR genes related to the artemisinin synthesis pathway. Seven genes were found to bear PTC in their IR isoforms. For instance, three IR isoforms of the LS (CTI12_AA094970) gene, i.e., CTI12_AA094970.6, CTI12_AA094970.7, and CTI12_AA094970.8, retain the second intron, leading to the PTC of these AS isoforms. Thus, all these three isoforms may produce a truncated protein which lacks the 3rd to 6th exons. PTC-present isoforms may also produce pre-mRNAs which will further subject to non-sense-mediated mRNA decay (NMD) and the expression of this gene thus could be appropriately regulated by these PTC-present isoforms induced decay (Isken and Maquat, 2008). These results imply that IR are involved in expression regulatory mechanism to control the metabolism of sesquiterpenes.

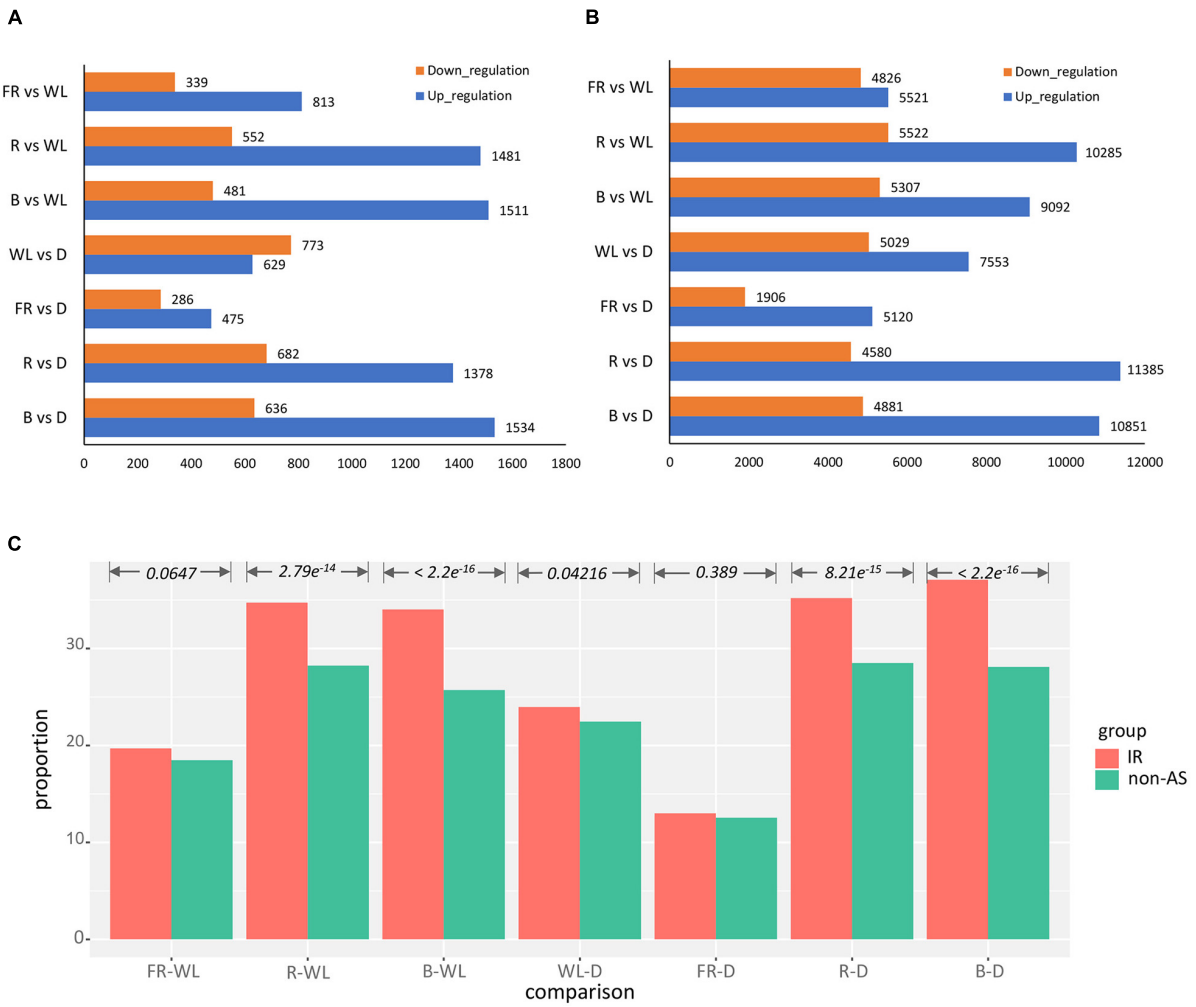

FIGURE 3 | Analysis of differential expression IR isoform expression pattern after light treatment. **(A,B)** Number of up- and down-regulated IR isoforms and non-AS genes after treatment, respectively. **(C)** Proportion of differentially expressed IR isoforms over all IR isoforms vs. the corresponding profortion of non-AS genes. B, blue light; R, red light; FR, far-red light; WL, white light; D, dark.

DISCUSSION

The accumulation of artemisinin is unique in *A. annua*, and the yield of artemisinin largely determines the medicinal value of *A. annua* (Graham et al., 2010; Czechowski et al., 2016, 2018). Since light has a positive effect on the accumulation of secondary metabolites (Li et al., 2017; Yoo et al., 2019; Zhang et al., 2019), the study of the molecular mechanism of the effect of light on artemisinin accumulation is of great significance for basic science and practical applications. In this study, we used both NGS and SMRT-based RNA-seq to identify transcripts of *A. annua* under different light conditions including blue, red, far-red, white light and dark treatments (Zhang et al., 2017), and analyzed the overall transcriptional level of each gene. By combining Illumina and SMRT platforms for transcriptome sequencing of leaf, flower, stem, root in *A. annua*, we generated a new isoform set. Our study identified 11,832 AS events in total, of which 5,854 were IR isoforms (**Figure 1** and **Table 2**). File of a total of 11,832 AS isoforms sequences is stored in Supplementary_AS_sequence.fasta. We found that IR isoforms accounted for 48.48% of all AS isoforms, representing the most frequent AS event is IR in *A. annua*. This result is consistent with previous findings in other plants (Filichkin et al., 2010; Chang et al., 2014; Gao H. et al., 2019). We found that IR isoform expression tends to be differentially expressed under light treatment. Comparing with the current annotation that records only 159 IR genes (**Table 2**), our new AS dataset is more reliable based on our knowledge of plant AS patterns and could sufficiently improve the *A. annua* genome annotation.

Former studies have shown that environmental stress can affect AS global pattern (Palusa et al., 2007; Filichkin et al., 2010, 2015; Duque, 2011; Reddy et al., 2013; Staiger and Brown, 2013; Ding et al., 2014). Light not only provides energy for plants, but also is a key environmental factor (Filichkin et al., 2010; Chang et al., 2014; Dietz, 2015; Gao H. et al., 2019). There are reported

TABLE 3 | Gene ontology (GO) functional enrichment of differentially expressed IR isoforms.

	ID	Description	Gene ratio	Bg ratio	*p*.adjust
IR_DE_B_D	GO: 0016020	Membrane	204/1,312	4,106/34,885	0.0015
	GO: 0006629	Lipid metabolic process	61/1,312	1,038/34,885	0.0182
	GO: 0009987	Cellular process	152/1,312	3,171/34,885	0.0268
	GO: 0006464	Cellular protein modification process	169/1,312	3,590/34,885	0.0268
	GO: 0005975	Carbohydrate metabolic process	82/1,312	1,565/34,885	0.0273
	GO: 0016787	Hydrolase activity	217/1,312	4,800/34,885	0.0279
IR_DE_R_D	GO: 0016020	Membrane	201/1,277	4,106/34,885	0.0008
	GO: 0006464	Cellular protein modification process	176/1,277	3,590/34,885	0.0015
	GO: 0003723	RNA binding	47/1,277	766/34,885	0.0123
	GO: 0016301	Kinase activity	136/1,277	2,832/34,885	0.0141
	GO: 0000166	Nucleotide binding	263/1,277	6,143/34,885	0.043
	GO: 0005623	Cell	22/1,277	315/34,885	0.043
IR_DE_WL_D	GO: 0016020	Membrane	142/896	4,106/34,885	0.0113
	GO: 0006629	Lipid metabolic process	44/896	1,038/34,885	0.0378
IR_DE_B_WL	GO: 0016020	Membrane	201/1,241	4,106/34,885	0.0001
	GO: 0006629	Lipid metabolic process	59/1,241	1,038/34,885	0.0132
	GO: 0006464	Cellular protein modification process	164/1,241	3,590/34,885	0.014
	GO: 0003723	RNA binding	44/1,241	766/34,885	0.0257
	GO: 0006810	Transport	141/1,241	3,102/34,885	0.0257
IR_DE_FR_WL	GO: 0016020	Membrane	120/729	4,106/34,885	0.0071
IR_DE_R_WL	GO: 0006464	Cellular protein modification process	170/1,272	3,590/34,885	0.019
	GO: 0016020	Membrane	188/1,272	4,106/34,885	0.0237
	GO: 0000166	Nucleotide binding	266/1,272	6,143/34,885	0.0313

Gene Ratio, The ratio of the number of differentially expressed genes associated with this term to the total number of differentially expressed genes; Bg Ratio, The ratio of the number of background genes associated with this term to the total number of all background genes; p.adjust, adjust p-values for multiple comparisons.

that the deletion of SAD1 which is a key gene involved in ABA signal pathway results in a genome-wide increase of AS (Cui et al., 2014). Our work also revealed that light possibly affect the production of AS particularly IR. Comparing with the non-AS isoforms, there is a greater proportion of AS gene expression regulated by light, which suggests that light can influence not only the production of AS but also its gene expression (**Figure 3C**). This finding could broaden our insight into how light regulates the behavior of plants. Ten genes were identified that produce IR type isoforms in the artemisinin pathway, but only one is in the artemisinin downstream pathway. This may be due to the upstream is the common pathway of many metabolites and can be affected by more environmental regulatory factors, so as to quick respond to the changes; while the downstream specific artemisinin synthesis pathway may not require too many regulatory changes. Moreover, we also found that the IR genes in the artemisinin pathway was basically high in the expression of reference isoform, while the expression of AS isoform was generally lower. The expression of AS reference and AS isoforms in the artemisinin pathway were higher in most light than in the dark, especially in red and blue light, which was consistent with the most obvious effect of blue and red light on the accumulation of artemisinin. This indicates that the regulation effect of AS on different transcripts is the same on the synthesis pathway of light, which is more conducive to the additive effect on the synthesis regulation of artemisinin and the rapid regulation of light on artemisinin.

Plants have distinct sets of photoreceptors for several parts of the light spectrum, ranging from near-UVB (280–315 nm) to far-red (FR) (∼750 nm) wavelengths. Plants mainly use red and blue light for photosynthesis. At the same time, red and blue light, as a signal, play an important role in many biological processes such as seed germination, de-etiolation, phototropism and flowering (Wit et al., 2016). In **Figure 3A**, red and blue light can induce more IR isoforms up-regulated than other light treatments, indicating that the transduction of red and blue light signals to plants may depend on the AS. Also, in **Figure 3C**, red and blue light treatments can induce more differentially expressed IR isoforms. Red and blue light can induce more physiological responses in plants and cause more changes in the expression of AS. Besides, our analysis show that lipid related functions such as lipid binding or lipid metabolic process are enriched in differentially expressed AS or IR genes (**Supplementary Tables 7, 8**). Lipids, which are major and essential constituents of all plant cells, not only provide structural integrity and energy for various metabolic processes but can also function as signal transduction mediators (Bigay and Antonny, 2012). There is a lot of lipid synthesis and metabolism in chloroplasts. Chloroplast is the site of photosynthesis in plants, and its growth and development are also regulated by light (Chen et al., 2018). Therefore, light changes can cause many lipids synthesis and metabolism gene expression changes. Also, PA, one of the central molecules in lipid biosynthesis, not only facilitates transport of lipids across membranes (Awai et al., 2006)

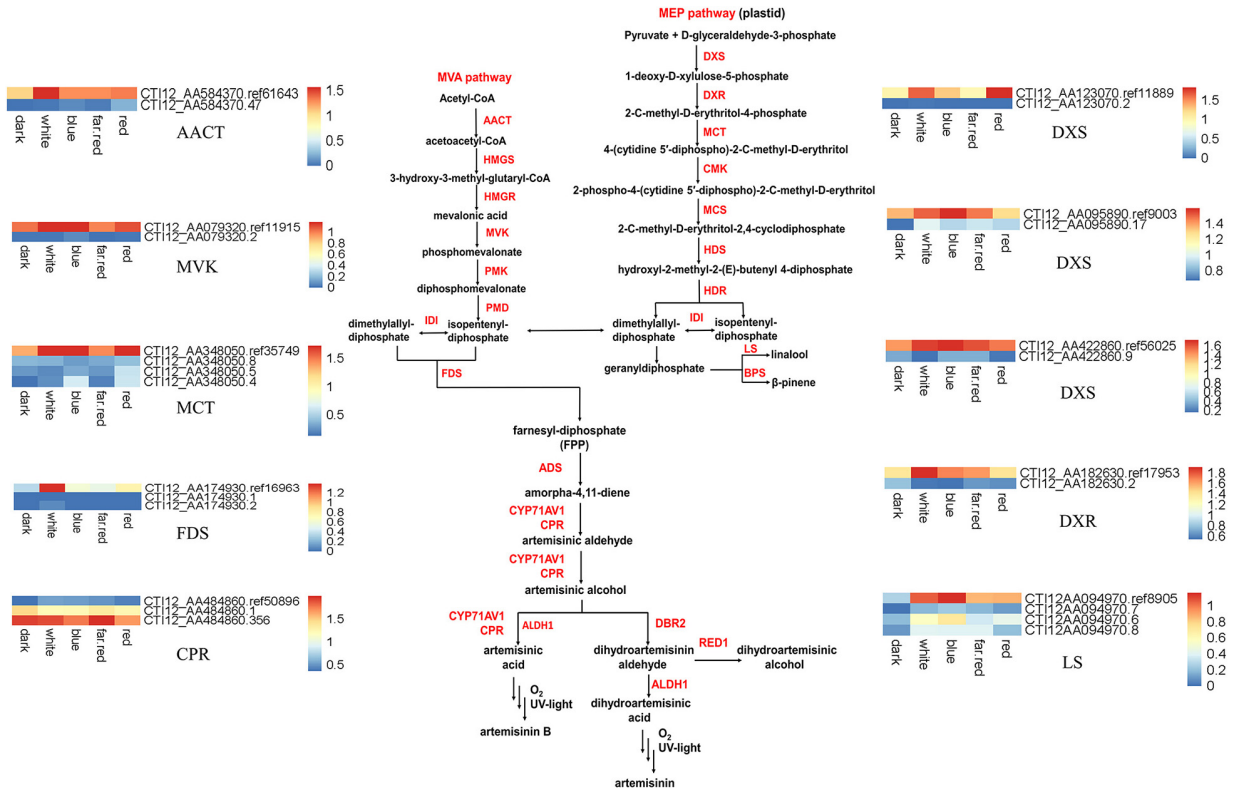

FIGURE 4 | Expression heatmap of the isoforms involved in artemisinin synthesis. The suffix "ref" indicates the reference isoform. For every gene, the reference isoform present in genome annotation is signed with the suffix "ref" or "rna" plus a series of number, while other isoforms newly identified are signed with pure number in its suffix. For example, CTI12_AA584370.ref61643 is the reference isoform of AACT while CTI12_AA584370.47 is a newly identified AS isoform. AACT, Acetyl-CoA C-acetyltransferase; HMGS, 3-Hydroxy-3-methylglutaryl-CoA synthase; HMGR, 3-Hydroxy-3-methylglutaryl-CoA reductase; MK, MVA kinase; PMK, Phospho-MVA kinase; MDC, Diphospho-MVA decarboxylase; DXS, 1-Deoxy-D-xylulose-5-phosphate synthase; DXR, 1-Deoxy-D-xylulose 5-phosphate reductoisomerase; MCT, 2-C-methyl-D-erythritol 4-phosphate cytidylyltransferase; CMK, 4-(Cytidine-5-diphospho)-2-C-methyl-D-erythritol kinase; MDS, 2-C-methyl-D-erythritol-2,4-cyclodiphosphate synthase; HDS, 4-Hydroxy-3-methylbut-2-enyl-diphosphate synthase; HDR, 4-Hydroxy-3-methylbut-2-enyl diphosphate reductase; GGPPS (E, E, E)-geranylgeranyl diphosphate synthase.

but also plays an important role in biotic and abiotic stress responses. Light is also a stress to plants, especially ultraviolet light. It is possible that light also mediates stress responses in plants through lipid signaling, and therefore, light may affect the expression of many genes related to lipid metabolism. Light is one of the important factors that regulate plant growth and development. Light exposure immediately induced alternative splicing, with many alternatively spliced transcripts expressed from genes with functions related to light signaling, suggesting a potential impact on pre-mRNA splicing and photomorphogenic gene regulation in response to light (Yoshimura et al., 2011; Petrillo et al., 2014a,b; Godoy Herz et al., 2019). Light promotes RNA polymerase II (Pol II) elongation in the affected genes, whereas in darkness, elongation is lower (Godoy Herz et al., 2019). Therefore, Photoreceptors strictly regulate gene expression to control light morphological response. These results jointly suggest that AS may play an important role in the transduction of light signals.

Overall, the number of up-regulated IR isoforms was more than the total number of down-regulated IR isoforms after blue, red, and far-red light treatments. GO enrichment indicated that some genes with special functions can produce multiple isoforms. In the artemisinin biosynthetic pathway, a total of 10 genes underwent AS to produce 26 isoforms, including 16 IR isoforms, two AA isoforms, and eight other isoforms (**Supplementary Tables 10, 11**). Our research suggests that the expression of IR isoforms is regulated by blue, red, and far-red light, which may also be involved in the biosynthesis of artemisinin and other plant secondary metabolite synthesis (Chen et al., 2013; Liu et al., 2018). For example, genes such as AACT and DXS in the MVA and MEP pathways exhibited IR isoforms (**Figure 4**). A recent study reported that most of the IR isoforms in Arabidopsis are predicted to be targets of NMD to regulate mRNA stability as they are subjected to NMD to eliminate incomplete transcripts (Filichkin et al., 2010; Syed et al., 2012; Ge and Porse, 2014; Zhu et al., 2020). These eliminated IR isoforms may contain functional domains important for artemisinin biosynthesis by influencing specific steps of the pathway.

The analysis of AS in *A. annua* has generated valuable insights regarding plant transcriptomes, and these findings provide a foundation for further analyses. In future work, functional verification of IR isoforms will be conducted in the artemisinin pathway and regulatory genes. In conclusion, this study provides not only new insights into the regulation of AS in artemisinin

biosynthesis, but also valuable genetic resources for further exploration of functional genomics in *A. annua*.

DATA AVAILABILITY STATEMENT

The raw sequencing datasets of *A. annua* reported in this paper have been submitted to the Sequence Read Archive from the NCBI under the accession number PRJNA752933.

AUTHOR CONTRIBUTIONS

SC, LX, and LL conceived the study. TM, HG, DZ, DD, LW, YYS, and GD performed the sample preparation of NGS and SMRT sequencing. HG, TM, DZ, LL, and TZ analyzed the data. WS, QY, LY, JW, ZX, and YHS contributed to discussion and language polishing. TM, HG, DZ, and LL wrote the manuscript. All authors contributed to the article and approved the submitted version.

FUNDING

This work was supported by the National Natural Science Foundation of China and Karst Science Research Center of Guizhou Province (U1812403-1), the China Postdoctoral Science Foundation (2021M690464), the National Natural Science Foundation of China (81903758, 31900258, and 81641002), the National Major Science and Technology Projects (2017ZX09101002-003-001, 2019ZX09201005-006-001, and 2019ZX09731-002), and the CACMS Innovation Fund (CI2021A05103).

ACKNOWLEDGMENTS

We would like to thank Yujun Zhang from Institute of the China Academy of Chinese Medical Sciences for the helpful discussion.

SUPPLEMENTARY MATERIAL

The Supplementary Material for this article can be found online at: https://www.frontiersin.org/articles/10.3389/fpls.2021.733505/full#supplementary-material

Supplementary Figure 1 | Sequence alignment of PTC-present isforms and their corresponding reference isoforms. Location of PTC is highlighted in red rectangle.

Supplementary Figure 2 | Gene structure of PTC-present isforms and their corresponding reference isoforms. Location of PTC is indicated by black arrow.

Supplementary Figure 3 | Expression heatmap of genes related to MVA, MEP and artemisinin synthesis pathways.

Supplementary Table 1 | Pre-processed of full-length reads and corrected full-length reads data in leaf, flowers, stem and root of *A. annua*.

Supplementary Table 2 | Summary of Illumina RNA-seq and single-molecule real-time (SMRT) full-length read and corrected full-length reads quality mapping to the reference genome as determined by STAR.

Supplementary Table 3 | The alternative splicing isoforms and splicing types identified by Isoform Detection and Prediction (IDP).

Supplementary Table 4 | The expression level of a total of 11,832 alternative splicing isoforms involved in the *A. annua*.

Supplementary Table 5 | Genome-wide quantitative analysis of alternative splicing isoforms produced by different light treatments. The table shows that blue, red, far red, white light and dark were used to treat *A. annua* seedlings for 48 h. There were three biological duplicates for each treatment. Kallisto was used to quantify 75,058 transcripts, and the mean value of TPM was taken as the expression of transcripts. Set TPM = 1 to the cut-off value, and the isoform (alternative splicing) of TPM $>$ 1 is considered to be expressed.

Supplementary Table 6 | The total number of up-regulated and down-regulated IR isoforms and non-AS genes after treatment with blue, red, far-red, white light and dark. The table shows the total number of up- and down-regulated IR isoforms and non-AS genes after different light treatments, which were used to **Supplementary Figure 3**.

Supplementary Table 7 | Functional enrichment of differentially expressed AS genes. The table shows gene enrichment results corresponding to all differentially expressed AS isoforms. Gene Ratio: The ratio of the number of differentially expressed genes associated with this term to the total number of differentially expressed genes; which had GO annotations; Bg Ratio: The ratio of the number of background genes associated with this term to the total number of all background genes which had GO annotations; *p*.adjust: adjust *p*-values for multiple comparisons.

Supplementary Table 8 | Alternative splicing isoforms of up-regulated and down-regulated genes in Gene ontology (GO) functional enrichment results. The table shows gene enrichment results corresponding to all differentially expressed IR isoforms were either up-regulated or down-regulated after blue, red, far-red, white light and dark treatment.

Supplementary Table 9 | The overlapping genes in Gene ontology (GO) enrichment analysis result.

Supplementary Table 10 | The alternative splicing type and expression level of the genes involved in the *A. annua* (dark as a control).

Supplementary Table 11 | The alternative splicing type and expression level of the genes involved in the *A. annua* (white as a control).

Supplementary_AS_sequence.fasta | Fasta-format sequence file of a total of 11,832 alternative splicing isoforms involved in the *A. annua*.

REFERENCES

Abdel-Ghany, S. E., Hamilton, M., Jacobi, J. L., Ngam, P., Devitt, N., Schilkey, F., et al. (2016). A survey of the sorghum transcriptome using single-molecule long reads. *Nat. Commun.* 7:11706.

Ardui, S., Ameur, A., Vermeesch, J. R., and Hestand, M. S. (2018). Single molecule real-time (SMRT) sequencing comes of age: applications and utilities for medical diagnostics. *Nucleic Acids Res.* 46, 2159–2168. doi: 10.1093/nar/gky066

Au, K. F., Jiang, H., Lin, L., Xing, Y., and Wong, W. H. (2010). Detection of splice junctions from paired-end RNA-seq data by SpliceMap. *Nucleic Acids Res.* 38, 4570–4578. doi: 10.1093/nar/gkq211

Au, K. F., Sebastiano, V., Afshar, P. T., Durruthy, J. D., Lee, L., Williams, B. A., et al. (2013). Characterization of the human ESC transcriptome by hybrid sequencing. *Proc. Natl. Acad. Sci. U. S. A.* 110, E4821–E4830.

Awai, K., Xu, C., Tamot, B., and Benning, C. (2006). A phosphatidic acid–binding protein of the chloroplast inner envelope membrane involved in lipid trafficking. *PNAS* 103, 10817–10822. doi: 10.1073/pnas.0602754103

Berlin, K., Koren, S., Chin, C. S., Drake, J. P., Landolin, J. M., and Phillippy, A. M. (2015). Assembling large genomes with single-molecule sequencing and locality-sensitive hashing. *Nat. Biotechnol.* 33, 623–630. doi: 10.1038/nbt.3238

Bigay, J., and Antonny, B. (2012). Curvature, lipid packing, and electrostatics of membrane organelles: defining cellular territories in determining specificity. *Dev. Cell* 23, 886–895. doi: 10.1016/j.devcel.2012.10.009

Bin, L., and Hong, Z. (2010). Advances on the study of the pharmacological effects of artemisinin and its derivatives. *Chin. J. Clin. Pharmacol. Ther.* 15, 572–576.

Bray, N. L., Pimentel, H., Melsted, P., and Pachter, L. (2016). Near-optimal probabilistic RNA-seq quantification. *Nat. Biotechnol.* 34, 525–527. doi: 10.1038/nbt.3519

Brett, D., Pospisil, H., Valcarcel, J., Reich, J., and Bork, P. (2002). Alternative splicing and genome complexity. *Nat. Genet.* 30, 29–30.

Chang, C. Y., Lin, W. D., and Tu, S. L. (2014). Genome-Wide Analysis of Heat-Sensitive Alternative Splicing in Physcomitrella patens. *Plant Physiol.* 165, 826–840. doi: 10.1104/pp.113.230540

Chen, J. F., Dong, X., Li, Q., Zhou, X., Gao, S. H., Chen, R. B., et al. (2013). Biosynthesis of the active compounds of isatis indigotica based on transcriptome sequencing and metabolites profiling. *BMC Genomics* 14:857. doi: 10.1186/1471-2164-14-857

Chen, Y., Zhou, B., Li, J., Tang, H., Tang, J., and Yang, Z. (2018). Formation and Change of Chloroplast-Located Plant Metabolites in Response to Light Conditions. *Int. J. Mol. Sci.* 19:654. doi: 10.3390/ijms19030654

Cui, P., Zhang, S., Ding, F., Ali, S., and Xiong, L. (2014). Dynamic regulation of genome-wide pre-mRNA splicing and stress tolerance by the Sm-like protein LSm5 in Arabidopsis. *Genome Biol.* 15:R1.

Cuong, D. M., Jeon, J., Morgan, A. M. A., Kim, C., Kim, J. K., Lee, S. Y., et al. (2017). Accumulation of Charantin and Expression of Triterpenoid Biosynthesis Genes in Bitter Melon (*Momordica charantia*). *J. Agric. Food Chem.* 65, 7240–7249. doi: 10.1021/acs.jafc.7b01948

Czechowski, T., Larson, T. R., Catania, T. M., Harvey, D., Brown, G. D., and Graham, I. A. (2016). *Artemisia annua* mutant impaired in artemisinin synthesis demonstrates importance of nonenzymatic conversion in terpenoid metabolism. *Proc. Natl. Acad. Sci. U. S. A.* 113, 15150–15155. doi: 10.1073/pnas.1611567113

Czechowski, T., Larson, T. R., Catania, T. M., Harvey, D., Wei, C. X., Essome, M., et al. (2018). Detailed phytochemical analysis of highand low artemisinin-producing chemotypes of *Artemisia annua*. *Front. Plant Sci.* 9:641. doi: 10.3389/fpls.2018.00641

Dietz, K. J. (2015). Efficient high light acclimation involves rapid processes at multiple mechanistic levels. *J. Exp. Bot.* 66, 2401–2414.

Ding, F., Cui, P., Wang, Z., Zhang, S., Ali, S., and Xiong, L. (2014). Genome-wide analysis of alternative splicing of pre-mRNA under salt stress in Arabidopsis. *BMC Genomics* 15:431. doi: 10.1186/1471-2164-15-431

Dobin, A., Davis, C. A., Schlesinger, F., Drenkow, J., Zaleski, C., Jha, S., et al. (2013). STAR: ultrafast universal RNA-seq aligner. *Bioinformatics* 29, 15–21. doi: 10.1093/bioinformatics/bts635

Duque, P. (2011). A role for SR proteins in plant stress responses. *Plant Signal. Behav.* 6, 49–54. doi: 10.4161/psb.6.1.14063

Filichkin, S. A., Cumbie, J. S., Dharmawardhana, P., Jaiswal, P., Chang, J. H., Palusa, S. G., et al. (2015). Environmental stresses modulate abundance and timing of alternatively spliced circadian transcripts in Arabidopsis. *Mol. Plant* 8, 207–227. doi: 10.1016/j.molp.2014.10.011

Filichkin, S. A., Priest, H. D., Givan, S. A., Shen, R., Bryant, D. W., Fox, S. E., et al. (2010). Genome-wide mapping of alternative splicing in Arabidopsis thaliana. *Genome Res.* 20, 45–58. doi: 10.1101/gr.093302.109

Gao, H., Li, F., Xu, Z., Huang, C., Xiong, C., Jiang, C., et al. (2019). Genome-wide analysis of methyl jasmonate-regulated isoform expression in the medicinal plant Andrographis paniculata. *Ind. Crops Prod.* 135, 39–48. doi: 10.1016/j.indcrop.2019.04.023

Gao, T., Xu, Z., Song, X., Huang, K., Li, Y., Wei, J., et al. (2019). Hybrid Sequencing of Full-Length cDNA Transcripts of the Medicinal Plant Scutellaria baicalensis. *Int. J. Mol. Sci.* 20:4426. doi: 10.3390/ijms20184426

Ge, Y., and Porse, B. T. (2014). The functional consequences of intron retention: alternative splicing coupled to NMD as a regulator of gene expression. *Bioessays* 36, 236–243. doi: 10.1002/bies.201300156

Godoy Herz, M. A., Kubaczka, M. G., Brzyzek, G., Servi, L., Krzyszton, M., Simpson, C., et al. (2019). Light Regulates Plant Alternative Splicing through the Control of Transcriptional Elongation. *Mol. Cell* 73, 1066–1074.e3.

Graham, I. A., Besser, K., Blumer, S., Branigan, C. A., Czechowski, T., Elias, L., et al. (2010). The genetic map of *Artemisia annua* L. identifies loci affecting yield of the antimalarial drug artemisinin. *Science* 327, 328–331. doi: 10.1126/science.1182612

Isken, O., and Maquat, L. E. (2008). The multiple lives of NMD factors: balancing roles in gene and genome regulation. *Nat. Rev. Genet.* 9, 699–712. doi: 10.1038/nrg2402

Jiao, X., Chang, J., Kilic, T., Tong, L., and Kiledjian, M. (2013). A mammalian pre-mrna 5' end capping quality control mechanism and an unexpected link of capping to pre-mrna processing. *Mol. Cell* 50, 104–115. doi: 10.1016/j.molcel.2013.02.017

Jin, H., Wan, Y. W., and Liu, Z. (2017). Comprehensive evaluation of RNA-seq quantification methods for linearity. *BMC Bioinformatics* 18:117. doi: 10.1186/s12859-017-1526-y

Keren, H., Lev-Maor, G., and Ast, G. (2010). Alternative splicing and evolution: diversification, exon definition and function. *Nat. Rev. Genet.* 11, 345–355. doi: 10.1038/nrg2776

Kim, H., and Yin, J. (2005). Effects of RNA splicing and post-transcriptional regulation on HIV-1 growth: a quantitative and integrated perspective. *Syst. Biol.* 152, 138–152. doi: 10.1049/ip-syb:20050004

Kochan, E., Balcerczak, E., Szymczyk, P., Sienkiewicz, M., Zielinska-Blizniewska, H., and Szymanska, G. (2019). Abscisic Acid Regulates the 3-Hydroxy-3-methylglutaryl CoA Reductase Gene Promoter and Ginsenoside Production in Panax quinquefolium Hairy Root Cultures. *Int. J. Mol. Sci.* 20:1310.

Kolde, R. (2015). *Pheatmap: Pretty Heatmaps. R package version 0.6 1: 2012*.

Koren, S., Schatz, M. C., Walenz, B. P., Martin, J., Howard, J. T., Ganapathy, G., et al. (2012). Hybrid error correction and de novo assembly of single-molecule sequencing reads. *Nat. Biotechnol.* 30, 693–700. doi: 10.1038/nbt.2280

Li, J., Ren, L., Gao, Z., Jiang, M., Liu, Y., Zhou, L., et al. (2017). Combined transcriptomic and proteomic analysis constructs a new model for light-induced anthocyanin biosynthesis in eggplant (*Solanum melongena* L.). *Plant Cell Environ.* 40, 3069–3087. doi: 10.1111/pce.13074

Li, Y., Wei, W., Feng, J., Luo, H., Pi, M., Liu, Z., et al. (2018). Genome re-annotation of the wild strawberry Fragaria vesca using extensive Illumina- and SMRT-based RNA-seq datasets. *DNA Res.* 25, 61–70. doi: 10.1093/dnares/dsx038

Li, Y. Q., Yang, S. H., Yang, H. J., and Hua, J. (2007). The TIR-NB-LRR gene SNC1 is regulated at the transcript level by multiple factors. *Mol. Plant Microbe Interact.* 20, 1449–1456. doi: 10.1094/mpmi-20-11-1449

Liu, G. F., Liu, J. J., He, Z. R., Wang, F. M., Yang, H., Yan, Y. F., et al. (2018). Implementation of CsLIS/NES in linalool biosynthesis involves transcript splicing regulation in Camellia sinensis. *Plant Cell Environ.* 41, 176–186. doi: 10.1111/pce.13080

Liu, Y. F., Wang, B., Shu, S. H., Li, Z., Song, C., and Liu, D. (2021). Analysis of the Coptis chinensis genome reveals the diversification of protoberberine-type alkaloids. *Nat. Commun.* 12:3276.

Lopes, E. M., Guimaraes-Dias, F., Gama, T., Macedo, A. L., Valverde, A. L., de Moraes, M. C., et al. (2019). *Artemisia annua* L. and photoresponse: from artemisinin accumulation, volatile profile and anatomical modifications to gene expression. *Plant Cell Rep.* 39, 101–117. doi: 10.1007/s00299-019-02476-0

Love, M. I., Huber, W., and Anders, S. (2014). Moderated estimation of fold change and dispersion for RNA-seq data with DESeq2. *Genome Biol.* 15:550.

Ma, T. Y., Xiang, L., Zhang, D., Shi, Y. H., Ding, D. D., Shen, X. F., et al. (2018). Statues and research strategy of molecular breeding in *Artemisia annua*. *Zhongguo Zhong Yao Za Zhi* 43, 3041–3050.

Martins, S. B., Rino, J., Carvalho, T., Carvalho, C., Yoshida, M., Klose, J. M., et al. (2011). Spliceosome assembly is coupled to RNA polymerase II dynamics at the 3' end of human genes. *Nat. Struct. Mol. Biol.* 18, 1115–1123. doi: 10.1038/nsmb.2124

Mason, C. E., and Elemento, O. (2012). Faster sequencers, larger datasets, new challenges. *Genome Biol.* 13:314. doi: 10.1186/gb-2012-13-3-314

Matlin, A. J., Clark, F., and Smith, C. W. (2005). Understanding alternative splicing: towards a cellular code. *Nat. Rev. Mol. Cell Biol.* 6, 386–398. doi: 10.1038/nrm1645

Maza, E. (2016). In Papyro Comparison of TMM (edgeR), RLE (DESeq2), and MRN Normalization Methods for a Simple Two-Conditions-Without-Replicates RNA-Seq Experimental Design. *Front. Genet.* 7:164. doi: 10.3389/fgene.2016.00164

Miller, L. H., and Su, X. (2011). Artemisinin: discovery from the Chinese herbal garden. *Cell* 146, 855–858. doi: 10.1016/j.cell.2011.08.024

Nagegowda, D. A. (2010). Plant volatile terpenoid metabolism: biosynthetic genes, transcriptional regulation and subcellular compartmentation. *FEBS Lett.* 584, 2965–2973. doi: 10.1016/j.febslet.2010.05.045

Nagegowda, D. A., Gutensohn, M., Wilkerson, C. G., and Dudareva, N. (2008). Two nearly identical terpene synthases catalyze the formation of nerolidol and linalool in snapdragon flowers. *Plant J.* 55, 224–239. doi: 10.1111/j.1365-313x.2008.03496.x

Nilsen, T. W., and Graveley, B. R. (2010). Expansion of the eukaryotic proteome by alternative splicing. *Nature* 463, 457–463. doi: 10.1038/nature08909

Ozsolak, F., and Milos, P. M. (2011). RNA sequencing: advances, challenges and opportunities. *Nat. Rev. Genet.* 12, 87–98.

Paddon, C. J., and Keasling, J. D. (2014). Semi-synthetic artemisinin: a model for the use of synthetic biology in pharmaceutical development. *Nat. Rev. Microbiol.* 12, 355–367. doi: 10.1038/nrmicro3240

Paddon, C. J., Westfall, P. J., Pitera, D. J., Benjamin, K., Fisher, K., McPhee, D., et al. (2013). High-level semi-synthetic production of the potent antimalarial artemisinin. *Nature* 496, 528–532.

Palusa, S. G., Ali, G. S., and Reddy, A. S. (2007). Alternative splicing of pre-mRNAs of Arabidopsis serine/arginine-rich proteins: regulation by hormones and stresses. *Plant J.* 49, 1091–1107. doi: 10.1111/j.1365-313x.2006.03020.x

Pan, Q., Shai, O., Lee, L. J., Frey, B. J., and Blencowe, B. J. (2008). Deep surveying of alternative splicing complexity in the human transcriptome by high-throughput sequencing. *Nat. Genet.* 40, 1413–1415. doi: 10.1038/ng.259

Peplow, M. (2013). Malaria drug made in yeast causes market ferment. *Nature* 494, 160–161.

Petrillo, E., Godoy Herz, M. A., Barta, A., Kalyna, M., and Kornblihtt, A. R. (2014a). Let there be light: regulation of gene expression in plants. *RNA Biol.* 11, 1215–1220. doi: 10.4161/15476286.2014.972852

Petrillo, E., Godoy Herz, M. A., Fuchs, A., Reifer, D., Fuller, J., Yanovsky, M. J., et al. (2014b). A chloroplast retrograde signal regulates nuclear alternative splicing. *Science* 344, 427–430. doi: 10.1126/science.1250322

Reddy, A. S., Marquez, Y., Kalyna, M., and Barta, A. (2013). Complexity of the alternative splicing landscape in plants. *Plant Cell* 25, 3657–3683.

Rhoads, A., and Au, K. F. (2015). PacBio Sequencing and Its Applications. *Genomics Proteomics Bioinformatics* 13, 278–289. doi: 10.1016/j.gpb.2015.08.002

Sharon, I., Morowitz, M. J., Thomas, B. C., Costello, E. K., Relman, D. A., and Banfield, J. F. (2013). Time series community genomics analysis reveals rapid shifts in bacterial species, strains, and phage during infant gut colonization. *Genome Res.* 23, 111–120.

Shen, Q., Lu, X., Yan, T., Fu, X., Lv, Z., Zhang, F., et al. (2016). The jasmonate-responsive AaMYC2 transcription factor positively regulates artemisinin biosynthesis in *Artemisia annua*. *New Phytol.* 210, 1269–1281. doi: 10.1111/nph.13874

Shen, Q., Zhang, L., Liao, Z., Wang, S., Yan, T., Shi, P., et al. (2018). The Genome of *Artemisia annua* Provides Insight into the Evolution of Asteraceae Family and Artemisinin Biosynthesis. *Mol. Plant* 11, 776–788. doi: 10.1016/j.molp.2018.03.015

Song, C., Liu, Y. F., Song, A. P., Dong, G. Q., Zhao, H. B., and Sun, W. (2018). The chrysanthemum nankingense genome provides insights into the evolution and diversification of chrysanthemum flowers and medicinal traits. *Mol. Plant* 11, 1482–1491. doi: 10.1016/j.molp.2018.10.003

Staiger, D., and Brown, J. W. S. (2013). Alternative Splicing at the Intersection of Biological Timing, Development, and Stress Responses. *Plant Cell* 25, 3640–3656. doi: 10.1105/tpc.113.113803

Sun, C., Deng, L., Du, M., Zhao, J., Chen, Q., Huang, T., et al. (2020). A Transcriptional Network Promotes Anthocyanin Biosynthesis in Tomato Flesh. *Mol. Plant* 13, 42–58. doi: 10.1016/j.molp.2019.10.010

Syed, N. H., Kalyna, M., Marquez, Y., Barta, A., and Brown, J. W. (2012). Alternative splicing in plants–coming of age. *Trends Plant Sci.* 17, 616–623. doi: 10.1016/j.tplants.2012.06.001

Tan, H. X., Ling, X., Gao, S. H., Li, Q., Chen, J. F., Xiao, Y., et al. (2015). Trichome and artemisinin regulator 1 is required for trichome development and artemisinin biosynthesis in *artemisia annua*. *Mol. Plant* 8, 1396–1411. doi: 10.1016/j.molp.2015.04.002

Thatcher, S. R., Zhou, W., Leonard, A., Wang, B. B., Beatty, M., Zastrow-Hayes, G., et al. (2014). Genome-wide analysis of alternative splicing in Zea mays: landscape and genetic regulation. *Plant Cell* 26, 3472–3487. doi: 10.1105/tpc.114.130773

Triemer, S., Gilmore, K., Vu, G. T., Seeberger, P. H., and Seidel-Morgenstern, A. (2018). Literally Green Chemical Synthesis of Artemisinin from Plant Extracts. *Angew. Chem. Int. Ed Engl.* 57, 5525–5528. doi: 10.1002/anie.201801424

Tu, Y. (2011). The discovery of artemisinin (qinghaosu) and gifts from Chinese medicine. *Nat. Med.* 17, 1217–1220. doi: 10.1038/nm.2471

Vashisth, D., Kumar, R., Rastogi, S., Patel, V. K., Kalra, A., Gupta, M. M., et al. (2018). Transcriptome changes induced by abiotic stresses in *Artemisia annua*. *Sci. Rep.* 8:3423.

Wang, E. T., Sandberg, R., Luo, S., Khrebtukova, I., Zhang, L., Mayr, C., et al. (2008). Alternative isoform regulation in human tissue transcriptomes. *Nature* 456, 470–476. doi: 10.1038/nature07509

Wang, Y., Cheong, C. G., Hall, T. M., and Wang, Z. (2009). Engineering splicing factors with designed specificities. *Nat. Methods* 6, 825–830. doi: 10.1038/nmeth.1379

Wit, M., Costa Galvão, V., and Fankhauser, C. (2016). Light-mediated hormonal regulation of plant growth and development. *Annu. Rev. Plant Biol.* 67, 513–537. doi: 10.1146/annurev-arplant-043015-112252

Xu, Z., Peters, R. J., Weirather, J., Luo, H., Liao, B., Zhang, X., et al. (2015). Full-length transcriptome sequences and splice variants obtained by a combination of sequencing platforms applied to different root tissues of Salvia miltiorrhiza and tanshinone biosynthesis. *Plant J.* 82, 951–961. doi: 10.1111/tpj.12865

Yoo, H. J., Kim, J. H., Park, K. S., Son, J. E., and Lee, J. M. (2019). Light-Controlled Fruit Pigmentation and Flavor Volatiles in Tomato and Bell Pepper. *Antioxidants* 9:14. doi: 10.3390/antiox9010014

Yoshimura, K., Mori, T., Yokoyama, K., Koike, Y., Tanabe, N., Sato, N., et al. (2011). Identification of alternative splicing events regulated by an Arabidopsis serine/arginine-like protein, atSR45a, in response to high-light stress using a tiling array. *Plant Cell Physiol.* 52, 1786–1805. doi: 10.1093/pcp/pcr115

Yu, G., Wang, L. G., Han, Y., and He, Q. Y. (2012). clusterProfiler: an R package for comparing biological themes among gene clusters. *OMICS* 16, 284–287. doi: 10.1089/omi.2011.0118

Yu, Z. X., Li, J. X., Yang, C. Q., Hu, W. L., Wang, L. J., and Chen, X. Y. (2012). The jasmonate-responsive AP2/ERF transcription factors AaERF1 and AaERF2 positively regulate artemisinin biosynthesis in *Artemisia annua* L. *Mol. Plant* 5, 353–365. doi: 10.1093/mp/ssr087

Zhang, D., Jiang, C., Huang, C., Wen, D., Lu, J., Chen, S., et al. (2019). The light-induced transcription factor FtMYB116 promotes accumulation of rutin in Fagopyrum tataricum. *Plant Cell Environ.* 42, 1340–1351. doi: 10.1111/pce.13470

Zhang, D., Sun, W., Shi, Y., Wu, L., Zhang, T., and Xiang, L. (2018). Red and Blue Light Promote the Accumulation of Artemisinin in *Artemisia Annua* L. *Molecules* 23:1329. doi: 10.3390/molecules23061329

Zhang, T., Song, C., Song, L., Shang, Z., Yang, S., Zhang, D., et al. (2017). RNA Sequencing and Coexpression Analysis Reveal Key Genes Involved in alpha-Linolenic Acid Biosynthesis in Perilla frutescens Seed. *Int. J. Mol. Sci.* 18:2433. doi: 10.3390/ijms18112433

Zhang, X., Chen, M. H., Wu, X., Kodani, A., Fan, J., Doan, R., et al. (2016). Cell-Type-Specific Alternative Splicing Governs Cell Fate in the Developing Cerebral Cortex. *Cell* 166, 1147–1162.e15.

Zhu, D., Mao, F., Tian, Y., Lin, X., Gu, L., Gu, H., et al. (2020). The Features and Regulation of Co-transcriptional Splicing in Arabidopsis. *Mol. Plant* 13, 278–294. doi: 10.1016/j.molp.2019.11.004

Conflict of Interest: YYS and GD were employed by the Amway (China) Botanical R&D Center.

The remaining authors declare that the research was conducted in the absence of any commercial or financial relationships that could be construed as a potential conflict of interest.

Publisher's Note: All claims expressed in this article are solely those of the authors and do not necessarily represent those of their affiliated organizations, or those of the publisher, the editors and the reviewers. Any product that may be evaluated in this article, or claim that may be made by its manufacturer, is not guaranteed or endorsed by the publisher.

frontiers in Plant Science

ORIGINAL RESEARCH
published: 25 November 2021
doi: 10.3389/fpls.2021.761068

Identification of Differentially Expressed Genes and Pathways Involved in Growth and Development of *Mesona chinensis* Benth Under Red- and Blue-Light Conditions

Danfeng Tang[1,2], Qinfen Huang[2], Kunhua Wei[1,2], Xiaonan Yang[1,2], Fan Wei[1,2] and Jianhua Miao[1,2]**

[1] Guangxi Key Laboratory of Medicinal Resources Protection and Genetic Improvement, Guangxi Botanical Garden of Medicinal Plants, Nanning, China, [2] Guangxi Engineering Research Center of TCM Resource Intelligent Creation, Guangxi Botanical Garden of Medicinal Plants, Nanning, China

OPEN ACCESS

Edited by:
Jordi Moreno-Romero,
Centre for Research in Agricultural Genomics (CRAG), Spain

Reviewed by:
Atsushi Fukushima,
Kyoto Prefectural University, Japan
Rongfang Guo,
Fujian Agriculture and Forestry University, China
Houcheng Liu,
South China Agricultural University, China

***Correspondence:**
Fan Wei
wfmanuscript@163.com
Jianhua Miao
mjh1962@vip.163.com

Specialty section:
This article was submitted to Plant Physiology, a section of the journal Frontiers in Plant Science

Received: 19 August 2021
Accepted: 26 October 2021
Published: 25 November 2021

Citation:
Tang D, Huang Q, Wei K, Yang X, Wei F and Miao J (2021) Identification of Differentially Expressed Genes and Pathways Involved in Growth and Development of Mesona chinensis Benth Under Red- and Blue-Light Conditions. Front. Plant Sci. 12:761068. doi: 10.3389/fpls.2021.761068

Mesona chinensis Benth (MCB) is an important Chinese herbal medicine. The plant factories might be one of the ways to solve the shortage of MCB supply. In this study, the MCB seedlings were treated under the red (R) and blue (B) lights in the plant factory. Results showed that the red light promoted the growth and development of MCB in comparison with the blue light. Under the red-light condition, the biomass, plant height, and root characteristics were significantly higher than those under blue-light condition, while the soil and plant analyzer development (SPAD) under the red-light treatment was significantly lower than that under the blue-light treatment. Red light also significantly promoted the content of soluble sugar and pectin of MCB compared with blue light. Transcriptome analysis showed that a total of 4,165 differentially expressed genes (DEGs) were detected including 2,034 upregulated and 2,131 downregulated. Of these, 1,112 DEGs including 410 upregulated and 702 downregulated genes were associated with 111 pathways. Moreover, a total of 8,723 differentially expressed transcription factors (TFs) were identified in R vs. B, and these TFs were distributed in 56 gene families. Metabonomic results revealed that a total of 184 metabolites and 99 differentially expressed metabolites (DEMs) (42 upregulated and 57 downregulated) were identified in the red- and blue-light treatments. Integrative analysis of transcriptome and metabolome unveiled that a total of 24 pathways included 70 compounds (metabolites) and were associated with 28 unigenes. In particular, these pathways included starch and sucrose metabolism, phenylpropanoid biosynthesis, cysteine and methionine metabolism, glycolysis/gluconeogenesis, and pentose and glucuronate interconversions. The unigenes included *asparagine synthetase* (*AS*), *thymidine kinase* (*TK*), *alpha, alpha-trehalose-phosphate synthase* (*TPS*), *phosphatase IMPL1* (*IMPL1*), *dihydroflavonol 4-reductase* (*D4R*), and *4-coumarate-CoA ligase-like 6* (*4CL6*), *bifunctional aspartokinase-homoserine dehydrogenase 1* (*thrA*), and *abscisic acid 8′-hydroxylase 2 isoform X1* (*ABA8*). It was indicated that these pathways and genes might play important roles in the growth and development of MCB. This study laid a foundation for the future research of MCB.

Keywords: ***Mesona chinensis*** **Benth, plant factory, LED, red and blue light, growth and development**

INTRODUCTION

Mesona chinensis Benth (MCB), belonging to the Lamiaceae family, is an annual or perennial herb. It is an economically important plant widely cultivated in South China and Southeast Asian countries (Ren et al., 2019; Tang et al., 2020). It includes polysaccharides, flavonoids, vitamins, amino acids, fat, fiber, and polyphenols (Su et al., 2011; Tang et al., 2020). *M. Chinensis* Benth polysaccharides (MCP) consist of eight monosaccharides, including galacturonic acid, glucose, galactose, xylose, mannose, rhamnose, ribose, and glucuronic acid, with the molar percentages of 28.4, 26.5, 16.4, 10.6, 7.4, 5.7, 4.2, and 0.9%, respectively (Zhang et al., 2013). As one of the functional active substances, MCP has attracted much attention owing to its various biological activities, including antitumor, antioxidant, antiviral, and hypoglycemic activities (Huang et al., 2018; Wang et al., 2019; Xiao et al., 2019). In addition to its medicinal values, MCB is used as a herbal beverage in China and Southeast Asian countries and also as a source of raw materials in food industries and packaging industries, such as natural food pigment, new refrigerant, food film, and coating agent (Cheng et al., 2015; Yang et al., 2015a,b; Huang et al., 2019; Ren et al., 2019). In recent years, due to a relatively high level of cultivation and management measures of MCB, farmers are not willing to plant it, resulting in the insufficient supply of MCB in China and a large import of MCB raw materials from Southeast Asian countries. Therefore, besides the traditional field cultivation, it is necessary to seek other cultural regimes of MCB.

The plant factory is a revolution for the traditional cropping system to deal with the issues of farmland area shrinkage and population growth (United Nations [UN], 2017). In a plant factory, electric-based equipment is used to control all involved environmental factors, for example, illumination condition, temperature, and nutrition supply (Kim et al., 2013; Zha and Liu, 2018). Light is one of the most important factors that regulate plant growth and development (He et al., 2020a) and that determine photosynthesis and subsequently carbohydrate production and accumulation (Wei et al., 2020). Light-emitting diode (LED) technology provides an essentially distinct and energy-effective approach for the agricultural industries (Ballare et al., 2012). The LED light system allows the regulation of spectrum, spectral composition, and light intensity to supply better growth conditions for commercial crops, fruits, flower plants, and even trees (Yeh and Chung, 2009; Tayebeh et al., 2020). Theoretically, in a plant factory framework, if all the factors are within the most favorable level, some specific plants can grow continuously and efficiently. As mentioned earlier, MCB is an annual or perennial herb and may be suitable for growing in plant factories.

Artificial light is essential in a plant factory, and red (R) and blue (B) lights are the two major wavelengths that drive photosynthesis (Tandeau de Marsac and Houmard, 1993; He et al., 2020c). Red light is a component of the solar spectrum that strongly affects plant tissues (Kuo et al., 2015), while blue light is an important environmental signal for various organisms regulating their growth and developmental processes through photoreceptors (Sano et al., 2009). Although the blue and red lights are essential for the growth of many plants, including potato (He et al., 2020c), watermelon (Bantis et al., 2020), birch (Saebo et al., 1995), lettuce, peanut plants (Poulet et al., 2014; Li et al., 2018), and kidney bean plants (Hiromichi and Kazuhiro, 2000), few studies have focused on the effects of each on the growth of MCB in a plant factory. In this study, we examined and analyzed the physiological, biochemical, cytological, and molecular responses to the red and blue lights in MCB. This study provides guidance for the cultivation of MCB in plant factories and lays a foundation for the future research of MCB molecular biology.

MATERIALS AND METHODS

Materials and Experimental Treatments

Mesona chinensis Benth cutting seedlings of about 10–15 cm height were used as plant materials. The seedlings were transplanted on the culture frame in the plant factory with a condition of 25°C room temperature and 70% humidity. The seedlings were exposed to blue (200 μmol m^{-2} s^{-1}) and red (200 μmol m^{-2} s^{-1}) lights at a day/night time of 16/8 h, respectively. All the plants were cultivated using the hydroponic method with 1/2 Hoagland nutrient solution. After 1 month, the data on the growth of MCB were measured and collected. Meanwhile, the three-fourth true leaves of apical meristem were collected and frozen at −80°C for the analysis of soluble sugar, soluble pectin, transcriptome, and metabolome (Suzhou PANOMIX Biomedical Tech Co. Ltd., Suzhou, China).

Determination of Agronomic Characters

Light-emitting diode meter equipment (UPRtek, MK350NPLUS) was used for spectrum measurement. At least three plants from each treatment were taken for the measurement of fresh weight, dry weight, plant height, and soil and plant analyzer development (SPAD) (SPAD-502 Chlorophyll Meter) values. Root morphological indexes were determined using the root analyze system (WinRHIZO, Regent, Canada) (Tang et al., 2019). Soluble sugar and soluble pectin were measured using Plant Soluble Sugar and Pectin Kits (Suzhou Grace Biotechnology Co. Ltd., Suzhou, China).

Transmission Electron Microscope Observation

The third true leaf of apical meristem was used, and the vein was removed. Transmission Electron Microscope (TEM) observation was referred by Tang et al. (2018). Leaves were cut into small size pieces (about 2 mm × 2 mm) and put into a 2.5% glutaraldehyde buffer solution. Then the samples were fixed at 4°C, rinsed in phosphate buffer, post-fixed in 1% osmium tetraoxide (OsO_4), dehydrated with a series of 50, 60, 70, 80, 90, and 100% ethanol, washed in 100% acetone, and embedded. Finally, the samples were observed under a TEM system of Hitachi.

cDNA Library Construction, Sequencing, *de novo* Assembly

The cDNA library was constructed and sequenced according to Santos et al. (2021). Briefly, RNA purity was checked, and RNA integrity was first assessed. Then, about 1 μg RNA per sample was employed for cDNA library construction using NEBNext® Ultra™ RNA Library Prep Kit for Illumina® (NEB, United States), following the instructions of the manufacturer. Consequently, the library quality was estimated using the Agilent Bioanalyzer 2100 system. Finally, the RNA-Seq library sequencing was performed using the Illumina Hiseq X Ten platform for a 150 bp paired-end read.

Trinity[1] was used for *de novo* assembly of transcriptomes. In brief, clean reads with a certain overlap length were initially combined to form contigs and then related contigs were clustered using the TGICL software (version 2.1) (Pertea et al., 2003) to yield unigenes that could not be extended on either end and redundancies were removed to obtain non-redundant unigenes.

Functional Annotation of the Assembled Unigenes

The sequences of unigenes were searched against the NR,[2] KEGG,[3] GO,[4] COG,[5] Swiss-Prot,[6] and TrEMBL databases (*E*-value ≤ 1E-5) using BLASTX to retrieve protein functional annotations based on sequence similarity. High-priority databases (followed by NR, Swiss-Prot, and KEGG) were selected to determine the direction of the unigene sequences. The best aligning results were used to predict the coding region sequences from unigenes, and the coding sequences (CDSs) were translated into amino sequences using the standard codon table. The ESTScan software (Iseli et al., 1999) was used to decide the sequence direction of the unigenes that could not be aligned to any of the above databases. GO terms were assigned to each sequence annotated using BLASTX against the Nr database using the Blast2GO program with the *E*-value threshold of 1E-5 for further functional categorization. The WEGO software (Ye et al., 2006) was used to plot the distribution of the GO functional classification of the unigenes. The unigene sequences were also aligned to the COG database to predict and classify possible functions and assigned to KEGG pathway annotations to analyze the inner-cell metabolic pathways and the related gene function using BLASTX.

Differential Expression Analysis and Functional Enrichment

HTSeq was used to calculate the number of reads mapped to each gene and the FPKM (fragments per kilobase of exon model per million mapped fragments) method was employed for the calculation of gene expression. Differential expression analysis was performed using the DgSeq2, *q*-value (or FDR) < 0.01, and | log 2 (fold change [FC])| > 1 was set as the threshold for significantly differential expression. GO enrichment analysis of differentially expressed genes (DEGs) was carried out using the GOseq, in which gene length bias was corrected. GO functional analysis included GO functional classification annotation for DEGs and GO functional enrichment analysis for DEGs (Gene Ontology database, see text footnote 4). The top 10 GO terms with the lowest *p*-value (the most significant enrichment) were selected from each GO category for display. KO-Based Annotation System (KOBAS) was used to test the statistical enrichment of DEGs in KEGG pathways (see text footnote 3). According to the results of DEGs of KEGG enrichment analysis, the top 30 pathways with the lowest *p*-value (the most significant enrichment) were selected for display.

Liquid Chromatography-Mass Spectrometry Detection

The extraction of metabolites was conducted as follows. All samples were taken in a 2 ml EP tube, two steel balls were added and ground in the tissue grinder at 50 Hz for 60 s, and then the samples were homogenized. Accurately weighed 100 mg (±1%) of the homogenized sample was taken in a 2 ml EP tube, accurately weighed 0.6 ml of methanol (including internal standard) was added, and the mixture was vortexed for 30 s. Two steel balls were added and ground in the tissue grinder for 60 s at 50 Hz. The mixture was centrifuged at 4°C for 10 min at 12,000 rpm, and the supernatant was filtered through 0.22 μm membrane to obtain the prepared samples for the detection of liquid chromatography-mass spectrometry (LC-MS). Of note, 20 μl from each sample was taken to the quality control (QC) samples (samples that were used to monitor deviations of the analytical results from these pool mixtures and compare them with the errors caused by the analytical instrument itself). The rest of the samples were used for the detection of LC-MS according to Zhang et al. (2020).

The raw LC-MS data were converted into mzXML format files by Proteowizard Data Analysis software (version v3.0.8789). Then, peaks identification, peaks filtration, and peaks alignment were processed using XCMS[7] with the following default set: ppm = 15, bw = 2, peak width = c(5, 30), mzdiff = 0.01, mzwid = 0.015, and method = centWave. Each metabolite was confirmed based on their exact molecular weights (MWs), and the possible empirical formulae of the metabolites were speculated (MW error < 20 ppm). Then, the exact MWs were employed to identify potential biomarkers using Metlin,[8] Human Metabolome Database (HMDB),[9]

[1] http://trinityrnaseq.sourceforge.net/, version 2.8.5.

[2] ftp://ftp.ncbi.nlm.nih.gov/blast/db/, version v0.8.37.99.

[3] http://www.genome.jp/kegg/, version 2.1.1.

[4] http://www.geneontology.org/, version 2.5.0.

[5] http://www.ncbi.nlm.nih.gov/COG/, version v0.8.37.99.

[6] http://web.expasy.org/docs/swiss-prot_guideline.html, version v0.8.37.99.

[7] www.bioconductor.org

[8] http://metlin.scripps.edu

[9] http://www.hmdb.ca

massbank,[10] mzCloud,[11] Lipid Maps,[12] and database built by Bionovogene Co. Ltd.

Quantitative Reverse Transcription-PCR Analysis

cDNA was synthesized using TransScript® One-Step gDNA Removal and cDNA Synthesis SuperMix, and quantitative reverse transcription-PCR (qRT-PCR) was conducted using PerfectStart® Green qPCR SuperMix (TransGen Biotech Co. Ltd.) on an applied biosystems (Thermo Fisher Scientific). The qPCR primers were designed and listed in **Supplementary Table 1**. The 20 μl qPCR reaction mixture contained 1.0 μl of cDNA, 0.4 μl of primers, 10 μl of PerfectStart® Green qPCR SuperMix, and 8.2 μl of nuclease-free water. The qPCR amplification procedure was as follows: 94°C for 30 s, followed by 40 cycles of 94°C for 5 s, 60°C for 15 s, and 72°C for 10 s. Each sample was analyzed in triplicate, and the relative gene expression was calculated using the $2^{-\Delta\Delta CT}$ method (Livak and Schmittgen, 2001).

Statistical Analysis

Means were compared using the least significant differences (Duncan) at the 5% probability level. GraphPad Prism 7, Microsoft Office PowerPoint, and Microsoft Excel were used for data processing and plotting figures.

RESULTS

Red Light Promoted the Growth and Development and Quality of *Mesona chinensis* Benth

In this study, to ensure the accuracy of the spectrum in the plant factory, the spectra of the red and blue lights were determined (**Figures 1A,B**). Red light promoted the growth and development of MCB in comparison with blue light (**Figures 1C,D**). Under the red-light condition, the biomass, plant height, and root characteristics of MCB were significantly higher than those under blue-light condition, while the SPAD of red-light treatment was significantly lower than that of blue-light treatment (**Figure 2**). Of these, the dry weight, fresh weight, and plant height increased by 96.90, 163.07, and 40.20%, respectively (**Figures 2A–C**). Compared with blue-light condition, the root length, root surface area, root volume, and root average diameter under red-light condition increased by 13.99, 93.05, 228.22, and 68.25%, respectively (**Figures 2E–H**). However, under red-light condition, the SPAD value was reduced by 57.50% in comparison with that under blue-light condition (**Figure 2D**). Moreover, red light also significantly promoted the content of soluble sugar and pectin of MCB compared with blue light (**Figures 2I,J**). The soluble sugar and soluble pectin contents of the red-light treatment increased by 299.48 and 217.71%, respectively.

[10]http://www.massbank.jp/

[11]https://www.mzcloud.org

[12]http://www.lipidmaps.org

Red Light Changed Chloroplast Ultrastructure of *Mesona chinensis* Benth Leaves

As mentioned earlier, the leaves turned light yellow under the red-light treatment, while it was green under the blue-light treatment. To further study the effects of red and blue lights on the leaf ultrastructure of MCB, TEM observation was performed in this study (**Figure 3**). The leaves under both treatments had intact cell walls and chloroplast structures. The osmiophilic granules and starch grains were also observed in the leaves under both treatments. Compared with the blue-light treatment, there were more starch grains in the leaves under the red-light treatment. However, they had different chloroplast ultrastructures. Remarkably, a large number of vesicles were found and the vesiculation phenomenon was observed in thylakoid lamellae under the red-light treatment in comparison with the blue-light treatment.

RNA Sequencing, *de novo* Assembly, and Functional Annotation

The RNA-Seq data generated in this study have been deposited in the Sequence Read Archive (SRA) database (accession number PRJNA741889). The *Q*30 values and the percentage of clean data of the six samples were more than 91 and 90%, respectively (**Supplementary Tables 2**, **3**). A total of 171,484 transcripts and 60,064 unigenes were identified with a total length of 224,909,017 and 64,130,649 bp, respectively (**Supplementary Table 4**), and then the unigenes were annotated against NR, GO, KEGG, eggNOG, Swiss-Prot, and Pfam databases (**Supplementary Tables 5**, **6**). Among these, 35,666 unigenes were annotated to the NR database, accounting for 59.38% of the transcripts, while 16,617 (27.67%), 14,347 (23.89%), 19,235 (32.02%), 34,247 (57.02%), and 26,555 (44.21%) unigenes could be annotated to GO, KEGG, Pfam, eggNOG, and Swissport, respectively (**Supplementary Table 7**). GO analysis revealed that a total of 24, 24, and 19 GO terms were involved in biological processes, cell components, and molecular functions, respectively (**Supplementary Figure 1**). Furthermore, we obtained the active biological functional pathways on MCB leaf unigenes from the KEGG pathway database. A total of 9,573 unigenes aligned with 35 classifications, and the pathways were divided into five categories containing metabolism, genetic information processing, environmental information processing, cellular processes, and organismal systems (**Supplementary Figure 2**).

Identification of Differentially Expressed Genes and Pathways

Using RSEM software and the transcript sequences as a reference, we aligned the clean reads of each sample to the reference sequence. Then, the number of reads aligned on each gene were counted in each sample and the FPKM values of each gene were calculated (**Supplementary Table 8**). The FPKM value between 1 and 10 was dominant in different ranges of expression levels (**Figures 4A,B**). Before DEGs analysis, the correlation of gene expression level among the samples was analyzed for checking the reliability of the experiment and the rationality of

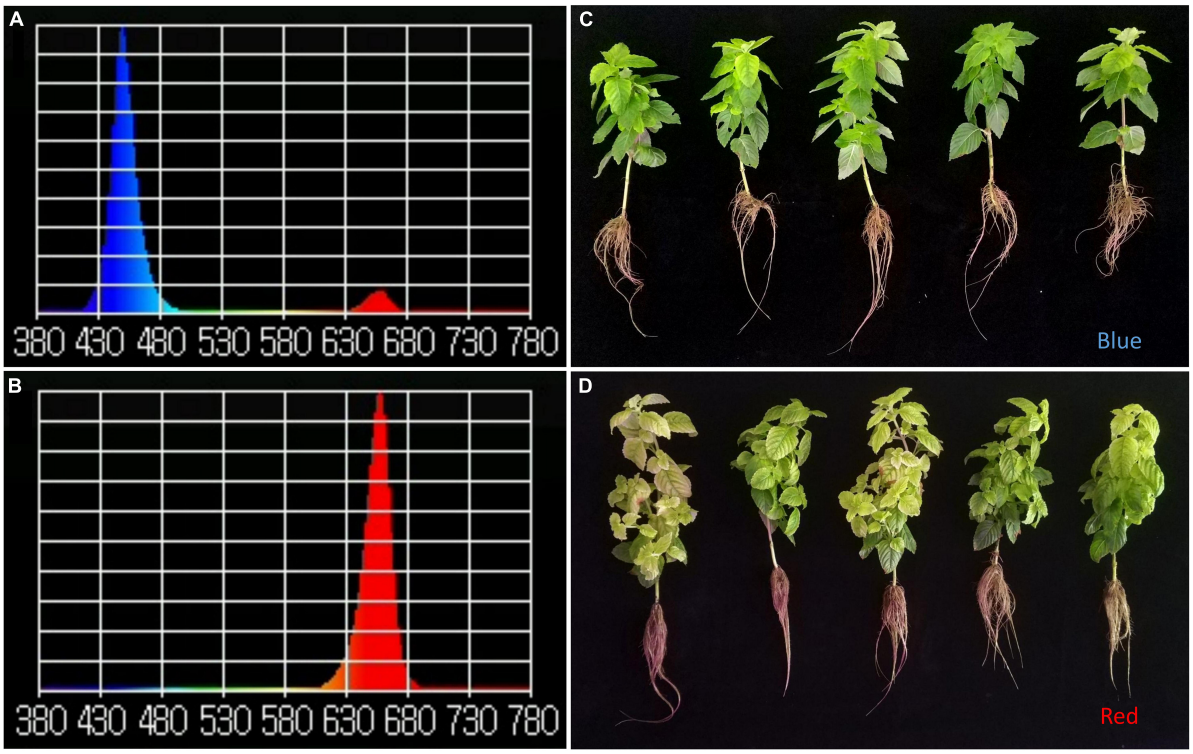

FIGURE 1 | Comparison of plant morphological characteristics and spectrum under the red and blue lights. **(A,B)** Blue- and red-light spectrum, respectively; Y-axis: λ.pv, X-axis: wavelength; **(C,D)** The plants grown under the blue- and red-light conditions, respectively.

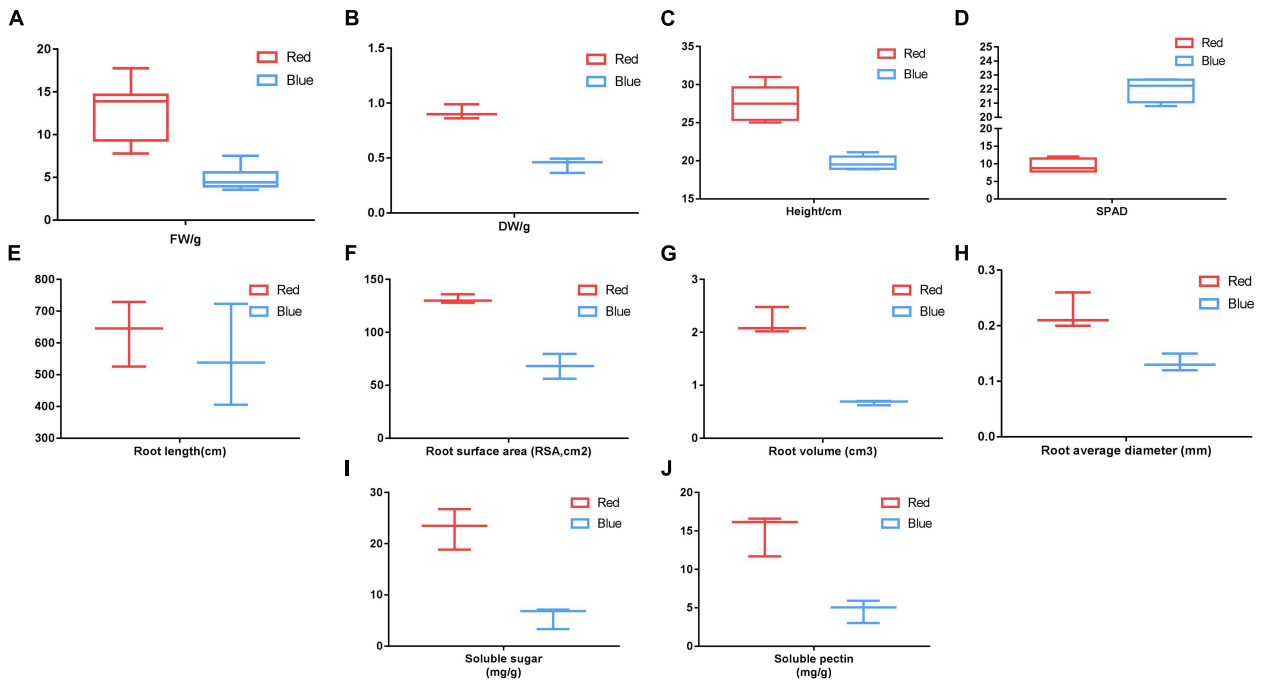

FIGURE 2 | Comparison of plant growth and development, soluble sugar, and soluble pectin under the red and blue lights. **(A–J)** Indiated the fresh weight, dry weight, plant height, SPAD, root length, root surface area, root volume, root average diameter, soluble sugar, and soluble pectin, respectively. FW: fresh weight; DW: dry weight; SPAD, soil and plant analyzer development.

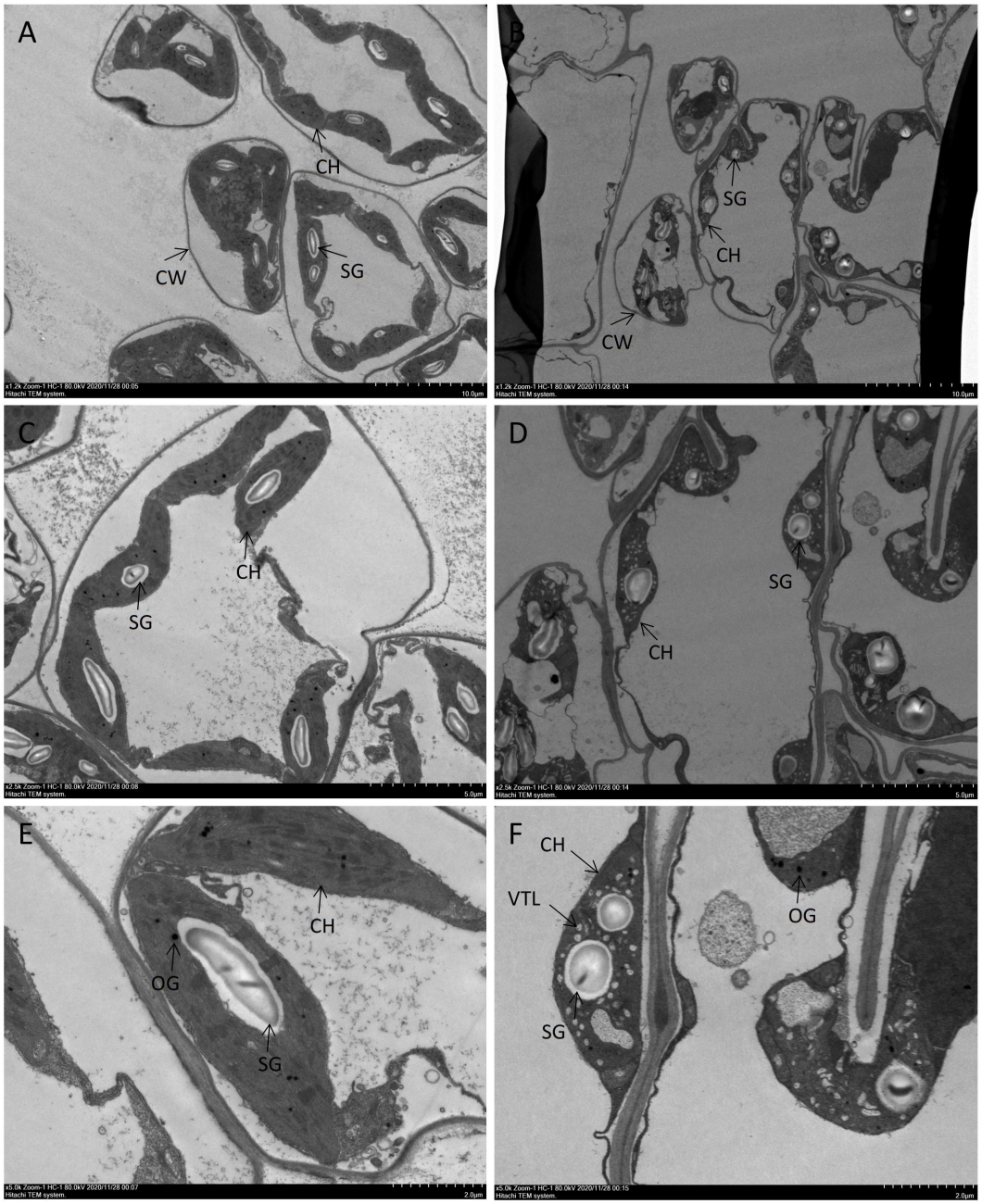

FIGURE 3 | Comparison of the ultrastructure of MCB leaves under the red and blue lights. **(A,C,E)** Represented the blue-light treatment; **(B,D,F)** Represented the red-light treatment. SG, starchgrains; OG, osmiophilicgranules; CH, chloroplast; CW, cellwall; VTL, vesiculation of thylakoid lamellar.

sample collection. The Pearson's correlation coefficient of gene expression levels under the blue-light condition ranged from 0.93 to 0.97, while under the red-light condition it ranged from 0.99 to 1.00 (**Figure 4C**). In addition, the samples under the two treatments also differed remarkably by the principal component analysis (PCA) (**Figure 4D**). Therefore, it was indicated that the data could be used for further DEG analysis.

To identify the genes involved in MCB growth, we analyzed the DEGs between the red-light and blue-light treatments with the following parameters: p-value < 0.05 and $|\log 2\ FC| \geq 1$. A total of 4,165 DEGs were detected including 2,034 upregulated and 2,131 downregulated (**Figure 5A**). Among these, 2–5 fold changes were noted in the expression of majority DEGs (1,518 upregulated and 1,718 downregulated) (**Figure 5B**).

GO analysis unveiled that the DEGs were categorized into certain cellular components, molecular functions, and biological processes (**Figure 5C**). Cellular component analysis showed that the most significant enrichment of DEGs was

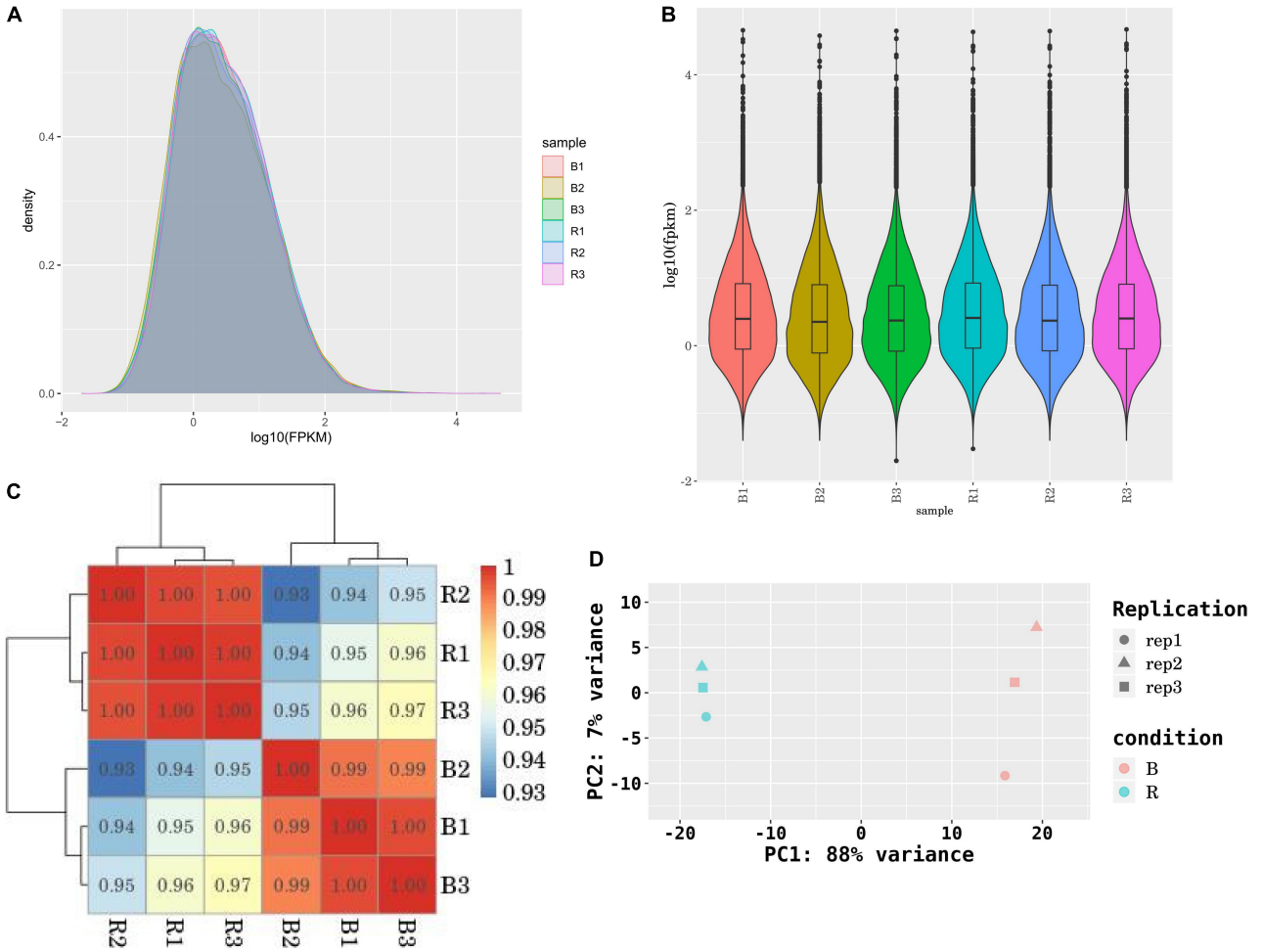

FIGURE 4 | Analysis of RNA sequencing data of six samples. **(A,B)** The density distribution of FPKM; **(C)** Correlation test of six samples; **(D)** PCA analysis of six samples.

involved in thylakoid, followed by chloroplast, plastid, and photosynthetic membrane. Regarding molecular functions, oxidoreductase activity was the most significant enrichment. In terms of biological processes, the oxidation-reduction process and photosynthesis were the significantly overrepresented items.

Further KEGG analysis uncovered that in total, 1,112 DEGs, including 410 upregulated and 702 downregulated genes, were associated with 111 pathways (**Supplementary Table 9**). All the top 30 most significant enrichment pathways were divided into environmental information processing, metabolism, and organismal systems (**Figure 5D**). Of these, only plant MAPK signaling pathways and plant hormone signal transduction were the most significant enrichment in environmental information processing, and the plant circadian rhythm and plant-pathogen interaction pathways were the two most representative pathways in organismal systems. Notably, the remaining 26 pathways, including starch and sucrose metabolism, pentose phosphate pathway, flavonoid biosynthesis, photosynthesis, and porphyrin and chlorophyll metabolism, were involved in metabolism.

Transcription factors regulate plant growth and development, environmental stress response, and biosynthesis of secondary metabolites by inhibiting or activating gene expression (Latchman, 1993; Chen et al., 2021). In this study, a total of 8,723 differentially expressed TFs were identified and they were distributed in 56 gene families (**Supplementary Figure 3** and **Supplementary Table 10**). It was indicated that these TFs might be associated with MCB growth.

Metabolome Profiling Between the Red- and Blue-Light Treatments

In this study, metabolites were extracted from leaf samples with six replicates and analyzed using LC-MS. A total of 184 metabolites were identified in the red- and blue-light treatments (**Supplementary Table 11** and **Supplementary Figure 4**). Based on these metabolites, the PCA and relative standard deviation (RSD) showed that the data were reliable (**Supplementary Figure 5**). The metabolites included carbohydrates and carbohydrate conjugates (CCC), alcohols and polyols (AP),

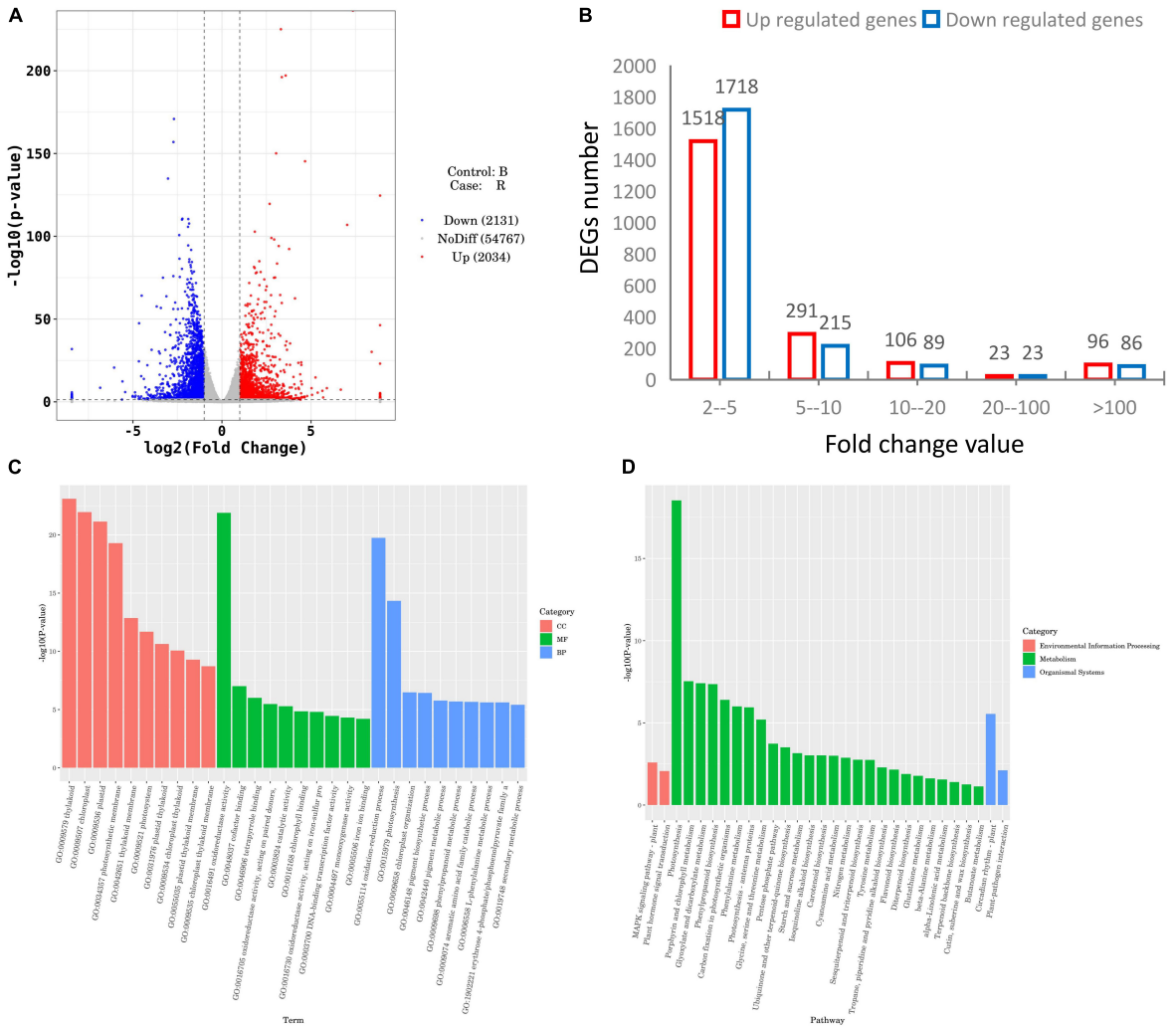

FIGURE 5 | Differentially expressed genes (DEGs) statistics and functional enrichment analysis between the red- and blue-light treatments. **(A)** DEGs statistical analysis; **(B)** Distribution of DEGs based on different fold change thresholds; **(C,D)** GO and KEGG enrichment analysis, respectively.

amino acids, peptides, and analogs (AAPA), fatty acids and conjugates (FAC), amines (A), eicosanoids (E), linoleic acids, and derivatives (LAD), 1-hydroxy-2-unsubstituted benzenoids (1H2UB), short-chain keto acids and derivatives (SKAD), tricarboxylic acids and derivatives (TAD), and cyclic purine nucleotides (CPN), accounting for 18.45, 19.42, 26.21, 11.65, 5.83, 3.88, 3.88, 2.91, 2.91, 2.91, and 1.94%, respectively (**Supplementary Figure 6**).

Furthermore, we found 99 DEMs between the red- and blue-light treatments, including 42 upregulated and 57 downregulated (**Figure 6A**). To illustrate the function of the metabolites involved in MCB growth, we analyzed the 99 DEMs using the KEGG database. A total of 53 pathways were found when the DEMs between the two treatments were introduced into KEGG (**Figure 6B**). Of these, based on the pathway impact scores (>0.1), we identified the 17 most relevant metabolic pathways (**Table 1**). Furthermore, seven pathways were at an extremely significant level ($p < 0.01$), including flavone and flavonol biosynthesis (FFB), aspartate and glutamate metabolism (AAGM), cysteine and methionine metabolism (CMM), galactose metabolism (GM), arginine and proline metabolism (APM), citrate cycle (TCA cycle), and lysine biosynthesis (LB). Only one pathway, glyoxylate and dicarboxylate metabolism, was at a significant level ($p < 0.05$). The remaining nine pathways were statistically non-significant ($p > 0.05$).

Integrative Analysis of Transcriptome and Metabolome

Based on the DEGs and DEMs data, we conducted an integrative analysis of transcriptome and metabolome between the red- and blue-light treatments. Results showed that a total of 24 pathways included 70 compounds (metabolites) and were involved in 28 unigenes (**Table 2**). These pathways included starch and sucrose metabolism (C00092 and C00185), phenylpropanoid biosynthesis (C00079), cysteine

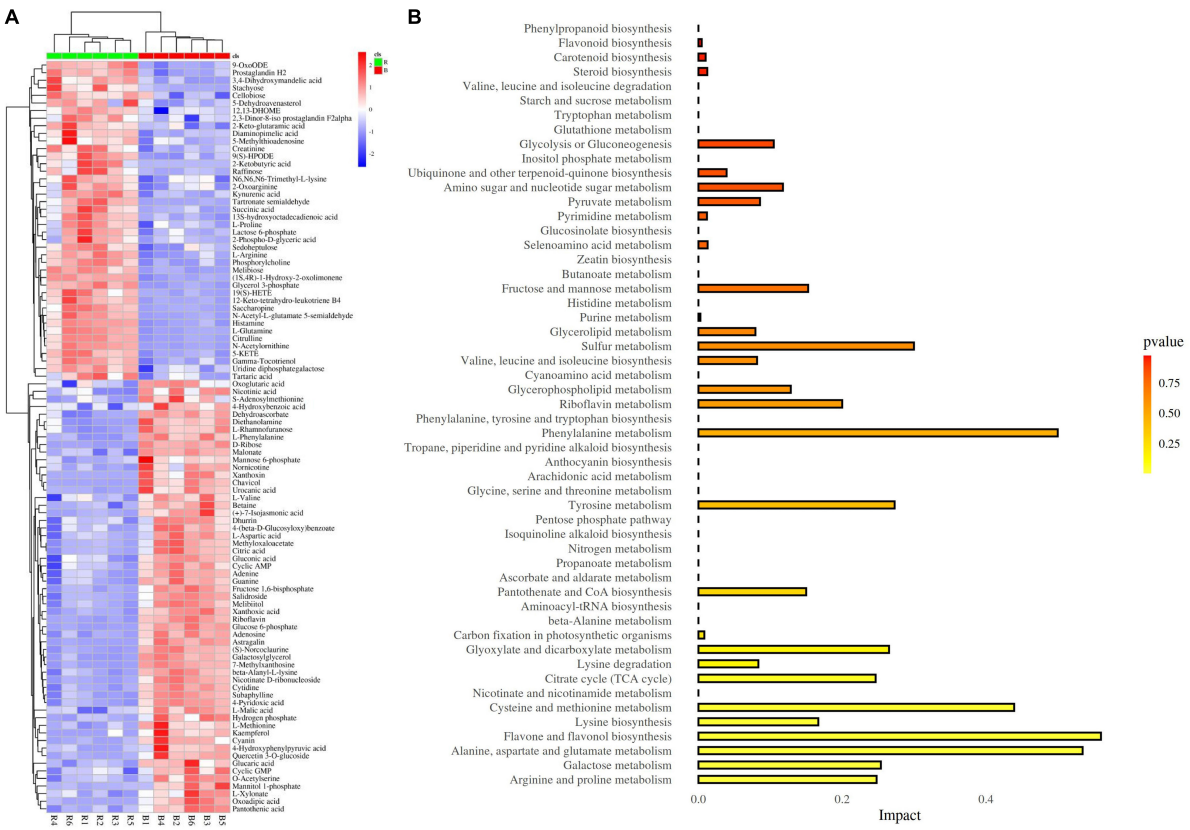

FIGURE 6 | Analysis of differentially expressed metabolites (DEMs) and KEGG pathway. **(A)** DEMs identified between the red- and blue-light treatments; **(B)** Analysis of KEGG pathway of DEMs.

TABLE 1 | Results from KEGG pathway analysis.

Pathway name	Total	Hits	Raw p	-Log(p)	Holm adjust	FDR	Impact
Flavone and flavonol biosynthesis	9	3	0.0263	3.6375	1.0000	0.5724	0.5600
Alanine, aspartate, and glutamate metabolism	22	5	0.0223	3.8038	1.0000	0.5724	0.5345
Phenylalanine metabolism	8	1	0.4736	0.7475	1.0000	1.0000	0.5000
Cysteine and methionine metabolism	34	6	0.0408	3.2001	1.0000	0.5910	0.4391
Sulfur metabolism	12	1	0.6187	0.4802	1.0000	1.0000	0.3000
Tyrosine metabolism	18	2	0.4085	0.8952	1.0000	1.0000	0.2727
Glyoxylate and dicarboxylate metabolism	17	3	0.1365	1.9912	1.0000	1.0000	0.2653
Galactose metabolism	26	6	0.0115	4.4636	0.9908	0.5012	0.2539
Arginine and proline metabolism	38	8	0.0065	5.0396	0.5635	0.5012	0.2480
Citrate cycle (TCA cycle)	20	4	0.0612	2.7936	1.0000	0.6656	0.2467
Riboflavin metabolism	10	1	0.5519	0.5944	1.0000	1.0000	0.2000
Lysine biosynthesis	10	3	0.0355	3.3373	1.0000	0.5910	0.1667
Fructose and mannose metabolism	16	1	0.7240	0.3229	1.0000	1.0000	0.1525
Pantothenate and CoA biosynthesis	14	2	0.2932	1.2270	1.0000	1.0000	0.1500
Glycerophospholipid metabolism	25	2	0.5852	0.5359	1.0000	1.0000	0.1283
Amino sugar and nucleotide sugar metabolism	41	2	0.8383	0.1764	1.0000	1.0000	0.1177
Glycolysis or Gluconeogenesis	25	1	0.8672	0.1425	1.0000	1.0000	0.1048

and methionine metabolism (C00019, C00049, C00073, C00109, C00170, C00979), glycolysis/gluconeogenesis (C00631), and pentose and glucuronate interconversions (C00026 and C05411). These genes included *asparagine synthetase* (*AS*), *thymidine kinase* (*TK*), *alpha, alpha-trehalose-phosphate synthase* (*TPS*), *phosphatase IMPL1* (*IMPL1*), *dihydroflavonol 4-reductase*

TABLE 2 | Results of integrative analysis of transcriptome and metabolome.

KEGG	Pathway description	Compounds_KO	Genes_ko
ath00960	Tropane, piperidine, and pyridine alkaloid biosynthesis	C00079;C00253;C06524;	K00276
ath00350	Tyrosine metabolism	C00042;C01179;C05580;C06046;	K00276
ath00240	Pyrimidine metabolism	C00064;C00383;C00475;	K00857
ath00592	alpha-Linolenic acid metabolism	C16317;	K08241
ath00650	Butanoate metabolism	C00026;C00042;	K01641
ath00500	Starch and sucrose metabolism	C00092;C00185;	K16055
ath00270	Cysteine and methionine metabolism	C00019;C00049;C00073;C00109;C00170;C00979;	K12524
ath00300	Lysine biosynthesis	C00026;C00049;C00322;C00449;C00666;	K12524
ath00230	Purine metabolism	C00064;C00147;C00212;C00242;C00575;C00942;	K00873
ath00562	Inositol phosphate metabolism	C00092;	K01092
ath00906	Carotenoid biosynthesis	C13453;C13454;	K09843
ath00950	Isoquinoline alkaloid biosynthesis	C01179;C06160;	K00276
ath00620	Pyruvate metabolism	C00149;	K00873
ath00360	Phenylalanine metabolism	C00042;C00079;C00156;	K00276;K10775
ath00010	Glycolysis/Gluconeogenesis	C00631;	K00873
ath00130	Ubiquinone and other terpenoid-quinone biosynthesis	C00156;C01179;C03993;	K01904
ath00250	Alanine, aspartate, and glutamate metabolism	C00026;C00042;C00049;C00064;C00940;	K01953
ath00410	beta-Alanine metabolism	C00049;C00383;C00864;C05341;	K00276
ath00941	Flavonoid biosynthesis	C05903;	K13082
ath00940	Phenylpropanoid biosynthesis	C00079;	K01904;K13066;K10775
ath00260	Glycine, serine and threonine metabolism	C00049;C00109;C00631;C00719;	K12524;K00276
ath00280	Valine, leucine, and isoleucine degradation	C00183;	K01641
ath00970	Aminoacyl-tRNA biosynthesis	C00049;C00062;C00064;C00073;C00079;C00148;C00183;	K04567
ath00040	Pentose and glucuronate interconversions	C00026;C05411;	K01051

(*D4R*), and *4-coumarate-CoA ligase-like 6* (*4CL6*), *bifunctional aspartokinase-homoserine dehydrogenase* (*thrA*), and *abscisic acid 8′-hydroxylase 2 isoform X1* (*ABA8* or *CYP707A2*), which were differentially expressed between the two treatments (**Figure 7**). It was indicated that these pathways and genes might play important roles in the growth and development of MCB.

Verification of Differentially Expressed Genes Using Quantitative Reverse Transcription -PCR

To verify the credibility of transcriptome sequencing data, eight candidate DEGs (*AS*, *TK*, *TPS*, *IMPL1*, *D4R*, *4CL*, *thrA*, and *ABA8*) were selected and analyzed using qRT-PCR. Results showed that our data were in line with those obtained with the RNA-Seq (**Figure 7**). These indicated the reliability of the results of DEGs analysis.

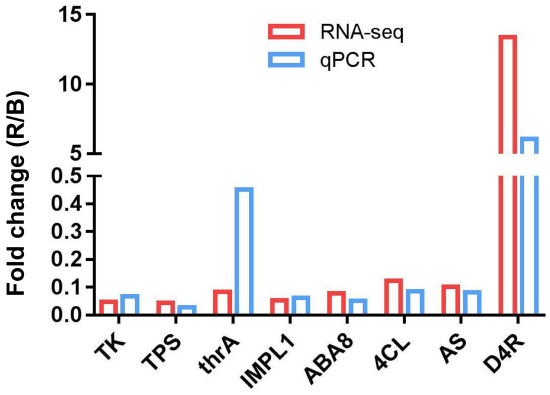

FIGURE 7 | The expression level of *AS*, *TK*, *TPS*, *IMPL1*, *D4R*, *4CL6*, *thrA*, and *ABA8* between the red- and blue-light treatments.

DISCUSSION

Red Light Promoted the Growth and Development and Quality of *Mesona chinensis* Benth

Light is the basic energy source of photosynthesis and the main environmental factor regulating plant growth and development throughout the plant life cycle (Devlin et al., 2007). The growth and development of plants are not only restricted by light intensity but also affected by light quality, that is, the light and radiation of different wavelengths (Paradiso and Proietti, 2021). The solar spectrum is roughly divided into ultraviolet radiation (ultraviolet, UV < 400 nm: UV-A, 320–400 nm; UV-B, 280–320 nm; UV-C, <280 nm, 100–280 nm), visible or photosynthetically active radiation (PAR) (PAR, 400–700 nm: blue light, 400–500 nm; green light, 500–600 nm; red light, 600–700 nm), and infrared radiation (700–800 nm) (Xu et al., 2015). Red light and blue light are the main energy sources for carbon dioxide assimilation and have primary impacts on carbohydrate

biosynthesis and plant growth (Lim and Eom, 2013; He et al., 2020b). Red light affected the height and leaf area of kidney bean plants (Hiromichi and Kazuhiro, 2000) and potato plantlets (Miyashita et al., 1997; Lee et al., 2011). Bantis et al. (2016) reported that the red light increased the dry weight of watermelon seedlings. Peanut and lettuce plants under a high proportion of red light also exhibited enhanced biomass accumulation (Poulet et al., 2014; Li et al., 2018). Red light determined better growth compared with blue light in lettuce (Yanagi et al., 1996). In this study, red light promoted the growth and development of MCB in comparison with blue light, specifically in the plant height, dry and fresh weight, and root growth (**Figures 2A–H**). It was consistent with the results mentioned earlier. The difference was that the red light reduced chlorophyll content in leaves of MCB compared with the blue light. It was consistent with the results of the study on Welsh onion (Gao et al., 2020). The reason might be that the chlorophyll content could be increased by the blue light (He et al., 2020b).

In response to the alterations in the light spectrum, plants are capable of adapting to environmental changes by accumulating a variety of metabolites, including polysaccharides, flavonoids, triterpenoids, and phenolic compounds (Ibrahim and Jaafar, 2012). Studies reported that the red light increased the number of phenolic compounds in the leaves of lettuce and tomato stems (Li and Kubota, 2009; Kim et al., 2013), *Ocimum basilicum* (Bantis et al., 2016), and *Perovskia* lamiaceae (Ghaffari et al., 2019), and it also promoted the anthocyanin content in *Brassica oleracea* L. *var*. acephala D.C. (Lefsrud et al., 2008) and red cabbage leaves (Mizuno et al., 2001). Meanwhile, under the red light, the contents of soluble sugar and total sugar significantly increased in tomatoes (Pu et al., 2005). In this study, the red light significantly promoted the contents of soluble sugar and pectin of MCB compared with the blue light (**Figures 2I,J**). Pectin was an important component of MCB polysaccharides, which was the standard to measure the quality of MCB. As the red light had positive effects on the biomass and quality of MCB, it might be feasible to supplement red light in production to promote the growth and development and quality of MCB.

Responses of Chloroplast Ultrastructure of *Mesona chinensis* Benth Leaves to the Red and Blue Lights

Chloroplasts contain chlorophyll and are rich in thylakoid membranes that can absorb and transform light energy (Kirchhoff, 2019) so that they are the sites of photosynthesis in plant cells (Barry et al., 2012; Tang et al., 2018). If the chlorophyll synthesis was decreased or impeded, the chloroplast ultrastructure would change (Zhang et al., 2014). The light quality was one of the important factors affecting chloroplast development. Under the blue light, the number of grana lamellae was the highest with the most stacked lamellae and the minimum starch grains in the chloroplast, while the leaves developed under red light alone displayed dysfunctional photosynthetic apparatus (Wang et al., 2015). In upland cotton, the seedlings that were grown under blue LEDs also showed high integrity of the chloroplast ultrastructure with a visible lamellar structure (Li et al., 2010). Gao et al. (2020) reported that the chloroplasts of leaves treated with blue and red lights were intact and contributed to photosynthesis, while yellow light inhibited chloroplast development. In our investigation, the leaves under both the red and blue light treatments also had intact chloroplast ultrastructure. However, compared with the blue-light treatment, there were more starch grains in the leaves under the red-light treatment, and a large number of vesicles were found in the thylakoid lamellar of the leaves under the red-light treatment (**Figure 3**). It could be concluded that the blue light was a key signal for chloroplast development (Wang et al., 2015). However, the red light had different effects on chloroplast development. These comparisons could support the hypothesis that there were species-specific responses to the light environment (Gao et al., 2020).

Contributing to Understanding the Chemical Components of *Mesona chinensis* Benth

Previous studies showed that MCB contained polysaccharides, flavonoids, triterpenoids, phenols, and other chemical components (Lin et al., 2013). MCP consisted of eight monosaccharides, including mannose, rhamnose, ribose, glucuronic acid, galacturonic acid, glucose, galactose, and xylose (Zhang et al., 2013). Quercetin was the main component of flavonoids (Liu, 1995), ursolic acid and oleanolic acid were the predominant components of triterpenoids (Shyu et al., 2008), and caffeic acid (the highest content) and epicatechin were the primary components of phenols (Qiu et al., 2010) in MCB. Besides the polysaccharides, flavonoids, triterpenoids, and phenols, MCB also contained minerals (such as iron, calcium, magnesium, manganese, zinc, and potassium) (Lin and Zhu, 1992), vitamin B, amino acids, cellulose, and plant pigments, etc. (Liu and Chen, 2004; Cao et al., 2007; Qiu et al., 2009). In this study, we identified 184 metabolites in MCB (**Supplementary Table 11** and **Supplementary Figure 4**), which positively contributed to understanding the chemical components of MCB and laid a foundation for the future study of chemical components in MCB.

Metabolites Involved in the Growth and Development of *Mesona chinensis* Benth

In this study, a total of 99 DEMs (42 upregulated and 57 downregulated) were found between the red- and blue-light treatments (**Figure 6A**). Furthermore, based on the KEGG analysis, seven pathways, including FFB, AAGM, CMM, GM, APM, TCA cycle, and LB, were at an extremely significant level ($p < 0.01$), and only the glyoxylate and dicarboxylate metabolism pathway was at a significant level ($p < 0.05$) (**Table 1**). Therefore, it was indicated that these pathways might be involved in the growth and development of MCB.

Genes Involved in the Growth and Development of *Mesona chinensis* Benth

Our integrative analysis of transcriptome and metabolome unveiled that 28 DEGs included *AS*, *TK*, *TPS*, *IMPL1*, *D4R*, and

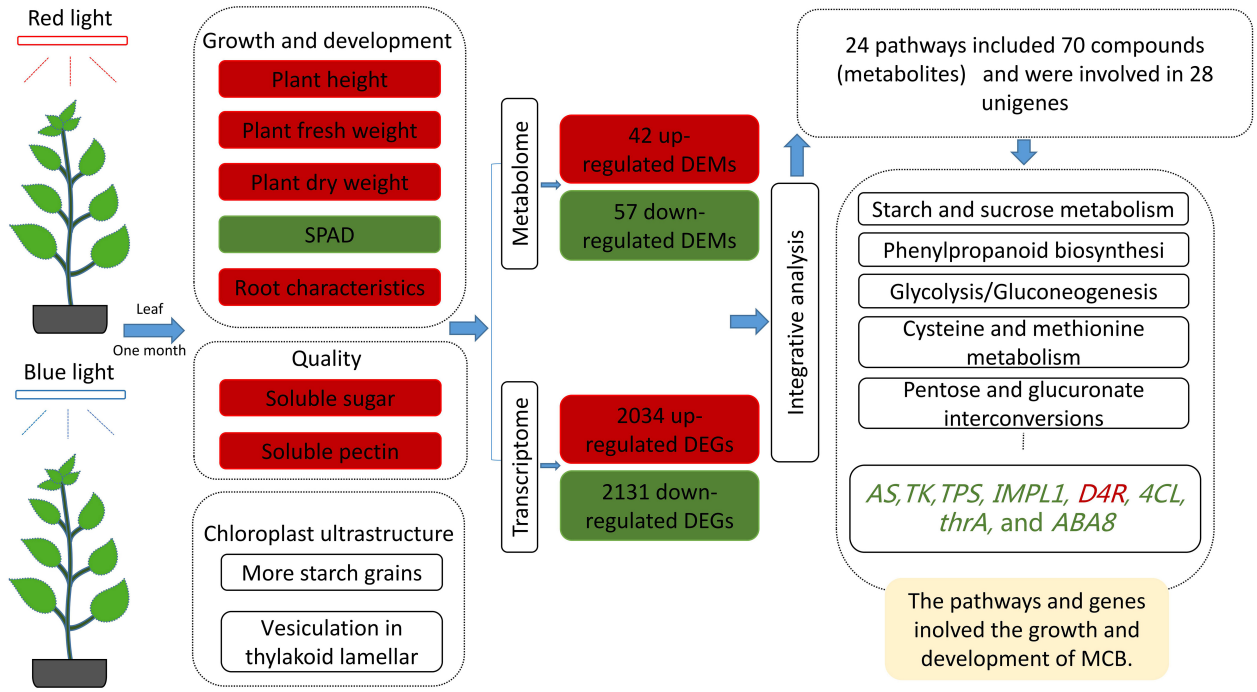

FIGURE 8 | Overview of the red light and blue light regulating the growth and development of MCB. Red boxes and words indicated upregulation; Green boxes and words indicated downregulation.

4CL6, *thrA*, and *ABA8* or *CYP707A2*. Asparagine (also known as aspartamide) was α-amino acid that was particularly found in plant proteins. Asparagine possessed a high nitrogen-to-carbon ratio and was the predominant nitrogen transport compound utilized when carbon sources were relatively limited in the dark (Sieciechowicz et al., 1988). The *AS* genes appeared to be encoded by a small gene family in most plant species, such as *Arabidopsis* (Lam et al., 1998), sunflower (Herrera-Rodriguez et al., 2002), *Triticum aestivum* (Gao et al., 2016), and *H. vulgare* (Avila-Ospina et al., 2015), and the *AS* gene expression in higher plants was regulated by many factors, for example, light, organ type, and development. Tsai and Coruzzi (1990) identified a family of genes (*AS1* and *AS2*) in *Pisum sativum*, and the *AS* genes were preferentially expressed in plants grown in the dark; moreover, the mRNA of the *AS* genes was negatively regulated by light at the transcriptional level and the expression of *AS* genes fluctuated sharply during a "normal" light/dark cycle. Wang et al. (2005) demonstrated that the *TaAsnS1* expression in bread wheat seedlings was significantly induced by osmotic and salinity stresses, probably through ABA-dependent pathways. *AsnS1* genes were downregulated in *N*-stressed roots, stems, and leaves during seedling growth and booting, while *AsnS2* genes were expressed in leaves, stems, and roots (Curci et al., 2018). In our investigation, the *AS* gene was differentially expressed between the leaves under the red- and blue-light conditions. The negative regulation of the *AS* gene expression by light was shown to be a general phenomenon in plants, which also occurs in non-legumes such as *Nicotiana tabacum* and *Nicotiana plumbaginifolia* (Tsai and Coruzzi, 1991).

Thymidine kinase (TK) catalyzed the first step by transferring a phosphate group to a thymidine molecule in the nucleotide salvage pathway. In *Oryza sativa*, the *TK1* gene expression was independent of cell-cycle regulation as the transcript was present in all developmental stages, and it was even more abundant in non-proliferating tissues (Ullah et al., 1999). In *Hevea brasiliensis*, the rubber tree, upregulation of the *TK1* gene was closely associated with resistance to mechanical wounding (Venkatachalam et al., 2010). There were two thymidine kinase genes, *AtTK1a* and *AtTK1b*, in *Arabidopsis thaliana*. *TK1a* was expressed in most tissues during plant development, and it was differentially induced by ultraviolet-C radiation because *TK1b* expression was unaffected (Pedroza-García et al., 2014). While mutants for each *TK1* gene showed normal growth, the double mutant developed poorly and plantlets died at an early stage, indicating that the function of *TK1* was essential for plant development (Clausen et al., 2012).

Myo-inositol was a key precursor of various phosphate metabolites in eukaryotes, for example, cell wall polysaccharides, phosphatidylinositol, phytic acid, and indole-3-acetic acid conjugate of myo-inositol (Loewus and Murthy, 2000). Myo-inositol monophosphatase (IMP) catalyzed the dephosphorylation of myo-inositol 3-phosphate in the last step of myo-inositol biosynthesis, which was also important in phosphate metabolism and was required for the biosynthesis of phytic acid, cell wall polysaccharides, and phosphatidylinositol. IMP was encoded by *VTC4*; however, *IMPL1* and *IMPL2* were the two additional and putative *IMP* genes in *A. thaliana*

(Torabinejad et al., 2009). Sato et al. (2011) demonstrated that the loss-of-function mutant *impl2* leads to embryonic lethality at the globular stage, and *IMPL2* was also involved in histidine biosynthesis during embryo development. In developing seeds of *A. thaliana*, the expression of *IMP* genes was not coupled with the expression of the genes encoding myo-inositol phosphate synthases, which supplied the substrate for IMPs, but was correlated with the expression of the gene for myoinositol polyphosphate 1-phosphatase (SAL1), which was involved in the myo-inositol salvage pathway, indicating a possible salvage pathway role in the seed development (Sato et al., 2011).

Trehalose metabolism was ubiquitous in plants, and the genes encoding trehalose pathway constituents were first reported in *A. thaliana* (Vogel et al., 1998). There were 11 trehalose phosphate synthase (TPS) homologs in *A. thaliana*. In particular, the *TPS* genes were expressed at very low levels (Schluepmann et al., 2003), and the *AtTPS1* gene was expressed in all tissues and was essential during embryogenesis (Eastmond et al., 2002), indicating an important role for trehalose metabolism in plants. *OtsA* encoded a TPS, and the expression of *OtsA* accumulated trehalose 6-phosphate (T6P). Moreover, the plant phenotype with T6P accumulation was significantly opposite to that of plants with low T6P levels and was consistent with the key role of T6P in growth and development (Schluepmann et al., 2003).

In addition, *D4R*, catalyzing the reduction of dihydroflavonols to leucoanthocyanins, was a key enzyme in the biosynthesis of anthocyanidins, proanthocyanidins, and other flavonoids, which was of great significance for plant development (Li et al., 2012). In *A. thaliana*, two 4-coumarate- CoA ligase (4CL)-like proteins (*At4g05160* and *At5g63380*) were targeted to leaf peroxisomes and could contribute to jasmonic acid biosynthesis (Schneider et al., 2005), which was a plant-signaling molecule closely associated with plant resistance to abiotic stress (Wang et al., 2020). In *Escherichia coli*, *thrA* catalyzes the commitment step involved in the regulation of the biosynthesis of threonine (Angeles and Viola, 1990), which can improve plant tolerance and promote the process of humification. Abscisic acid (ABA) is a plant stress hormone, and *ABA 8′-hydroxylase* (CYP707A) is the major and key P450 enzyme in ABA catabolism in plants (Ueno et al., 2007).

Taken together, in this study, compared with the blue-light treatment, the *AS*, *TK*, *TPS*, *IMPL1*, *4CL*, *thrA*, and *ABA8* genes were downregulated, while the *D4R* gene was upregulated under the red-light condition (**Figure 7**). The expression of these genes from the leaves of MCB could be regulated by light quality, indicating that these genes might be closely related to the growth and development of MCB.

CONCLUSION

The red light promoted the growth and development and quality of MCB in comparison with the blue light. The plant phenotype and leaf chloroplast ultrastructure responded differently to the red and blue lights. Transcriptome analysis showed 410 upregulated and 702 downregulated unigenes. The results of metabonomics revealed that a total of 184 metabolites and 99 DEMs were identified between the red- and blue-light treatments. Integrative analysis of transcriptome and metabolome unveiled that *AS*, *TK*, *TPS*, *IMPL1*, *4CL*, *D4R*, *thrA*, and *ABA8* genes were differentially expressed (**Figure 8**). Therefore, these pathways and genes might be involved in the growth and development of MCB.

DATA AVAILABILITY STATEMENT

"The original contributions presented in the study are publicly available. This data can be found here: National Center for Biotechnology Information (NCBI) BioProject database under accession number PRJNA741889."

AUTHOR CONTRIBUTIONS

DT was involved in conceptualization, methodology, investigation, formal analysis, writing original draft, and writing—reviewing and editing. FW and JM were involved in funding acquisition. FW, QH, KW, and XY were involved in writing—reviewing and editing. All authors approved the submitted version.

FUNDING

This study was supported by the Guangxi Innovation-Driven Development Project (GuiKe AA18242040), Scientific Research Funding Project of Guangxi Botanical Garden of Medicinal Plants (GuiYaoJi202011), Natural Science Foundation of Guangxi (2020JJA140312), China Agricultural Research System (CARS-21), Bagui Scholor Program of Guangxi Zhuang Autonomous Region and Research Innovation Team Project (GuiYaoChuang 2019005), and Innovation team project of Guangxi Botanical Garden of Medicinal Plants (GuiYaoChuang2019010).

SUPPLEMENTARY MATERIAL

The Supplementary Material for this article can be found online at: https://www.frontiersin.org/articles/10.3389/fpls.2021.761068/full#supplementary-material

REFERENCES

Angeles, T. S., and Viola, R. E. (1990). The kinetic mechanisms of the bifunctional enzyme aspartokinase- homoserine dehydrogenase I from *Escherichia coli*. *Arch. Biochem. Biophys.* 283, 96–101. doi: 10.1016/0003-9861(90)90617-8

Avila-Ospina, L., Marmagne, A., Talbotec, J., and Krupinska, K. (2015). The identification of new cytosolic glutamine synthetase and *Asparagine synthetase*

genes in barley (*Hordeum vulgare* L.), and their expression during leaf senescence. *J. Exp. Bot.* 66, 2013–2026. doi: 10.1093/jxb/erv003

Ballare, C. L., Mazza, C. A., Austin, A. T., and Pierik, R. (2012). Canopy light and plant health. *Plant Physiol.* 160, 145–155. doi: 10.1104/pp.112.200733

Bantis, F., Koukounaras, A., Siomos, A. S., Fotelli, M. N., and Kintzonidis, D. (2020). Bichromatic red and blue LEDs during healing enhance the vegetative growth and quality of grafted watermelon seedlings. *Sci. Hortic.* 261:109000. doi: 10.1016/j.scienta.2019.109000

Bantis, F., Ouzounis, T., and Radoglou, K. (2016). Artificial LED lighting enhances growth characteristics and total phenolic content of *Ocimum basilicum*, but variably affects transplant success. *Sci. Hortic.* 198, 277–283. doi: 10.1016/j.scienta.2015.11.014

Barry, C. S., Aldridge, G. M., Herzog, G., Ma, Q., McQuinn, R. P., Hirschberg, J., et al. (2012). Altered chloroplast development and delayed fruit ripening caused by mutations in a Zinc metalloprotease at the lutescent2 locus of Tomato. *Plant Physiol.* 159, 1086–1098. doi: 10.1104/pp.112.197483

Cao, C. J., Liu, X. G., and Wang, X. J. (2007). The extraction of the pigment from *Mesona chinensis* benth. *Food Res. Dev.* 28, 64–67.

Chen, C., Geng, Z., Juan, C., Liu, X. H., Lu, X. Y., Chen, H. M., et al. (2021). Integrated metabolome and transcriptome analysis unveils novel pathway involved in the formation of yellow peel in Cucumber. *Int. J. Mol. Sci.* 22:1494. doi: 10.3390/ijms22031494

Cheng, W. W., Li, J. G., Jiang, A. M., Zhang, D. L., Fan, M. M., Shen, X. L., et al. (2015). Effects of Hsian-tsao gum on rheological property, sensory quality and antioxidant activity of Chinese-style meatball. *Food Sci. Technol.* 40, 11–15.

Clausen, A. R., Girandon, L., Ali, A., Knecht, W., Rozpedowska, E., Sadrini, M., et al. (2012). Two thymidine kinases and one multisubstrate deoxyribonucleoside kinase salvage DNA precursors in *Arabidopsis thaliana*. *FEBS J.* 279, 3889–3896. doi: 10.1111/j.1742-4658.2012.08747.x

Curci, P. L., Bergès, H., Marande, W., Maccaferri, M., Tuberosa, R., and Sonnante, G. (2018). *Asparagine synthetase* genes (*AsnS1* and *AsnS2*) in durum wheat: structural analysis and expression under nitrogen stress. *Euphytica* 214:36. doi: 10.1007/s10681-017-2105-z

Devlin, P. F., Christie, J. M., and Terry, M. J. (2007). Many hands make light work. *J. Exp. Bot.* 58, 3071–3077. doi: 10.1093/jxb/erm251

Eastmond, P. J., van Dijken, A. J., Spielman, M., Kerr, A., Tissier, A. F., Dickinson, H. G., et al. (2002). Trehalose-6-phosphate synthase 1, which catalyses the first step in trehalose synthesis, is essential for *Arabidopsis* embryo maturation. *Plant J.* 29, 225–235. doi: 10.1046/j.1365-313x.2002.01220.x

Gao, R., Curtis, T. Y., and Powers, S. J. (2016). Food safety: structure and expression of the *Asparagine synthetase* gene family of wheat. *J. Cereal Sci.* 68, 122–131. doi: 10.1016/j.jcs.2016.01.010

Gao, S., Liu, X. N., Liu, Y., Cao, B. L., Chen, Z. J., and Xu, K. (2020). Photosynthetic characteristics and chloroplast ultrastructure of welsh onion (*Allium fistulosum* L.) grown under different LED wavelengths. *BMC Plant Biol.* 20:78. doi: 10.1186/s12870-020-2282-0

Ghaffari, Z., Rahimmalek, M., and Sabzalian, M. R. (2019). Variation in the primary and secondary metabolites derived from the isoprenoid pathway in the Perovskia species in response to different wavelengths generated by light emitting diodes (LEDs). *Ind. Crops Prod.* 140:111592. doi: 10.1016/j.indcrop.2019.111592

He, D. X., Yan, Z. Y., Sun, X., and Yang, P. (2020a). Leaf development and energy yield of hydroponic sweet potato seedlings using single-node cutting as influenced by light intensity and LED spectrum. *J. Plant Physiol.* 254:153274. doi: 10.1016/j.jplph.2020.153274

He, W., Pu, M., Li, J., Xu, Z. G., and Gan, L. J. (2020c). Potato tuber growth and yield under red and blue LEDs in plant factories. *J. Plant Growth Regul.* doi: 10.1007/s00344-020-10277-z

He, W., Miao, C., You, J., Gan, L. J., and Xu, Z. G. (2020b). Effects of red and blue light with supplemental white light on growth, carbohydrate metabolism, and yield of virus-free potato in plant factories. *Am. J. Potato Res.* 97, 554–564. doi: 10.1007/s12230-020-09803-2

Herrera-Rodriguez, M. B., Carrasco-Ballesteros, S., and Maldonado, J. M. (2002). Three genes showing distinct regulatory patterns encode the *Asparagine synthetase* of sunflower (*Helianthus annuus*). *New Phytol.* 155, 33–45. doi: 10.1046/j.1469-8137.2002.00437.x

Hiromichi, H., and Kazuhiro, S. (2000). Effects of blue light and red light on kidney bean plants grown under combined radiation from narrowband light sources. *Environ. Control Biol.* 38, 13–24. doi: 10.2525/ecb1963.38.13

Huang, L. X., Huang, M., Shen, M. Y., Wen, P. W., Wu, T., Hong, Y. Z., et al. (2019). Sulfated modification enhanced the antioxidant activity of *Mesona chinensis* Benth polysaccharide and its protective effect on cellular oxidative stress. *Int. J. Biol. Macromol.* 136, 1000–1006. doi: 10.1016/j.ijbiomac.2019.06.199

Huang, L. X., Shen, M. Y., Zhang, X. W., Jiang, L., Song, Q. Q., and Xie, J. H. (2018). Effect of high pressure microfluidization treatment on the physicochemical properties and antioxidant activities of polysaccharide from *Mesona chinensis* Benth. *Carbohyd. Polym.* 200, 191–199. doi: 10.1016/j.carbpol.2018.07.087

Ibrahim, M. H., and Jaafar, H. Z. (2012). Primary, secondary metabolites, H_2O_2, malondialdehyde and photosynthetic responses of *Orthosiphon stimaneus* Benth. to different irradiance levels. *Molecules* 17, 1159–1176. doi: 10.3390/molecules17021159

Iseli, C., Jongeneel, C. V., and Bucher, P. (1999). ESTScan: a program for detecting, evaluating, and reconstructing potential coding regions in EST sequences. *Proc. Int. Conf. Intell. Syst. Mol. Biol.* 99, 138–148.

Kim, K., Kook, H., Jang, Y., Lee, W., Kamala-Kannan, S., and Lee, K. (2013). The effect of blue-light-emitting diodes on antioxidant properties and resistance to *Botrytis cinerea* in tomato. *Plant Pathol. Microbiol.* 4, 203–212.

Kirchhoff, H. (2019). Chloroplast ultrastructure in plants. *New Phytol.* 223, 565–574. doi: 10.1111/nph.15730

Kuo, T. C. Y., Chen, C. H., Chen, S. H., Lu, I. H., Chu, M. J., Huang, L. C., et al. (2015). The effect of red light and far-red light conditions on secondary metabolism in *Agarwood*. *BMC Plant Biol.* 15:139. doi: 10.1186/s12870-015-0537-y

Lam, H. M., Hsieh, M. H., and Coruzzi, G. (1998). Reciprocal regulation of distinct *Asparagine synthetase* genes by light and metabolites in *Arabidopsis thaliana*. *Plant J.* 16, 345–353. doi: 10.1046/j.1365-313x.1998.00302.x

Latchman, D. S. (1993). Transcription factors: an overview. *Int. J. Exp. Pathol.* 74, 417–422.

Lee, Y. I., Fang, W., and Chen, C. C. (2011). Histological observation on the growth of potato plantlets *in vitro* under six different led light qualities. *Acta Hortic.* 907, 393–395. doi: 10.17660/ActaHortic.2011.907.66

Lefsrud, M. G., Kopsell, D., and Sams, C. E. (2008). Irradiance from distinct wavelength light-emitting diodes affect secondary metabolites in kale. *HortScience* 43, 2243–2244. doi: 10.21273/HORTSCI.43.7.2243

Li, C., Liu, D., Li, L. L., Hu, S. X., Xu, Z. G., and Tang, C. M. (2018). Effects of light emitting diodes on the growth of peanut plants. *Agron. J.* 110, 2369–2377. doi: 10.2134/agronj2017.11.0674

Li, H. H., Qiu, J., Chen, F. D., Lv, X. F., Fu, C. X., Zhao, D. X., et al. (2012). Molecular characterization and expression analysis of dihydroflavonol 4-reductase (DFR) gene in *Saussurea medusa*. *Mol. Biol. Rep.* 39, 2991–2999. doi: 10.1007/s11033-011-1061-2

Li, H. M., Xu, Z. G., and Tang, C. M. (2010). Effect of light-emitting diodes on growth and morphogenesis of upland cotton (*Gossypium hirsutum* L.) plantlets *in vitro*. *Plant Cell Tissue Organ Cult.* 103, 155–163. doi: 10.1007/s11240-010-9763-z

Li, Q., and Kubota, C. (2009). Effects of supplemental light quality on growth and phytochemicals of baby leaf lettuce. *Environ. Exp. Bot.* 67, 59–64. doi: 10.1016/j.envexpbot.2009.06.011

Lim, Y. J., and Eom, S. H. (2013). Effects of different light types on root formation of *Ocimum basilicum* L. cuttings. *Sci. Hortic.* 164, 552–555. doi: 10.1016/j.scienta.2013.09.057

Lin, L. S., Zhang, K., Zhan, Y. L., Wang, Z. K., and Lin, H. T. (2013). A review of chemical constituents and medicinal function of *Mesona chinensis* Benth. *Curr. Biotechnol.* 3, 448–452.

Lin, S. Q., and Zhu, S. M. (1992). Determination of trace elements in *Mesona chinensis* Benth. *Fu. Med. J.* 14:58.

Liu, S. L. (1995). Oleanolic acid and quercetin from Mesona chinensis. *J. Chinese Med. Mat.* 18:247.

Liu, X. G., and Chen, M. M. (2004). Study on the development and utilization of *Mesona chinensis*. *Food Res. Dev.* 25, 109–112.

Livak, K. J., and Schmittgen, T. D. (2001). Analysis of relative gene expression data using real-time quantitative PCR and the 2(-Delta Delta C(T)) method. *Methods* 25, 402–408. doi: 10.1006/meth.2001.1262

Loewus, F. A., and Murthy, P. P. N. (2000). Myo-inositol metabolism in plants. *Plant Sci.* 150, 1–19. doi: 10.1016/S0168-9452(99)00150-8

Miyashita, Y., Kimura, T., Kitaya, Y., Kubota, C., and Kozai, T. (1997). Effects of red light on the growth and morphology of potato plantlets in vitro: using light emitting diodes (LEDs) as a light source for micropropagation. *Acta Hortic.* 418, 169–173. doi: 10.17660/ActaHortic.1997.418.23

Mizuno, T., Amaki, W., and Watanabe, H. (2001). Effects of monochromatic light irradiation by LED on the growth and anthocyanin contents in leaves of cabbage seedlings. *Acta Hortic.* 907, 179–184. doi: 10.17660/ActaHortic.2011.907.25

Paradiso, R., and Proietti, S. (2021). Light-Quality manipulation to control plant growth and photomorphogenesis in greenhouse horticulture: the state of the art and the opportunities of modern LED systems. *J. Plant Growth Regul.* doi: 10.1007/s00344-021-10337-y

Pedroza-García, J. A., Nájera-Martínez, M., de la Paz Sanchez, M., and Plasencia, J. (2014). *Arabidopsis thaliana* thymidine kinase 1a is ubiquitously expressed during development and contributes to confer tolerance to genotoxic stress. *Plant Mol. Biol.* 87, 303–315. doi: 10.1007/s11103-014-0277-7

Pertea, G., Huang, X. Q., Liang, F., Antonescu, V., Sultana, R., Karamycheva, S., et al. (2003). TIGR Gene Indices clustering tools (TGICL): a software system for fast clustering of large EST datasets. *Bioinformatics* 19, 651–652. doi: 10.1093/bioinformatics/btg034

Poulet, L., Massa, G. D., Morrow, R. C., Bourget, C. M., Wheeler, R. M., and Mitchell, C. A. (2014). Significant reduction in energy for plant-growth lighting in space using targeted LED lighting and spectral manipulation. *Life Sci. Space Res.* 2, 43–53. doi: 10.1016/j.lssr.2014.06.002

Pu, G. M., Liu, S. Q., Liu, L., and Ren, L. H. (2005). Effects of different light qualities on growth and physiological characteristics of tomato seedlings. *Acta Hortic. Sin.* 32, 420–425.

Qiu, T., Lin, X. C., and Wang, B. Y. (2010). Identification of Epicatechin from *Mesona procumbens* Hemsl. *Nat. Prod. Res.* 22, 798–800.

Qiu, T., Wang, B. Y., Lin, X. C., and Wu, Y. X. (2009). Study on preparation of sodium zinc chlorophyllin from Hsian-tsao (*mesona procumbens* hemsl) and its stability. *J. Fuzhou Univ.* 37, 435–438.

Ren, Y. M., Jiang, L., Wang, W. J., Xiao, Y. H., Liu, S. C., Luo, Y., et al. (2019). Effects of *Mesona chinensis* Benth polysaccharide on physicochemical and rheological properties of sweet potato starch and its interactions. *Food Hydrocoll.* 99:105371. doi: 10.1016/j.foodhyd.2019.105371

Saebo, A., Krekling, T., and Appelgren, M. (1995). Light quality affects photosynthesis and leaf anatomy of birch plantlets *in vitro*. *Plant Cell Tissue Organ Cult.* 41, 177–185. doi: 10.1007/BF00051588

Sano, H., Kaneko, S., Sakamoto, Y., Sato, T., and Shishido, K. (2009). The basidiomycetous mushroom Lentinula edodes white collar-2 homolog PHRB a partner of putative blue-light photoreceptor PHRA, binds to a specific site in the promoter region of the L. edodes tyrosinase gene. *Fungal Genet. Biol.* 46, 333–341. doi: 10.1016/j.fgb.2009.01.001

Santos, L., Ugun-Klusek, A., Coveney, C., and Boocock, D. J. (2021). Multiomic analysis of stretched osteocytes reveals processes and signalling linked to bone regeneration and cancer. *NPJ Regen. Med.* 32, 1–7. doi: 10.1038/s41536-021-00141-3

Sato, Y., Yazawa, K., Yoshida, S., Tamaoki, M., Nakajima, N., Iwai, H., et al. (2011). Expression and functions of myo-inositol monophosphatase family genes in seed development of *Arabidopsis*. *J. Plant Res.* 124, 385–394. doi: 10.1007/s10265-010-0381-y

Schluepmann, H., Pellnyt, T., van Dijken, A., Smeekens, S., and Pau, M. (2003). Trehalose 6-phosphate is indispensable for carbohydrate utilization and growth in *Arabidopsis thaliana*. *Proc. Natl. Acad. Sci. U. S. A.* 100, 6849–6854. doi: 10.1073/pnas.1132018100

Schneider, K., Kienow, L., Schmelzer, E., Colby, T., Bartsch, M., Miersch, O., et al. (2005). A new type of peroxisomal acyl-coenzyme a synthetase from *Arabidopsis thaliana* has the catalytic capacity to activate biosynthetic precursors of jasmonic acid. *J. Biol. Chem.* 14, 13962–13972. doi: 10.1074/jbc.M413578200

Shyu, M. H., Kao, T. C., and Yen, G. C. (2008). Hsian-tsao *(Mesona procumbens* Heml) prevents against rat liver fibrosis induced by CCl4 via inhibition of hepatic stellate cells activation. *Food Chem. Toxicol.* 46:3707371. doi: 10.1016/j.fct.2008.09.051

Sieciechowicz, K. A., Joy, K. W., and Ireland, R. J. (1988). The metabolism of asparagine in plants. *Phytochemistry* 27, 663–671. doi: 10.1016/0031-9422(88)84071-8

Su, H. L., Huang, Y. Z., and Chen, J. Y. (2011). Comparative analysis of amino acids content in *Mesona chinensis* from different producing areas. *Chin. Wild Plant Resour.* 5:19.

Tandeau de Marsac, N., and Houmard, J. (1993). Adaptation of cyanobacteria to environmental stimuli: new steps towards molecular mechanisms. *FEMS Microbiol. Rev.* 104, 119–190. doi: 10.1111/j.1574-6968.1993.tb05866.x

Tang, D. F., Wei, F., Cai, Z. Q., Wei, Y. Y., Aziz, K., Miao, J. H., et al. (2020). Analysis of codon usage bias and evolution in the chloroplast genome of *Mesona chinensis* Benth. *Dev. Genes Evol.* 231, 1–9. doi: 10.1007/s00427-020-00670-9

Tang, D. F., Wei, F., Muhammad, H. K., Aziz, K., Li, Z. Q., Shi, Q. Q., et al. (2018). Analysis of chloroplast differences in leaves of rice isonuclear alloplasmic lines. *Protoplasma* 255, 863–871. doi: 10.1007/s00709-017-1189-6

Tang, D. F., Wei, F., Qin, S. X., Aziz, K., Muhammad, H. K., and Zhou, R. Y. (2019). Polyethylene glycol induced drought stress strongly influences seed germination, root morphology and cytoplasm of different kenaf genotypes. *Ind. Crop Prod.* 137, 180–186. doi: 10.1016/j.indcrop.2019.01.019

Tayebeh, A., Leila, S., and Mohammad, R. S. (2020). LED light mediates phenolic accumulation and enhances antioxidant activity in *Melissa officinalis* L. under drought stress condition. *Protoplasma* 257, 1231–1242. doi: 10.1007/s00709-020-01501-4

Torabinejad, J., Donahue, J. L., Gunesekera, B. N., Allen-Daniels, M. J., and Gillaspy, G. E. (2009). VTC4 is a bifunctional enzyme that affects myoinositol and ascorbate biosynthesis in plants. *Plant Physiol.* 150, 951–961. doi: 10.1104/pp.108.135129

Tsai, F. Y., and Coruzzi, G. (1991). Light represses transcription of *Asparagine synthetase* genes in photosynthetic and nonphotosynthetic organs of plants. *Mol. Cell. Biol.* 11, 4966–4972. doi: 10.1128/MCB.11.10.4966

Tsai, F. Y., and Coruzzi, G. M. (1990). Dark-induced and organspecific expression of two *Asparagine synthetase* genes in *Pisum sativum*. *EMBO J.* 9, 323–332. doi: 10.1002/j.1460-2075.1990.tb08114.x

Ueno, K., Yoneyama, H., Mizutani, M., Hirai, N., and Todoroki, Y. (2007). Asymmetrical ligand binding by abscisic acid 8' -hydroxylase. *Bioorg. Med. Chem.* 15, 6311–6322. doi: 10.1016/j.bmc.2007.06.010

Ullah, H. M., Robertson, D., and Fites, R. C. (1999). A gene for thymidine kinase in plants. *Plant Physiol.* 119, 1567–1568. doi: 10.1104/pp.119.4.1567

United Nations [UN] (2017). *World Population Prospects: The 2017 Revision*. New York: United Nations.

Venkatachalam, P., Geetha, N., and Priya, P. (2010). Identification of a differentially expressed thymidine kinase gene related to tapping panel dryness syndrome in the rubber tree (*Hevea brasiliensis* Muell. Arg.) by random amplified polymorphic DNA screening. *Int. J Plant Biol.* 1, 33–39. doi: 10.4081/pb.2010.e7

Vogel, G., Aeschbacher, R. A., Muller, J., Boller, T., and Wiemken, A. (1998). Trehalose-6-phosphate phosphatases from *Arabidopsis thaliana*: identification by functional complementation of the yeast tps2 mutant. *Plant J.* 13, 673–683. doi: 10.1046/j.1365-313X.1998.00064.x

Wang, H., Liu, D., Sun, J., and Zhang, A. (2005). *Asparagine synthetase* gene *TaASN1* from wheat is up-regulated by salt stress, osmotic stress and ABA. *J. Plant Physiol.* 162, 81–89. doi: 10.1016/j.jplph.2004.07.006

Wang, J., Song, L., Gong, X., Xu, J. F., and Li, M. H. (2020). Functions of Jasmonic acid in plant regulation and response to abiotic stress. *Int. J. Mol. Sci.* 21:1446. doi: 10.3390/ijms21041446

Wang, W. J., Jiang, L., Ren, Y. M., Shen, M. Y., and Xie, J. H. (2019). Characterizations and hepatoprotective effect of polysaccharides from *Mesona blumes* against tetrachloride induced acute liver injury in mice. *Int. J. Biol. Macromol.* 124, 788–795. doi: 10.1016/j.ijbiomac.2018.11.260

Wang, X. Y., Xu, X. M., and Cui, J. (2015). The importance of blue light for leaf area expansion, development of photosynthetic apparatus, and chloroplast ultrastructure of *Cucumis sativus* grown under weak light. *Photosynthetica* 53, 213–222. doi: 10.1007/s11099-015-0083-8

Wei, H. X., Zhao, H. T., Chen, X., and He, X. Y. (2020). Secondary metabolites, carbohydrate accumulation, and nutrient uptake in *Aralia elata* (Miq.) seem seedlings exposed to shoot cutting and different LED spectra. *Acta Physiol. Plant.* 42:162. doi: 10.1007/s11738-020-03149-2

Xiao, Y. H., Liu, S. C., Shen, M. Y., Jiang, L., Ren, Y. M., and Luo, Y. (2019). Physicochemical, rheological and thermal properties of *Mesona chinensis* polysaccharides obtained by sodium carbonate assisted and cellulase assisted extraction. *Int. J. Biol. Macromol.* 126, 30–36. doi: 10.1016/j.ijbiomac.2018.12.211

Xu, D. W., Gao, W., and Ruan, J. (2015). Effects of light quality on plant growth and development. *Plant Physiol. J.* 51, 1217–1234.

Yanagi, T., Okamoto, K., and Takita, S. (1996). Effect of blue, red, and blue/red lights of two different PPF levels on growth and morphogenesis of lettuce plants. *Acta Hortic.* 440, 117–122. doi: 10.17660/ActaHortic.1996.440.21

Yang, H., Li, J. G., Wu, N. F., Fan, M. M., Shen, X. L., Chen, M. T., et al. (2015a). Effect of hsian-tsao gum (HG) content upon rheological properties of film-forming solutions (FFS) and physical properties of soy protein/hsian-tsao gum films. *Food Hydrocoll.* 50, 211–218. doi: 10.1016/j.foodhyd.2015.03.028

Yang, H., Wen, X. L., Guo, S. G., Chen, M. T., Jiang, A. M., and Lai, L. S. (2015b). Physical, antioxidant and structural characterization of blend films based on hsian-tsao gum (HG) and casein (CAS). *Carbohydr. Polym.* 134, 222–229. doi: 10.1016/j.carbpol.2015.07.021

Ye, J., Fang, L., Zheng, H., Zhang, Y., Chen, J., Zhang, Z., et al. (2006). WEGO: a web tool for plotting GO annotations. *Nucleic Acids Res.* 34, W293–W297. doi: 10.1093/nar/gkl031

Yeh, N., and Chung, J. P. (2009). High-brightness LED-energy efficient lighting sources and their potential in indoor plant cultivation. *Renew. Sust. Energ. Rev.* 13, 2175–2180. doi: 10.1016/j.rser.2009.01.027

Zha, L., and Liu, W. (2018). Effects of light quality, light intensity, and photoperiod on growth and yield of cherry radish grown under red plus blue LEDs. *Hortic. Environ. Biotech.* 59, 511–518. doi: 10.1007/s13580-018-0048-5

Zhang, C. Y., Wang, M. H., Chen, J. J., Gao, X. Z., Shao, C. Y., Lv, Z. D., et al. (2020). Survival strategies based on the hydraulic vulnerability segmentation hypothesis, for the tea plant [*Camellia sinensis* (L.) O. Kuntze] in long-term drought stress condition. *Plant Physiol. Biochem.* 156, 489–493. doi: 10.1016/j.plaphy.2020.09.034

Zhang, F. J., Zhang, K. K., Du, C. Z., Li, J., Xing, Y. X., Yang, L. T., et al. (2014). Effect of drought stress on anatomical structure and chloroplast ultrastructure in leaves of sugarcane. *Sugar Tech.* 17, 41–48. doi: 10.1007/s12355-014-0337-y

Zhang, W. B., Wang, Z. C., Zhang, L. Y., and Qian, J. H. (2013). Analysis of monosaccharide composition and content in *Mesona Chinensis* Benth polysaccharides by precolumn derivatization ultra-high performance liquid chromatography-tandem quadrupole mass spectrometry. *J. Instrumental Anal.* 32, 143–149.

Conflict of Interest: The authors declare that the research was conducted in the absence of any commercial or financial relationships that could be construed as a potential conflict of interest.

Publisher's Note: All claims expressed in this article are solely those of the authors and do not necessarily represent those of their affiliated organizations, or those of the publisher, the editors and the reviewers. Any product that may be evaluated in this article, or claim that may be made by its manufacturer, is not guaranteed or endorsed by the publisher.

frontiers in Plant Science

ORIGINAL RESEARCH
published: 23 February 2022
doi: 10.3389/fpls.2022.828529

Phytochrome A Mediates the Disassembly of Processing Bodies in Far-Red Light

Philipp Schwenk[1,2] *and Andreas Hiltbrunner*[1,3]*

[1] Faculty of Biology, Institute of Biology II, University of Freiburg, Freiburg, Germany, [2] Spemann Graduate School of Biology and Medicine, University of Freiburg, Freiburg, Germany, [3] Signalling Research Centres BIOSS and CIBSS, University of Freiburg, Freiburg, Germany

Phytochromes are red- and far-red light receptors that control the growth and development of plants, enabling them to respond adequately to changing light conditions. It has been shown that halted mRNAs stored in RNA granules called processing bodies are released upon light perception and contribute to the adaptation to the light environment. However, the photophysiological background of this process is largely unknown. We found that light of different wavelengths can trigger the disassembly of processing bodies in a dose- and time-dependent manner. We show that phytochromes control this process in red- and far-red light and that cytoplasmic phytochrome A is sufficient and necessary for the far-red light-induced disassembly of processing bodies. This adds a novel, unexpected cytoplasmic function to the processes controlled by phytochrome A. Overall, our findings suggest a role of phytochromes in the control of translationally halted mRNAs that are stored in processing bodies. We expect our findings to facilitate understanding of how light and environmental cues control the assembly and disassembly of processing bodies, which could have broader implications for the regulation of non-membranous organelles in general.

Keywords: phytochrome, p-bodies, photomorphogenesis, light signalling, liquid-liquid-phase-separation

OPEN ACCESS

Edited by:
Jordi Moreno-Romero, Universitat Autònoma de Barcelona, Spain

Reviewed by:
Jeong-Il Kim, Chonnam National University, South Korea
Ruohe Yin, Shanghai Jiao Tong University, China

***Correspondence:**
Andreas Hiltbrunner
andreas.hiltbrunner@biologie.uni-freiburg.de

Specialty section:
This article was submitted to Plant Physiology, a section of the journal Frontiers in Plant Science

Received: *03 December 2021*
Accepted: *18 January 2022*
Published: *23 February 2022*

Citation:
Schwenk P and Hiltbrunner A (2022) Phytochrome A Mediates the Disassembly of Processing Bodies in Far-Red Light. Front. Plant Sci. 13:828529. doi: 10.3389/fpls.2022.828529

INTRODUCTION

Throughout their life cycle, plants are subject to constantly changing environmental conditions at the place where they germinated. In order to cope with fluctuations in the surrounding, plants sense and integrate environmental cues and react with a high level of plasticity to adapt their growth and development accordingly (Chevin and Lande, 2015). This integration happens at different levels, including gene expression (Peschke and Kretsch, 2011), translation, and degradation of proteins (Wu et al., 2019), as well as modifications of mechanical properties of cell walls (Falcioni et al., 2020). Environmental cues can change rapidly, therefore reaction time is a critical factor. A mechanism to overcome the need for mRNA synthesis prior to protein translation is the storage of mRNAs in translationally inactive state (Merchante et al., 2017). The formation and disassembly of processing bodies (p-bodies), a sub-class of RNA granules, is a mechanism to store translationally halted mRNAs and release them in response to specific conditions that has recently gained attention in different model organisms and contexts (Decker and Parker, 2012; Wang et al., 2018; Jang et al., 2019).

RNA granules are cytoplasmic non-membranous organelles formed by phase separation (Sachdev et al., 2019). They can be roughly subdivided into stress granules, p-bodies, and neuronal granules (Anderson and Kedersha, 2006). To our knowledge, the first morphological description of RNA granules dates back to 1865 (Mecznikoff, 1865), though their composition and function remained unknown. Later, yeast p-bodies have been characterised and shown to consist mainly of RNA and proteins supposedly involved in degradation of mRNA (Sheth and Parker, 2003; Parker and Sheth, 2007). Experiments also suggested that primarily mRNA degrading proteins are present in plant p-bodies, indicating a conserved role throughout the phylum of eukaryotes (Maldonado-Bonilla, 2014).

Pioneering work from Hubstenberger et al. (2017) was of particular importance for understanding the protein composition of p-bodies. Increasing evidence suggests that the primary role of p-bodies is the storage of halted mRNAs. P-bodies can be disassembled upon diverse stimuli, releasing these halted mRNAs, and enabling the translation of the transcripts initially stored in p-bodies (Brengues et al., 2005; Aizer et al., 2014; Hubstenberger et al., 2017). This provides a shortcut for rapid changes of the proteome in response to environmental cues, avoiding the need for *de novo* transcribing, splicing, exporting, and maturating mRNA. In plants, this stimulus-induced disassembly plays a role in developmental processes and adaptions to the environment. It has been shown that the light conditions to which plants are exposed determine the number and size of p-bodies and thus the release of mRNAs for translation, including *GUN5* and *OE33* (Jang et al., 2019). The proteins encoded by these mRNAs are relevant for the establishment of fully developed chloroplasts and help plants to adapt to light.

Light is one of the most important factors determining a plant's life (Paik and Huq, 2019). In order to acquire information about the light conditions in the ambient environment, plants have evolved a set of photoreceptors that monitor the light spectrum from UV-B to far-red (FR) light. Phytochromes mediate light signalling in the red (R) and FR light range of the light spectrum (Legris et al., 2019). They are synthesised in the inactive Pr form and can undergo conversion to the active Pfr form upon light absorption. Pfr can revert to Pr either upon light absorption or via thermal relaxation (Klose et al., 2015a). This behaviour forms a molecular toggle switch allowing phytochromes to determine the R:FR ratio in the surrounding environment. PhyB plays a dominant role in R light, whereas phyA is the only photoreceptor in *Arabidopsis thaliana* that mediates responses to FR light. Photoactivated phytochromes translocate to the nucleus where they interact with a plethora of signalling components to control gene expression (Legris et al., 2019). A canonical, well-investigated pathway of phytochrome signalling depends on the PHYTOCHROME INTERACTING FACTORs (PIFs), a set of bHLH transcription factors. Upon binding of PIFs to phytochromes in the nucleus, the DNA-binding activity of PIFs is suppressed (Legris et al., 2019). Another key component in phytochrome signalling is the CONSTITUTIVELY PHOTOMORPHOGENIC 1/SUPPRESSOR OF PHYA-105 (COP1/SPA) complex, which targets positive factors of photomorphogenesis, such as ELONGATED HYPOCOTYL 5 (HY5), for degradation in darkness. This complex is reorganised and inactivated upon binding of photoactivated phytochromes, allowing positive factors of photomorphogenesis to accumulate (Sheerin and Hiltbrunner, 2017). Jang et al. (2019) showed that the *hy2* mutant is unable to react to white light with a reduction of p-body numbers. This mutant is deficient in the synthesis of phytochromobilin and therefore lacks photoactive phytochromes (Kohchi et al., 2001). Additionally, it was shown that a mutation in *COP1*, *cop1-6*, leads to decreased p-body numbers in darkness. This is in line with the light-independent activation of light signalling in the *cop1-6* mutant (Ma et al., 2002). These results indicate an involvement of the phytochrome signalling system in the disassembly of p-bodies in response to light. Yet, the wavelength- and fluence rate-dependency of p-body disassembly has not been investigated and it is still unknown which specific phytochromes are involved in this process.

In our recent work, we described NOT9B as a p-body localised protein. NOT9B is part of the CCR4-NOT complex, a multi-protein complex described to be localised in p-bodies and the nucleus (Maldonado-Bonilla, 2014; Collart, 2016). This complex fulfils a multitude of different functions in plants and has gained attention in plant science over the last years. Only recently, the complex as such was shown to exist in plants (Arae et al., 2019; Zhou et al., 2020; Schwenk et al., 2021). Components of the complex have been described as regulators of transcription and integrators of environmental stresses (Liang et al., 2009; Walley et al., 2010; Suzuki et al., 2015). Here, we used YFP-tagged NOT9B as marker for p-bodies to further investigate the role of light signalling in the disassembly of p-bodies. We determined the basic physiological parameters that control this process, such as the light intensity and quality. P-body disassembly in different mutant and transgenic backgrounds was analysed to evaluate photoreceptor dependency of this process.

RESULTS

Light of Different Wavelengths Triggers p-Body Disassembly

As demonstrated by Jang et al. (2019), prolonged exposure to white light triggers a reduction of the number of p-bodies in cotyledons. To further investigate this effect, we performed similar experiments using *Arabidopsis thaliana* lines stably expressing the p-body localised protein NOT9B N-terminally fused to HA-YFP. We found that 4 h of exposure to FR or R light reduced p-body numbers in hypocotyl epidermis cells (**Figure 1A**). This effect is tissue independent, as we also observed an FR light-dependent reduction of p-body numbers in roots and cotyledons of the HA-YFP-NOT9B transgenic line (**Figures 1B,C**). The effect of FR light on p-bodies is possibly independent of photosynthesis and the energy status, since FR light is poorly photosynthetically active. Supporting this notion, we found that supplementing the growth medium with sucrose does not have any effect on the number of p-bodies (**Supplementary Figure 1**). To investigate the possibility that

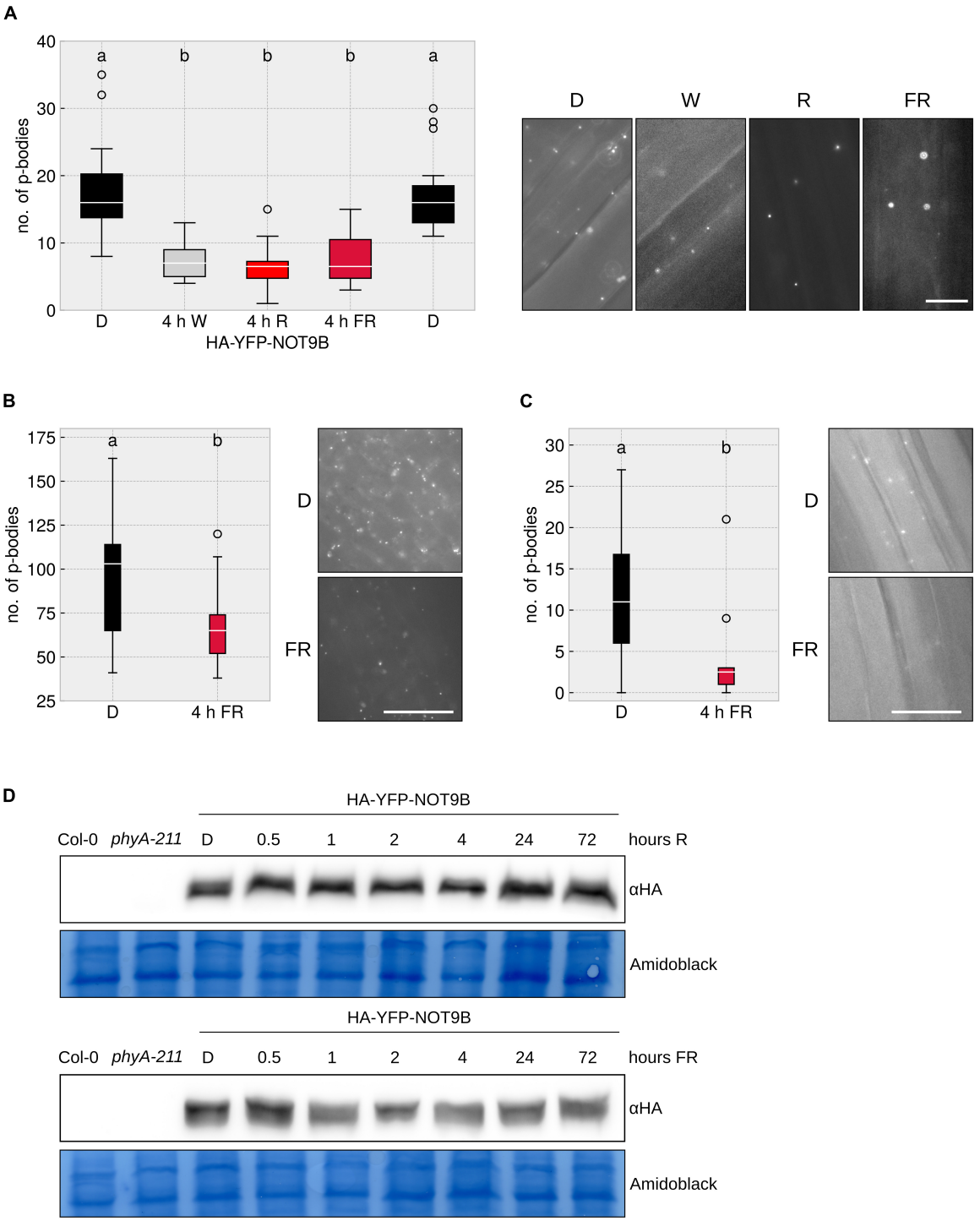

FIGURE 1 | Different wavelengths trigger p-body disassembly. **(A–C)** HA-YFP-NOT9B tagged p-bodies in different light conditions in different tissues. *p35S:HA-YFP-NOT9B* expressing seedlings were grown for 4 days in darkness, followed by 4 h of indicated light quality at a fluence rate of 40 μmol m^{-2} s^{-1} (FR) or 20 μmol m^{-2} s^{-1} (R). Seedlings were imaged and 15 pictures were evaluated. One representative experiment out of three independent experiments is shown. Representative microscope pictures for each treatment are displayed. Different letters indicate significant differences between groups as determined by one-way ANOVA, followed by Tukey's HSD. $P < 0.05$. Scale bar represents 10 μm. Number of p-bodies was quantified in **(A)** hypocotyl epidermal cells, **(B)** cotyledon mesophyll cells, and **(C)** root epidermal cells. **(D)** Protein levels of HA-YFP-NOT9B remain constant under light treatments. 4-day old, dark-grown HA-YFP-NOT9B expressing seedlings were treated with light (40 μmol m^{-2} s^{-1} FR or 20 μmol m^{-2} s^{-1} R) for the indicated time. Total protein was extracted and analysed by Western blotting; HA-YFP-NOT9B was detected using αHA antibody; the Amido Black stained membrane is shown as loading control.

light has an effect on the protein level of NOT9B, we analysed the stability of HA-YFP-NOT9B in R and FR light by western blotting. The amount of NOT9B is not or only slightly affected by light treatments that trigger p-body disassembly. Differences in HA-YFP-NOT9B levels did not exceed 30% and there was no trend toward lower levels after longer exposure to light (**Supplementary Figure 2**). Therefore, the lower abundance of p-bodies in light cannot be explained by reduced levels of HA-YFP-NOT9B (**Figure 1D**).

Using another p-body marker, DCP1-CFP, we also observed a reduction in p-body numbers in response to FR light, similar to HA-YFP-NOT9B marked p-bodies. This indicates that light does not specifically trigger the exclusion of HA-YFP-NOT9B from p-bodies but rather promotes a general disassembly of p-bodies (**Supplementary Figure 3**).

P-Body Disassembly in Far-Red and Red Light Is Dependent on Phytochrome A and B, Respectively

So far, it was unclear which photoreceptor mediates the disassembly of p-bodies in response to different light qualities. We crossed the HA-YFP-NOT9B expressing line into *phyA-211*, *phyB-9*, and *phyA-211 phyB-9* mutants and quantified p-body number reduction in response to R and FR light. The reduction of p-body numbers in response to R light was dependent on phyB, whereas the reduction in FR light required phyA. The *phyA-211 phyB-9* double mutant was not able to react to any of these light qualities in terms of reduction of p-body numbers (**Figures 2A–C**). This behaviour is in line with the canonical function of phyA and phyB as primary FR and R light receptors, respectively.

NOT9B directly interacts with phyA, raising the possibility that the phyA-induced disassembly of p-bodies depends on this interaction. Therefore, we took advantage of a point mutant of NOT9B, NOT9B ΔPNB, which lacks phyA binding capability, to examine the effect of direct physical interaction of phyA with the p-body marker NOT9B (Schwenk et al., 2021). As shown in **Supplementary Figure 4**, the number of p-bodies in FR light was reduced to a similar degree in lines expressing HA-YFP-NOT9B ΔPNB or HA-YFP-NOT9B, indicating that the disassembly of p-bodies in FR light is independent of NOT9B's direct interaction with phyA, even though it is dependent on the presence of phyA.

P-Body Disassembly in Response to Light Is Dependent on the Time and Intensity of Illumination

Many responses mediated by phytochromes, e.g., the inhibition of hypocotyl elongation, are dependent on the fluence rate and the light quality (Casal et al., 2014). To investigate these characteristics in the context of p-body disassembly, we treated plants for different time-spans with R, FR, or W light. Illumination for 1 h did not lead to a significant reduction in p-body number, yet 4 h exposure to either R, FR, or W light triggered an approx. 50% reduction in p-body abundance; exposing the seedlings for 24 h to light did not further reduce the number of p-bodies (**Figure 3A**). A reaction after 4 h is known for some phytochrome mediated responses, e.g., upregulation of gene expression (*ELIP1/2*, *CHS*) (Peschke and Kretsch, 2011) or the unfolding of cotyledons (Kretsch, 2010). To investigate whether the reduction of p-body disassembly is dependent on the intensity of FR light used for illumination, we treated the plants for 4 h with FR light of different intensities. A clear dose-dependency was observed, with a saturation point between 5 and 20 μmol m^{-2} s^{-1} (**Figure 3B**). This is similar to canonical responses such as inhibition of hypocotyl growth in FR light. The non-saturating effect of lower intensities might be due to a reduced total fluence. To assay this, we increased illumination to 24 h, yielding very similar results as 4 h (**Supplementary Figure 5**). This indicates that the fluence rate rather than the total fluence is determining the degree of p-body disassembly in FR light, suggesting that this response is a high-irradiance response (HIR) mediated by phyA.

Cytoplasmic phyA Is Sufficient to Reduce the Number of Processing Bodies

To date, by far the most phyA-mediated responses that have been investigated are dependent on nuclear localised, light-activated phyA, whereas only very few responses, such as the control of translation of *PORA* mRNA, are described to be mediated by cytoplasmic phyA (Paik et al., 2012; Hughes, 2013). Since p-bodies are localised to the cytoplasm, the question arises whether the disassembly of p-bodies is mediated by a cytoplasmic signalling pathway or routed through the nucleus, e.g., via transcription of a factor that is active in the cytoplasm. PhyA nuclear import upon light perception depends on FHY1 and FHL (Hiltbrunner et al., 2006), making the *fhy1-3 fhl-1* mutant an ideal tool to tackle this question.

A line expressing HA-YFP-NOT9B in the *fhy1-3 fhl-1* mutant background was evaluated for FR dependent reduction of p-body abundance. Lack of nuclear transport of phyA had no significant effect on the total number of p-bodies and the reduction in response to a 4 h FR light treatment was in the range of the line expressing HA-YFP-NOT9B in WT background (**Figure 4A**). This indicated that cytoplasmic phyA is sufficient to induce p-body disassembly. To test if cytoplasmic phyA is required for this response, we investigated p-body disassembly in a double transgenic Arabidopsis line co-expressing *p35S:HA-YFP-NOT9B* and *pPHYA:PHYA-NLS-YFP* in the *phyA-211* background. We could not observe any reduction of p-body numbers in response to exposure to FR light in this line containing exclusively nuclear localised phyA (Rausenberger et al., 2011). This indicated that the nuclear fraction of phyA does not play a role in this process in FR light (**Figure 4A**). In order to confirm that a C-terminally tagged version of phyA is generally capable of mediating the disassembly of p-bodies, we crossed *p35S:HA-YFP-NOT9B* into *phyA-211 pPHYA:PHYA-CFP*. In this line, the reduction of p-body numbers in response to light was similar to the Col-0 background (**Supplementary Figure 6**).

The dependency of p-body disassembly on phytochromes raises the possible involvement of canonical phytochrome

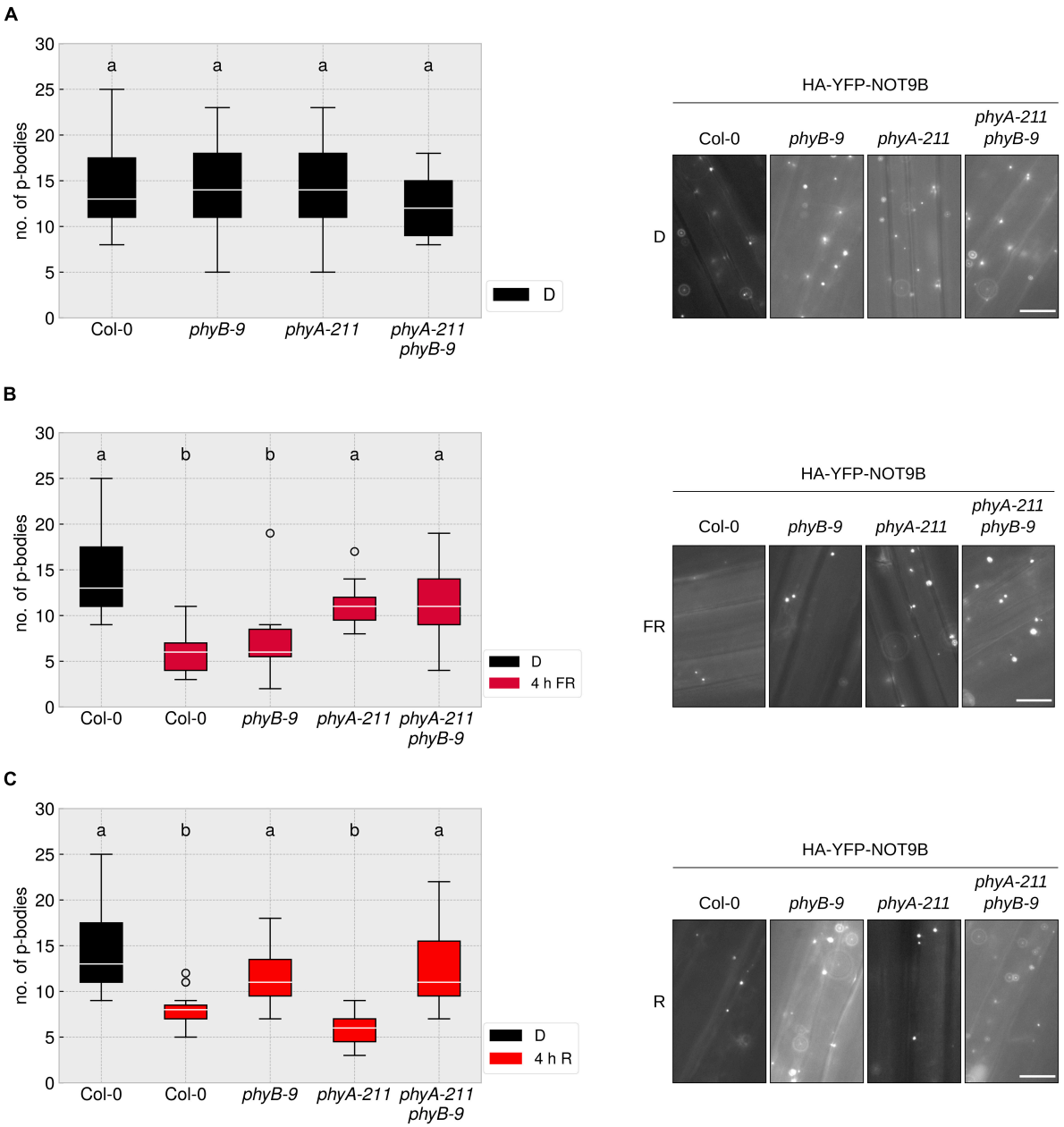

FIGURE 2 | R and FR light-induced reduction of p-body abundance is dependent on phytochromes. **(A–C)** *p35S:HA-YFP-NOT9B* expressing seedlings in the indicated genetic backgrounds were grown for 4 days in darkness. Abundance of p-bodies was quantified before exposure to light **(A)**, or following 4 h exposure to FR **(B)** or R **(C)** light. Light intensity was set to a fluence rate of 40 μmol m^{-2} s^{-1} (FR) or 20 μmol m^{-2} s^{-1} (R). Epidermis cells of hypocotyls of seedlings were imaged and 15 pictures were evaluated. One representative experiment out of three independent experiments is shown. Representative microscope pictures for each treatment are displayed. Different letters indicate significant differences between groups as determined by one-way ANOVA, followed by Tukey's HSD. $P < 0.05$. Scale bar represents 10 μm.

downstream signalling pathways. One of the key factors that mediate signalling events downstream of phyA and phyB is HY5. Therefore, we crossed the line expressing HA-YFP-NOT9B into the *hy5-215* mutant and evaluated the response to FR light. As shown in **Supplementary Figure 7**, the lack of functional HY5 has no effect on the reduction of p-body numbers in response to FR light. Taken together, we conclude that the effect of phyA on p-bodies is exclusively mediated by the cytoplasmic fraction of phyA (**Figure 4B**). Knock-out of one of the most prominent transcription factors in light signalling, HY5, did not affect the p-body disassembly. This would be in line with the notion that there is no need for an indirect signalling via *de novo* transcription in the nucleus. In conclusion, cytoplasmic phyA might exert control over p-body number directly.

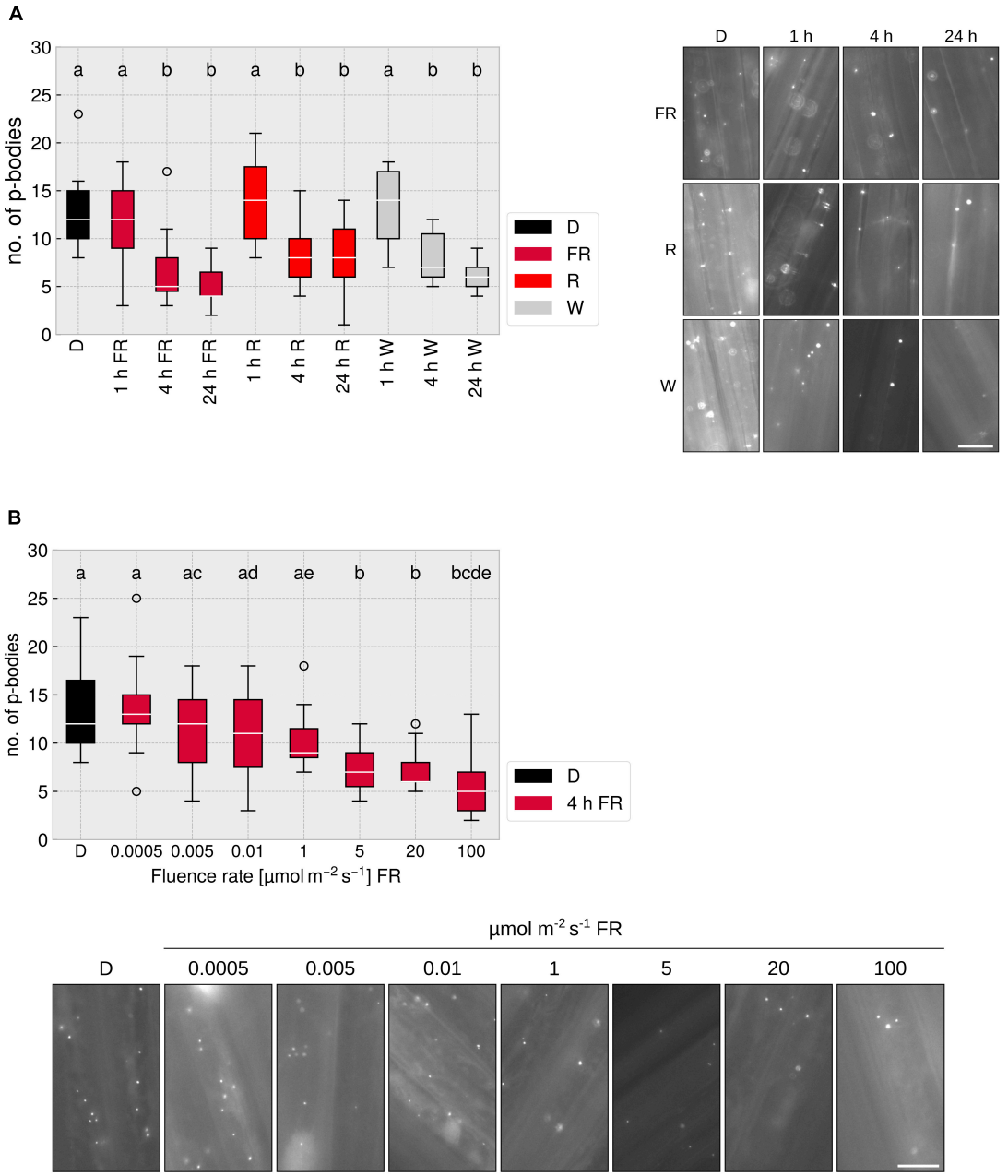

FIGURE 3 | FR light-dependent reduction of p-body abundance is time- and fluence rate dependent. **(A)** p-body disassembly kinetics. 4-day old, dark-grown *p35S:HA-YFP-NOT9B* expressing seedlings were grown under indicated light conditions for different time spans. Light intensity was set to a fluence rate of 40 µmol m^{-2} s^{-1} (FR) or 20 µmol m^{-2} s^{-1} (R). Epidermis cells of hypocotyls of seedlings were imaged and 15 pictures were evaluated. One representative experiment out of three independent experiments is shown. Representative micrograph pictures for each treatment are displayed. Different letters indicate significant differences between groups as determined by one-way ANOVA, followed by Tukey's HSD. $P < 0.05$. Scale bar represents 10 µm. **(B)** Fluence rate dependency of p-body disassembly. 4-day old, dark-grown *p35S:HA-YFP-NOT9B* expressing seedlings were exposed to FR light of different fluence rates for 4 h. Epidermis cells in hypocotyls of seedlings were imaged and 15 pictures were evaluated. One representative experiment out of three independent experiments is shown. Representative microscope pictures for each treatment are displayed. Different letters indicate significant differences between groups as determined by one-way ANOVA, followed by Tukey's HSD. $P < 0.05$. Scale bar represents 10 µm.

DISCUSSION

Light signalling mediated by phytochromes has been researched for more than 70 years, and still our knowledge of these processes is incomplete. In their pioneering work, Jang et al. (2019) showed that mRNAs crucial for kickstarting photosynthesis are halted and stored in DCP2-marked p-bodies and released upon light irradiation, thereby initiating translation of these mRNAs. So far,

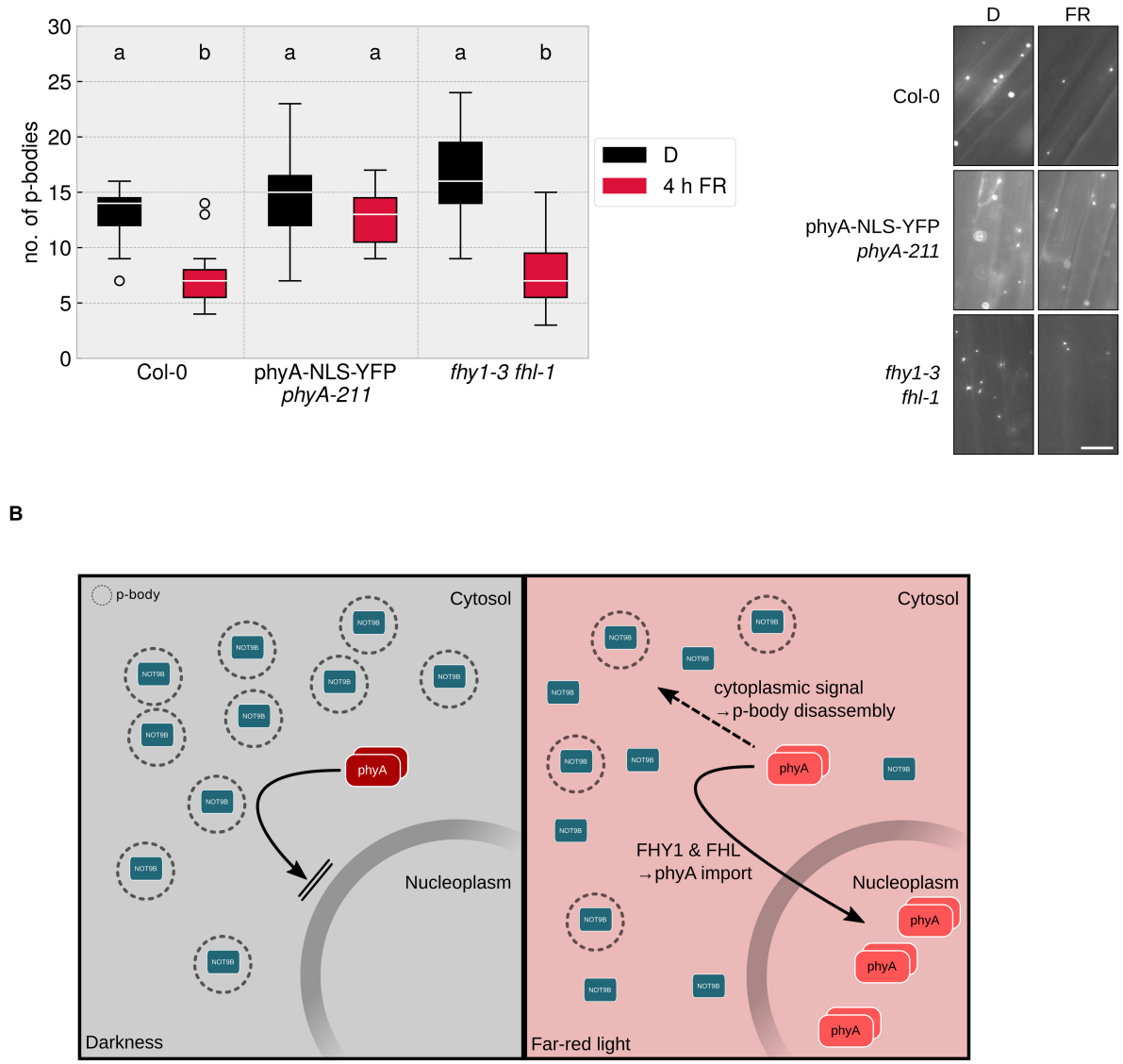

FIGURE 4 | Cytoplasmic phyA is sufficient and necessary for FR light-dependent reduction of p-body numbers. **(A)** *p35S:HA-YFP-NOT9B* expressing plant lines were crossed into *phyA-211 pPHYA:PHYA-NLS-YFP* and *fhy1-3 fhl-1*. 4-day old, dark-grown seedlings were treated for 4 h with FR light (40 μmol m^{-2} s^{-1}) and analysed. Epidermis cells in hypocotyls of seedlings were imaged and 15 pictures were evaluated, focusing on the cytoplasmic p-body fraction marked by HA-YFP-NOT9B. One representative experiment out of three independent experiments is shown. Representative microscope pictures for each treatment are displayed. Different letters indicate significant differences between groups as determined by one-way ANOVA, followed by Tukey's HSD. $P < 0.05$. Scale bar represents 10 μm. **(B)** Hypothetical model of phyA mediated p-body disassembly. In darkness, phyA is localised to the cytoplasm in its inactive Pr form; FHY1 and FHL transport part of the active phyA into the nucleus, while the remaining, cytoplasmic Pfr phyA is triggering p-body disassembly via a cytoplasmic signalling cascade.

it was only shown that the marker protein DCP2 is excluded from p-bodies in response to light. Here, we provide evidence that other p-body markers (DCP1 and NOT9B) display a similar behaviour as DCP2. This supports the notion that the p-bodies indeed disassemble, rather than that specific factors are selectively excluded. Our data demonstrate that the process of p-body disassembly is controlled by phytochromes in R and FR light, with phyB playing a dominant role in R and phyA in FR light. Future work will have to unravel the mechanism by which the signal perceived by photoreceptors is transduced to a change in the composition and disassembly of p-bodies.

We used transgenic and mutant lines containing exclusively nuclear or cytoplasmic localised phyA to investigate which fraction of phyA is required and sufficient for the disassembly

of p-bodies in response to FR light. As the cytoplasmic fraction of phyA is sufficient and the nuclear fraction does not elicit a disassembly of p-bodies, we conclude that the mechanism is not routed through nuclear phytochrome signalling. Until today, only few cytoplasmic phytochrome responses have been reported (Hughes, 2013). For example, it has been shown that phytochrome in the active Pfr state binds to PENTA 1 (PNT1) and thereby represses the translation of mRNAs, e.g., *PORA* mRNA (Paik et al., 2012).

It is still unclear if cytoplasmic phyB exerts a similar effect on p-bodies in response to R light as phyA does in response to FR light. Unfortunately, experimentally addressing this question for phyB is much more difficult than for phyA, because the nucleo-cytoplasmic partitioning of phyB is much less strict than for phyA (Klose et al., 2015b). Further studies could include crossing of p-body marker lines into a line expressing *p35S:PHYB-NLS-GFP* in *phyB-9* background to evaluate if nuclear phyB is able to trigger p-body disassembly. As no specific importer for phyB nuclear transport has been identified, the inverse, much more conclusive experiment is difficult. Here, fusions of phyB to GR could be of value to retain phyB in the cytosol and control nuclear import by application of DEX (Huq et al., 2003). Many responses mediated by phyA and phyB depend on the same signalling components (e.g., PIFs and COP1/SPA), so one can speculate that signal transduction downstream of these two photoreceptors also converges when it comes to regulation of p-body disassembly. Additionally, it will be of interest if the disassembly of p-bodies in response to R and FR light affects the translatome in a similar way, or if there are wavelength-specific effects. Jang et al. (2019) showed that mRNAs encoding OE33 and GUN5, proteins relevant for the establishment of chloroplasts, are released by p-body disassembly in light and undergo translation. As FR light plays a minor role in photosynthesis compared to R light, it will be interesting to evaluate if a different set of mRNAs is released from p-bodies in response to R and FR light.

In the dark, nuclear-localised COP1, together with SPA proteins, tags specific proteins for degradation by the proteasome. However, COP1 is also present in the cytosol (Balcerowicz et al., 2017) and therefore one could speculate that also cytosolic COP1 could be active and target a hypothetical protein X that degrades RNAs or proteins in p-bodies required for the structural integrity of p-bodies. When cytosolic COP1 is inhibited by photoactivated phytochromes in the cytosol, such a protein X would accumulate and could affect p-body composition and number (**Supplementary Figure 8**). To date, however, the identity of protein X is unknown and it is also unknown if COP1 has E3 ubiquitin ligase activity in the cytosol. Evidence for an involvement of COP1 in p-body disassembly is the fact that in a *cop1-6* mutant, the total p-body number is reduced and no further reduction takes place after light irradiation (Jang et al., 2019). Elucidating the mechanism of p-body disassembly will be crucial to understanding how light affects mRNA translation. Recent advancements in proteomic measurements of p-body contents purified from mammalian cell cultures might be useful to establish an experimental protocol to compare p-bodies isolated from light- and dark-grown plants (Hubstenberger et al., 2017).

As membraneless organelles, p-bodies are being formed by liquid-liquid-phase-separation (LLPS). The ability to undergo LLPS is depending on different factors, including an elevated local concentration of proteins that are of high intrinsic disorder. Additionally, *in vitro* studies showed that ribonucleoproteins (RNPs) bound to mRNAs can confer phase separation potential (Garcia-Jove Navarro et al., 2019). A process that disassembles p-bodies is presumably reducing this potential for phase separation by either selective or general removal of factors conferring phase separation potential. Identifying these factors will help understand how environmental cues, such as light, affect this process.

Even though NOT9B is a component of p-bodies implicated in light signalling and directly interacting with the FR photoreceptor phyA, there is no evidence that it is mechanistically involved in the assembly or disassembly of p-bodies. The phyA-binding capability of NOT9B is not relevant for the assembly of NOT9B into p-bodies, as mutating the PNB site that confers phyA binding capability of NOT9B does not lead to an altered pattern of p-body formation or disassembly. Since for the human homologue of NOT9B, CNOT9, a nucleotide-binding capacity was demonstrated *in vitro* (Garces et al., 2007), one could speculate that tethering of NOT9B to halted mRNAs localised to p-bodies might contribute to NOT9B's dynamic association with p-bodies. Another potential mechanism for the association of NOT9B with p-bodies might be the interaction with GW-repeat proteins, a class of proteins that contain glycine/tryptophane repeats known to interact with AGOs and the human NOT9B homologue CNOT9 (Chen et al., 2014). A mutant version of NOT9B that lacks GW binding sites shows reduced association with p-bodies (Schwenk et al., 2021).

Structurally, CNOT9 consists of an Armadillo repeat (ARM) domain flanked by an N-terminal and a C-terminal unstructured, flexible region (Garces et al., 2007), a structure conserved in NOT9B. These regions of high intrinsic disorder could be considered as low-complexity domains, similar to low-complexity domains implicated in the formation of LLPS granules. The unstructured N-terminal domain of NOT9B was found to be phosphorylated in high-throughput studies (Heazlewood et al., 2008; Reiland et al., 2009). Phosphorylation might contribute to the nucleo-cytoplasmic partitioning, but also to the association with p-bodies under different light conditions. Experiments using different truncated and/or mutated versions of NOT9B will help elucidate whether it is a structural component of processing bodies.

With a saturation after approximately 4 h, the disassembly of p-bodies is a fast response. The initial release of mRNAs for translation is probably even faster, as we only observe the final disappearance of p-bodies. The fast kinetics is in line with the proposed purpose of releasing mRNAs quickly in order to adapt to a changing environment. Investigating the kinetics of p-body disassembly is therefore of considerable interest and FISH probes for identified p-body localised mRNAs or miRNAs could help understand the kinetics of their release.

It is tempting to speculate about why only approximately 50% of p-bodies disassemble after irradiation with light, irrespective of the duration and intensity of the light treatment. Literature

describes a heterogeneous composition of p-bodies, which might contain different structural elements with different sensitivities to different stimuli, for example to hypoxia and light (Sorenson and Bailey-Serres, 2014; Jang et al., 2019). The term "processing body" presumably describes a heterogeneous class of different granules that have partially specific, partially overlapping contents and functions. This could explain how different sets of RNAs can be released in response to different stimuli and why only approximately 50% of p-bodies disassemble in response to light. Fluorescent Activated Particle Sorting (FAPS) could be used to purify p-bodies from plant tissue and separate them from the diffuse fraction. These purified bodies can be analysed for their protein and RNA content using MS/MS and RNA-seq techniques. Performing these experiments following treatments of plants with different stimuli that reduce the number of p-bodies could help distinguish between potential subclasses of p-bodies and identify their RNA and protein contents. Again, FISH probes could turn out to be an indispensable tool to investigate whether mRNA species are distributed equally throughout these different p-bodies. Not knowing the content and not knowing how the content is released from p-bodies is a current shortcoming in this fascinating field of research and one can expect great insight into the function of p-bodies once these questions are solved.

Taken together, our results reveal a novel cytoplasmic function of phyA in releasing mRNAs by disassembly of p-bodies in response to light. Our understanding of p-bodies is currently focussed on their RNA content, yet the molecular mechanism of the disassembly of p-bodies is still unclear. It will be interesting to find out whether light is the only stimulus that triggers the release of mRNA from p-bodies, or if this is a general mechanism in the regulation of plant development.

MATERIALS AND METHODS

Plant Growth

For experimental purposes, plants were grown on 1/2 MS, 1.2% agar. Seeds were surface sterilised by incubating in 1 ml 70% EtOH for 10 min, followed by incubation in 1 ml 100% EtOH for 10 min. Seeds were left to dry in sterile conditions. After sowing, plates were kept for 48–72 h in 4°C for stratification. For germination induction, seeds were treated with 70 μmol m^{-2} s^{-1} white light for 6–8 h and transferred back to D for 4 days. Further light treatments were performed as described in the figure legends.

For breeding and propagation purposes, plants were grown on standard soil in a growth chamber in 100 μmol m^{-2} s^{-1} PAR in long-day conditions (16 h W, 22°C; 8 h D, 18°C).

Light Treatments and Light Sources

For experiments, 740 nm LEDs have been used for FR light, 656 nm LEDs for R light, and fluorescent bulbs mounted in a Sanyo cabinet (Sanyo, Osaka, Japan) for W light. For plant cultivation, plants were kept under fluorescent light bulbs. Spectra of all light sources can be found in **Supplementary Figure 9**.

Imaging and Counting of Processing Bodies

Seedlings were mounted in ddH_2O in green light conditions and subjected to epifluorescence microscopy. Microscopic images were acquired using a Zeiss Axioplan 2 MOT (Carl Zeiss, Göttingen, Germany) equipped with a Photometrics CoolSNAP-HQ 12-bit monochrome CCD camera (Roper Scientific, Tucson, AZ, United States), external filter wheels (LUDL, Hawthorne, NY, United States), and filter sets for YFP (F31-028, excitation 500 nm, emission 515 nm; AHF Analysentechnik, Tübingen, Germany), or CFP (F31-044, excitation 436 nm, emission 455 nm; AHF Analysentechnik, Tübingen, Germany).

The upper third of the hypocotyl was used for imaging. Here, the uppermost layer of the epidermis was focused and three consecutive images along the hypocotyl were taken. A 350 × 200 px area was chosen of each picture in a way that as many p-bodies as possible were included. Using ImageJ, the number of p-bodies was counted.

Protein Extraction and Western Blotting

Plants were grown for 4 days in D, followed by the indicated light treatments. 100 mg of plant material was harvested and ground in liquid nitrogen. 250 μl of 95°C SDS sample buffer [65 mM Tris/HCl pH 7.3, 4 M Urea, 3% SDS, 10% Glycerol, 0.05% Bromphenol blue, 20 mM DTT, 1× Protease Inhibitor Cocktail (Sigma-Aldrich, Cat-No: I3911)] was added and samples were incubated under vigorous shaking at 95°C for 10 min. Insoluble debris was pelleted by centrifugation (15 min, 20,000 × *g*). The supernatant was transferred to a new tube and protein content was determined using the Amido Black method (Popov et al., 1975).

Equal amounts of proteins were separated on a 10% SDS-PAGE and transferred to PVDF membrane. Membranes were blocked with 5% skim milk powder in PBS-T (137 mM NaCl, 2.7 mM KCl, 10 mM Na_2HPO_3, 1.8 mM KH_2PO_4, pH 7.4, 0.5% Tween-20). Equal loading was shown by Amido Black staining or detection of ACT. Membranes were probed with anti-HA-antibody (mouse, monoclonal, 1:1,000 in PBS-T, BioLegend, San Diego, CA, United States, Cat-No: 901533) or anti-ACT-antibody (mouse, monoclonal, 1:5,000 in PBS-T, Sigma-Aldrich, St. Louis, MO, United States, Cat-No: A0480) followed by secondary anti-mouse antibody (1:7,500 in PBS-T, Vector Laboratories, Burlingame, CA, United States, Cat-No: AP-2000-1). Immunodetection was performed using CDP-STAR (Sigma-Aldrich, Cat-No: 11759051001) according to manufacturers instructions. Quantification was done as described previously (Schwenk et al., 2021).

Data Visualisation

Microscopy images were cropped and brightness/contrast adjusted using ImageJ. Plots were created using the Matplotlib package in Python 3.7.6 using Spyder IDE v4.0.1. Box plots display the following features of the data sets: White line indicates the median value, and box indicates the limits of quartile 1 (Q1) and quartile 3 (Q3). Interquartile range (IQR) is defined

as Q3 – Q1. Whiskers indicate Q1–1.5 × IQR and Q3 + 1.5 × IQR. Circles indicate outliers that do not fall into the whisker range.

Figures were assembled using Inkscape. Statistical analysis was performed as indicated in the figure legends.

Plasmid Constructs and Plant Lines Used in This Study

All plasmid constructs and plant lines used in this study are listed in **Supplementary Tables 1**, **2** (Genoud et al., 2008; Rausenberger et al., 2011; Menon et al., 2020; Schwenk et al., 2021).

DATA AVAILABILITY STATEMENT

The original contributions presented in the study are included in the article/**Supplementary Material**, further inquiries can be directed to the corresponding author/s.

AUTHOR CONTRIBUTIONS

PS and AH: conceptualisation, visualisation, writing – original draft, writing – review and editing, and funding acquisition. PS: investigation. AH: project administration. Both authors contributed to the article and approved the submitted version.

FUNDING

This study was supported by the German Research Foundation (DFG) under Germany's Excellence Strategy (GSC-4/Spemann Graduate School of Biology and Medicine to PS; CIBSS – EXC-2189 – Project ID 390939984, project C1 and CIBSS Impulse Funds to AH), HI 1369/10-1 (Project ID 453030721), and in part by the Ministry of Science, Research and the Arts Baden-Württemberg.

ACKNOWLEDGMENTS

We are grateful to M. Krenz and T. Albonetti for technical assistance. We acknowledge support by the Open Access Publication Fund of the University of Freiburg.

SUPPLEMENTARY MATERIAL

The Supplementary Material for this article can be found online at: https://www.frontiersin.org/articles/10.3389/fpls.2022.828529/full#supplementary-material

Supplementary Table 1 | List of plasmid constructs used in this study.

Supplementary Table 2 | List of *A. thaliana* plant lines used in this study.

REFERENCES

Aizer, A., Kalo, A., Kafri, P., Shraga, A., Ben-Yishay, R., Jacob, A., et al. (2014). Quantifying mRNA targeting to P-bodies in living human cells reveals their dual role in mRNA decay and storage. *J. Cell Sci.* 127, 4443–4456. doi: 10.1242/jcs.152975

Anderson, P., and Kedersha, N. (2006). RNA granules. *J. Cell Biol.* 172, 803–808.

Arae, T., Morita, K., Imahori, R., Suzuki, Y., Yasuda, S., Sato, T., et al. (2019). Identification of Arabidopsis CCR4-NOT complexes with Pumilio RNA-binding proteins, APUM5 and APUM2. *Plant Cell Physiol.* 60, 2015–2025. doi: 10.1093/pcp/pcz089

Balcerowicz, M., Kerner, K., Schenkel, C., and Hoecker, U. (2017). SPA proteins affect the subcellular localization of COP1 in the COP1/SPA ubiquitin ligase complex during photomorphogenesis. *Plant Physiol.* 174, 1314–1321. doi: 10.1104/pp.17.00488

Brengues, M., Teixeira, D., and Parker, R. (2005). Movement of eukaryotic mRNAs between polysomes and cytoplasmic processing bodies. *Science* 310, 486–489. doi: 10.1126/science.1115791

Casal, J. J., Candia, A. N., and Sellaro, R. (2014). Light perception and signalling by phytochrome a. *J. Exp. Bot.* 65, 2835–2845. doi: 10.1093/jxb/ert379

Chen, Y., Boland, A., Kuzuoðlu-Öztürk, D., Bawankar, P., Loh, B., Chang, C.-T., et al. (2014). A DDX6-CNOT1 complex and W-binding pockets in CNOT9 reveal direct links between miRNA target recognition and silencing. *Mol. Cell* 54, 737–750. doi: 10.1016/j.molcel.2014.03.034

Chevin, L.-M., and Lande, R. (2015). Evolution of environmental cues for phenotypic plasticity. *Evolution* 69, 2767–2775. doi: 10.1111/evo.12755

Collart, M. A. (2016). The Ccr4-not complex is a key regulator of eukaryotic gene expression. *WIREs RNA* 7, 438–454. doi: 10.1002/wrna.1332

Decker, C. J., and Parker, R. (2012). P-bodies and stress granules: possible roles in the control of translation and mRNA degradation. *Cold Spring Harb. Perspect. Biol.* 4:a012286. doi: 10.1101/cshperspect.a012286

Falcioni, R., Moriwaki, T., Perez-Llorca, M., Munné-Bosch, S., Gibin, M. S., Sato, F., et al. (2020). Cell wall structure and composition is affected by light quality in tomato seedlings. *J. Photochem. Photobiol. B* 203:111745. doi: 10.1016/j.jphotobiol.2019.111745

Garces, R. G., Gillon, W., and Pai, E. F. (2007). Atomic model of human Rcd-1 reveals an armadillo-like-repeat protein with in vitro nucleic acid binding properties. *Protein Sci.* 16, 176–188. doi: 10.1110/ps.062600507

Garcia-Jove Navarro, M., Kashida, S., Chouaib, R., Souquere, S., Pierron, G., Weil, D., et al. (2019). RNA is a critical element for the sizing and the composition of phase-separated RNA-protein condensates. *Nat. Commun.* 10:3230. doi: 10.1038/s41467-019-11241-6

Genoud, T., Schweizer, F., Tscheuschler, A., Debrieux, D., Casal, J. J., Schäfer, E., et al. (2008). FHY1 mediates nuclear import of the light-activated phytochrome A photoreceptor. *PLoS Genet.* 4:e1000143. doi: 10.1371/journal.pgen.1000143

Heazlewood, J. L., Durek, P., Hummel, J., Selbig, J., Weckwerth, W., Walther, D., et al. (2008). PhosPhAt: a database of phosphorylation sites in Arabidopsis thaliana and a plant-specific phosphorylation site predictor. *Nucleic Acids Res.* 36, D1015–D1021. doi: 10.1093/nar/gkm812

Hiltbrunner, A., Tscheuschler, A., Viczián, A., Kunkel, T., Kircher, S., and Schäfer, E. (2006). FHY1 and FHL act together to mediate nuclear accumulation of the phytochrome A photoreceptor. *Plant Cell Physiol.* 47, 1023–1034. doi: 10.1093/pcp/pcj087

Hubstenberger, A., Courel, M., Bénard, M., Souquere, S., Ernoult-Lange, M., Chouaib, R., et al. (2017). P-Body purification reveals the condensation of repressed mRNA regulons. *Mol. Cell* 68, 144–157.e5. doi: 10.1016/j.molcel.2017.09.003

Hughes, J. (2013). Phytochrome cytoplasmic signaling. *Annu. Rev. Plant Biol.* 64, 377–402. doi: 10.1146/annurev-arplant-050312-120045

Huq, E., Al-Sady, B., and Quail, P. H. (2003). Nuclear translocation of the photoreceptor phytochrome B is necessary for its biological function in seedling photomorphogenesis. *Plant J.* 35, 660–664. doi: 10.1046/j.1365-313x.2003.01836.x

Jang, G.-J., Yang, J.-Y., Hsieh, H.-L., and Wu, S.-H. (2019). Processing bodies control the selective translation for optimal development of Arabidopsis young seedlings. *Proc. Natl. Acad. Sci. U. S. A.* 116, 6451–6456. doi: 10.1073/pnas.1900084116

Klose, C., Venezia, F., Hussong, A., Kircher, S., Schäfer, E., and Fleck, C. (2015a). Systematic analysis of how phytochrome B dimerization determines its specificity. *Nat. Plants* 1:15090.

Klose, C., Viczián, A., Kircher, S., Schäfer, E., and Nagy, F. (2015b). Molecular mechanisms for mediating light-dependent nucleo/cytoplasmic partitioning of phytochrome photoreceptors. *New Phytol.* 206, 965–971. doi: 10.1111/nph.13207

Kohchi, T., Mukougawa, K., Frankenberg, N., Masuda, M., Yokota, A., and Lagarias, J. C. (2001). The Arabidopsis HY2 gene encodes phytochromobilin synthase, a ferredoxin-dependent biliverdin reductase. *Plant Cell* 13, 425–436. doi: 10.1105/tpc.13.2.425

Kretsch, T. (2010). Phenotypic characterization of photomorphogenic responses during plant development. *Methods Mol. Biol.* 655, 189–202. doi: 10.1007/978-1-60761-765-5_13

Legris, M., Ince, Y. Ç, and Fankhauser, C. (2019). Molecular mechanisms underlying phytochrome-controlled morphogenesis in plants. *Nat. Commun.* 10:5219. doi: 10.1038/s41467-019-13045-0

Liang, W., Li, C., Liu, F., Jiang, H., Li, S., Sun, J., et al. (2009). The Arabidopsis homologs of CCR4-associated factor 1 show mRNA deadenylation activity and play a role in plant defence responses. *Cell Res.* 19, 307–316. doi: 10.1038/cr.2008.317

Ma, L., Gao, Y., Qu, L., Chen, Z., Li, J., Zhao, H., et al. (2002). Genomic evidence for COP1 as a repressor of light-regulated gene expression and development in Arabidopsis. *Plant Cell* 14, 2383–2398. doi: 10.1105/tpc.004416

Maldonado-Bonilla, L. D. (2014). Composition and function of P bodies in *Arabidopsis thaliana*. *Front. Plant Sci.* 5:201.

Mecznikoff, E. (1865). Über die Entwicklung der Cecidomyienlarve aus dem Pseudovum. *Arch. Naturgesch.* 31, 304–311.

Menon, C., Klose, C., and Hiltbrunner, A. (2020). Arabidopsis FHY1 and FHY1-LIKE are not required for phytochrome A signal transduction in the nucleus. *Plant Commun.* 1:100007. doi: 10.1016/j.xplc.2019.100007

Merchante, C., Stepanova, A. N., and Alonso, J. M. (2017). Translation regulation in plants: an interesting past, an exciting present and a promising future. *Plant J.* 90, 628–653. doi: 10.1111/tpj.13520

Paik, I., and Huq, E. (2019). Plant photoreceptors: multi-functional sensory proteins and their signaling networks. *Semin. Cell Dev. Biol.* 92, 114–121. doi: 10.1016/j.semcdb.2019.03.007

Paik, I., Yang, S., and Choi, G. (2012). Phytochrome regulates translation of mRNA in the cytosol. *Proc. Natl. Acad. Sci. U. S. A.* 109, 1335–1340. doi: 10.1073/pnas.1109683109

Parker, R., and Sheth, U. (2007). P bodies and the control of mRNA translation and degradation. *Mol. Cell* 25, 635–646. doi: 10.1016/j.molcel.2007.02.011

Peschke, F., and Kretsch, T. (2011). Genome-wide analysis of light-dependent transcript accumulation patterns during early stages of Arabidopsis seedling deetiolation. *Plant Physiol.* 155, 1353–1366. doi: 10.1104/pp.110.166801

Popov, N., Schmitt, M., Schulzeck, S., and Matthies, H. (1975). Eine störungsfreie Mikromethode zur Bestimmung des Proteingehaltes in Gewebehomogenaten. *Acta Biol. Med. Ger.* 34, 1441–1446.

Rausenberger, J., Tscheuschler, A., Nordmeier, W., Wüst, F., Timmer, J., Schäfer, E., et al. (2011). Photoconversion and nuclear trafficking cycles determine phytochrome A's response profile to far-red light. *Cell* 146, 813–825. doi: 10.1016/j.cell.2011.07.023

Reiland, S., Messerli, G., Baerenfaller, K., Gerrits, B., Endler, A., Grossmann, J., et al. (2009). Large-scale Arabidopsis phosphoproteome profiling reveals novel chloroplast kinase substrates and phosphorylation networks. *Plant Physiol.* 150, 889–903. doi: 10.1104/pp.109.138677

Sachdev, R., Hondele, M., Linsenmeier, M., Vallotton, P., Mugler, C. F., Arosio, P., et al. (2019). Pat1 promotes processing body assembly by enhancing the phase separation of the DEAD-box ATPase Dhh1 and RNA. *eLife* 8:e41415. doi: 10.7554/eLife.41415

Schwenk, P., Sheerin, D. J., Ponnu, J., Staudt, A.-M., Lesch, K. L., Lichtenberg, E., et al. (2021). Uncovering a novel function of the CCR4-NOT complex in phytochrome A-mediated light signalling in plants. *eLife* 10:e63697. doi: 10.7554/eLife.63697

Sheerin, D. J., and Hiltbrunner, A. (2017). Molecular mechanisms and ecological function of far-red light signalling. *Plant Cell Environ.* 11, 2509–2529. doi: 10.1111/pce.12915

Sheth, U., and Parker, R. (2003). Decapping and decay of messenger RNA occur in cytoplasmic processing bodies. *Science* 300, 805–808. doi: 10.1126/science.1082320

Sorenson, R., and Bailey-Serres, J. (2014). Selective mRNA sequestration by OLIGOURIDYLATE-BINDING PROTEIN 1 contributes to translational control during hypoxia in Arabidopsis. *Proc. Natl. Acad. Sci. U. S. A.* 111, 2373–2378. doi: 10.1073/pnas.1314851111

Suzuki, Y., Arae, T., Green, P. J., Yamaguchi, J., and Chiba, Y. (2015). AtCCR4a and AtCCR4b are involved in determining the poly(A) length of Granule-bound starch synthase 1 transcript and modulating sucrose and starch metabolism in *Arabidopsis thaliana*. *Plant Cell Physiol.* 56, 863–874. doi: 10.1093/pcp/pcv012

Walley, J. W., Kelley, D. R., Nestorova, G., Hirschberg, D. L., and Dehesh, K. (2010). Arabidopsis deadenylases AtCAF1a and AtCAF1b play overlapping and distinct roles in mediating environmental stress responses. *Plant Physiol.* 152, 866–875. doi: 10.1104/pp.109.149005

Wang, C., Schmich, F., Srivatsa, S., Weidner, J., Beerenwinkel, N., and Spang, A. (2018). Context-dependent deposition and regulation of mRNAs in P-bodies. *eLife* 7:e29815.

Wu, G.-Z., Meyer, E. H., Richter, A. S., Schuster, M., Ling, Q., Schöttler, M. A., et al. (2019). Control of retrograde signalling by protein import and cytosolic folding stress. *Nat. Plants* 5, 525–538. doi: 10.1038/s41477-019-0415-y

Zhou, H., Lin, R., Huang, H., Li, L., Cai, T., Zhu, J., et al. (2020). The CCR4-NOT complex component NOT1 regulates RNA-directed DNA methylation and transcriptional silencing by facilitating Pol IV-dependent siRNA production. *Plant J.* 103, 1503–1515. doi: 10.1111/tpj.14818

Conflict of Interest: The authors declare that the research was conducted in the absence of any commercial or financial relationships that could be construed as a potential conflict of interest.

Publisher's Note: All claims expressed in this article are solely those of the authors and do not necessarily represent those of their affiliated organizations, or those of the publisher, the editors and the reviewers. Any product that may be evaluated in this article, or claim that may be made by its manufacturer, is not guaranteed or endorsed by the publisher.

frontiers in Plant Science

ORIGINAL RESEARCH
published: 02 March 2022
doi: 10.3389/fpls.2022.829121

ZEITLUPE Promotes ABA-Induced Stomatal Closure in Arabidopsis and *Populus*

*Manuela Jurca[1], Johan Sjölander[1†], Cristian Ibáñez[1,2†], Anastasia Matrosova[3], Mikael Johansson[1,4], Iwanka Kozarewa[1], Naoki Takata[1,5], Laszlo Bakó[1], Alex A. R. Webb[6], Maria Israelsson-Nordström[3] and Maria E. Eriksson[1,6]**

[1]Umeå Plant Science Centre, Department of Plant Physiology, Umeå University, Umeå, Sweden, [2]Departamento de Biología Universidad de La Serena, La Serena, Chile, [3]Umeå Plant Science Centre, Department of Forest Genetics and Plant Physiology, Swedish University of Agricultural Sciences, Umeå, Sweden, [4]RNA Biology and Molecular Physiology, Faculty for Biology, Bielefeld University, Bielefeld, Germany, [5]Forest Bio-Research Center, Forestry and Forest Products Research Institute, Hitachi, Japan, [6]Department of Plant Sciences, University of Cambridge, Cambridge, United Kingdom

OPEN ACCESS

Edited by:
Andres Romanowski, Utrecht University, Netherlands

Reviewed by:
Uriel Urquiza-Garcia, Heinrich Heine University of Düsseldorf, Germany
Eva Farre, Michigan State University, United States

***Correspondence:**
Maria E. Eriksson
maria.eriksson@umu.se

†These authors have contributed equally to this work

Specialty section:
This article was submitted to Plant Physiology, a section of the journal Frontiers in Plant Science

Received: *04 December 2021*
Accepted: *26 January 2022*
Published: *02 March 2022*

Citation:
Jurca M, Sjölander J, Ibáñez C, Matrosova A, Johansson M, Kozarewa I, Takata N, Bakó L, Webb AAR, Israelsson-Nordström M and Eriksson ME (2022) ZEITLUPE Promotes ABA-Induced Stomatal Closure in Arabidopsis and Populus. Front. Plant Sci. 13:829121. doi: 10.3389/fpls.2022.829121

Plants balance water availability with gas exchange and photosynthesis by controlling stomatal aperture. This control is regulated in part by the circadian clock, but it remains unclear how signalling pathways of daily rhythms are integrated into stress responses. The serine/threonine protein kinase OPEN STOMATA 1 (OST1) contributes to the regulation of stomatal closure *via* activation of S-type anion channels. OST1 also mediates gene regulation in response to ABA/drought stress. We show that ZEITLUPE (ZTL), a blue light photoreceptor and clock component, also regulates ABA-induced stomatal closure in *Arabidopsis thaliana*, establishing a link between clock and ABA-signalling pathways. ZTL sustains expression of *OST1* and ABA-signalling genes. Stomatal closure in response to ABA is reduced in *ztl* mutants, which maintain wider stomatal apertures and show higher rates of gas exchange and water loss than wild-type plants. Detached rosette leaf assays revealed a stronger water loss phenotype in *ztl-3*, *ost1-3* double mutants, indicating that ZTL and OST1 contributed synergistically to the control of stomatal aperture. Experimental studies of *Populus* sp., revealed that ZTL regulated the circadian clock and stomata, indicating ZTL function was similar in these trees and Arabidopsis. PSEUDO-RESPONSE REGULATOR 5 (PRR5), a known target of ZTL, affects ABA-induced responses, including stomatal regulation. Like ZTL, PRR5 interacted physically with OST1 and contributed to the integration of ABA responses with circadian clock signalling. This suggests a novel mechanism whereby the PRR proteins—which are expressed from dawn to dusk—interact with OST1 to mediate ABA-dependent plant responses to reduce water loss in time of stress.

Keywords: abiotic stress, abscisic acid, circadian clock, stomatal closure, ZEITLUPE, OPEN STOMATA 1, PSEUDO-RESPONSE REGULATORs

INTRODUCTION

As plants are sessile, their survival depends upon their ability to balance growth against stress mitigation. Plants must time their growth and modulate their water use on daily, seasonal and yearly timescales. Perennial plants, such as trees, may live for hundreds or even thousands of years (Burian et al., 2016) and must therefore inhibit growth under unfavourable conditions and manage a multitude of seasonal stresses over this lifespan. The timing of reproduction and growth is coordinated by the circadian clock, which uses light quality, photoperiod and temperature cues to entrain plants to local conditions (Millar, 2016). Arabidopsis (*Arabidopsis thaliana*) accessions coordinate germination and flowering with the seasonal patterns of their local environment, maximising survival, reproduction and seed yield (Green et al., 2002; Johansson et al., 2015; Rubin et al., 2017).

The plant hormone abscisic acid (ABA) controls many aspects of growth and development, including seed dormancy and germination, seedling growth and responses to abiotic and biotic stresses (Finkelstein, 2013). In *Populus*, ABA regulates seasonal growth (Tylewicz et al., 2018) and, in Arabidopsis, ABA controls cell growth by inhibiting the TARGET OF RAPAMYCIN (TOR) kinase (Wang et al., 2017).

Plants control water loss by opening or closing their stomata. Stomatal movements are therefore critical for balancing the conflicting needs of photosynthesis, gas exchange and water stress mitigation (Lawson and Vialet-Chabrand, 2018). In addition to its roles in controlling growth, ABA plays an important role in regulating stomata. ABA is produced during drought or light stress and evokes the local and systemic signals regulating stomatal aperture (Munemasa et al., 2015; Devireddy et al., 2018). In response to ABA, levels of osmotically active ions are reduced in guard cells, which leads to loss of turgor and stomatal closure (MacRobbie, 2000).

In the absence of stress, the PYRABACTIN RESISTANCE 1 (PYR1) / PYR1-LIKE (PYL)/REGULATORY COMPONENTS OF ABA RECEPTORS (RCAR) associates with type-2C protein phosphatases (PP2Cs), such as ABSCISIC ACID INSENSITIVE 1 (ABI1), ABI2, HYPERSENSITIVE TO ABA 1 (HAB1) or HAB2, in the cytosol to inhibit the two SUCROSE NONFERMENTING 1-related protein kinases SnRK2.2 (SRK2D), OPEN STOMATA 1 (OST1/SnRK2.6/SRK2E) and SnRK2.3 (SRK2I) (Baumann, 2010; Hubbard et al., 2010). Binding of ABA to PYR/PYL/RCAR (in the complex with PP2Cs) releases SnRK2s, thus enabling SnRK2 autophosphorylation and subsequent target protein phosphorylation (Vlad et al., 2010). Once activated, SnRK2s inhibit the inward rectifying ion channel K^+ TRANSPORTER OF ARABIDOPSIS THALIANA 1 (KAT1) and activate the SLOW ANION CHANNEL-ASSOCIATED 1 (SLAC1) efflux of Cl^- and $NO3^-$ anions (Hubbard et al., 2010). Calcium-dependent protein kinases activated by an ABA-induced elevation of cytosolic calcium are also required, phosphorylating and activating SLAC1 (Brandt et al., 2012, 2015; Munemasa et al., 2015). Therefore, the guard cell osmotic pressure is reduced, water is lost and stomata close. In the nucleus, OST1-dependent phosphorylation of b-ZIP transcription factors, such as ABSCISIC ACID INSENSITIVE3 (ABI3) and ABI5, mediates ABA-induced transcriptional change (Nakashima et al., 2009; Hubbard et al., 2010; Dai et al., 2013).

The circadian clock enables an organism to anticipate regular changes in its environment and modulate its development, growth, metabolism and even defence against predators (Sanchez and Kay, 2016). The plant circadian system is reset daily to local time *via* receptors detecting environmental cues of light and temperature (Millar, 2016), as well as by changes in metabolic sugar levels (Knight et al., 2008; Haydon et al., 2013; Shor et al., 2017). The plant oscillator consists of a large network of transcription factors of mainly repressive interlocking feedback transcription-translation circuits between the homologous proteins CIRCADIAN CLOCK ASSOCIATED 1 (CCA1), and LATE ELONGATED HYPOCOTYL (LHY), which show peak abundance in the morning, and TIMING OF CAB2 EXPRESSION 1 (TOC1)/PSEUDO-RESPONSE REGULATOR 1 (PRR1), which has an evening peak [see reviews (Farré and Liu, 2013; Millar, 2016; Sanchez and Kay, 2016; McClung, 2019)], and studies by Millar et al., (1995), Wang and Tobin (1998), Matsushika et al., (2000), Strayer et al., (2000), Alabadí et al., (2001), Locke et al., (2005), Gendron et al., (2012). These plant oscillator components are embedded in a wider network of interlocking feedback loops that ensure robust clock function with a period (cycle; τ) length close to 24 h (Fogelmark and Troein, 2014; Urquiza-García and Millar, 2021). The basic structure of the clock is conserved across plant species; thus, the clock of *Populus* spp. appears to function similarly to the 'model' clock developed from studies of Arabidopsis (Ramos et al., 2005; Zdepski et al., 2008; Takata et al., 2009; Hoffman et al., 2010; Ibáñez et al., 2010; Takata et al., 2010; Filichkin et al., 2011).

The period of the plant circadian oscillator is negatively related to the level of TOC1, whose phosphorylation and nuclear import are modulated by PRR5 (Millar et al., 1995; Strayer et al., 2000; Eriksson et al., 2003; Más et al., 2003; Fujiwara et al., 2008; Wang et al., 2010). ZEITLUPE (ZTL), a central F-box clock protein and blue light receptor, acts in an E3-ligase complex that controls proteasomal degradation of both TOC1 and a structurally similar protein, PRR5, that is expressed slightly earlier in the day (Han et al., 2004; Somers et al., 2004; Kevei et al., 2006; Kiba et al., 2007; Fujiwara et al., 2008). ZTL levels show a rhythmic pattern over 24 h, with troughs and peaks occurring near dawn (i.e. lights-on in a controlled environment) and dusk (lights-off), respectively (Kim et al., 2007; Lee et al., 2018), as a result of its interaction with GIGANTEA (GI). GI stabilises ZTL *in vivo* by a direct protein-protein interaction *via* the amino-terminal flavin-binding LIGHT, OXYGEN OR VOLTAGE (LOV) domain. This interaction is stabilised by blue light. Mutations within the LOV domain, such as *ztl-21* (Kevei et al., 2006), significantly reduce the interaction between ZTL and GI, decreasing ZTL levels (Kim et al., 2007). GI also recruits deubiquitylases to modulate ZTL-complex function (Lee et al., 2019).

Daily rhythms of stomatal aperture are subject to direct regulation by light *via* blue and red light photoreceptors that control the activities of H^+-ATPase and other ion channels (Hubbard et al., 2010). Multiple signals, such as ABA, CO_2 and extracellular calcium, converge to control stomatal guard

cells (Webb and Hetherington, 1997; Israelsson et al., 2006). ABA-signal transduction initiates stomatal closing and inhibits stomatal opening. The Arabidopsis circadian mutant *toc1-1* has a short period rhythm of stomatal opening under constant conditions, indicating the involvement of the circadian clock in regulating stomatal aperture (Somers et al., 1998); conversely, a long period *ztl-1* mutation delays the daily rhythms of carbon assimilation and stomatal conductance (Dodd et al., 2004), and also affects water use efficiency (Simon et al., 2020).

Mathematical modelling suggests the circadian period changes upon application of ABA (Pokhilko et al., 2013). Experimentally, this prediction is supported by the finding that MYB96 feeds back into the oscillator through the transcriptional activation of TOC1 (Lee et al., 2016).

Stress responses involving the induction of ABA interact in several ways with circadian signalling pathways. Interestingly, the clock protein PRR5 contributes to ABA regulation and signalling, as well as to several ABA-regulated responses, and was recently shown to promote germination synergistically with ABI5 in the presence of ABA (Yang et al., 2021). Overexpression of PRR5 enhances the effect of ABA signalling, inhibiting seed germination in the presence of ABA, while underexpression reduces it.

We addressed the integration of the circadian clock with ABA-dependent stress responses by testing ABA-induced stomatal closure. We reasoned that stomatal closure in the evening was critical to stress and growth regulation, and thus assayed Arabidopsis plants carrying mutations in evening-expressed circadian clock proteins. Consistent with earlier findings (Dodd et al., 2004; Simon et al., 2020), mutations at the *ZTL* locus significantly affected stomatal closure. We also established that ZTL-mediated regulation of stomata was conserved across species by analysing stomata in *Populus tremula* L. × *P. tremuloides* Michx. (*Populus; Ptt*) lines with reduced expression of *PttZTL* orthologues. The role of ZTL in ABA-induced signalling was investigated; it showed that ZTL function is necessary to sustain expression of *AREB/ABF/ABI5* gene expression in response to ABA.

Stomatal movements in both species indicated that the circadian clock acted *via* ZTL to modulate water use efficiency (Simon et al., 2020) and ABA signalling (Adams et al., 2018). We therefore undertook further genetic, physiological and biochemical analyses to determine if an interaction between ZTL and OST1 controlled stomatal closure. ZTL and OST1 interacted physically in plant cells. ABA-induced gene expression in the Arabidopsis mutant *ztl-3* resembled the effect of the strong *ost1-3* allele (Mustilli et al., 2002).

As ZTL post-translationally regulates PRR5, changes to diel regulation of stomata as well as their stress regulation and may be affected by accumulation of PRR5. Hence, we examined stomatal aperture and water loss in *prr5* mutants. Stomatal aperture was affected by loss of PRR5, and PRR5 could interact with OST1 in plant cells. *ztl-3 and ost1-3* double mutants showed an increased sensitivity to drought compared to both single mutants, suggesting these proteins acted in a synergistic manner and may be affected by PRR5 accumulation. Studies of their genetic interactions showed that PRR5 was involved in stomatal closure and suggested the circadian and ABA-signalling pathways converged at ZTL and the control of PRR5, with both proteins interacting with OST1 to control stomatal movements. The circadian signalling and ABA-stress response pathways are thus closely integrated, each modulating the other to enable plants to balance the trade-off between managing growth and mitigating environmental stress in a timely manner.

MATERIALS AND METHODS

Arabidopsis Germplasm

Seeds of Arabidopsis [*Arabidopsis thaliana* (L.) Heynh.] containing the T-DNA insertion allele *ztl-3* (SALK_035701) in the Columbia-0 (Col-0) background (Jarillo et al., 2001; Kim et al., 2003) were obtained from the Salk collection[1] at the Arabidopsis Biological Resource Centre (ABRC), Ohio State University, Ohio, United States *via* the Nottingham Arabidopsis Stock Centre (NASC), Nottingham, United Kingdom. Seed of the *ost1-3*/*snrk2.6*/*srk2e* mutant (SALK_008068; Yoshida et al., 2002) was provided by Dr. Kazuko Yamaguchi-Shinozaki (University of Tokyo, Japan) to the Israelsson-Nordström laboratory. The Webb laboratory received seed of the *ztl-4, fkf1-2 and lkp2-1* triple mutant (Baudry et al., 2010) from Dr. Steve Kay (Keck School of Medicine, University of Southern California, United States) and of the *prr5-11* mutant (Nakamichi et al., 2005) from Dr. Takeshi Mizuno (Nagoya University, Japan). The *ztl-1* mutant in the C24 background, the *ztl-21* mutant in the Wassilewskija-2 (Ws-2) background and *prr5-1* (SALK_006280) have all been described previously (Eriksson et al., 2003; Kevei et al., 2006; Kiba et al., 2007).

The *ztl-3 and ost1-3* double mutant in the Col-0 background were generated using *ztl-3* as the pollen recipient and *ost1-3* as the pollen donor. The *ztl-3, prr5-1 and ost1-3* triple mutant, and combinations thereof, were generated using *ztl-3; prr5-1* (Norén et al., 2016) as the pollen recipient and *ost1-3* as the pollen donor.

To complement the loss-of-function mutant *ztl-3*, we generated transgenic *ztl-3* plants expressing *ZTL* under the control of the 35S CaMV constitutive promoter. *Agrobacterium tumefaciens* GV3101 (pMP90RK-pSoup) was transformed with the *p35S::HA::ZTL* construct in pGreenII 0229. The construct was introduced into *ztl-3* mutant Arabidopsis plants by floral dipping (Bechtold et al., 1993). The pGreenII 0229 construct contains the bialaphos resistance gene (*BAR*) that confers resistance to glufosinate-ammonium (Hellens et al., 2000). Seeds from dipped plants were sterilised and plated on full-strength Murashige and Skoog (MS) medium supplemented with vitamins (Duchefa, BH Haarlem, Netherlands), 3% w/v sucrose (SIGMA-Aldrich, Saint Louis, MO, United States) and 0.8% agar (E1674, Duchefa), pH 5.7, plus 10 mg/l glufosinate-ammonium (SIGMA-Aldrich). Resistant plants were allowed to self-fertilise and next-generation seeds were again screened on glufosinate-ammonium. Expression

[1]http://signal.salk.edu

of the *p35S::HA::ZTL* construct was confirmed by Western blotting (not shown), prior to phenotyping.

Radicle Emergence Assay

Radicle emergence assays were conducted using seeds sown on plates containing half-strength MS medium with 0.8% agar, pH 5.7. Seeds of the different genotypes were grown and harvested at the same time under the same conditions and stored for least 3 months after harvest as seed age and storage affect germination responses. Seeds were surface-sterilised by consecutive washes with 15% hypochlorite, 70% ethanol with 0.1% tween and 95% ethanol before plating. Plated seeds (60 seeds per genotype per replicate; **Supplementary Figure S1**) were stratified at 4°C for 2 days and transferred to a growth chamber (LD 16:8 at 22°C; light intensity during day: 150 μmol m^{-2} s^{-1}) to initiate germination. Germination was determined by the appearance of the testa, endosperm rupture and radicle protrusion (Wu et al., 2012). Radicle emergence was scored every 12 h, starting at 24 h, and calculated as a percentage of the plated seeds.

Populus Material and Growth Assays

In vitro-cultivated, rooted cuttings of *PttZTL1,2* RNA interference (RNAi) lines and wild-type (WT) *Populus tremula* L. × *P. tremuloides* Michx. cv. T89 (Nilsson et al., 1992; *Populus; Ptt*) plants were potted in a 3:1 mix of fertilised peat and perlite, and established under long day cycles consisting of light:dark (LD) 18:6 at constant temperature (18°C) and 80% relative humidity for 4 weeks; light intensity during the day was 200 μmol m^{-2} s^{-1} (Osram Powerstar HQI-T 400 W/D lamps; Osram, München, Tyskland). After this point, temperature, humidity and irradiance during the day were maintained but the photoperiod was shortened to LD 15:9 at 18°C, keeping the time of dawn unchanged.

A sub-set of lines (1, 3, 4, 5 and 7) with variable levels of *ZTL1,2* downregulation were selected and samples for analysis taken twice a week subsequent to the shift from LD 18:6 to LD 15:9. Growth cessation, which refers to the elongation of shoots ceasing, was scored according to a predefined scale (score 2), as previously described (Ibáñez et al., 2010).

Gene Constructs

Populus ZTL RNA Interference

The *ZTL* RNAi fragment from *Populus* was used to construct RNAi lines; this fragment targets two homologous genes, *PttZTL1* and *PttZTL2* [Potrx050857g15511 and Potrx063764g24087 (Sjödin et al., 2009)].[2] Template cDNA from wild-type (WT) *Populus* was amplified by PCR using Platinum Pfx DNA polymerase (Invitrogen, Carlsbad, CA, United States) and gene-specific primers (**Supplementary Material**).

The amplified fragment was cloned into the Gateway entry vector pDONOR201, followed by recombination into the binary vector pHELLSGATE8 (Helliwell et al., 2002) using Gateway BP Clonase enzyme mix (Invitrogen, Carlsbad, CA, United States). WT trees were transformed with the resulting binary vector that contained the RNAi construct, using *Agrobacterium tumefaciens* C58 strain GV3101 (pMP90RK; Nilsson et al., 1992, 1996). Transgenic plants were selected using kanamycin and regenerated, as described previously (Eriksson et al., 2000). This produced 10 independent, stable and first-generation *PttZTL1,2* RNAi transgenic lines.

RNA was extracted from a pool of leaves collected from the 10th internode of different *PttZTL1,2* RNAi lines; leaf samples were collected at five time points from trees of each line, with one leaf sampled every 4 h, starting at ZT 0 (dawn) under a 24 h cycle (**Supplementary Figure S2A**) or pools from the 8, 9 and 10th internode collected at ZT 12 (**Supplementary Figure S2B**). An RT-qPCR analysis with gene-specific primers (**Supplementary Material**) determined the extent of downregulation of *PttZTL1* and *PttZTL2* in each independent line.

Arabidopsis ZTL Over Expression Construct

To produce constructs overexpressing ZTL, the *ZTL* coding sequence under the control of the 35S CaMV promoter and fused in frame with the 3×HA-epitope tag (*p35S::HA::ZTL*) was obtained from pRT104-HA-ZTL (Johansson et al., 2011) by SbfI restriction digest. The *p35S::HA::ZTL* fragment was then subcloned into the PstI site of the promoter-less pGreenII 0229 plasmid (Hellens et al., 2000). Positive colonies were selected by colony PCR using primers that amplified the ZTL ORF. The cloned construct was sequenced and used to transform competent *A. tumefaciens* GV3101 (pMP90RK-pSoup). *A. tumefaciens* clones containing the *p35S::HA::ZTL* construct were selected in medium containing 25 μg/ml kanamycin and confirmed by colony PCR; a single confirmed clone was used to transform Arabidopsis plants *via* the floral dip method (Bechtold et al., 1993). Independent lines of T_3 transgenic seeds were used in experiments.

Delayed Fluorescence of *Populus* and Period Analysis

Young leaves from internodes four to six were dissected from sterile cuttings grown in jars on half-strength Murashige and Skoog (MS) medium, supplemented with vitamins (Duchefa) and 0.8% agar (E1674, Duchefa), pH 5.7, under 18 h light:6 h dark (LD 18:6) cycles. The light intensity during the day was 100–120 μmolm^{-2} s^{-1}. The light:dark cycle was reinforced by warm:cold (W:C) temperature cycles (20°C during light:18°C during dark).

Excised leaves, together with a clean-cut petiole to sustain growth, were placed on square plates (12×12 cm) containing MS medium. Plates were transferred at Zeitgeber time (ZT) 0 (i.e. 'dawn' or lights-on) to constant light (LL), consisting of equal parts blue (470 nm) and red light (660 nm) from 20 μmolm^{-2} s^{-1} light-emitting diodes (MD Electronics, Warwick, United Kingdom) at a constant temperature of 22°C. Rhythms of delayed fluorescence were recorded following lights-off using a cooled ORCA-IIERG 1024 camera (Hamamatsu Photonics, Hamamatsu City, Japan) with medium gain, a 900 ms delay

[2]https://popgenie.org/

and 1 min exposure. Imaging data were analysed using BRASS Fourier analysis software (Plautz et al., 1997; Locke et al., 2005), as described previously (Ibáñez et al., 2010). Only data collected 24–120 h after the transfer to LL were included in the analysis. Plants were considered rhythmic when the relative amplitude error was ≤0.6.

Water Loss Assay

Water loss assays were performed in detached leaves of similar developmental stage and size from 3-week-old Arabidopsis or 12- to 13-week-old *Populus* plants. Arabidopsis plants were grown on soil under controlled conditions (LD 16:8 cycles; light intensity during the day: 100–120 μmol m^{-2} s^{-1}) at 22°C. For Arabidopsis assays, a single leaf per plant (six to eight plants per genotype) was detached and the loss in fresh weight monitored over time. For *Populus*, plants from WT and RNAi lines were grown under controlled conditions (LD 18:6 cycles; light intensity during the day: 250 μmol m^{-2} s^{-1}) at 18°C. Three expanded young leaves from internodes eight to 10 (counted from the first leaf at least 1 cm long) were detached from each plant (six plants per genotype) and the loss in fresh weight monitored over time. Water loss was expressed as a percentage of the initial fresh weight.

Stomatal Conductance

Arabidopsis and *Populus* plants were grown as described for the water loss assay. Stomatal conductance (gs = mmol H_2O m^{-2} s^{-1}) was measured in intact 3-week-old wild-type, *ztl-3* and *ost1-3* Arabidopsis plants using a steady-state Leaf Porometer (Decagon Devices, Pullman, United States). Measurements were made on the abaxial leaf surface from four leaves per plant, and from eight to 10 plants per genotype. Conductance was measured in *Populus* in three expanded young leaves from internodes eight to 10, as defined above, and from seven to eight plants per genotype.

Stomatal Aperture and Density Measurements

The stomatal ratio is a better measure than aperture as it accounts for differences in stomatal size that may occur in expanding leaves with different growth rates. To calculate the stomatal ratio, measurements of stomata opening were made, as previously described (Conn et al., 2011). Plants were cultivated *in vitro* in Petri dishes (Arabidopsis) or in jars (*Populus*) for 3 to 4 weeks on half-strength MS with 0.8% agar, pH 5.7, under LD 16:8 (*Populus*) or LD 12:12 (Arabidopsis) at 20°C, light intensity during day ~200 μmol m^{-2} s^{-1}. Leaves were collected and transferred to 20 ml 10 mM MES pH 6.2 (adjusted with KOH) and blended in pulses (3 × 30 s) with 10 s intervals between pulses. The suspension was filtered through a mesh (pore size: 100 μm) and epidermal fragments were collected in 10 ml 10 mM MES. Samples were incubated in the dark for 1 h at 20°C before the epidermal fragments were filtered and collected in 20 ml buffer (5 mM KCl, 0.1 mM $CaCl_2$ in 10 mM MES pH 6.2). The samples were divided into two equal parts; 10 μl 10 mM ABA dissolved in 70% ethanol was added to one part and 10 μl 70% ethanol to the other as a control (both aliquots were diluted in 10 ml 10 mM MES). Both treatment and control samples were incubated for 3 h in a water bath at 20°C under cold fluorescence light and CO_2-free aeration (Conn et al., 2011). Measurements were made on stomata from plants treated either at ZT 8–9 or at a time adjusted to circadian time (CT) 9 for each genotype to accommodate the longer circadian period (~28–29 h) of *ztl-3* (Somers et al., 2004) and shorter (~22–23 h) period of *prr5-11* (Yamamoto et al., 2003); the circadian phenotype of *prr5-11* is comparable to *prr5-1* (Eriksson et al., 2003; Michael et al., 2003). In each case, the experimenter was blinded to genotype and treatment until the analysis was completed. Plant tissues were incubated in the presence/absence of ABA for 3 h in light, under CO_2-free aeration (Conn et al., 2011), and stomatal closure was scored at ZT 8–9, i.e. 8–9 h after dawn.

Stomatal density was measured in leaves from 3- to 4-week-old soil-grown Arabidopsis plants cultivated under long photoperiods (LD 16:8) and concomitant temperature cycles (WC 20°C:18°C). Plants were grown and treated in the same manner as the plants subjected to stomatal conductance measurements, described above. Measurements were made from one leaf per plant and from eight to 10 plants per genotype. Stomatal density in *Populus* wild type and RNAi lines was measured in fully expanded young leaves from internodes eight to 10 from soil-grown plants cultivated under long photoperiods (LD 18:6) at 18°C. For density measurements in both species, the abaxial surface of leaves from three plants per genotype was peeled off and visualised using an Axiocam digital camera attached to an Axioplan light microscope (Carl Zeiss Microscopy GmbH, Oberkochen, Germany). The number of stomata per mm^2 of leaf area was counted using the software provided.

Protein Expression Constructs

Expression vectors to express epitope-tagged proteins in protoplasts were obtained by cloning full length coding sequences into pRT104 plasmids carrying 3 × HA or 3 × Myc epitopes under the constitutive CaMV35S promoter (Fülöp et al., 2005). Epitope-tagged ZTL and TOC1 were obtained as described previously (Johansson et al., 2011).

To obtain epitope-tagged OST1 and PRR5, the full length cDNAs clones were obtained from ABRC,[3] inserted into either pENTR D-TOPO (*OST1*) or pUNI51 (*PRR5*), and used as templates for PCR. The OST1 PCR amplified coding sequence was cloned into pRT104 at the EcoRI/SalI sites and PRR5 at the BamHI/KpnI sites.

All constructs were confirmed by sequencing before use. The primer sequences are listed in **Supplementary Material**.

Transient Protoplast Expression Assays

An Arabidopsis Col-0 cell suspension culture was grown under LD 16:8 with concomitant WC 22°C:18°C cycles; light intensity during day: 150 μmol $m^{-2}s^{-1}$. Protoplasts were co-transfected with HA or Myc-tagged proteins in the combinations ZTL + OST1, ZTL + TOC1 and OST1 + PRR5 prior to co-immunoprecipitation

[3]www.Arabidopsis.org/abrc/

assays (Meskiene et al., 2003). Protoplasts were harvested for protein extraction 18 h post-transfection and suspended in immunoprecipitation buffer [25 mM Tris–HCl, pH 7.8, 10 mM $MgCl_2$, 75 mm NaCl, 5 mM EGTA, 60 mM β-glycerophosphate, 1 mM dithiothreitol, 10% glycerol, 0.2% Igepal CA-630 and 1× Protein Inhibitor Cocktail (SIGMA-Aldrich)]. The samples were frozen in liquid nitrogen until use.

For immuno-analysis, samples were thawed on ice and centrifuged. Supernatants were mixed with 1.5 µl 5 M NaCl, 1.5 µl anti-Myc antibody (9E10; Covance, Princeton, NJ, United States), 1 µl 20 mg/ml BSA and immunoprecipitation buffer to a final volume of 100 µl. The mixtures were incubated for 2 h at 4°C on a rotating wheel. Immune complexes were captured by adding 10 µl Protein G-Sepharose beads (Wu et al., 2009) to the mixtures and incubating for a further 2 h at 4°C with rotation. The beads were washed three times with ice-cold immunoprecipitation wash buffer (25 mM sodium phosphate, 150 mM NaCl, 5% glycerol and 0.2% Igepal CA-630). Immune complexes were eluted from beads using 25 µl 1× SDS buffer. Proteins were separated by electrophoresis on 8% SDS polyacrylamide gels and blotted into Immobilon-P PVDF membranes (Millipore Corporation, Billerica, MA, United States). The presence of HA-tagged proteins in the immune complexes was determined by probing blots with anti-HA-POD antibody (3F10; Roche Diagnostics, Basel, Switzerland). Subsequently, blots were stripped for 15 min at 70°C in buffer (100 mM β-mercaptoethanol, 2% SDS and 62.5 mM TRIS pH 6.8) and incubated with anti-c-Myc chicken antibody (A21281; Thermo Fisher Scientific) to confirm the presence of Myc-tagged proteins in the complex. Co-IP results, where quantified, were measured using ImageJ software (Schneider et al., 2012). Measurements of immunoprecipitated HA-tagged protein bands were made on acquired images in ImageJ after background subtraction. The values indicated are the ratio of the HA-tagged pull-down protein density to input samples, with loaded input ~40% of the total reaction. The results are average of three independent experiments.

Mesophyll protoplasts were isolated according to the tape-Arabidopsis sandwich procedure (Wu et al., 2009). Plants were grown as described for the water loss assay and 8–10 leaves were collected from 3- to 4-week-old plants. Protoplasts were transfected using a modified TEAMP to investigate whether binding method (Yoo et al., 2007). For protein stability assays, transfected protoplasts were incubated for 3 h with 100 µM cycloheximide (CHX), an inhibitor of protein synthesis, before sample collection at the indicated time points. Monoclonal anti-PSTAIR CDKA antibody was hybridised at 1:5000 dilution (SIGMA-Aldrich). The protein stability assays in mesophyll protoplasts were performed using 50 µM MG132 (SIGMA-Aldrich), a proteasome inhibitor. Protoplasts were incubated with MG132 or DMSO (control) for 4 h. An antibody detecting the RUBISCO small subunit antibody (AS07 259, Agrisera AB, Vännäs, Sweden) was used as a loading control.

Quantitative Reverse Transcription PCR

To characterise *PttZTL* RNAi lines, plants were grown in a greenhouse under controlled conditions (LD 18:6 at 18°C; light intensity during day: 250 µmol m^{-2} s^{-1}). Leaf samples were collected 8 h after dawn (ZT 8) and frozen in liquid nitrogen. RNA was extracted from one fully developed leaf per sample, using the CTAB method (Le Provost et al., 2007), and treated with DNase (TURBO DNA-free kit; Ambion, Austin, United States). cDNA was synthesised from 1 µg RNA using the iScript cDNA Synthesis Kit (Bio-Rad Laboratories). Quantitative reverse transcription PCR (RT-qPCR) was performed using a CFX96 Real-Time detection system (Bio-Rad Laboratories) and gene-specific primers (**Supplementary Material**).

The increase in SYBR Green fluorescence (Bio-Rad Laboratories) was used to visualise the accumulation of PCR products in real time. All RT-qPCR reactions were performed using three or four biological repetitions with duplicate technical samples. *PttZTL* expression levels were normalised against expression of the reference genes *ELONGATION FACTOR 1 ALPHA* (*EF1a*) or 18S rRNA using the $2^{-\Delta\Delta CT}$ method incorporating the primer efficiencies obtained by experiment, which ranged from 98 to 100% (Livak and Schmittgen, 2001; Pfaffl, 2001). Expression data are presented relative to expression in wild-type *Populus*. Data were log2 transformed to obtain a normal distribution and analysed using Student's *t*-test. Primer sequences are listed (**Supplementary Material**); primers for *PttZTL* amplified both *ZTL* homologues. For gene expression analyses in Arabidopsis, seeds were surface-sterilised, plated *in vitro* and grown as described above for 3–4 weeks. Seedlings were sprayed with 10 µM ABA (10 µl ABA stock dissolved in 70% ethanol) and diluted in 10 ml water or control (equal amount of 70% etanol dissolved in water) 3 h prior to harvesting at ZT 8. Gene expression levels were determined using RT-qPCR, as described above, with gene-specific primers (**Supplementary Material**). Expression of each gene was normalised against expression of *EF1a* using the $2^{-\Delta\Delta CT}$ method (Livak and Schmittgen, 2001; Pfaffl, 2001). The efficiency of each primer pair was included in the analysis (efficiency ranged from 95.3 to 100%). Gene expression levels are shown relative to expression in wild-type plants without ABA treatment, which was set as 1. Log2-transformed values were analysed by two-way ANOVA followed by Sidak's multiple comparison test.

Statistical Analyses

The statistical significance of results was tested using one- or two-way ANOVA followed by *post-hoc* comparisons (Tukey's test or Sidak's test, each corrected for multiple comparisons) or unpaired Student's *t*-tests, as indicated, using GraphPad Prism version 6.0 for Windows (GraphPad Software, La Jolla, CA, United States). In each case, significance was taken at alpha <0.05.

RESULTS

ABA-Induced Stomatal Closure Is Impaired in *ztl* Mutants

In Arabidopsis, sensitivity to ABA, which induces stomatal closure, increases in the late afternoon (Correia and Pereira, 1995). This timing correlates with high levels of ZTL (Kim et al., 2007). We therefore investigated the sensitivity of *ztl*

mutants to ABA. As defects in the different protein domains affect different aspects of ZTL function (Kevei et al., 2006; Kim et al., 2007), we measured sensitivity to ABA in *ztl-3* (complete loss-of-function mutant), *ztl-1* (Kelch domain mutant) and *ztl-21* (LOV domain mutant). Although ABA evoked stomatal closure in *ztl* mutants, the response was significantly greater in wild-type (WT) plants (**Figures 1A–C**).

Mutations in *ZTL* and *OST1* Have Similar Effects

We measured stomatal conductance in *ztl-3* and *ost1-3* leaves using a handheld SC-1 leaf porometer (Decagon). Stomatal conductance levels were higher in *ztl-3* and *ost1-3* than in WT controls (**Figure 1D**). *ost1-3* mutants have the same stomatal density as WT plants (Engineer et al., 2014; Jalakas et al., 2018). Stomatal density was similar in WT (208 stomata/mm^2) and *ztl-3* plants (210 stomata/mm^2; Student's *t*-test $p = 0.727$, $n = 3$ biological replicates, each containing 71–93 measurements/genotype). Thus, the increased water loss of *ztl-3* and *ost1-3* mutants was not caused by an increase in the number of stomata. The higher stomatal conductance in *ztl-3* (**Figure 1D**) observed is consistent with their reduced response to ABA (**Figures 1A–C**). Overall, the ABA sensitivity and stomatal conductance phenotypes of *ztl-3* resembled the strong *ost1-3* phenotype.

A detached-leaf assay revealed that *ztl-3* and *ost1-3* leaves have significantly higher rates of water loss than WT leaves at ZT 8–9 (**Figure 1E**).

To further determine the role of ZTL in the drought response, we measured the water loss phenotype of *ztl-3* plants overexpressing *ZTL* under the control of the 35*S* CaMV promoter (*p35S::HA::ZTL*). There were no differences in the rates of water loss between WT plants and three independent T_3 lines overexpressing ZTL in the *ztl*-3 background (**Figure 1F**); thus, *ZTL* could rescue the leaf water loss phenotype of *ztl-3*. This indicated that ZTL and OST1 are both needed for stomatal closure under stress.

We also analysed seed germination time (determined by radicle emergence), a developmental phase transition, to establish whether ZTL and OST1 showed shared effects across biological responses (Penfield and Hall, 2009). Both *ztl-3* and *ost1-3* mutants showed a similar significant delay in radicle emergence compared to WT seeds (**Supplementary Figure S1**).

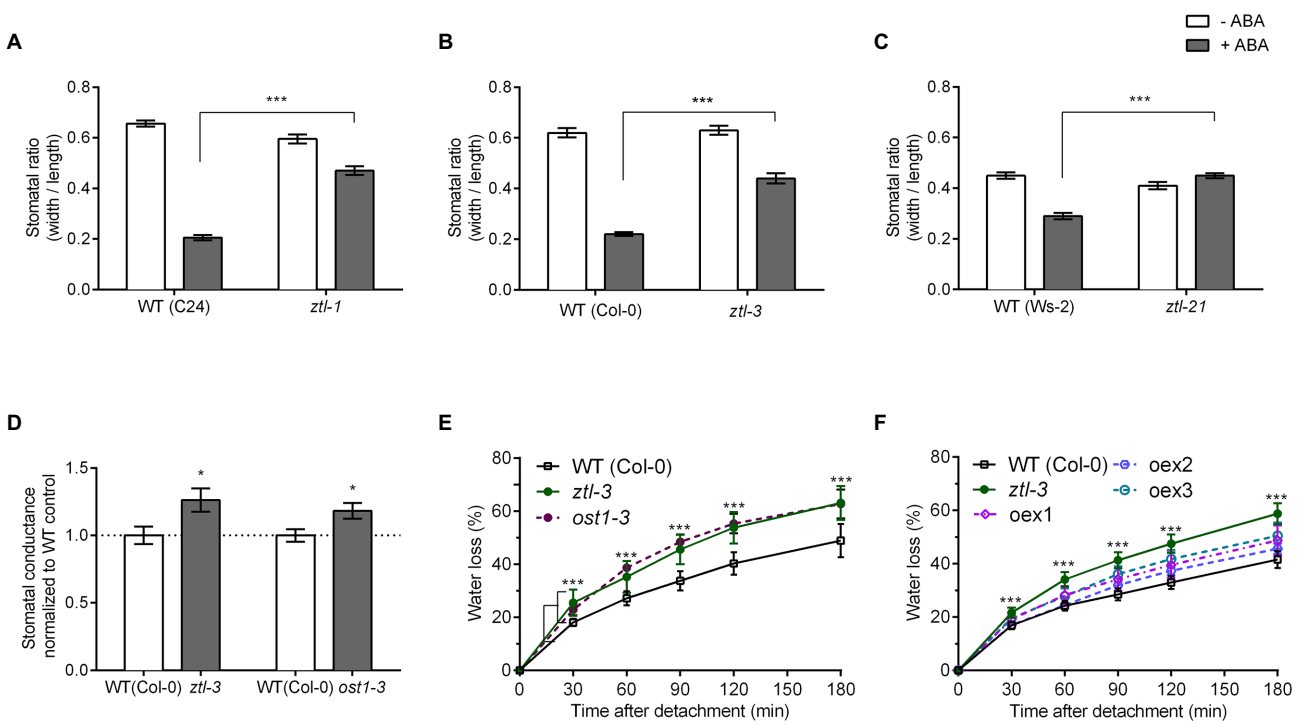

FIGURE 1 | Stomatal opening and water loss phenotypes of detached Arabidopsis leaves. **(A–C)** Stomatal aperture in epidermal strips from leaves of 4-week-old seedlings treated with or without 10 μM ABA measured at ZT 8–9 under CO_2-free aeration. **(A)** *ztl-1* and WT (C24) plants; **(B)** *ztl-3* and WT (Col-0); and **(C)** *ztl-21* and WT (Ws-2). **(D)** Stomatal conductance (gs) in leaves of 4-week-old Arabidopsis plants. Conductance was normalised against the WT means. **(E,F)** Rates of water loss in detached rosette leaves from 3-week-old Arabidopsis plants. Values are means ± SE of three biological replicates, each containing one leaf from six to eight plants of each genotype. **(E)** Rates of water loss in WT (Col-0); *ztl-3* and *ost1-3*. Asterisks in **(E)** refer to both the comparison between WT and *ztl-3* and between WT and *ost1-3* (Student's *t*-test); both mutants showed the same level of statistical difference from WT. **(F)** Rates of water loss in WT (Col-0); *ztl-3* and *ztl-3:p35S::HA::ZTL* (oex1-3: independent lines of *ztl-3* overexpressing ZTL). Asterisks in **(F)** represent the comparison between WT and *ztl-3* plants (Student's *t*-test); water loss from all other mutants did not differ statistically from that of WT plants. WT and *ztl-3* plants (Student's *t*-test); water loss from all other mutants did not differ statistically from that of WT plants. **(A–F)** $^*p < 0.05$ and $^{***}p < 0.001$ (Student's *t*-test).

Circadian Clock Function Depends on ZTL in *Populus* Trees

Circadian components and ABA-signalling pathways are largely conserved between Arabidopsis and *Populus* (Ibáñez et al., 2010; Kozarewa et al., 2010; Cai et al., 2017; Yu et al., 2017; Tylewicz et al., 2018; Rigoulot et al., 2019). We hypothesised that ZTL's roles in regulating the circadian clock and physiological responses to drought and ABA would also be conserved. The role of ZTL was examined in transgenic *Populus* trees in which expression of both *PttZTL1* and *PttZTL2* was downregulated by RNAi (*PttZTL1,2* RNAi lines). RNAi line 5, which had a strong reduction in *PttZTL* (**Figures 2A**,**B**; **Supplementary Figure S2**), leading to earlier growth cessation (**Supplementary Figure S3**), and RNAi line 7, which also showed a strong, significant reduction of *PttZTL* transcript (**Figures 2A**,**B**; **Supplementary Figure S2**), were selected for further analysis. Microarray expression profiles from short period (*lhy-10* RNAi) and WT *Populus* trees (Edwards et al., 2018) were examined for comparison (**Supplementary Figure S4**), together with an RT-qPCR analysis of time-series data from WT trees (**Supplementary Figure S5**). These data show *PttZTL1,2* expression appears disrupted in *lhy-10* trees in LD cycles (**Supplementary Figure S4**); thus, disruption of *PttLHY 1* and *PttLHY2*, expressed in the morning clock loop, apparently affects expression of *PttZTL1* and *2*, an evening gene, in *Populus* as in Arabidopsis. *PttZTL* expression is rhythmic in WT *Populus* leaves (**Supplementary Figure S5**).

Clock function was analysed in *PttZTL1,2* RNAi lines 5 and 7. Their circadian periods were measured in detached leaves using delayed fluorescence from photosystem II (Gould et al., 2009; Johansson et al., 2015). The normalised fluorescence traces (Best Y) showed both RNAi lines had significantly longer circadian periods than WT trees (**Figure 2A**; **Table 1**). The associated relative amplitude error (RAE) values indicate the level of rhythmicity associated with an individual leaf (**Figure 2B**); values ≥0.6 (dotted line) indicate arrhythmia. These results are in line with the downregulation of *PttZTL1,2* in RNAi lines 5 and 7 (**Supplementary Figures S2A,B**). Downregulation of *PttZTL1,2* expression resulted in a slower running but still strongly rhythmic circadian clock, as shown by the longer periods and low RAE values, indicating that the phenotypes of *PttZTL1,2* RNAi trees resembled those of Arabidopsis *ztl* mutants (Kevei et al., 2006).

Thus, these lines provided suitable material for further studies comparing ZTL-dependent function in ABA-related stress responses across plant species.

ZTL's Role in Stomatal Movements Is Conserved

To investigate whether ABA-induced stomatal closure was conserved between Arabidopsis and *Populus*, we confirmed downregulation of ZTL at ZT 8–9 in *Populus* (i.e. at dusk, when ZTL levels peak and sensitivity to ABA are high in WT Arabidopsis) using an additional reference gene (*Ef1a*; **Figure 3A**). This confirmed that *PttZTL1* and *PttZTL2* were reduced to at least ~40% of WT levels in both lines at ZT 8–9. Further, we measured stomatal aperture in leaves from *Populus* trees grown *in vitro* (**Figure 3B**). Stomatal closure in response to ABA was reduced in RNAi lines 5 and 7, relative to WT plants. In addition, stomatal conductance in leaves from both *PttZTL1,2* RNAi lines was significantly higher than that of WT leaves (**Figure 3C**). These results resembled those from Arabidopsis *ztl* mutants (**Figures 1A–D**).

Next, we investigated water loss using detached-leaf assays. Both *PttZTL1,2* RNAi lines 5 and 7 showed significantly higher rates of water loss than WT plants (**Figure 3D**), similar to the Arabidopsis *ztl-3* mutant (**Figures 1E**,**F**). Stomatal density measurements revealed leaves from *PttZTL1,2* RNAi line 5

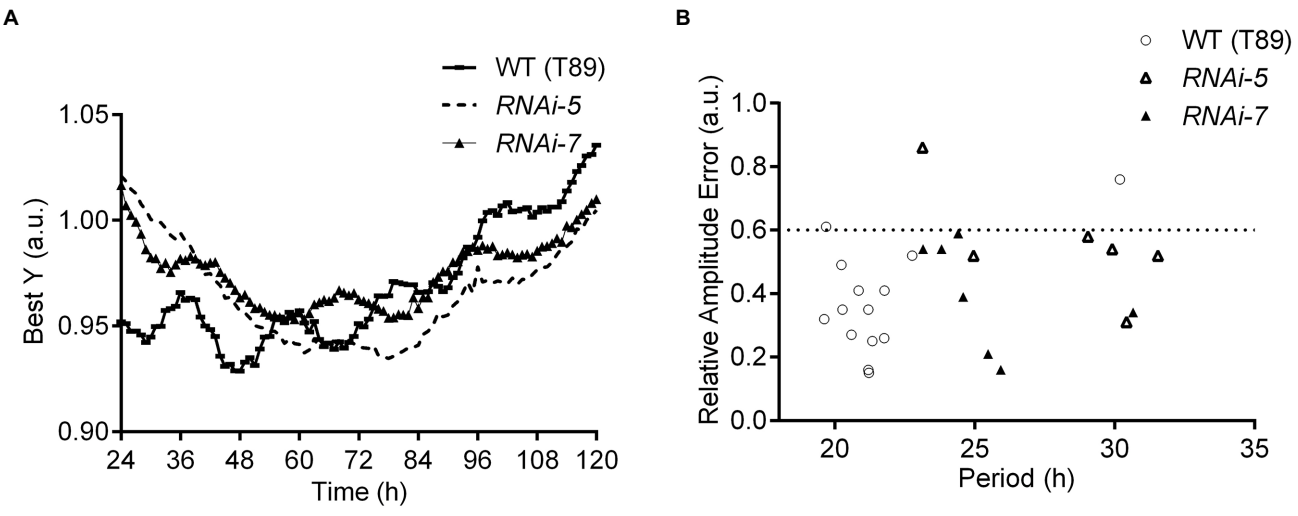

FIGURE 2 | Delayed fluorescence (DF) in *Populus* leaves from WT (T89) trees and *PttZTL 1,2* RNAi lines assayed under continuous light. **(A)** Best fitted Y traces of DF rhythms in leaves in constant conditions following entrainment in LD 18:6 cycles. **(B)** Values of circadian period and relative amplitude errors (RAE) of individual leaves included in the experiment shown in **(A)**. RAE of rhythmic plants ≤0.6; period estimates are shown in **Table 1**.

TABLE 1 | Free-running periods of delayed fluorescence in leaves of wild-type (WT; T89) *Populus* trees and *PttZTL1,2* RNAi lines 5 and 7 measured under continuous light.

Genotype	Period (h)	Error ± 1SE	Number of leaves ($^{\$}$Rhythmic/total)	Sidak's *post-hoc* test ($\alpha < 0.05$)
WT	21.1	±0.2	12/18	N/A
RNAi-5	29.2	±1.1	5/9	****
RNAi-7	25.4	±0.9	7/9	***

Populus trees were grown under LD 18:6 cycles; light intensity (equal parts blue and red light): 20 µmol m^{-2} s^{-1}. Plants were transferred to continuous light (LL) at ZT 0 (dawn). Free-running rhythms (24–120 h after transfer to LL) were analysed using BRASS. $^{\$}$Only rhythmic traces (relative amplitude error (RAE) ≤0.6) were included. Significance levels of the effects identified by one-way ANOVA ($p < 0.0001$) were determined using Sidak's multiple comparisons post-hoc test; ***$p < 0.001$; ****$p < 0.0001$. N/A, not applicable.

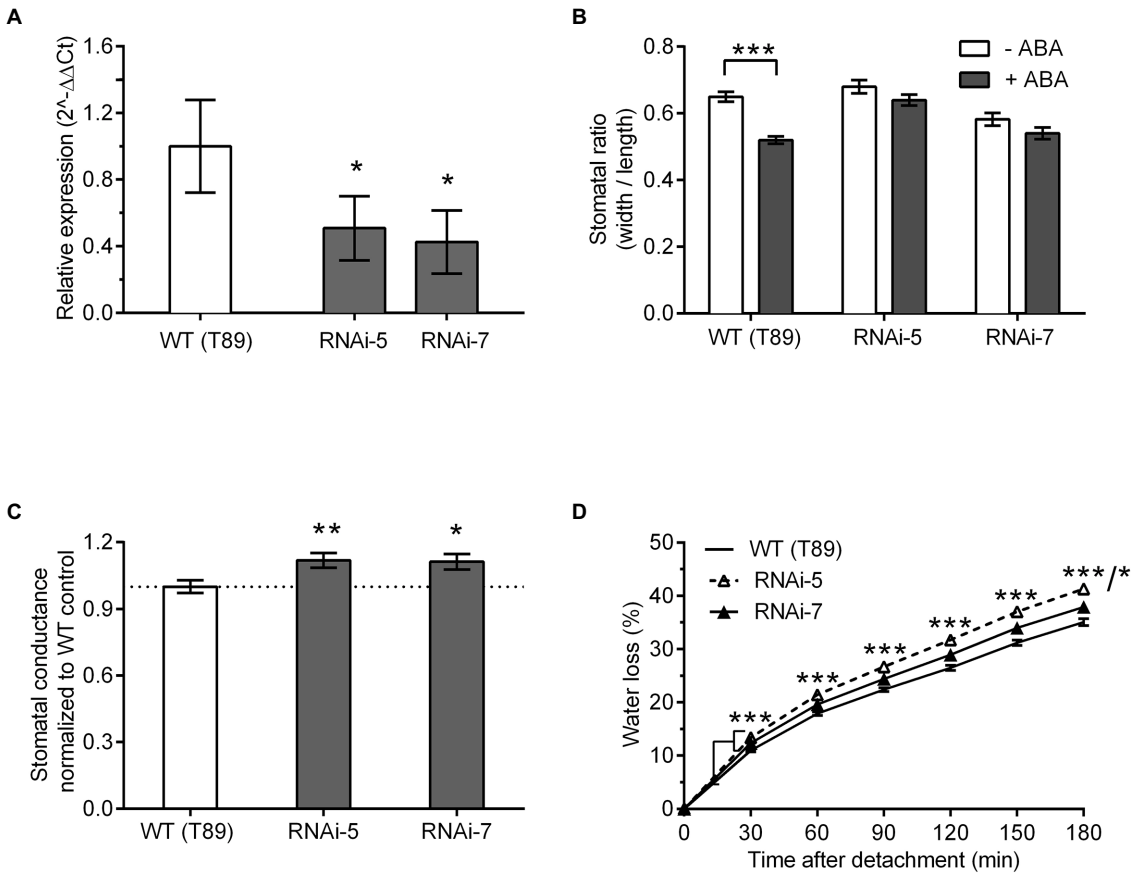

FIGURE 3 | Effect of ZTL expression on stomatal phenotype in *Populus*. **(A)** Relative expression levels of *PttZTL* at ZT 8 in two *PttZTL 1,3* RNAi lines of *Populus*. Expression levels of *PttZTL* were normalised against expression of *EF1a* and the ratio was set at 1 in WT (T89) trees. Values are means ± SE of three or four biological replicates. **(B)** Effect of ABA treatment on stomatal ratios (width:length) in epidermal strips from wild-type and *PttZTL 1,2* RNAi lines measured at ZT 8–9 under CO_2-free aeration. Data are means ± SE of three biological replicates, each containing 20 to 22 stomata. **(C)** Stomatal conductance (gs) in leaves from intact 6 to 9-week-old WT and *PttZTL 1,2* RNAi trees. Values are means ± SE of three biological replicates, each containing six to eight plants with three leaves/genotype. Conductance was normalised against the WT means. **(D)** Rates of water loss from detached leaves from 13-week-old *PttZTL* RNAi and wild-type trees. Values are means ± SE of three leaves per biological replicates, from six plants per genotype. In **(D)**, both RNAi lines differed from WT all time points: *** thus represents both the RNAi-5 vs. WT and RNAi-7 vs. WT comparisons at time points where RNAi lines differed from WT at the same level of significance. At 180 min, WT vs. RNAi line 5 differed from WT at $p < 0.001$ and RNAi line 7 differed from WT at $p < 0.05$; this is represented by ***/* on the Figure. **(A–D)** Differences between WT compared with both mutants are indicated where statistically significant at *$p < 0.05$; **$p < 0.01$; and ***$p < 0.001$ (Student's *t*-test).

(135 stomata/mm^2) differed significantly from WT leaves (141 stomata/mm^2; Student's *t*-test; $p = 0.04$; $n = 3$ biological replicates, each containing 120 to 144 measurements); however, there was no significant difference in stomatal density between WT leaves and leaves from *PttZTL1,2* RNAi line 7 (141 stomata/mm^2; Student's *t*-test $p = 0.89$; $n = 3$ biological replicates, each containing 120 to 144 measurements). These results indicated the increased water loss resulted from greater stomatal openness,

not changed stomatal density. The lower sensitivity to ABA, increased stomatal aperture and conductance, and higher water loss observed in both *PttZTL1,2* RNAi lines (**Figure 3**) indicated they phenocopied Arabidopsis *ztl* mutants (**Figure 1**), supporting a conserved role for ZTL between the two species.

Expression of ABA-Signalling Genes Is Impaired in Arabidopsis *ztl* Mutants

Given stomatal closure in response to ABA was impaired in *ztl* mutants (**Figures 1A–C**) and the similar changes in stomatal regulation in Arabidopsis and *Populus* trees with reduced ZTL function (**Figures 2, 3**), we evaluated whether ZTL modulated expression of early and late ABA-signalling components and ABA-responsive genes in Arabidopsis. We analysed expression of key ABA response and signalling genes in *ztl-3* and WT plants treated with ABA for 3 h (**Figure 4**). *PYL5* was selected as a representative of an ABA reception gene, *ABI2, HAB1, OST1*, *ABI5*, *ABF3* and *ABF4* as examples of early and progressing ABA-signalling genes, and *RAB18* and *RD29A* as late ABA-responsive genes (Santiago et al., 2009; Raghavendra et al., 2010; Gonzalez-Guzman et al., 2012).

Analysis by two-way ANOVA indicated there were no treatment (T), genotype (G) and treatment × genotype (T × G) effects on *PYL5* expression (**Figure 4A**). Analysis of expression of ABI2 and HAB1 (**Figures 4B,C**), two negative regulators of ABA signalling (Saez et al., 2004, 2006), revealed that genotype had a significant effect on *ABI2*, with a significant reduction in transcript level in *ztl-3* (**Figure 4B**), but not on *HAB1*, which only showed a treatment effect (**Figure 4C**). Both treatment and genotype had significant effects on *OST1*, expression of which was significantly reduced in *ztl-3* relative to wild-type plants (**Figure 4D**). Expression of the later ABA-signalling gene *ABI5* was severely diminished in response to ABA in *ztl-3* plants, with significant effects of both treatment and genotype, as well as a treatment × genotype interaction (**Figure 4E**). Only treatment affected *ABF3* expression (**Figure 4F**), but both treatment and genotype affected expression of *ABF4* (**Figure 4G**). Expression of another ABA-responsive gene, *RAD29A*, showed significant treatment and genotype effects (**Figure 4H**). Both treatment and genotype had significant effects on expression of *RAB18* (**Figure 4I**), and these factors interacted to produce a further significant effect. All these data show that ZTL was required for ABA sensitivity and significantly promoted the expression of major ABA-signalling components (**Table 2**).

ZTL Interacts With OST1 in Plant Cells

Given the function of ZTL in stomata closure and in ABA-induced gene expression, we tested if it has the capacity to interact with OST1 when expressed in plant cells. Co-immunoprecipitation (Co-IP) assays following expression of tagged ZTL and OST1 proteins in protoplasts revealed an interaction between ZTL and OST1 (**Figure 5A**). The ratios of signal from Co-IP bands to input, measured from three experiments, showed a strong signal from HA-OST1, when it was coexpressed with Myc-OST1 (**Figure 5B**). Co-IP of the known interactors, ZTL and TOC1, showed a similar result (**Supplementary Figures S6A,B**; Johansson et al., 2011).

The effect of ZTL on OST1 stability was investigated using mesophyll protoplasts obtained from the triple mutant *ztl-4, fkf1-2 and lkp2-1* (**Supplementary Figure S7**). This mutant lacks all three members of the ZTL F-box protein family [ZTL, FLAVIN-BINDING, KELCH REPEAT, F BOX 1 (FKF1) and LOV KELCH PROTEIN 2 (LKP2)] (Baudry et al., 2010). ZTL-like activities were diminished in this background, as expected. No ZTL-dependent degradation of OST1 was detected in protoplasts transfected with OST1 and ZTL, regardless of whether the proteasome inhibitor MG132 was present (**Supplementary Figures S7A,B, S8**). The effect of proteasome inhibition was also tested using TOC1, and in contrast, coexpression of TOC1 and ZTL led to lower TOC1 expression at time 0 (**Supplementary Figures S7C,D**). Although the effect on TOC1 in blue light was not entirely consistent with the current model, wherein ZTL acts to degrade TOC1 in the dark (Más et al., 2003), the lack of activity of the ZTL family members FKF1 and LKP2 in the triple mutant protoplasts affected TOC1 expression (**Supplementary Figures S7C,D**), consistent with the results of Baudry et al. (2010). OST1 stability, on the other hand, showed no effect of ZTL coexpression or proteasome inhibition (**Figures 6A,B**), which supports our conclusion that ZTL does not regulate OST1 protein levels. OST1 stability was not negatively affected in protoplast suspension cultures, regardless of the presence of ZTL, light or CHX (**Supplementary Figure S8**).

Both ZTL and PRR5 Interact With OST1 to Modulate Stomatal Regulation

The genetic data suggested that ZTL and OST1 both severely and similarly affected stomatal closure in response to ABA (**Figure 1E**). In order to determine if additional factors were involved, we investigated the role of PRR5, a ZTL substrate that affects ABA metabolism and induced responses (Yang et al., 2021). We adjusted ABA treatment time to match the circadian period of each genotype (*ztl-3*: 28 h; *prr5-11*: 23 h and WT: 24 h) and scored the stomatal ratio at Circadian Time (CT) 8–9 for each genotype to confirm that the phenotypic change resulted from ABA treatment rather than circadian mistiming. Under these conditions, the stomata of *ztl-3* mutants failed to close following ABA treatment, while stomata of *prr5-11* closed more readily (**Figure 7A**). The responses of both mutants to ABA differed significantly from WT plants, albeit in opposite directions, consistent with the changes in endogenous period.

Given that ZTL mediates proteasomal degradation and several *ztl* mutants show alterations in PRR5 protein stability and other alterations that may affect PRR5 function (Kiba et al., 2007; Fujiwara et al., 2008), we hypothesised that altered ZTL-dependent regulation, for instance stabilisation of PRR5 in the *ztl-3* mutant, might increase stomatal opening. Consistent with this, PRR5 appeared to be required for normal stomatal responses. Although *prr5-1* mutants remained sensitive to ABA and showed stomatal closure in response to ABA treatment,

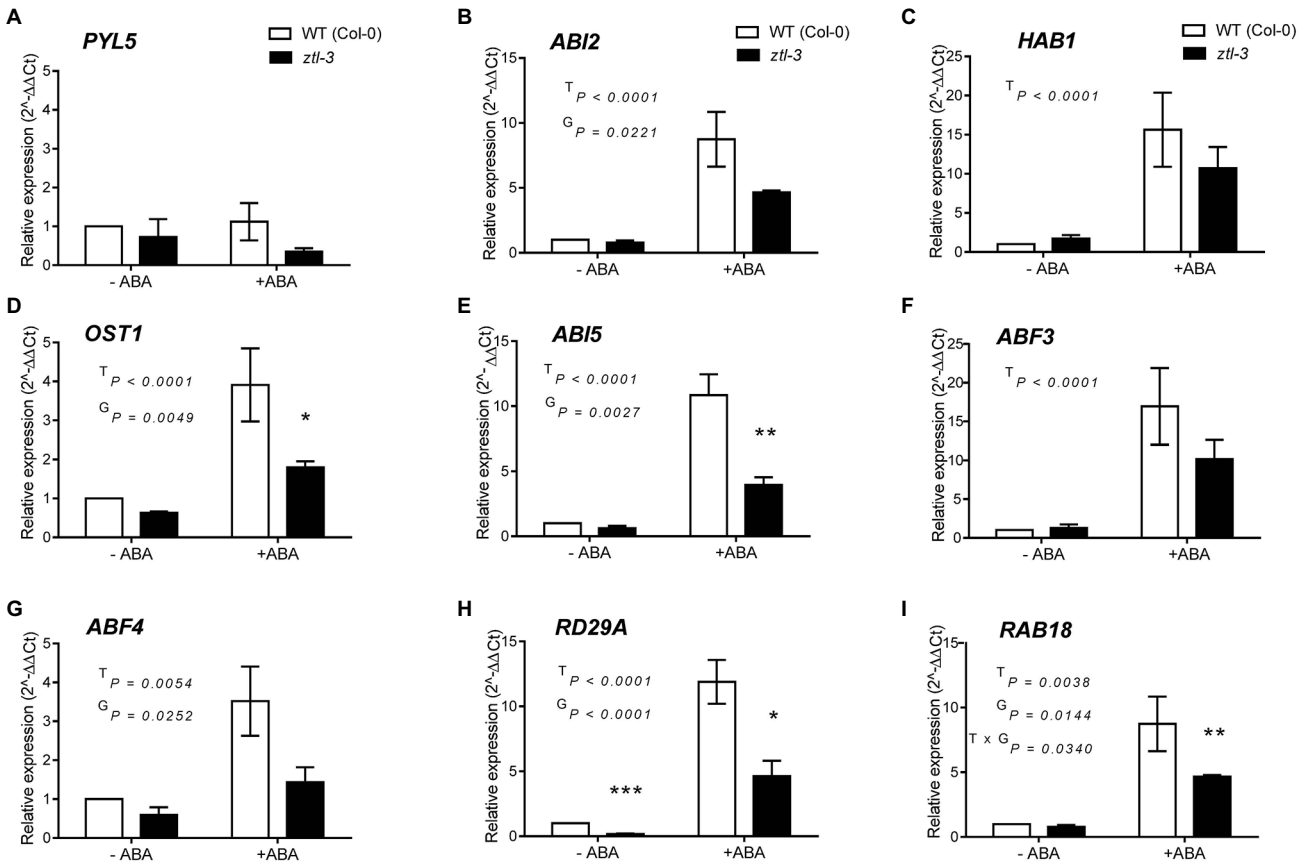

FIGURE 4 | Effects of genotype and ABA on expression of early and late ABA-signalling components and ABA-responsive genes in Arabidopsis. **(A)** ABA reception gene *PYL5*. **(B–G)** Early and progressing ABA-signalling genes. **(B)** *ABI2*. **(C)** *HAB1*. **(D)** *OST1*. **(E)** *ABI5*. **(F)** *ABF3*. **(G)** *ABF4*. **(H,I)** Late responsive ABA-signalling genes. **(H)** *RD29A*. **(I)** *RAB18*. Gene expression was measured in samples collected at ZT 8 from WT (Col-0) and *ztl-3* plants treated with ABA or ethanol (control). Values are the means ± SE of pooled seedlings from three biological replicates, each containing two technical replicates. Expression levels were normalised against expression of *EF1a* and the ratio was set at 1 in untreated WT (Col-0). Results were analysed by two-way ANOVA to determine the effects of treatment (T), genotype **(G)** and the T × G interaction. Significance levels of the effects were determined using Sidak's multiple comparisons *post-hoc* test; $^{*}p < 0.05$; $^{**}p < 0.01$; and $^{***}p < 0.001$.

in the absence of exogenous ABA, their stomata were more open than those of WT plants (**Figure 7A**). This may result from an increase in ZTL levels in *prr5-1* in the absence of ABA. We found a clear interaction between PRR5 and OST1 in plant cells (**Figure 7B**).

To understand how OST1, ZTL and PRR5 interacted to regulate stomata (i.e. responsiveness to ABA), we performed water loss assays using detached leaves from a series of single, double and triple mutants carrying different combinations of the *ztl-3*, *ost1-3* and *prr5-1* alleles to determine their physiological responses to drought (**Figure 6A**). The *ztl-3* and *ost1-3* single mutants had a similar phenotype that differed from that of WT plants, consistent with previous data implicating both ZTL and OST1 in stomatal regulation; moreover, each single mutant differed significantly from the double mutant, *ztl-3 and ost1-3*. The increased severity of the loss-of-function phenotype in the *ztl-3 and ost1-3* double mutant indicated both ZTL and OST1 were required for stomatal control and potentially acted additively to each other.

Leaves from *prr5-1* single mutants showed rates of water loss similar to WT with slight deviations (**Figures 6A**,**B**). The double mutant *ztl-3 and prr5-1* behaved as WT (**Figure 6B**). The double mutant *prr5-1 and ost1-3* behaved like *ost1-3* (**Figure 6A**). The *ztl-3 and ost1-3* double mutant had the strongest water loss phenotype, indicating that retaining PRR5 in the absence of OST1 and ZTL partially blocked regulation of stomatal aperture by ABA. The *ztl-3, prr5-1 and ost1-3* triple mutant showed a significantly lower rate of water loss than the *ztl-3 and ost1-3* double mutant between 90 and 150 min, and again at 180 min, which is consistent with the suggestion that PRR5 is involved in ABA signalling in the absence of ZTL and OST1.

These results taken together suggest that inhibition of the ABA-signalling pathway by PRR5 is opposed by ZTL and OST1. The *ztl-3, prr5-1 and ost1-3* triple mutant had a significantly stronger water loss phenotype than the *ost1-3* single mutant, indicating that ZTL can oppose the inhibitory effect of PRR5 in the absence of OST1. By contrast, the *prr5-1 and ost1-3* double mutant and the *ost1-3* and *ztl-3* single mutants all showed

TABLE 2 | Summary of *post-hoc* analysis using Sidak's multiple comparisons test of RT-qPCR analysis of gene expression in Arabidopsis wild-type (Col-0) and *ztl-3* plants ± ABA (**Figure 4**).

Gene	Treatment	Mean diff. (WT – *ztl-3*)	95% CI of diff.	Significance level α <0.05
PYL5	–ABA	1.040	–1.605 to 3.685	ns
	+ABA	1.294	–1.351 to 3.938	ns
ABI2	–ABA	0.3944	–0.4455 to 1.234	ns
	+ABA	0.832	–0.007819 to 1.672	ns
HAB1	–ABA	–0.6830	–2.069 to 0.7031	ns
	+ABA	0.4794	–0.9068 to 1.866	ns
OST1	–ABA	0.6713	–0.1823 to 1.525	ns
	+ABA	1.024	0.1703 to 1.878	Yes, *
ABI5	–ABA	0.8129	–0.2108 to 1.837	ns
	+ABA	1.449	0.4254 to 2.473	Yes, **
ABF3	–ABA	–0.1650	–1.707 to 1.377	ns
	+ABA	0.6919	–0.8497 to 2.233	ns
ABF4	–ABA	0.9553	–0.6202 to 2.531	ns
	+ABA	1.276	–0.2995 to 2.852	ns
RD29A	–ABA	2.567	1.498 to 3.636	Yes, ***
	+ABA	1.440	0.3710 to 2.509	Yes, *
RAB18	–ABA	0.1204	–0.7153 to 0.9561	ns
	+ABA	1.221	0.3849 to 2.056	Yes, **

*Statistical significances indicated *p<0.05; **p<0.01; and ***p<0.001 (post-hoc analysis).*

very similar phenotypes that were less extreme than the *ztl-3, prr5-1 and ost1-3* triple mutant (**Figure 6A**), indicating the importance of the interactions between ZTL, OST1 and PRR5.

DISCUSSION

Water Loss Is Regulated by Both Clock and ABA-Signalling Pathways

In Arabidopsis, light and the circadian clock act *via* ZTL to regulate the daily pattern of stomatal opening (Somers et al., 1998; Salomé et al., 2002; Dodd et al., 2004). Many metabolic processes and enzymes associated with photosynthesis are under circadian control (Dodd et al., 2014). We show that ZTL was also required for circadian clock function (**Figure 2; Table 1**) in *Populus*, and ZTL regulated stomatal closure in both Arabidopsis and *Populus* (**Figures 1, 3**). In Arabidopsis, both OST1- and ABA-dependent gene expression and integration of ABA-signalling require ZTL (**Figure 4; Table 2**). ZTL regulated the physiological responses of guard cells to ABA and drought by acting in synergy with OST1 (**Figures 1, 5, 6**).

OST1 is a central component of ABA signalling and stomatal closure. The increased rate of water loss from Arabidopsis *ztl* mutants as well as their impaired stomatal regulation in response to ABA (**Figure 1**) suggests a requirement of ZTL for normal *OST1* function. The similar phenotypes observed in *Populus* trees with reduced ZTL function (**Figure 3**) indicates a similar mechanism operates in *Populus*.

OST1 Interacts With the Clock Proteins ZTL and PRR5

We showed that ZTL bound directly to OST1 in plant cells. Loss-of-function *prr5-11* mutants showed an opposite stomatal phenotype to *ztl-3*, a null mutant (Somers et al., 2004) that does not produce mRNA or protein (**Figure 7A**). The water loss phenotype of the *prr5-1* mutant (a low level of water loss comparable to WT) was as expected, given the *prr5-11* mutant showed high levels of stomatal closure in the presence of ABA (**Figure 7A**). In contrast, the stomata of the *ztl-3* and *ost1-3* single mutants remained more open in response to ABA (**Figure 7A**), which matched the high levels of water loss shown by these mutants (**Figures 6A,B**). The genetic data confirmed that a triple mutant that combined the loss-of-function *prr5-1* allele with the *ztl-3* and *ost1-3* alleles had a lower rate of water loss than a *ztl-3 and ost1-3* double mutant but did not completely phenocopy it (**Figure 6A**). This may result from TOC1 accumulation, in the triple mutant as TOssC1 is a substrate of ZTL that affects ABA responses (Legnaioli et al., 2009); moreover, overexpression of TOC1 slightly increases stomatal apertures and reduces water use efficiency (Legnaioli et al., 2009; Simon et al., 2020).

We hypothesised that an increased level of PRR5 in the absence of ZTL would exacerbate the water loss phenotype. Thus, we carried out physiological, biochemical and genetic assays to probe PRR5 function in stomatal closure, rate of water loss and interaction with OST1 (**Figures 6, 7**). Direct interactions between ZTL and OST1 (**Figure 5**), and between PRR5 and OST1 (**Figure 7B**), occurred in plant cells. In addition, the level of PRR5 affected stomatal aperture (**Figure 7A**). Removing both OST1 and ZTL function (*ztl-3 and ost1-3* double mutant) produced a strong water loss phenotype (**Figure 6A**); however, a triple mutant (*ztl-1, prr5-1 and ost1*-3) showed a less extreme water loss phenotype (**Figure 6A**), indicating that, in the absence of ZTL and OST1, PRR5 partially blocked the ABA pathways controlling stomatal aperture. The interactions between OST1, ZTL and PRR5 are thus essential for ABA-signalling and water regulation under stressful conditions. ABA treatment may produce a change in circadian period which is dependent on genotype and thus, the effect of ZTL on ABA-signalling gene expression may result from a phase shift (Legnaioli et al., 2009; Liu et al., 2013), although, in our hands, treatment with 20 µM ABA did not significantly alter the phase in the first 24 h (**Supplementary Figure S9**) or period of WT and *ztl-21* seedlings (**Supplementary Figure S9; Supplementary Tables 1, 2**).

These findings suggest that both ZTL and PRR5 interact with OST1 to regulate stomata and ABA-dependent responses. As the loss of PRR5 did not influence the *ost1-3* water loss phenotype (**Figure 6A**), PRR5 appears to act upstream of OST1. In contrast, the loss of PRR5 strongly influenced the water loss phenotype of *ztl-3* mutants (**Figure 6B**). PRR5 acting downstream of ZTL but upstream of OST1 would also explain the phenotype of the *ztl-3, prr5-1 and ost1-3* triple mutant. These physical and genetic interactions provide a biochemical framework linking ZTL directly to ABA-regulated components. ZTL thus acts with OST1 as a circadian short-cut to help phosphorylate and/or degrade PRR5 enabling osmotic regulation of guard cells and connecting the clock with responses essential for water conservation.

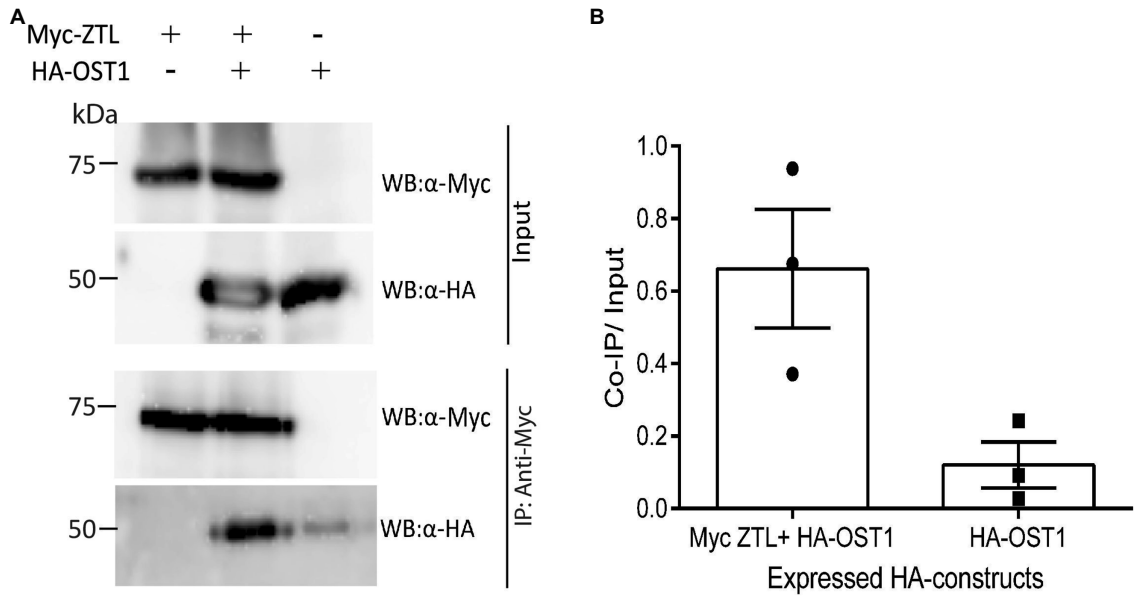

FIGURE 5 | Coexpression of ZTL and OST1 in plant cells indicates a strong interaction between the proteins. **(A)** Representative co-immunoprecipitation assay showing *in vivo* interaction between ZTL and OST1. Tagged versions of ZTL and OST1 proteins were expressed in Arabidopsis protoplasts, singly or in combination. Proteins were immunoprecipitated using mouse anti-Myc antibody (IP: α-Myc) and subsequently analysed by Western blotting with an anti-HA-POD antibody (WB: α-HA) and anti-c-Myc chicken antibody (WB: α-Myc). The experiment was repeated three times in different Western blots and produced similar results. **(B)** Mean values ($n=3$) ± SEM of the ratio of Co-IP signal to sample signal from the input reaction (40% of sample used in Co-IP) of the three different co-immunoprecipitation assays described in **(A)**. The individual results from each experiment are shown on the plot: Filled circles (left-hand side): Myc-OST1 + HA-ZTL; filled squares (right-hand side): HA-ZTL.

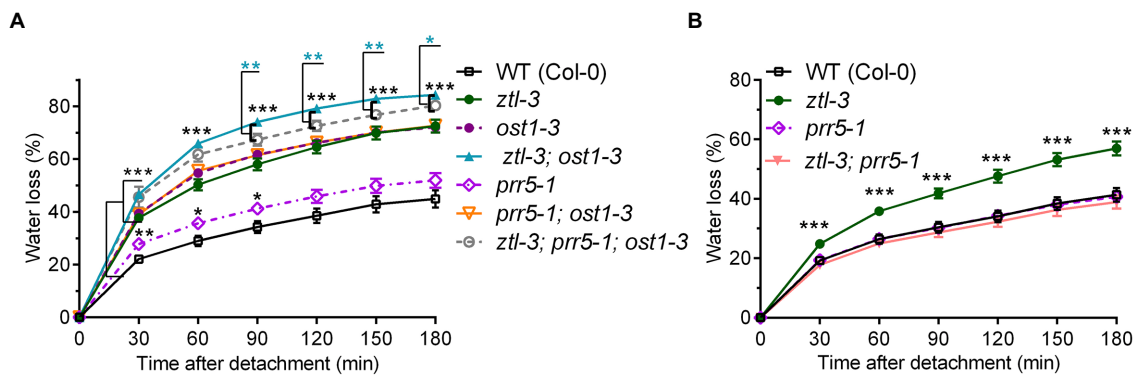

FIGURE 6 | ZTL and OST1 act synergistically to promote stomatal closure, and PRR5 partially blocks ABA signalling in the absence of both ZTL and OST1. **(A, B)** Water loss from detached rosette leaves of 3-week-old WT (Col-0) Arabidopsis and single, double and triple mutants carrying different combinations of alleles at the *ZTL* (*ztl-3*), *PRR5* (*prr5-1*) and *OST1* (*ost1-3*) loci. Values are means ± SE of two to three biological replicates, each containing one leaf from six to eight plants of each genotype. In **(A)**, significant differences between the *ztl-3 and ost1-3* double mutant and the *ztl-3, prr5-1 and ost1-3* triple mutant are shown by cyan-coloured asterisks. As all the mutants differed from WT at $p<0.001$ (Student's *t*-test) at all time points, all the pairwise mutant vs. WT comparisons represented by three black asterisks for simplicity. In **(B)**, pairwise comparisons found that *ztl-3* differed significantly from WT but *prr5-1* and the *prr5-1 and ztl-3* double mutant did not. The result for *ztl-3 vs* WT (Student's *t*-test) is represented by three black asterisks. Statistical levels in **(A)** and **(B)**: *$p<0.05$; **$p<0.01$; and ***$p<0.001$.

The Roles of ZTL and OST1 in Regulating Water Loss Are Conserved Across Plant Species

There is a significant overlap between ABA and cold signalling pathways and control by the circadian clock (Eriksson and Webb, 2011); for instance, the circadian MYB-transcription factors CCA1 and LHY contribute to cold responses in both Arabidopsis and *Populus* sp. (Espinoza et al., 2010; Ibáñez et al., 2010; Dong et al., 2011). The circadian clock regulates ABA signalling *via* transcriptional changes induced by TOC1 (Legnaioli et al., 2009; Huang et al., 2012). Mutations at the circadian clock-associated *EARLY BIRD/NFX1-LIKE 2* locus also increase resistance to salt and drought stress (Lisso et al., 2006), as well as inducing hypersensitive responses to ABA

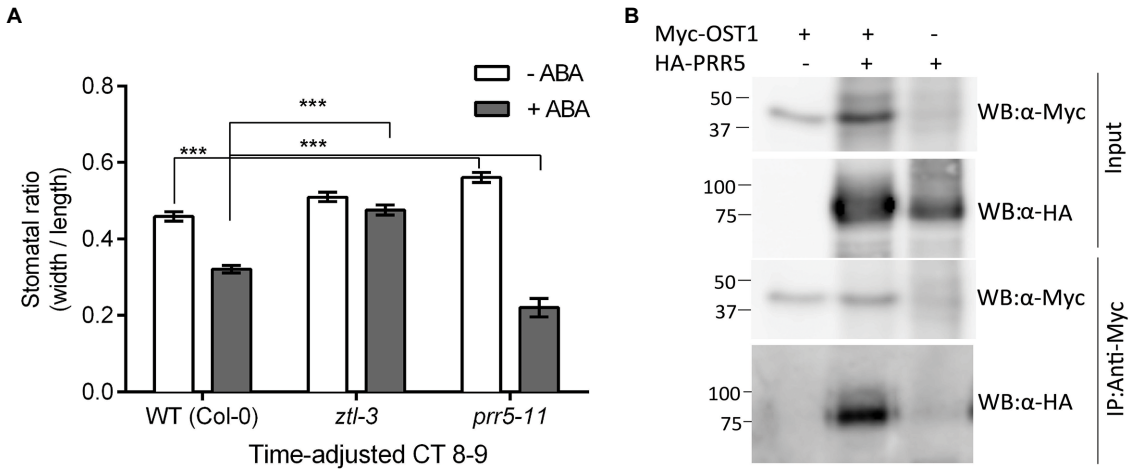

FIGURE 7 | The circadian clock protein PRR5 interacts with ZTL and OST1 to regulate stomatal responses in Arabidopsis. **(A)** *ztl-3* and *prr5-11* mutants show opposite stomatal aperture phenotypes in response to ABA. Time of ABA treatment was adjusted to an equivalent point in the circadian cycle to accommodate the difference in period (τ) between *ztl-3* (τ = ~ 28 h), *prr5-11* (τ = ~ 23 h) and wild-type (τ = 24 h) plants. Values are means ± SE of three biological replicates, each containing 20 stomata/genotype. (***$p < 0.001$; Student's *t*-test). **(B)** PRR5 and OST1 interact *in vivo*. Co-immunoprecipitation assay showing an interaction between PRR5 and OST1 in Arabidopsis protoplasts. Tagged versions of PRR5 and OST1 proteins were expressed in Arabidopsis protoplasts. Proteins were immunoprecipitated using mouse anti-Myc antibody (IP: α-Myc) and subsequently analysed by Western blotting with an anti-HA-POD antibody (WB: α-HA) and anti-c-Myc chicken antibody (WB: α-Myc).

(Lisso et al., 2012). Genome-wide analysis of Arabidopsis recently showed that LHY controlled expression of ABA biosynthesis and receptor genes, as well as other aspects of signalling (Adams et al., 2018). We investigated several of these genes, including *ABI2*, *OST1*, *ABI5, ABF4* and *RD29A*, and found ZTL affected their expression (**Figure 4**).

The receptors regulating ABA responses have increased in number since plants first colonised dry land (Umezawa et al., 2010) in response to the need to manage water status and detect and respond to heat and drought stresses. Such stresses are largely managed by controlling stomata. Stomata provide a means of CO_2 entry, thus enabling photosynthesis, and also of controlling water loss through transpiration. They thus are critical regulators of plant growth.

Stomatal conductance is a crucial trait affecting water status and photosynthetic capacity that directly impacts biomass accumulation of trees. Stomatal conductance is under diurnal regulation in field-grown *Eucalyptus sp.*, and thus likely controlled by the clock (Resco de Dios et al., 2013). We found previously that *Eucalyptus sp.* exhibit robust circadian rhythms under constant conditions (Johansson et al., 2015), and our present data suggest that ZTL acts in similar ways in both Arabidopsis and *Populus* to link the clock to stomatal control. Thus, the important roles of ZTL and OST1 in controlling stomata is conserved across species.

Our work highlights plants' dependence on the circadian clock to respond to drought stress. Studies in *Populus balsamifera (Pb)* suggest that *PbZTL2* is under local climatic selection, as are ABA-related signalling components, *PbGIs* and additional clock-associated genes (Keller et al., 2017). In addition, in *Populus trichocarpa*, *PtPRR5*, *PtPRR7* and other clock genes are associated with biomass, phenology and physiological traits in Genome-Wide Association Studies (GWAS) and appear to have undergone selection (McKown et al., 2014); for example, *PtPRR5* is part of an adaptive introgression of genes on Chromosome 15 transferred from *P. balsamifera* into *P. trichocarpa* (Suarez-Gonzalez et al., 2016).

OST1 is a kinase and thus a target for both phosphorylation and ubiquitination (Kim et al., 2013). The partnership between ZTL and OST1 underlies changes in ubiquitination and/or phosphorylation. Their associations with PRR5 may facilitate localisation of PRR5 to the nucleus and its interactions with, for instance, ABI5. The circadian clock PRR proteins are expressed sequentially between dawn and dusk in the order PRR9, PRR7, PRR5 and TOC1/PRR1. This may provide a set of 'cogs' enabling interactions with OST1, with or without ZTL, to be integrated into circadian clock and ABA-signalling pathways and respond to abiotic stresses occurring at different times across the day. Other circadian genes including *PRR7* influence ABA signalling (Liu et al., 2013). Future efforts to resolve the underlying mechanisms controlling stomatal regulation and stress tolerance will benefit from consideration of the interaction between OST1, ZTL and the PRRs. Further studies in both Arabidopsis and *Populus* will determine the detailed mechanisms controlling diel stomatal closure and ABA-signalling responses.

DATA AVAILABILITY STATEMENT

The original contributions presented in the study are included in the article/**Supplementary Material**, further questions can be directed to the corresponding author.

AUTHOR CONTRIBUTIONS

AARW and MEE conceived the research. MJu, MJo, IK, LB, AARW, MI-N, and MEE designed the experiments. MJu, AM, MJo, CI, IK, JS, NT, and MEE carried out the experiments and analysed the data. All authors interpreted the results and contributed to writing the manuscript.

FUNDING

This research was funded by Carl Trygger Foundation for Scientific Research, the Kempe Foundations, the Swedish Governmental Agency for Innovation Systems (VINNOVA), the Swedish Research Council (VR), the Swedish Research Council Formas, Stiftelsen Nils and Dorthi Troëdsson Forskningsfond, Trees and Crops 4 the Future, Knut and Alice Wallenberg Foundation, and the Berzelii Centre for forest biotechnology. MI-N as VINNMER fellow was funded by VINNOVA. ME as VINNMER Marie Curie International Qualification Fellow was funded by VINNOVA and European Union and supported by an Umeå University career grant and also received support from Churchill College, Cambridge University, Cambridge, United Kingdom.

ACKNOWLEDGMENTS

We wish to thank Takeshi Mizuno, Kazuko Yamaguchi-Shinozaki and Steve Kay for their gifts of seeds; Göran Samuelsson for the gift of the RbCS antibody; and Dave Somers for the gift of the pPZP vector containing the *ztl-1* coding sequence. We thank Sofia Österberg, Olga Mielczarek and Matthew Stancombe for excellent technical assistance. We are thankful for help from the transgenic facilities and greenhouse staff at UPSC and to NASC and ABRC facilities for providing materials. Thanks are also due for the award of the By-Fellowship (2011-14) from Churchill College, Cambridge University to MEE. We gratefully acknowledge financial support from the funding agencies outlined above.

SUPPLEMENTARY MATERIAL

The Supplementary Material for this article can be found online at: https://www.frontiersin.org/articless/10.3389/fpls.2022.829121/full#supplementary-material

REFERENCES

Adams, S., Grundy, J., Veflingstad, S. R., Dyer, N. P., Hannah, M. A., Ott, S., et al. (2018). Circadian control of abscisic acid biosynthesis and signalling pathways revealed by genome-wide analysis of LHY binding targets. *New Phytol.* 220, 893–907. doi: 10.1111/nph.15415

Alabadí, D., Oyama, T., Yanovsky, M. J., Harmon, F. G., Mas, P., and Kay, S. A. (2001). Reciprocal regulation between TOC1 and LHY/CCA1 within the Arabidopsis circadian clock. *Science* 293, 880–883. doi: 10.1126/science.1061320

Baudry, A., Ito, S., Song, Y. H., Strait, A. A., Kiba, T., Lu, S., et al. (2010). F-box proteins FKF1 and LKP2 act in concert with ZEITLUPE to control *Arabidopsis* clock progression. *Plant Cell* 22, 606–622. doi: 10.1105/tpc.109.072843

Baumann, K. (2010). ABA's greatest hits. *Nat. Rev. Mol. Cell Biol.* 11:2. doi: 10.1038/nrm2826

Bechtold, N., Ellis, J., and Pelletier, G. (1993). In-planta agrobacterium-mediated gene-transfer by infiltration of adult *Arabidopsis thaliana* plants. *Compt. Rendus Acad. Sci. III Sci. Vie* 316, 1194–1199.

Brandt, B., Brodsky, D. E., Xue, S., Negi, J., Iba, K., Kangasjärvi, J., et al. (2012). Reconstitution of abscisic acid activation of SLAC1 anion channel by CPK6 and OST1 kinases and branched ABI1 PP2C phosphatase action. *Proc. Natl. Acad. Sci. U. S. A.* 109, 10593–10598. doi: 10.1073/pnas.1116590109

Brandt, B., Munemasa, S., Wang, C., Nguyen, D., Yong, T., Yang, P. G., et al. (2015). Calcium specificity signaling mechanisms in abscisic acid signal transduction in Arabidopsis guard cells. *Elife* 4:e03599. doi: 10.7554/eLife.03599

Burian, A., Barbier de reuille, P., and Kuhlemeier, C. (2016). Patterns of stem cell divisions contribute to plant longevity. *Curr. Biol.* 26, 1385–1394. doi: 10.1016/j.cub.2016.03.067

Cai, S., Chen, G., Wang, Y., Huang, Y., Marchant, D. B., Wang, Y., et al. (2017). Evolutionary conservation of ABA signaling for stomatal closure. *Plant Physiol.* 174, 732–747. doi: 10.1104/pp.16.01848

Conn, S. J., Gilliham, M., Athman, A., Schreiber, A. W., Baumann, U., Moller, I., et al. (2011). Cell-specific vacuolar calcium storage mediated by *CAX1* regulates Apoplastic calcium concentration, gas exchange, and plant productivity in *Arabidopsis*. *Plant Cell* 23, 240–257. doi: 10.1105/tpc.109.072769

Correia, M. J., and Pereira, J. S. (1995). The control of leaf conductance of white lupin by xylem ABA concentration decreases with the severity of water deficits. *J. Exp. Bot.* 46, 101–110. doi: 10.1093/jxb/46.1.101

Dai, M., Xue, Q., Mccray, T., Margavage, K., Chen, F., Lee, J.-H., et al. (2013). The PP6 phosphatase regulates ABI5 phosphorylation and abscisic acid signaling in *Arabidopsis*. *Plant Cell* 25, 517–534. doi: 10.1105/tpc.112.105767

Devireddy, A. R., Zandalinas, S. I., Gómez-Cadenas, A., Blumwald, E., and Mittler, R. (2018). Coordinating the overall stomatal response of plants: rapid leaf-to-leaf communication during light stress. *Sci. Signal.* 11:eaam9514. doi: 10.1126/scisignal.aam9514

Dodd, A. N., Kusakina, J., Hall, A., Gould, P. D., and Hanaoka, M. (2014). The circadian regulation of photosynthesis. *Photosynth. Res.* 119, 181–190. doi: 10.1007/s11120-013-9811-8

Dodd, A. N., Parkinson, K., and Webb, A. A. R. (2004). Independent circadian regulation of assimilation and stomatal conductance in the ztl-1 mutant of Arabidopsis. *New Phytol.* 162, 63–70. doi: 10.1111/j.1469-8137.2004.01005.x

Dong, M. A., Farre, E. M., and Thomashow, M. F. (2011). CIRCADIAN CLOCK-ASSOCIATED 1 and LATE ELONGATED HYPOCOTYL regulate expression of the C-REPEAT BINDING FACTOR (CBF) pathway in Arabidopsis. *Proc. Natl. Acad. Sci. U. S. A.* 108, 7241–7246. doi: 10.1073/pnas.1103741108

Edwards, K. D., Takata, N., Johansson, M., Jurca, M., Novák, O., Hényková, E., et al. (2018). Circadian clock components control daily growth activities by modulating cytokinin levels and cell division-associated gene expression in Populus trees. *Plant Cell Environ.* 41, 1468–1482. doi: 10.1111/pce.13185

Engineer, C. B., Ghassemian, M., Anderson, J. C., Peck, S. C., Hu, H., and Schroeder, J. I. (2014). Carbonic anhydrases, EPF2 and a novel protease mediate CO_2 control of stomatal development. *Nature* 513, 246–250. doi: 10.1038/nature13452

Eriksson, M. E., Hanano, S., Southern, M. M., Hall, A., and Millar, A. J. (2003). Response regulator homologues have complementary, light-dependent functions in the Arabidopsis circadian clock. *Planta* 218, 159–162. doi: 10.1007/s00425-003-1106-4

Eriksson, M. E., Israelsson, M., Olsson, O., and Moritz, T. (2000). Increased gibberellin biosynthesis in transgenic trees promotes growth, biomass production and xylem fiber length. *Nat. Biotechnol.* 18, 784–788. doi: 10.1038/77355

Eriksson, M. E., and Webb, A. A. R. (2011). Plant cell responses to cold are all about timing. *Curr. Opin. Plant Biol.* 14, 731–737. doi: 10.1016/j.pbi.2011.08.005

Espinoza, C., Degenkolbe, T., Caldana, C., Zuther, E., Leisse, A., Willmitzer, L., et al. (2010). Interaction with diurnal and circadian regulation results in

dynamic metabolic and transcriptional changes during cold acclimation in Arabidopsis. *PLoS One* 5:e14101. doi: 10.1371/journal.pone.0014101

Farré, E. M., and Liu, T. (2013). The PRR family of transcriptional regulators reflects the complexity and evolution of plant circadian clocks. *Curr. Opin. Plant Biol.* 16, 621–629. doi: 10.1016/j.pbi.2013.06.015

Filichkin, S. A., Breton, G., Priest, H. D., Dharmawardhana, P., Jaiswal, P., Fox, S. E., et al. (2011). Global profiling of rice and poplar transcriptomes highlights key conserved circadian-controlled pathways and *cis*-regulatory modules. *PLoS One* 6:e16907. doi: 10.1371/journal.pone.0016907

Finkelstein, R. (2013). Abscisic acid synthesis and response. *The Arabidopsis Book* 11:e0166. doi: 10.1199/tab.0166

Fogelmark, K., and Troein, C. (2014). Rethinking transcriptional activation in the *Arabidopsis* circadian clock. *PLoS Comput. Biol.* 10:e1003705. doi: 10.1371/journal.pcbi.1003705

Fujiwara, S., Wang, L., Han, L. Q., Suh, S. S., Salome, P. A., Mcclung, C. R., et al. (2008). Post-translational regulation of the Arabidopsis circadian clock through selective proteolysis and phosphorylation of pseudo-response regulator proteins. *J. Biol. Chem.* 283, 23073–23083. doi: 10.1074/jbc.M803471200

Fülöp, K., Pettkó-Szandtner, A., Magyar, Z., Miskolczi, P., Kondorosi, E., Dudits, D., et al. (2005). The Medicago CDKC;1-CYCLINT;1 kinase complex phosphorylates the carboxy-terminal domain of RNA polymerase II and promotes transcription. *Plant J.* 42, 810–820. doi: 10.1111/j.1365-313X.2005.02421.x

Gendron, J. M., Pruneda-Paz, J. L., Doherty, C. J., Gross, A. M., Kang, S. E., and Kay, S. A. (2012). Arabidopsis circadian clock protein, TOC1, is a DNA-binding transcription factor. *Proc. Natl. Acad. Sci. U. S. A.* 109, 3167–3172. doi: 10.1073/pnas.1200355109

Gonzalez-Guzman, M., Pizzio, G. A., Antoni, R., Vera-Sirera, F., Merilo, E., Bassel, G. W., et al. (2012). Arabidopsis PYR/PYL/RCAR receptors play a major role in quantitative regulation of stomatal aperture and transcriptional response to abscisic acid. *Plant Cell* 24, 2483–2496. doi: 10.1105/tpc.112.098574

Gould, P. D., Diaz, P., Hogben, C., Kusakina, J., Salem, R., Hartwell, J., et al. (2009). Delayed fluorescence as a universal tool for the measurement of circadian rhythms in higher plants. *Plant J.* 58, 893–901. doi: 10.1111/j.1365-313X.2009.03819.x

Green, R. M., Tingay, S., Wang, Z.-Y., and Tobin, E. M. (2002). Circadian rhythms confer a higher level of fitness to Arabidopsis plants. *Plant Physiol.* 129, 576–584. doi: 10.1104/pp.004374

Han, L. Q., Mason, M., Risseeuw, E. P., Crosby, W. L., and Somers, D. E. (2004). Formation of an SCFZTL complex is required for proper regulation of circadian timing. *Plant J.* 40, 291–301. doi: 10.1111/j.1365-313X.2004.02207.x

Haydon, M. J., Mielczarek, O., Robertson, F. C., Hubbard, K. E., and Webb, A. A. R. (2013). Photosynthetic entrainment of the Arabidopsis circadian clock. *Nature* 502, 689–692. doi: 10.1038/nature12603

Hellens, R. P., Edwards, E. A., Leyland, N. R., Bean, S., and Mullineaux, P. M. (2000). pGreen: a versatile and flexible binary Ti vector for agrobacterium-mediated plant transformation. *Plant Mol. Biol.* 42, 819–832. doi: 10.1023/a:1006496308160

Helliwell, C. A., Wesley, S. V., Wielopolska, A. J., and Waterhouse, P. M. (2002). High-throughput vectors for efficient gene silencing in plants. *Funct. Plant Biol.* 29, 1217–1225. doi: 10.1071/fp02033

Hoffman, D. E., Jonsson, P., Bylesjö, M., Trygg, J., Antti, H., Eriksson, M. E., et al. (2010). Changes in diurnal patterns within the Populus transcriptome and metabolome in response to photoperiod variation. *Plant Cell Environ.* 33, 1298–1313. doi: 10.1111/j.1365-3040.2010.02148.x

Huang, W., Pérez-García, P., Pokhilko, A., Millar, A. J., Antoshechkin, I., Riechmann, J. L., et al. (2012). Mapping the core of the Arabidopsis circadian clock defines the network structure of the oscillator. *Science* 336, 75–79. doi: 10.1126/science.1219075

Hubbard, K. E., Nishimura, N., Hitomi, K., Getzoff, E. D., and Schroeder, J. I. (2010). Early abscisic acid signal transduction mechanisms: newly discovered components and newly emerging questions. *Genes Dev.* 24, 1695–1708. doi: 10.1101/gad.1953910

Ibáñez, C., Kozarewa, I., Johansson, M., Ögren, E., Rohde, A., and Eriksson, M. E. (2010). Circadian clock components regulate entry and affect exit of seasonal dormancy as well as winter hardiness in Populus trees. *Plant Physiol.* 153, 1823–1833. doi: 10.1104/pp.110.158220

Israelsson, M., Siegel, R. S., Young, J., Hashimoto, M., Iba, K., and Schroeder, J. I. (2006). Guard cell ABA and CO_2 signaling network updates and Ca^{2+} sensor priming hypothesis. *Curr. Opin. Plant Biol.* 9, 654–663. doi: 10.1093/aob/mcr252

Jalakas, P., Merilo, E., Kollist, H., and Brosché, M. (2018). ABA-mediated regulation of stomatal density is OST1-independent. *Plant Direct* 2:e00082. doi: 10.1002/pld3.82

Jarillo, J. A., Capel, J., Tang, R.-H., Yang, H.-Q., Alonso, J. M., Ecker, J. R., et al. (2001). An Arabidopsis circadian clock component interacts with both CRY1 and phyB. *Nature* 410, 487–490. doi: 10.1038/35068589

Johansson, M., Mcwatters, H. G., Bakó, L., Takata, N., Gyula, P., Hall, A., et al. (2011). Partners in time: EARLY BIRD associates with ZEITLUPE and regulates the speed of the Arabidopsis clock. *Plant Physiol.* 155, 2108–2122. doi: 10.1104/pp.110.167155

Johansson, M., Ramos-Sanchez, J. M., Conde, D., Ibáñez, C., Takata, N., Allona, I., et al. (2015). "Role of the circadian clock in cold acclimation and winter dormancy in perennial plants," in *Advances in Plant Dormancy*. ed. J. V. Anderson (Netherlands: Springer International Publishing), 51–74.

Keller, S. R., Chhatre, V. E., and Fitzpatrick, M. C. (2017). Influence of range position on locally adaptive gene–environment associations in Populus flowering time genes. *J. Hered.* 109, 47–58. doi: 10.1093/jhered/esx098

Kevei, E., Gyula, P., Hall, A., Kozma-Bognar, L., Kim, W. Y., Eriksson, M. E., et al. (2006). Forward genetic analysis of the circadian clock separates the multiple functions of ZEITLUPE. *Plant Physiol.* 140, 933–945. doi: 10.1104/pp.105.074864

Kiba, T., Henriques, R., Sakakibara, H., and Chua, N. H. (2007). Targeted degradation of PSEUDO-RESPONSE REGULATOR5 by an SCFZTL complex regulates clock function and photomorphogenesis in Arabidopsis thaliana. *Plant Cell* 19, 2516–2530. doi: 10.1105/tpc.107.053033

Kim, W. Y., Fujiwara, S., Suh, S. S., Kim, J., Kim, Y., Han, L. Q., et al. (2007). ZEITLUPE is a circadian photoreceptor stabilized by GIGANTEA in blue light. *Nature* 449, 356–360. doi: 10.1038/nature06132

Kim, W.-Y., Geng, R., and Somers, D. E. (2003). Circadian phase-specific degradation of the F-box protein ZTL is mediated by the proteasome. *Proc. Natl. Acad. Sci. U. S. A.* 100, 4933–4938. doi: 10.1073/pnas.0736949100

Kim, D.-Y., Scalf, M., Smith, L. M., and Vierstra, R. D. (2013). Advanced proteomic analyses yield a deep catalog of Ubiquitylation targets in *Arabidopsis*. *Plant Cell* 25, 1523–1540. doi: 10.1105/tpc.112.108613

Knight, H., Thomson, A. J. W., and Mcwatters, H. G. (2008). SENSITIVE TO FREEZING6 integrates cellular and environmental inputs to the plant circadian clock. *Plant Physiol.* 148, 293–303. doi: 10.1104/pp.108.123901

Kozarewa, I., Ibáñez, C., Johansson, M., Ögren, E., Mozley, D., Nylander, E., et al. (2010). Alteration of PHYA expression change circadian rhythms and timing of bud set in Populus. *Plant Mol. Biol.* 73, 143–156. doi: 10.1007/s11103-010-9619-2

Lawson, T., and Vialet-Chabrand, S. (2018). Speedy stomata, photosynthesis and plant water use efficiency. *New Phytol.* 221, 93–98. doi: 10.1111/nph.15330

Le Provost, G., Herrera, R., Paiva, J. A., Chaumeil, P., Salin, F., and Plomion, C. (2007). A micromethod for high throughput RNA extraction in forest trees. *Biol. Res.* 40, 291–297. doi: 10.4067/S0716-97602007000400003

Lee, C.-M., Feke, A., Li, M.-W., Adamchek, C., Webb, K., Pruneda-Paz, J., et al. (2018). Decoys untangle complicated redundancy and reveal targets of circadian clock F-box proteins. *Plant Physiol.* 177, 1170–1186. doi: 10.1104/pp.18.00331

Lee, C.-M., Li, M.-W., Feke, A., Liu, W., Saffer, A. M., and Gendron, J. M. (2019). GIGANTEA recruits the UBP12 and UBP13 deubiquitylases to regulate accumulation of the ZTL photoreceptor complex. *Nat. Commun.* 10, 3750–3750. doi: 10.1038/s41467-019-11769-7

Lee, H. G., Mas, P., and Seo, P. J. (2016). MYB96 shapes the circadian gating of ABA signaling in Arabidopsis. *Sci. Rep.* 6:17754. doi: 10.1038/srep17754

Legnaioli, T., Cuevas, J., and Mas, P. (2009). TOC1 functions as a molecular switch connecting the circadian clock with plant responses to drought. *EMBO J.* 28, 3745–3757. doi: 10.1038/emboj.2009.297

Lisso, J., Altmann, T., and Müssig, C. (2006). The AtNFXL1 gene encodes a NF-X1 type zinc finger protein required for growth under salt stress. *FEBS Lett.* 580, 4851–4856. doi: 10.1016/j.febslet.2006.07.079

Lisso, J., Schröder, F., Schippers, J. H. M., and Müssig, C. (2012). NFXL2 modifies cuticle properties in Arabidopsis. *Plant Signal. Behav.* 7, 551–555. doi: 10.4161/psb.19838

Liu, T., Carlsson, J., Takeuchi, T., Newton, L., and Farré, E. M. (2013). Direct regulation of abiotic responses by the Arabidopsis circadian clock component PRR7. *Plant J.* 76, 101–114. doi: 10.1111/tpj.12276

Livak, K. J., and Schmittgen, T. D. (2001). Analysis of relative gene expression data using real-time quantitative PCR and the 2(-Delta Delta C(T)) method. *Methods* 25, 402–408. doi: 10.1006/meth.2001.1262

Locke, J. C. W., Southern, M. M., Kozma-Bognar, L., Hibberd, V., Brown, P. E., Turner, M. S., et al. (2005). Extension of a genetic network model by iterative experimentation and mathematical analysis. *Mol. Syst. Biol.* 1:2005.0013. doi: 10.1038/msb4100018

MacRobbie, E. A. (2000). ABA activates multiple Ca(2+) fluxes in stomatal guard cells, triggering vacuolar K(+)(Rb(+)) release. *Proc. Natl. Acad. Sci. U. S. A.* 97, 12361–12368. doi: 10.1073/pnas.220417197

Más, P., Kim, W. Y., Somers, D. E., and Kay, S. A. (2003). Targeted degradation of TOC1 by ZTL modulates circadian function in *Arabidopsis thaliana*. *Nature* 426, 567–570. doi: 10.1038/nature02163

Matsushika, A., Makino, S., Kojima, M., and Mizuno, T. (2000). Circadian waves of expression of the APRR1/TOC1 family of pseudo-response regulators in *Arabidopsis thaliana*: insight into the plant circadian clock. *Plant Cell Physiol.* 41, 1002–1012. doi: 10.1093/pcp/pcd043

McClung, C. R. (2019). The plant circadian oscillator. *Biology* 8:14. doi: 10.3390/biology8010014

McKown, A. D., Klápště, J., Guy, R. D., Geraldes, A., Porth, I., Hannemann, J., et al. (2014). Genome-wide association implicates numerous genes underlying ecological trait variation in natural populations of *Populus trichocarpa*. *New Phytol.* 203, 535–553. doi: 10.1111/nph.12815

Meskiene, I., Baudouin, E., Schweighofer, A., Liwosz, A., Jonak, C., Rodriguez, P. L., et al. (2003). Stress-induced protein phosphatase 2C is a negative regulator of a mitogen-activated protein kinase. *J. Biol. Chem.* 278, 18945–18952. doi: 10.1074/jbc.M300878200

Michael, T. P., Salome, P. A., Yu, H. J., Spencer, T. R., Sharp, E. L., McPeek, M. A., et al. (2003). Enhanced fitness conferred by naturally occurring variation in the circadian clock. *Science* 302, 1049–1053. doi: 10.1126/science.1082971

Millar, A. J. (2016). The intracellular dynamics of circadian clocks reach for the light of ecology and evolution. *Annu. Rev. Plant Biol.* 67, 595–618. doi: 10.1146/annurev-arplant-043014-115619

Millar, A. J., Carre, I. A., Strayer, C. A., Chua, N. H., and Kay, S. A. (1995). Circadian clock mutants in Arabidopsis identified by luciferase imaging. *Science* 267, 1161–1163. doi: 10.1126/science.7855595

Munemasa, S., Hauser, F., Park, J., Waadt, R., Brandt, B., and Schroeder, J. I. (2015). Mechanisms of abscisic acid-mediated control of stomatal aperture. *Curr. Opin. Plant Biol.* 28, 154–162. doi: 10.1016/j.pbi.2015.10.010

Mustilli, A. C., Merlot, S., Vavasseur, A., Fenzi, F., and Giraudat, J. (2002). Arabidopsis OST1 protein kinase mediates the regulation of stomatal aperture by abscisic acid and acts upstream of reactive oxygen species production. *Plant Cell* 14, 3089–3099. doi: 10.1105/tpc.007906

Nakamichi, N., Kita, M., Ito, S., Sato, E., Yamashino, T., and Mizuno, T. (2005). The Arabidopsis pseudo-response regulators, PRR5 and PRR7, coordinately play essential roles for circadian clock function. *Plant Cell Physiol.* 46, 609–619. doi: 10.1093/pcp/pci061

Nakashima, K., Fujita, Y., Kanamori, N., Katagiri, T., Umezawa, T., Kidokoro, S., et al. (2009). Three Arabidopsis SnRK2 protein kinases, SRK2D/SnRK2.2, SRK2E/SnRK2.6/OST1 and SRK2I/SnRK2.3, involved in ABA signaling are essential for the control of seed development and dormancy. *Plant Cell Physiol.* 50, 1345–1363. doi: 10.1093/pcp/pcp083

Nilsson, O., Aldén, T., Sitbon, F., Anthony Little, C. H., Chalupa, V., Sandberg, G., et al. (1992). Spatial pattern of cauliflower mosaic virus 35S promoter-luciferase expression in transgenic hybrid aspen trees monitored by enzymatic assay and non-destructive imaging. *Transgenic Res.* 1, 209–220. doi: 10.1007/BF02524751

Nilsson, O., Moritz, T., Sundberg, B., Sandberg, G., and Olsson, O. (1996). Expression of the agrobacterium rhizogenes rolC gene in a deciduous forest tree alters growth and development and leads to stem fasciation. *Plant Physiol.* 112, 493–502. doi: 10.1104/pp.112.2.493

Norén, L., Kindgren, P., Stachula, P., Rühl, M., Eriksson, M. E., Hurry, V., et al. (2016). Circadian and plastid signaling pathways are integrated to ensure correct expression of the CBF and COR genes during photoperiodic growth. *Plant Physiol.* 171, 1392–1406. doi: 10.1104/pp.16.00374

Penfield, S., and Hall, A. (2009). A role for multiple circadian clock genes in the response to signals that break seed dormancy in Arabidopsis. *Plant Cell* 21, 1722–1732. doi: 10.1105/tpc.108.064022

Pfaffl, M. W. (2001). A new mathematical model for relative quantification in real-time RT–PCR. *Nucleic Acids Res.* 29:e45. doi: 10.1093/nar/29.9.e45

Plautz, J. D., Straume, M., Stanewsky, R., Jamison, C. F., Brandes, C., Dowse, H. B., et al. (1997). Quantitative analysis of drosophila period gene transcription in living animals. *J. Biol. Rhythm.* 12, 204–217. doi: 10.1177/074873049701200302

Pokhilko, A., Mas, P., and Millar, A. J. (2013). Modelling the widespread effects of TOC1 signalling on the plant circadian clock and its outputs. *BMC Systems Biol.* 7:23. doi: 10.1186/1752-0509-7-23

Raghavendra, A. S., Gonugunta, V. K., Christmann, A., and Grill, E. (2010). ABA perception and signalling. *Trends Plant Sci.* 15, 395–401. doi: 10.1016/j.tplants.2010.04.006

Ramos, A., Perez-Solis, E., Ibanez, C., Casado, R., Collada, C., Gomez, L., et al. (2005). Winter disruption of the circadian clock in chestnut. *Proc. Natl. Acad. Sci. U. S. A.* 102, 7037–7042. doi: 10.1073/pnas.0408549102

Resco de Dios, V., Díaz-Sierra, R., Goulden, M. L., Barton, C. V. M., Boer, M. M., Gessler, A., et al. (2013). Woody clockworks: circadian regulation of night-time water use in *Eucalyptus globulus*. *New Phytol.* 200, 743–752. doi: 10.1111/nph.12382

Rigoulot, S. B., Petzold, H. E., Williams, S. P., Brunner, A. M., and Beers, E. P. (2019). Populus trichocarpa clade A PP2C protein phosphatases: their stress-induced expression patterns, interactions in core abscisic acid signaling, and potential for regulation of growth and development. *Plant Mol. Biol.* 100, 303–317. doi: 10.1007/s11103-019-00861-7

Rubin, M. J., Brock, M. T., Davis, A. M., German, Z. M., Knapp, M., Welch, S. M., et al. (2017). Circadian rhythms vary over the growing season and correlate with fitness components. *Mol. Ecol.* 26, 5528–5540. doi: 10.1111/mec.14287

Saez, A., Apostolova, N., Gonzalez-Guzman, M., Gonzalez-Garcia, M. P., Nicolas, C., Lorenzo, O., et al. (2004). Gain-of-function and loss-of-function phenotypes of the protein phosphatase 2C HAB1 reveal its role as a negative regulator of abscisic acid signalling. *Plant J.* 37, 354–369. doi: 10.1046/j.1365-313x.2003.01966.x

Saez, A., Robert, N., Maktabi, M. H., Schroeder, J. I., Serrano, R., and Rodriguez, P. L. (2006). Enhancement of abscisic acid sensitivity and reduction of water consumption in Arabidopsis by combined inactivation of the protein phosphatases type 2C ABI1 and HAB1. *Plant Physiol.* 141, 1389–1399. doi: 10.1104/pp.106.081018

Salomé, P. A., Michael, T. P., Kearns, E. V., Fett-Neto, A. G., Sharrock, R. A., and McClung, C. R. (2002). The *out of phase 1* mutant defines a role for PHYB in circadian phase control in Arabidopsis. *Plant Physiol.* 129, 1674–1685. doi: 10.1104/pp.003418

Sanchez, S. E., and Kay, S. A. (2016). The plant circadian clock: from a simple timekeeper to a complex developmental manager. *Cold Spring Harb. Perspect. Biol.* 8:a027748. doi: 10.1101/cshperspect.a027748

Santiago, J., Rodrigues, A., Saez, A., Rubio, S., Antoni, R., Dupeux, F., et al. (2009). Modulation of drought resistance by the abscisic acid receptor PYL5 through inhibition of clade A PP2Cs. *Plant J.* 60, 575–588. doi: 10.1111/j.1365-313X.2009.03981.x

Schneider, C. A., Rasband, W. S., and Eliceiri, K. W. (2012). NIH image to ImageJ: 25 years of image analysis. *Nat. Methods* 9, 671–675. doi: 10.1038/nmeth.2089

Shor, E., Paik, I., Kangisser, S., Green, R., and Huq, E. (2017). PHYTOCHROME INTERACTING FACTORS mediate metabolic control of the circadian system in Arabidopsis. *New Phytol.* 215, 217–228. doi: 10.1111/nph.14579

Simon, N. M. L., Graham, C. A., Comben, N. E., Hetherington, A. M., and Dodd, A. N. (2020). The circadian clock influences the long-term water use efficiency of Arabidopsis. *Plant Physiol.* 183, 317–330. doi: 10.1104/pp.20.00030

Sjödin, A., Street, N. R., Sandberg, G., Gustafsson, P., and Jansson, S. (2009). The Populus genome integrative explorer (PopGenIE): a new resource for exploring the *Populus* genome. *New Phytol.* 182, 1013–1025. doi: 10.1111/j.1469-8137.2009.02807.x

Somers, D. E., Kim, W. Y., and Geng, R. S. (2004). The F-box protein ZEITLUPE confers dosage-dependent control on the circadian clock, photomorphogenesis, and flowering time. *Plant Cell* 16, 769–782. doi: 10.1105/tpc.016808

Somers, D. E., Webb, A. A., Pearson, M., and Kay, S. A. (1998). The short-period mutant, *toc1-1*, alters circadian clock regulation of multiple outputs throughout development in *Arabidopsis thaliana*. *Development* 125, 485–494. doi: 10.1242/dev.125.3.485

Strayer, C., Oyama, T., Schultz, T. F., Raman, R., Somers, D. E., Mas, P., et al. (2000). Cloning of the Arabidopsis clock cone TOC1, an autoregulatory response regulator homolog. *Science* 289, 768–771. doi: 10.1126/science.289.5480.768

Suarez-Gonzalez, A., Hefer, C. A., Christe, C., Corea, O., Lexer, C., Cronk, Q. C. B., et al. (2016). Genomic and functional approaches reveal a case of adaptive introgression from *Populus balsamifera* (balsam poplar) in *P. trichocarpa* (black cottonwood). *Mol. Ecol.* 25, 2427–2442. doi: 10.1111/mec.13539

Takata, N., Saito, S., Saito, C., Nanjo, T., Shinohara, K., and Uemura, M. (2009). Molecular phylogeny and expression of poplar circadian clock genes, LHY1 and LHY2. *New Phytol.* 181, 808–819. doi: 10.1111/j.1469-8137.2008.02714.x

Takata, N., Saito, S., Saito, C., and Uemura, M. (2010). Phylogenetic footprint of the plant clock system in angiosperms: evolutionary processes of pseudo-response regulators. *BMC Evol. Biol.* 10:126. doi: 10.1186/1471-2148-10-126

Tylewicz, S., Petterle, A., Marttila, S., Miskolczi, P., Azeez, A., Singh, R. K., et al. (2018). Photoperiodic control of seasonal growth is mediated by ABA acting on cell-cell communication. *Science* 360, 212–215. doi: 10.1126/science.aan8576

Umezawa, T., Nakashima, K., Miyakawa, T., Kuromori, T., Tanokura, M., Shinozaki, K., et al. (2010). Molecular basis of the core regulatory network in ABA responses: sensing, signaling and transport. *Plant Cell Physiol.* 51, 1821–1839. doi: 10.1093/pcp/pcq156

Urquiza-García, U., and Millar, A. J. (2021). Testing the inferred transcription rates of a dynamic, gene network model in absolute units. *is Plant* 3:diab022. doi: 10.1093/insilicoplants/diab022

Vlad, F., Droillard, M.-J., Valot, B., Khafif, M., Rodrigues, A., Brault, M., et al. (2010). Phospho-site mapping, genetic and in planta activation studies reveal key aspects of the different phosphorylation mechanisms involved in activation of SnRK2s. *Plant J.* 63, 778–790. doi: 10.1111/j.1365-313X.2010.04281.x

Wang, L., Fujiwara, S., and Somers, D. E. (2010). PRR5 regulates phosphorylation, nuclear import and subnuclear localization of TOC1 in the Arabidopsis circadian clock. *EMBO J.* 29, 1903–1915. doi: 10.1038/emboj.2010.76

Wang, Z., and Tobin, E. (1998). Constitutive expression of the CIRCADIAN CLOCK ASSOCIATED 1 (CCA1) gene disrupts circadian rhythms and suppresses its own expression. *Cell* 93, 1207–1217. doi: 10.1016/s0092-8674(00)81464-6

Wang, P., Zhao, Y., Li, Z., Hsu, C.-C., Liu, X., Fu, L., et al. (2017). Reciprocal regulation of the TOR kinase and ABA receptor balances plant growth and stress response. *Mol. Cell* 69, 100–112.e6. doi: 10.1016/j.molcel.2017.12.002

Webb, A. A., and Hetherington, A. M. (1997). Convergence of the abscisic acid, CO_2, and extracellular calcium signal transduction pathways in stomatal guard cells. *Plant Physiol.* 114, 1557–1560. doi: 10.1104/pp.114.4.1557

Wu, C., Feng, J., Wang, R., Liu, H., Yang, H., Rodriguez, P. L., et al. (2012). HRS1 acts as a negative regulator of abscisic acid signaling to promote timely germination of Arabidopsis seeds. *PLoS One* 7:e35764. doi: 10.1371/journal.pone.0035764

Wu, F.-H., Shen, S.-C., Lee, L.-Y., Lee, S.-H., Chan, M.-T., and Lin, C.-S. (2009). Tape-Arabidopsis Sandwich– a simpler Arabidopsis protoplast isolation method. *Plant Methods* 5:16. doi: 10.1186/1746-4811-5-16

Yamamoto, Y., Sato, E., Shimizu, T., Nakamich, N., Sato, S., Kato, T., et al. (2003). Comparative genetic studies on the APRR5 and APRR7 genes belonging to the APRR1/TOC1 quintet implicated in circadian rhythm, control of flowering time, and early photomorphogenesis. *Plant Cell Physiol.* 44, 1119–1130. doi: 10.1093/pcp/pcg14

Yang, M., Han, X., Yang, J., Jiang, Y., and Hu, Y. (2021). The Arabidopsis circadian clock protein PRR5 interacts with and stimulates ABI5 to modulate abscisic acid signaling during seed germination. *Plant Cell* 33, 3022–3041. doi: 10.1093/plcell/koab168

Yoo, S.-D., Cho, Y.-H., and Sheen, J. (2007). Arabidopsis mesophyll protoplasts: a versatile cell system for transient gene expression analysis. *Nat. Protoc.* 2, 1565–1572. doi: 10.1038/nprot.2007.199

Yoshida, R., Hobo, T., Ichimura, K., Mizoguchi, T., Takahashi, F., Aronso, J., et al. (2002). ABA-activated SnRK2 protein kinase is required for dehydration stress signaling in Arabidopsis. *Plant Cell Physiol.* 43, 1473–1483. doi: 10.1093/pcp/pcf188

Yu, J., Li, H., Peng, Y., Yang, L., Zhao, F., Luan, S., et al. (2017). A survey of the pyrabactin resistance-like abscisic acid receptor gene family in poplar. *Plant Signal. Behav.* 12:e1356966. doi: 10.1080/15592324.2017.1356966

Zdepski, A., Wang, W., Priest, H. D., Ali, F., Alam, M., Mockler, T. C., et al. (2008). Conserved daily transcriptional programs in *Carica papaya*. *Trop. Plant Biol.* 1, 236–245. doi: 10.1007/s12042-008-9020-3

Conflict of Interest: MEE is a member and CEO of the holding company Woodheads AB, a part-owner of SweTree Technologies (STT), which played no part in this work and she is also a board member of STT.

The remaining authors declare that the research was conducted in the absence of any commercial or financial relationships that could be construed as a potential conflict of interest.

Publisher's Note: All claims expressed in this article are solely those of the authors and do not necessarily represent those of their affiliated organizations, or those of the publisher, the editors and the reviewers. Any product that may be evaluated in this article, or claim that may be made by its manufacturer, is not guaranteed or endorsed by the publisher.

frontiers in Plant Science

ORIGINAL RESEARCH
published: 24 March 2022
doi: 10.3389/fpls.2022.829336

Ultraviolet-B Radiation Represses Primary Root Elongation by Inhibiting Cell Proliferation in the Meristematic Zone of Arabidopsis Seedlings

*Maria Luján Sheridan, Lucio Simonelli, Marisol Giustozzi and Paula Casati**

Centro de Estudios Fotosintéticos y Bioquímicos, Universidad Nacional de Rosario, Rosario, Argentina

In *Arabidopsis thaliana* plants, exposure to UV-B induces an inhibition of primary root elongation. Different mutants have been isolated that are deficient in this response; however, little is known about the cellular and molecular mechanisms that regulate inhibition of root elongation in seedlings exposed to UV-B. In this work, we investigated the effect UV-B irradiation of different organs on primary root elongation. Our results demonstrate that irradiation of the leaves and shoots only induce a partial inhibition of primary root elongation, while when only roots are exposed to this radiation, primary root inhibition is similar as that measured when the complete seedling is irradiated. The consequences of exposure at different root developmental stages and times after the end of the treatment was also studied. We here show that inhibition of primary root elongation is a consequence of a decrease in cell proliferation in the meristematic zone of the primary roots, while the elongation zone size is not affected by the treatment. The decrease in cell number after UV-B exposure is partially compensated by an increase in cell length in the root meristem; however, this compensation is not enough to maintain the meristem size. We also here demonstrate that, similarly as what occurs in developing leaves, GROWTH REGULATING FACTOR 3 (GRF3) transcription factor regulates cell proliferation in UV-B irradiated roots; however, and in contrast to what occurs in the leaves, this response does not depend on the presence of MITOGEN ACTIVATED PROTEIN KINASE 3 (MPK3). Inhibition of primary root elongation by UV-B under our experimental conditions is also independent of the UV-B photoreceptor UV RESISTANT LOCUS 8 (UVR8) or ATAXIA TELANGIECTASIA MUTATED (ATM); but a deficiency in *ATM AND RAD3-RELATED* (*ATR*) expression increases UV-B sensitivity in the roots. Finally, our data demonstrate that UV-B affects primary root growth in various Arabidopsis accessions, showing different sensitivities to this radiation.

Keywords: cell elongation, cell proliferation, primary root, programmed cell death, UV-B radiation

OPEN ACCESS

Edited by:
John Christie,
University of Glasgow,
United Kingdom

Reviewed by:
Gary Gardner,
University of Minnesota, Twin Cities,
United States
Miroslava Konstantinova Zhiponova,
Sofia University "St. Kliment Ohridski",
Bulgaria

***Correspondence:**
Paula Casati
casati@cefobi-conicet.gov.ar;
paulacasati@gmail.com

Specialty section:
This article was submitted to Plant Physiology, a section of the journal Frontiers in Plant Science

Received: *05 December 2021*
Accepted: *28 February 2022*
Published: *24 March 2022*

Citation:
Sheridan ML, Simonelli L, Giustozzi M and Casati P (2022) Ultraviolet-B Radiation Represses Primary Root Elongation by Inhibiting Cell Proliferation in the Meristematic Zone of Arabidopsis Seedlings. Front. Plant Sci. 13:829336. doi: 10.3389/fpls.2022.829336

INTRODUCTION

Plants are continually exposed to a changing environment, and this influences their developmental programs. Light is probably the most important environmental factor that affects plant growth and development. Ultraviolet-B (UV-B) radiation (280–315 nm) represents only a small proportion of the solar radiation that reaches the Earth; however, plants respond to exposure to wavelengths in

the UV-B range, for example showing changes in plant morphology, physiology and producing secondary metabolites (Dotto and Casati, 2017).

Ultraviolet-B radiation effects on plant growth include specific photomorphogenic responses, mostly mediated by the UV-B specific photoreceptor UV RESISTANT LOCUS 8 (UVR8), and non-specific stress or genotoxic responses (Hu et al., 2016; Podolec et al., 2021). UVR8 is so far the only UV-B specific photoreceptor identified in plants (for a review, see Podolec et al., 2021), this receptor modulates plant responses to UV-B interacting with CONSTITUTIVELY PHOTOMORPHOGENIC 1 (COP1) after UV-B exposure to activate transcription of UV-B responsive genes, initiating UV-B acclimation pathways. On the other hand, the non-specific effects include the formation of reactive oxygen species (ROS), DNA damage and the activation of the DNA damage response, membrane changes and protein crosslinking, these effects are usually produced after exposure to high UV-B doses or long exposure times (Manova and Gruszka, 2015; Parihar et al., 2015). These high UV-B activated responses are usually independent of UVR8 and involve signaling pathways that are partially conserved among different organisms (Hu et al., 2016). One of these pathways is the DNA damage response (DDR), which is induced after DNA damage; in this pathway the protein kinases ATAXIA TELANGIECTASIA MUTATED (ATM) and ATM AND RAD3-RELATED (ATR) function as a key regulators of the DNA damage response, activating SUPPRESSOR OF GAMMA RESPONSE 1 (SOG1; Furukawa et al., 2010), a transcription factor that regulates the expression of genes that encode proteins in this pathway (Bourbousse et al., 2018). A second UV-B pathway that acts independently of UVR8 requires the action of mitogen activated protein kinases (MAPK) MPK3 and MPK6, which are also triggered after exposure to DNA-damaging agents in Arabidopsis; thus, the MPK3/MPK6 cascade is an additional important pathway contributing to UV-B-induced DNA damage (González Besteiro and Ulm, 2013; Hu et al., 2016).

One plant response to UV-B is the reduction in the leaf area (Dotto and Casati, 2017). This decrease can be a consequence of an inhibition of cell division and/or to a decrease in cell expansion, and these different effects are due to different experimental conditions, developmental stages or plant species. For example, UV-B conditions that produce DNA damage in general inhibit cell proliferation, while lower doses and/or chronic UV-B exposure can produce both inhibition of cell proliferation and expansion. In Arabidopsis, the decrease in leaf size in UV-B irradiated plants is a consequence of inhibition of cell proliferation mediated by the microRNA miR396, which downregulates the expression of *GROWTH REGULATING FACTORS* (*GRF*) transcription factors (Casadevall et al., 2013). miRNA396 is upregulated by UV-B in proliferating leaves, and this induces the decrease in *GRF1*, *GRF2,* and *GRF3* levels. Induction of miR396 results in an inhibition of cell proliferation without affecting cell expansion. Interestingly, this response is independent of the UVR8 photereceptor and ATR, but depends on the presence of MPK3 (Casadevall et al., 2013). Interestingly, the role of miR396 in primary root elongation after UV-B exposure was also demonstrated (Gómez et al., 2019). Arabidopsis transgenic plants expressing an artificial target mimic directed against miR396 (*MIM396*) and showing a decrease in the endogenous microRNA activity, had a shorter primary root than WT plants, but they showed a lower inhibition of primary root elongation after UV-B exposure. In this way, inhibition of primary root elongation in Arabidopsis seedlings by UV-B is also regulated by this microRNA.

In addition, different reports have shown that Arabidopsis plants have a UV-B-sensing mechanism in the roots that regulate morphogenesis (Tong et al., 2008; Leasure et al., 2009). Moreover, after UV-B exposure at high intensity, in Arabidopsis roots, there is an upregulation of the expression of cell cycle regulatory and DNA damage genes, suggesting that UV-B-induced DNA damage in this organ may induce a delay of the G1-to-S transition of the cell cycle (Jiang et al., 2011). Thus, this delay in the progression of the cell cycle may be a protective mechanism to prevent cells with damaged DNA from dividing. Despite this, little is known about the cellular and molecular mechanisms that regulate the inhibition of root elongation in seedlings exposed to UV-B. Here, we investigated the effect UV-B irradiation of different organs on primary root elongation. We also analyzed the consequences of exposure at different root developmental stages and times after the end of the treatment. Our data show that inhibition of primary root elongation is a consequence of an inhibition of cell proliferation in the meristematic zone of the primary roots, while the elongation zone size is not affected by the treatment. The decrease in cell number after UV-B exposure is partially compensated by an increase in cell length in the root meristem; however, this compensation is not enough to maintain the meristem size of control roots grown in the absence of UV-B. The role of GRF3 was also analyzed, demonstrating that similarly as what occurs in developing leaves, transcription factors from this family regulate cell proliferation in the roots under UV-B conditions; however, and in contrast to what occurs in the leaves, this response does not depend on the presence of MPK3. We here also demonstrate that inhibition of primary root elongation by UV-B under the conditions of our experiments is independent of the UV-B photoreceptor UVR8 or ATM; but a deficiency in *ATR* expression significantly increases UV-B sensitivity in the roots. Finally, our data demonstrate that UV-B affects primary root growth in various Arabidopsis accessions, showing different sensitivities to this radiation.

MATERIALS AND METHODS

Plant Material, Growth Conditions, and Irradiation Protocols

Arabidopsis thaliana ecotypes Columbia (accessions Col-0, Col-3, and Col-4), Landsberg erecta (Ler) and Wassilewskija (Ws) were used for all experiments. *uvr8*, *mpk3*, *atm,* and *atr* seeds were a gift from Roman Ulm (University of Geneva, Switzerland). *rGRF3* plants were previously described by Rodriguez et al. (2010). *msh6* mutants in a Col-0 background were previously described in Lario et al. (2011).

For all the experiments, Arabidopsis seeds were grown on Murashige and Skoog (MS) growth medium supplemented with

0.7% agar in Petri dishes, and they were kept in a vertical position in the growth chamber at 22°C under a 16 h/8 h light/dark photoperiod (100 μEm^{-2} s^{-1}). In most experiments, 5 days after germination, full seedlings were irradiated for 1 h using UV-B lamps on fixtures mounted 30 cm above the plants (9 μmol m^{-2} s^{-1} UV-B and 2.9 μmol m^{-2} s^{-1} UV-A, Bio-Rad ChemiDoc^{TM} XRS UV-B lamps, catalog 1708097). These lamps have a peak at 302 nm and an emission spectra from 290 to 310 nm, and they were covered using cellulose acetate filters (CA, 100 mm extra-clear cellulose acetate plastic, Tap Plastics, Mountain View, CA, United States). The CA filter absorbs wavelengths lower than 290 nm; this control was done in case some lower wavelength radiation was produced with lamps aging. As a control without UV-B, plants were exposed for the same time under the lamps also covered with a polyester plastic that absorbs UV-B at wavelengths lower than 320 nm (PE, 100 mm clear polyester plastic; Tap Plastics). UV radiation was recorded using a UV-B/UV-A radiometer (UV203 AB radiometer; Macam Photometrics). Alternatively, during the UV-B treatment, the roots or the aerial parts of the seedlings (cotyledons and hypocotyl) were covered using a black paper, so as that only some parts of the seedlings are UV-B irradiated. After the UV-B treatment, seedlings were kept in the growth chamber under a 16 h/8 h light/dark photoperiod in the absence of UV-B. Alternatively, control and UV-B treated seedlings were kept in the dark to analyze the effect of photoreactivation in primary root elongation.

For fluence response analysis of primary root elongation, seedlings were irradiated for 1 h as described above at 4.5, 6.75, 9, or 11.25 μmol m^{-2} s^{-1} UV-B. After the UV-B treatment, seedlings were kept in the growth chamber under a 16 h/8 h light/dark photoperiod in the absence of UV-B.

Primary Root Length Measurements

Seedlings were grown for 5 or 9 days in MS-agar plates, they were UV-B irradiated as described above and they were then kept in the growth chamber in the absence of UV-B for 4 days. Plates were photographed before the treatment and 1, 2, 3, and 4 days after. Primary root length was measured using the ImageJ software version 1.52p.

Primary Root Meristem Analysis and Programmed Cell Death After Ultraviolet-B Exposure

Five days after stratification, MS-agar plate grown seedlings were irradiated with UV-B or kept under control conditions. Then, seedlings were maintained in the growth chamber under control conditions without UV-B for 24 or 96 h, and meristem length, cell number, average cell length in the meristematic zone and programmed cell death (PCD) were quantified by staining the root tips with a modified pseudo-Schiff propidium iodide (PI) staining protocol (Furukawa et al., 2010). Primary roots were analyzed by confocal laser scanning microscopy (Nikon C1) under water with 40X. The excitation wavelength for PI-stained samples was 488 nm and emission was collected at 520–720 nm. The meristematic zone characteristics were analyzed using the Image J software version 1.52p.

DNA Damage Analysis

Cyclobutane pyrimidine dimers (CPD) were measured using monoclonal antibodies by dot-blot analysis (TDM-2; Cosmo Bio Co., Ltd., Japan). Twelve-day-old plants were treated with UV-B for 1 or 4 h as described above, and samples (0.1 g) were collected after the treatment. 2 μg of the extracted DNA by a modified cetyltrimethylammonium bromide (CTAB) method was then denatured using 0.3 M NaOH for 10 min. Samples were analyzed using a nylon membrane (PerkinElmer Life Sciences, Inc.) in sextuplicate. The membrane was incubated at 80°C for 2 h and blocked with a buffer containing 20 mM Tris–HCl, pH 7.6, 137 mM NaCl (TBS) and 5% (p/v) dried milk for 1 h at room temperature. The membrane was finally washed with TBS and incubated with anti-CPDs antibodies (1:2000 in TBS) overnight at 4°C with agitation. Unbound antibodies were washed away and secondary antibodies conjugated to alkaline phosphatase (1:3000; Bio-Rad) were added. The blot was washed and finally developed by the addition of 5-bromo-4-chloro-3-indolyl phosphate and nitroblue tetrazolium. Dots were quantified by densitometry using ImageQuant software version 5.2. Total DNA was quantified fluorometrically using the Qubit dsDNA assay kit (Invitrogen).

Statistical Analysis

Comparisons between one independent variable were done using One-Way ANOVA (Dunn Test), while comparisons between more than two variables were analyzed using Two-Way ANOVA (Tukey's Test), using non-transformed data. These statistical analyses were performed using Sigma Plot 7.0. Dead meristematic cells were analyzed using the mixed generalized linear model with a Poisson distribution ($p > 0.05$), these analysis were performed using Infostat.

RESULTS

Full Inhibition of Primary Root Elongation in Col-0 Seedlings by Ultraviolet-B Requires Direct Exposure of the Roots and It Is a Consequence of Decreased Cell Proliferation in the Meristematic Zone

As described in the section "Introduction," in Arabidopsis seedlings, UV-B exposure produces an inhibition of primary root elongation. Because Arabidopsis plants have UV-B specific sensing and responsive mechanisms in the roots (Tong et al., 2008; Leasure et al., 2009), and as they also express the UV-B photoreceptor UVR8 in this organ (van Gelderen et al., 2018), we first investigated whether primary root inhibition after UV-B exposure requires full exposure of roots, or if it can also occur when only the shoots and leaves are irradiated, as it generally happens in nature. **Figure 1** shows that 1 day after a UV-B treatment, primary roots are significantly shorter than those

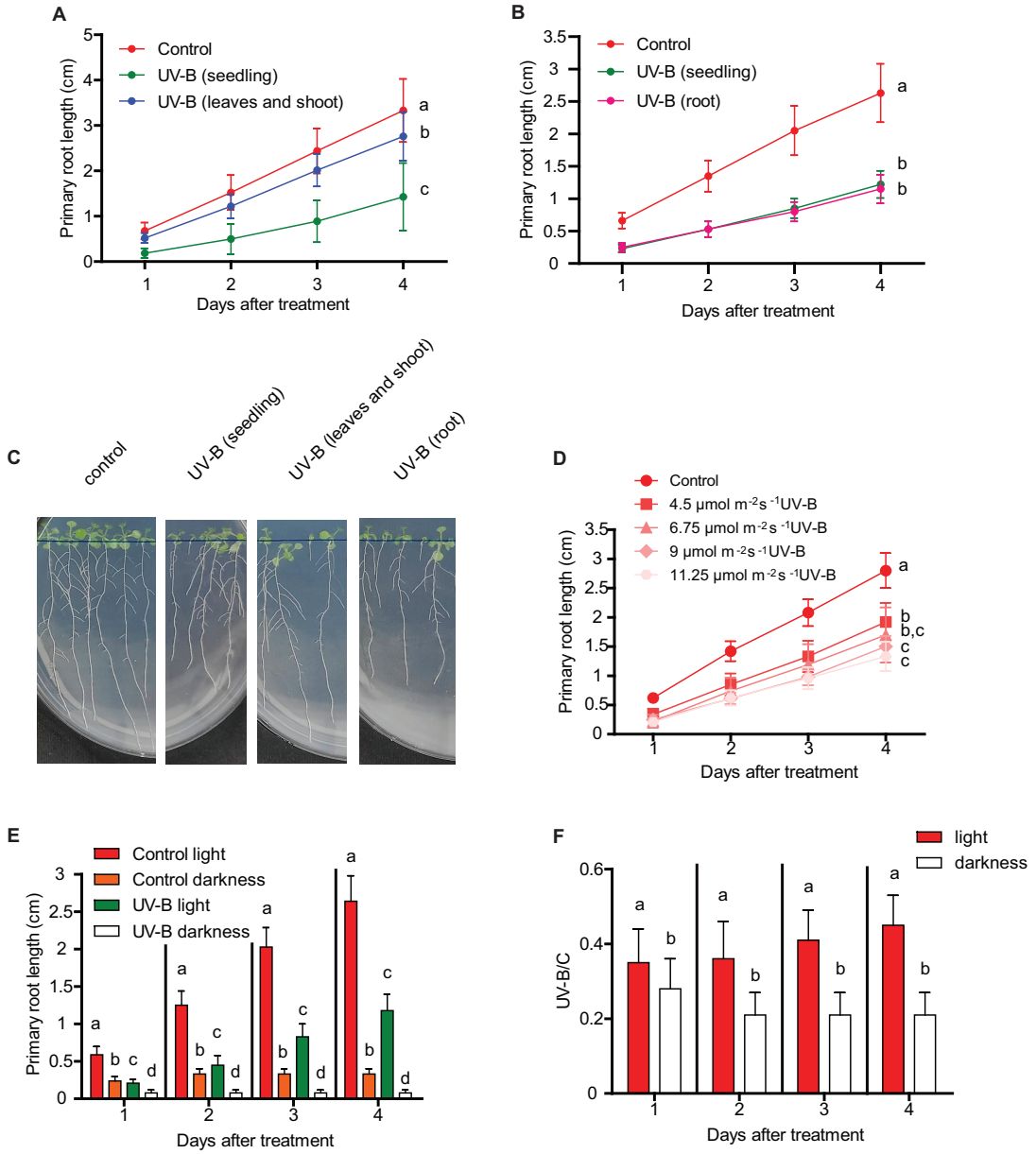

FIGURE 1 | Primary root growth inhibition assays in WT Col-0 after UV-B exposure. **(A)** Graphs of average root lengths of Col-0 seedlings that were grown in the absence of UV-B (control), after UV-B irradiation for 1 h at 9 µmol m^{-2} s^{-1} UV-B of the full seedlings or when only the shoot and leaves were irradiated. **(B)** Graphs of average root lengths of Col-0 seedlings that were grown in the absence of UV-B (control), after UV-B irradiation for 1 h at 9 µmol m^{-2} s^{-1} UV-B of the full seedlings or when only the roots were irradiated. **(C)** Representative pictures of one experiment showing primary roots from WT Col-0 seedlings under the different experimental conditions analyzed in **(A,B)**. **(D)** Fluence response curves of primary root inhibition by UV-B in Col-0 seedlings. Seedlings were irradiated at 4.5, 6.75, 9, or 11.25 µmol m^{-2} s^{-1} UV-B for 1 h. **(E)** Graphs of average root lengths of Col-0 seedlings that were grown in the absence of UV-B (control), after UV-B irradiation for 1 h at 9 µmol m^{-2} s^{-1} UV-B and were then kept under normal photoperiod (light) or in the darkness (dark). **(F)** Ratio between root lengths after UV-B exposure vs. under control conditions shown in **(E)**. Results show the individual values and the average from at least 20 biological replicates ± S.D. from one experiment. Three independent experiments were performed with similar results. Different letters indicate statistically significant differences applying one-way ANOVA (Dunn test, $P < 0.05$).

from non-irradiated plants when they are irradiated for 1 h at an intensity of 9 µmol m^{-2} s^{-1}. Interestingly, when only the shoots and leaves were exposed to a similar UV-B treatment, primary roots still showed a significant inhibition of elongation; however, this inhibition was much lower than that measured in fully exposed seedlings (**Figures 1A,C**). On the contrary, when only roots were UV-B irradiated, the decrease in primary root elongation was similar to that observed in fully irradiated seedlings (**Figures 1B,C**). Together, these results suggest that although a partial inhibition of primary root elongation by UV-B

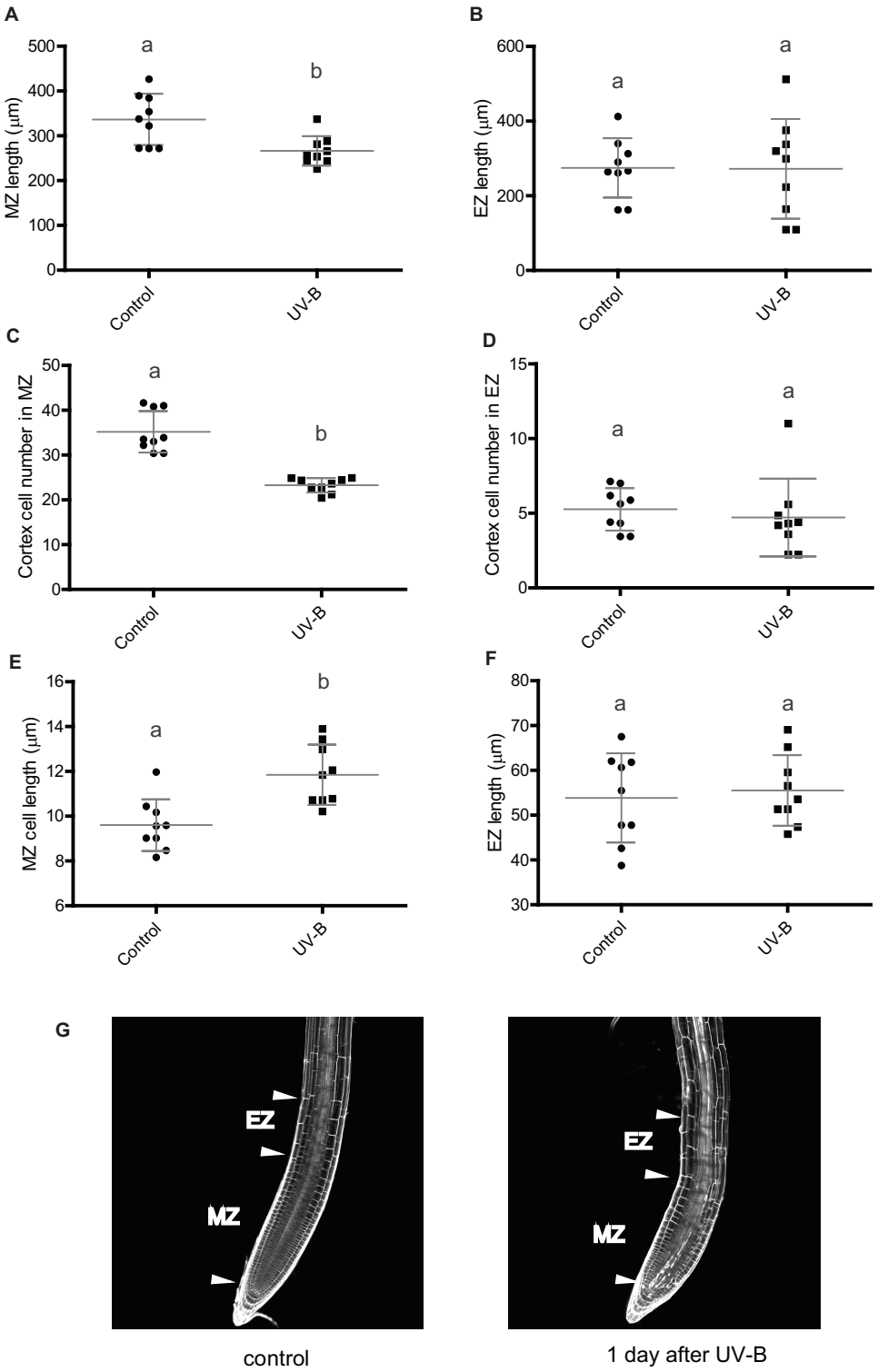

FIGURE 2 | UV-B inhibits cell proliferation in the primary root meristematic zone and does not affect the elongation zone of WT Col-0 seedlings. **(A)** Root meristematic zone length, **(C)** cortex cell number, and **(E)** cortex cell length from control or UV-B treated for 1 h at 9 μmol m^{-2} s^{-1} UV-B WT Col-0 seedlings 1 day after the treatment. **(B)** Root elongation zone length, **(D)** cortex cell number, and **(F)** cortex cell length from UV-B treated or control WT Col-0 seedlings. Results show the individual values and the average from at least eight independent biological replicates ± S.D. from one experiment. Different letters indicate statistically significant differences applying one-way ANOVA (Dunn test, $P < 0.05$). Three independent experiments were performed with similar results. **(G)** Representative images of primary roots of WT Col-0 seedlings 1 day after a UV-B treatment or kept in the absence of UV-B (control).

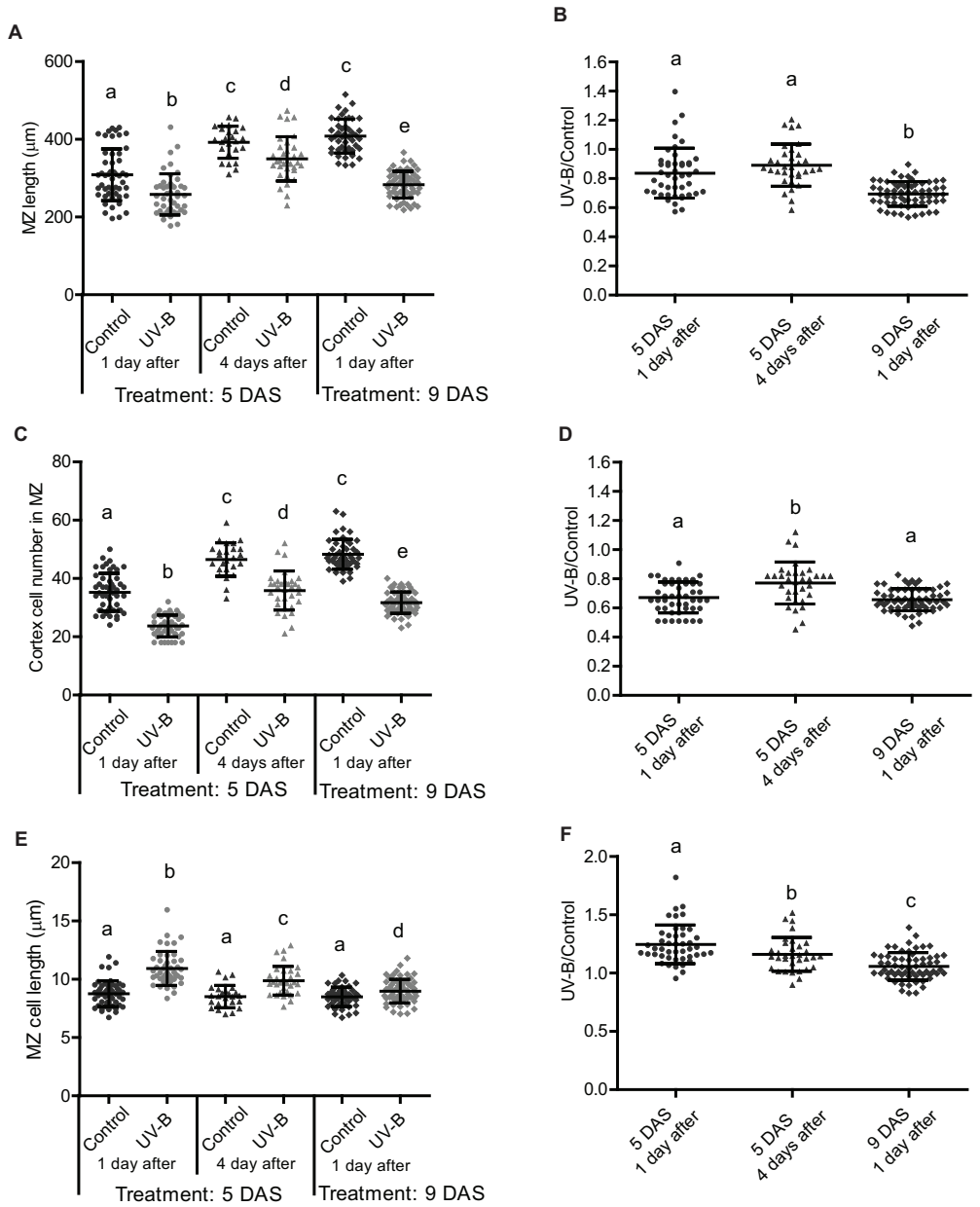

FIGURE 3 | UV-B differently affects cell proliferation in the root meristematic zone of WT Col-0 seedlings at different developmental stages or times after exposure. **(A)** Meristematic zone length, **(C)** cortex cell number, and **(E)** cortex cell length in the primary roots from UV-B treated or control WT Col-0 seedlings 1 or 4 days after the treatment in plants irradiated 5 or 9 days after sowing (DAS). Different letters indicate statistically significant differences applying two-way ANOVA (Tukey's test, $P < 0.05$). **(B)** Ratio between meristematic zone length, **(D)** cortex cell number, and **(F)** cortex cell length values measured after UV-B exposure vs. those under control conditions in primary roots are shown. Different letters indicate statistically significant differences applying one-way ANOVA (Dunn test, $P < 0.05$). Results show the individual values and the average from at least eight independent biological replicates ± S.D. from one experiment. Three independent experiments were performed with similar results.

could be activated from signals from usually directly exposed tissues, such as the shoots and leaves, full inhibition requires direct UV-B exposure of the roots.

Next, we analyzed how primary root inhibition was affected by UV-B treatments at different fluences. Our results show that when seedlings were UV-B irradiated for 1 h at an intensity of 4.5 μmol m^{-2} s^{-1}, primary root elongation was less affected than when the experiment was done for the same time using 9 μmol m^{-2} s^{-1} (**Figure 1D**). However, higher UV-B doses produced a similar inhibition of primary root elongation (**Figure 1D**), suggesting that at 9 μmol m^{-2} s^{-1} this response gets its maximal inhibitory effect.

The consequence of UV-B exposure in primary root elongation was also studied when irradiated plants were allowed

to recover under dark conditions. **Figure 1E** shows that darkness not only affected primary root elongation in UV-B irradiated plants, but also in control non-irradiated seedlings. However, growth under dark conditions was more affected in UV-B irradiated plants, suggesting that white light is required to improve root elongation in UV-B irradiated seedlings.

Arabidopsis primary roots can be divided in three different regions: the meristematic zone, which contains cells that actively divide and elongate; the elongation zone, which includes cells that no longer divide but only elongate (**Figure 2G**); and the mature zone, containing cells that no longer divide nor elongate (Fiorani and Beemster, 2006). Thus, we investigated whether the decrease in primary root length was a consequence of an inhibition of the growth of either or both the meristematic and the elongation zones, which are those that could affect primary root elongation. One day after a UV-B treatment, while the elongation zone size was not affected by the treatment in WT Col-0 plants, the meristematic zone length was significantly decreased, showing a significant lower number of cortex cells after the treatment (**Figures 2A–C**). Interestingly, in UV-B irradiated roots, cell length in the meristems was increased compared to that under control conditions (**Figure 2E**), suggesting that a compensating effect may be taking place to counteract the inhibition of cell proliferation measured. Despite this, this compensation did not completely revert the decrease in the meristem length measured. In contrast, cortex cell number and cortex cell length in the elongation zone was not affected by the UV-B treatment (**Figures 2D,F**); thus, inhibition of primary root elongation by UV-B is probably due to an inhibition of cell proliferation in the meristem of Col-0 seedlings.

When the effect of a UV-B treatment on the primary root meristematic and elongating zones was analyzed 4 days after the treatment, the results showed that there is still a decrease in the size of the meristem of UV-B treated seedlings, with a lower number of cells with longer sizes, suggesting that the inhibitory effect persists several days after the end of the treatment (**Supplementary Figure 1**). On the contrary, the elongation zone was not affected 4 days after the treatment, similarly as shown 1 day after the treatment (**Supplementary Figure 1**).

Ultraviolet-B Affects Cell Expansion, Cell Division, and Programmed Cell Death in the Primary Root Meristems at Different Root Developmental Stages

Next, we compared how cell expansion and cell elongation in the meristematic zone was affected at 1 and 4 days after recovery from a UV-B treatment, or when irradiation was done at different stages of primary root development. Our results show that 4 days after a UV-B treatment, the primary root meristematic zone is still shorter than that from non-irradiated plants (**Figures 3A,B**). However, the decrease in cell number is lower than that measured 1 day after the treatment, and this lower decrease in cell proliferation is accompanied with a lower increase in cell expansion (**Figures 3C–F**), suggesting that inhibition of cell proliferation is recovered over time after the end of the treatment.

In the primary root meristems of Arabidopsis plants, proliferating and expanding cells coexist and are primarily separated in space. At early stages of development, primary root meristem size increases as a consequence of coordinated cell division and elongation, until the meristem size reaches to a maximal size (Fiorani and Beemster, 2006). As shown in **Figure 3**, the size of the primary root meristems 5 days after sowing in control seedlings not exposed to UV-B is still growing, as 9 days after sowing the size of the meristems is longer; with more cortex cells. Thus, we investigated the effect of UV-B exposure in Arabidopsis seedlings where the meristem has completely expanded, and primary root elongation is mostly achieved by increased number of mature cells (Fiorani and Beemster, 2006). **Figure 3B** shows that the decrease in meristem size 1 day after the UV-B treatment at 9 DAS was more important than when it was applied 5 DAS. Interestingly, inhibition of cell proliferation 1 day after the treatment was similar when seedlings were irradiated at 5 and 9 DAS (**Figures 3C,D**). However, the decrease in the meristem size was larger in these plants because at this developmental stage, cell elongation was less increased by UV-B (**Figures 3E,F**).

After Arabidopsis seedlings are exposed to UV-B radiation, there is also an activation of programmed cell death (PCD) in the primary root meristematic zone (Furukawa et al., 2010). Dead cells are stained when incubated with propidium iodide (PI), while live cells exclude this compound (Furukawa et al., 2010). Thus, we next analyzed how PCD activation was affected at different times after exposure or when UV-B irradiation was done at different developmental stages. **Figure 4** shows that when UV-B irradiation was done when the meristematic zone is still growing (5 DAS), the number of dead cells was significantly higher than when the treatment was done after the meristem has reached its final size. Interestingly, 4 days after UV-B exposure, primary roots from irradiated seedlings at 5 DAS showed a significant reduction of dead cells, as previously reported (Johnson et al., 2018; Maulión et al., 2019).

Together, these results demonstrate that in the primary root meristems, inhibition of cell proliferation, increase in cell expansion and PCD after UV-B exposure take place at different developmental stages and remain several days after the treatment. However, the degree to which these processes are affected depend on the developmental stage of the primary roots and the time after exposure.

Growth Regulating Factor 3 Regulates Primary Root Elongation, Inhibition of Cell Proliferation and Programmed Cell Death in the Meristematic Zone After Ultraviolet-B Exposure

Previously, we demonstrated that after UV-B exposure, inhibition of leaf growth was mediated by the miR396 and the Growth Regulating Factors (GRFs), including GRF3. Therefore, we investigated if transcription factors from this family also participate in the inhibition of primary root elongation in UV-B irradiated seedlings. For these experiments, we analyzed the effect of UV-B radiation in cell proliferation in transgenic plants

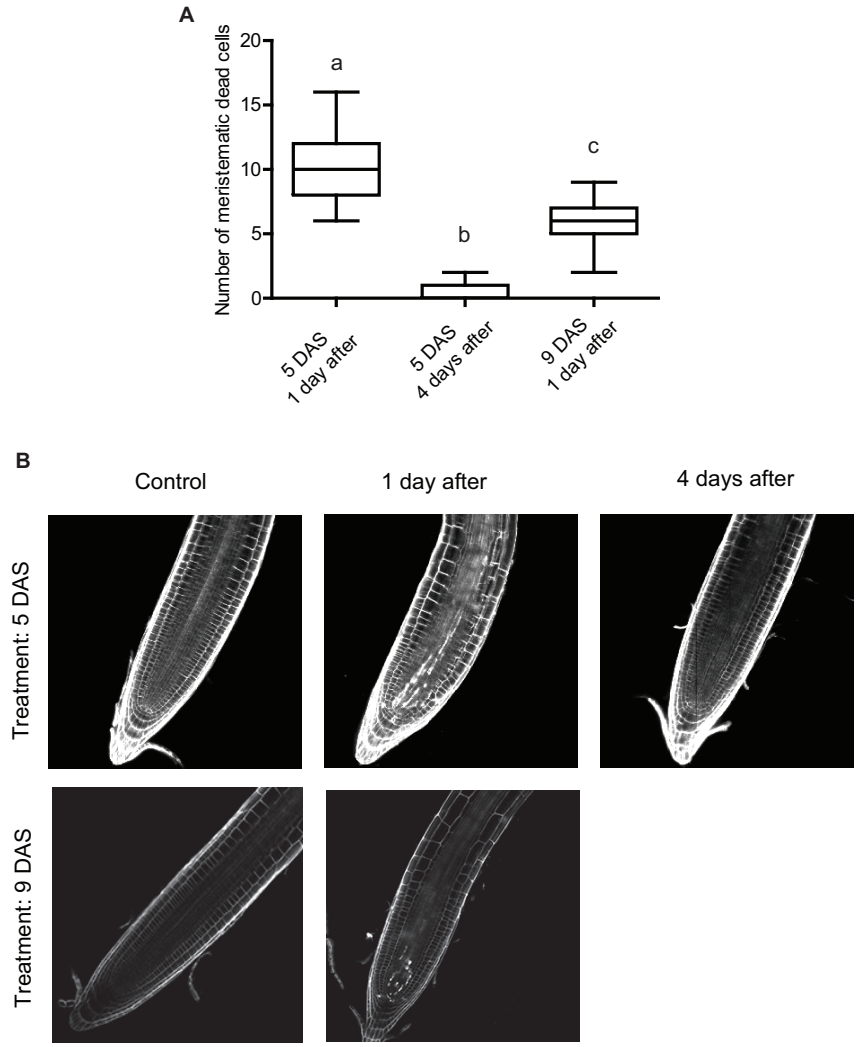

FIGURE 4 | UV-B affects programmed cell death in the root meristematic zone of WT Col-0 seedlings. **(A)** Number of stem cells that are dead after UV-B exposure in WT Col-0 primary root meristems 1 and 4 days after the treatment 5 days after sowing (DAS), or 1 day after the treatment 9 DAS. Results show the individual values and the average from at least 15 independent biological replicates ± S.D. from one experiment. Different letters represent statistically significant differences applying a mixed generalized linear model with a Poisson distribution ($p > 0.05$). Three independent experiments were performed with similar results.
(B) Representative images of primary roots of WT Col-0 seedlings in which stem cells and adjacent daughter cells were PI staining to count dead stem cells per root 1 or 4 days after UV-B exposure or in control conditions 5 or 9 DAS.

expressing a miR396-resistant version of GRF3 under its own promoter (*rGRF3*). This transgene was prepared by introducing synonymous mutations in the miR396 binding site of GRF3 (Casadevall et al., 2013). Primary roots from *rGRF3* plants were shorter than those from WT Col-0 plants when grown under control conditions as previously reported (Rodriguez et al., 2015; **Figure 5**). After UV-B exposure, *rGRF3* roots were still shorter than WT roots (**Figure 5A**), but showed a lower inhibition of elongation by UV-B (**Figure 5B**).

When the effect of UV-B on primary root meristems was compared in WT and *rGRF3* seedlings, the results showed that, in the transgenic plants, inhibition of cell proliferation in the primary roots was reduced compared to WT roots, while cell elongation was not affected (**Figure 6**). As previously reported, *rGRF3* primary root meristems were shorter with less cells than those from WT seedlings (Rodriguez et al., 2015; **Figure 6**). Together, our results suggest that similarly as what it was previously reported in proliferating leaves, inhibition of cell proliferation in the roots requires the activity of GRF3. Because *rGRF3* primary root meristems were shorter than WT meristems, the number of dead cells 1 day after the treatment were calculated relative to the cortex cells in this zone, showing that *rGRF3* primary roots had less dead cells after the treatment (**Figure 7**). This result suggests that GRF3 not only regulates cell proliferation but also PCD after UV-B exposure. Four days after the treatment, both WT and *rGRF3* primary roots showed undetectable levels of dead cells; thus, roots from both lines are similarly recovered in the absence of UV-B (**Figure 7B**).

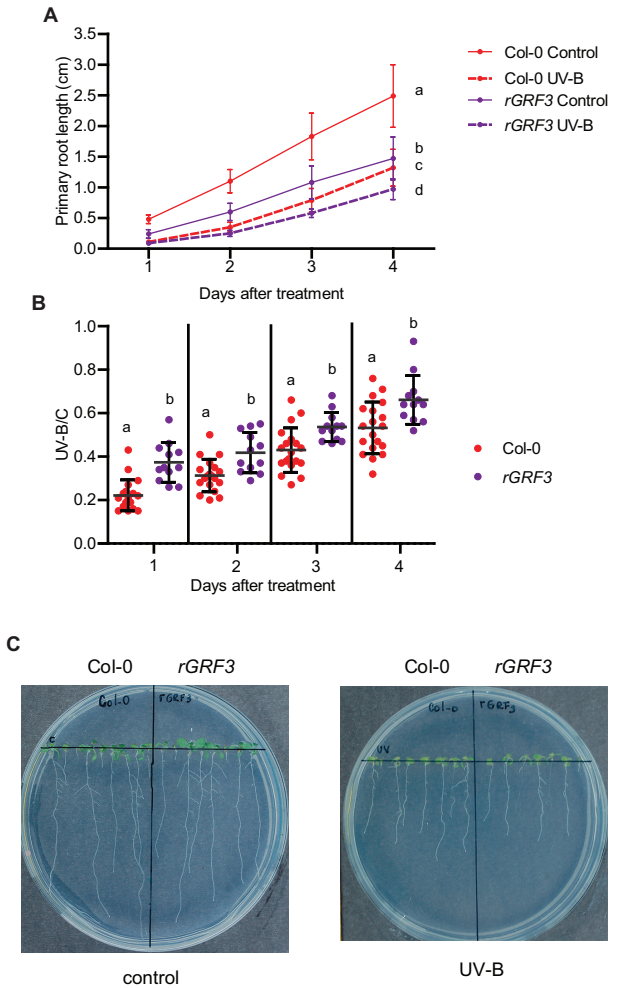

FIGURE 5 | Primary root growth inhibition assays in WT Col-0 and *rGRF3* seedlings after UV-B exposure. **(A)** Graphs of average root lengths of WT Col-0 and *rGRF3* seedlings after UV-B exposure or grown under control conditions without UV-B. **(B)** Ratio between root lengths after UV-B exposure vs. under control conditions. Results show the individual values and the average from at least 20 biological replicates ± S.D. from one experiment. Three independent experiments were performed with similar results. Different letters indicate statistical significant differences applying one-way ANOVA (Dunn test, $P < 0.05$). **(C)** Representative pictures of one experiment showing primary roots from control and UV-B irradiated WT Col-0 and *rGRF3* seedlings.

Regulation of Cell Number in the Primary Root Meristems by Ultraviolet-B Is Not Mediated by UVR8, MPK3 or Ataxia Telangiectasia Mutated, but Requires ATM and Rad3-Related and It Is Not Affected in DNA Repair Deficient Mutants

As described in the section "Introduction," UV-B responses activated by low-fluence UV-B radiation are mostly regulated by the UV-B specific UVR8 photoreceptor (Rizzini et al., 2011). Nevertheless, some responses to higher UV-B doses are independent of UVR8 and require the activation of different pathways that involve the activity of several protein kinases, for example MPK3, ATM, or/and ATR (Ulm, 2003). Previously, we showed that inhibition of cell division by UV-B in proliferating leaves of Arabidopsis by miR396 and GRFs depended on the activation of MPK3 but was independent of UVR8, MPK6, ATM, and ATR (Casadevall et al., 2013). Thus, we further investigated if a similar regulation occurs in the primary roots. As shown in **Figure 8A**, *uvr8* mutants showed a similar inhibition of root elongation after UV-B exposure; with a similar reduction of the meristematic zone length after the treatment (**Supplementary Figure 2**). The decrease in the number of cortex cells and increase in cell length after the treatment was also similar as that in WT roots, suggesting that this response to UV-B is independent of the photoreceptor. Interestingly, a similar response was measured when experiments were done using *mpk3* mutants (**Figure 8B** and **Supplementary Figure 3**). This demonstrates that inhibition of cell proliferation in the roots by UV-B is activated by a different pathway as that occurring in leaves, independently of MPK3.

On the other hand, while primary roots from *atm* mutants also showed a similar inhibition of elongation after a UV-B treatment by UV-B as WT plants, elongation of *atr* primary roots was more inhibited than WT or *atm* roots (**Figure 8C**). Under control conditions, the meristematic zone length from *atr* roots was similar to that from WT roots, with a similar number of cells of similar length (**Figures 8D–F**). However, 1 day after a UV-B treatment, the meristem size was significantly more shortened, showing a larger decrease in the number of cortex cells than that in the meristematic zone of WT Col-0 seedlings, but a similar increase in cell length (**Figures 8D–F**). Moreover, *atr* mutants accumulated more dead cells after UV-B exposure, both 1 and 4 days after the treatment (**Figure 8G**), while neither *uvr8* nor *mpk3* mutants showed differences in the number of dead cells compared to WT seedlings (**Supplementary Figures 2D,E, 3D**). Therefore, while inhibition of cell proliferation by UV-B in the leaves and in the primary roots require the activity of GRF3, MPK3 only regulates cell proliferation in the leaves while ATR is required for proper inhibition of cell division in the roots.

In previous studies, mutants in DNA repair enzymes involved in Nucleotide Excision Repair showed a more important decrease in hypocotyl elongation by UV-B than WT seedlings (Gardner et al., 2009; Biever et al., 2014). These results suggested that direct damage to DNA may regulate photomorphogenic responses. In our lab, we previously demonstrated that Arabidopsis mutants in *MSH2* and *MSH6*, encoding two proteins that participate in the Mismatch Repair DNA pathway, were deficient in DNA repair after UV-B exposure (Lario et al., 2011). Thus, we investigated whether *msh6* primary roots were more affected by UV-B than WT roots. Our results showed that elongation of primary roots from *msh6* mutants was similarly inhibited by UV-B radiation as those from WT seedlings, and this was also true when irradiation was done using different UV-B fluences (**Figure 8H**). Interestingly, elongation of *msh6* primary roots was similarly inhibited by UV-B exposure when seedlings were allowed to recover under normal photoperiod in the presence of

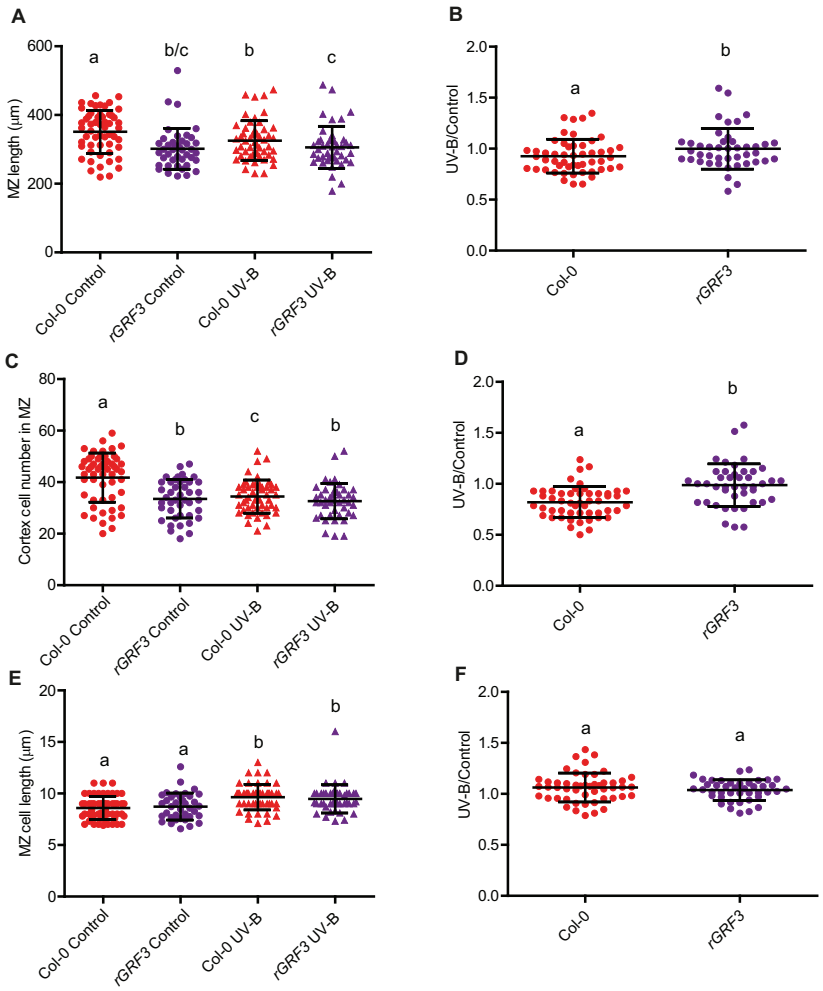

FIGURE 6 | UV-B differently affects cell proliferation in the primary root meristematic zone of WT Col-0 and *rGRF3* seedlings. **(A)** Root meristematic zone length, **(C)** cortex cell number, and **(E)** cortex cell length from UV-B treated or control WT Col-0 and *rGRF3* seedlings 4 days after the treatment. Different letters indicate statistically significant differences applying two-way ANOVA (Tukey's test, $P < 0.05$). **(B)** Ratio between meristematic zone length, **(D)** cortex cell number, and **(F)** cortex cell area values measured after UV-B exposure vs. those under control conditions in primary roots are shown. Different letters indicate statistically significant differences applying one-way ANOVA (Dunn test, $P < 0.05$). Results show the individual values and the average from at least eight independent biological replicates ± S.D. from one experiment. Three independent experiments were performed with similar results.

white light that allow photorepair of damaged DNA, or under darkness (**Supplementary Figure 4**). These results demonstrate that although *msh6* mutants accumulate more DNA damage after UV-B exposure than WT plants, they show a similar inhibition of root growth at similar UV-B fluences and also under conditions that do not allow photorepair, suggesting that levels of DNA damage accumulated in WT plants after UV-B exposure are sufficient to activate inhibition of cell proliferation in the primary root meristems.

Ultraviolet-B Inhibition of Root Elongation Differ in Arabidopsis Ecotypes and Accessions

Finally, we analyzed weather the different primary root phenotypes in Col-0 seedlings after UV-B exposure were also observed in other Arabidopsis accessions and ecotypes. When primary root elongation was compared in Col-0, Col-3, Col-4, Ws, and Ler seedlings after UV-B exposure, all lines showed a significant inhibition of growth (**Figure 9**). However, while primary roots from Col-3 were longer than those from Col-0 seedlings, after UV-B exposure at different fluences, primary roots from both accessions showed a similar length (**Figures 9A–D**). It is interesting to note that higher inhibition of primary root elongation in Col-3 seedlings occurs even at low UV-B fluences, and the inhibitory effect is similar under all UV-B conditions investigated (**Figure 9D**). Thus, elongation of Col-3 primary roots is more affected by UV-B. In contrast; primary roots from all other accessions/ecotypes analyzed showed a similar inhibition of elongation after a UV-B treatment as Col-0 (**Figures 9E–H**).

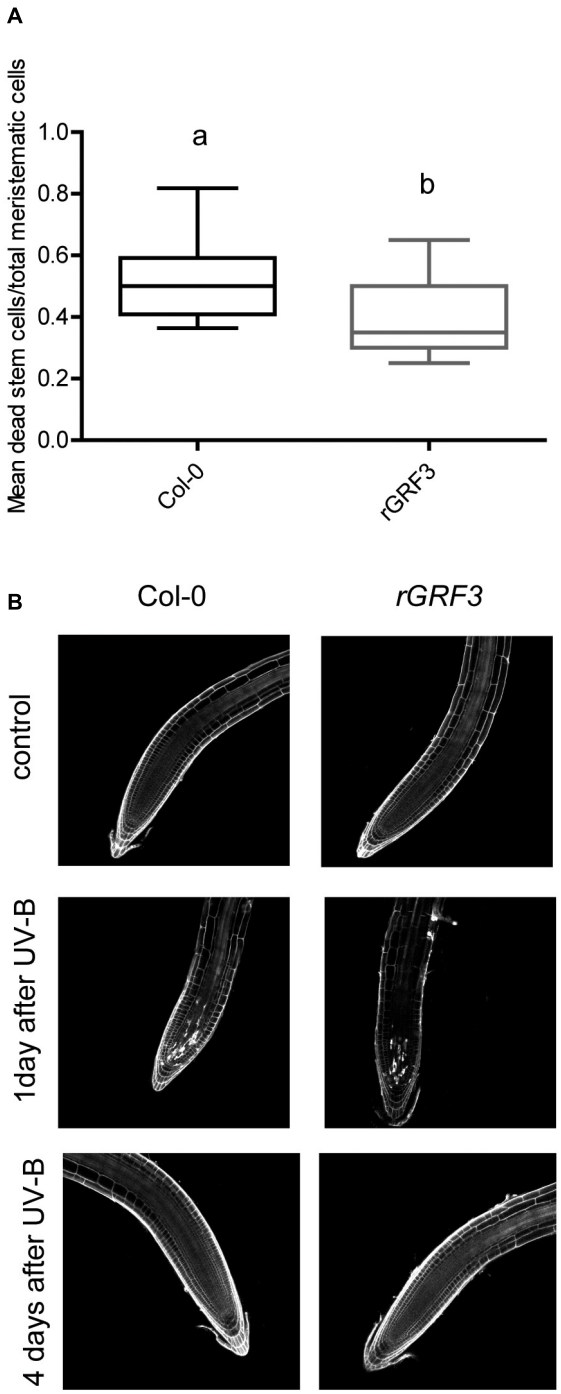

FIGURE 7 | UV-B affects programmed cell death in the root meristematic zone of *rGRF3* seedlings. **(A)** Number of stem cells that are dead 1 day after UV-B exposure in WT Col-0 and *rGRF3* primary root meristems. Results show the individual values and the average from at least 15 independent biological replicates ± S.D. from one experiment. Different letters represent statistically significant differences applying a mixed generalized linear model with a Poisson distribution ($p > 0.05$). Three independent experiments were performed with similar results. **(B)** Representative images of primary roots of WT Col-0 and *rGRF3* seedlings in which stem cells and adjacent daughter cells were PI staining to count dead stem cells per root 1 and 4 days after UV-B exposure or in control conditions without UV-B.

In addition, all accessions except Col-3 showed a similar inhibition of the meristematic zone length after UV-B exposure, with a similar decrease in cell proliferation after the treatment (**Figure 10** and **Supplementary Figure 5**). In contrast, Col-3 meristematic zone was longer than that from Col-0 roots, but after the treatment, meristems from both accessions showed a similar length (**Figure 10A**). The higher decrease in the meristem size in Col-3 was a consequence of a higher inhibition of cell proliferation after the treatment (**Figures 10C,D**), while the increase in cell length was similar in both accessions (**Figures 10E,F**). Together, Col-3 primary roots are more sensitive to UV-B than those from the other accessions and ecotypes analyzed.

Interestingly, when PCD was studied 1 day after a UV-B exposure, not only Col-3 but also Col-4 primary roots meristems showed decreased number of dead cells compared to Col-0, while Ler and Ws roots showed similar PCD as Col-0 (**Figures 10G,H** and **Supplementary Figure 5**). Interestingly, all accessions showed similar DNA damage accumulation after UV-B exposure (**Supplementary Figures 5J,K**). These results demonstrate that while primary roots from all accessions analyzed are affected by a UV-B, there is natural variation in the responses measured.

DISCUSSION

In the primary roots of *Arabidopsis thaliana* plants, the meristematic zone located in the root tips contains cells that actively divide and elongate; while the elongation zone includes cells that no longer divide but only elongate, and the mature zone has cells that no longer divide nor elongate (Fiorani and Beemster, 2006). Cells are generally organized in parallel files along which one-dimensional developmental gradients are present. Therefore, primary root elongation is mostly a consequence of cell proliferation in the meristematic zone, and cell expansion in the meristematic and elongation zones. In this work, we investigated the effect of a single UV-B radiation treatment on the primary roots of Arabidopsis seedlings, and we demonstrated that UV-B exposure can inhibit its elongation by decreasing cell proliferation in the meristematic zone. We also here show that the decrease in cell proliferation is accompanied with an increase in cell elongation; thus, a compensating effect occurs to balance the inhibition of cell proliferation measured. However, the effect of UV-B on cell proliferation is more important than that on cell expansion, and the consequence of this is that the meristem size of irradiated primary roots is smaller than that from control roots (**Figure 2**). In contrast, cortex cell number and cortex cell length in the elongation zone was not affected by the UV-B treatment (**Figure 2**); thus, inhibition of primary root elongation by UV-B is probably mostly due to an inhibition of cell proliferation in the meristematic zone of Col-0 seedlings. Interestingly, when we previously studied the effect of a UV-B treatment on Arabidopsis leaves, which were grown at similar intensities as those used in this study, our results showed that in proliferating leaves, only cell division was affected, while cell size was not modified (Casadevall et al., 2013). Moreover, similar experiments using maize plants also demonstrated that

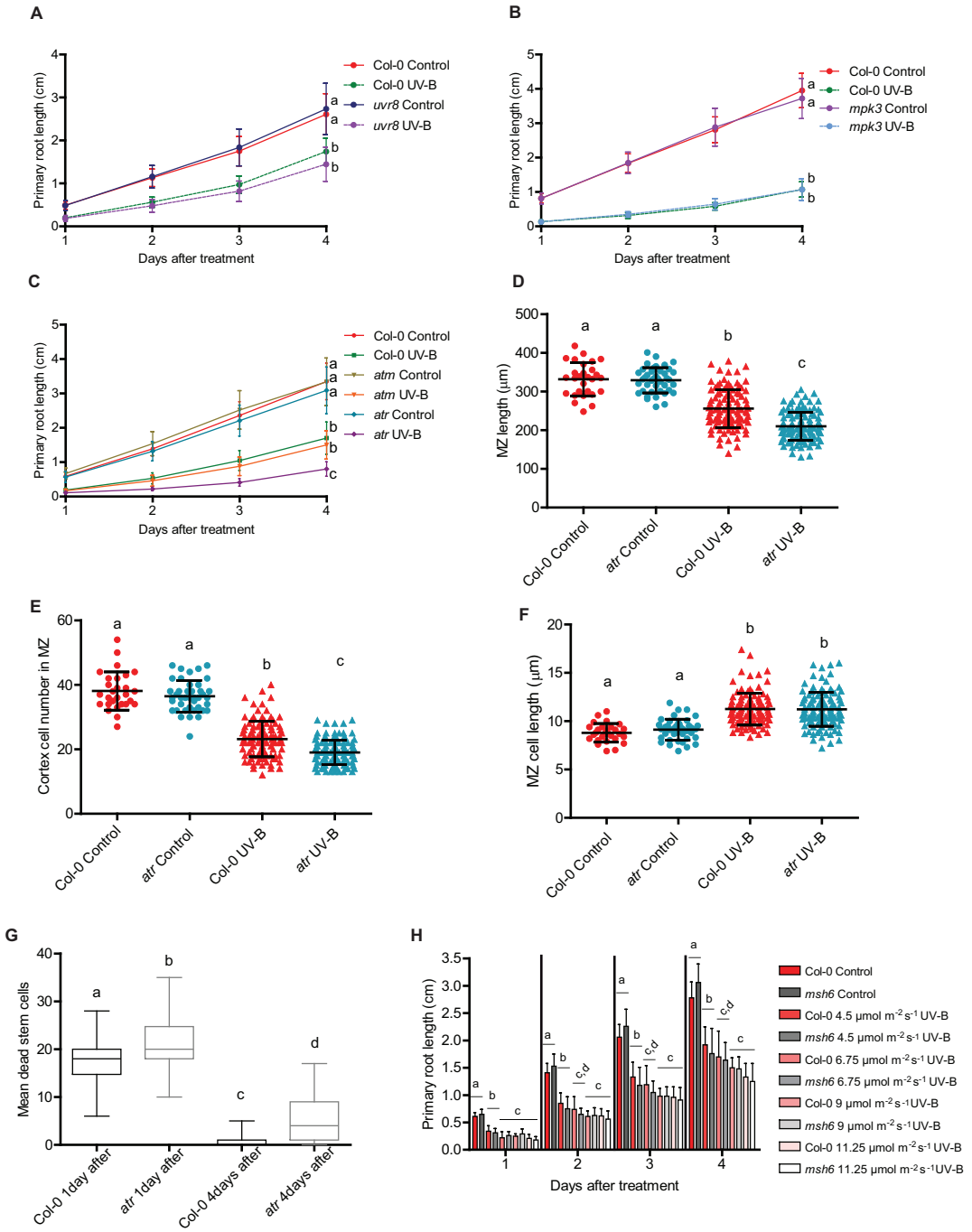

FIGURE 8 | Primary root growth inhibition assays in WT Col-0, *uvr8*, *mpk3*, *msh6*, *atm,* and *atr* seedlings after UV-B exposure. **(A–C)** Graphs of average root lengths in WT Col-0, *uvr8* **(A)**, *mpk3* **(B)**, *atm* and *atr* **(C)** seedlings after UV-B exposure for 1 h at 9 µmol m^{-2} s^{-1} UV-B at or grown under control conditions without UV-B. Results show the individual values and the average from at least 20 biological replicates ± S.D. from one experiment. Three independent experiments were performed with similar results. Different letters indicate statistically significant differences applying two-way ANOVA (Tukey's test, $P < 0.05$). **(D)** Root meristematic zone length, **(E)** cortex cell number, and **(F)** cortex cell length from UV-B treated or control WT Col-0 and *atr* seedlings 1 day after the treatment. Different letters indicate statistically significant differences applying two-way ANOVA (Tukey's test, $P < 0.05$). **(G)** Number of stem cells that are dead 1 and 4 days after UV-B exposure in WT Col-0 and *atr* primary root meristems. Different letters represent statistically significant differences applying a mixed generalized linear model with a Poisson distribution ($p > 0.05$). Results show the individual values and the average from at least 15 independent biological replicates ± S.D. from one experiment. Three independent experiments were performed with similar results. **(H)** Fluence response curves of primary root inhibition by UV-B in Col-0 and *msh6* seedlings. Seedlings were irradiated at 4.5, 6.75, 9, or 11.25 µmol m^{-2} s^{-1} UV-B for 1 h. Results show the individual values and the average from at least 20 biological replicates ± S.D. from one experiment. Three independent experiments were performed with similar results. Different letters indicate statistically significant differences applying two-way ANOVA (Tukey's test, $P < 0.05$).

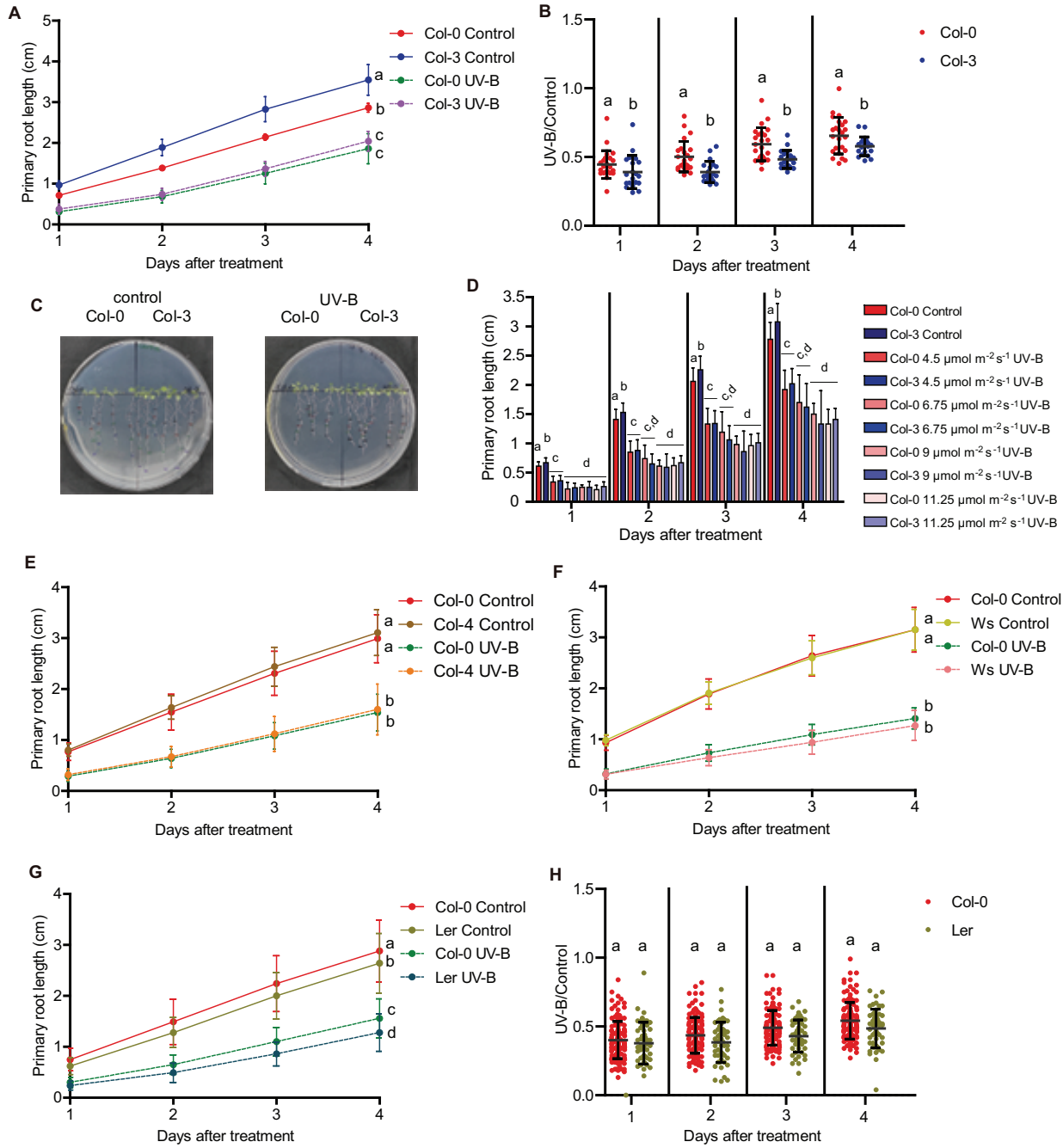

FIGURE 9 | Primary root growth inhibition assays in WT Col-0, Col-3, Col-4, Ws, and Ler seedlings after UV-B exposure. **(A)** Graphs of average root lengths in WT Col-0 and Col-3 seedlings after UV-B exposure for 1 h at 9 μmol m^{-2} s^{-1} UV-B or grown under control conditions without UV-B. **(B)** Ratio between root lengths after UV-B exposure vs. under control conditions. **(C)** Representative pictures of one experiment showing primary roots from control and UV-B irradiated WT Col-0 and Col-3 seedlings. **(D)** Fluence response curves of primary root inhibition by UV-B in Col-0 and Col-3 seedlings. Seedlings were irradiated at 4.5, 6.75, 9, or 11.25 μmol m^{-2} s^{-1} UV-B for 1 h. **(E–G)** Graphs of average root lengths in WT Col-0 and Col-4 **(E)**, Ws **(F)**, and Ler **(G)** seedlings after UV-B exposure or grown under control conditions without UV-B. Results show the individual values and the average from at least 20 biological replicates ± S.D. from one experiment. **(H)** Ratio between Col-0 and Ler root lengths after UV-B exposure vs. under control conditions. Three independent experiments were performed with similar results. Different letters indicate statistically significant differences applying one-way ANOVA (Dunn test, $P < 0.05$).

cell number in the meristematic zone of growing leaves was decreased by UV-B but not cell size, and this decrease in cell number caused a decrease in the meristematic zone size (Fina et al., 2017). Maize is a monocot plant, and elongation of growing leaves occurs in a similar way as primary root elongation in Arabidopsis (Fiorani and Beemster, 2006; Fina et al., 2017).

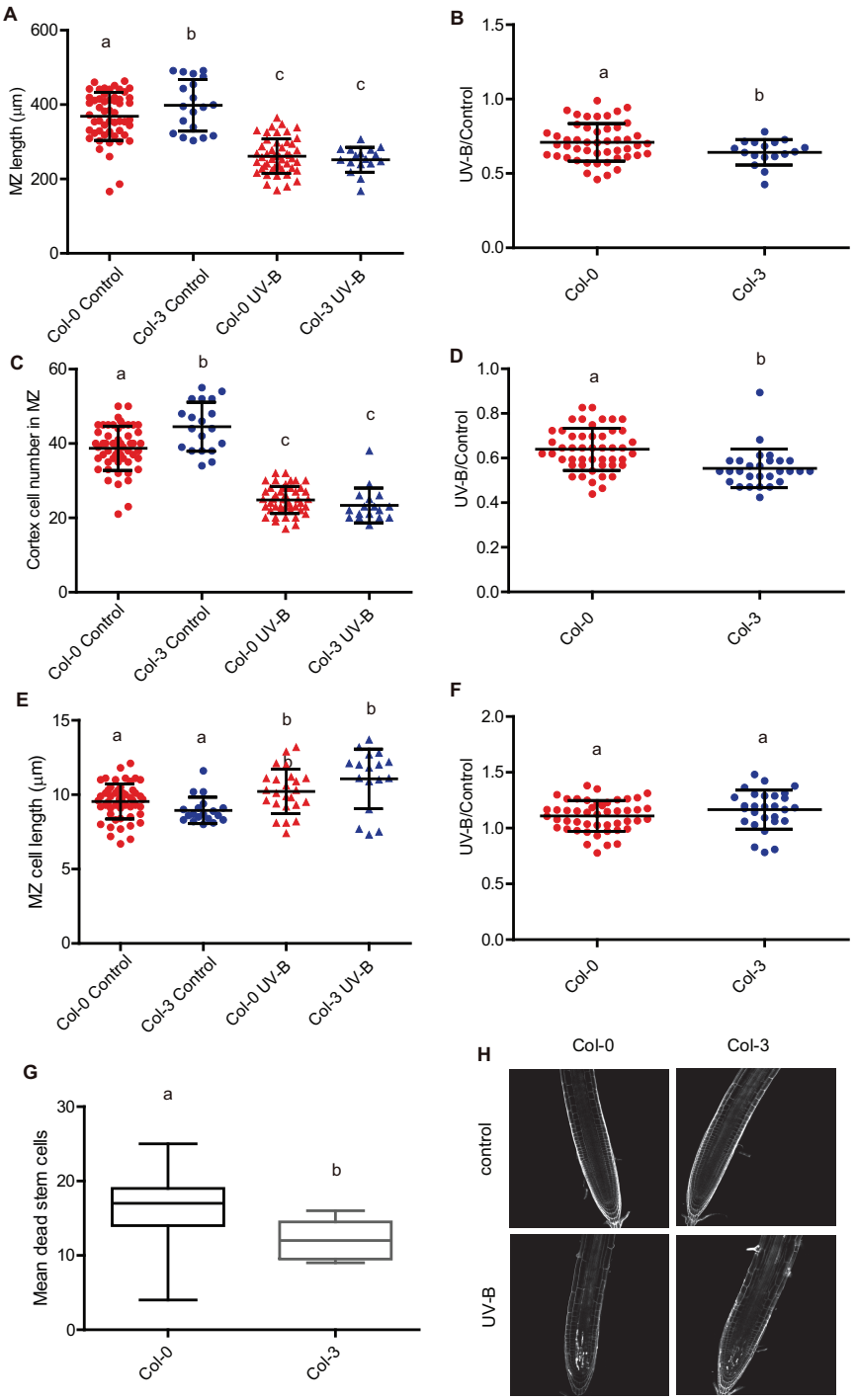

FIGURE 10 | UV-B differently affects cell proliferation and PCD in the root meristematic zone of WT Col-0 and Col-3 seedlings. **(A)** Root meristematic zone length, **(C)** cortex cell number, and **(E)** cortex cell length from UV-B treated or control WT Col-0 and Col-3 seedlings 1 day after the treatment. Different letters indicate statistical significant differences applying two-way ANOVA (Tukey's test, $P < 0.05$). **(B)** Ratio between meristematic zone length, **(D)** cortex cell number, and **(F)** cortex cell area values measured after UV-B exposure vs. those under control conditions in primary roots are shown. Different letters indicate statistically significant differences applying one-way ANOVA (Dunn test, $P < 0.05$). Results show the individual values and the average from at least eight independent biological replicates ± S.D. from one experiment. **(G)** Number of stem cells that are dead 1 day after UV-B exposure in WT Col-0 and Col-3 primary root meristems. Different letters represent statistically significant differences applying a mixed generalized linear model with a Poisson distribution ($p > 0.05$). Results show the individual values and the average from at least 15 independent biological replicates ± S.D. from one experiment. Three independent experiments were performed with similar results. **(H)** Representative images of primary roots of WT Col-0 and Col-3 seedlings in which stem cells and adjacent daughter cells were PI staining to count dead stem cells per root 1 day after UV-B exposure or in control conditions without UV-B.

Our previous study using maize leaves showed that UV-B affected the meristematic zone size without changing the elongation zone, similarly as what is now described for primary roots from *Arabidopsis thaliana* seedlings (Fina et al., 2017; **Figure 2**). Together, these results demonstrate that exposure to UV-B at our experimental conditions affects cell proliferation in leaves and roots but only cell expansion in the root meristems. The increase in cell size could be a consequence of changes in the cell wall structure or composition occurring after exposure, as previously described in the leaf cell walls of mutants with altered sensitivity to this radiation (Maulión et al., 2019), to changes in endoreduplication levels in the cells, which are sometimes measured after UV-B exposure in leaf cells (Radziejwoski et al., 2011), or to other UV-B modulated mechanisms that could specifically affect cell size in the roots not yet characterized.

On the other hand, our results also show that UV-B inhibits cell division in the primary root meristems at different developmental stages, but the degree of inhibition and the effect in cell elongation varies according to the development stage of the meristematic zone. Interestingly, 4 days after irradiation, meristems from UV-B exposed plants were still smaller than those control plants, with less but longer cells (**Figure 3**), demonstrating that the developmental consequences of a UV-B treatment are maintained several days in the absence of the stress. On the contrary, while the number of dead cells in the meristems 1 day after a UV-B treatment was substantial, 4 days after the treatment most roots showed a significant recovery with very low number of dead cells (**Figure 4**). Therefore, in the root meristematic zone there is a faster recovery from PCD than from developmental changes that occur after UV-B exposure. In agreement with the results presented here, Johnson et al. (2018) showed that, after DNA damage occurs, programmed cell death in the root meristematic cells triggers its regeneration and enables growth recovery. This process is regulated by the activity of the transcription factor SUPPRESSOR OF GAMMA RESPONSE 1 (SOG1), which activates DNA damage-induced programmed cell death. In this way, proper activation and then recovery of PCD after DNA damage from UV-B is required to undergo normal cell division rates. Thus, and as also proposed by Johnson et al. (2018), recovery from programmed cell death could be a signal employed by plants to restore growth after repair of DNA damage following UV-B exposure. Previously, Gardner et al. (2009) showed that, similarly as what we here report occurs in Arabidopsis seedlings primary roots, UV-B exposure induces growth inhibition of etiolated seedlings. As a consequence, inhibition of hypocotyl elongation was observed, which depended on photon fluence. In our experiments, the degree of primary root inhibition also depended on UV-B fluence. Mutants in DNA repair enzymes involved in Nucleotide Excision Repair showed a more important decrease in hypocotyl elongation by UV-B than WT seedlings, suggesting that direct damage to DNA may regulate photomorphogenic responses, probably repressing cell cycle progression (Gardner et al., 2009; Biever et al., 2014). In contrast, in our experiments, *msh6* mutants, which are deficient in DNA repair after UV-B exposure (Lario et al., 2011) showed a similar inhibition of primary root elongation as WT seedlings at all UV-B fluences studied, and even under dark conditions that do not allow photorepair of the DNA by photolyases. This suggests that levels of DNA damage accumulated in WT plants after UV-B exposure are sufficient to inhibit cell proliferation in the primary root meristems. Thus, inhibition of cell proliferation caused by UV-B are probably a consequence of an activation of the DNA damage response that could occur at different fluences in the different organs. It is important to note that, as reviewed by Biever and Gardner (2016), it is evident that some photomorphogenic responses, such as the inhibition of hypocotyl and primary root elongation in Arabidopsis seedlings, respond to UV-B-induced DNA damage and do not require the activation of the UVR8 photoreceptor, and this could also be dependent on the UV-B fluence used during the irradiation treatments.

Interestingly, while complete inhibition of the primary root elongation by UV-B requires full exposure of this organ, irradiation of the leaves and shoots provokes a partial but significant decrease in the root length (**Figure 1**). Thus, it is possible that signals from these tissues could be transmitted to the roots. Previously, we demonstrated that maize plants that were irradiated with UV-B lamps at similar intensities used in the experiments described here showed transcriptome changes in the roots, which were not directly exposed to UV-B (Casati and Walbot, 2004). In this previous study, transcriptome changes were also measured in different types of maize shielded tissues besides roots, such as immature ears and shielded leaves, and these different tissues all displayed altered transcriptome profiles after exposure of the plant to UV-B (Casati and Walbot, 2004). Thus, some signal(s) must be transmitted from irradiated to shielded tissues in different plants species, and in Arabidopsis, these signals could regulate root growth in the absence of direct exposure.

Our data provides evidence that primary root inhibition by UV-B is at least in part regulated by GRF3, a transcription factor from the Growth regulating family that is a target of the microRNA miR396. In the experiments presented here, the decrease in cortex cell number after a UV-B exposure in the primary root meristems was partially compensated by an increase in cell length, but the regulation of cell elongation was independent of GRF3, as cells from *rGRF3* roots were similarly elongated as those from WT after a treatment. The role of GRF3 and other GRFs in root growth has been previously described (Rodriguez et al., 2015; Ercoli et al., 2018). While decreased levels of GRFs and their co-activators GRF-INTERACTING FACTORS (GIFs) leads to an increased size of the primary root meristem, a reduction in miR396 levels, *rGRF2* or *3* expression or *GIF* overexpression decrease the meristem size. In agreement, primary roots from *rGRF3* seedlings in our experiments were also shorter, with smaller meristematic zones (**Figures 5**, **6**). In the roots, GRFs and GIFs regulate *PLETHORA* genes, which are transcription factors that control root growth (Rodriguez et al., 2015; Ercoli et al., 2018). GRF2/3 are expressed in actively dividing cells in the root meristems, and together with GIFs directly decrease *PLETHORA* genes transcription (Rodriguez et al., 2015; Ercoli et al., 2018). Thus, the regulation of cell proliferation by GRFs after UV-B exposure in the roots may also involve the participation of PLETHORA transcription factors.

In Arabidopsis and maize, inhibition of cell proliferation in the leaves by UV-B is regulated by the microRNA miR396 (Casadevall et al., 2013; Fina et al., 2017). miR396 also regulates primary root elongation after UV-B exposure in Arabidopsis (Gómez et al., 2019). Interestingly, it was recently reported that a different microRNA, miR5642, has a potential role regulating UV-B responses during early development in Arabidopsis seedlings (Dukowic-Schulze et al., 2021). This microRNA seems to participate in hypocotyl growth inhibition after UV-B exposure, regulating transcript levels of putative target mRNAs. Both miR396 and miR5642 participate in DNA damage responses activated by UV-B, in particular regulating cell cycle arrest (Casadevall et al., 2013; Dukowic-Schulze et al., 2021). Thus, it would be interesting to investigate whether these two miRNAs participate in a common pathway in response to UV-B.

We have previously showed that, in the leaves, inhibition of cell division by UV-B required the presence of MPK3 (Casadevall et al., 2013). This MPK, together with MPK6 and their phosphatase MKP1, participates in UV-B stress responses in Arabidopsis leaves (González Besteiro and Ulm, 2013). In this species, both MPK3 and MPK6 are activated by UV-B–induced DNA damage. Our results show that, in the primary root meristems, inhibition of cell proliferation by UV-B is independent of MPK3 (**Figure 8** and **Supplementary Figure 3**). However, roots from *atr* seedlings are highly sensitive to a UV-B treatment, showing a higher inhibition of root elongation with a larger decrease in the meristem size of irradiated seedlings (**Figure 8**). In the leaves of Arabidopsis plants exposed to UV-B, *atr* mutants did not show differences in cell proliferation with WT leaves (Casadevall et al., 2013). ATR participates in a different UV-B activated pathway from MPK3 and MPK6, which seems to be mainly present in the roots (González Besteiro and Ulm, 2013). Thus, the results presented here demonstrate that while GRF3 regulates cell proliferation under UV-B conditions both in the leaves and roots, MPK3 is only required for this regulation in the leaves; and a deficiency in ATR expression significantly affects cell division in UV-B exposed roots. Interestingly, *rGRF3* roots showed a lower number of dead cells after UV-B than WT roots (**Figure 7**), suggesting the GRF3 not only regulates cell proliferation but also other DNA damage responses. Finally, we here also demonstrate that, in our experimental conditions, inhibition of cell proliferation in the roots and leaves after UV-B exposure is independent of the activity of the UV-B photoreceptor UVR8 and the protein kinase ATM (Casadevall et al., 2013; **Figure 8** and **Supplementary Figure 2**). Interestingly, inhibition of hypocotyl elongation by UV-B was previously reported to be independent of the presence of any of the known photoreceptors including UVR8 (Gardner et al., 2009; Biever et al., 2014); which is in agreement with our results. Thus, it is possible that inhibition of hypocotyl and primary root elongation may share at least some components of a common pathway.

Last, we investigated the effect of UV-B exposure in the roots of different Arabidopsis accessions and ecotypes. Our results demonstrate that despite there are differences in the responses to UV-B analyzed between some accessions; all genotypes responded to the treatment, showing an inhibition of cell proliferation in the root meristems that produced, at least in part, an inhibition in primary root elongation. Moreover, UV-B exposure provoked an induction of PCD in the primary root meristems of all plants studied, and they all showed a similar accumulation of DNA damage after UV-B exposure. These data demonstrate that primary roots from all accessions analyzed are affected by UV-B; however, there is natural variation in the UV-B responses in some ecotypes.

CONCLUSION

We here show that inhibition of primary root elongation is a consequence of an inhibition of cell proliferation in the meristematic zone of the primary roots that is regulated by GRF3, while the elongation zone size is not affected by the treatment. The decrease in cell number after UV-B exposure is partially compensated by an increase in cell length in the root meristem; however, this compensation is not enough to maintain the meristem size of control roots grown in the absence of UV-B. Our data also demonstrates that there is natural variation in the root responses to UV-B.

DATA AVAILABILITY STATEMENT

The original contributions presented in the study are included in the article/**Supplementary Material**, further inquiries can be directed to the corresponding author.

AUTHOR CONTRIBUTIONS

MS and PC conceived and designed the study. MS, LS, and MG performed the experiments. MS, LS, MG, and PC analyzed the data. PC wrote the manuscript. All authors contributed to the article and approved the submitted version.

FUNDING

This research was supported by the Argentina FONCyT grants PICT 2018-798 and 2019-167 to PC.

ACKNOWLEDGMENTS

We thank Mariana Giro (CEFOBI) for confocal microscopy analysis and Javier Palatnik and Ramiro Rodriguez Virasoro for their discussions on the results and experiments.

SUPPLEMENTARY MATERIAL

The Supplementary Material for this article can be found online at: https://www.frontiersin.org/articles/10.3389/fpls.2022.829336/full#supplementary-material

REFERENCES

Biever, J. J., Brinkman, D., and Gardner, G. (2014). UV-B inhibition of hypocotyl growth in etiolated *Arabidopsis thaliana* seedlings is a consequence of cell cycle arrest initiated by photodimer accumulation. *J. Exp. Bot.* 65, 2949–2961. doi: 10.1093/jxb/eru035

Biever, J. J., and Gardner, G. (2016). The relationship between multiple UV-B perception mechanisms and DNA repair pathways in plants. *Environ. Exp. Bot.* 124, 89–99. doi: 10.1016/j.envexpbot.2015.12.010

Bourbousse, C., Vegesna, N., and Law, J. A. (2018). SOG1 activator and MYB3R repressors regulate a complex DNA damage network in *Arabidopsis*. *Proc. Natl. Acad. Sci. U. S. A.* 115, E12453–E12462. doi: 10.1073/pnas.1810582115

Casadevall, R., Rodriguez, R. E., Debernardi, J. M., Palatnik, J. F., and Casati, P. (2013). Repression of growth regulating factors by the microRNA396 inhibits cell proliferation by UV-B radiation in *Arabidopsis* leaves. *Plant Cell* 25, 3570–3583. doi: 10.1105/tpc.113.117473

Casati, P., and Walbot, V. (2004). Rapid transcriptome responses of maize to UV-B in irradiated and shielded tissues. *Genome Biol.* 5:R16.

Dotto, M., and Casati, P. (2017). Developmental reprogramming by UV-B radiation in plants. *Plant Sci.* 267, 96–101. doi: 10.1016/j.plantsci.2017.09.006

Dukowic-Schulze, S., Harvey, A., Garcia, N., Chen, C., and Gardner, G. (2021). UV-B Irradiation Results in Changes in Elongation, Cell Cycle, and Decreased Endoreduplication Mediated by miR5642. *Photochem. Photobiol.* [Online ahead of print] doi: 10.1111/php.13574

Ercoli, M. F., Ferela, A., Debernardi, J. M., Perrone, A. P., Rodriguez, R. E., and Palatnik, J. F. (2018). GIF transcriptional co-regulators control root meristem homeostasis. *Plant Cell* 30, 347–359. doi: 10.1105/tpc.17.00856

Fina, J. P., Casadevall, R., AbdElgawad, H., Prinsen, E., Markakis, M., Beemster, G. T., et al. (2017). UV-B inhibits leaf growth through changes in growth regulating factors and gibberellin levels. *Plant Physiol.* 174, 1110–1126. doi: 10.1104/pp.17.00365

Fiorani, F., and Beemster, G. T. S. (2006). Quantitative analyses of cell division in plants. *Plant Mol. Biol.* 60, 963–979. doi: 10.1007/s11103-005-4065-2

Furukawa, T., Curtis, M. J., Tominey, C. M., Duong, Y. H., Wilcox, B. W. L., Aggoune, D., et al. (2010). A shared DNA-damage-response pathway for induction of stem-cell death by UVB and by gamma irradiation. *DNA Repair* 9, 940–948. doi: 10.1016/j.dnarep.2010.06.006

Gardner, G., Lin, C., Tobin, E. M., Loehrer, H., and Brinkman, D. (2009). Photobiological properties of the inhibition of etiolated *Arabidopsis* seedling growth by ultraviolet-B irradiation. *Plant Cell Environ.* 32, 1573–1583. doi: 10.1111/j.1365-3040.2009.02021.x

Gómez, M. S., Falcone Ferreyra, M. L., Sheridan, M. L., and Casati, P. (2019). *Arabidopsis* E2Fc is required for the DNA damage response under UV-B radiation epistatically over the microRNA396 and independently of E2Fe. *Plant J.* 97, 749–764. doi: 10.1111/tpj.14158

González Besteiro, M. A., and Ulm, R. (2013). ATR and MKP1 play distinct roles in response to UV-B stress in *Arabidopsis*. *Plant J.* 73, 1034–1043. doi: 10.1111/tpj.12095

Hu, Z., Cools, T., and De Veylder, L. (2016). Mechanisms Used by Plants to Cope with DNA Damage. *Annu. Rev. Plant Biol.* 67, 439–462. doi: 10.1146/annurev-arplant-043015-111902

Jiang, L., Wang, Y., Bjorn, L. O., and Li, S. (2011). UV-B-induced DNA damage mediates expression changes of cell cycle regulatory genes in *Arabidopsis* root tips. *Planta* 233, 831–841. doi: 10.1007/s00425-010-1340-5

Johnson, R. A., Conklin, P. A., Tjahjadi, M., Missirian, V., Toal, T., Brady, S. M., et al. (2018). SUPPRESSOR OF GAMMA RESPONSE1 Links DNA Damage Response to Organ Regeneration. *Plant Physiol.* 176, 1665–1675. doi: 10.1104/pp.17.01274

Lario, L. D., Ramirez-Parra, E., Gutierrez, C., Casati, P., and Spampinato, C. P. (2011). Regulation of plant MSH2 and MSH6 genes in the UV-B induced DNA damage response. *J. Exp. Bot.* 62, 2925–2937. doi: 10.1093/jxb/err001

Leasure, C. D., Tong, H., Yuen, G., Hou, X., Sun, X., and He, Z.-H. (2009). ROOT UV-B SENSITIVE2 Acts with ROOT UV-B SENSITIVE1 in a Root Ultraviolet B-Sensing Pathway. *Plant Physiol.* 150, 1902–1915. doi: 10.1104/pp.109.139253

Manova, V., and Gruszka, D. (2015). DNA damage and repair in plants – from models to crops. *Front. Plant Sci.* 6:885. doi: 10.3389/fpls.2015.00885

Maulión, E., Gomez, M. S., Bustamante, C. A., and Casati, P. (2019). AtCAF-1 mutants show different DNA damage responses after ultraviolet-B than those activated by other genotoxic agents in leaves. *Plant Cell Environ.* 42, 2730–2745. doi: 10.1111/pce.13596

Parihar, P., Singh, S., Singh, R., Singh, V. P., and Prasad, S. M. (2015). Changing scenario in plant UV-B research: UV-B from a generic stressor to a specific regulator. *J. Photochem. Photobiol. B.* 153, 334–343. doi: 10.1016/j.jphotobiol.2015.10.004

Podolec, R., Demarsy, E., and Ulm, R. (2021). Perception and Signaling of Ultraviolet-B Radiation in Plants. *Annu. Rev. Plant Biol.* 72, 793–822. doi: 10.1146/annurev-arplant-050718-095946

Radziejwoski, A., Vlieghe, K., Lammens, T., Berckmans, B., Maes, S., Jansen, M. A. K., et al. (2011). Atypical E2F activity coordinates PHR1 photolyase gene transcription with endoreduplication onset. *EMBO J.* 30, 355–363. doi: 10.1038/emboj.2010.313

Rizzini, L., Favory, J.-J., Cloix, C., Faggionato, D., O'Hara, A., Kaiserli, E., et al. (2011). Perception of UV-B by the *Arabidopsis* UVR8 Protein. *Science* 332, 103–106. doi: 10.1126/science.1200660

Rodriguez, R. E., Ercoli, M. F., Debernardi, J. M., Breakfield, N. W., Mecchia, M. A., Sabatini, M., et al. (2015). MicroRNA miR396 regulates the switch between stem cells and transit-amplifying cells in *Arabidopsis* roots. *Plant Cell* 27, 3354–3366. doi: 10.1105/tpc.15.00452

Rodriguez, R. E., Mecchia, M. A., Debernardi, J. M., Schommer, C., Weigel, D., and Palatnik J. F. (2010). Control of cell proliferation in *Arabidopsis thaliana* by microRNA miR396. *Development* 137, 103–112.

Tong, H., Leasure, C. D., Hou, X., Yuen, G., Briggs, W., and He, Z.-H. (2008). Role of root UV-B sensing in *Arabidopsis* early seedling development. *Proc. Natl. Acad. Sci. U. S. A.* 105, 21039–21044. doi: 10.1073/pnas.0809942106

Ulm, R. (2003). "Molecular genetics of genotoxic stress signalling in plants," in *Plant Responses to Abiotic Stress. Topics in Current Genetics*, eds H. Heribert and K. Shinozaki (Heidelberg: Springer), 217–240. doi: 10.1007/978-3-540-39402-0_9

van Gelderen, K., Kang, C., and Pierik, R. (2018). Light Signaling, Root Development, and Plasticity. *Plant Physiol.* 176, 1049–1060. doi: 10.1104/pp.17.01079

Conflict of Interest: The authors declare that the research was conducted in the absence of any commercial or financial relationships that could be construed as a potential conflict of interest.

frontiers in Plant Science

ORIGINAL RESEARCH
published: 31 March 2022
doi: 10.3389/fpls.2022.840720

Low Fluence Ultraviolet-B Promotes Ultraviolet Resistance 8-Modulated Flowering in *Arabidopsis*

*Anna Zioutopoulou, Eirini Patitaki, Liz O'Donnell and Eirini Kaiserli**

College of Medical, Veterinary and Life Sciences, Institute of Molecular, Cell and Systems Biology, University of Glasgow, Glasgow, United Kingdom

Ultraviolet-B (UV-B) irradiation (280–320 nm) is an integral part of sunlight and a pivotal environmental cue that triggers various plant responses, from photoprotection to photomorphogenesis and metabolic processes. UV-B is perceived by ULTRAVIOLET RESISTANCE 8 (UVR8), which orchestrates UV-B signal transduction and transcriptional control of UV-B-responsive genes. However, there is limited information on the molecular mechanism underlying the UV-B- and UVR8-dependent regulation of flowering time in plants. Here, we investigate the role of UV-B and UVR8 in photoperiodic flowering in *Arabidopsis thaliana*. Our findings suggest that UV-B controls photoperiodic flowering in an ecotype-specific manner and that UVR8 acts as a negative regulator of UV-B-induced flowering. Overall, our research shows that UV-B modulates flowering initiation through the action of UVR8 at the transcriptional level.

Keywords: light, UV-B, *Arabidopsis*, flowering, photoperiod

OPEN ACCESS

Edited by:
Andres Romanowski, Utrecht University, Netherlands

Reviewed by:
Maria Jose De Leone, Consejo Nacional de Investigaciones Científicas y Técnicas (CONICET), Argentina
Agnieszka Katarzyna Banas, Jagiellonian University, Poland

***Correspondence:**
Eirini Kaiserli
eirini.kaiserli@glasgow.ac.uk

Specialty section:
This article was submitted to Plant Physiology, a section of the journal Frontiers in Plant Science

Received: *21 December 2021*
Accepted: *09 February 2022*
Published: *31 March 2022*

Citation:
Zioutopoulou A, Patitaki E, O'Donnell L and Kaiserli E (2022) Low Fluence Ultraviolet-B Promotes Ultraviolet Resistance 8-Modulated Flowering in Arabidopsis. Front. Plant Sci. 13:840720. doi: 10.3389/fpls.2022.840720

INTRODUCTION

Plants are sessile organisms that have evolved to adapt to environmental variation in order to ensure survival. Light, in particular, is an external stimulus that affects every aspect of a plant's life, from seed germination to the transition to the reproductive state by floral initiation (Sullivan and Deng, 2003). Plants are able to perceive the intensity, quality, duration, and even direction of light in order to phenotypically adjust according to their ever-changing environment (Montgomery and Lagarias, 2002). However, since plants have not evolved eyesight like organisms that belong to the animal kingdom, they employ proteins called photoreceptors which perceive light cues, allowing plants to respond to diurnal and seasonal light shifts (Briggs and Olney, 2001). This sophisticated mechanism grants the ability for plants to timely coordinate crucial developmental processes such as flowering initiation (Fornara et al., 2010). *Arabidopsis thaliana* is a facultative long-day plant and its flowering time is mediated through the function of two master orchestrators: FLOWERING LOCUS T (FT) and CONSTANS (CO) that are regulated by light, circadian rhythms, temperature, and hormones (Fornara et al., 2010). CO induces the expression of *FT* in a long-day-dependent fashion, through direct association with its promoter (Fornara et al., 2010). *CO* gene expression and protein stability is tightly regulated by light and circadian clock components (Imaizumi et al., 2005; Sawa et al., 2007; Song et al., 2012). For instance, FLAVIN-BINDING, KELCH REPEAT, F-BOX 1 (FKF1) and GIGANTEA (GI) facilitate the degradation of CYCLING DOF FACTOR (CDF) proteins which suppress the expression of *CO* and *FT* (Sawa et al., 2007; Song et al., 2012). Furthermore, GI stabilizes FKF1 and ZEITLUPE (ZTL), which act in synergy with their homolog

LOV KELCH PROTEIN 2 (LKP2) to degrade the DOF transcription factor CDF2 (Kim et al., 2007; Fornara et al., 2009). An additional circadian clock component that controls CO abundance is EARLY FLOWERING 3 (ELF3) (Hicks et al., 2001; Nusinow et al., 2011). In particular, ELF3 forms a complex with CONSTITUTIVE PHOTOMORPHOGENIC 1 (COP1) and GI which leads to the inactivation of GI and ultimately the repression of *CO* expression (Zhao et al., 2021).

Ultraviolet-B irradiation is an integral part of sunlight that reaches the earth and ranges from 280 to 315 nm. Although UV-B can be harmful to most living organisms, it simultaneously triggers various photomorphogenic responses in plants depending on the intensity (Jenkins, 2014). Plants perceive UV-B light through the function of UVR8, the only photoreceptor identified so far absorbing and mediating responses to UV-B light (Brown et al., 2005; Favory et al., 2009; Rizzini et al., 2011; Jenkins, 2014). Upon UV-B exposure, dimeric UVR8 undergoes structural alterations that lead to the photo-induced dissociation of the dimer into a monomeric active state (Heilmann et al., 2016). UVR8 activation is negatively regulated by REPRESSOR OF UV-B PHOTOMORPHOGENESIS 1 and 2 (RUP1 and RUP2), which facilitate the re-dimerization of the UVR8 monomers (Gruber et al., 2010; Heijde and Ulm, 2012). Upon monomerization, UVR8 translocates from the cytosol to the nucleus, where it interacts with COP1 an E3 ubiquitin ligase, to mediate photomorphogenic and photoprotection responses through the transcriptional activation of UV-B-responsive genes (Kaiserli and Jenkins, 2007; Cloix and Jenkins, 2008; Heijde and Ulm, 2012). In addition, the physical interaction between UVR8 and COP1 leads to the stabilization of bZIP transcription factor ELONGATED HYPOCOTYL 5 (HY5), granting the activation of HY5-induced genes involved in UV-B-associated photomorphogenic responses (Ulm et al., 2004; Huang et al., 2012).

UVR8 has been reported to antagonize shade avoidance and thermomorphogenic responses through the deactivation of PHYTOCHROME INTERACTING FACTOR 4 and 5 (PIF4 and PIF5) (Hayes et al., 2014, 2017). A recent study demonstrated that even in the absence of shade conditions the UVR8-mediated degradation of PIF4 and PIF5 is an essential step in UV-B signal transduction and UVR8-dependent hypocotyl growth inhibition (Tavridou et al., 2020).

Apart from photomorphogenic responses, low intensity UV-B also mediates circadian clock entrainment through the synergistic function of UVR8 and COP1 (Feher et al., 2011). However, circadian clock components can in turn attenuate UV-B responsiveness by repressing *UVR8*, *COP1,* and UV-B-induced genes to limit energy expenses (Feher et al., 2011). Indicatively, studies on arrhythmic *elf3* mutants showed elevated levels of UV-B-associated gene activation, however, this response did not promote UV-B stress tolerance (Feher et al., 2011).

Studies on the role of UV-B and/or UVR8 in regulating flowering time in plants are limited. *Landsberg erecta* (*Ler*) wild type plants subjected to UV-B irradiation demonstrated a delayed flowering phenotype, whilst the opposite was observed in *uvr8* mutants which flower earlier than their wild type counterparts (Hayes et al., 2014). In addition, the delay in flowering time in the *Arabidopsis Columbia-0* (*Col-0*) ecotype under long day (LD) and short day (SD) photoperiodic conditions has also been attributed to the UVR8-signaling trajectory. Flowering time analysis demonstrated that *uvr8* did not show a significant change in flowering time compared to a late flowering phenotype observed in *Col-0* in response to WL (white light) supplemented with short-time interval high fluence rate UV-B in LD (Dotto et al., 2018). Interestingly, the UVR8-repressor, RUP2, was shown to inhibit CO from binding to the *FT* promoter leading to a significant delay in flowering time in plants under a SD photoperiod supplemented with UV-B (Arongaus et al., 2018).

Although a lot of effort has been invested in elucidating how UVR8 and UV-B regulate plant responses, the molecular mechanism through which the aforementioned factors regulate flowering time under LDs remains largely uncharted. Our results indicate that constant low levels of UV-B (0.5 μmol $m^{-2}s^{-1}$) promote flowering initiation under LD photoperiodic conditions in *Col-0* and *Ler Arabidopsis* ecotypes. Additionally, UV-B induces early flowering of mutants lacking key flowering (*co*), UV-B (*uvr8* and *rup1rup2*) and light signaling (*cop1, pif4,* and *ztl*) components. Furthermore, we show that UVR8 acts as a negative regulator of UV-B-induced early flowering since *uvr8* mutants exhibited early flowering phenotypes under white light supplemented with UV-B. Overall, our data uncover that UV-B can modulate flowering initiation through the action of UVR8 at the transcriptional level.

MATERIALS AND METHODS

Plant Materials and Growth Conditions

The following wild type *Arabidopsis thaliana* ecotypes of *Col-0*, *Ler,* and *Cape Verde Islands* (*Cvi*) were used. Additionally, mutant and transgenic lines were used for flowering and gene expression studies in *Col-0* background [*rup1rup2* (Gruber et al., 2010; Vanhaelewyn et al., 2016), *cop1-4* (McNellis et al., 1994), *constans-10 (co-10)* (Laubinger, 2006), *ztl lkp2 fkf1* (*zlf*) (Baudry et al., 2010), *elf3-1* (Zagotta et al., 1992), *pif4* (Koini et al., 2009), *pif4pif5* (Lucas et al., 2008), and *OX-PIF4-HA* (Kumar et al., 2012)], or *Ler* [*uvr8-1* (Kliebenstein et al., 2002), *uvr8-2* (Brown et al., 2005) and *OX-GFPUVR8*/*uvr8-1* (Kaiserli and Jenkins, 2007)]. The UVR8 over-expressing line will be referenced in the text as OXUVR8. Seeds used for flowering and gene expression experiments were stratified in sterile distilled dH_2O for 3–4 days at 4°C and were sown on soil (Phytotron growth chambers) under long day (LD) photoperiods (16 h light and 8 h dark) with an illumination intensity of white light (50 μmol $m^{-2}s^{-1}$) $\pm$ UV-B (0.5 μmol $m^{-2}s^{-1}$) for UV-B experiments. The WL in these experiments was provided by LED lights (CEC). UV-B was provided by narrowband fluorescent lights (PHILIPS NARROWBAND TL 40W/0I-PS). The temperature of the chamber plants were grown was 22°C.

RNA Extraction and Quantitative Gene Expression Analysis

Total RNA was extracted from 12-day-old (until they reached the juvenile phase, before transition to reproductive growth) plants

grown under LD photoperiodic conditions at zeitgeber ZT 0.5 (30 min after light onset) and ZT 15 (15 h after light onset). The tissue was rapidly frozen in liquid nitrogen and disrupted using a TissueLyser by Qiagen (1 min with 18.0 m/s frequency). RNA was extracted using the RNeasy plant mini kit (Qiagen) according to the manufacturer's instructions and the total amount of RNA was quantified using a spectrophotometer nanodrop (Implen). Complementary DNA synthesis was performed on 1 μg of total RNA using the QuantiTect Reverse Transcription Kit by Qiagen according to the manufacturer's instructions. Real-time quantitative PCR was performed using the StepOnePlus™ Real-Time PCR System (Applied Biosystems, Life Technologies) and the Brilliant III Ultra-Fast SYBR® Green QPCR Master Mix (Agilent Technologies) using the following thermocycler (Step 1: Incubate at 95°C for 2 min, Step 2: Incubate at 95°C for 3 s, Step 3: Incubate at 59.5°C for 30 s, Step 4: Repeat Step 2 and 3 for 50 cycles, Step 5: Incubate at 95°C for 1 min, Step 6: Incubate at 60°C for 30 s, Step 7: Incubate at 95°C for 30 s). Expression of one of two abundantly expresses housekeeping genes was used for normalization. These genes were either *IRON-SULFUR CLUSTER ASSEMBLY PROTEIN 1* (*ISU1*), a well-established house-keeping gene which is involved in iron-sulfur cluster biogenesis (Perrella et al., 2018) or *ISOPENTENYL DIPHOSPHATE ISOMERASE 2* (*IPP2*), another well-established house-keeping gene used as a control for clock and light signaling gene expression studies as its expression is not regulated by diurnal rhythms (Farre et al., 2005; Zhu et al., 2016; Hwang et al., 2017). The amplification efficiency of each sample was calculated by StepOne™ Software v2.2 (Life Technologies) by using the slope of the regression line in the standard curve. The normalization of the data was achieved by geometric averaging of *ISU1* or *IPP2* as internal reference genes. A complete list of primers used for qRT-PCR are listed in **Supplementary Table 1**.

Flowering Time Measurements

Flowering time was monitored by either (a) counting the total number of rosette leaves of each plant on the day it bolted (appearance of the first flower bud with a stem of 2 cm) or (b) by calculating the number of days after germination at the time of bolting.

Statistical Analysis

The statistical analysis of the results acquired in the current research was performed using Student's *t*-test provided by Excel. ANOVA analysis was performed using GraphPad Prism 8.4.1 and Tukey's *Post hoc* test was conducted.

RESULTS

Ultraviolet-B Accelerates Photoperiodic Flowering in an Ecotype-Specific Manner

Environmental regulation of flowering time is a complex process that requires signal integration (Fornara et al., 2010). In order to better understand the effect of UV-B irradiation in *Arabidopsis thaliana*, we conducted flowering experiments on different ecotypes, mutants and overexpressing lines of light signaling and flowering components under a LD photoperiod of WL (50 μmol $m^{-2}s^{-1}$) or WL supplemented with physiologically relevant UV-B irradiation (0.5 μmol $m^{-2}s^{-1}$). The intensity of UV-B irradiation was calculated based on the intensity of UV-B on a sunny day at the University of Glasgow campus (0.5–1 μmol $m^{-2}s^{-1}$). Separate measurements were conducted in the months of March, April, May, June, July, and September and a mean of total UV-B intensity at floral level was calculated based on the aforementioned measurements. Three possible UV-B intensities were initially tested (0.3, 0.5, and 1 μmol $m^{-2}s^{-1}$) and one of them was chosen (0.5 μmol $m^{-2}s^{-1}$) based on its efficiency in mediating UV-B-dependent photomorphogenesis, by monitoring the expression of *HY5*, a marker gene for UV-B mediated photomorphogenic responses (Brown et al., 2005) and was therefore used as an indicator that our UV-B treatment efficiently induced physiological UV-B responses (**Supplementary Figures 1A,B**). From the intensities we tested 0.3 μmol $m^{-2}s^{-1}$ was not able to initiate plant photomorphogenic responses (**Supplementary Figure 1C**). Moreover, the UV-B intensity selected (0.5 μmol $m^{-2}s^{-1}$) did not cause any damaging effects on the plants, in order to avoid stress-induced responses (**Supplementary Figure 2**). The constant UV-B irradiation of 1 μmol $m^{-2}s^{-1}$ was too damaging for plants to survive and could therefore not reach the floral induction stage. Three common *Arabidopsis* ecotypes were tested in our experiments: *Landsberg erecta* (*Ler*), *Columbia-0* (*Col-0*) and *Cape Verde islands* (*Cvi*). In order to assess flowering time two variables were taken into consideration: (a) the number of rosette leaves each plant had on the day the bolt reached approximately 2 cm in height and (b) the number of days after germination when the first bud emerged. From these two parameters the number of rosette leaves was selected as the most reliable assay in order to investigate changes regarding flowering initiation in response to UV-B. This decision was based mainly on two factors. Firstly, flowering experiments in published literature use primarily the number of rosette leaves at the time of bolting to avoid any growth rate defects presented in many mutant genotypes (Wollenberg et al., 2008; Hayes et al., 2014). Furthermore, it is well-established that UV-B inhibits hypocotyl elongation (Gruber et al., 2010) but also delays plant growth altogether which can result in an increase in the number of days that have passed before bolting, which is not directly related to flowering initiation but to growth rate. Nevertheless our conclusions were formed after investigating both of these factors along with data from gene expression analysis.

Our data showed that flowering time under WL supplemented with UV-B was induced early in *Col-0* wild-type ecotype compared to non-UV-B treated plants, since a statistically significant decrease both in the number of rosette leaves as well as in the number of days before plants bolted was observed under WL supplemented with UV-B versus WL treatments (**Figures 1B,E**). Wild type *Ler* ecotype also depicted a milder early flowering phenotype, since there was a statistically significant decrease in the number of rosette leaves plants had at the day of bolting but not in the number of days at bolting under UV-B irradiation compared to WL treatment only (**Figures 1A,D**). Flowering time under UV-B irradiation compared to WL treatment was delayed in the *Cvi* ecotype, more specifically a

statistically significant increase was observed in both the number of rosette leaves as well as in the number of days before plants bolted (**Figures 1C,F**). To further investigate the molecular mechanism underlying the early flowering phenotypes observed in the *Col-0* and *Ler* ecotypes, gene expression analysis was performed monitoring master integrators of the photoperiodic pathway, which is controlled by the day length and the circadian clock. The zeitgeber time point (ZT 0.5) was chosen based on the expression patterns of the monitored genes (Fornara et al., 2010) and at the time point where the maximal UV-B effect was observed. Specifically under LD both *FT* and *CO* expression peaks after dawn (ZT 0.5) and at dusk (ZT 15) (Yanovsky and Kay, 2003). Our results suggest that *FT* and *CO* are significantly upregulated in *Col-0* and *Ler* grown under WL supplemented with UV-B, in comparison to the ones grown solely under WL (**Figures 2A–D**) indicating that FT and CO are mediating the early induced flowering phenotype observed in *Col-0* and *Ler* under WL supplemented UV-B. On the other hand, *Cvi* plants show a downregulation in *FT* transcript levels (**Supplementary Figure 3**).

Ultraviolet Resistance 8 Acts as a Negative Regulator of Flowering

Since UVR8 is the only identified UV-B photoreceptor to date (Tilbrook et al., 2013), we were interested in further investigating its role in photoperiodic-controlled flowering initiation, by examining *uvr8* mutant and UVR8 over-expressing lines. We conducted flowering experiments under a LD photoperiod of WL (50 μmol $m^{-2}s^{-1}$) or WL supplemented with UV-B (0.5 μmol $m^{-2}s^{-1}$), in *Ler* wild-type plants, two different *uvr8* mutant alleles (*uvr8-1* and *uvr8-2*) and a UVR8 over-expressing line. More specifically, to examine the *Ler* ecotype we used a UVR8 over-expressing line in an *uvr8* mutant background [OXUVR8 = *35Spro*GFP-UVR8/uvr8-1 (Kaiserli and Jenkins, 2007)] and two different *uvr8* mutant alleles: *uvr8-1* and *uvr8-2*. *Uvr8-1* mutants have a single recessive mutation leading to a deletion of 15 nucleotides, which results in the absence of UVR8 protein production (null allele) (Kliebenstein et al., 2002). *Uvr8-2* mutants contain a premature stop codon on the 400th amino acid (Brown et al., 2005; Yin et al., 2015), therefore these mutants are still able to produce truncated but non-functional UVR8 protein (Cloix et al., 2012). The data from the flowering experiments depicted that UV-B induces an early flowering phenotype in *uvr8-1* and *uvr8-2*, but does not significantly affect flowering of OXUVR8 (**Figure 3A**). Additionally, under WL *uvr8-1* flowers earlier than wild type, while *uvr8-2*, OXUVR8 and wild type (*Ler*) flower simultaneously (**Figure 3A**). When *uvr8-1* and *uvr8-2* mutants were exposed to WL + UV-B, they flowered earlier compared to wild type, while OXUVR8 had a late flowering phenotype (**Figure 3A**). In order to investigate these responses at the molecular level, we examined once more the transcript levels of genes encoding the key flowering regulators *FT* and *CO* (Fornara et al., 2010) in WT, *uvr8-1* and OXUVR8 backgrounds. Our results indicate that *FT* and *CO* genes are significantly upregulated in *uvr8-1* mutants grown under WL supplemented with UV-B (**Figures 3B,C**). *FT* transcript levels are also significantly downregulated in the OXUVR8 line in plants grown under WL supplemented with UV-B compared to the ones grown solely under WL, while *CO* levels do not depict significant change (**Figures 3B,C**). As demonstrated in **Figures 3B,C**, there is a greater induction of *FT* in *uvr8-1* compared to the wild type and an overall higher level of *FT* transcripts over *CO* in both wild type and mutant plants.

Ultraviolet-B Affects Flowering in Photoperiodic and Light Signaling Mutant and Over-Expressing Lines

To understand how UV-B regulates photoperiodic flowering in Arabidopsis, we examined flowering time initiation of mutant and transgenic lines of key light signaling and/or photoperiodic flowering components. More specifically, *co*, *zlf* and *elf3-1* mutants, lacking photoperiodic flowering components CO (Fornara et al., 2010), ZTL/LKP2/FKF1 (Kim et al., 2007) and ELF3 (Hicks et al., 2001) were examined. *Pif4pif5* mutants lacking the key light signaling proteins PIF4 and PIF5 (Hayes et al., 2014), as well as OXPIF4 over-expressing PIF4 (Kumar et al., 2012) were also examined. Finally, we tested how UV-B dependent flowering in *cop1-4* and *rup1rup2* mutants which lack important UV-B signaling mediating proteins COP1 (Oravecz, 2006; Yin and Ulm, 2017), and RUP1 and RUP2 (Arongaus et al., 2018). The research findings from our flowering experiments showed that UV-B can still induce early flowering in the late flowering *co* and *zlf* mutants, in a similar manner to *Col-0* (**Figure 4A**). On the contrary, UV-B exposure slightly delayed the early flowering phenotype of *elf3-1* (**Figure 4D**). Furthermore, UV-B induced an early flowering phenotype in the light signaling *pif4pif5* mutants, which was comparable to the response observed in wild type *Col-0* plants (**Figure 4B**). Early flowering OX-PIF4 grown under WL and WL supplemented with UV-B, showed a reversion of the early flowering phenotype induced by UV-B that is observed in the wild type *Col-0* (**Figure 4E**), therefore UV-B is found to also slightly delay flowering initiation in OXPIF4 plants. Finally, differences in flowering time between UV-B signaling *cop1-4* and *rup1rup2* mutants grown under WL and WL supplemented with UV-B, suggest that UV-B induces early photoperiodic flowering in those lines, a similar response to the one observed in wild type *Col-0* plants (**Figure 4C**).

DISCUSSION

The Effect of Ultraviolet-B on Photoperiodic Flowering Is Ecotype-Specific

Understanding the molecular trajectory and components that modulate photoperiodic flowering is key for acquiring the ability to improve plant yield in agricultural production systems. Although UV-B is an integral part of sunlight, the impact of UV-B radiation on photoperiodic flowering has not yet been extensively studied. Flowering experiments were conducted under the presence or absence of non-damaging UV-B levels. The intensity of the irradiation was selected to simulate natural

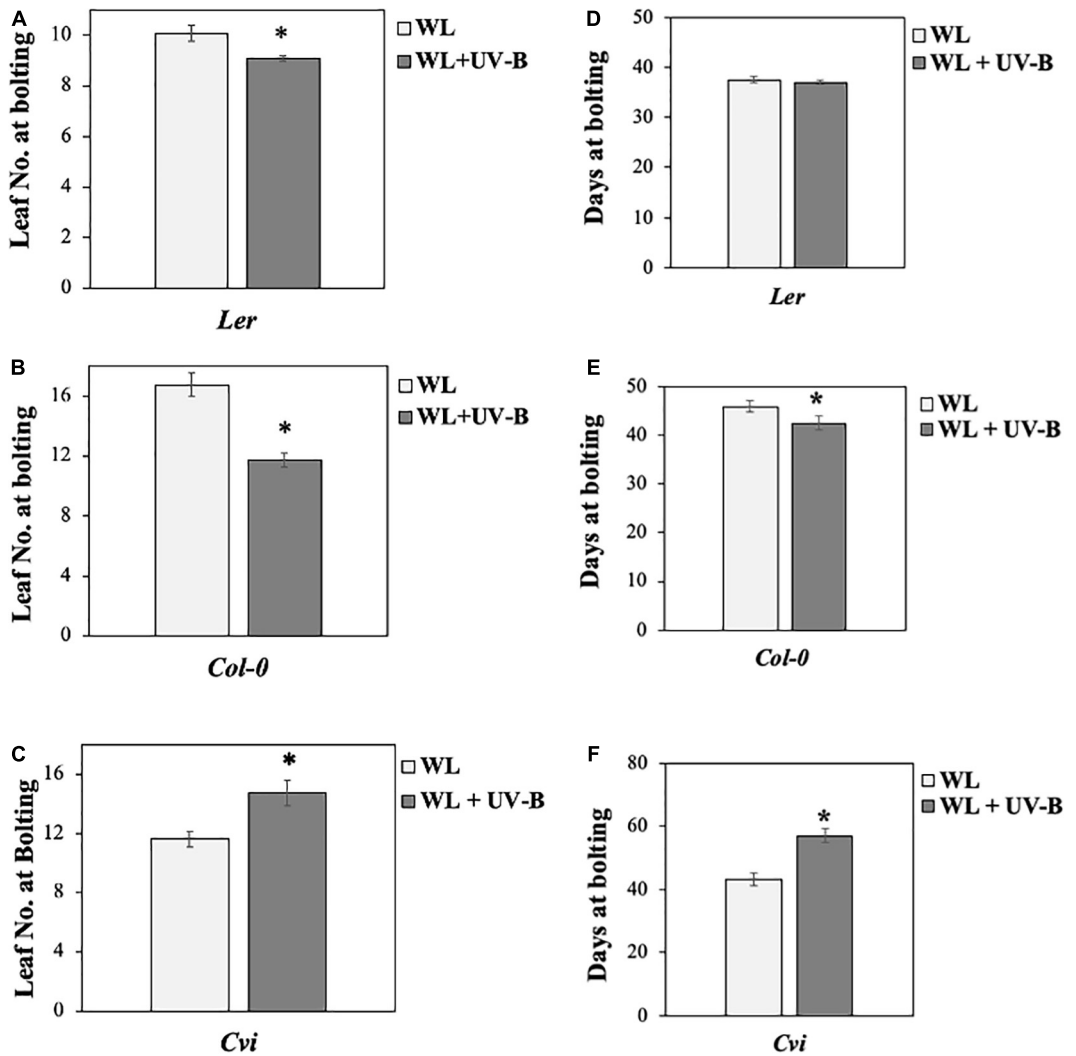

FIGURE 1 | UV-B induces early flowering in *Col-0* and *Ler* but delays it in *Cvi*. **(A–C)** Flowering times (as measured by rosette leaf number) of *Col-0* **(A)**, *Ler* **(B)**, and *Cvi* **(C)** ecotypes grown under a LD photoperiod in WL (50 μmol $m^{-2}s^{-1}$) or WL supplemented with UV-B (0.5 μmol $m^{-2}s^{-1}$). Data are represented as mean ± SEM ($n \geq 15$ plants recorded) and an asterisk (*) indicates statistically significant differences ($P < 0.05$) between means. **(D–F)** Flowering times (as measured by the number of days prior to bolting) of *Col-0* **(D)**, *Ler* **(E)**, and *Cvi* **(F)** ecotypes grown under a LD photoperiod in WL (50 μmol $m^{-2}s^{-1}$) or WL supplemented with UV-B (0.5 μmol $m^{-2}s^{-1}$). Data are represented as mean ± SEM ($n \geq 15$ plants recorded) and an asterisk (*) indicates statistically significant differences ($P < 0.05$) between means. Data are representative of three biological repeats including all genotypes represented above, a minimum number of 15 plants was assayed per genotype per condition.

UV-B conditions, since it was measured as the intensity a plant would receive on a moderately sunny day in Glasgow. The chosen amount of UV-B irradiation did not induce any stress responses which could potentially cause early flowering, as depicted from the low transcript levels of stress gene *COLD-REGULATED 15* (*COR15*) (Lin and Thomashow, 1992; **Supplementary Figure 2**). From these results it is observed that *Col-0* and *Ler* ecotypes have different stress expression gene responses under UV-B, probably due to their different environmental origins, a common cause for *Arabidopsis* species to develop phenotypic and genetic variations (Alonso-blanco and Koornneef, 2000; **Supplementary Figure 2**). Our results suggest that out of the three *Arabidopsis* accessions that were tested two of them (*Ler* and *Col-0*) demonstrated an early flowering phenotype when irradiated with low UV-B, more specifically in *Col-0* ecotype a stronger early flowering phenotype was observed compared to a milder one in *Ler* (**Figures 1A,B,D,E**). On the other hand the third ecotype tested (*Cvi*), depicted a delay in flowering time in response to UV-B (**Figures 1C,F**). Furthermore, transcript expression analysis of the key flowering regulating genes *FT* and *CO* suggested that a concomitant UV-B dependent upregulation of *FT* and *CO* is observed in *Ler* and *Col-0* ecotypes (**Figures 2A–D**), while a UV-B dependent downregulation of *FT* occurs in *Cvi* (**Supplementary Figure 3**). The aforementioned data indicate that different environments of origin are crucial for adaptation of different *Arabidopsis*

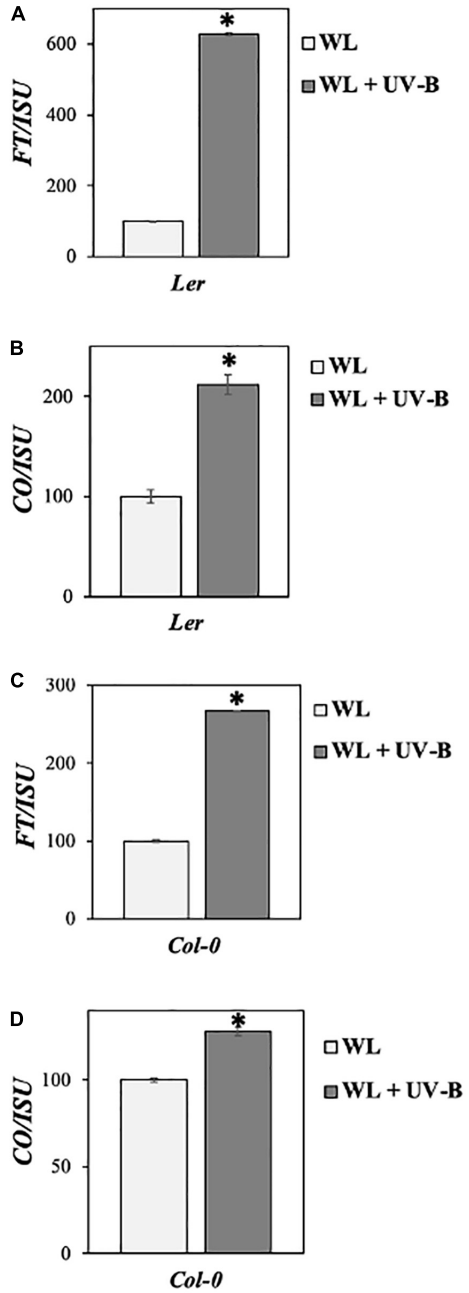

FIGURE 2 | UV-B induces photoperiodic pathway genes *FT* and *CO* in *Col-0* and *Ler* ecotypes. **(A–D)** qRT-PCR analysis of *FT* and *CO* transcript levels in *Ler* **(A,B)** and *Col-0* **(C,D)** normalized with the housekeeping gene *ISU.* Plant tissue was collected at ZT 0.5 12 days after germination. Plants were grown under a LD photoperiod of WL (50 μmol $m^{-2}s^{-1}$) or WL supplemented with UV-B (0.5 μmol $m^{-2}s^{-1}$). Plants grown under WL were used as reference (100%). Data are represented as mean ± SEM. Data are representative of three biological repeats including all genotypes represented above. For each biological repeat three technical qPCR replicates were conducted. *indicates a statistically significant difference.

responses, considering that all three ecotypes originate from very different environmental conditions. *Cvi* is an islandic population (Alonso-blanco and Koornneef, 2000) and Cape Verde islands are known to exhibit a particular geography and a photoperiod of 12 h of light and 12 h of darkness all year long. This contrasts *Col-0* and *Ler* which were originally identified in the United States and Europe, respectively (Koornneef et al., 2010) and are subjected to either a SD (8 h light/16 h darkness) or LD (16 h light/8 h darkness) photoperiod depending on the time of year. Moreover, *Cvi* is generally found in higher altitudes compared to *Col-0* and shorter latitudes compared to *Col-0* and *Ler*, which exhibit very similar altitudes to each other (data acquired from The *Arabidopsis* Information Resource). A possible explanation could be that *Col-0* and *Ler* interpret UV-B irradiation signals as a probable harmful factor even when the intensity of the irradiation is not harmful but could potentially increase, especially if these ecotypes experience a variation of photoperiodic length during the course of a year. In this case early flowering might be triggered as a way for the plant to ensure successful reproduction. On the other hand, ecotypes like *Cvi,* which face little or no changes in photoperiodic length and probably experience less variation in the sunlight they perceive, might have adapted differently in interpreting UV-B irradiation signals. In any case it has been found that it is very common for *Arabidopsis thaliana* species to develop variations both phenotypically and genetically, due to their wide distribution (Alonso-blanco and Koornneef, 2000). Thus, it would be interesting to further examine the genetic variations exhibited in the *UVR8* locus in the *Cvi* ecotype.

Two previous studies reported that under UV-B irradiation both *Ler* and *Col-0* exhibit a late flowering phenotype compared to the corresponding plants grown solely under WL (Hayes et al., 2014; Dotto et al., 2018). The experimental conditions used in the previous studies were significantly different from the ones employed by this research work, as we were interested in testing photoperiodic flowering initiation under a continuous and non-harmful UV-B regime. Previous flowering time analysis conducted in *Col-0* was in response to an irradiation intensity almost 20 times greater than the one utilized in this study, with a duration of 1 h during a SD or LD photoperiod (Dotto et al., 2018). The conditions where *Ler* exhibited a late flowering phenotype under UV-B irradiation, were also different than the growth conditions in our own experiments, since the intensity of the irradiation and the commencement of the UV-B treatment differed; plants were subjected to 9 days of continuous UV-B irradiation after exposure to WL for 10 days (Hayes et al., 2014). The UV-B intensity that was used in the aforementioned study could lead to non-specific stress responses if used long-term. In a more recent study a lower UV-B regime led to a delay in flowering time induction in *Col-0* under a SD photoperiod (Arongaus et al., 2018). Thus, we can conclude that the variability and intensity of the UV-B regime used in flowering time experiments is crucial for inducing flowering initiation, since different UV-B irradiation intensities initiate different UV-B-mediated responses, which subsequently lead to diverse outcomes regarding the initiation of flowering.

Gene expression analysis on the potential mechanism of early flowering initiation further solidifies our results, as both *Col-0* and *Ler* showed significant upregulation of *FT* and *CO* transcript levels under WL supplement with UV-B (**Figures 2A–D**),

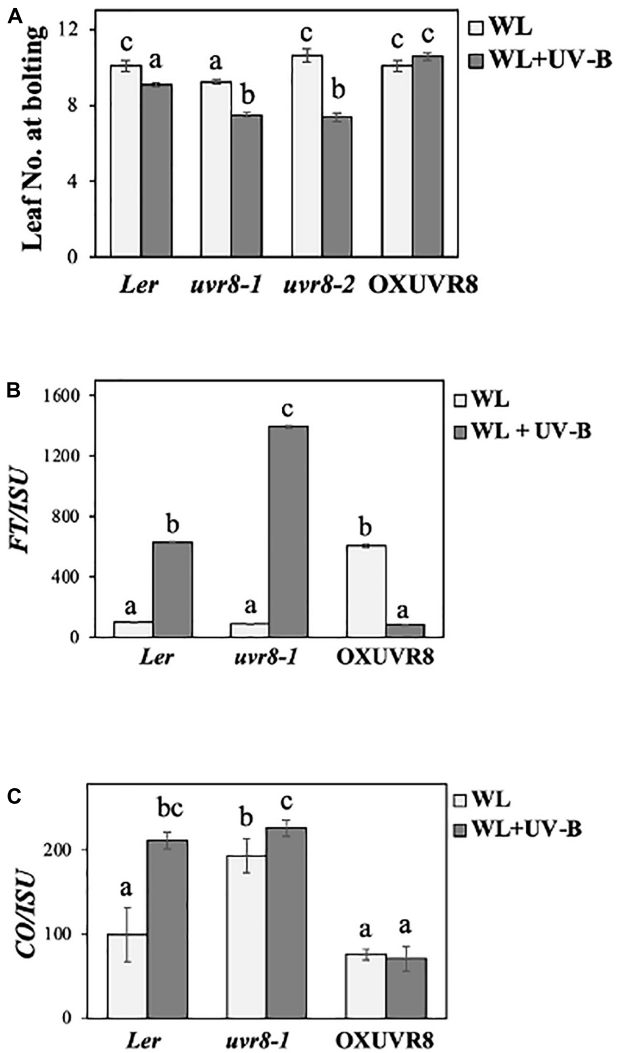

FIGURE 3 | UVR8 acts as a negative regulator of flowering initiation. **(A)** Flowering time of wild-type (*Ler*), *uvr8-1*, *uvr8-2, and* OX-UVR8 plants grown under a LD photoperiod in WL (50 μmol $m^{-2}s^{-1}$) or WL supplemented with UV-B (0.5 μmol $m^{-2}s^{-1}$). Data are represented as mean ± SEM ($n \geq 15$). Different letters indicate statistically significant differences ($P < 0.05$) between means. **(B,C)** qRT-PCR analysis of *FT* **(B)** and *CO* **(C)** transcript levels normalized with the housekeeping gene *ISU* in wild-type (*Ler*), *uvr8-1*, *uvr8-2* and OX-UVR8 plants. Plant tissue was collected at ZT 0.5 12 days after germination. Plants were grown under a LD photoperiod of WL (50 μmol $m^{-2}s^{-1}$) or WL supplemented with UV-B (0.5 μmol $m^{-2}s^{-1}$). Plants grown under WL were used as reference (100%). Data are representative of three biological repeats including all genotypes represented above, a minimum number of 15 plants was assayed per genotype. For qPCR experiments for each biological repeat three technical qPCR replicates were conducted.

suggesting that components of the photoperiodic pathway (Fornara et al., 2010) are involved in the early flowering response.

Ultraviolet Resistance 8 Acts as a Negative Regulator of Flowering

To better understand if the UV-B receptor UVR8 affects flowering initiation, we investigated flowering time of plants that either lack or over-express UVR8. Our results suggest that UVR8 acts as a negative regulator of flowering under UV-B irradiation. This conclusion was based on the early flowering phenotype that *uvr8* mutant plants demonstrate when grown under WL that was supplemented with UV-B compared to wild type *Ler* (**Figure 3A**). On the other hand, *uvr8-1* plants flower significantly earlier than wild type *Ler* under WL, while *uvr8-2* mutant plants flower around the same time as *Ler*, suggesting that the type of mutation of UVR8 (*uvr8-1* is a null mutant while in *uvr8-2* the produced protein is impaired) plays a role in their observed flowering phenotype (**Figure 3A**). These observations are in agreement with our transcript analysis findings, since transcript abundance of both flowering inducers *FT* and *CO* was significantly upregulated in *uvr8* mutants, whilst *FT* levels were significantly downregulated in UVR8 overexpressors (**Figures 3B,C**), suggesting that CO and FT are involved in UV-B dependent regulation of flowering. Under WL conditions wild type *Ler* and *uvr8-1* mutant plants depict similar transcript levels of *FT* (**Figure 3B**), with *uvr8-1* flowering earlier (**Figure 3A**), suggesting that other flowering regulators such as CO are important since *CO* is increased in *uvr8-1* plants compared to wild type *Ler* under WL (**Figure 3C**). An upregulation of *FT* transcript levels in *uvr8* grown under WL + UV-B compared to WL, has also been observed in a recent study investigating the effects of UV-B in flowering via changes in the activity of the PRC2 complex and miR156 levels (Dotto et al., 2018). The aforementioned research work focused mainly on the potential mechanism that leads to *FLC* upregulation through the control of the age flowering pathway that ultimately delays flowering in their experimental conditions under UV-B irradiation (Dotto et al., 2018).

The significance of our findings is that we provide evidence of an additional flowering pathway in *Arabidopsis*, the photoperiodic, that is involved in the regulation of flowering time under UV-B irradiation, through UVR8-specific mediated responses.

Ultraviolet-B Accelerates Flowering in Key Flowering and Signaling Mutants

The effect of UV-B on the flowering time of different *Arabidopsis* mutants of key protein components of photoperiodic flowering and/or light signaling, was also analyzed through flowering experiments. UV-B irradiation was found to induce early flowering in *co*, *zlf*, *pif4pif5*, *cop1-4,* and *rup1rup2* leading to the conclusion that these factors may not be essential for UV-B specific acceleration of flowering.

A UV-B induced acceleration of flowering was observed in the late flowering mutants *co* (Wu et al., 2014) and *zlf* (Baudry et al., 2010; **Figure 4A**). The aforementioned observation for the *co* mutant line would suggest that even if the photoperiodic pathway is most likely involved in UV-B specific acceleration of flowering (**Figures 2A–D**), it may require additional factors other than CO for the subsequent induction of *FT*. This could imply a putative mechanism where UVR8 bypasses CO in the photoperiodic flowering pathway by interacting directly with the *FT* promoter or by interacting with another transcription factor

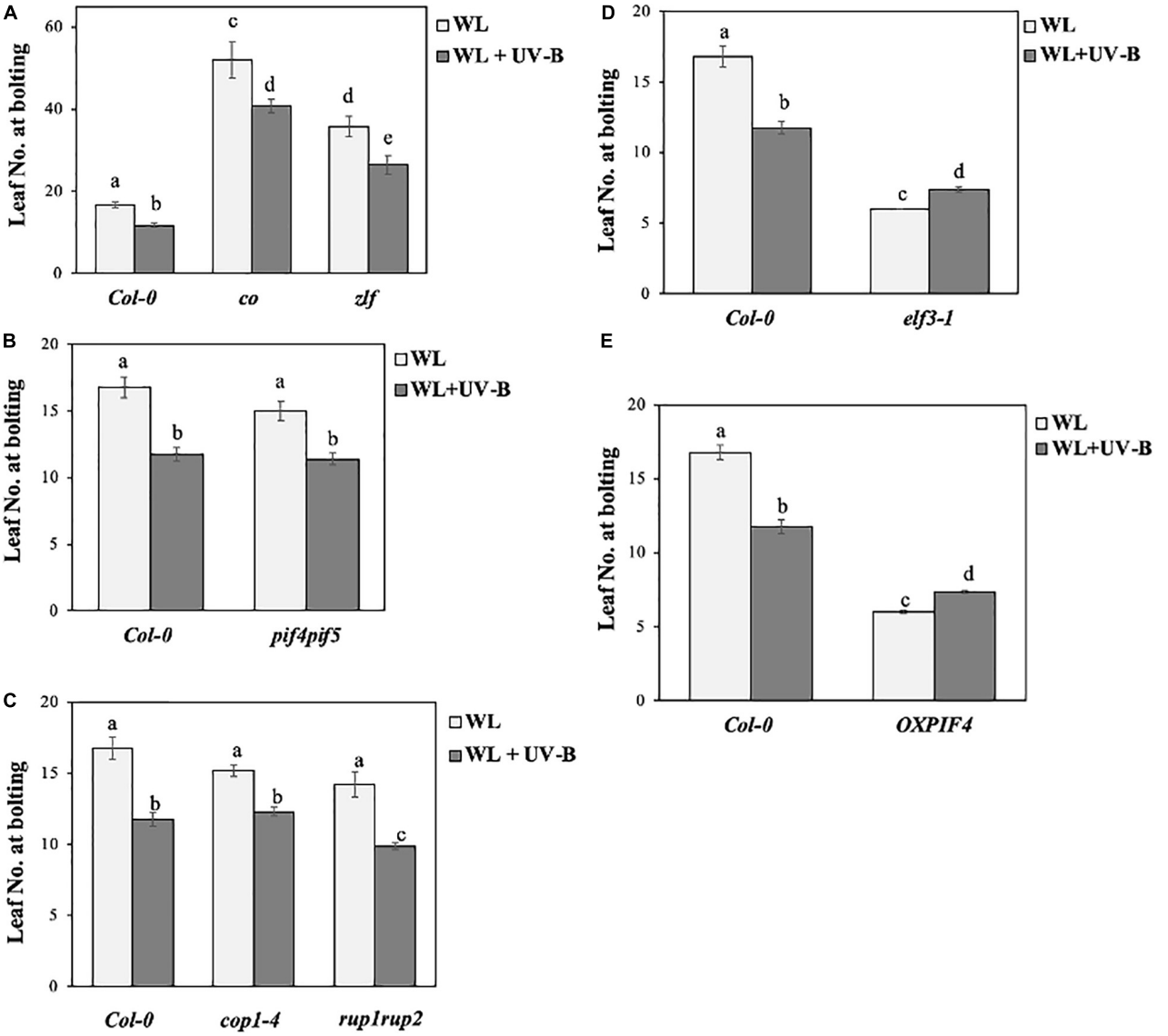

FIGURE 4 | UV-B accelerates flowering of *co*, *zlf*, *pif4pif5*, *cop1-4,* and *rup1rup2* but delays flowering of *elf3-1* and OXPIF4. **(A–C)** Flowering time of wild-type *Col-0*, *co* and *zlf* **(A)**, *pif4pif5* **(B)**, *and cop1-4* and *rup1rup2* **(C)** plants grown under a LD photoperiod in WL (50 μmol $m^{-2}s^{-1}$) or WL supplemented with UV-B (0.5 μmol $m^{-2}s^{-1}$). Data are represented as mean ± SEM ($n \geq 15$). Different letters indicate statistically significant differences ($P < 0.05$) between means. **(D,E)** Flowering time of wild-type *Col-0*, *elf3-1* **(D)** and OXPIF4 **(E)** plants grown under a LD photoperiod in WL (50 μmol $m^{-2}s^{-1}$) or WL supplemented with UV-B (0.5 μmol $m^{-2}s^{-1}$). Data are represented as mean ± SEM ($n \geq 15$). Different letters indicate statistically significant differences ($P < 0.05$) between means. Data are representative of three biological repeats including all genotypes represented above, a minimum number of 15 plants was assayed per genotype.

that induces *FT* expression. This hypothesis is further supported by evidence showing that the *FT* expression is still significantly induced under WL supplemented with UV-B in *co* mutant plants (**Supplementary Figure 4**).

Another component that has been shown to be involved in flowering induction especially in a temperature-dependent manner is PIF4 (Tavridou et al., 2020). In particular, PIF4 and PIF5 are degraded under UV-B in an UVR8-specific manner (Tavridou et al., 2020). Our results suggest that *pif4pif5* (Lucas et al., 2008) mutants demonstrate the same early flowering phenotype under UV-B conditions as WT (**Figure 4B**), thus indicating that PIF4 is not essential for UV-B-induced early flowering.

Early flowering time under WL supplemented with UV-B of mutants for UV-B signaling components *cop1-4* (McNellis et al., 1994) and *rup1rup2* (Gruber et al., 2010; Vanhaelewyn et al., 2016) was also induced compared to WL (**Figure 4C**). RUP2 has been associated with flowering regulation under UV-B conditions (Wang et al., 2011; Arongaus et al., 2018). Previous studies showed that RUP1 and RUP2 play a role in regulating floral transition under WL (Wang et al., 2011). While RUP1 does not regulate flowering, RUP2 was found to repress flowering, under

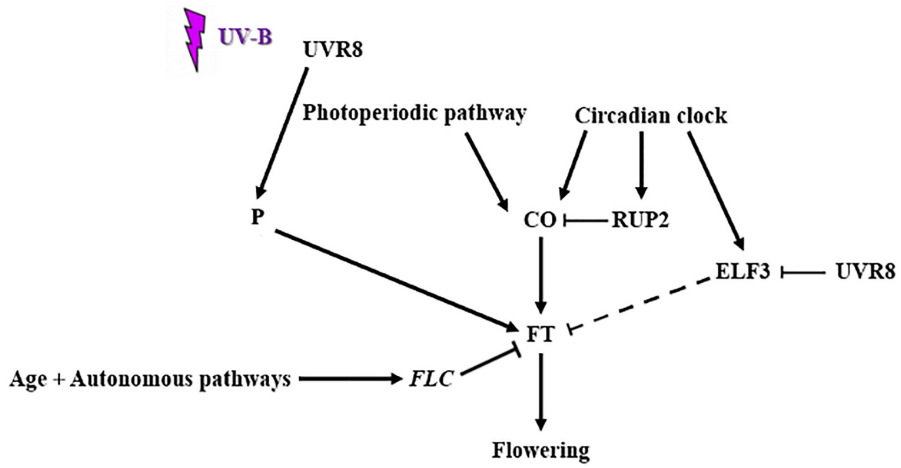

FIGURE 5 | Schematic representation of UV-B mediated control of flowering time (factors and flowering pathways involved). Upon UV-B irradiation multiple flowering pathways control flowering time. The age and autonomous pathways lead to an upregulation of *FLC* [as demonstrated by Dotto et al. (2018)], which acts as an *FT* repressor. CO and FT are flowering promoting factors of the photoperiodic pathway. CO is repressed by RUP2, a negative regulator of UVR8 signaling [as demonstrated by Arongaus et al. (2018)] and a circadian clock component. ELF3, another circadian clock component also represses *FT*, indirectly by targeting CO for degradation. UVR8 represses *ELF3* and possibly interacts with another protein factor (P) in order to promote *FT* gene expression.

WL conditions (Wang et al., 2011). Intriguingly, over-expression of RUP1 or RUP2 accelerated flowering in plants grown under LD photoperiodic conditions subjected solely to WL irradiation (Wang et al., 2011). *Rup2* mutants demonstrated an early flowering phenotype as well as RUP2 over-expressing plants, indicating a more complex regulatory mechanism affecting photoperiodic flowering, whilst both factors were found to be controlled by the circadian clock (Wang et al., 2011). A more recent study indicated that *rup2* mutants flower at the same time as WT under WL LD conditions (Arongaus et al., 2018), a phenotype similar to our findings where under WL *rup1rup2* flowering time is not statistically different to the one of wild type *Col-0* (**Figure 4C**). Under SD WL supplemented with UV-B, *rup2* and *rup1rup2* flower earlier than wild type plants in a UVR8 dependent manner (Arongaus et al., 2018). Interestingly, this observation correlates with our own findings from flowering experiments conducted under a LD photoperiod for *rup1rup2* (**Figure 4C**). Moreover, it was demonstrated that RUP2 and CO can interact directly and that the early phenotype of *rup2* is dependent on both *FT* and *CO* (Arongaus et al., 2018), suggesting that factors of the photoperiodic flowering pathway are indeed essential for mediating the early UV-B dependent flowering initiation response under both LD and SD photoperiods.

Ultraviolet-B Delays the Early Flowering Phenotype of *elf3-1* and OXPIF4

In contrast to the other genotypes examined, *elf3-1* (Zagotta et al., 1992) and OXPIF4 (Kumar et al., 2012), demonstrated a slight delay in flowering initiation under WL + UV-B compared to WL (**Figures 4D,E**). This data would suggest that ELF3 could potentially act as a key regulator of the UV-B mediated flowering initiation response downstream of UVR8. Our results altogether indicate that UV-B has clearly a different effect on flowering initiation of early flowering mutants. Thus, it would be particularly interesting to further examine the molecular mechanism underlying these responses and examine the effect of UV-B on additional early flowering [possibly *SUCpro*::CO-HA also known as the over-expressing CO line (Mizuno et al., 2014)]. Flowering time regulation is a very complex process regulated by many different protein factors and pathways (Fornara et al., 2010), therefore it is possible that in mutant or transgenic plants exhibiting an early flowering phenotype under WL, UV-B signal affects differently photoperiodic flowering responses.

Based on all of the above conclusions a preliminary and simplified model of UVR8 action can be formulated (**Figure 5**). More specifically upon UV-B irradiation multiple flowering pathways control flowering time. The age and autonomous pathways lead to an upregulation of *FLC* (Dotto et al., 2018), which acts as an *FT* repressor. CO and FT are flowering promoting factors of the photoperiodic pathway. CO is repressed by RUP2, a negative regulator of UVR8 signaling (Arongaus et al., 2018). ELF3, a circadian clock component also represses *FT*, indirectly by targeting CO for degradation. UVR8 represses *ELF3* and possibly interacts with a protein factor that has not yet been identified in order to promote *FT* gene expression. However, further investigation need to be performed in order to identify the mechanism and factors that are involved in the UV-B specific control of flowering time in *Arabidopsis thaliana*, through the action of UVR8.

Our experiments have provided further insights on the way UV-B irradiation affects flowering initiation in *Arabidopsis thaliana*. However, future experiments need to be performed in order to fully elucidate the molecular mechanism, as well as the physiological significance of these flowering time alternations. Uncovering the mechanism underlying UV-B-mediated flowering initiation, including all the factors

and pathways that integrate the UV-B-specific photoperiodic flowering, as well as determining the role of UVR8 in this process, will further advance our abilities on designing more efficient agricultural practices which will contribute to the goal of improving global food security. Developing strategies to improve crop resilience and increase yield according to environmental stimuli such as UV-B, can provide the tools to maximize global crop production. Deciphering these mechanisms primarily in *Arabidopsis thaliana* consists an integral part of this process since it is the most universally used model plant organism, due to its many advantages and the ability to identify homologs in many commercial crops.

DATA AVAILABILITY STATEMENT

The original contributions presented in the study are included in the article/**Supplementary Material**, further inquiries can be directed to the corresponding author/s.

AUTHOR CONTRIBUTIONS

AZ and EK designed and performed the research, and analyzed the data. AZ, EP, and EK wrote the manuscript. AZ performed genotyping, western blot analysis, and all qRT-PCR experiments and analysis. EP performed RNA extraction and assisted with flowering experiments. LO'D assisted with the performance of flowering experiments. All authors contributed to the article and approved the submitted version.

FUNDING

AZ was supported by a Medical, Veterinary and Life Sciences Doctoral Studentship from the University of Glasgow. EK is grateful to the BBSRC (BB/M023079/1).

ACKNOWLEDGMENTS

We are grateful to the Jenkins Lab for discussions and reagents provided. We thank Silviya Dimova and Adam Gauley for performing preliminary experiments related to this study.

SUPPLEMENTARY MATERIAL

The Supplementary Material for this article can be found online at: https://www.frontiersin.org/articles/10.3389/fpls.2022.840720/full#supplementary-material

REFERENCES

Alonso-blanco, C., and Koornneef, M. (2000). Naturally occurring variation in *Arabidopsis*: an underexploited resource for plant genetics. *Trends Plant Sci.* 5, 22–29. doi: 10.1016/s1360-1385(99)01510-1

Arongaus, A. B., Chen, S., Pireyre, M., Glöckner, N., Galvão, V. C., Albert, A., et al. (2018). *Arabidopsis* RUP2 represses UVR8-mediated flowering in noninductive photoperiods. *Genes Dev.* 32, 1332–1343. doi: 10.1101/gad.318592.118

Baudry, A., Ito, S., Song, Y. H., Strait, A. A., Kiba, T., Lu, S., et al. (2010). F-box proteins FKF1 and LKP2 act in concert with ZEITLUPE to control *Arabidopsis* clock progression. *Plant Cell* 22, 606–622. doi: 10.1105/tpc.109.072843

Briggs, W. R., and Olney, M. A. (2001). Photoreceptors in plant photomorphogenesis to date . five phytochromes, two cryptochromes, one phototropin, and one superchrome. *Plant Physiol.* 125, 85–88. doi: 10.1104/pp.125.1.85

Brown, B. A., Cloix, C., Jiang, G. H., Kaiserli, E., Herzyk, P., Kliebenstein, D. J., et al. (2005). A UV-B-specific signaling component orchestrates plant UV protection. *Proc. Natl. Acad. Sci. U.S.A.* 102, 18225–18230. doi: 10.1073/pnas.0507187102

Cloix, C., and Jenkins, G. I. (2008). Interaction of the *Arabidopsis* UV-B-specific signaling component UVR8 with chromatin. *Mol. Plant* 1, 118–128. doi: 10.1093/mp/ssm012

Cloix, C., Kaiserli, E., Heilmann, M., Baxter, K. J., Brown, B. A., O'Hara, A., et al. (2012). C-terminal region of the UV-B photoreceptor UVR8 initiates signaling through interaction with the COP1 protein. *Proc. Natl. Acad. Sci. U.S.A.* 109, 16366–16370. doi: 10.1073/pnas.1210898109

Dotto, M., Gómez, M. S., Soto, M. S., and Casati, P. (2018). UV - B radiation delays flowering time through changes in the PRC2 complex activity and MiR156 levels in *Arabidopsis thaliana*. *Plant Cell Environ.* 41, 1394–1406. doi: 10.1111/pce.13166

Farre, E. M., Harmer, S. L., Harmon, F. G., Yanovsky, M. J., and Kay, S. A. (2005). Overlapping and distinct roles of PRR7 and PRR9 in the *Arabidopsis* circadian clock. *Curr. Biol.* 15, 47–54. doi: 10.1016/j.cub.2004.12.067

Favory, J. J., Stec, A., Gruber, H., Rizzini, L., Oravecz, A., Funk, M., et al. (2009). Interaction of COP1 and UVR8 regulates UV-B induced photomorphogenesis and stress acclimation in *Arabidopsis*. *EMBO J.* 28, 591–601. doi: 10.1038/emboj.2009.4

Feher, B., Bognar, L. K., Hajdu, A., Binkert, M., Jon Davis, S. J., Schafer, E., et al. (2011). Functional interaction of the circadian clock and UV RESISTANCE LOCUS 8-controlled UV-B signaling pathways in *Arabidopsis thaliana*. *Plant J.* 67, 37–48. doi: 10.1111/j.1365-313X.2011.04573.x

Fornara, F., de Montaigu, A., and Coupland, G. (2010). SnapShot: control of flowering in *Arabidopsis*. *Cell* 141, 550–550.e2.

Fornara, F., Panigrahi, K. C. S., Gissot, L., Sauerbrunn, N., Rühl, M., Jarillo, J. A., et al. (2009). *Arabidopsis* DOF transcription factors act redundantly to reduce CONSTANS expression and are essential for a photoperiodic flowering response. *Dev. Cell* 17, 75–86. doi: 10.1016/j.devcel.2009.06.015

Gruber, H., Heijde, M., Heller, W., Albert, A., Seidlitz, H. K., and Ulm, R. (2010). Negative feedback regulation of UV-B-induced photomorphogenesis and stress acclimation in *Arabidopsis*. *Proc. Natl. Acad. Sci. U.S.A.* 107, 20132–20137. doi: 10.1073/pnas.0914532107

Hayes, S., Sharma, A., Fraser, D. P., Trevisan, M., Cragg-Barber, C. K., Tavridou, E., et al. (2017). UV-B perceived by the UVR8 photoreceptor inhibits plant thermomorphogenesis. *Curr. Biol.* 27, 120–127. doi: 10.1016/j.cub.2016.11.004

Hayes, S., Velanis, C. N., Jenkins, G. I., and Franklin, K. A. (2014). UV-B detected by the UVR8 photoreceptor antagonizes auxin signaling and plant shade avoidance. *Proc. Natl. Acad. Sci. U.S.A.* 111, 11894–11899. doi: 10.1073/pnas.1403052111

Heijde, M., and Ulm, R. (2012). UV-B photoreceptor-mediated signalling in plants. *Trends Plant Sci.* 17, 230–237. doi: 10.1016/j.tplants.2012.01.007

Heilmann, M., Velanis, C. N., Cloix, C., Smith, B. O., Christie, J. M., and Gareth, I. J. (2016). Dimer/Monomer status and in vivo function of salt-bridge mutants of the plant UV-B photoreceptor UVR8. *Plant J.* 88, 71–81. doi: 10.1111/tpj.13260

Hicks, K. A., Albertson, T. M., and Wagner, D. R. (2001). EARLY FLOWERING3 encodes a novel protein that regulates circadian clock function and flowering in *Arabidopsis*. *Plant Cell* 13:1281. doi: 10.1105/tpc.13.6.1281

Huang, X., Ouyang, X., Yang, P., Lau, O. S., Li, G., Li, J., et al. (2012). *Arabidopsis* FHY3 and HY5 positively mediate induction of COP1 transcription in response to photomorphogenic UV-B light. *Plant Cell* 24, 4590–4607. doi: 10.1105/tpc.112.103994

Hwang, G., Zhu, J., Lee, Y. K., Kim, S., Nguyen, T. T., Kim, J., et al. (2017). PIF4 promotes expression of LNG1 and LNG2 to induce thermomorphogenic growth in *Arabidopsis*. *Front. Plant Sci.* 8:1320. doi: 10.3389/fpls.2017.01320

Imaizumi, T., Schultz, T. F., Harmon, F. G., Ho, L. A., and Kay, S. A. (2005). FKF1 F-box protein mediates cyclic degradation of a repressor of CONSTANS in *Arabidopsis*. *Science* 309, 293–297. doi: 10.1126/science.1110586

Jenkins, G. I. (2014). Structure and function of the UV-B photoreceptor UVR8. *Curr. Opin. Struct. Biol.* 29, 52–57. doi: 10.1016/j.sbi.2014.09.004

Kaiserli, E., and Jenkins, G. I. (2007). UV-B promotes rapid nuclear translocation of the UV-B–specific signaling component UVR8 and activates its function in the nucleus. *Plant Cell* 19, 2662–2673. doi: 10.1105/tpc.107.053330

Kim, W. Y., Fujiwara, S., Suh, S. S., Kim, J., Kim, Y., Han, L., et al. (2007). ZEITLUPE is a circadian photoreceptor stabilized by GIGANTEA in blue light. *Nature* 449, 356–360. doi: 10.1038/nature06132

Kliebenstein, D. J., Lim, J. E., Landry, L. G., and Last, R. L. (2002). *Arabidopsis* regulates Ultraviolet-B signal transduction and tolerance and contains sequence similarity to human regulator of chromatin condensation 1. *Plant Physiol.* 130, 234–243. doi: 10.1104/pp.005041

Koini, M. A., Alvey, L., Allen, T., Tilley, C. A., Harberd, N. P., Whitelam, G. C., et al. (2009). High temperature-mediated adaptations in plant architecture require the BHLH transcription factor PIF4. *Curr. Biol.* 19, 408–413. doi: 10.1016/j.cub.2009.01.046

Koornneef, M., Meink, D., Linne, C., and Radix West, R. (2010). The development of *Arabidopsis* as a model plant. *Plant J.* 61, 909–921. doi: 10.1111/j.1365-313x.2009.04086.x

Kumar, S. V., Lucyshyn, D., Jaeger, K. E., Alós, E., Alvey, E., Harberd, N. P., et al. (2012). Transcription factor PIF4 controls the thermosensory activation of flowering. *Nature* 484:242. doi: 10.1038/nature10928

Laubinger, S. (2006). *Arabidopsis* SPA proteins regulate photoperiodic flowering and interact with the floral inducer CONSTANS to regulate its stability. *Development* 133, 3213–3222. doi: 10.1242/dev.02481

Lin, C., and Thomashow, M. F. (1992). DNA sequence analysis of a complementary DNA for cold-regulated *Arabidopsis* gene Cor15 and characterization of the COR15 polypeptide. *Plant Physiol.* 99, 519–525.

Lucas, M. D., Jean-michel Daviere, J.-M., Rodriguez-Falcon, M., Pontin, M., Iglesias-Pedraz, J. M., Lorrain, S., et al. (2008). A molecular framework for light and gibberellin control of cell elongation. *Nature* 451, 480–484. doi: 10.1038/nature06520

McNellis, T. W., von Arnim, G., Araki, T., Komeda, Y., Miséra, S., and Deng, X. W. (1994). Genetic and molecular analysis of an allelic series of Cop1 mutants suggests functional roles for the multiple protein domains. *Plant Cell* 6, 487–500. doi: 10.1105/tpc.6.4.487

Mizuno, T., Nomoto, Y., Oka, H., Kitayama, M., Takeuchi, A., Tsubouchi, M., et al. (2014). Ambient temperature signal feeds into the circadian clock transcriptional circuitry through the EC night-time repressor in *Arabidopsis thaliana*. *Plant Cell Physiol.* 55, 958–976. doi: 10.1093/pcp/pcu030

Montgomery, B. L., and Lagarias, J. C. (2002). "Phytochrome ancestry: sensors of bilins and light phytochromes: a definition. *Trends Plants Sci.* 1385, 1–10.

Nusinow, D. A., Helfer, A., Hamilton, E. E., King, J. J., Imaizumi, T., Schultz, T. M., et al. (2011). The ELF4–ELF3–LUX complex links the circadian clock to diurnal control of hypocotyl growth. *Nature* 475:398. doi: 10.1038/nature10182

Oravecz, A. (2006). CONSTITUTIVELY PHOTOMORPHOGENIC1 is required for the UV-B response in *Arabidopsis*. *Plant Cell Online* 18, 1975–1990. doi: 10.1105/tpc.105.040097

Perrella, G., Davidson, M. L. H., O'Donnell, L., Nastase, A.-M., Herzyk, P., Breton, G., et al. (2018). ZINC-FINGER interactions mediate transcriptional regulation of Hypocotyl growth in *Arabidopsis*. *Proc. Natl. Acad. Sci. U.S.A.* 115, E4503–E4511. doi: 10.1073/pnas.1718099115

Rizzini, L., Favory, J. J., Cloix, C., Faggionato, D., O'Hara, A., Kaiserli, E., et al. (2011). Perception of UV-B by the *Arabidopsis* UVR8 protein. *Science* 332, 103–106.

Sawa, M., Nusinow, D. A., Kay, S. A., and Takato Imaizumi, T. (2007). FKF1 and GIGANTEA complex formation is required for day-length measurement in *Arabidopsis*. *Science* 318, 261–265. doi: 10.1126/science.1146994

Song, Y. H., Smith, R. W., To, B. J., Millar, A. J., and Imaizumi, T. (2012). FKF1 conveys timing information for CONSTANS stabilization in photoperiodic flowering. *Science* 336, 1045–1050. doi: 10.1126/science.1219644

Sullivan, J. A., and Deng, X. W. (2003). From seed to seed: the role of photoreceptors in *Arabidopsis* development. *Dev. Biol.* 260, 289–297. doi: 10.1016/s0012-1606(03)00212-4

Tavridou, E., Pireyre, M., and Ulm, R. (2020). Degradation of the transcription factors PIF4 and PIF5 under UV-B promotes UVR8-mediated inhibition of Hypocotyl growth in *Arabidopsis*. *Plant J.* 101, 507–517. doi: 10.1111/tpj.14556

Tilbrook, K., Arongaus, A. B., Binkert, M., Heijde, M., Yin, R., and Ulm, R. (2013). The UVR8 UV-B photoreceptor: perception, signaling and response. *Arabidopsis Book* 11:e0164. doi: 10.1199/tab.0164

Ulm, R., Baumann, A., Oravecz, A., Máté, Z., Ádám, E., Oakeley, E. J., et al. (2004). Genome-wide analysis of gene expression reveals function of the BZIP transcription factor HY5 in the UV-B response of *Arabidopsis*. *Proc. Natl. Acad. Sci. U.S.A.* 101, 1397–1402. doi: 10.1073/pnas.0308044100

Vanhaelewyn, L., Schumacher, P., Poelman, D., Fankhauser, C., Van Der Straeten, D., and Vandenbussche, F. (2016). REPRESSOR OF ULTRAVIOLET-B PHOTOMORPHOGENESIS function allows efficient phototropin mediated Ultraviolet-B phototropism in etiolated seedlings. *Plant Sci.* 252, 215–221. doi: 10.1016/j.plantsci.2016.07.008

Wang, W., Yang, D., and Feldmann, K. A. (2011). EFO1 and EFO2, encoding putative WD-domain proteins, have overlapping and distinct roles in the regulation of vegetative development and flowering of *Arabidopsis*. *J. Exp. Bot.* 62, 1077–1088. doi: 10.1093/jxb/erq336

Wollenberg, A. C., Strasser, B., Cerdan, P. D., and Amasino, R. M. (2008). Acceleration of flowering during shade avoidance in *Arabidopsis* alters the balance between FLOWERING LOCUS C -mediated repression and photoperiodic induction of flowering. *Plant Physiol.* 148, 1681–1694. doi: 10.1104/pp.108.125468

Wu, F., Price, B. W., Haider, W., Seufferheld, G., Nelson, R., and Hanzawa, Y. (2014). Functional and evolutionary characterization of the CONSTANS Gene family in short-day photoperiodic flowering in soybean. *PLoS One* 9:e85754. doi: 10.1371/journal.pone.0085754

Yanovsky, M. J., and Kay, S. A. (2003). Living by the calendar: how plants know when to flower. *Nat. Rev. Mol. Cell Biol.* 4, 265–275. doi: 10.1038/nrm1077

Yin, R., and Ulm, R. (2017). How plants cope with UV-B: from perception to response. *Curr. Opin. Plant Biol.* 37, 42–48. doi: 10.1016/j.pbi.2017.03.013

Yin, R., Arongaus, A. B., Binkert, M., and Ulm, R. (2015). Two distinct domains of the UVR8 photoreceptor interact with COP1 to initiate UV-B signaling in *Arabidopsis*. *Plant Cell Online* 27, 202–213. doi: 10.1105/tpc.114.133868

Zagotta, M. T., Shannon, S., Jacobs, C., and Meeks-Wagner, D. R. (1992). Early-flowering mutants of *Arabidopsis thaliana*. *Australian J. Plant Physiol.* 19, 411–418.

Zhao, H., Xu, D., Tian, T., Kong, F., Lin, K., Gan, S., et al. (2021). Molecular and functional dissection of EARLY-FLOWERING 3 (ELF3) and ELF4 in *Arabidopsis*. *Plant Sci.* 303:110786. doi: 10.1016/j.plantsci.2020.110786

Zhu, J.-Y., Oh, E., Wang, T., and Wang, Z. Y. (2016). TOC1 – PIF4 interaction mediates the circadian gating of thermoresponsive growth in *Arabidopsis*. *Nat. Commun.* 7:13692. doi: 10.1038/ncomms13692

Conflict of Interest: The authors declare that the research was conducted in the absence of any commercial or financial relationships that could be construed as a potential conflict of interest.

Publisher's Note: All claims expressed in this article are solely those of the authors and do not necessarily represent those of their affiliated organizations, or those of the publisher, the editors and the reviewers. Any product that may be evaluated in this article, or claim that may be made by its manufacturer, is not guaranteed or endorsed by the publisher.

frontiers | Frontiers in Plant Science

ORIGINAL RESEARCH
published: 06 May 2022
doi: 10.3389/fpls.2022.855243

Transcriptomic and Metabolomic Response to High Light in the Charophyte Alga *Klebsormidium nitens*

*Emma Serrano-Pérez[1,2†], Ana B. Romero-Losada[1,2†], María Morales-Pineda[1], M. Elena García-Gómez[1], Inmaculada Couso[1], Mercedes García-González[1] and Francisco J. Romero-Campero[1,2]**

[1] Microalgae Systems Biology and Biotechnology Research Group, Institute for Plant Biochemistry and Photosynthesis, Universidad de Sevilla – Consejo Superior de Investigaciones Científicas, Seville, Spain, [2] Department of Computer Science and Artificial Intelligence, Universidad de Sevilla, Seville, Spain

OPEN ACCESS

Edited by:
Jordi Moreno-Romero,
Universitat Autònoma de Barcelona, Spain

Reviewed by:
Jan de Vries,
University of Göttingen, Germany
Burkhard Becker,
University of Cologne, Germany

***Correspondence:**
Francisco J. Romero-Campero
fran@us.es

[†] These authors have contributed equally to this work and share first authorship

Specialty section:
This article was submitted to Plant Physiology, a section of the journal Frontiers in Plant Science

Received: 14 January 2022
Accepted: 28 March 2022
Published: 06 May 2022

Citation:
Serrano-Pérez E, Romero-Losada AB, Morales-Pineda M, García-Gómez ME, Couso I, García-González M and Romero-Campero FJ (2022) Transcriptomic and Metabolomic Response to High Light in the Charophyte Alga Klebsormidium nitens. Front. Plant Sci. 13:855243. doi: 10.3389/fpls.2022.855243

The characterization of the molecular mechanisms, such as high light irradiance resistance, that allowed plant terrestralization is a cornerstone in evolutionary studies since the conquest of land by plants played a pivotal role in life evolution on Earth. Viridiplantae or the green lineage is divided into two clades, Chlorophyta and Streptophyta, that in turn splits into Embryophyta or land plants and Charophyta. Charophyta are used in evolutionary studies on plant terrestralization since they are generally accepted as the extant algal species most closely related to current land plants. In this study, we have chosen the facultative terrestrial early charophyte alga *Klebsormidium nitens* to perform an integrative transcriptomic and metabolomic analysis under high light in order to unveil key mechanisms involved in the early steps of plants terrestralization. We found a fast chloroplast retrograde signaling possibly mediated by reactive oxygen species and the inositol polyphosphate 1-phosphatase (SAL1) and 3′-phosphoadenosine-5′-phosphate (PAP) pathways inducing gene expression and accumulation of specific metabolites. Systems used by both Chlorophyta and Embryophyta were activated such as the xanthophyll cycle with an accumulation of zeaxanthin and protein folding and repair mechanisms constituted by NADPH-dependent thioredoxin reductases, thioredoxin-disulfide reductases, and peroxiredoxins. Similarly, cyclic electron flow, specifically the pathway dependent on proton gradient regulation 5, was strongly activated under high light. We detected a simultaneous co-activation of the non-photochemical quenching mechanisms based on LHC-like stress related (LHCSR) protein and the photosystem II subunit S that are specific to Chlorophyta and Embryophyta, respectively. Exclusive Embryophyta systems for the synthesis, sensing, and response to the phytohormone auxin were also activated under high light in *K. nitens* leading to an increase in auxin content with the concomitant accumulation of amino acids such as tryptophan, histidine, and phenylalanine.

Keywords: light stress, Charophyta, omics integration, plant evolution, carotenoids, chloroplast retrograde signaling, linear/cyclic electron flow, PsbS/LHCSR NPQ systems

INTRODUCTION

The evolutionary history of the green plants kingdom or Viridiplantae splits into two different lineages Chlorophyta and Streptophyta. Chlorophyta are primarily constituted by marine and freshwater green microalgae. In turn, Streptophyta are divided into two different clades Charophyta and Embryophyta. Whereas Embryophyta comprises mainly land plants, Charophyta are still considered algae with a preference for freshwater and with some facultative terrestrial species (Becker and Marin, 2009). It is widely accepted that the primary adaptation of Charophyta to freshwater played a key role facilitating their transition to dry land in contrast to marine Chlorophyta. Plant terrestralization constitutes a key milestone in life evolution on Earth since it led to a massive increase in land biomass resulting in a substantial atmospheric CO_2 drop, oxygen increase and terrestrial habitat stabilization promoting land colonization by animals and fungi (Lenton et al., 2016; Morris et al., 2018). Present-day Charophyta are generally accepted as the extant algal species most closely related to the aquatic ancestors of land plants or Embryophyta. Accordingly, the molecular systems that potentially allowed this group of photosynthetic organisms to evolve toward terrestrial land plants are under intense analysis (Nishiyama et al., 2018). These studies focus mainly on genomic data. The lack of multi-omic data such as transcriptomic and metabolomic data for Charophyta under specific conditions relevant to the terrestralization process is preventing the full characterization of the molecular systems that promoted the transition to the first land plants (Hori et al., 2014). During this transition, the evolution of response molecular systems to terrestrial environmental stresses was critical. Some terrestrial physiological adaptations, such as desiccation resistance and tolerance to UV radiation are present in Charophyta from which current land plant mechanisms supposedly evolved (Becker and Marin, 2009). Multiple cellular features such as phragmoplast, plasmodesmata, hexameric cellulose synthase, and oogamous sexual reproduction with zygote retention first evolved in Streptophytic algae or Charophyta leading to multicellularity (Umen, 2014). A tight retrograde signaling communicating the chloroplast state to the nucleus making plastids more dependent on the nucleus has been reported in Charophyta under cold and high light stresses (De Vries et al., 2018). Other systems found in Embryophyta such as abscisic acid (ABA) and auxin biosynthesis and transport, photoprotective capacity, and adaptation to transient light changes have been identified in Charophyta as *Zygnema circumcarinatum* (Ohtaka et al., 2017; Pierangelini et al., 2017). Biosynthetic pathways sources of metabolites relevant to abiotic stresses typical of terrestrial environments such as the phenylpropanoid pathway has been described to first emerged in Charophyta (de Vries et al., 2021). In this study, we have chosen the freshwater facultative terrestrial Charophyte alga *Klebsormidium nitens* (*K. nitens*) as model organism to study the transcriptomic and metabolomic response to high light intensity recreating at least one of the most critical environmental changes faced by plants during terrestralization. *Klebsormidium* cultures consist of multicellular and non-branching filaments without specialized cells with a single chloroplast. Many *Klebsormidium* species are cosmopolitan distributed in terrestrial environments as soil crusts and rocks as well as freshwater habitats like streams and rivers where they contribute to important ecological roles as primary producers and soil stabilizers (Karsten et al., 2016). Their presence in these environments expose cells to extreme conditions including high light irradiance (Holzinger and Pichrtová, 2016). Physiological studies under such conditions have been carried out reporting photosynthetic resistance against intense light meditated by the presence of photoprotective mechanisms dissipating energy as heat (non-photochemical quenching, NPQ) (Gerotto and Morosinotto, 2013) and/or by the activation of alternative electron routes to reduce reactive oxygen species (ROS) production (Alboresi et al., 2019). Several comparative genomic analyses have been carried out providing evidence about *K. nitens* possessing fundamental molecular mechanisms required for the adaptation and survival in terrestrial environments including wax-related genes (Kondo et al., 2016), phytohormone signaling (Holzinger and Becker, 2015), and transcription factors involved in resistance to high light and UV radiation (Kitzing and Karsten, 2015; Domozych et al., 2016). Nonetheless, there are very few transcriptomic studies integrating gene expression with physiological data aiming at the characterization of *K. nitens* responses to abiotic stresses such as desiccation, cold, and heat (Holzinger et al., 2014; Rippin et al., 2019a; de Vries et al., 2020; Monte et al., 2020). Furthermore, *K. nitens* is also of interest for its biotechnological applications in the removal of nutrients from horticultural wastewater (Liu et al., 2016a) and in the production of polyunsaturated fatty acids and lipids (Liu et al., 2016b; Xu et al., 2021).

The goal of the current study consists in identifying the molecular mechanisms underlying the response to high light intensity in the Charophyte alga *K. nitens*. The similarity of these systems with those used by Embryophyta and Chlorophyta is discussed in order to elucidate the key mechanisms that allowed the transition from aquatic environments to dry land during plant evolution. Our results were obtained from an integrative analysis combining gene expression and metabolite profiles. Further validation of our results were carried out using pulse-amplitude-modulation fluorometry (PAM), Western blotting, and confocal microscopy.

MATERIALS AND METHODS

Algal Material, Growth Conditions, and Sample Collection

Klebsormidium nitens (strain NIES-2285) was obtained from the National Institute for Environmental Studies (Japan). Cells were grown photoautotrophically in Bold's Basal Medium using photobioreactors containing 0.8 L of cell suspension and bubbled with air supplemented with 1% (v/v) CO_2 as carbon source. Photobioreactors were continuously illuminated with white light lamps at 50 $\mu E\ m^{-2}\ s^{-1}$ and maintained at 20°C. Defoamer (Antifoam 204) was added to avoid the contamination of the aeration systems. Cultures at exponential phase with 45 μg/mL

chlorophyll content were used in our experiments. Control cultures were kept under a light irradiance of 50 μE m^{-2} s^{-1} whereas high light cultures were illuminated for 3 h with an irradiance of 1500 μE m^{-2} s^{-1}. Cells were collected by centrifugation at 3500 × *g* for 5 min at 4°C. Cell pellets were washed with PBS, flash frozen with liquid Nitrogen and stored at −80°C.

RNA-Seq Data Generation and Processing

Two independent biological replicates were considered for both low and high light irradiance conditions. RNA extraction was performed using mechanical disruption of the frozen cell pellets in a Mini Bead Beater (Biospe Products) mixed with 2.7 mm glass beads for filament fragmentation and 0.5 mm glass beads for individual cell lysis (ratio 1/3) in the presence of an extraction buffer consisting of phenol:chloroform (1:1, v/v). Subsequently, RNA was purified using ISOLATE II RNA Plant Kit (Bioline) following manufacturer's instructions. RNA integrity number (RIN) was computed using an Agilent 2100 Bioanalyzer producing values greater than 8 per sample. Sequencing libraries were generated according to Illumina TruSeq Stranded mRNA protocol and sequenced on an Illumina NextSeq 500 sequencer producing approximately 17 million 50 nt long reads per sample. The computational pipeline MARACAS (Romero-Losada et al., 2022) was used to determine differentially expressed genes according to a log2FC of ±1 and a *q*-value or false discovery rate (FDR) threshold of 0.05. MARACAS uses the *K. nitens* genome sequence assembly and annotation v1.0 (accession number DF236950) as reference genome (Hori et al., 2014). The software tool AlgaeFUN[1] was used to perform functional enrichment analysis based on Gene Ontology (GO) terms and Kyoto Encyclopedia of Genes and Genomes (KEGG) pathways over the sets of differentially expressed genes.

Specifically, in our study, MARACAS was set to run using fastqc, HISAT2 and Stringtie for quality control, read mapping, transcript assembly, and gene expression quantification, respectively (Pertea et al., 2016). Normalization is carried out in MARACAS based on the Bioconductor R package NormalyzerDE (Willforss et al., 2019). In our study, gene expression was normalized using quantile normalization. Differentially expressed genes were determined in MARACAS using the bioconductor R package limma based on linear models with a moderated t-student (Ritchie et al., 2015). This method estimates individual gene expression variance using information from all genes and can be applied in analysis with two replicates in contrast to R packages such as DESeq2 based on binomial negative distribution that require at least three replicates (Love et al., 2014). Several studies comparing the performance of limma (linear models with a moderated *t*-student) and DEseq2 (negative binomial distribution) conclude that, although they are mostly equivalent, limma outperforms DESeq2 at reducing batch effects and false positives (Seyednasrollah et al., 2013; Stupnikov et al., 2021). The presence of low levels of noise in our two replicates was confirmed in MARACAS using scatterplots and principal components analysis (PCA), **Supplementary Figure 1**. We also checked that our sequencing coverage (or depth) with more than 17 million reads per sample was enough to detect gene expression and determine differentially expressed genes using a saturation analysis that identified around 12 million read as the saturation point for RNA-seq data in *K. nitens* (**Supplementary Figure 1**). In conclusion, the read coverage, level of noise in our data and use of linear models with a moderated *t*-student would guarantee the reliability of our analysis based on two replicates.

[1]https://greennetwork.us.es/AlgaeFUN/

Metabolomic Data Generation and Processing

Six independent biological replicates were considered for low and high light irradiance metabolomic data generation. Significant differences were determined using the non-parametric Wilcoxon signed-rank test implemented in the wilcox.test function from the stats R package.

For metabolite content determination, cell pellets were lyophilized (Skadi-Europe TFD 8503), flushed with a nitrogen stream to prevent oxidation and stored at −20°C. Primary metabolites were determined from 20 mg of lyophilized biomass subjected to mechanical disruption in a Mini Bead Beater (Biospe Products) with a mixture of 2.7 and 0.5 mm glass beads (ratio 1/3) in the presence of 1 mL extraction buffer consisting of chloroform:methanol (3:7, v/v). As internal standard, 5 μL of ribitol 4 mM were added. Following centrifugation at 5000 × *g* for 5 min at RT (room temperature) the supernatant was collected. This process was repeated adding 1 mL of extraction buffer until the supernatant was colorless. The combined supernatants were dried under nitrogen stream, resuspended in Milli-Q water and submitted for analysis. Primary metabolite determination was carried out by ultra high performance liquid chromatography system coupled with mass spectrometry (UPLC/MS) as described in Mccloskey and Ubhi (2015).

Phytohormone content was determined from 50 mg of lyophilized biomass following the protocol presented in Salem et al. (2020). Cellular lysis and sample homogenization was performed as described above for RNA and primary metabolite extraction using, in this case, 1 mL of an extraction buffer consisting of methyl tert-butyl ether (MTBE):methanol (3:1, v/v). Samples were incubated for 30 min at 4°C in a rotating mixer, followed by sonication for 15 min at 4°C and centrifugation at 10,000 × *g* for 10 min. The supernatant was mixed with 0.1% HCl (1:1, v/v) and 20 μL of paracetamol added as internal standard at 4°C. Subsequently, samples were first vigorously vortexed for 1 min and then gently shaken in a rotating mixer for 30 min at 4°C and centrifuged again. The supernatant was dried overnight in spin vacuum and finally resuspended in water:methanol (1:1, v/v) and filtered for determination using UPLC/MS.

Carotenoid content was determined by high-performance liquid chromatography (HPLC) coupled to an UV-visible scanning spectrophotometer from 5 mg of lyophilized biomass using acetone extracts subjected to mechanical disruption for cell lysis and sample homogenization as described in Del Campo et al. (2004).

Pulse-Amplitude-Modulation Fluorometry

Photosynthetic parameters were determined by pulse-amplitude-modulation fluorometry (PAM) with a DUAL-PAM-100 (Walz). Samples were dark adapted for 10 min before fluorescence was measured. Values for basal fluorescence level, F_0, were determined after 5 min in the presence of non-actinic light 450 nm. Values for maximal fluorescence (F_m) were determined by applying a pulse of saturating red light 655 nm, 2.4 μE for 40 s. Values for photosystem II (PSII) maximal efficiency (F_v/F_m) were calculated as $(F_m–F_0)/F_m$. Cyclic electron flow (CEF) was detected by subjecting dark adapted samples to constant actinic light (500 μE) for 5 min and subsequently turning off light and measuring fluorescence.

Total Protein Extraction, Sodium Dodecyl Sulfate-Polyacrylamide Gel Electrophoresis, and Western Blotting Analysis

Cells were pelleted by centrifugation at 3500 × *g* for 5 min at 4°C, washed with PBS and resuspended in 50 mM Tris pH 8, SDS 9%, PID, PMSF 0.1 M and NaCl 150 mM. Total protein extracts were obtained by freeze/thaw cycles in liquid nitrogen followed by another mechanical disruption procedure as described above. Protein extracts were separated by sodium dodecyl sulfate-polyacrylamide gel electrophoresis (SDS-PAGE), stained with Comassie blue, and transferred onto a PVDF membrane (Immobilon®-P, pore size 0.45 μm) using a power blotting station (Invitrogen™, Thermo Fischer). Immunoblotting analysis was performed with an antibody against photosystem II subunit S (PsbS) at 1:1000 (Agrisera). Anti-rabbit secondary antibody was used at 1:10,000 (Invitrogen). Immunoblots were visualized using IQ800 Control software (ImageQuant 800, Amersham).

RESULTS AND DISCUSSION

Transcriptomic and Metabolomic Analysis Unveil a Response to High Light Intensity

Nuclear gene expression responses to high light in *K. nitens* were studied using RNA-seq data. We detected expression in 68.4% of the 17,290 genes in the current *K. nitens* genome annotation (Hori et al., 2014). We found that after 3 h of high light treatment 7.84% of the entire *K. nitens* genome was differentially expressed with respect to low light conditions. Specifically, we identified 677 activated and 678 repressed genes (**Figure 1** and **Supplementary Table 1**). Using AlgaeFUN (microALGAE FUNctional enrichment tool), we performed functional enrichment analysis based on GO terms to identify the cellular components and biological processes significantly affected by high light (**Figure 1**). The proteins encoded by differentially expressed genes, both activated and repressed genes, were significantly localized in the chloroplast thylakoid membranes indicating the initiation of a major chloroplast reprogramming. Specifically, proteins encoded by repressed genes were significantly associated with photosystems and cellular structures present during cell division such as condensed nuclear chromosomes and microtubules. Accordingly, photosynthesis, hexose biosynthesis, cell cycle, and DNA metabolism were significantly enriched processes in the repressed genes. This points to an arrest in the photosynthetic machinery and cell cycle progression as response to high light. Proteins encoded by activated genes are, in turn, significantly localized in cellular structures involved in *de novo* protein biosynthesis such as preribosomes and translation initiation factor 3′ complex. In particular, categories encompassing ribosome biogenesis, cytoplasmic translation initiation, and protein folding were significantly enriched in the activated genes. Moreover, response to oxidative stress, response to high light intensity, tetraterpenoid and carotenoid metabolism were identified as significantly activated processes. This suggests an activation of repair and protective mechanisms to damages caused by high light.

Metabolomic responses to 3 h of high light treatment in *K. nitens* were also analyzed. Six independent biological replicates were considered for both, high and low light conditions. We detected 69 different primary and secondary metabolites including most amino acids and some phytohormones, **Supplementary Table 2**. Significant differentially abundant metabolites were identified by performing the non-parametric Wilcoxon test using a *p*-value threshold of 0.05. We found 12 significantly more abundant and 8 less abundant metabolites under high light when compared to low light (**Figure 2**). For instance, under high light, we detected significant changes in specific carotenoids, accumulation of the amino acid tryptophan and the phytohormone indole-3-acetic acid (IAA).

An Activation of the Carotenoid Biosynthesis β-Branch and Xanthophyll Cycle Is Observed

Here, we present an integrated transcriptomic and metabolomic analysis of this specific photoprotective response to high light in *K. nitens* (**Figure 3**). The gene encoding the first enzyme in the carotenoid pathway and the main rate-limiting step, phytoene synthase (PSY, *kfl00019_0320*) was 1.53-fold activated after 3 h of high light treatment. Similarly, the genes encoding the next enzymes in the pathway producing lycopene, phytoene desaturase (PDS, *kfl00103_0130*), and ζ-carotene desaturase (ZDS, *kfl00496_0070*), were 1.88- and 1.64-fold activated, respectively. At this point carotenoid biosynthesis bifurcates into the ε-branch leading to lutein and the β-branch proceeding to β-carotene and the xanthophyll cycle. These two branches showed antagonist regulation in the response to high light in *K. nitens*. On the one hand, a strong gene repression of 7.49-fold was found for the enzyme funneling lycopene into the ε-branch, lycopene epsilon cyclase (LCYε, *kfl00536_0070*). Nonetheless, no significant change was observed in the carotenoids produced in this branch, α-carotene and lutein in contrast to the massive increase in this latest carotenoid observed in Chlorophyta as Chlamydomonas under

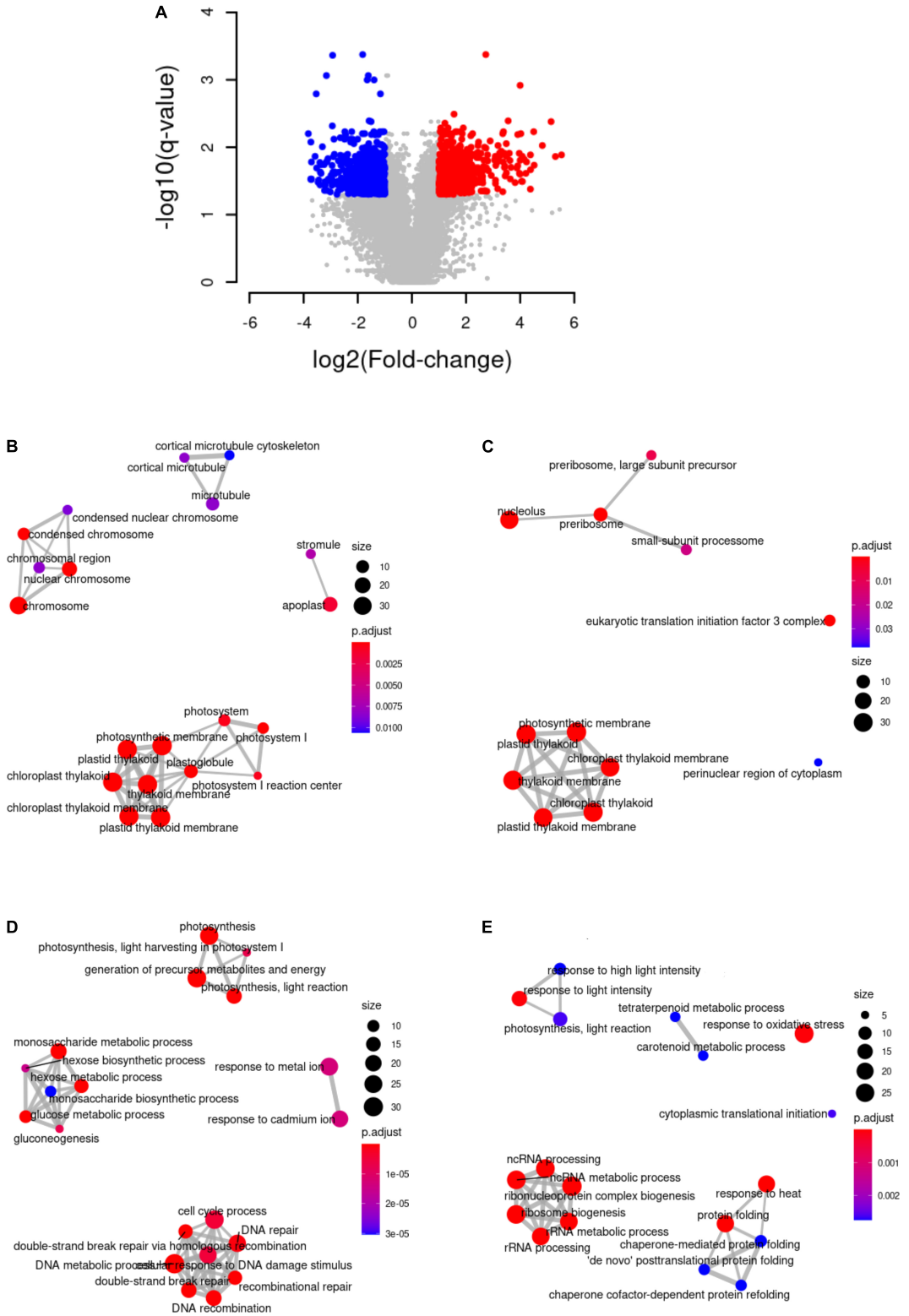

FIGURE 1 | Differential gene expression analysis under high light intensity and functional enrichment analysis. **(A)** Volcano plot representing differentially activated (red), repressed (blue), and unaltered (gray) genes under high light when compared to low light. **(B)** Cellular components to which the proteins encoded by repressed genes are significantly associated. **(C)** Cellular components to which the proteins encoded by the activated genes are significantly associated. **(D)** Biological processes in which the proteins encoded by the repressed genes are significantly involved. **(E)** Biological processes in which the proteins encoded by the activated genes are significantly involved.

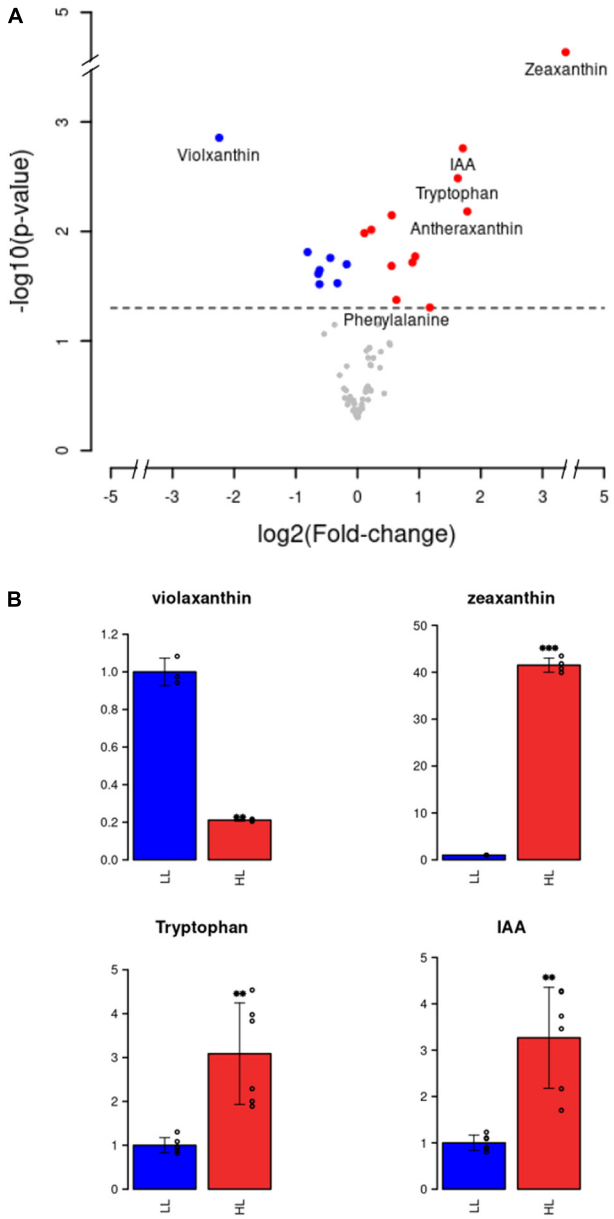

FIGURE 2 | Differential metabolite abundance analysis under high light intensity. **(A)** Volcano plot representing more abundant (red), less abundant (blue), and equally abundant (gray) metabolites under high light when compared to low light. **(B)** Barplots representing the relative metabolite abundance under high light in red (HL) with respect to low light in blue (LL) for violaxanthin, zeaxanthin, tryptophan, and indole-3-acetic acid (IAA).

high light (Ma et al., 2019). On the other hand, simultaneously, a strong gene activation of 2.52-fold was detected for the enzyme channeling lycopene into the β-branch, lycopene beta cyclase (LCYβ, *kfl00003_0600*) and of 2.24-fold for the enzyme β-carotene hydroxylase (BCH, *kfl00515_0050*) that converts β-carotene into zeaxanthin. This response has been also observed in Chlorophyta (Couso et al., 2012). Although, β-carotene content was similar under low and high light conditions, significant changes were found in the carotenoids constituting the xanthophyll cycle. Violaxanthin content decreased 4.73-fold whereas antheraxanthin and zeaxanthin contents were increased 3.44- and 41.5-fold, respectively, under high light when compared to low light. Accordingly, the gene encoding the enzyme involved in the xanthophyll cycle, violaxanthin de-epoxidase (VDE, *kfl00604_0070*) converting violaxanthin into antheraxanthin and zeaxanthin was activated 1.86-fold. Furthermore, the gene encoding zeaxanthin epoxidase (ZEP, *kfl00092_0060*) that catalyzes the synthesis of violaxanthin from zeaxanthin and antheraxanthin was 3.84-fold repressed under high light. In the xanthophyll cycle, the interconversion of violaxanthin into antheraxanthin and zeaxanthin, constitutes one of the major photoprotective mechanism in Embryophyta (Latowski et al., 2011) and Chlorophyta (Goss and Jakob, 2010). High light induces the mobilization of violaxanthin to zeaxanthin whereas low light or darkness produce the reverse reaction. De-epoxidation of violaxanthin to zeaxanthin enhances dissipation of excess excitation energy (NPQ) in the PSII antenna, thereby preventing inactivation and damage to the photosynthetic apparatus. NPQ is considered a fundamental mechanism for Streptophyta adaptation to terrestrial habitats (Pierangelini et al., 2017). Here, we specifically show that the xanthophyll cycle is part of the early transcriptomic and metabolomic response to high light intensity in the Charophyta *K. nitens*.

Chloroplast Retrograde Signaling Triggered by Oxidative Stress and Protein Misfolding Is Identified as a Response to High Light

Under high light conditions exceeding photosynthetic capacity, production of harmful ROS is unavoidable associated with electron transport in the photosystems. Excess electron leakage to molecular oxygen and incomplete water oxidation produce singlet oxygen ($^1O_2$), superoxide ($O_2^{\cdot -}$), hydrogen peroxide (H_2O_2), and hydroxyl radical ($HO^{\cdot}$) (Pospíšil, 2016). This triggers a signaling cascade communicating the chloroplast state to the nucleus termed retrograde signaling that ultimately induces the expression of nuclear genes. The evolution of this system has played a central role in plant terrestralization (Zhao et al., 2019; Calderon and Strand, 2021). Retrograde signaling induced by ROS is dependent on executer (EX, *kfl00184_0040*), whose gene expression was not affected in our experiment, and on the FtsH2 protease (*kfl00201_0150*) strongly activated in our study (Dogra et al., 2017, 2019b; Kim, 2020). Indeed, response to oxidative stress was one of the most significant GO term in our functional enrichment analysis over the activated genes in a response to high light treatment in *K. nitens*. More than twofold activation was detected in genes encoding chloroplast targeted antioxidant enzymes such as catalase (CAT, *kfl01057_0030*) and peroxiredoxins Q (PRXQ, *kfl00014_0230* and *kfl00014_0250*) that, together with carotenoids such as zeaxanthin, contribute to ROS scavenging (Pinnola and Bassi, 2018). Under these conditions proteins suffer oxidative damage specifically but not limited to the active thiol groups of cysteine residues, which are oxidized to disulfide bonds (Cejudo et al., 2021). This

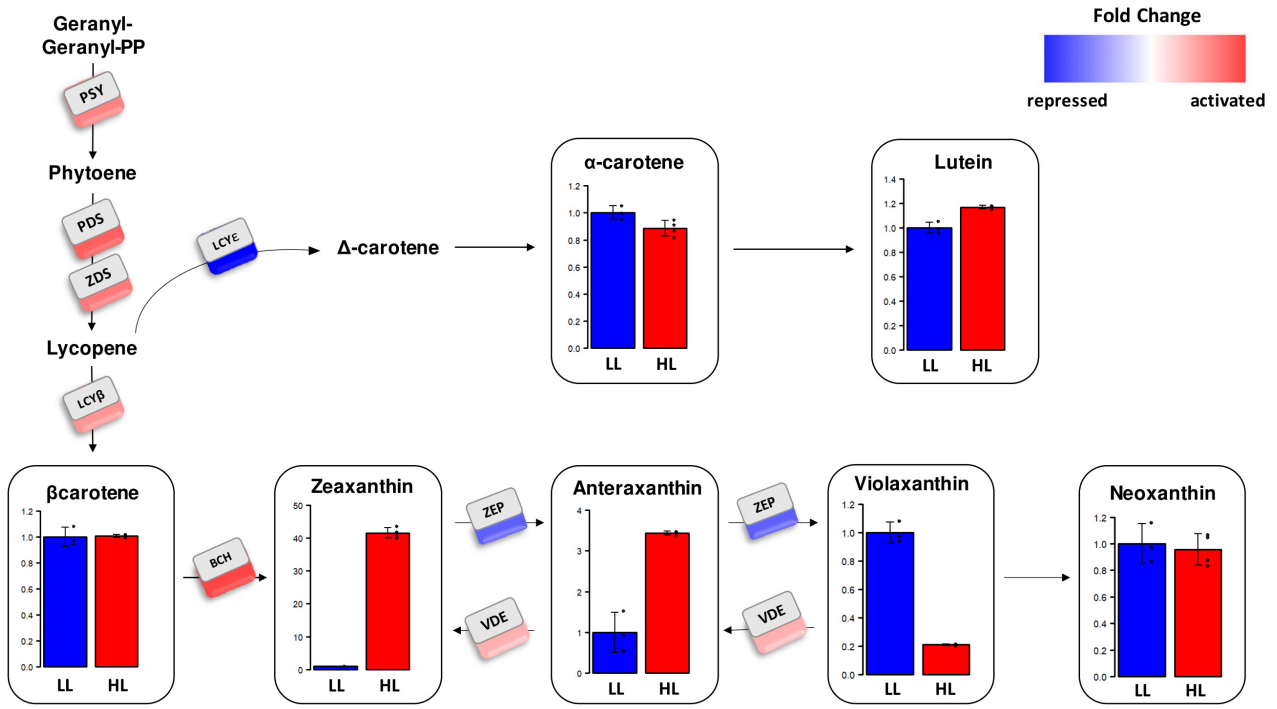

FIGURE 3 | Gene expression level and relative carotenoid content in the carotenoid biosynthesis pathway in *Klebsormidium nitens* under high light (HL) and low light (LL). Expression fold change under high light compared to low light is represented for genes corresponding to the different enzymes involved in carotenogenesis in *Klebsormidium nitens*: phytoene synthase (PSY), phytoene desaturase (PDS), ζ-carotene desaturase (ZDS), lycopene epsilon cyclase (LCYε), lycopene beta cyclase (LCYβ), β-carotene hydroxylase (BCH), violaxanthin de-epoxidase (VDE), and zeaxanthin epoxidase (ZEP). Red squares represent strong activation whereas blue squares stand for strong repression. Barplots show relative carotenoid content under high light in red (HL) compared to low light in blue (LL).

produces major modifications in protein structure that can lead to misfolding and loss of function. The accumulation in the chloroplast of aberrant misfolded proteins also contributes to initiate retrograde signaling (Dogra et al., 2019a). In this respect, activation was identified for genes such as *kfl00120_0050* and *kfl00573_0030* encoding several thioredoxin-disulfide reductases (TRX) and *kfl00021_0420* corresponding to NADPH-dependent thioredoxin reductase (NTR). These enzymes constitute a system involved in oxidative damage avoidance by supplying reducing power to reductases repairing oxidized proteins (Vieira Dos Santos and Rey, 2006; **Figure 4**). Moreover, we found the activation of multiple chloroplast targeted chaperones, co-chaperones and chaperonins that would contribute to restore misfolded proteins, such as heat shock proteins 90 and 101 (HSP90, *kfl00002_0530* and HSP101, *kfl00387_0020*); chloroplast chaperonin 60 alpha and beta subunits (CPN60A, *kfl00113_0150* and CPN60B, *kfl00076_0150*), specifically involved in Rubisco correct folding (Zhao and Liu, 2018), and chloroplast GrpE involved in correct oligomerization of the photosynthesis-related light harvesting complex II (LHCII) in *Arabidopsis* (de Luna-Valdez et al., 2019). An example of a protein that suffers severe oxidative damage under high light stress is the D1 protein (PsbA) located at PSII reaction center. Specific tryptophan residues undergo oxidation in this protein triggering protein repair mechanisms (Dogra et al., 2019a). It has been shown that the aminoacids trypthophan and histidine easily suffer photooxidation (Huvaere and Skibsted, 2009). Recent studies have shown accumulation of tryptophan and phenylalanine under several environmental conditions as high light, drought, and temperature stress in Embryophyta (Galili et al., 2016). In this respect, our analysis shows that similar accumulation of the amino acids tryptophan, phenylalanine, and histidine takes place in a response to high light stress in Charophyta, like *K. nitens*, **Supplementary Table 2**.

Concomitant to the activation of protein repair mechanisms we found significant activation of ribosome biogenesis and cytoplasmic translation initiation (**Figure 1**). For example, genes encoding nuclear enzymes involved in 18S, 40S, and 60S rRNA biogenesis (UTP15 *kfl00593_0050*, NOB1 *kfl00104_0280*, and MDN1 *kfl00198_0260*) were strongly activated. Similarly, the genes CRM1 (*kfl00518_0070*) and NMD3 (*kfl00006_0030*), encoding nuclear export systems of these ribosomal components, were also detected as more than twofold activated. Additional activation was identified, for instance, in genes corresponding to eukaryotic translation initiation factor 2 (eIF2 *kfl00434_0020*) and 3 (eIF3 *kfl00078_0290*) (**Figure 4**). These strongly activated processes are required for *de novo* protein synthesis and, together with the previously described protein repair mechanisms, constitute part of the response to high light in *K. nitens*, contributing to maintain proteome homeostasis under this stress.

Besides, the retrograde signaling pathways induced by ROS and aberrant misfolded proteins discussed above,

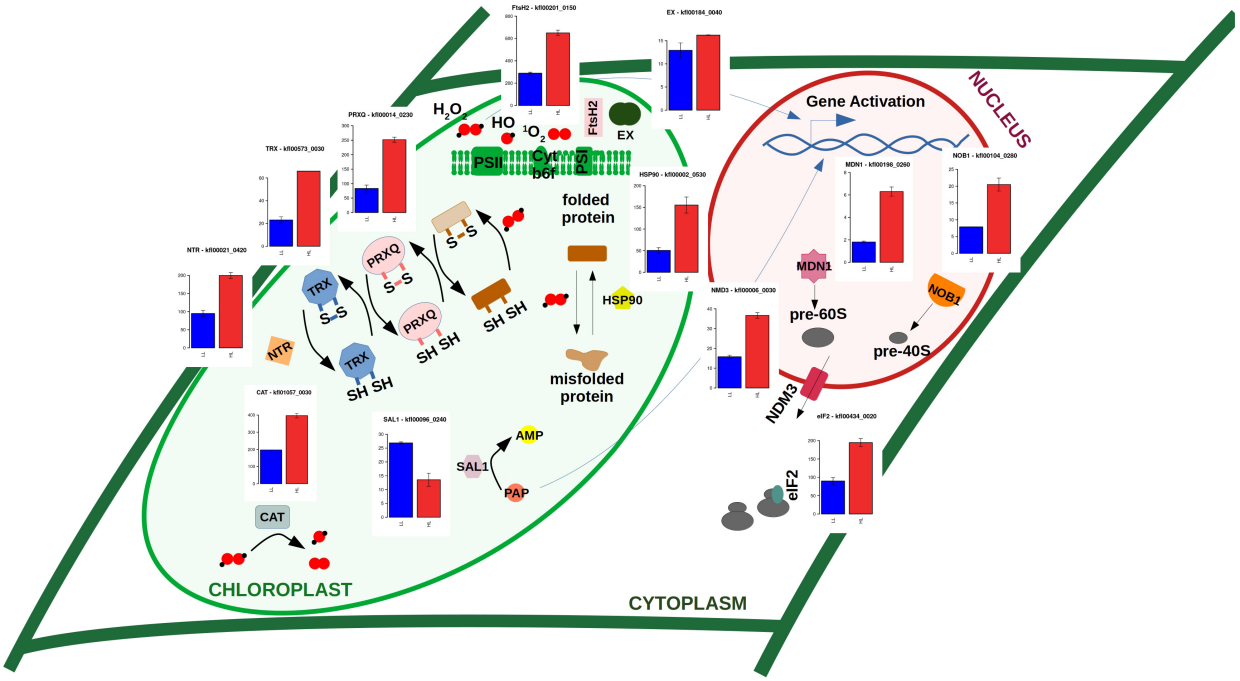

FIGURE 4 | Gene expression level for enzymes involved in retrograde signaling triggered by high light oxidative stress inducing gene activation of protein repair mechanisms and *de novo* protein synthesis. Barplots represent gene expression measured in FPKM (Fragments per Kilobase of exon and million of Mapped reads) under high light in red (HL) and low light in blue (LL) for enzymes EX (executer), protease FtsH2, PRXQ (peroxiredoxin Q), TRX (thioredoxin), NTR (NADPH-dependent thioredoxin reductase), HSP90 (heat shock protein 90), CAT (catalase), SAL1 (inositol polyphosphate 1-phosphatase), midasin AAA ATPase 1 (MDN1), NIN/RPN12 binding protein (NOB1), nonsense-mediated decay 3 (NMD3), and eukaryotic translation initiation factor 2 (eIF2).

there exists another pathway regulated by the accumulation of 3′-phosphoadenosine-5′-phosphate (PAP). The inositol polyphosphate 1-phosphatase (SAL1) removes PAP preventing its accumulation. The gene encoding this enzyme *kfl00096_0240* was twofold repressed indicating a possible accumulation of PAP and an activation of the SAL1-PAP retrograde signaling pathway, as a response to high light intensity in *K. nitens*.

Cyclic Electron Flow Is Strongly Induced as a Response to High Light

Photosynthetic electron flow operates in two modes, linear and cyclic (Suorsa, 2015). Our transcriptomic analysis unveiled an antagonist regulation of these two systems as a response to high light in *K. nitens*. The major route of electron transport in oxygenic photosynthesis is linear electron flow (LEF) initiated from water by harvesting sunlight and transferring excitation energy by LHCII to PSII and then through cytochrome b6f (Cytb6f) to photosystem I (PSI) and NADP+ toward the Calvin–Benson cycle. Proteins encoded by repressed genes during the response to high light in *K. nitens* were significantly associated with both photosystems resulting in a strong repression of photosynthesis and hexose biosynthesis (**Figure 1**). For example, we found more than twofold repression for genes corresponding to the LHCII protein LHCB1 (*kfl00098_0080*); to the PSII proteins PsbP (*kfl00239_0120*) and PsbW (*kfl00638_0030*); to the Cytb6f protein PetC (*kfl00433_0020*); and to the PSI proteins PsaD (*kfl00193_0150*) and PsaO (*kfl00283_0090*) (**Figure 5**). Funneling electrons from PSI to the Calvin–Benson cycle we found similarly repressed genes encoding ferredoxin-NADP-reductase (FNR, *kfl00169_0050*) and ferredoxin (Fd, *kfl00017_0060*). Correspondingly, gene repression was identified for all the enzymes involved in CO_2 assimilation from the Calvin–Benson cycle. This indicates a strong repression of LEF in *K. nitens* under high light stress overexciting photosystems and producing electron excess that would damage them. Certainly, we observed lower values for PSII maximal efficiency (F_v/F_m) under high light 0.49, when compared to low light 0.66. As described in the previous section an excess of electrons at the PSI acceptor side results in reduction of molecular oxygen and generation of superoxide ($O_2^{\cdot -}$). The Mehler reaction or water–water cycle removes this harmful anion radical. In our transcriptomic analysis, we detected gene activation for enzymes in this cycle as superoxide dismutase (SOD, *kfl00631_0030*), converting $O_2^{\cdot -}$ to H_2O_2, and ascorbate peroxidase (APX, *kfl00460_0010*), which scavenges H_2O_2 with the aid of ascorbate to produce H_2O and monodehydroascorbate radical (MDA). In turn, MDA is reduced by the MDA reductase (MDAR, *kfl00196_0050*) (Cardol et al., 2011). Nonetheless, the corresponding gene was found underexpressed in high light when compared to low light conditions. Flavodiiron proteins (Flv, *kfl00041_0060*) constitute another enzymatic system involved in the water–water cycle photoreducing O_2 to H_2O. Although Flv genes can be found in Charophyta genomes (Chaux et al., 2017) no activation

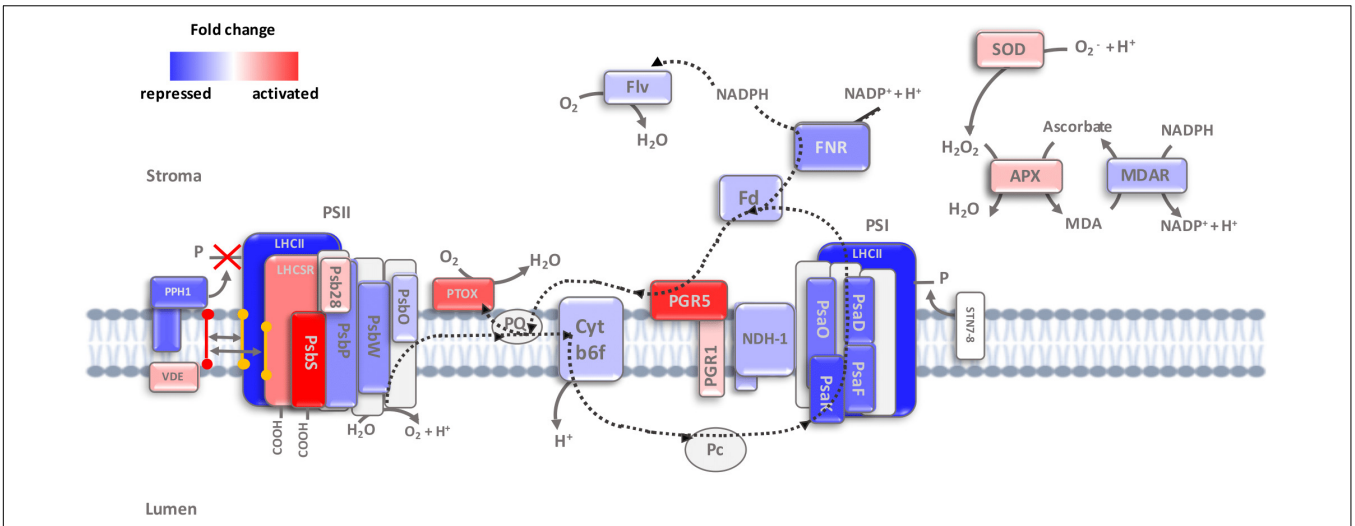

FIGURE 5 | Electron flow through photosystems and non-photochemical quenching mechanisms dissipating excess light energy. Expression fold change under high light compared to low light is represented for genes corresponding to the different proteins involved in linear and cyclic electron flow, NPQ, state transitions and water-water cycle: violaxanthin de-epoxidase (VDE), light harvesting complex II (LHCII), LHC-like stress related (LHCSR) protein, photosystem II subunit S (PsbS), photosystem II subunit 28 (Psb28), photosystem II subunit P (PsbP), photosystem II subunit W (PsbW), photosystem II subunit O (PsbO), plastid terminal oxidase (PTOX), plastoquinone (PQ), cytochrome b6f (Cytb6f), proton gradient regulation 5 (PGR5), PGR-like 1 (PRGL1), NADH dehydrogenase-like complex (NDH), photosystem I subunit O (PsaO), photosystem I subunit K (PsaK), photosystem I subunit D (PsaD), photosystem I subunit F (PsaF), photosystem I subunit D (PsaD), photosystem I subunit F (PsaF), ferredoxin (Fd), ferredoxin-NADP-reductase (FNR), flavodiiron proteins (Flv), protein phosphatase 1 (PPH1), state transition 7/8 (STN7/8), superoxide dismutase (SOD), ascorbate peroxidase (APX) and monodehydroascorbate radical reductase (MDAR). Red represents strong activation whereas blue stands for strong repression under high light.

was identified suggesting their expression is not related to the response to high light in *K. nitens* (**Figure 5**).

In contrast to LEF, our transcriptomic analysis unveiled a strong activation in CEF around PSI. In this route, electrons are recycled from Fd back to plastoquinone (PQ), creating a transthylakoid proton gradient, and leading to the production of only ATP (**Figure 5**). Indeed, we detected CEF activity as a clear transient increase in chlorophyll fluorescence after turning off actinic light by PAM in *K. nitens* cultures under high light that was not observed under low light (**Figure 6**). CEF has been identified as an essential regulatory process governing light acclimation and photosystems protection from ROS after high light exposure in Chlorophyta and Embryophyta (Iwai et al., 2010; Ma et al., 2021). Two different CEF pathways have been identified based on their different sensitivity to antimycin (Ravenel et al., 1994). The antimycin-insensitive CEF pathway is dependent on the NADH dehydrogenase-like complex (NDH). Even though this is the major pathway in cyanobacteria (Miller et al., 2021) and it plays crucial roles at low light intensity in Embryophyta such as rice (Yamori et al., 2015) and *Marchantia polymorpha* (Ueda et al., 2012), Ndh genes have disappeared from most Chlorophyta species including *Chlamydomonas*, *Chlorella*, *Scenedesmus*, and *Ostreococcus*. Nonetheless, Ndh genes are present in Charophytic genomes as *Chara* and *Mesostigma* (Peltier et al., 2010). Specifically, in *K. nitens*, several Ndh isoforms have been detected (Hori et al., 2014). However, all the Ndh subunits encoded by nuclear genes such as Ndh M/N/O (*kfl00053_0440*, *kfl00564_0070*, and *kfl00414_0120*) presented strong downregulation under high light (**Figure 5**). This suggests that the major CEF pathway in *K. nitens* under this stress is not dependent on the Ndh complex. In the antimycin-sensitive CEF pathway, the proteins proton gradient regulation 5 (PGR5, *kfl00020_0020*) and PGR-Like 1 (PRGL1, *kfl00342_0140*) are essential components. Genes corresponding to these proteins have been identified across Chlorophyta, Charophyta, and Embryophyta (Peltier et al., 2010; Hori et al., 2014; Yamamoto and Shikanai, 2019) which supports their relevance in the physiology of photosynthetic organisms. Although PGR5 plays a pivotal role in CEF, its function is not fully characterized. PGRL1 is a transmembrane protein with an iron cofactor, which is probably responsible for electron transfer from Fd to PQ (Ma et al., 2021). Both proteins PGR5 and PGRL1 need to operate jointly for efficient CEF to take place. Our analysis unveiled a strong activation of 5-fold in the gene encoding PGR5 and a mild activation of 1.24-fold in the gene for PGRL1 indicating that this is the major CEF pathway in response to high light in *K. nitens*.

The redistribution of excitation energy between PSII and PSI by reversible phosphorylation of LHCII, known as state transitions, plays an important role in light response in plants (Mekala et al., 2015). In state I, LHCII is phosphorylated by the kinases State Transition 7/8 (STN7/8, *kfl00129_0080* and *kfl00018_0210*) separated from PSII and adhered to PSI. In state II, LHCII is dephosphorylated by protein phosphatase 1 (PPH1, *kfl00753_0080*), and moved back to PSII. In our transcriptomic data, we found a strong repression greater than threefold in the gene encoding PPH1 and no significant changes in the genes for STN7/8 (**Figure 6**). This suggests that, in a response to high light,

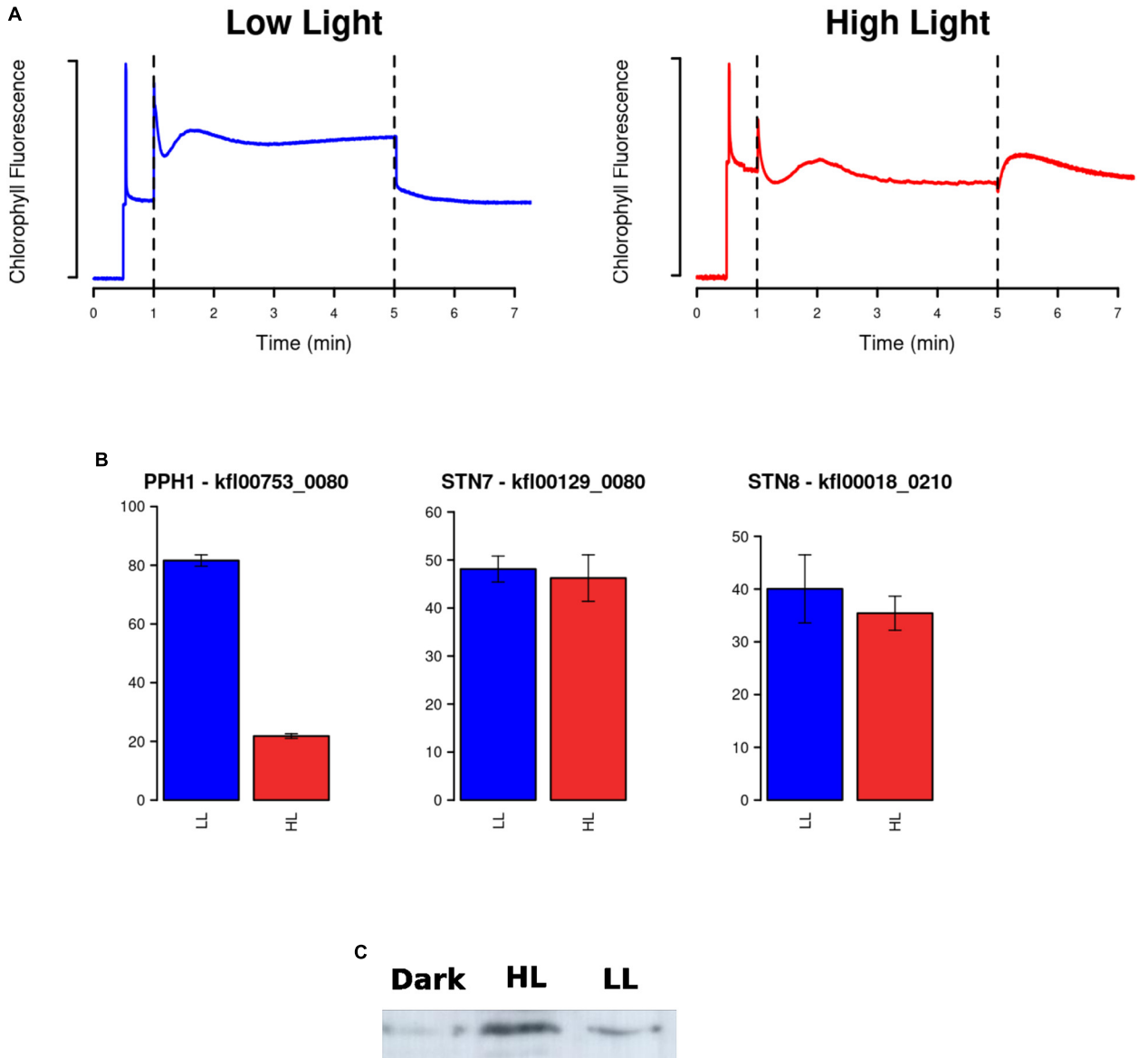

FIGURE 6 | Measurement of cyclic electron flow (CEF), gene expression of enzymes involved in state transitions and identification of the response in PsbS protein abundance to light intensity. **(A)** Dark adapted *Klebsormidium nitens* cultures exposed to low light (blue) or high light (red) were subjected to actinic light after the first minute. CEF activity was detected after 5 min when actinic light was turn off and a clear transient increase in chlorophyll fluorescence was observed only for the high light cultures (red) using pulse-amplitude-modulation fluorometry. **(B)** Barplots representing gene expression measured in FPKM (Fragments per Kilobase of exon and million of Mapped reads) under high light in red (HL) and low light in blue (LL) for enzymes involved in state transitions: protein phosphatase 1 (PPH1) involved in dephosphorylation of light harvesting complex II (LHCII) associating it with photosystem II (PSII) and kinases State Transition 7/8 (STN7/8) involved in phosphorylation of LHCII associating it with photosystem I (PSI). **(C)** Identification of the PsbS protein abundance response using Western blotting with anti-PsbS antibody. Almost no PsbS protein was detected from cultures maintained under constant dark for 24 h (dark), whereas for cultures under high light (HL) greater PsbS protein abundance was observed when compared to low light (LL).

K. nitens locks photosystems in state I maintaining LHCII bound to PSI which would protect PSII from excess light and allocate light energy to PSI further enhancing CEF.

Another system contributing to adjust the redox poise of the photosynthetic electron transport chain tuning the ratios between LEF and CEF is constituted by the concerted operation between plastid terminal oxidase (PTOX, *kfl00009_0280*) and NADH dehydrogenase (Rumeau et al., 2007). Our transcriptomic analysis showed 3.5-fold upregulation of the corresponding gene for PTOX in high light cultures similar to a common adaptation strategy in marine phytoplankton to high light conditions (Cardol et al., 2008). This system has also been proposed to act as a safety valve during photosynthesis, preventing over reduction of the PQ pool during light stress (Niyogi, 2000).

Photosystem II Subunit S and LHC-Like Stress Related Systems Are Simultaneously Activated Under High Light

Non-photochemical quenching plays an essential role in photoprotection dissipating excessive absorbed light energy as heat. Two different proteins for NPQ activation are known in Chlorophyta and Embryophyta, namely, the LHC-like stress related (LHCSR) protein and the PsbS. These two systems induce NPQ through different molecular mechanisms. LHCSRs are grouped under the so-called stress-induced chlorophyll-binding proteins (Dittami et al., 2010). The abundance of LHCSR increases under high light just as NPQ is induced (Peers et al., 2009). LHCSR homologs have been shown to be involved in NPQ in diatoms (Bailleul et al., 2010; Zhu et al., 2010). LHCSR binds pigments and is capable of efficiently dissipate excitation energy as heat. PsbS induces a reorganization of the photosynthetic apparatus by interfering with the formation of aggregates of thylakoid membrane proteins, thus allowing easy exchange and incorporation of xanthophyll cycle pigments into such structures. The structures formed in the presence of violaxanthin are characterized by minimized dissipation of excitation energy, whereas the structures formed in the presence of zeaxanthin show enhanced excitation quenching (Welc et al., 2021). It has been reported that NPQ relies mainly on PsbS in Embryophyta (Li et al., 2000) whereas in Chlorophyta the major role is played by LHCSR (Peers et al., 2009). Our study aims at contributing to the elucidation of these two systems in Charophyta as *K. nitens*.

Our transcriptomic analysis identified a strong overexpression of both systems under high light when compared to low light in *K. nitens*. Specifically, we detected a 3-fold activation of the gene *kfl00478_0030* corresponding to LHCSR and a massive upregulation of 114-fold in the gene encoding PsbS, *kfl00093_0070* (**Figure 5**). Although the PsbS transcript has been detected previously in *K. nitens*, the identification of the corresponding protein remained elusive (Hori et al., 2014). Accumulation of the PsbS protein has only been detected in Charophyta, such as *Zygnema* and *Mesotaenium* (Gerotto and Morosinotto, 2013) and so, it was discussed that the PsbS system is only operational in late and not in early Charophyta as *K. nitens*. In contrast to these previous negative results, we were able to detect the protein PsbS in *K. nitens* protein extracts using Western blotting (**Figure 6**). We observed almost no detectable PsbS protein from cultures maintained under constant dark for 24 h whereas for cultures under low light a band corresponding to PsbS was detected whose level was increased in cultures under high light supporting a response of this system to increasing levels of light intensity (**Figure 6**).

Our results support the fact that, as a response to high light, both systems based on LHCSR and PsbS are strongly activated for efficient NPQ in early Charophyta as *K. nitens*. A similar response has been described for the Bryophyta *Physcomitrium patens* (Gerotto et al., 2012), which diverged from vascular plants early after land colonization. In this specie, both systems are also active, contributing to efficient NPQ. This suggests the co-existence of these two NPQ mechanisms from early Charophyta to Bryophyta during plant evolution, before the emergence of vascular land plants that eventually lost LHCSR while retaining PsbS instead (Pinnola, 2019).

Genes Present Only in Streptophyta Are Induced as a Response to High Light Intensity

Based on sequence similarity, specific genes only found in Streptophyta were identified in *K. nitens*, as those without a significant homolog in Chlorophyta genomes (Hori et al., 2014). These genes could have played important roles in the adaptation of Charophyta to terrestrial environments, promoting land colonization by Streptophyta. According to this classification, we found 70 specific Streptophyta activated genes corresponding to 10% of the whole activated transcriptome in *K. nitens*. Several genes with significant sequence homology to transcription factors involved in development in Embryophyta were identified. For example, potential homolog genes of transcription factors regulating floral transition in *Arabidopsis* were found activated as *kfl00088_0250* (Homeobox 51), *kfl00396_0130* (Protodermal Factor 2), and *kfl00882_0020* (Terminal Flower 1). Similarly, we identified, as significantly activated, the genes *kfl00186_0090* and *kfl00862_0040* potential homologs of the transcription factors growth regulating factor 2 (grf2) and homeobox 2 (HB-2), respectively (**Figure 7**). These are regulators of cell growth, expansion and proliferation as a response to phytohormones in *Arabidopsis* (He et al., 2020). Genomic studies have unveiled certain types of primitive land plant signaling pathways for phytohormone response in *K. nitens* (Holzinger and Becker, 2015; Holzinger and Pichrtová, 2016). These primitive phytohormone systems may be involved in various responses to harsh environmental stresses on land in this early Charophyta (Hori et al., 2014). Our metabolomic analysis identified the presence of the phytohormones salicylic acid (SA), gamma-aminobutyric acid (GABA), ABA, indole-3-carboxylic acid (ICA), and IAA in *K. nitens* cultures, **Supplementary Table 2**. None of these phytohormones changed significantly except IAA with a threefold increase under high light (**Figure 2**). Auxins are synthesized from tryptophan through a pathway where the protein YUCCA plays a central role. As described previously, our metabolomic analysis found a significant threefold increase in tryptophan abundance under high light that could be related to the increase in IAA content. Moreover, the gene *kfl00109_0340* encoding YUCCA exhibited a large 16-fold increase in expression in a response to high light in *K. nitens*. Other Streptophyta specific genes involved in auxin sensing and response such as the receptor *kfl00434_0030* (auxin signaling F-box 3, AFB3) and *kfl00426_0080* (expansin, EXP) were also significantly activated under high light (**Figure 7**). Nevertheless, no significant change was observed in the gene *kfl00071_0010* encoding the single PIN auxin transporter protein identified in *K. nitens*. However, the expression of the related gene *kfl00192_0040*, encoding a sterol 4-alpha-methyl-oxidase (SMO), was also increased under high light. It has been suggested that SMO enzymes affect the polar localization of PIN altering developmental processes in Embryophyta (Zhang and Li, 2016). Auxins has been described to

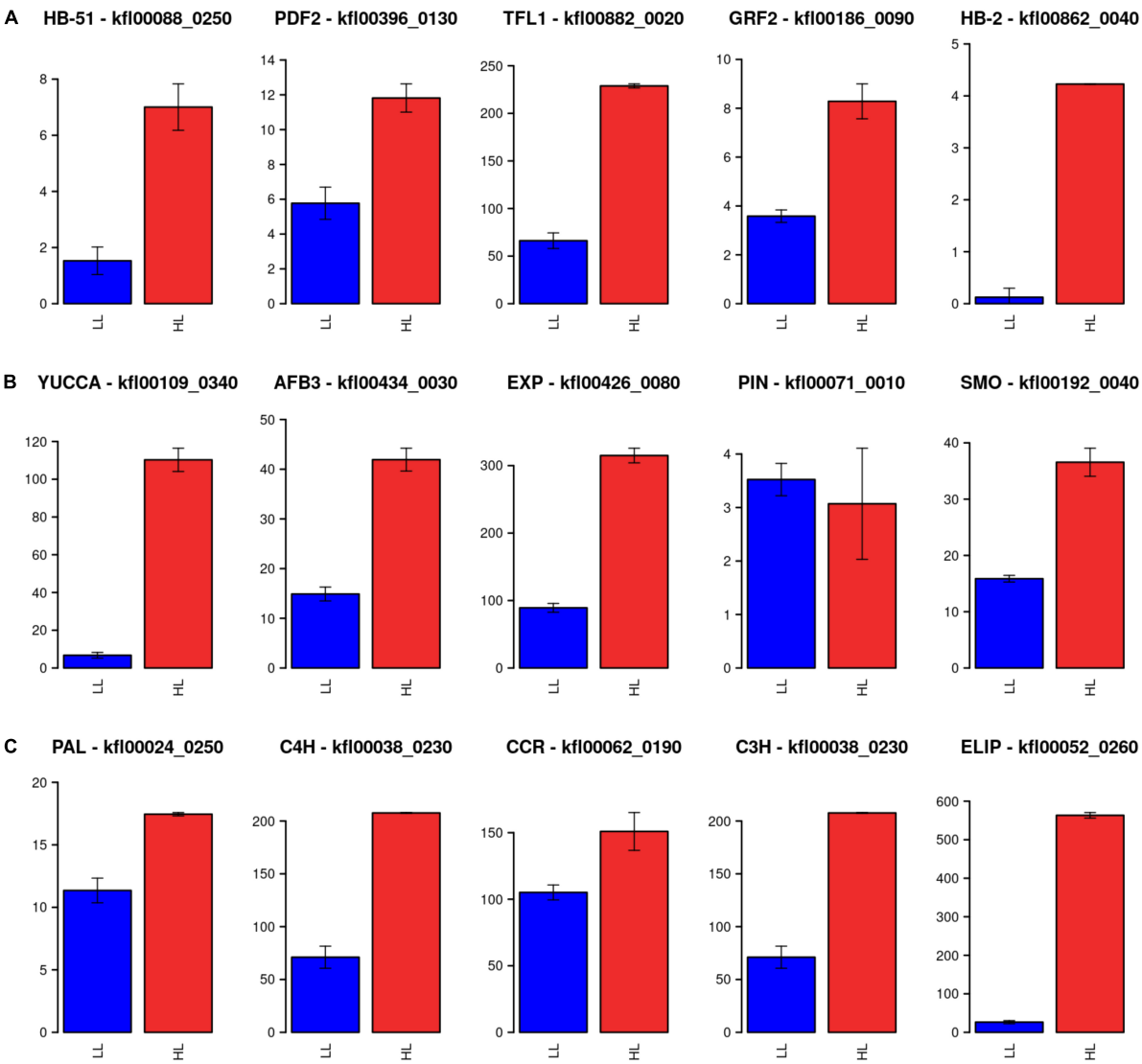

FIGURE 7 | Expression level for Streptophyta exclusive genes. **(A)** Barplots representing gene expression measured in FPKM (Fragments per Kilobase of exon and million of Mapped reads) under high light in red (HL) and low light in blue (LL) for potential homolog genes of transcription factors regulating floral transition in *Arabidopsis*: Homeobox 51 (HB-51), Protodermal Factor 2 (PDF2), and Terminal Flower 1 (TFL1). **(B)** Barplots representing gene expression measured in FPKM (Fragments per Kilobase of exon and million of Mapped reads) under high light in red (HL) and low light in blue (LL) for potential homolog genes involved in auxin biosynthesis, sensing, and response in *Arabidopsis*: YUCCA, auxin signaling F-box 3 (AFB3), expansin (EXP), PIN, and sterol 4-alpha-methyl-oxidase (SMO). **(C)** Barplots representing gene expression measured in FPKM (Fragments per Kilobase of exon and million of Mapped reads) under high light in red (HL) and low light in blue (LL) for potential homolog genes involved in the phenylpropanoid pathway: phenylalanine ammonia-lyase (PAL), cinnamate 4-hydroxylase (C4H), cinnamoyl-CoA reductase (CCR), and 4-coumarate 3-hydroxylase (C3H). The high activation of early light induced protein (ELIP) is also shown.

induce cell elongation in plants (Ma and Li, 2019). Although no phenotypic change was apparent after 3 h of high light treatment, we could observe significant cell elongations (p-vale 1.3×10^{-11}) in *K. nitens* filaments after 72 h (**Figure 8**). Nonetheless, the observed cell elongation could be produced by the arrest in cell cycle identified in our functional enrichment analysis (**Figure 1**) rather than on the activation of IAA responsive genes such as EXP (Ohtaka et al., 2017).

The phenylpropanoid pathway was considered to be an important Embryophyta specific source for metabolites relevant to environmental stresses. Nonetheless, candidate homologous genes codifying for enzymes acting at different steps in this pathway have recently been identified in *K. nitens* (de Vries et al., 2021). Concomitant to an increase in the aromatic amino acid phenylalanine, input to this pathway (**Figure 2**), some of these genes were found activated under high light stress in our study (**Figure 7**). Specifically, one of the candidate genes encoding phenylalanine ammonia-lyase (PAL) *kfl00024_0250* was 1.53-fold activated. Although no clear cinnamate 4-hydroxylase (C4H) homolog has been determined in *K. nitens* one of the candidates

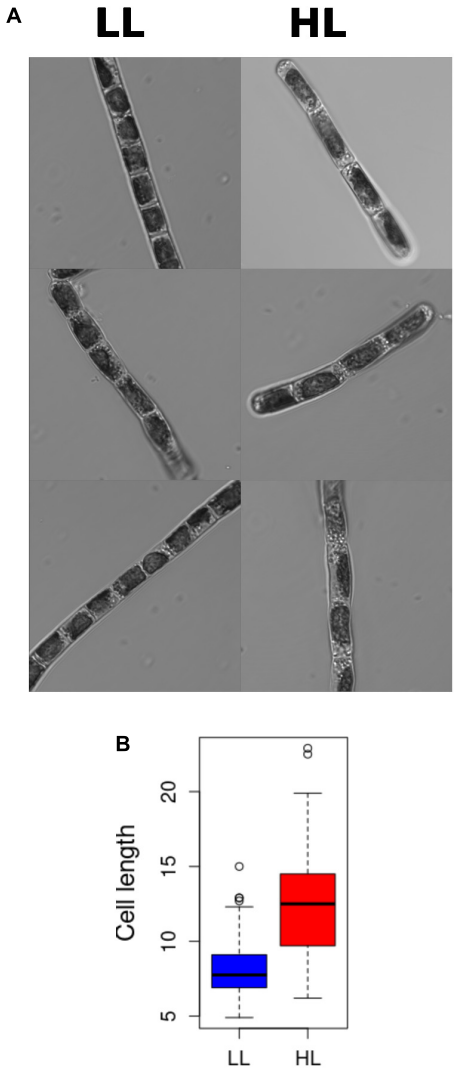

FIGURE 8 | *Klebsormidium nitens* cell elongation under high light. **(A)** Confocal images of *Klebsormidium nitens* cells under low light (LL) on the left and high light (HL) on the right. **(B)** Boxplot representing the significative increase in cell elongation under high light (HL) in red when compared to low light (LL) in blue.

kfl00038_0230 was 3-fold activated. Similarly, candidates for 4-coumarate 3-hydroxylase (C3H), *kfl00038_0230*, and cinnamoyl-CoA reductase (CCR), *kfl00062_0190*, were 2.92- and 1.43-fold activated, respectively.

Early light induced proteins (ELIPs) were thought to be Embryophyta specific stress responsive mechanisms (Adamska et al., 1992). Nonetheless, ELIPs have been found activated in Charophyta under abiotic stresses such as heat and desiccation (Holzinger et al., 2014; De Vries et al., 2018; Rippin et al., 2019b; de Vries et al., 2020). In our study, genes codifying for ELIPs were among the most activated ones under high light stress, for example, *kfl00052_0260* was more than 21-fold activated (**Figure 7**).

CONCLUSION

Klebsormidium nitens, as a representative of early Charophyta, exhibit the co-existence of high light response mechanisms that are also detected in Chlorophyta and Embryophyta. Assuming that these systems have not independently arisen in *K. nitens*, our results support a model by which the streptophyte ancestor of land plants conserved features of its chlorophyte relatives and also developed new signaling responses to high light that promoted the transition to land and the emergence of Embryophyta. *K. nitens* possesses a tight and fast chloroplast retrograde signaling, possibly mediated by ROS and the SAL1-PAP pathways, as suggested by the downregulation of the *SAL1* gene. This system, after only 3 h of high light, induces gene expression and accumulation of specific metabolites to overcome this stress, especially relevant in terrestrial environments. Precisely, mechanisms common to Chlorophyta and Embryophyta are induced such as the xanthophyll cycle, with VDE activation and ZEP repression, leading to the accumulation of zeaxanthin; and protein repair mechanisms based on the NTR-TRX-PRX system. Further photoprotective mechanisms were identified such as the downregulation of LEF and the upregulation of CEF, with the specific activation of PGR5 and repression of Ndh components, and PPH1 locking LHCII in state I associated with PSI. More interestingly, the simultaneous strong activation of NPQ mechanisms specific to Chlorophyta, as LHCSR, and to Embryophyta, as PsbS, were detected. Finally, specific Embryophyta systems for auxin synthesis, sensing, and response were activated leading to an increase in auxin content with the concomitant accumulation of amino acids such as tryptophan, histidine, and phenylalanine. Moreover, specific genes in the phenylpropanoid pathway and ELIPs were also activated in our study. All these systems could have been major facilitators for plants conquest of terrestrial environments since they would have enabled an adaptation of land plants algal ancestors to high light, one of the major stressors for Charophyta in terrestrial habitats.

DATA AVAILABILITY STATEMENT

The raw and processed datasets generated and analyzed in this study can be found in the Gene Expression Omnibus data base identified with the accession number GSE198330 (https://www.ncbi.nlm.nih.gov/geo/). Raw sequencing data can be accessed from the Sequence Read Archive (https://www.ncbi.nlm.nih.gov/sra) identified with the accession number PRJNA814727. Raw UPLC/MS metabolomic data can be accessed from the database MetaboLights (https://www.ebi.ac.uk/metabolights/) using the identifier MTBLS4467.

AUTHOR CONTRIBUTIONS

MM-P and MEG-G performed the experiment, collected the samples, processed them for metabolomic analysis,

and generated and analyzed the confocal microscopy images. ES-P and AR-L extracted and purified the RNA for sequencing. ES-P, AR-L, and FR-C performed the transcriptomic and metabolomic data analysis, visualization of the results, and carried out PAM measurements and analysis. IC, ES-P, and AR-L performed the protein extraction, SDS-PAGE, and Western blotting analysis. FR-C and MG-G designed the experiments, supervised the research, interpreted the results, and wrote the manuscript. All authors read and approved the manuscript.

FUNDING

This work was supported by the research projects MINOTAUR (BIO2017-84066-R) funded by the Spanish Ministry of Science and Innovation granted to FR-C and TORINS&CO2 (2021/00001525) funded by FEDER US – Junta de Andalucía granted to IC.

ACKNOWLEDGMENTS

We would like to acknowledge Bruno Catarino and Miguel A. Blázquez for critical reading of the manuscript and discussions; Manuel J. Mallén-Ponce for his advice and discussions on PAM measurements; Carlos A. Parejo-Pérez for his technical guidance on metabolomic data generation; Alica Orea for her technical assistance in confocal microscopy; and Eloisa Andújar-Pulido and Mónica Pérez from the Genomics Unit (CABIMER) for their assistance in RNA-seq data generation.

SUPPLEMENTARY MATERIAL

The Supplementary Material for this article can be found online at: https://www.frontiersin.org/articles/10.3389/fpls.2022.855243/full#supplementary-material

REFERENCES

Adamska, I., Ohad, I., and Kloppstechtt, K. (1992). Synthesis of the early light-inducible protein is controlled by blue light and related to light stress. *Proc. Natl. Acad. Sci. U.S.A.* 89, 2610-2613.

Alboresi, A., Storti, M., and Morosinotto, T. (2019). Balancing protection and efficiency in the regulation of photosynthetic electron transport across plant evolution. *New Phytol.* 221, 105–109. doi: 10.1111/nph.15372

Bailleul, B., Rogato, A., De Martino, A., Coesel, S., Cardol, P., Bowler, C., et al. (2010). An atypical member of the light-harvesting complex stress-related protein family modulates diatom responses to light. *Proc. Natl. Acad. Sci. U.S.A.* 107, 18214–18219. doi: 10.1073/pnas.1007703107

Becker, B., and Marin, B. (2009). Streptophyte algae and the origin of embryophytes. *Ann. Bot.* 103, 999–1004. doi: 10.1093/aob/mcp044

Calderon, R. H., and Strand, Å (2021). How retrograde signaling is intertwined with the evolution of photosynthetic eukaryotes. *Curr. Opin. Plant Biol.* 63:102093. doi: 10.1016/j.pbi.2021.102093

Cardol, P., Bailleul, B., Rappaport, F., Derelle, E., Béal, D., Breyton, C., et al. (2008). An original adaptation of photosynthesis in the marine green alga Ostreococcus. *Proc. Natl. Acad. Sci. U.S.A.* 105, 7881–7886. doi: 10.1073/pnas.0802762105

Cardol, P., Forti, G., and Finazzi, G. (2011). Regulation of electron transport in microalgae. *Biochim. Biophys. Acta Bioenerg.* 1807, 912–918. doi: 10.1016/J.BBABIO.2010.12.004

Cejudo, F. J., González, M. C., and Pérez-Ruiz, J. M. (2021). Redox regulation of chloroplast metabolism. *Plant Physiol.* 186, 9–21. doi: 10.1093/plphys/kiaa062

Chaux, F., Burlacot, A., Mekhalfi, M., Auroy, P., Blangy, S., Richaud, P., et al. (2017). Flavodiiron proteins promote fast and transient O2 photoreduction in chlamydomonas. *Plant Physiol.* 174, 1825–1836. doi: 10.1104/pp.17.00421

Couso, I., Vila, M., Vigara, J., Cordero, B. F., Vargas, M. Á, Rodríguez, H., et al. (2012). Synthesis of carotenoids and regulation of the carotenoid biosynthesis pathway in response to high light stress in the unicellular microalga Chlamydomonas reinhardtii. *Eur. J. Phycol.* 47, 223–232. doi: 10.1080/09670262.2012.692816

de Luna-Valdez, L. A., Villaseñor-Salmerón, C. I., Cordoba, E., Vera-Estrella, R., León-Mejía, P., and Guevara-García, A. A. (2019). Functional analysis of the Chloroplast GrpE (CGE) proteins from Arabidopsis thaliana. *Plant Physiol. Biochem.* 139, 293–306. doi: 10.1016/j.plaphy.2019.03.027

De Vries, J., Curtis, B. A., Gould, S. B., and Archibald, J. M. (2018). Embryophyte stress signaling evolved in the algal progenitors of land plants. *Proc. Natl. Acad. Sci. U.S.A.* 115, E3471–E3480. doi: 10.1073/pnas.1719230115

de Vries, J., de Vries, S., Curtis, B. A., Zhou, H., Penny, S., Feussner, K., et al. (2020). Heat stress response in the closest algal relatives of land plants reveals conserved stress signaling circuits. *Plant J.* 103, 1025–1048. doi: 10.1111/tpj.14782

de Vries, S., Fürst-Jansen, J. M. R., Irisarri, I., Dhabalia Ashok, A., Ischebeck, T., Feussner, K., et al. (2021). The evolution of the phenylpropanoid pathway entailed pronounced radiations and divergences of enzyme families. *Plant J.* 107, 975–1002. doi: 10.1111/tpj.15387

Del Campo, J. A., Rodríguez, H., Moreno, J., Vargas, M. Á, Rivas, J., and Guerrero, M. G. (2004). Accumulation of astaxanthin and lutein in Chlorella zofingiensis (Chlorophyta). *Appl. Microbiol. Biotechnol.* 64, 848–854. doi: 10.1007/s00253-003-1510-5

Dittami, S. M., Michel, G., Collén, J., Boyen, C., and Tonon, T. (2010). Chlorophyll-binding proteins revisited - A multigenic family of light-harvesting and stress proteins from a brown algal perspective. *BMC Evol. Biol.* 10:365. doi: 10.1186/1471-2148-10-365

Dogra, V., Li, M., Singh, S., Li, M., and Kim, C. (2019b). Oxidative post-translational modification of EXECUTER1 is required for singlet oxygen sensing in plastids. *Nat. Commun.* 10:2834. doi: 10.1038/s41467-019-10760-6

Dogra, V., Duan, J., Lee, K. P., and Kim, C. (2019a). Impaired PSII proteostasis triggers a UPR-like response in the var2 mutant of Arabidopsis. *J. Exp. Bot.* 70, 3075–3088. doi: 10.1093/jxb/erz151

Dogra, V., Duan, J., Lee, K. P., Lv, S., Liu, R., and Kim, C. (2017). FtsH2-dependent proteolysis of EXECUTER1 is essential in mediating singlet oxygen-triggered retrograde signaling in Arabidopsis thaliana. *Front. Plant Sci.* 8:1145. doi: 10.3389/fpls.2017.01145

Domozych, D. S., Popper, Z. A., and Sørensen, I. (2016). Charophytes: evolutionary giants and emerging model organisms. *Front. Plant Sci.* 7:1470. doi: 10.3389/fpls.2016.01470

Galili, G., Amir, R., and Fernie, A. R. (2016). The Regulation of Essential Amino Acid Synthesis and Accumulation in Plants. *Annu. Rev. Plant Biol.* 67, 153–178. doi: 10.1146/annurev-arplant-043015-112213

Gerotto, C., Alboresi, A., Giacometti, G. M., Bassi, R., and Morosinotto, T. (2012). Coexistence of plant and algal energy dissipation mechanisms in the moss Physcomitrella patens. *New Phytol.* 196, 763–773. doi: 10.1111/j.1469-8137.2012.04345.x

Gerotto, C., and Morosinotto, T. (2013). Evolution of photoprotection mechanisms upon land colonization: evidence of PSBS-dependent NPQ in late Streptophyte algae. *Physiol. Plant* 149, 583–598. doi: 10.1111/PPL.12070

Goss, R., and Jakob, T. (2010). Regulation and function of xanthophyll cycle-dependent photoprotection in algae. *Photosynth. Res.* 106, 103–122. doi: 10.1007/s11120-010-9536-x

He, G., Liu, P., Zhao, H., and Sun, J. (2020). The HD-ZIP II transcription factors regulate plant architecture through the auxin pathway. *Int. J. Mol. Sci.* 21:3250. doi: 10.3390/ijms21093250

Holzinger, A., and Becker, B. (2015). Desiccation tolerance in the streptophyte green alga Klebsormidium: the role of phytohormones. *Commun. Integr. Biol.* 8:e1059978. doi: 10.1080/19420889.2015.1059978

Holzinger, A., Kaplan, F., Blaas, K., Zechmann, B., Komsic-Buchmann, K., and Becker, B. (2014). Transcriptomics of desiccation tolerance in the streptophyte green alga Klebsormidium reveal a land plant-like defense reaction. *PLoS One* 9:e110630. doi: 10.1371/journal.pone.0110630

Holzinger, A., and Pichrtová, M. (2016). Abiotic stress tolerance of charophyte green algae: new challenges for omics techniques. *Front. Plant Sci.* 7:678. doi: 10.3389/fpls.2016.00678

Hori, K., Maruyama, F., Fujisawa, T., Togashi, T., Yamamoto, N., Seo, M., et al. (2014). Klebsormidium flaccidum genome reveals primary factors for plant terrestrial adaptation. *Nat. Commun.* 5:3978. doi: 10.1038/ncomms4978

Huvaere, K., and Skibsted, L. H. (2009). Light-induced oxidation of tryptophan and histidine. Reactivity of aromatic N-heterocycles toward triplet-excited flavins. *J. Am. Chem. Soc.* 131, 8049–8060. doi: 10.1021/ja809039u

Iwai, M., Takizawa, K., Tokutsu, R., Okamuro, A., Takahashi, Y., and Minagawa, J. (2010). Isolation of the elusive supercomplex that drives cyclic electron flow in photosynthesis. *Nature* 464, 1210–1213. doi: 10.1038/nature08885

Karsten, U., Herburger, K., and Holzinger, A. (2016). Living in biological soil crust communities of African deserts-Physiological traits of green algal Klebsormidium species (Streptophyta) to cope with desiccation, light and temperature gradients. *J. Plant Physiol.* 194, 2–12. doi: 10.1016/j.jplph.2015.09.002

Kim, C. (2020). ROS-Driven Oxidative Modification: its Impact on Chloroplasts-Nucleus Communication. *Front. Plant Sci.* 10:1729. doi: 10.3389/fpls.2019.01729

Kitzing, C., and Karsten, U. (2015). Effects of UV radiation on optimum quantum yield and sunscreen contents in members of the genera Interfilum, Klebsormidium, Hormidiella and Entransia (Klebsormidiophyceae, Streptophyta). *Eur. J. Phycol.* 50, 279–287. doi: 10.1080/09670262.2015.1031190

Kondo, S., Hori, K., Sasaki-Sekimoto, Y., Kobayashi, A., Kato, T., Yuno-Ohta, N., et al. (2016). Primitive extracellular lipid components on the surface of the charophytic alga Klebsormidium flaccidum and their possible biosynthetic pathways as deduced from the genome sequence. *Front. Plant Sci.* 7:952. doi: 10.3389/fpls.2016.00952

Latowski, D., Kuczyńska, P., and Strzałka, K. (2011). Xanthophyll cycle - a mechanism protecting plants against oxidative stress. *Redox Rep.* 16, 78–90. doi: 10.1179/174329211X13020951739938

Lenton, T. M., Dahl, T. W., Daines, S. J., Mills, B. J. W., Ozaki, K., Saltzman, M. R., et al. (2016). Earliest land plants created modern levels of atmospheric oxygen. *Proc. Natl. Acad. Sci. U.S.A.* 113, 9704–9709. doi: 10.1073/pnas.1604787113

Li, X. P., Björkman, O., Shih, C., Grossman, A. R., Rosenquist, M., Jansson, S., et al. (2000). A pigment-binding protein essential for regulation of photosynthetic light harvesting. *Nature* 403, 391–395. doi: 10.1038/35000131

Liu, J., Danneels, B., Vanormelingen, P., and Vyverman, W. (2016a). Nutrient removal from horticultural wastewater by benthic filamentous algae Klebsormidium sp., Stigeoclonium spp. and their communities: from laboratory flask to outdoor Algal Turf Scrubber (ATS). *Water Res.* 92, 61–68. doi: 10.1016/j.watres.2016.01.049

Liu, J., Vanormelingen, P., and Vyverman, W. (2016b). Fatty acid profiles of four filamentous green algae under varying culture conditions. *Bioresour. Technol.* 200, 1080–1084. doi: 10.1016/j.biortech.2015.11.001

Love, M. I., Huber, W., and Anders, S. (2014). Moderated estimation of fold change and dispersion for RNA-seq data with DESeq2. *Genome Biol.* 15:550. doi: 10.1186/s13059-014-0550-8

Ma, L., and Li, G. (2019). Auxin-dependent cell elongation during the shade avoidance response. *Front. Plant Sci.* 10:914. doi: 10.3389/fpls.2019.00914

Ma, M., Liu, Y., Bai, C., Yang, Y., Sun, Z., Liu, X., et al. (2021). The Physiological Functionality of PGR5/PGRL1-Dependent Cyclic Electron Transport in Sustaining Photosynthesis. *Front. Plant Sci.* 12:1313. doi: 10.3389/fpls.2021.702196

Ma, R., Zhao, X., Xie, Y., Ho, S. H., and Chen, J. (2019). Enhancing lutein productivity of Chlamydomonas sp. via high-intensity light exposure with corresponding carotenogenic genes expression profiles. *Bioresour. Technol.* 275, 416–420. doi: 10.1016/j.biortech.2018.12.109

Mccloskey, D., and Ubhi, B. K. (2015). *Quantitative and Qualitative Metabolomics for the Investigation of Intracellular Metabolism*. Framingham: SCIEX.

Mekala, N. R., Suorsa, M., Rantala, M., Aro, E. M., and Tikkanen, M. (2015). Plants actively avoid state transitions upon changes in light intensity: role of light-harvesting complex ii protein dephosphorylation in high light. *Plant Physiol.* 168, 721–734. doi: 10.1104/pp.15.00488

Miller, N. T., Vaughn, M. D., and Burnap, R. L. (2021). Electron flow through NDH-1 complexes is the major driver of cyclic electron flow-dependent proton pumping in cyanobacteria. *Biochim. Biophys. Acta Bioenerg.* 1862:148354. doi: 10.1016/j.bbabio.2020.148354

Monte, I., Kneeshaw, S., Franco-Zorrilla, J. M., Chini, A., Zamarreño, A. M., García-Mina, J. M., et al. (2020). An Ancient COI1-Independent Function for Reactive Electrophilic Oxylipins in Thermotolerance. *Curr. Biol.* 30, 962.e–971.e. doi: 10.1016/j.cub.2020.01.023

Morris, J. L., Puttick, M. N., Clark, J. W., Edwards, D., Kenrick, P., Pressel, S., et al. (2018). The timescale of early land plant evolution. *Proc. Natl. Acad. Sci. U.S.A.* 115, E2274–E2283. doi: 10.1073/pnas.1719588115

Nishiyama, T., Straeten, D., Van Der Gould, S. B., Rensing, S. A., Nishiyama, T., Sakayama, H., et al. (2018). The Chara Genome : secondary Complexity and Implications for Plant Terrestrialization. *Cell* 174, 448–464.

Niyogi, K. K. (2000). Safety valves for photosynthesis. *Curr. Opin. Plant Biol.* 3, 455–460. doi: 10.1016/S1369-5266(00)00113-8

Ohtaka, K., Hori, K., Kanno, Y., Seo, M., and Ohta, H. (2017). Primitive auxin response without TIR1 and Aux/IAA in the charophyte alga Klebsormidium nitens. *Plant Physiol.* 174, 1621–1632. doi: 10.1104/pp.17.00274

Peers, G., Truong, T. B., Ostendorf, E., Busch, A., Elrad, D., Grossman, A. R., et al. (2009). An ancient light-harvesting protein is critical for the regulation of algal photosynthesis. *Nature* 462, 518–521. doi: 10.1038/nature08587

Peltier, G., Tolleter, D., Billon, E., and Cournac, L. (2010). Auxiliary electron transport pathways in chloroplasts of microalgae. *Photosynth. Res.* 106, 19–31. doi: 10.1007/s11120-010-9575-3

Pertea, M., Kim, D., Pertea, G. M., Leek, J. T., and Salzberg, S. L. (2016). Transcript-level expression analysis of RNA-seq experiments with HISAT, StringTie and Ballgown. *Nat. Protoc.* 11, 1650–1667. doi: 10.1038/nprot.2016.095

Pierangelini, M., Ryšánek, D., Lang, I., Adlassnig, W., and Holzinger, A. (2017). Terrestrial adaptation of green algae Klebsormidium and Zygnema (Charophyta) involves diversity in photosynthetic traits but not in CO2 acquisition. *Planta* 246, 971–986. doi: 10.1007/s00425-017-2741-5

Pinnola, A. (2019). The rise and fall of Light-Harvesting Complex Stress-Related proteins as photoprotection agents during evolution. *J. Exp. Bot.* 70, 5527–5535. doi: 10.1093/jxb/erz317

Pinnola, A., and Bassi, R. (2018). Molecular mechanisms involved in plant photoprotection. *Biochem. Soc. Trans.* 46, 467–482. doi: 10.1042/BST20170307

Pospíšil, P. (2016). Production of reactive oxygen species by photosystem II as a response to light and temperature stress. *Front. Plant Sci.* 7:1950. doi: 10.3389/FPLS.2016.01950/ABSTRACT

Ravenel, J., Peltier, G., and Havaux, M. (1994). The cyclic electron pathways around photosystem I in Chlamydomonas reinhardtii as determined in vivo by photoacoustic measurements of energy storage. *Planta* 193, 251–259. doi: 10.1007/BF00192538

Rippin, M., Borchhardt, N., Karsten, U., and Becker, B. (2019a). Cold acclimation improves the desiccation stress resilience of polar strains of Klebsormidium (Streptophyta). *Front. Microbiol.* 10:1730. doi: 10.3389/fmicb.2019.01730

Rippin, M., Pichrtová, M., Arc, E., Kranner, I., Becker, B., and Holzinger, A. (2019b). Metatranscriptomic and metabolite profiling reveals vertical heterogeneity within a Zygnema green algal mat from Svalbard (High Arctic). *Environ. Microbiol.* 21, 4283–4299. doi: 10.1111/1462-2920.14788

Ritchie, M. E., Phipson, B., Wu, D., Hu, Y., Law, C. W., Shi, W., et al. (2015). Limma powers differential expression analyses for RNA-sequencing and microarray studies. *Nucleic Acids Res.* 43:e47. doi: 10.1093/nar/gkv007

Romero-Losada, A. B., Arvanitidou, C., De Los Reyes, P., García-González, M., Romero-Campero, F. J., and Romero, F. J. (2022). ALGAEFUN with MARACAS, microALGAE FUNctional enrichment tool for MicroAlgae RnA-seq and Chip-seq analysis. *BMC Bioinform.* 23:113. doi: 10.1186/s12859-022-04639-5

Rumeau, D., Peltier, G., and Cournac, L. (2007). Chlororespiration and cyclic electron flow around PSI during photosynthesis and plant stress response. *Plant Cell Environ.* 30, 1041–1051. doi: 10.1111/j.1365-3040.2007.01675.x

Salem, M. A., Yoshida, T., Perez de Souza, L., Alseekh, S., Bajdzienko, K., Fernie, A. R., et al. (2020). An improved extraction method enables the comprehensive analysis of lipids, proteins, metabolites and phytohormones from a single sample of leaf tissue under water-deficit stress. *Plant J.* 103, 1614–1632. doi: 10.1111/tpj.14800

Seyednasrollah, F., Laiho, A., and Elo, L. L. (2013). Comparison of software packages for detecting differential expression in RNA-seq studies. *Brief. Bioinform.* 16, 59–70. doi: 10.1093/bib/bbt086

Stupnikov, A., McInerney, C. E., Savage, K. I., McIntosh, S. A., Emmert-Streib, F., Kennedy, R., et al. (2021). Robustness of differential gene expression analysis of RNA-seq. *Comput. Struct. Biotechnol. J.* 19, 3470–3481. doi: 10.1016/j.csbj.2021.05.040

Suorsa, M. (2015). Cyclic electron flow provides acclimatory plasticity for the photosynthetic machinery under various environmental conditions and developmental stages. *Front. Plant Sci.* 6:800. doi: 10.3389/fpls.2015.00800

Ueda, M., Kuniyoshi, T., Yamamoto, H., Sugimoto, K., Ishizaki, K., Kohchi, T., et al. (2012). Composition and physiological function of the chloroplast NADH dehydrogenase-like complex in Marchantia polymorpha. *Plant J.* 72, 683–693. doi: 10.1111/j.1365-313X.2012.05115.x

Umen, J. G. (2014). Green Algae and the Origins of Multicellularity in the Plant Kingdom. *Cold Spring Harb. Perspect. Biol.* 6:a016170. doi: 10.1101/cshperspect.a016170

Vieira Dos Santos, C., and Rey, P. (2006). Plant thioredoxins are key actors in the oxidative stress response. *Trends Plant Sci.* 11, 329–334. doi: 10.1016/j.tplants.2006.05.005

Welc, R., Luchowski, R., Kluczyk, D., Zubik-Duda, M., Grudzinski, W., Maksim, M., et al. (2021). Mechanisms shaping the synergism of zeaxanthin and PsbS in photoprotective energy dissipation in the photosynthetic apparatus of plants. *Plant J.* 107, 418–433. doi: 10.1111/tpj.15297

Willforss, J., Chawade, A., and Levander, F. (2019). NormalyzerDE: online Tool for Improved Normalization of Omics Expression Data and High-Sensitivity Differential Expression Analysis. *J. Proteome Res.* 18, 732–740. doi: 10.1021/acs.jproteome.8b00523

Xu, Z., He, Q., Gong, Y., Wang, Y., Chi, Q., Liu, G., et al. (2021). Assessment of a Novel Oleaginous Filamentous Microalga Klebsormidium sp. Lgx80 (Streptophyta, Klebsormidiales) for Biomass and Lipid Production1. *J. Phycol.* 57, 1151–1166. doi: 10.1111/jpy.13137

Yamamoto, H., and Shikanai, T. (2019). PGR5-dependent cyclic electron flow protects photosystem I under fluctuating light at donor and acceptor sides. *Plant Physiol.* 179, 588–600. doi: 10.1104/pp.18.01343

Yamori, W., Shikanai, T., and Makino, A. (2015). Photosystem i cyclic electron flow via chloroplast NADH dehydrogenase-like complex performs a physiological role for photosynthesis at low light. *Sci. Rep.* 5:13908. doi: 10.1038/srep13908

Zhang, X., and Li, H. (2016). Role of Arabidopsis sterol 4α-methyl oxidase2 family in embryo and postembryonic development. *Plant Signal. Behav.* 11:e1249081. doi: 10.1080/15592324.2016.1249081

Zhao, C., Wang, Y., Chan, K. X., Marchant, D. B., Franks, P. J., Randall, D., et al. (2019). Evolution of chloroplast retrograde signaling facilitates green plant adaptation to land. *Proc. Natl. Acad. Sci. U.S.A.* 116, 5015–5020. doi: 10.1073/pnas.1812092116

Zhao, Q., and Liu, C. (2018). Chloroplast chaperonin: an intricate protein folding machine for photosynthesis. *Front. Mol. Biosci.* 4:98. doi: 10.3389/fmolb.2017.00098

Zhu, X. G., Long, S. P., and Ort, D. R. (2010). Improving photosynthetic efficiency for greater yield. *Annu. Rev. Plant Biol.* 61, 235–261. doi: 10.1146/annurev-arplant-042809-112206

Conflict of Interest: The authors declare that the research was conducted in the absence of any commercial or financial relationships that could be construed as a potential conflict of interest.

Publisher's Note: All claims expressed in this article are solely those of the authors and do not necessarily represent those of their affiliated organizations, or those of the publisher, the editors and the reviewers. Any product that may be evaluated in this article, or claim that may be made by its manufacturer, is not guaranteed or endorsed by the publisher.

frontiers | Frontiers in Plant Science

ORIGINAL RESEARCH
published: 01 June 2022
doi: 10.3389/fpls.2022.846262

Phytochrome-Dependent Regulation of *ZFP6* and *ZFPH* Impacts Photomorphogenesis in *Arabidopsis thaliana*

*Keni Cota-Ruiz[1], Sookyung Oh[1] and Beronda L. Montgomery[1,2,3]**

[1] MSU DOE-Plant Research Laboratory, Michigan State University, East Lansing, MI, United States, [2] Department of Biochemistry and Molecular Biology, Michigan State University, East Lansing, MI, United States, [3] Department of Microbiology and Molecular Genetics, Michigan State University, East Lansing, MI, United States

OPEN ACCESS

Edited by:
Gabriela Toledo-Ortiz, Lancaster University, United Kingdom

Reviewed by:
Miguel De Lucas, Durham University, United Kingdom
Eugenio Gómez Minguet, Polytechnic University of Valencia, Spain

***Correspondence:**
Beronda L. Montgomery
montg133@msu.edu

Specialty section:
This article was submitted to Plant Physiology, a section of the journal Frontiers in Plant Science

Received: *31 December 2021*
Accepted: *10 May 2022*
Published: *01 June 2022*

Citation:
Cota-Ruiz K, Oh S and Montgomery BL (2022) Phytochrome-Dependent Regulation of ZFP6 and ZFPH Impacts Photomorphogenesis in Arabidopsis thaliana. Front. Plant Sci. 13:846262. doi: 10.3389/fpls.2022.846262

Phytochromes (phy) are key regulators of photomorphogenesis in plants. Among the different phys characterized in higher plants (i.e., phyA to phyE), phyA and phyB primarily regulate phenotypic responses in plants under far-red (FR) and red (R) conditions, respectively. Recent findings suggest that some zinc finger proteins (ZFPs) are involved in plant light-modulated morphogenesis. However, the interaction(s) between phyA, phyB and ZFP homologs potentially involved in photomorphogenesis, as well as their phenotypic and molecular effects in Arabidopsis seedlings exposed to R and FR light remain to be elucidated fully. Prior analyses with phytochrome chromophore deficient lines indicated that *ZFP6* expression is misregulated compared to levels in Col-0 wild type (WT). Here, we used plants with phytochrome chromophore or apoprotein (specifically phyA and phyB) deficiencies, lines with mutations in *ZFP6* and *ZFP6 HOMOLOG* (*ZFPH*) genes, and plants overexpressing *ZFP6* to examine regulatory interactions between phytochromes, ZFP6, and ZFPH. Our results indicate that phytochromes are required for downregulation of *ZFP6* and *ZFPH* and suggest a role for light-regulated control of *ZFP* levels in phytochrome-dependent photomorphogenesis. Conversely, *PHYB* is downregulated in *zfp6* mutants under R light. Analyses of a *zfp6zfph* double mutant confirmed disruption in photomorphogenic phenotypes, including the regulation of hypocotyl elongation in seedlings grown under FR light. In addition, *PIF3* and *PIF4* levels are transcriptionally regulated by ZFP6 and ZFPH in a gibberellic acid-dependent manner. *ZFP6* overexpression resulted in opposite phenotypic responses to those observed in the *zfp6* and *zfph* mutants grown in FR and R light, as well as a reduction in the rosette size of mature *ZFP6* OX plants relative to WT under white light. Based on these observations, we provide insight into how phy and ZFPs interact to regulate specific aspects of light-dependent processes in Arabidopsis.

Keywords: phytochrome, *ZFP6*, *ZFPH*, gibberellic acid, PIF, DELLA, far-red light

INTRODUCTION

Light controls multiple and critical processes throughout the plant life cycle. Aspects of plant growth and development regulated by light include seed germination, etiolation or de-etiolation behaviors in seedlings, responses to neighboring plants in competition for light, and the shift between vegetative and reproductive stages, among others (Fankhauser and Chory, 1997). These light-dependent growth and developmental processes are mediated by light perception by photoreceptors throughout the life cycle of plants, including phytochromes, cryptochromes, phototropins, and UVR8 (Legris et al., 2019). Phytochrome (phy) A (phyA) and phyB are the most extensively studied photoreceptors; they are the predominant phytochromes that control photomorphogenic responses in the presence of far-red (FR) and red (R) light, respectively (Li et al., 2011; Cheng et al., 2021; Kim et al., 2021). Encoded by genes in the nucleus, phy proteins are synthesized and the chromophore covalently attached in the cytoplasm; holophytochromes remain in the cytosol in their inactive form (Pr) if no activating light is present, or upon light-activated conversion to their active form (Pfr) are translocated into the nucleus (Kevei et al., 2007). In the nucleus, phytochromes control distinct classes of regulatory genes, including those encoding transcription factors.

Zinc finger proteins (ZFPs) are one class of transcription factor families that are widely distributed in plants. ZFPs participate in numerous biological processes, including flowering, light-mediated morphogenesis, disease suppression, and activation of defense mechanisms in response to abiotic stress (Feurtado et al., 2011; Noman et al., 2019; Xie et al., 2019). They are classified into nine families based on their conserved cysteine-histidine-amino acid motif, which coordinates with a zinc atom (Xie et al., 2019). The largest group comprises 176 C_2H_2-type ZFP proteins (Englbrecht et al., 2004). ZFPs have been shown to have DNA-binding activity in plants, indicating roles for these proteins in transcriptional regulation (Han et al., 2020). While one of the larger protein families, this group of regulatory proteins have been underexplored *in planta* (Fedotova et al., 2017). *ZFP6* and closely related *ZFP6 HOMOLOG* (*ZFPH*) are of particular interest in this current research given their identification as differentially regulated genes in prior transcriptomic analyses of phytochrome-deficient plant lines (Oh et al., 2013).

Prior experimental analyses demonstrated that *ZFP6* overexpression in 35S:*ZFP6* transgenic lines led to an increased number of trichomes on the sepals of flowers, in addition to ectopic trichome formation on carpels in Arabidopsis (Zhou et al., 2013). Of note, exogenous gibberellic acid (GA) application induced significantly higher *ZFP6* expression compared to untreated plants, indicating interaction between GA signaling and ZFP6 function (Zhou et al., 2013). The GA hormone is implicated in several plant development stages in Arabidopsis, including control of seed germination, promotion of stem elongation and leaf expansion, and the induction of flowering (Phillips, 1998). In addition to ZFP6, ZFP5 also aids in the GA pathway to induce trichome initiation on shoots in Arabidopsis (Zhou et al., 2011). Molecular-based approaches suggested that ZFP6 regulates *ZFP5* expression (Zhou et al., 2013) and ZFP5 in turn induces *GLABROUS INFLORESCENCE STEMS 1* (*GIS1*), *GLABROUS INFLORESCENCE STEMS 2* (*GIS2*), and *ZFP8* expression (Zhou et al., 2011). *GIS* genes also encode C_2H_2-type ZFPs. *ZFPH* was previously identified as *GIS3* and also was demonstrated to increase trichome density when overexpressed (Sun et al., 2015). *ZFPH/GIS3*, however, exerts its impact on trichomes independent of ZFP6 and ZFP5; yet, impacts *GIS1*, *GIS2*, and *ZFP8* similar to ZFP5 (Sun et al., 2015). Another *ZFP* family member, i.e., *ZFP3*, impacts seedling development, but through a distinct mechanism. Overexpression of *ZFP3* interfered with the ABA signaling pathway in Arabidopsis, rendering the seeds unable to germinate. Additionally, seedlings overexpressing *ZFP3* displayed shorter hypocotyls both in light and dark conditions (Joseph et al., 2014). Together, these results indicate multiple roles for *ZFP* homologs in plant growth and development, including some phenotypes that overlap with those controlled by light and phytochromes.

PIFs (Phytochrome-Interacting Factors) are phytochrome-dependent transcription factors that have been shown to physically interact with phytochromes and to activate organ-elongation genes and promote etiolation (Leivar and Monte, 2014), i.e., the dark-dependent development of seedlings with long stems and small, yellow-colored cotyledons. During de-etiolation, R light-dependent activation of phyB leads to degradation of PIFs and characteristic inhibition of stem elongation and promotion of leaf development and greening (Leivar and Monte, 2014). In addition to impacting PIFs, phyB inhibits the morphogenetic repressor COP1 (CONSTITUTIVE PHOTOMORPHOGENIC 1) in a light-dependent manner, restraining its ability to target the transcription factor ELONGATED HYPOCOTYL 5 (HY5) for proteasome-mediated degradation (Osterlund and Deng, 1998). Thus, HY5 accumulates in the light and promotes photomorphogenesis in plants (Osterlund et al., 2000; Shi et al., 2018). Conversely to its R-dependent movement into the nucleus, phyB remains in its inactive red-light absorbing form (Pr) in the cytoplasm under FR light conditions. When phyB remains in the cytosol in FR, PIF molecules are able to accumulate in the nucleus where they function to transcribe PIF target genes, including those that promote elongation (Ejaz et al., 2021). PIF proteins intersect with hormone-based regulation of growth as targets of the GA signaling pathway (Hernández-García et al., 2021). PIFs are targeted for inactivation by DELLA proteins, which are molecules that suppress growth (Kusnetsov et al., 2020). DELLAs restrain PIFs (PIF1, PIF3, PIF4, and PIF5) by targeting them for proteasome-mediated degradation in a light-independent manner (Li et al., 2016).

Given the prior associations of ZFP6 as a target of transcriptional regulation by phytochromes and GA regulation, as well as roles for both phytochromes and GA in light-dependent growth and development in Arabidopsis, we investigated light and phytochrome-dependent transcript accumulation for *ZFP6* and *ZFPH*, light and GA-dependent phenotypic and molecular responses of *zfp6* and *zfph* mutants, and the consequence of overexpressing the *ZFP6* gene on light-dependent plant growth and development. To gain specific insights into the crosstalk between phytochromes, PIFs, and ZFP6 during the regulation

of growth, we assessed expression of select genes within the phytochrome, GA, and organ elongation pathways. Considering these observations collectively, we describe specific aspects of phytochrome-dependent processes that are mediated via ZFP6 and closely related ZFPH in Arabidopsis.

MATERIALS AND METHODS

Plant Materials

Col-0 wild type (WT) ecotype of *Arabidopsis thaliana* (hereafter Arabidopsis) was obtained from the Arabidopsis Biological Resource Center (ABRC).[1] An Arabidopsis *phyAphyB* (*PHYA*: *AT1G09570*; *PHYB*: *AT2G18790*) double mutant line was previously constructed and described (Mayfield et al., 2007; Ruckle et al., 2007). *zfp6* (SALK_200865; *AT1G68360*) and *zfph* (SALK_043793; *AT1G68360*) mutant lines were also obtained from ABRC, and the *zfp6zfph* double mutant was isolated from a genetic cross between the two single mutants. The production of transgenic BVR lines was previously described (Montgomery et al., 1999; Warnasooriya and Montgomery, 2009).

For *ZFP6* overexpression lines, *ZFP6* cDNA was amplified from a cDNA clone for *ZFP6* (U13157) from ABRC using forward primer 5′-ATGGCGACTGAAACATCTTCTT-3′ and reverse primer 5′-TCATGGCCCAAGGCTTAAAT-3′ and recombined into the pCR^{TM}8/GW/TOPO^{TM} vector using a TA Cloning Kit according to manufacturer's instructions (Thermo Fisher Scientific, Waltham, MA, United States). Insertion of the full-length *ZFP6* cDNA fragment into the vector was confirmed via *Eco*RI digestion and validated by DNA sequencing. The recombinant vector was cloned into One Shot^{TM} TOP10 *E. coli* cells (Thermo Fisher Scientific, Waltham, MA, United States) following the manufacturer's directions. Full-length *ZFP6* cDNA was recombined into the 35S promoter-containing pEarlyGate 100 vector using LR Clonase II enzyme according to manufacturer's instructions (Thermo Fisher Scientific, Waltham, MA, United States) to generate the 35S:ZFP6 construct, which was introduced into GV3101 Agrobacterium to transform Col-0 WT plants via a standard floral-dip transformation protocol (Clough and Bent, 1998). *ZFP6* overexpression was confirmed by RT-PCR as described below.

Plant Growth and Light Sources

Arabidopsis seeds were sterilized with 2.88% (v/v) sodium hypochlorite including 0.025% (v/v) SDS for 15 min. Chlorine was removed by rinsing seeds with sterilized ddH_2O five times. Then, the seeds were planted on 0.5 × Murashige and Skoog (MS) medium (Caisson Laboratories, Smithfield, UT, United States) containing 0.9% (w/v) Phytoblend (Caisson Laboratories) and 1% (w/v) sucrose (Thermo Fisher Scientific, Waltham, MA, United States). Seeds were stratified on agar plates at 4°C for 4 days in darkness and then replicate plates were incubated in white (W), far-red (FR) and red (R) light for 7 days at 22°C. Additional treatments included germination and/or growth of seedlings on plates with 10 μM GA and GA biosynthesis inhibitor paclobutrazol (PAC) at a concentration of 100 nM. For W light, a Percival chamber model no. CU36LA irradiating light at 110 μmol m^{-2} s^{-1} was used; for the rest of the tested lights (see below), Percival LED chambers (model E30LED; Percival, Perry, IA, United States) were employed. For continuous FR (FR; λmax ∼735 nm) light, the light was emitted at 5 μmol m^{-2} s^{-1}; for R conditions (λmax ∼670 nm), the fluence rate was ∼25 to 50 μmol m^{-2} s^{-1}; and for blue (B) conditions (λmax ∼ 470 nm), the fluence rate was ∼50 μmol m^{-2} s^{-1}.

Phenotypic Analyses

Hypocotyl and root lengths of 7-days-old *zfp6*, *zfph,* and *zfp6zfph* mutant seedlings were measured using the ruler tool in Photoshop 2021 or using Image J. Similar measurements were performed on single copy, homozygous lines overexpressing *ZFP6* grown for 7 days in MS media containing 1% sucrose and 0.7% agar, pH 5.7, under FR (5 μmol m^{-2} s^{-1}), R (50 μmol m^{-2} s^{-1}), and blue (50 μmol m^{-2} s^{-1}) lights at 22°C. To document additional phenotype characteristics of mature lines overexpressing *ZFP6*, Col-0 WT and 35S:*ZFP6* overexpression lines were grown in soil for 21 days at 22°C in W at ∼125 μmol m^{-2} s^{-1} under a 16 h light/8 h dark cycle. Plants were photographed to evaluate rosette architecture and trichome formation.

RNA Extraction and RT-PCR

Seven-day-old seedlings incubated in R and FR light at 22°C were harvested in green light conditions, while those grown in W light were harvested under room light. Collected seedlings were immediately submerged in liquid nitrogen and stored at –70°C. Total RNA was extracted using the E.Z.N.A. Plant RNA Kit (Omega Bio-Tek, Norcross, GA, United States), following the manufacturer's instructions and including the DNase I digestion protocol. An additional DNA digestion was performed using DNase I RNase-free (Thermo Fisher Scientific, Waltham, MA, United States) using 1 unit per microgram of RNA. Total RNA (500 ng) was reverse-transcribed using a qScript cDNA SuperMix kit (Quantabio, Beverly, MA, United States). Real-time quantitative PCR (qPCR) was performed on an ABI 7500 Fast Real-Time PCR System (Applied Biosystems, Foster City, CA, United States). The primers (at a final concentration of 200–500 nm) and cycling conditions are specified in **Supplementary Table 1**. A melting curve protocol was performed at the end of the PCR starting at 60°C with increments of 0.5°C/20 s. Three biological replicates along with three technical replicates were used. The *UBC21* gene was used for normalizing purposes and gene expression analyses were conducted using the $2^{-\Delta CT}$ method. To confirm overexpression of *ZFP6*, standard RT-PCR was performed with *UBC21* as the internal control using primers (final primer concentration 400 nm) and cycling conditions indicated in **Supplementary Table 1**.

In silico Promoter Analyses

Analyses of the *ZFP6* and *ZFPH* promoter regions were performed using the PlantCare database[2] to identify

[1] https://abrc.osu.edu/

[2] http://bioinformatics.psb.ugent.be/webtools/plantcare/html/

conserved *cis*-elements potentially involved in gene regulation. Approximately 1,000 nucleotides upstream of the start codon of each gene were analyzed to search for transcription start (TS) sites using the neural network promoter prediction with a minimum promoter score of 0.9[3] and for predicted transcription factor binding sites using the PlantCare database. In parallel, the TF2Network database (Kulkarni et al., 2018)[4] was used to investigate potential light- and/or phytochrome-dependent regulators for *ZFP6* and *ZFPH*.

Statistical Analysis

ANOVA analysis was performed to examine significant differences in the means. A normal distribution of the data was evaluated by the Kolmogorov-Smirnov test. Data that did not follow a normal distribution were transformed using the Box-Cox algorithm. The Fisher test at $p \leq 0.05$ was conducted to evaluate significant differences among population means. All statistical analyses and graphs were generated on OriginPro 2018.

RESULTS

Phytochrome A and Phytochrome B Negatively Regulate *ZFP6* and *ZFPH* Transcript Levels

Mining of previous transcriptomic data indicated that *ZFP6* and *ZFPH* were differentially regulated in phytochrome chromophore-deficient transgenic *BVR* lines grown in FR light conditions (Oh et al., 2013). BVR (biliverdin IX reductase) inactivates the tetrapyrrole precursors required for synthesis of the phytochrome chromophore, phytochromobilin; thus, BVR induces a chromophore deficiency in transgenic plants (Montgomery et al., 1999). The mRNA levels for both *ZFP6* and *ZFPH* were significantly higher in FR-grown CAB3:pBVR lines that lack the accumulation of photoactive phytochromes in mesophyll cells of leaves (**Figures 1A,B**; Oh et al., 2013). To confirm this finding for *ZFP6*, we assessed its expression by quantitative, real-time PCR (qRT-PCR) analysis. *ZFP6* mRNA levels were ∼2.6-fold higher in a CAB3:pBVR line than in Col-0 WT grown in FR light (**Figure 1C**). As the lack of phytochrome chromophore results in a lack of all holophytochromes, we used a *phyAphyB* mutant lacking the two predominant phytochromes to confirm that it was the lack of phytochromes in the BVR line which directly contributed to a disruption in transcript accumulation for *ZFP* homologs. Consistent with the phenotype for chromophore-deficient *BVR*-expressing plants, *ZFP6* transcripts levels also were increased ∼2.5 fold in a *phyAphyB* T-DNA mutant line (**Figure 1D**), compared to Col-0 WT. These findings suggest that phyA and phyB are the primary phytochromes required to downregulate *ZFP6*.

ZFP6 and *ZFPH* Are Expressed in Different Tissues and in Response to Distinct Light Conditions

Given the role of phys in regulating *ZFP6* and *ZFPH*, we examined the expression of these genes and the closely related *ZFP5* in different tissues and light conditions utilizing public microarray data for Col-0 WT from AtGenExpress[5] (**Figures 2A,B**). We chose to examine expression of *ZFP5* in parallel given that it is regulated by ZFP6 (Zhou et al., 2013), shares regulation of similar GA-dependent phenotypic responses as *ZFP6* (Zhou et al., 2011), and controls expression of some of the same genes as ZFPH (Sun et al., 2015). *ZFP5* shared some overlap with *ZFP6* and *ZFPH* in terms of tissues in which it was expressed, including roots and hypocotyls; yet, *ZFP5* was expressed to relatively higher levels in roots than either *ZFP6* or *ZFPH* (**Figure 2A**). *ZFP6* and *ZFPH* are highly expressed in roots, hypocotyls, and internodes, with *ZFPH* also exhibiting some expression in the shoot apex and inflorescence tissues (**Figure 2A**). We focused our subsequent analyses on the most closely related *ZFP6* and *ZFPH*.

Using qRT-PCR, we confirmed the differential accumulation of *ZFP6* mRNA in roots and hypocotyls, but not in cotyledons (**Figure 2C**). Additionally, *ZFP6* is upregulated by light, with significant upregulation after 4 h of FR (10 μmol m^{-2} s^{-1}) exposure according to public microarray data (**Figure 2B**). By comparison, *ZFPH* exhibits more moderate light-dependent changes in expression, with UV-A/B having the most significant impact. Given the association of multiple wavelengths of light that are correlated with phytochrome activity having a greater impact on *ZFP6* induction, we documented that *ZFP6* expression was 3. 1-, 1. 72-, and 2.7-fold downregulated in Col-0 WT exposed to continuous R, FR, and W light conditions, respectively, compared to Col-0 WT grown in dark (**Figure 2D**).

ZFP6 and ZFPH-Deficient Lines Exhibit Defects in Light-Dependent Phenotypes

Aiming to evaluate the phenotypic impact conferred by *ZFP6* and *ZFPH*, we identified homozygous T-DNA mutants for *ZFP6* (i.e., *zfp6*) and *ZFPH* (i.e., *zfph*). We also created a homozygous *zfp6zfph* double mutant via a genetic cross. Given the regulation of *ZFP6* and *ZFPH* mRNA accumulation by phytochromes and by light for *ZFP6*, we examined seedling photomorphogenic phenotypes in R and FR light grown seedlings. In FR light, the *zfp6*, *zfph*, and *zfp6zfph* mutant lines all exhibited significantly longer hypocotyls (∼1.2-fold longer) than Col-0 WT (**Figure 3A**). Although mutant seedlings trended longer that WT under R light conditions, hypocotyl elongation was not significantly different in R conditions (**Figure 3B**). Noted differences in hypocotyl elongation were light-specific as there was no difference among WT, *zfp6*, *zfph*, and *zfp6zfph* for seedlings grown in darkness (**Supplementary Figure 1**).

In addition to the impact of light, seedling growth is tightly regulated by plant hormones. For instance, auxins and GA promote plant growth while abscisic acid is generally known

[3]https://www.fruitfly.org/seq_tools/promoter.html

[4]http://bioinformatics.psb.ugent.be/webtools/TF2Network/

[5]https://www.arabidopsis.org/portals/expression/microarray/ATGenExpress.jsp

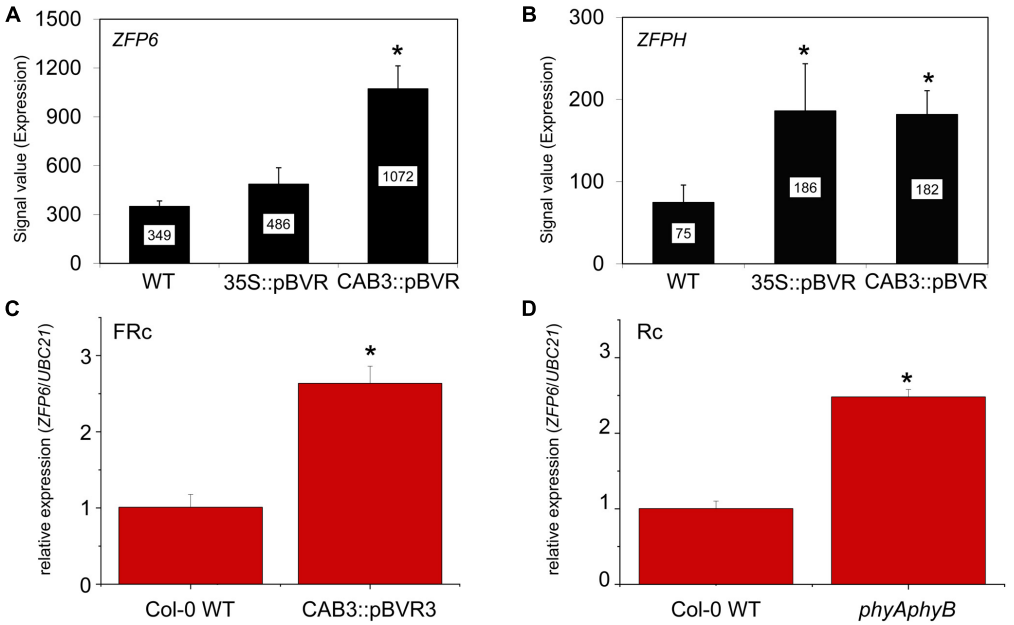

FIGURE 1 | Relative expression of *ZFP6* homologs in Arabidopsis seedlings. Expression levels (signal value) of **(A)** *ZFP6* and **(B)** *ZFPH* in wild-type (WT), 35S:pBVR, and CAB3:pBVR seedlings grown under continuous far-red (FRc) from published data set (Oh et al., 2013) are shown (± SD, $n = 3$). Signal value indicates signal intensity on the ATH1 array as calculated by Affymetrix Microarray Suite (MAS). **(C)** *ZFP6* relative expression in CAB3:pBVR3 line (Warnasooriya and Montgomery, 2009) in FRc light compared to WT. **(D)** *ZFP6* relative expression in *phyAphyB* mutant in continuous red (Rc) light conditions compared to WT. **(C,D)** Seedlings were stratified at 4°C for 4 days in MS plates with 1% sucrose and then incubated in FRc or Rc light for 7 days. Gene expression data were obtained following the $2^{-\Delta CT}$ method using *UBC21* as the reference gene. Means ± SD were calculated from at least three biological replicates. *$p \leq 0.05$, relative to WT.

as a plant-growth inhibitor. Given the importance of GA in promoting elongation in seedlings and the prior report of GA regulation of *ZFP6* (Zhou et al., 2013), we evaluated the effect of GA or inhibition of GA accumulation using the pharmacological agent paclobutrazol (PAC) on *zfp6*, *zfph*, and *zfp6zfph* mutant lines. Seedling hypocotyl length was significantly increased by ∼1.3-fold on average in *zfp6*, *zfph*, and *zfp6zfph* seedlings treated with GA compared to their corresponding untreated seedlings in FR, which was slightly less than the 1.4-fold longer seedlings observed for GA-treated WT seedlings (**Figure 3C**). Adding the GA biosynthesis inhibitor PAC disrupted the germination process in all seedlings exposed to FR light, including Col-0 WT. To overcome this, seeds were stratified on MS media without PAC and grown under W light for ∼2 d to allow germination, after which, they were exposed to PAC under FR conditions. All FR-grown, PAC-treated seedlings exhibited significantly shorter hypocotyls than their untreated counterparts, with no significant differences observed between WT and mutants (**Supplementary Figure 2A**). For R light-grown seedlings, we observed a moderate increase in hypocotyl lengths for GA-treated seedlings compared to control conditions for all lines including WT (**Figure 3D**), although these differences were not statistically significant as they were under FR. R-light, PAC-treated seedlings exhibited significantly shorter hypocotyls than untreated seedlings for all lines tested inclusive of WT (**Supplementary Figure 2B**). We also assessed hypocotyl lengths of seedlings under W light, where there were no significant changes in hypocotyl length observed among Col-0 WT and the *zfp6* mutants (**Supplementary Figure 3A**). There were also no significant changes in root lengths for any of the seedlings lines grown in R, FR, or W light (**Supplementary Figures 3B–D**).

ZFP6 Overexpression Is Sufficient to Inhibit Hypocotyl Elongation in R and Far-Red Light-Grown Seedlings

An absence of *ZFP6* and *ZFPH* expression resulted in longer hypocotyls in FR light compared to WT; hence, we hypothesized that overexpression of *ZFP6* or *ZFPH* may inversely result in shorter hypocotyls in seedlings. As expected, elongated hypocotyls observed in *zfp6* seedlings were inversely shortened in *ZFP6*-overexpression (OX) lines (**Figure 4**). In multiple transgenic lines exhibiting elevated levels of *ZFP6* mRNA (**Figure 4A**), the inhibition of hypocotyl elongation was impacted compared to WT and vector control (VC) lines (**Figures 4B,C**), particularly under R and FR conditions. The strongest reduction occurred under R light conditions for the homozygous *ZFP6* #7-2 OX line, compared to Col-0 WT and VC seedlings. Hypocotyl elongation phenotypes were not affected in *ZFP6* OX seedlings treated with blue light, with the exception of a reduction observed for *ZFP6* #7-2 OX in blue light, suggesting a direct interaction between phys and *ZFP6* in the regulation of hypocotyl length. There were no differences for any lines grown in darkness.

Besides the marked reductions in the lengths of hypocotyls observed for seedlings overexpressing *ZFP6*, we also noted other phenotypic changes for *ZFP6* OX plants. Mature 21 day-old *ZFP6*

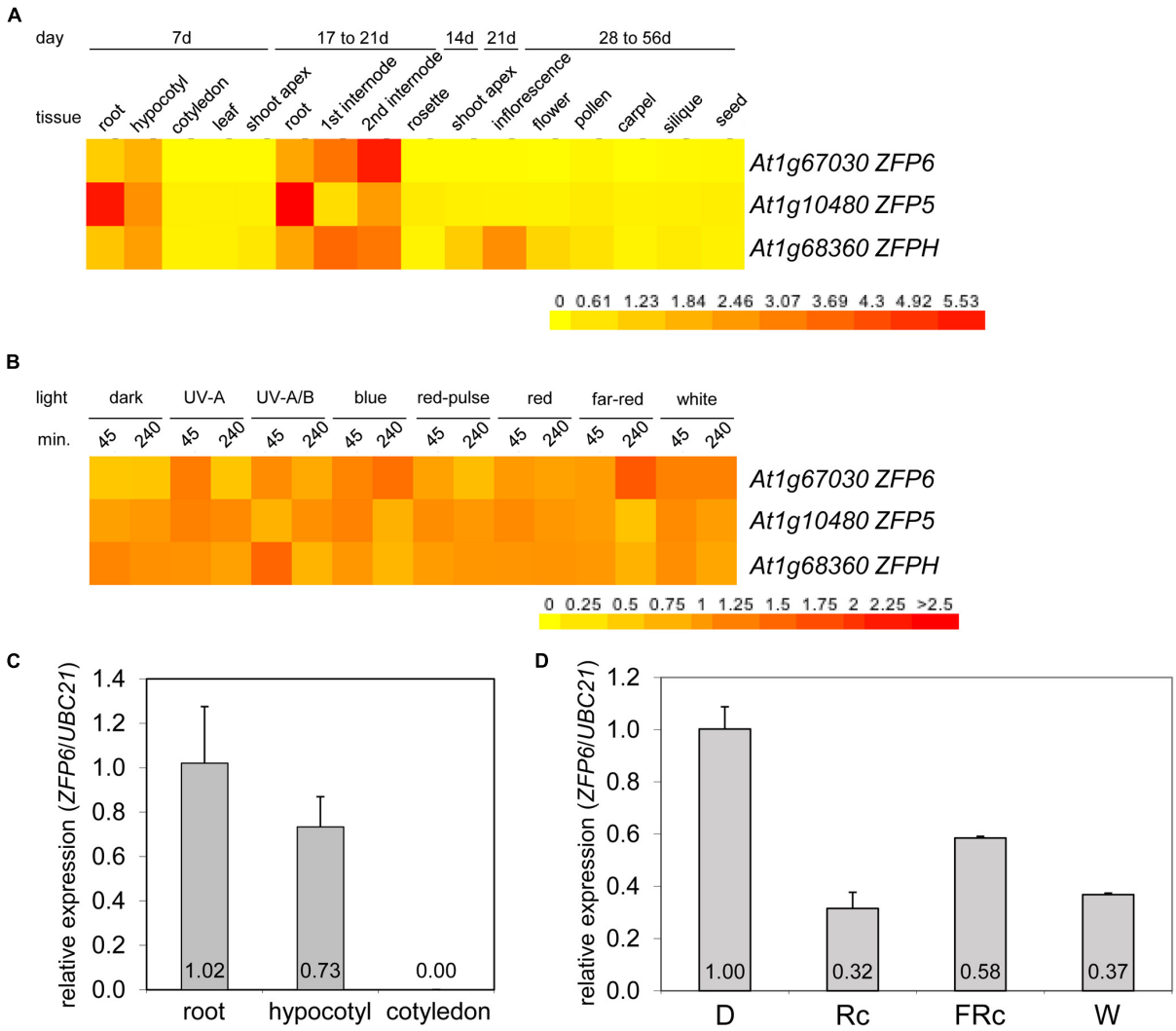

FIGURE 2 | Expression of *ZFP6*, *ZFP5*, and *ZFPH* in different tissues and light conditions. Heat map showing the expression of *ZFP6*, *ZFP5*, and *ZFPH* in **(A)** different tissues or **(B)** different light conditions for Arabidopsis. For heat map, mean-normalized values of Col-0 WT from AtGenExpress expression library and BAR Heatmapper Plus (bar.utoronto.ca) were used. For light experiments in panel **(B)**, aerial parts (hypocotyl and cotyledons) of 4-days-old Col-0 WT seedling grown on MS medium were treated with different light for either 45 or 240 min. **(C)** qRT-PCR analysis of *ZFP6* expression in Col-0 WT root, hypocotyl, or cotyledon tissues from seedlings grown on MS medium containing 1% sucrose and 0.7% Phytoblend agar at 22°C for 7 days under white light (W) at 100 μmol m^{-2} s^{-1}. **(D)** *ZFP6* expression analyses in Col-0 WT grown as mentioned in **(C)** but under dark, continuous red (Rc; 50 μmol m^{-2} s^{-1}), continuous far-red (FRc; 5 μmol m^{-2} s^{-1}), or W (100 μmol m^{-2} s^{-1}) light conditions. Relative *ZFP6* expression level compared with *UBC21* is shown (± SD, $n = 3$).

OX plants grown on soil at 22°C under long days (16 h light, 8 h dark) developed smaller rosettes than Col-0 WT or empty vector plants (**Figure 5**). Moreover, *ZFP6* OX lines developed more trichomes on their rosette leaves than Col-0 WT plants, which is consistent with a previous report (Zhou et al., 2013).

Light- and Growth-Responsive Genes Are Differentially Regulated in *ZFP6*- and *ZFPH*-Deficient Lines

Using qRT-PCR, we evaluated the expression of *PIF3*, *PIF4*, *PHYB*, and *RGA1* (*Repressor of GA1*), key genes participating in the light- or hormone-dependent regulation of tissue growth (**Figure 6**; de Lucas et al., 2008; Leivar et al., 2008; Oh et al., 2014). RGA1 is one member of the DELLA family of proteins that binds to PIF3 and PIF4, inhibiting DNA binding activity of these PIF proteins and thus affecting the expression of PIF3- and PIF4-regulated genes (de Lucas et al., 2008; Feng et al., 2008). In R light, target gene *PIF3* was ∼2.6-fold upregulated in Col-0 WT compared to W light-treated Col-0 WT (**Figure 6A**). Notably, *PIF3* mRNA levels were significantly reduced in the *zfph* and *zfp6zfph* mutants (**Figure 6A**). This result indicated a positive role for ZFPH in R-dependent *PIF3* mRNA accumulation.

In FR and R light conditions, *PIF4* mRNA levels significantly increased in Col-0 WT by ∼3.7- and ∼5-fold, respectively, compared to W light (**Figure 6B**). These findings align with

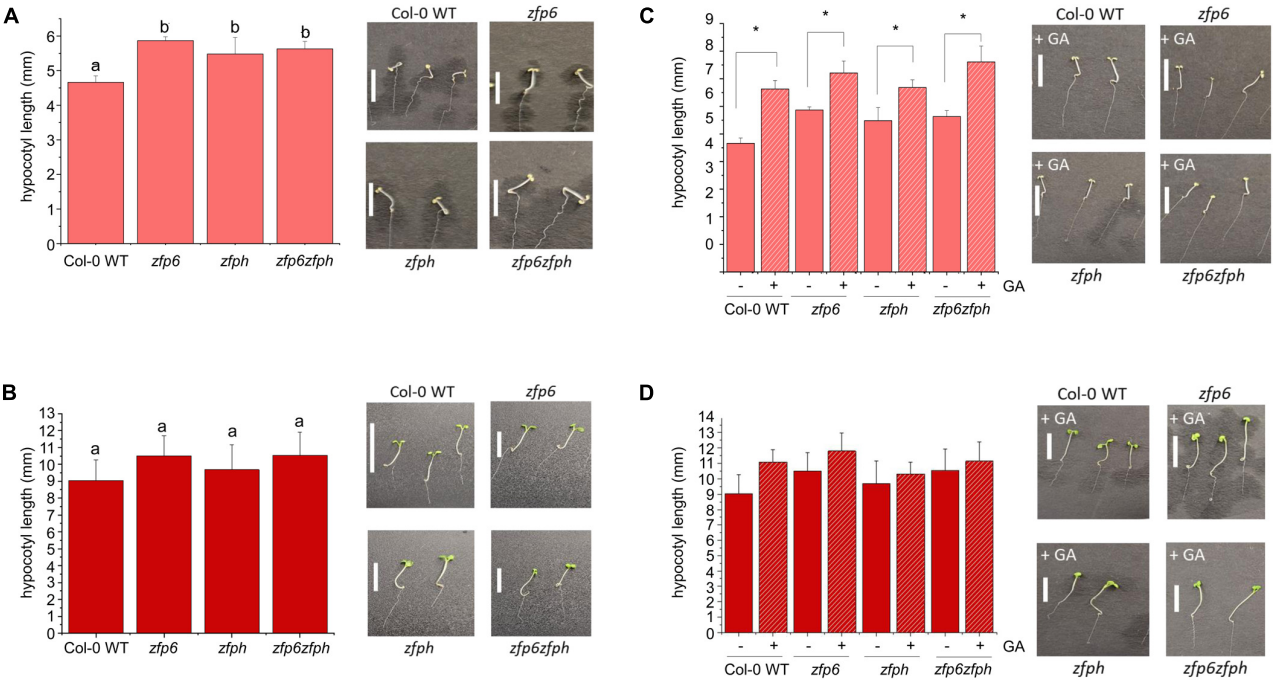

FIGURE 3 | Hypocotyl measurements in FR and R light-exposed seedlings. Seedlings were stratified at 4°C for 4 days in dark on MS plates with 1% sucrose, and subsequently incubated in continuous far-red FR light or R light for 7 days at 22°C. **(A,B)** Untreated seedlings on MS plates exposed to **(A)** FR or **(B)** R light. **(C,D)** Seedlings on MS plates with (+) or without (–) the addition of 10 μM GA under **(C)** FR or **(D)** R light. Hypocotyl measurements were performed using Photoshop 2021 with 3 plates per treatment, each containing 10 seedlings ($n = 30$). Significant differences are highlighted with different letters **(A,B)** or asterisks **(C,D)** at $p \leq 0.05$. Representative images of seedlings under each condition are shown to the right of bar graphs and the bar in the images equals 1 cm.

a previous report where *PIF4* mRNA levels in Arabidopsis seedlings grown for 6 days in long days (16 h light, 8 h dark) increased ∼1.7–fold after the seedlings were incubated in continuous R light (Zhai et al., 2020), and prior reported upregulation of *PIF4* in both R and FR (Huq and Quail, 2002). Under FR light, *PIF4* expression was ∼1.5-fold reduced in *zfp6* homolog mutant lines compared to Col-0 WT, although the difference was only significant for *zfph*. In *zfp6* and *zfph* single mutant lines treated with R light, *PIF4* transcripts were significantly upregulated by ∼1.3-fold compared to mRNA levels for R light-treated Col-0 WT seedlings.

PHYB expression levels were significantly higher in R light-treated seedlings than for W or FR light-exposed plants by an average of ∼3.1-fold (**Figure 6C**). It has been documented that *PHY* genes are generally constitutively expressed under different light conditions (Clack et al., 1994); however, another report suggests that *PHYB* is transcriptionally regulated (Somers and Quail, 1995). In R light, single and double *zfp6* homolog mutants showed lower *PHYB* expression levels (∼1.7-fold reduction) than Col-0-WT, suggesting that ZFP6 is involved in upregulating *PHYB*.

RGA1 mRNA levels significantly increased in all R light-treated seedlings by ∼4.4-fold in comparison to W and FR light, with the exception of the *zfp6zfph* double mutant that had an increase but it was only marginally significant. However, no significant differences were detected among R light-treated Col-0 WT and R light-treated *zfp6* mutant lines (**Figure 6D**).

Given that some *ZFP* genes exhibit cascade or reciprocal regulation and to facilitate interpretation of results for target genes, we tested whether *ZFPH* expression was impacted in a *zfp6* mutant, as well as whether *ZFP6* expression was impacted in the *zfph* mutant background. *ZFP6* does not directly control *ZFPH* expression as *ZFPH* transcripts were present at near WT levels in *zfp6* lines (**Supplementary Figure 4**). Likewise, *ZFPH* does not act upstream to impact *ZFP6* as *ZFP6* transcripts were present at near WT levels in *zfph* lines (**Supplementary Figure 4**).

Gibberellic Acid Modulates Light-Dependent mRNA Levels of Light- and Growth-Responsive Genes in *ZFP6* and *ZFPH* Deficient Lines

Given the prior association of GA with an induction of *ZFP6* expression and the noted impact of light and phytochromes on *ZFP6* and *ZFPH*, we examined the impact of GA on the light- and growth-responsive genes assessed in WT, *zfp6*, *zfph*, and *zfp6zfph* lines. The addition of GA to the growth media resulted in a modulation of *PIF3*, *PIF4*, *PHYB*, and *RGA1* expression levels in a light-dependent manner (**Figure 6**). The mRNA levels of *PIF3* were not different among lines grown in the presence of GA; yet, this result in the presence of GA represents a loss of R light-associated induction of *PIF3* mRNA levels in WT and *zfp6* lines compared to growth in R light in the absence of GA (**Figure 6A** vs. **Figure 6E**). Thus, the

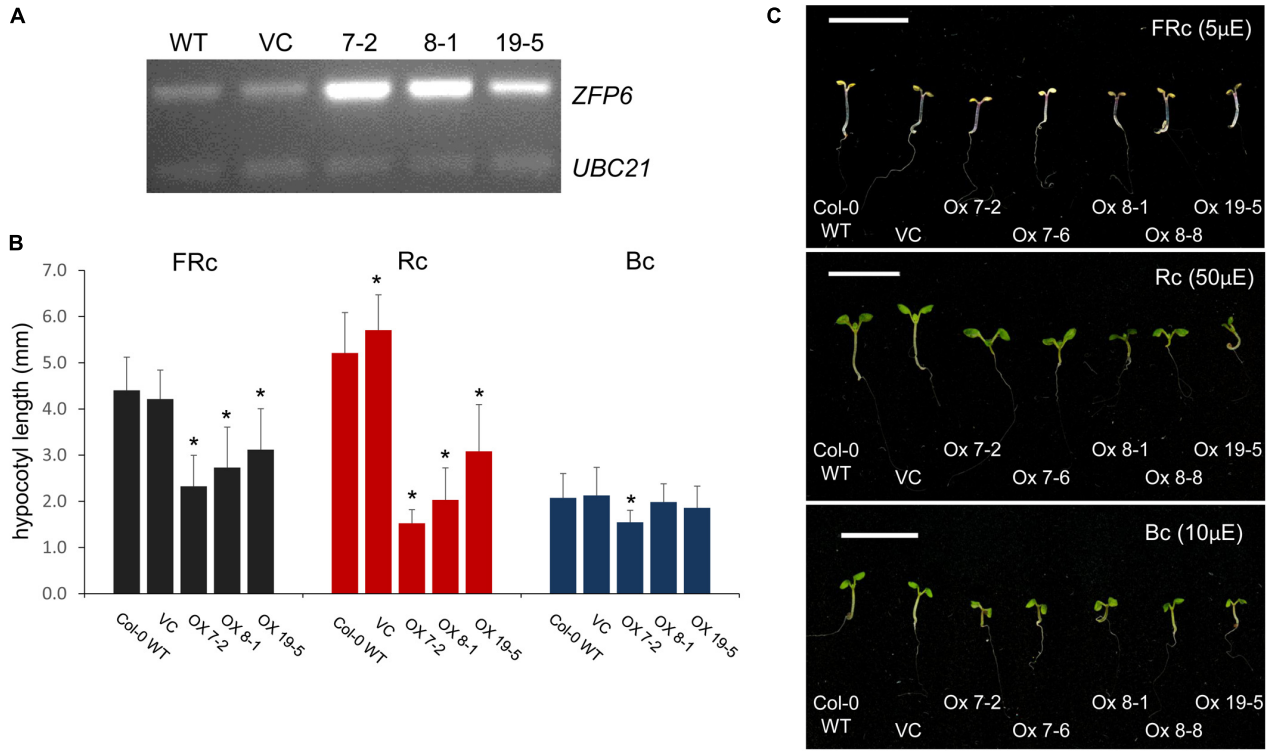

FIGURE 4 | *ZFP6* Overexpression and analyses of hypocotyl lengths of seedlings under different light conditions. **(A)** RT-PCR of *ZFP6* mRNA levels relative to control gene *UBC21* for wild-type, control lines transformed with an empty vector or vector control (VC), and three independent *ZFP6* overexpression lines. **(B,C)** Seedlings were stratified at 4°C for 4 days in the dark, grown in MS plates with 1% sucrose, 0.7% agar, and subsequently incubated in different light conditions for 7 days at 22°C. Seedlings (Col-0 WT, VC lines, and different *ZFP6* overexpression (OX) lines (i.e., OX 7-2, OX 7-6, OX 8-1, OX 8-8, and OX 19-5) were grown under continuous far-red (FRc; 5 μmol m^{-2} s^{-1} or μE), red (Rc; 50 μmol m^{-2} s^{-1} or μE), and blue (Bc; 10 μmol m^{-2} s^{-1} or μE) light. **(B)** Hypocotyl measurements were performed using Image J with at least 25 seedlings per line. Significant differences are shown with asterisks at $p \leq 0.05$. **(C)** Representative images of seedlings are shown. Bar, 1 cm.

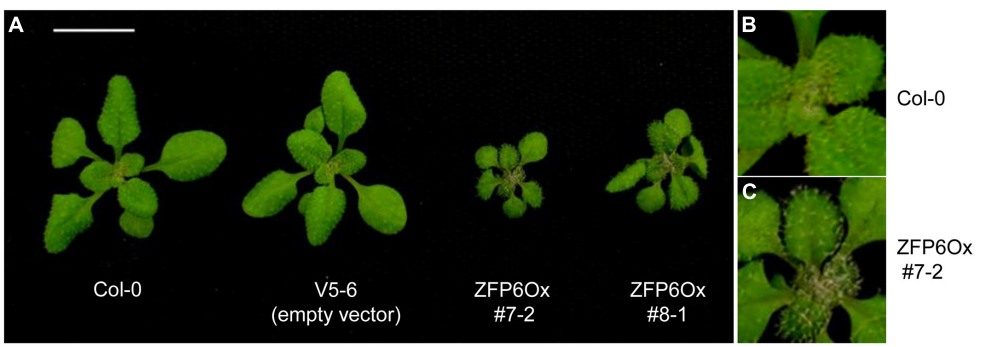

FIGURE 5 | Phenotypes of *35S:ZFP6* overexpression (OX) transgenic lines. **(A)** Rosette structure of Arabidopsis Col-0 WT, vector control (empty vector, i.e., V5-6), and the *35S:ZFP6* OX transgenic lines 7-2 and 8-1. Trichome formation in **(B)** Col-0 WT and **(C)** *ZFP6* OX 7-2 line.

R-induced accumulation of *PIF3* appears to be dependent on both GA and ZFPH.

The mRNA levels of *PIF4* were significantly upregulated in FR light-exposed seedlings compared to seedlings grown in R and W light in the presence of GA by ∼7.7- and 4-fold, respectively (**Figure 6F**). Notably, the pattern of *PIF4* transcript levels in FR and R light-treated seedlings were inverted when the seedlings grew in the presence of GA (**Figure 6B** vs. **Figure 6F**). *PIF4* mRNA levels were only significantly different in the *zfp6zfph* double mutant for GA-treated seedlings in FR light, suggesting a redundant role for the two factors under this condition.

By comparison, *PHYB* transcript levels were significantly lower in GA-treated *zfp6*, *zfph*, and *zfp6zfph* mutant seedlings

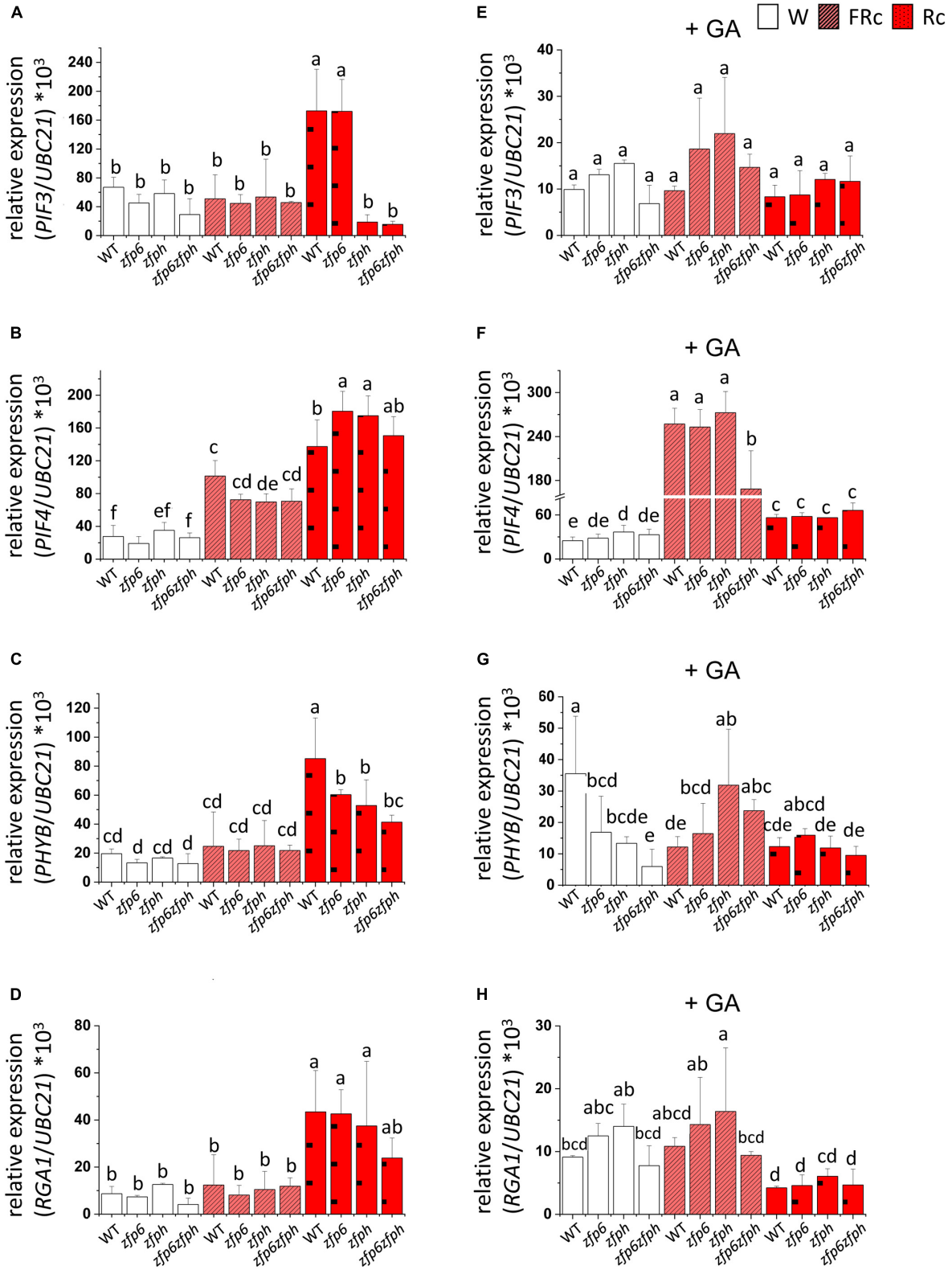

FIGURE 6 | *PIF3*, *PIF4*, *PHYB*, and *RGA1* expression in seedlings grown in white, far-red, and red light conditions with or without GA. Seedlings were stratified at 4°C for 4 days in darkness and then incubated for 7 days at 22°C in white (W; 110 μmol m^{-2} s^{-1}), continuous far-red (FRc; λmax ~735 nm at 5 μmol m^{-2} s^{-1}), or continuous red (Rc; λmax ~670 nm at a fluence ~25 μmol m^{-2} s^{-1}) in the absence **(A–D)** or presence of GA (+ GA; **E–H**). *UBC21* was used as the reference gene and the expression data was calculated using the $2^{-\Delta CT}$ method. Bars with different letters are significantly different.

Gene	Motif	Position Strand (from transcription start)	Strand	Sequence
ZFP6	G-Box	-213	-	TACGTG
	GA	-310	-	ATAGATAA
	GATA	-46	-	AAGATAAGATT
	GT1	-133 and -140	-	GGTTAA
	TCT	-417 and -655	-	TCTTAC
ZFPH	TCT	-323	-	TCTTAC
	Box4	-459	+	ATTAAT

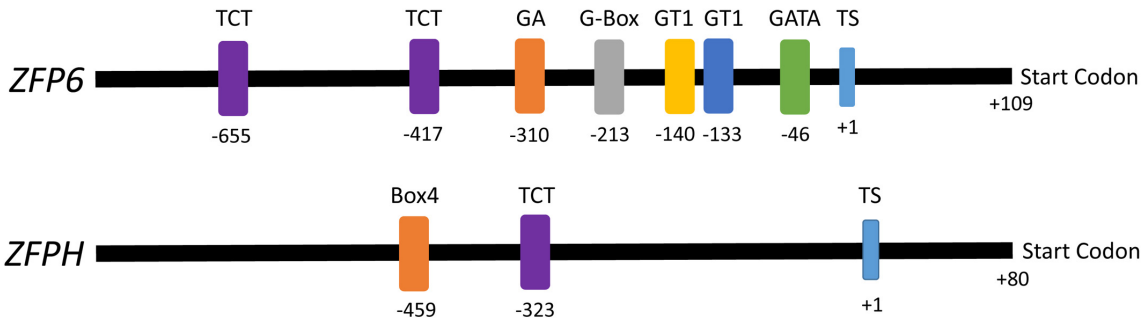

FIGURE 7 | Promoter analyses for *ZFP6* and *ZFPH* genes. The transcription start (TS) was identified using the neural network promoter prediction website and the putative light-responsive promoter regions were found using the PlantCare database (see text for details). Numbers indicate the motif and start codon positions. Sequence of the motif and the strand of DNA on which it is found (–, negative; +, positive) is indicated in the table.

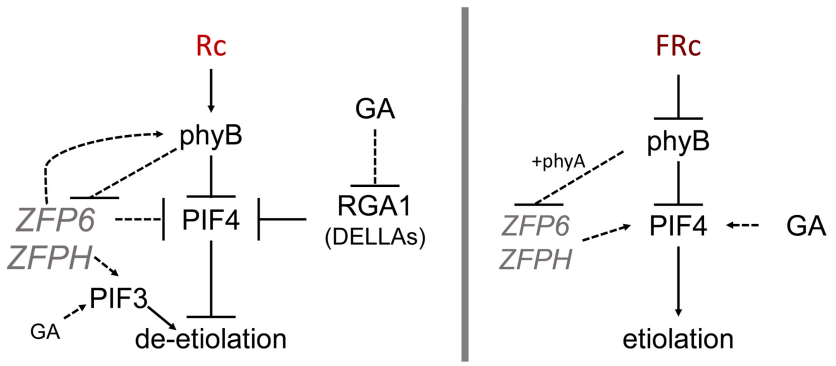

FIGURE 8 | Model showing ZFP6 genetic interactions in red and far-red light. Published literature has demonstrated that phyB destabilizes PIFs while RGA1 (a DELLA family protein) blocks PIF4 (prior relationships represented with solid black lines). In red (R) light (left), phyB reduces *ZFP6* expression. In turn, ZFP6 downregulates *PIF4* and induces *PHYB* (relationships established in this work represented with dotted lines) in R light likely providing a feedback loop to aptly modulate hypocotyl lengths in response to light. ZFPH serves to promote *PIF3* in R light, and *PIF3* is also promoted by GA in R. In the presence of the growth-promoting GA hormone in R light, GA reduces *RGA1* transcripts, which allows PIF4 accumulation and promotion of elongation in presence of GA. In far-red (FR) light (right), phyB together with phyA reduce *ZFP6* (and *ZFPH*) expression. In the presence of the growth-promoting GA hormone in FR, GA promotes *PIF4* accumulation leading to elongation typical of etiolation.

under W light compared to WT (**Figure 6G**). While there were no significant differences in *PHYB* mRNA levels for any seedlings including WT when treated with GA under R light, *PHYB* levels were significantly reduced (∼4.8-fold) in GA-treated, R light-exposed seedlings compared to their untreated counterparts grown in R light (**Figure 6C** vs. **Figure 6G**). In FR light, *PHYB* was ∼2.6-fold upregulated in GA-treated *zfph* seedlings compared to GA-treated FR light-grown Col-0 WT, and also significantly upregulated in the *zfp6zph* double mutant (**Figure 6G**).

There was no significant impact of GA treatment on *RGA* mRNA levels in W or FR light conditions (**Figure 6H**). However, *RGA1* mRNA levels were significantly reduced (∼7.5-fold) in GA-treated R-light exposed seedlings compared to R light-exposed seedlings grown without the addition of GA (**Figure 6D** vs. **Figure 6H**).

Together, these results indicate interactions between light, GA and, ZFP6/ZFPH in regulating the expression of some genes, including *PIF3* and *RGA1*.

ZFP6 and *ZFPH* Promoters Contain Light-Responsive Elements and Are Potentially Regulated by Light-Induced Genes

Analyses of the *ZFP6* and *ZFPH* promoter regions were conducted to identify cis-elements potentially involved in light responsiveness. Potential transcription start (TS) sites for *ZFP6* and *ZFPH* were found at nucleotide −109 (score cutoff 0.98) and −80 (score cutoff 1.0), respectively, from the start codon. *ZFP6* and *ZFPH* promoter region analyses resulted in the identification of different light-responsive motifs (**Figure 7**). For *ZFP6*, elements identified included G-Box, GA, GATA, GT1, and TCT motifs. The *ZFPH* promoter possessed two consensus sequences belonging to the TCT and Box 4 motifs. All these motifs have been previously documented as light-responsive elements (Shariatipour and Heidari, 2018).

To determine whether *ZFP6* and *ZFPH* genes are potentially regulated by proteins encoded by light-responsive genes, an additional *in silico* analysis was performed using the TF2Network database (see text footnote 4). We compared the *ZFP6* and *ZFPH* genes vs. 3,290 genes previously reported as light-responsive genes (**Table 1**; Bechtold et al., 2008; Shi et al., 2018). We found 9 and 17 genes that may encode proteins that bind and potentially regulate expression of *ZFP6* and *ZFPH*, respectively. One notable factor predicted to regulate ZFPH is PIF4, which together with altered *PIF4* levels in the *zfph* mutant in FR and R light conditions (**Figure 6A**) suggests an interesting potential feedback loop between ZFPH and PIF4. Many of the identified genes belong to the *ZFP* family, which indicates a cascade regulation among *ZFP* genes, as previously reported (Zhou et al., 2013). In addition, among genes predicted to encode factors that regulate *ZFP6* and *ZFPH* are an overrepresentation of hormone-inducible genes, mainly those regulated by ABA (**Supplementary Figure 2**).

DISCUSSION

Phytochromes negatively regulate *ZFP6* and *ZFPH* expression. We, thus, investigated whether phytochrome-dependent regulation of *ZFP6* and *ZFPH* is involved in controlling aspects of photomorphogenesis. To examine the interplay between phytochromes and *ZFP6* and *ZFPH* during development, we analyzed the development of *zfp6*, *zfph* and *zfp6zfph* mutants under distinct light conditions. Given the prior association of *ZFP6* induction by GA, we also examined the impact of modulating GA levels on development through treatment of seedlings with exogenous GA or a GA inhibitor. The *zfp6*, *zfph*, and *zfp6zfph* mutant lines exhibited significantly longer hypocotyls than Col-0 WT under FR light conditions. There was no specific effect of GA treatment or inhibition of GA accumulation on *zfp6*, *zfph*, or *zfp6zfph* seedling relative to WT in either R or FR light, indicating that the impacts of GA and phytochromes on these *ZFP* homologs may occur independently.

In FR light, PIFs escape phyB-mediated degradation as phyB remains in the cytosol and thus its transcriptional activity is blocked (Kevei et al., 2007); this FR-associated block of phyB translocation and a lack of associated phyB activity such as the downregulation of *PIF4* in the nucleus promotes PIF4 accumulation and elongated hypocotyls (Fiorucci and Fankhauser, 2017). In line with this, we observed that *PIF4* transcripts significantly increased in response to FR light in Col-0 WT (**Figure 6B**). As previously reported, *PIF4* mRNA levels also increase in R light (**Figure 6A**; Zhai et al., 2020). Of note, the phytochrome-dependent regulation of a transcription factor that results in downregulation of *PIF4* mRNA levels in FR light and upregulation in R light in deficient mutants was previously reported for *sig2* mutants (Oh and Montgomery, 2013), which parallels the response noted here for *zfp6* and *zfph* mutants. Of note, SIG2 is a regulatory factor also controlled by phyA and phyB and that impacts both *PIF4* mRNA levels and hypocotyl elongation among other phenotypes (Oh and Montgomery, 2013). However, the regulation of *PIF4* levels did not correspond with significantly longer hypocotyls in R or FR light for *zfp6* and *zfph* mutants. Thus, although ZFP6 and ZFPH appear to exert positive transcriptional regulation on *PIF4* under FR light and negative regulation under R light, this does not explain in full the significant disruption in hypocotyl elongation under FR. This finding may suggest that other members of the PIF family, or other factors altogether, may be involved in coordinating the observed etiolated responses in FR light where the hypocotyls of *ZFP6* and *ZFPH*-deficient seedlings were significantly longer than WT. We also checked *PIF3* mRNA levels in FR and its expression was not significantly changed under these conditions.

Under R light, our results imply that ZFP6 may limit hypocotyl elongation in part in WT by blocking *PIF4* mRNA accumulation in R light (**Figure 8**), taking into consideration previous research that has shown consistency at the level of transcript levels and protein accumulation for PIF (Lee et al., 2021) and DELLAs (Zentella et al., 2007; Achard et al., 2008). To demonstrate whether *ZFP6* is sufficient to inhibit hypocotyl elongation in seedlings, we created transgenic plants overexpressing *ZFP6*. The *ZFP6* OX plants exhibited shorter hypocotyls than Col-0 WT Arabidopsis seedlings, especially those exposed to FR and R light conditions (**Figure 4**). These results confirm a key regulatory role of *ZFP6* in restraining tissue elongation.

We observed elongated hypocotyls in all cases when GA was added. Additionally, Col-0 WT and all mutant seedlings treated with PAC displayed the same phenotypes independent of whether grown in R or FR light. These results indicate that DELLAs exert their impact on seedling elongation via an independent mechanism compared to *ZFP6* and *ZFPH*, and that DELLAs likely serve as master regulators in response to GA.

As we observed increased *ZFP6* mRNA levels for *phyB* mutants, we were also interested in evaluating the expression of *PHYB* in *zfp6* mutant lines to test for reciprocal regulation. *PHYB* was downregulated in *zfp6* and *zfph* mutant lines grown in R light, suggesting that ZFP6 is implicated in upregulating *PHYB* under these conditions (**Figure 8**). Indeed, by performing *in silico*

analysis of the *ZFP6* and *ZFPH* promoters, we identified several light-regulated motifs in the *ZFP6* and *ZFPH* promoters. We also identified several proteins encoded by light-regulated genes that can potentially regulate *ZFP6* and *ZFPH*. This finding aligns with prior analyses in which some members of the ZFP family have been previously associated with photomorphogenesis in plants (Ito et al., 2018).

Here, we report that hypocotyl elongation can be modulated at the seedling stage depending on *ZFP6* and *ZFPH* phytochrome-dependent regulation. In addition to *ZFP6* and *ZFPH* being regulated by light and phytochrome activity, ZFP6 and ZFPH regulate *PHYB* and *PIF4* and *PIF3*, key components of the photomorphogenesis signaling cascade that can impact organ elongation genes. In mature plants, the rosette architecture is markedly reduced in lines overexpressing *ZFP6*, while the hairy trichomes become denser as previously reported (Zhou et al., 2013). Additional research is needed to fully elucidate the phytochrome and *ZFP6/ZFPH*-dependent regulatory network(s) that target organ-elongation genes and, ultimately, control light-dependent morphogenesis *in planta*.

DATA AVAILABILITY STATEMENT

The original contributions presented in the study are included in the article/**Supplementary Material**, further inquiries can be directed to the corresponding author/s.

AUTHOR CONTRIBUTIONS

KC-R and SO designed and conducted the research, analyzed and interpreted data, and contributed to writing and editing the article. BM designed the research, analyzed and interpreted the data, and contributed to writing and editing article. All authors approved the submitted article.

FUNDING

This work was supported by the National Science Foundation (NSF; MCB-1243983 to BM) and the Office of Science of the U.S. Department of Energy (DE-FG02-91ER20021 to BM).

ACKNOWLEDGMENTS

We are grateful to Hussien Alameldin for his assistance with genotyping experiments and growing plants.

SUPPLEMENTARY MATERIAL

The Supplementary Material for this article can be found online at: https://www.frontiersin.org/articles/10.3389/fpls.2022.846262/full#supplementary-material

REFERENCES

Achard, P., Gong, F., Cheminant, S., Alioua, M., Hedden, P., and Genschik, P. (2008). The cold-inducible CBF1 factor-dependent signaling pathway modulates the accumulation of the growth-repressing DELLA proteins via its effect on gibberellin metabolism. *Plant Cell* 20, 2117–2129. doi: 10.1105/tpc.108.058941

Bechtold, U., Richard, O., Zamboni, A., Gapper, C., Geisler, M., Pogson, B., et al. (2008). Impact of chloroplastic- and extracellular-sourced ROS on high light-responsive gene expression in *Arabidopsis*. *J. Exp. Bot.* 59, 121–133. doi: 10.1093/jxb/erm289

Cheng, M.-C., Kathare, P. K., Paik, I., and Huq, E. (2021). Phytochrome signaling networks. *Annu. Rev. Plant Biol.* 72, 217–244. doi: 10.1146/annurev-arplant-080620-024221

Clack, T., Mathews, S., and Sharrock, R. A. (1994). The phytochrome apoprotein family in *Arabidopsis* is encoded by five genes: the sequences and expression of PHYD and PHYE. *Plant Mol. Biol.* 25, 413–427. doi: 10.1007/BF00043870

Clough, S. J., and Bent, A. F. (1998). Floral dip: a simplified method for Agrobacterium-mediated transformation of *Arabidopsis thaliana*. *Plant J.* 16, 735–743. doi: 10.1046/j.1365-313X.1998.00343.x

de Lucas, M., Daviere, J. M., Rodriguez-Falcon, M., Pontin, M., Iglesias-Pedraz, J. M., Lorrain, S., et al. (2008). A molecular framework for light and gibberellin control of cell elongation. *Nature* 451, 480–484. doi: 10.1038/nature06520

Ejaz, M., Bencivenga, S., Tavares, R., Bush, M., and Sablowski, R. (2021). *Arabidopsis thaliana* HOMEOBOX GENE 1 controls plant architecture by locally restricting environmental responses. *Proc. Natl. Acad. Sci. U.S.A* 118, 1–6. doi: 10.1073/pnas.2018615118

Englbrecht, C. C., Schoof, H., and Böhm, S. (2004). Conservation, diversification and expansion of C2H2 zinc finger proteins in the *Arabidopsis thaliana* genome. *BMC Genomics* 5:39. doi: 10.1186/1471-2164-5-39

Fankhauser, C., and Chory, J. (1997). Light control of plant development. *Annu. Rev. Cell Dev. Biol.* 13, 203–229. doi: 10.1146/annurev.cellbio.13.1.203

Fedotova, A. A., Bonchuk, A. N., Mogila, V. A., and Georgiev, P. G. (2017). C2H2 zinc finger proteins: the largest but poorly explored family of higher eukaryotic transcription factors. *Acta Nat.* 9, 47–58.

Feng, S., Martinez, C., Gusmaroli, G., Wang, Y., Zhou, J., Wang, F., et al. (2008). Coordinated regulation of *Arabidopsis thaliana* development by light and gibberellins. *Nature* 451, 475–479. doi: 10.1038/nature06448

Feurtado, J. A., Huang, D., Wicki-Stordeur, L., Hemstock, L. E., Potentier, M. S., Tsang, E. W. T., et al. (2011). The *Arabidopsis* C2H2 zinc finger INDETERMINATE DOMAIN1/ENHYDROUS promotes the transition to germination by regulating light and hormonal signaling during seed maturation. *Plant Cell* 23, 1772–1794. doi: 10.1105/tpc.111.085134

Fiorucci, A. S., and Fankhauser, C. (2017). Plant strategies for enhancing access to sunlight. *Curr. Biol.* 27, R931–R940. doi: 10.1016/j.cub.2017.05.085

Han, G., Lu, C., Guo, J., Qiao, Z., Sui, N., Qiu, N., et al. (2020). C2H2 zinc finger proteins: master regulators of abiotic stress responses in plants. *Front. Plant Sci.* 11:115. doi: 10.3389/fpls.2020.00115

Hernández-García, J., Briones-Moreno, A., and Blázquez, M. A. (2021). Origin and evolution of gibberellin signaling and metabolism in plants. *Semin. Cell Dev. Biol.* 109, 46–54. doi: 10.1016/j.semcdb.2020.04.009

Huq, E., and Quail, P. H. (2002). PIF4, a phytochrome-interacting bHLH factor, functions as a negative regulator of phytochrome B signaling in *Arabidopsis*. *EMBO J.* 21, 2441–2450. doi: 10.1093/emboj/21.10.2441

Ito, T., Okada, K., Fukazawa, J., and Takahashi, Y. (2018). DELLA-dependent and -independent gibberellin signaling. *Plant Signal. Behav.* 13:e1445933. doi: 10.1080/15592324.2018.1445933

Joseph, M. P., Papdi, C., Kozma-Bognár, L., Nagy, I., López-Carbonell, M., Rigó, G., et al. (2014). The *Arabidopsis* ZINC FINGER PROTEIN3 interferes with abscisic acid and light signaling in seed germination and plant development. *Plant Physiol.* 165, 1203–1220. doi: 10.1104/pp.113.234294

Kevei, E., Schafer, E., and Nagy, F. (2007). Light-regulated nucleo-cytoplasmic partitioning of phytochromes. *J. Exp. Bot.* 58, 3113–3124. doi: 10.1093/jxb/erm145

Kim, J. Y., Lee, J. H., and Park, C. M. (2021). A multifaceted action of phytochrome B in plant environmental adaptation. *Front. Plant Sci.* 12:659712. doi: 10.3389/fpls.2021.659712

Kulkarni, S. R., Vaneechoutte, D., Van De Velde, J., and Vandepoele, K. (2018). TF2Network: predicting transcription factor regulators and gene regulatory networks in *Arabidopsis* using publicly available binding site information. *Nucleic Acids Res.* 46:e31. doi: 10.1093/nar/gkx1279

Kusnetsov, V. V., Doroshenko, A. S., Kudryakova, N. V., and Danilova, M. N. (2020). Role of phytohormones and light in de-etiolation. *Russ. J. Plant Physiol.* 67, 971–984. doi: 10.1134/S1021443720060102

Lee, S., Wang, W., and Huq, E. (2021). Spatial regulation of thermomorphogenesis by HY5 and PIF4 in *Arabidopsis*. *Nat. Commun.* 12:3656. doi: 10.1038/s41467-021-24018-7

Legris, M., Ince, Y. Ç, and Fankhauser, C. (2019). Molecular mechanisms underlying phytochrome-controlled morphogenesis in plants. *Nat. Commun.* 10:5219. doi: 10.1038/s41467-019-13045-0

Leivar, P., and Monte, E. (2014). PIFs: systems integrators in plant development. *Plant Cell* 26, 56–78. doi: 10.1105/tpc.113.120857

Leivar, P., Monte, E., Oka, Y., Liu, T., Carle, C., Castillon, A., et al. (2008). Multiple phytochrome-interacting bHLH transcription factors repress premature seedling photomorphogenesis in darkness. *Curr. Biol.* 18, 1815–1823. doi: 10.1016/j.cub.2008.10.058

Li, J., Li, G., Wang, H., and Deng, X. W. (2011). Phytochrome signaling mechanisms. *Arabidopsis Book* 9:e0148. doi: 10.1199/tab.0148

Li, K., Yu, R., Fan, L.-M., Wei, N., Chen, H., and Deng, X. W. (2016). DELLA-mediated PIF degradation contributes to coordination of light and gibberellin signalling in *Arabidopsis*. *Nat. Commun.* 7:11868. doi: 10.1038/ncomms11868

Mayfield, J. D., Folta, K. M., Paul, A.-L., and Ferl, R. J. (2007). The 14-3-3 proteins μ and υ influence transition to flowering and early phytochrome response. *Plant Physiol.* 145, 1692–1702. doi: 10.1104/pp.107.108654

Montgomery, B. L., Yeh, K.-C., Crepeau, M. W., and Lagarias, J. C. (1999). Modification of distinct aspects of photomorphogenesis via targeted expression of mammalian biliverdin reductase in transgenic *Arabidopsis* plants. *Plant Physiol.* 121, 629–640. doi: 10.1104/pp.121.2.629

Noman, A., Aqeel, M., Khalid, N., Islam, W., Sanaullah, T., Anwar, M., et al. (2019). Zinc finger protein transcription factors: integrated line of action for plant antimicrobial activity. *Microb. Pathog.* 32, 141–149. doi: 10.1016/j.micpath.2019.04.042

Oh, E., Zhu, J.-Y., Bai, M.-Y., Arenhart, R. A., Sun, Y., and Wang, Z.-Y. (2014). Cell elongation is regulated through a central circuit of interacting transcription factors in the *Arabidopsis* hypocotyl. *Elife* 3:e03031. doi: 10.7554/eLife.03031

Oh, S., and Montgomery, B. L. (2013). Phytochrome-induced SIG2 expression contributes to photoregulation of phytochrome signaling and photomorphogenesis in *Arabidopsis thaliana*. *J. Exp. Bot.* 64, 5457–5472. doi: 10.1093/jxb/ert308

Oh, S., Warnasooriya, S. N., and Montgomery, B. L. (2013). Downstream effectors of light- and phytochrome-dependent regulation of hypocotyl elongation in *Arabidopsis thaliana*. *Plant Mol. Biol.* 81, 627–640. doi: 10.1007/s11103-013-0029-0

Osterlund, M. T., and Deng, X.-W. (1998). Multiple photoreceptors mediate the light-induced reduction of GUS-COP1 from *Arabidopsis* hypocotyl nuclei. *Plant J.* 16, 201–208. doi: 10.1046/j.1365-313x.1998.00290.x

Osterlund, M. T., Hardtke, C. S., Wei, N., and Deng, X. W. (2000). Targeted destabilization of HY5 during light-regulated development of *Arabidopsis*. *Nature* 405:462. doi: 10.1038/35013076

Phillips, A. L. (1998). Gibberellins in *Arabidopsis*. *Plant Physiol. Biochem.* 36, 115–124. doi: 10.1016/S0981-9428(98)80096-X

Ruckle, M. E., DeMarco, S. M., and Larkin, R. M. (2007). Plastid signals remodel light signaling networks and are essential for efficient chloroplast biogenesis in *Arabidopsis*. *Plant Cell* 19, 3944–3960. doi: 10.1105/tpc.107.054312

Shariatipour, N., and Heidari, B. (2018). Investigation of drought and salinity tolerance related genes and their regulatory mechanisms in *Arabidopsis* (*Arabidopsis thaliana*). *Open Bioinform. J.* 11, 12–28. doi: 10.2174/1875036201811010012

Shi, H., Lyu, M., Luo, Y., Liu, S., Li, Y., He, H., et al. (2018). Genome-wide regulation of light-controlled seedling morphogenesis by three families of transcription factors. *Proc. Natl. Acad. Sci. U.S.A* 115, 6482–6487. doi: 10.1073/pnas.1803861115

Somers, D. E., and Quail, P. H. (1995). Temporal and spatial expression patterns of PHYA and PHYB genes in *Arabidopsis*. *Plant J.* 7, 413–427. doi: 10.1046/j.1365-313X.1995.7030413.x

Sun, L., Zhang, A., Zhou, Z., Zhao, Y., Yan, A., Bao, S., et al. (2015). GLABROUS INFLORESCENCE STEMS3 (GIS3) regulates trichome initiation and development in *Arabidopsis*. *New Phytol.* 206, 220–230. doi: 10.1111/nph.13218

Warnasooriya, S. N., and Montgomery, B. L. (2009). Detection of spatial-specific phytochrome responses using targeted expression of biliverdin reductase in *Arabidopsis*. *Plant Physiol.* 149, 424–433. doi: 10.1104/pp.108.127050

Xie, M., Sun, J., Gong, D., and Kong, Y. (2019). The roles of *Arabidopsis* C1-2i subclass of C2H2-type zinc-finger transcription factors. *Genes* 10:653. doi: 10.3390/genes10090653

Zentella, R., Zhang, Z.-L., Park, M., Thomas, S. G., Endo, A., Murase, K., et al. (2007). Global analysis of DELLA direct targets in early gibberellin signaling in *Arabidopsis*. *Plant Cell* 19, 3037–3057. doi: 10.1105/tpc.107.054999

Zhai, H., Xiong, L., Li, H., Lyu, X., Yang, G., Zhao, T., et al. (2020). Cryptochrome 1 inhibits shoot branching by repressing the self-activated transciption loop of PIF4 in *Arabidopsis*. *Plant Commun.* 1:100042. doi: 10.1016/j.xplc.2020.100042

Zhou, Z., An, L., Sun, L., Zhu, S., Xi, W., Broun, P., et al. (2011). Zinc finger protein5 is required for the control of trichome initiation by acting upstream of zinc finger protein8 in *Arabidopsis*. *Plant Physiol.* 157, 673–682. doi: 10.1104/pp.111.180281

Zhou, Z., Sun, L., Zhao, Y., An, L., Yan, A., Meng, X., et al. (2013). Zinc Finger Protein 6 (ZFP6) regulates trichome initiation by integrating gibberellin and cytokinin signaling in *Arabidopsis thaliana*. *New Phytol.* 198, 699–708. doi: 10.1111/nph.12211

Conflict of Interest: The authors declare that the research was conducted in the absence of any commercial or financial relationships that could be construed as a potential conflict of interest.

Publisher's Note: All claims expressed in this article are solely those of the authors and do not necessarily represent those of their affiliated organizations, or those of the publisher, the editors and the reviewers. Any product that may be evaluated in this article, or claim that may be made by its manufacturer, is not guaranteed or endorsed by the publisher.

frontiers | Frontiers in Plant Science

ORIGINAL RESEARCH
published: 09 June 2022
doi: 10.3389/fpls.2022.862387

Dual Role for FHY3 in Light Input to the Clock

*Bruce M. Rhodes, Hamad Siddiqui, Safina Khan and Paul F. Devlin**

Department of Biological Sciences, Royal Holloway, University of London, Egham, United Kingdom

The red-light regulated transcription factors FHY3 and FAR1 form a key point of light input to the plant circadian clock in positively regulating expression of genes within the central clock. However, the *fhy3* mutant shows an additional red light-specific disruption of rhythmicity which is inconsistent with this role. Here we demonstrate that only *fhy3* and not *far1* mutants show this red specific disruption of rhythmicity. We examined the differences in rhythmic transcriptome in red versus white light and reveal differences in patterns of rhythmicity among the central clock proteins suggestive of a change in emphasis within the central mechanism of the clock, changes which underlie the red specificity of the *fhy3* mutant. In particular, changes in enrichment of promoter elements were consistent with a key role for the HY5 transcription factor, a known integrator of the ratio of red to blue light in regulation of the clock. Examination of differences in the rhythmic transcriptome in the *fhy3* mutant in red light identified specific disruption of the CCA1-regulated *ELF3* and *LUX* central clock genes, while the CCA1 target TBS element, TGGGCC, was enriched among genes that became arrhythmic. Coupled with the known interaction of FHY3 but not FAR1 with CCA1 we propose that the red-specific circadian phenotype of *fhy3* may involve disruption of the previously demonstrated moderation of CCA1 activity by FHY3 rather than a disruption of its own transcriptional regulatory activity. Together, this evidence suggests a conditional redundancy between FHY3 and HY5 in the integration of red and blue light input to the clock in order to enable a plasticity in response to light and optimise plant adaptation. Furthermore, our evidence also suggests changes in CCA1 activity between red and white light transcriptomes. This, together with the documented interaction of HY5 with CCA1, leads us to propose a model whereby this integration of red and blue signals may at least partly occur *via* direct FHY3 and HY5 interaction with CCA1 leading to moderation of CCA1 activity.

Keywords: circadian, clock, light, photoreceptor, transcriptome, mutant

OPEN ACCESS

Edited by:
Karen Halliday,
The University of Edinburgh,
United Kingdom

Reviewed by:
Ana M. Casas,
Aula Dei Experimental Station (CSIC),
Spain
Francisco J. Romero-Campero,
Institute of Plant Biochemistry
and Photosynthesis (CSIC), Spain

***Correspondence:**
Paul F. Devlin
paul.devlin@rhul.ac.uk

Specialty section:
This article was submitted to
Plant Physiology,
a section of the journal
Frontiers in Plant Science

Received: *25 January 2022*
Accepted: *16 May 2022*
Published: *09 June 2022*

Citation:
Rhodes BM, Siddiqui H, Khan S
and Devlin PF (2022) Dual Role for
FHY3 in Light Input to the Clock.
Front. Plant Sci. 13:862387.
doi: 10.3389/fpls.2022.862387

INTRODUCTION

The circadian clock is an internal regulator of biological processes that enhances fitness by ensuring living organisms are optimally in sync with the daily cycle of day and night (Creux and Harmer, 2019). A wide range of behaviours and metabolic reactions, environmental responses and even biotic interactions has been found to oscillate with a circadian rhythm that continues

even under constant environmental conditions. In plants, circadian clock outputs control seedling establishment (Gommers and Monte, 2018), development (Henriques et al., 2018) and rhythms of leaf movement (Woodley Of Menie et al., 2019). Replenishment of the photosynthetic machinery is maximised around dawn (Dodd et al., 2015) while usage of starch reserves overnight is carefully timed to coincide with the duration of night (Graf et al., 2010). The clock also forms the basis of timekeeping for the measurement of day length in the regulation of flowering time, tuber formation and bud dormancy (Rodriguez-Falcon et al., 2006; Ibanez et al., 2010; Song et al., 2015) and, consequently, has a significant impact upon agriculture. Many plant responses also vary in magnitude at different times of day. Triggers received at certain times of day may be better indicators of environmental information than those received at other times. In such cases, the clock acts as a "gate" which closes at certain times, constraining these responses. For example, response to temperature is much greater around subjective dusk (Grundy et al., 2015). Light induction of gene expression is much more prominent during the subjective day (Millar and Kay, 1996; Fraser et al., 2021) and even responses to plant hormones is gated to be maximal at certain times of day (Covington and Harmer, 2007).

The circadian clock, itself, is acutely responsive to light. Light forms the most prominent indicator of dawn and dusk and so light, along with temperature, forms a key input to entrain the clock (Oakenfull and Davis, 2017). Although circadian clocks run with a precisely repeating period of approximately 24 h, a limited range of different period lengths can be observed within a population meaning that most individuals require minor adjustments to the phase of their clock to keep it in time with the diurnal cycle. Equally, latitudinal clines can be observed in circadian period length. Differences in period length within a species are thought to be an advantage in dealing with the varying stresses associated with different latitudes but this also requires an ability to reset the clock on a daily basis (Michael et al., 2003). Finally, as daylength changes through the year, minor adjustments are needed and the final pattern of the circadian cycle may be a combination of resetting signals at dawn and dusk that enable optimal adaptation to the different seasons (Hearn et al., 2018).

The photoreceptors mediating light input to the clock have been well characterised. Both red and blue wavelengths can adjust the clock, perceived by the red-absorbing phytochromes and blue-absorbing cryptochromes and Zeitlupe photoreceptor (Somers et al., 1998; Devlin and Kay, 2000; Yan et al., 2021). As an indication of how important light input is within the plant circadian system, the majority of the genes that make up the plant central clock have been demonstrated to be light regulated (Oakenfull and Davis, 2017). The plant clock, itself, consists of interlocked transcriptional feedback loops (Hsu and Harmer, 2014). Two morning-phased myb transcription factors, CCA1 and LHY, act to repress evening-phased genes, *ELF3*, *LUX*, and *ELF4*, which encode the constituents of an evening complex that, in turn acts to repress a series of pseudo response regulator genes. *PRR9*, *PRR7*, *PRR5*, and *TOC1* (*PRR1*). The PRR proteins peak in that order in a sequence ranging through the day, and act to complete the loop by repressing *CCA1* and *LHY* expression. The action of TOC1 in regulation of *CCA1* expression has been shown to involve interaction with the TPS transcription factor, CHE (Pruneda-Paz et al., 2009), which binds a TCP binding site (TBS), GGTCC (or GGACC). At the same time, positive acting factors including RVE8, another myb transcription factor related to CCA1 and LHY, act in response to light to activate expression of many of the central clock genes including the *PRR* genes, *PRR9*, *PRR5*, and *TOC1*, and the evening complex genes, *LUX* and *ELF4*. The *RVE8* gene also shows circadian regulation, with its expression peaking at dawn and, like *CCA1* and *LHY*, being repressed by the PRR proteins.

As well as driving oscillation of the central clock, the clock components are also responsible for output from the central clock, targeting a significant proportion of the transcriptome (Michael et al., 2008). Both the negative actions of CCA1 and LHY and the positive actions of RVE8 are mediated by their association with evening elements in the promoters of their target genes and the evening element has been found to be highly enriched in the promoters of rhythmic genes. CCA1 also binds to another TBS, GGCCCA (or TGGGCC) as well as GA (or CT) motif elements and potentially G-boxes (CACGTG) to mediate output from the clock (Kamioka et al., 2016).

We are also now beginning to understand more about how the mechanism of light input affects the genes of the central clock, itself. A number of signal transduction components acting downstream of the phytochromes and cryptochromes have been shown to act on central clock gene expression. The HY5 transcription factor acts downstream of both phytochromes and cryptochromes in light signalling. HY5 protein accumulates in response to light and associates with the ACE (ACGT) promoter element, which forms the core of the G-box, whereby it activates gene expression as part of a dimer with the related protein, HYH. HY5 associates with the promoters of most of the central clock genes but particularly acts in blue light input to the clock. The *hy5* mutant has a short period in blue light but not red or white light. It was recently demonstrated that HY5 levels are higher in blue light and considerably reduced in red light. Hence, HY5 confers information about the ratio of red and blue light (Hajdu et al., 2018). The light-signalling transcription factors, FHY3 and FAR1, also act a dimer to positively regulate expression of the central clock genes, *ELF4*, and *CCA1*, by binding to the FHY3/FAR1 binding site (fbs), CACGCGC, in the promoters of these target genes (Li et al., 2011; Liu et al., 2020). Consistent with this, loss of either FHY3 or FAR1 causes an almost complete loss of *ELF4* expression in white light. However, only a slight loss of the amplitude of *CCA1* and LHY expression was observed under the same conditions (Li et al., 2011), indicating that loss of either FHY3 or FAR1 does not stop the clock altogether in white light. However, the *fhy3* mutation does cause a much more dramatic effect in red light. In red light there is an almost complete loss of *CCA1* and *LHY* expression (Allen et al., 2006). Furthermore, analysis of the output gene, *CAB2*, also showed a wavelength-specific phenotype. *CAB2* expression in *fhy3* is arrhythmic in red light but shows limited rhythmicity in white light and completely normal circadian rhythmicity in blue light (Allen et al., 2006), indicating that action of FHY3 is also dependent

on the proportions of red and blue light incident on the plant. Interestingly, FHY3 but not FAR1 protein directly interacts with HY5. Additionally, FHY3 interacts with a number of central clock proteins. FHY3 but not FAR1 also directly interacts with CCA1 and LHY in the regulation of *ELF4* expression, while both FHY3 and FAR1 directly interact with TOC1 and PIF5 in the regulation of *CCA1* expression.

Here we have further investigated the role of FHY3 and FAR1 in light input to the clock. We confirmed that the red-specific disruption of rhythmicity of the *fhy3* mutant extends to a wide range of clock outputs and to several central clock genes. However, the *far1* mutant showed normal rhythmicity in all light conditions. Given the requirement for both FHY3 and FAR1 dimer components for transcriptional activation of *ELF4* expression *via* the fbs, this suggested that the red-specific disruption of rhythmicity in *fhy3* likely reflects and additional role for FHY3, possibly related to its specific protein interactions. A microarray analysis comparing the circadian transcriptome in white light and red light revealed a series of coherent changes in the patterns of rhythmicity, which may explain the greater severity of the *fhy3* phenotype in red versus white light. Most notably, the proportion of the transcriptome showing rhythmicity was considerably reduced in red, while the amplitude of the expression of a number of clock genes was also reduced. Specifically, the morning-phased genes, *CCA1*, *RVE8*, and *PRR9*, and the evening phased genes, *LUX* and *ELF4*, damped low, while *PRR5* damped high. Simultaneously, the importance of the evening element and the G-box among rhythmic genes in red light was reduced. A general decrease in mean expression among rhythmic genes peaking during the night was also observed in red light, while genes showing reduced mean expression in red were also found to be strongly enriched in G-box elements. The importance of the G-box among genes showing differential expression patterns in white and red light, coupled with the known variation in HY5 levels in response to changes in the proportion of red and blue light, is consistent with a key role for HY5 in this transition between white and red light configurations. A similar investigation of the *fhy3* transcriptome revealed a loss of rhythmicity in the majority of output genes in red light. At the same time, almost all central clock genes showed a dramatic loss of amplitude, with *ELF3* and *LUX* becoming completely arrhythmic. In contrast, *PRR5*, uniquely, showed an increase in amplitude. Genes becoming arrhythmic in *fhy3* showed enrichment of the CCA1-targetted TBS site, TGGGCC, suggesting that CCA1 action is disrupted in *fhy3*. In contrast, the fbs element was only found to be enriched among genes showing a reduction in mean expression in *fhy3* and was not enriched among those losing rhythmicity, supporting the proposal that the red-specific arrhythmicity of *fhy3* is not simply related to the role of FHY3 as a transcription factor in directly activating clock genes. Rather, our findings point to the specific interaction of FHY3 but not FAR1 with CCA1 being a potential explanation for this phenotype. On that basis, we propose that FHY3 and HY5, respectively, may form a key mechanism for integration of red and blue light signals to the clock, with FHY3 acting in red and white light and HY5 in blue, possibly *via* their interaction as a complex with the CCA1 central clock protein.

MATERIALS AND METHODS

Plant Materials and Growth Conditions

The *fhy3*-4, *far1*-2, and *fhy3*-4 *far1*-2 mutants of *Arabidopsis thaliana* and their isogenic wild type in the No-0 ecotype have been described previously, as have the *fhy3*-4, *far1*-2, and *fhy3*-4 *far1*-2 mutant and isogenic wild type luciferase reporter lines containing *CAB2:LUC* and *CAT3:LUC*, *TOC1:LUC* and *ELF4:LUC*, also in the No-0 ecotype (Wang and Deng, 2002; Li et al., 2011). In all experiments, seeds were sterilised in 30% bleach, 0.02% Triton X-100, sown on Murashige and Skoog (MS) medium containing 2% sucrose, then stratified for 3 days in darkness at 4 C. Following stratification, seeds were germinated and grown in 12 h white light/12 h dark cycles for 7 days prior to treatment conditions. White light for this consisted of equally mixed red light (λ-max 660 nm, 60 μmol m^{-2} s^{-1}), blue light (λ-max 450 nm, 60 μmol m^{-2} s^{-1}) provided by LEDs within Fytoscope FS80-RGBIR Minicabinets (Photon Systems International, Brno, Czechia). All experiments were carried out at 21 C.

Light conditions during luciferase bioluminescence imaging experiments were provided within the imaging chamber by a custom-made LED rig providing red light (λ-max 660 nm, 40 μmol m^{-2} s^{-1}), blue light (λ-max 450 nm, 40 μmol m^{-2} s^{-1}) or white light consisting of equally mixed red and blue light (total 40 μmol m^{-2} s^{-1}).

For microarray analysis and for RT-qPCR analysis of *CCA1*, *LHY*, and *ELF4* rhythms, lighting conditions were provided by red light (λ-max 660 nm, 120 μmol m^{-2} s^{-1}) LEDs within Fytoscope FS80-RGBIR Minicabinets (Photon Systems International, Brno, Czechia).

All light measurements were made using a StellarNet EPP2000-HR spectroradiometer.

Luciferase Imaging

Luciferase imaging was carried out using a NightOwl ultra Cooled CCD (charge-coupled device) camera (Berthold Technologies, United Kingdom) as described by Siddiqui et al. (2016). Data were analysed by using Winlight image analysis software version 2.17 (Berthold Technologies, United Kingdom). Using this software, uniform, circular regions of interest were manually placed over the seedlings and quantification of bioluminescence counts from within these regions was automatically collected from the sequence of images taken and imported into a Microsoft Excel spreadsheet along with data for time of collection. Mean and standard error for bioluminescence for each seedling were then calculated. All data represent the findings of at least two independent experiments.

Microarray Analysis

RNA extraction was carried out as described previously (Wang et al., 2011). Samples for our microarray analysis in red light in wild type and the *fhy3* mutant were taken at 24, 32, 40, and 48 h after the transfer to red light. Approximately 100 seedlings were collected for each sample. Our microarray hybridisation was carried out by the Nottingham Arabidopsis

Stock Centre (Nottingham, United Kingdom) using Affymetrix ATH1 arrays. To enable the comparison of rhythmic gene expression in Arabidopsis in continuous white light, the publicly available Affymetrix ATH1 dataset, NCBI GSE8365 (Covington and Harmer, 2007) was selected. Following normalisation with our own microarray data, this was analysed for the identification of rhythmic gene expression alongside our microarray data using the methods developed here for this study. As in our assay, these seedlings in the NCBI GSE8365 dataset had been entrained in 12 h white light/12 h dark cycles for 7 days. These NCBI GSE8365 samples had been transferred to constant white light (120 μ mol m^{-2} s^{-1}) and, after 24 h in constant light, 12 samples were harvested at 4-h intervals over the next 44 h. All data from both microarray experiments was normalised as a single dataset using the D-chip programme (Li and Wong, 2001). Probes lacking a corresponding AGI code in the Arabidopsis genome TAIR10 version of the Affymetrix ATH1 probe assignment were excluded prior to subsequent analyses as were probes corresponding to mitochondrial genes and chloroplastic genes. In order to exclude non-expressed genes, those probes which had a mean expression for every genotype/treatment considered that was below 5% of the mean expression value of all probes across all arrays were discounted.

Rhythm Analysis

Rhythmicity was determined based on a combination of two criteria: correlation to a sine wave with a period of 24 h and a minimum change in expression from peak to trough. The correlation approach was based on that described by Devlin et al. (2003) for the analysis of co-expression patterns in microarray data. This was adapted for the analysis of rhythmic gene expression as follows. A Pearson correlation was performed to assess the degree of correlation to sine waves with period 24 h with mean and amplitude equal to 60 phased 1 h apart. The phase giving the highest r value for correlation was selected for each gene. A t-test for correlation (r) was then performed and genes showing a p-value of <0.01 were selected (H_0: $r = 0$). Selected genes were then tested to determine whether they exceeded a minimum change in expression level from peak to trough. Genes showing either a predicted 1.5-fold change in expression from peak to trough or an absolute change in expression between minimum and maximum sample points of 250 times mean expression value of all probes across all arrays were selected. The predicted fold change in expression from peak to trough was calculated based on a comparison of the fold change between the nearest sample points to the calculated peak and trough and the predicted values at those same points for a sine wave with the same phase, the same mean expression level and a peak to trough variation of 1.5-fold. All calculations involved in selection were performed in Microsoft Excel and automated using visual basic.

Cis Element Analysis

Cis element analysis was carried out using the MEME and DREME modules of the MEME Suite software package (version 4.12.0) (Bailey and Elkan, 1994; Bailey, 2011). The region 500 base pairs upstream of the transcription start site was used for analysis and MEME suite was run using the Cygwin interface https://www.cygwin.com on the Microsoft Windows operating system.

Z-scores for overrepresentation of specific phases among rhythmic genes containing recognised *cis* elements were calculated based on a rolling window of four phases. A bootstrapping approach was used to generate the background population for each phase window. A total of 100 random groups of rhythmic genes containing the same number of genes as were found within that phase window were selected from among all of the rhythmic genes in that same dataset. The number of occurrences of the element in question within the genes in the phase window was compared to the average from within the 100 random groups. All z-score calculations were performed in Microsoft Excel and automated using visual basic.

Gene Ontology Analysis

Ontological analysis was performed using the PAGEMAN module of the MAPMAN software suite (Usadel et al., 2006), applying the defaults parameters. For data entry, genes within a selected group were given a score of 1 in place of the expected value for log2(expression change). Z-scores for over- or under-represented biological processes were then represented using the conditional formatting function in Microsoft Excel.

RNA Extraction and qRT-PCR

RNA extraction and qRT-PCR were carried both out exactly as described previously (Wang et al., 2011). All gene expression values are expressed relative to an Arabidopsis *ACTIN2* housekeeping control. All data represent the findings of at least two independent experiments. The following primers were used for qRT-PCR: *CCA1*, TCGAAAGACGGGAAGTGGAA CG and GTCGATCTTCATTGGCCATCTCAG; *LHY*, AGTC TCCGAAGAGGGTCGTATAGC and TCACATTCTCTGCCAC TTGAGGAG; *ACTIN2*, TCCCTCAGCACATTCCAGCAGAT and AACGATTCCTGGACCTGCCTCATC.

RESULTS

fhy3 but Not *far1* Shows Specific Arrhythmicity in Constant Red Light for Multiple Non-direct Target Genes

To examine the impact of both FHY3 and FAR1, individually and in conjunction, on the function of the circadian clock in various light conditions, we used luciferase reporter constructs to examine the circadian expression patterns of two clock output genes and one central clock gene in the *fhy3*, *far1*, and *fhy3 far1* double mutants in constant red, white and blue light. Seedlings were entrained to light dark cycles before release into constant light. The evening-phased central clock gene, *TOC1*, showed robust rhythmicity in wild type seedlings in red, white, and blue light. Similarly, *TOC1* expression was robustly rhythmic in all conditions in *far1* mutant seedlings. In contrast, although *fhy3* single mutant and *fhy3 far1* double mutant seedlings showed

robust *TOC1* rhythmicity in constant blue light, both lines displayed a severe disruption of *TOC1* rhythmicity after two cycles of oscillation following release into constant white or red light (**Figure 1**). The evening-phased output gene, *CAT3*, and the morning-phased output gene, *CAB2*, behaved very similarly to *TOC1* in that circadian rhythmicity was dramatically disrupted in red or white light in the *fhy3* and *fhy3 far1* mutants but not in *far1* mutants (**Figure 1**). *CAT3* expression in *fhy3* and *fhy3 far1* was disrupted after only a single cycle in red or white light, ultimately resulting in an apparent arrhythmic phenotype in these mutant lines. None of *TOC1*, *CAT3*, and *CAB2* contain the fbs promoter element, meaning that these are not direct target genes for FHY3 and FAR1. These observations demonstrate that the disruption of rhythmicity of these non-target genes is specific to the absence of FHY3 only, and is not affected by absence of FAR1. Furthermore, the patterns of rhythmicity of these three genes confirm that the phenotype only occurs in the presence of red light in each case. These patterns reinforce the proposal that the previously observed red-light specific role for FHY3 in the circadian clock is distinct from its function as a positive acting transcription factor as part of a dimer with FAR1, where loss of either component has been shown to result in reduced function.

Global Circadian Gene Expression Patterns Differ in Red Light

In order to further examine the nature of the red-light specific circadian defect in *fhy3* mutants, we carried out a microarray analysis of gene expression over a 24 h period in constant red light in wild type and *fhy3* mutant seedlings. Seedlings were entrained in 12 h/12 h white light/dark cycles for seven days before transfer to constant red light and tissue collection. RNA extraction was carried out at 24, 32, 40 and 48 h after transfer. Our data for *CAB:LUC* oscillation in red and white light (**Figure 1**) corroborated our previous observation that the loss of rhythmicity was more extreme in red light than in white light (Allen et al., 2006). Consequently, we also took the opportunity to compare the wild type transcriptome in red light to that previously published for seedlings in white light in otherwise identical conditions of entrainment and light intensity. Our aim here was to look for potential differences which could underlie

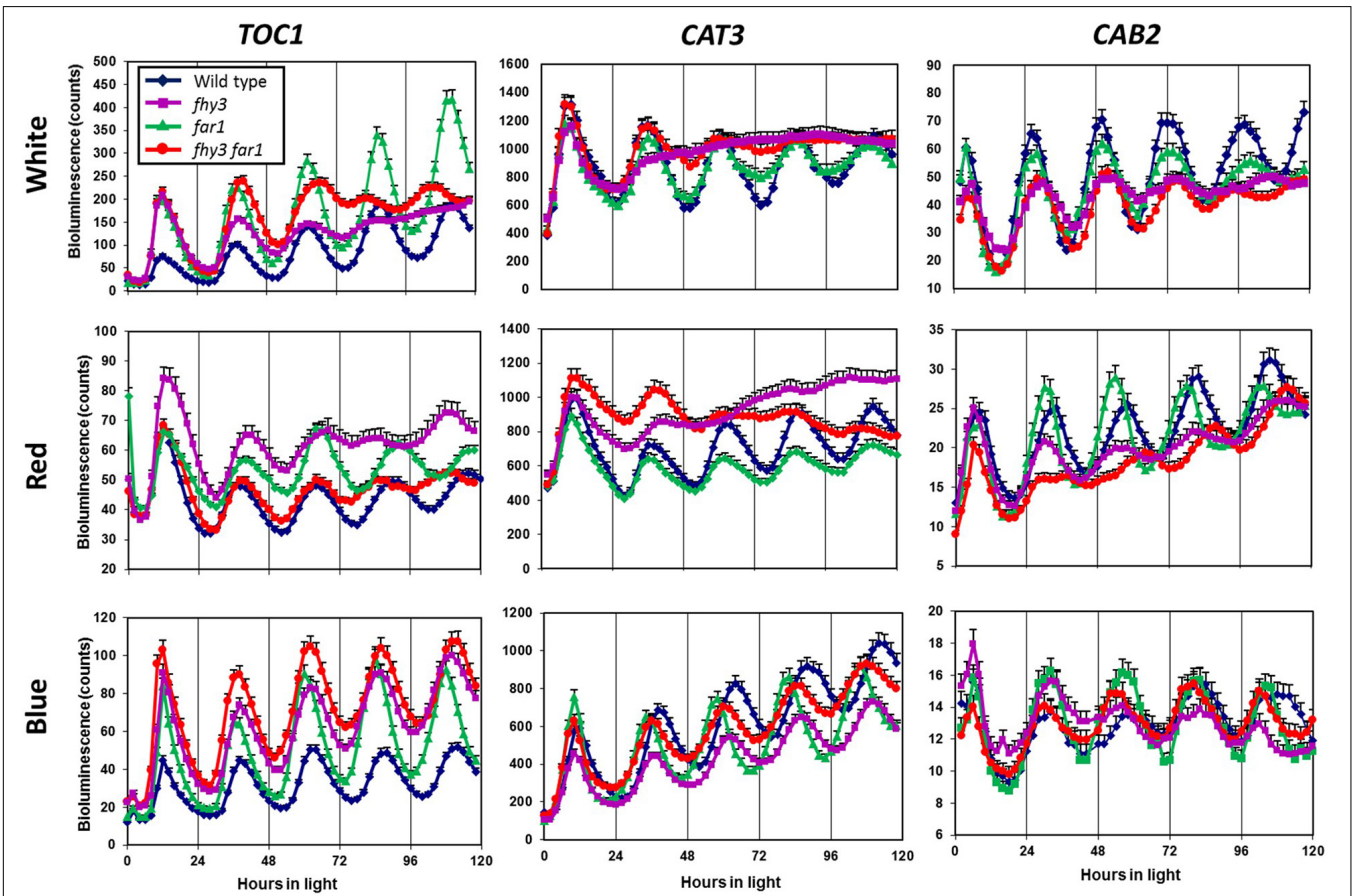

FIGURE 1 | Loss of FHY3 but not FAR1 results in arrhythmic expression of non-target genes in the presence of red light. Wild type, *fhy3*, *far1*, and *fhy3 far1* mutant seedlings containing either the *TOC1:LUC*, *CAT3:LUC*, or *CAB2:LUC* transgenes were germinated and entrained in 12 h white light: 12 h dark cycles for 1 week before transfer to either constant white (red + blue), red or blue light. Luciferase bioluminescence was then recorded every 2 h. Data represent the means of at least 11 seedlings ±SE.

the impact of light wavelength on the *fhy3* phenotype. For this, we examined the publicly available white light microarray dataset of Covington and Harmer (2007). After normalisation of both white light and all red light data as a single dataset and removal of data for ambiguous probes, non-nuclear genes and non-expressed genes, analysis of circadian gene expression patterns was performed using a method modified from Devlin et al. (2003). For this, the Pearson correlation coefficient was calculated for each gene to a series of sine waves of period 24 phased 1 h apart across one whole circadian cycle. The sine wave giving maximum correlation coefficient (r) for each gene was recorded. To ensure high stringency in light of the low sampling resolution for the red light data, only those genes for which the maximum correlation gave a p-value of less than 0.01 using a t-test for correlation coefficient (H_0: $r = 0$) and met minimum extrapolated peak-to-trough expression change criteria (1.5-fold change or an absolute change of 250 times the mean expression of all genes on the array across all timepoints) were accepted as circadian. The phase of the sine wave giving the maximum correlation was then recorded as being the phase of expression for that gene. Applying these criteria to the white light data revealed 2,438 genes displaying a circadian rhythm (**Supplementary Table 1**). This represents 13% of expressed genes which agrees with previous analyses which range between 6 and 31% (Harmer et al., 2000; Edwards et al., 2006; Michael et al., 2008).

Applying these criteria to our red light data revealed 5,915 genes displaying a circadian rhythm (31% of expressed genes, **Supplementary Table 2**). Analysis of the reasons for failure of genes to meet our selection criteria in either white or red light conditions indicate that lower numbers of genes in the white light data meet each of the two criteria (correlation and fold-change). A total of 79% of expressed genes in the white light dataset do not meet the expression change criteria compared to 60% of expressed genes in the red light dataset, consistent with the white light dataset collected by Covington and Harmer (2007) having a lower median dynamic range (median min–max range white = 1.26, red = 1.42; **Supplementary Figure 1**). At the same time, 69% of expressed genes in the white light dataset do not meet the correlation criterion, compared to 36% of expressed genes in the red light dataset. Despite the consistent 0.01 p-value cut-off used in both cases, it is probable that there would still be a reduced likelihood of a correlation for genes within the white light dataset given the fact that it covers two cycles rather than just one. Genes must, therefore, show good correlation with a sine wave over both cycles in the white light data to achieve the cut-off. The variable nature of the data means that there is likely to be a difference in the correlation of each cycle of actual data with a consistent sine wave applied across both cycles and the final correlation would represent a best fit "compromise" between the two cycles, reducing the r value that could be achieved by fitting a sine wave to a single cycle. We can, however, have a greater confidence in genes correlating in the white light data as a result. Given the latter, we considered the white light rhythmic transcriptome as our baseline for comparison between white and red light and looked at the way in which genes identified as rhythmic in white light changed their behaviour in red light. Primarily, it is notable that only 46% of the genes (1,129) identified as rhythmic in white light were also identified as rhythmic in red light suggesting considerable loss of rhythmicity in red light (**Supplementary Table 3**). However, a comparison of the phases of expression of genes that were identified as rhythmic in both conditions revealed that these genes showed a similar phase in both conditions; though, the vast majority were shifted slightly later by 2–3 h in red light (**Figure 2A**). Consistent with this, in both conditions, the most frequent times of peak expression for all rhythmic genes was also similar, with high numbers of rhythmic genes peaking during the afternoon or late night. Again, though, these maxima were on average 2–3 h later in red light than in white light (**Figure 2B**), suggesting that the absence of blue light results in a delay in phase; though, this could equally be caused by a lengthening of period, given the single cycle of data available for red light.

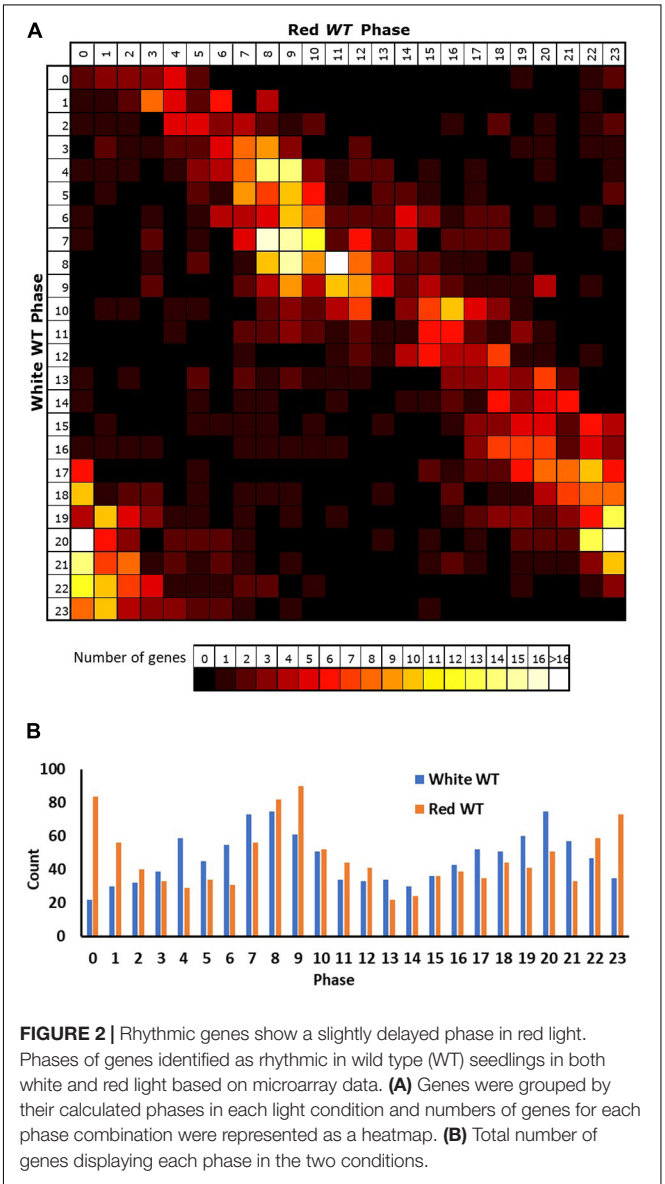

FIGURE 2 | Rhythmic genes show a slightly delayed phase in red light. Phases of genes identified as rhythmic in wild type (WT) seedlings in both white and red light based on microarray data. **(A)** Genes were grouped by their calculated phases in each light condition and numbers of genes for each phase combination were represented as a heatmap. **(B)** Total number of genes displaying each phase in the two conditions.

Given the loss of rhythmicity in red light observed for 54% of rhythmic genes in white light, we then investigated the reasons for failure to meet our criteria for rhythmicity among these genes. The most common reason behind loss of rhythmicity in red light was revealed to be a failure to meet our expression change criteria (67% of genes), suggesting that the absence of blue light resulted in a loss of amplitude. An analysis of the change in mean expression in red versus white light revealed that the majority of rhythmic genes in white light also showed a reduction in mean expression in the absence of blue despite the consistent light intensity in both conditions (**Figure 3**). Interestingly, the majority of these genes showing reduced expression in red were genes peaking during the subjective night (**Figure 3**), suggesting an important positive role for blue light at this time. The smaller group of genes showing an increase in mean expression in red showed a preference for genes peaking during the subjective day, the 180° phase difference, suggesting these may, indeed, include genes that are normally negatively regulated by those night time genes which now show lower expression in red.

We also observed differences in the enrichment of gene ontology terms that were associated with various biological processes among rhythmic genes in white versus red light. Rhythmic process terms enriched in white light included photosynthesis, major carbohydrate metabolism, amino acid synthesis, various aspects of secondary metabolism, as well as stress and redox signalling (**Supplementary Figure 2**). Photosynthesis and major carbohydrate degradation continued to be enriched among genes that were rhythmic in red light as did stress responses. However, minor carbohydrate metabolism (raffinose/trehalose), amino acid synthesis, and many secondary metabolic processes were no longer enriched. Instead, these processes were enriched among genes which became arrhythmic in red light (**Supplementary Figure 2**).

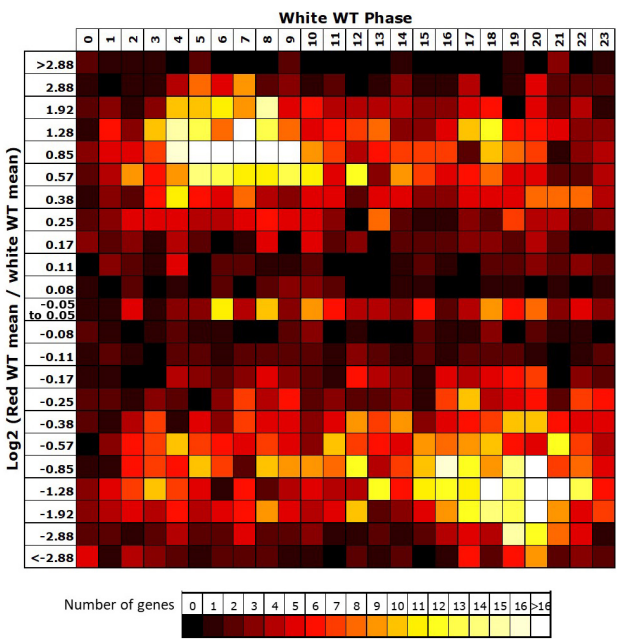

FIGURE 3 | Night-phased genes in white light show a loss of mean expression in red. For all genes identified as rhythmic in wild type (WT) in white light, the change in mean expression in red light was plotted against calculated phase in white light. Bins for log2 change in mean expression also follow a log2 progression. Each expression change bin covers the range up to the value indicated, starting from the value of the preceding bin.

Central Circadian Clock Gene Expression Patterns Differ Between White and Red Light

We then compared the expression patterns of the central clock genes in white light and red light-grown seedlings. The raw data and fitted sine waves are shown in **Figure 4**. All clock genes analysed continued to be rhythmic in red light and, consistent with global patterns of gene expression, most of the clock genes showed a slightly delayed phase in red (**Figure 4** and **Supplementary Table 4**). However, more noticeable differences were observed in amplitude of expression of specific central clock genes in red. Amplitude was reduced in the morning-phased genes, *CCA1* and *RVE8*; in the daytime-phased genes, *PRR9*, *PRR5*, and *CHE*; and in the evening-phased genes, *LUX* and *ELF4* (**Figure 4** and **Supplementary Table 4**). *ELF4*, particularly, showed a dramatic decrease in amplitude and mean expression. This very low *ELF4* expression in red was confirmed by analysis of bioluminescence in seedlings containing an *ELF4:LUC* transgene (**Supplementary Figure 3**). It is also notable that, while the amplitude reduction seen in *CCA1*, *PRR9*, *LUX*, and *ELF4* was a result of decreased peak expression, the reduced amplitude observed in *PRR5* was distinct in being the result of an increased trough value. The pattern of *ELF3* expression was also remarkable in showing a dramatic increase in mean expression level without showing any change in amplitude. In this comparison, both assays were carried out in the same light intensity suggesting that these changes in central clock gene expression are result of the specific absence in blue wavelengths and that this non-redundant nature of red and blue light input pathways to the clock may be the result of differential regulation of distinct groups target genes within the clock by the two pathways.

Promoter Element Enrichment Differs Between the White and Red Light Circadiome

Promoter element enrichment analysis using DREME and MEME (Bailey and Elkan, 1994; Bailey, 2011) for the white light circadiome revealed several previously characterised circadian clock-associated *cis* elements within the region 500 bp upstream of the transcription start sites of rhythmic genes: the evening element (AAAATATC), bound by CCA1 and LHY (Harmer et al., 2000); two TCP binding sites (TBS): the core GGTCC (or GGACC) which is bound by CHE (Pruneda-Paz et al., 2009) and the GGCCCA (or TGGGCC) site, bound by CCA1 (Kamioka et al., 2016); and a G-box variant (CACGTG), associated with binding of HY5, PIFs and PILs (Toledo-Ortiz et al., 2003; **Figure 5A**).

Both TBS elements and the G-box showed significant enrichment, more specifically, in the region 50–100 bp upstream

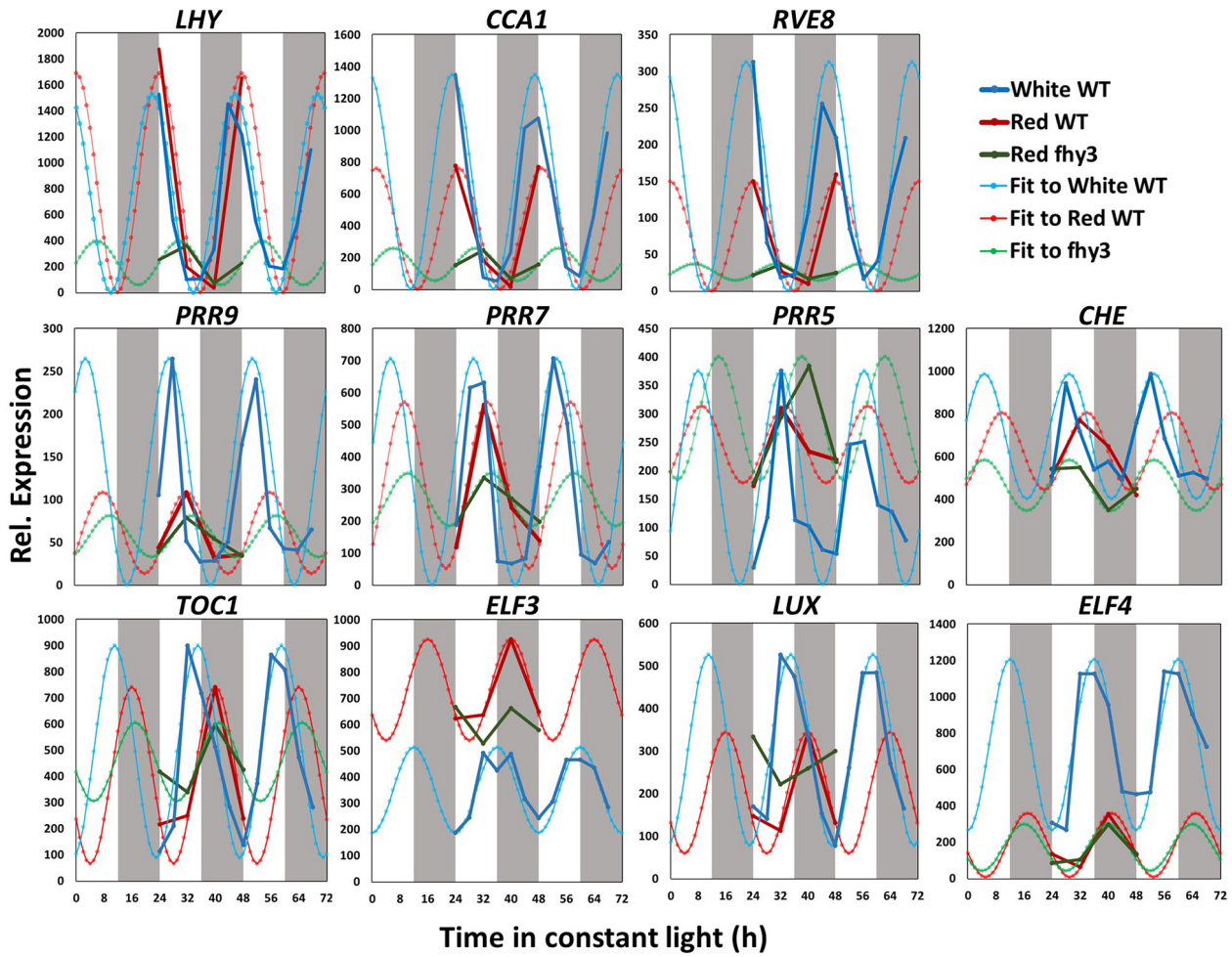

FIGURE 4 | Changes in central clock gene expression in white light, red light and in the *fhy3* mutant. Mean microarray data values and mathematically fitted waveforms are shown for central clock genes in wild type (WT) seedlings in constant white and in wild type and *fhy3* seedlings in constant red light. Grey bars represent subjective day and night.

of the transcription start sites of rhythmic genes (**Supplementary Figure 4**). Analysis of the phase of genes containing each of these elements revealed that the genes possessing the evening element were significantly more likely to display a phase of peak expression in a window centred on phase 8 (afternoon), while genes containing a G-box were significantly enriched in a window centred around dawn (**Figure 5B**), consistent with previous observations (Michael et al., 2008). Those containing the TBS element, TGGGCC, were significantly enriched in a window centred on phase 14 (early night) (**Figure 5B**).

Promoter element enrichment analysis for the red light circadiome revealed only a partially overlapping set of enriched elements. The TBS element, TGGGCC, was again found; though, genes containing it showed a later peak of phase enrichment than was observed in white light, at around phase 19 (**Figures 5A,C**), consistent with the slightly later phase of expression of rhythmic genes in red. Curiously, neither the evening element nor the G-box were enriched in the red circadiome. Instead, two additional GA motifs were observed (GAGAGAGAGA and RRAGAAGAAG) (**Figure 5A**). Both are very similar to elements that are bound by CCA1 (Kamioka et al., 2016). Genes containing the GA element were also shown to be upregulated as a result of TOC1 over expression (Gendron et al., 2012). Genes possessing the GA motif were significantly more likely to display a phase of peak expression in a window centred on phase 8 (**Figure 5C**). Intriguingly, the disappearance of G-box enrichment in the red circadiome is accompanied by the observation that those genes which were rhythmic in white light and which showed a decrease in mean expression in red light (>1.5-fold decrease) did show an enrichment of the G-box (**Figure 5A**). The G-box is a target of HY5 which has been shown to bind to the promoters of a number of clock genes, with binding enhanced by blue light. It specifically regulates *PRR5*, *LUX*, and *ELF4* and has been predicted to regulate *CCA1* (Li et al., 2011; Hajdu et al., 2018), all of which show reduced amplitude in red. Finally, those genes showing an increase in mean expression in red light (>1.5-fold increase) showed a specific enrichment for presence of a morning element-related *cis* motif (**Figure 5A**), the morning element,

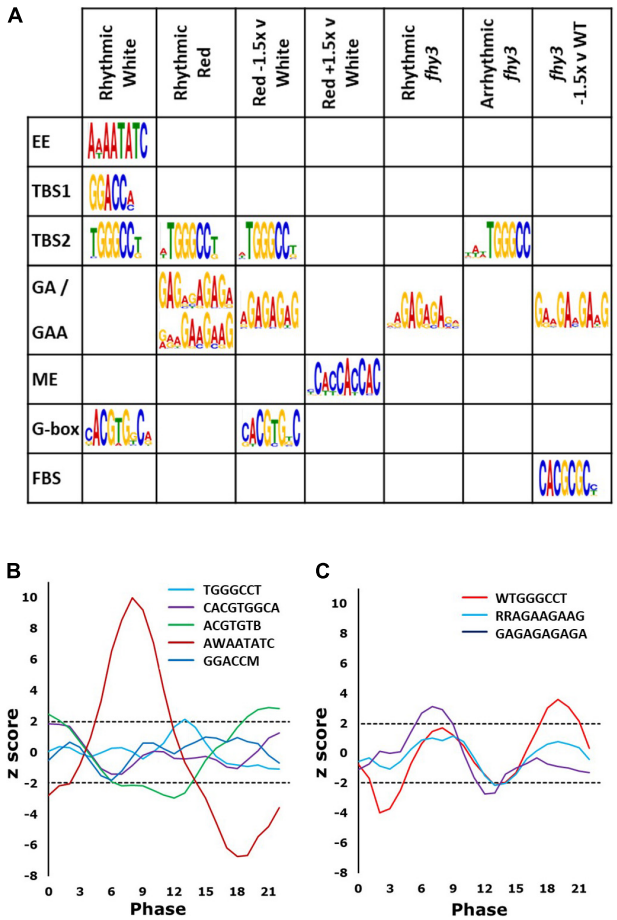

FIGURE 5 | Promoter elements enriched in rhythmic genes. **(A)** Recognised elements enriched in genes in the categories indicated. Rhythmic White (rhythmic in wild type in white light); Rhythmic Red (rhythmic in wild type in red light); Red −1.5x v White (rhythmic genes in white light showing mean expression in red light ≤1.5-fold that in white light); Red +1.5 v White (rhythmic genes in white light showing mean expression in red light ≥1.5-fold that in white light); Rhythmic *fhy3* (genes which maintain rhythmicity in *fhy3* in red light); Arrhythmic *fhy3* (genes which lose rhythmicity in *fhy3* in red light); *fhy3* −1.5 v WT (genes with mean expression in *fhy3* in red light ≤1.5-fold that in wild type in red light). **(B)** Phase enrichment among Rhythmic White genes containing the elements indicated. Note two variants of the G-box are shown. **(C)** Phase enrichment among the Rhythmic Red genes containing elements indicated. Phase enrichment is represented by *z*-score and plotted as a three-point moving average. Dotted lines indicate *z*-scores corresponding to $p = 0.05$. *Z*-scores greater than 1.96 or less than −1.96 indicate significant enrichment for a given phase.

enriched in the promoters of morning-phased genes (Harmer and Kay, 2005) which is consistent with the observation that the majority of genes showing upregulation in white versus red showed a morning phased expression (**Figure 3**).

In all, this suggests that the changes in patterns of circadian expression in the absence of blue light may be related to the role of HY5 in integrating the relative quantities of red and blue light. It is also notable that the evening element, which was specifically enriched in genes rhythmic in white light in many studies (Harmer et al., 2000; Michael et al., 2008), was not enriched among genes showing rhythmicity in red light. Along with the analysis of clock gene expression, this further indicates the difference in the relative importance of the central clock proteins responsible for rhythmicity, itself, for plants growing in the absence of blue light. This is, furthermore, consistent with our proposal that the relative importance of FHY3 may be greatly enhanced as a result of the loss of some redundancy in the clock system under the specific conditions created by the relative reduction in blue versus red light input.

The *fhy3* Mutation Causes Dramatic Changes in the Circadian Transcriptome in Red Light

Comparison of the circadiome of the wild type and *fhy3* mutant in red light revealed a dramatic reduction in the number of genes which remained rhythmic in *fhy3* (2,258 of the 5,915 rhythmic genes identified in wild type; **Supplementary Table 5**). Thus, although the majority of genes that were rhythmic in wild type lost rhythmicity, *fhy3* was not completely arrhythmic. Comparative analysis of the phases of peak expression of genes that remained rhythmic revealed an unexpected profile. Rather than a consistent phase relationship between wild type and *fhy3*, rhythmic genes in *fhy3* appear concentrated in one of two windows of peak phase, centred on phases 4 and 16 (4 h after subjective dawn and 16 h after subjective dawn), with the majority of genes that were phased at other times in wild type, shifting to one of these two phase windows in *fhy3* (**Figure 6**). Genes peaking around subjective dawn or phase 0 in wild type shifted slightly later to phase 4, genes peaking around late night in wild type shifting to phase 16 and genes peaking during the afternoon in wild type shifting to either phase 4 or phase 16 in approximately equal proportions (**Supplementary Figure 5**).

The vast majority (3,465 of 3,657) of the genes which lost rhythmicity in *fhy3* failed our rhythmic selection criteria on the basis of fold change in expression, suggesting severe loss of amplitude among the majority of cycling genes was the primary cause of arrhythmicity. We also analysed the change in mean expression in *fhy3* in all genes that were rhythmic in wild type in red light. Curiously, though, we observed that approximately equal proportions of genes showed increased and decreased mean expression in *fhy3*, suggesting that this loss of rhythmicity in *fhy3* was not simply a general loss of positive regulation of gene expression due to the loss of a light signalling component. Furthermore, there was a marked association between phase of expression in wild type and the occurrence of either an increase or decrease in mean expression in *fhy3*. The majority of those genes which showed a decrease in mean expression in *fhy3* showed a daytime phase in wild type, whilst the majority of those genes which showed an increase in mean expression in *fhy3* showed a night time or dawn phase in wild type (**Figure 7**).

In terms of biological processes among genes that became arrhythmic in *fhy3* versus those that maintained rhythmicity, an ontology enrichment analysis suggested that photosynthetic processes, minor carbohydrate metabolism (raffinose/trehalose), and brassinosteroid metabolism became arrhythmic in *fhy3*. Cell wall proteins, gibberellic acid metabolism and stress

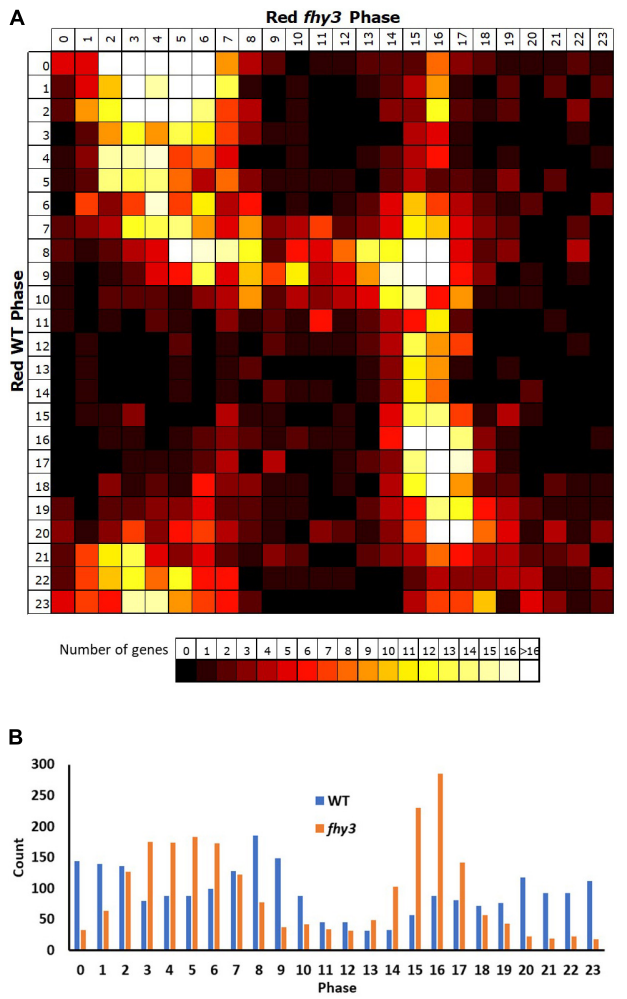

FIGURE 6 | Rhythmic genes show a concentration in morning and early night phases in *fhy3* in red light. Phases of genes identified as rhythmic in both wild type and *fhy3* in red light based on microarray data. **(A)** Genes were grouped by their calculated phases in each genotype and numbers of genes for each phase combination were represented as a heatmap. **(B)** Total number of genes displaying each phase in the two genotypes.

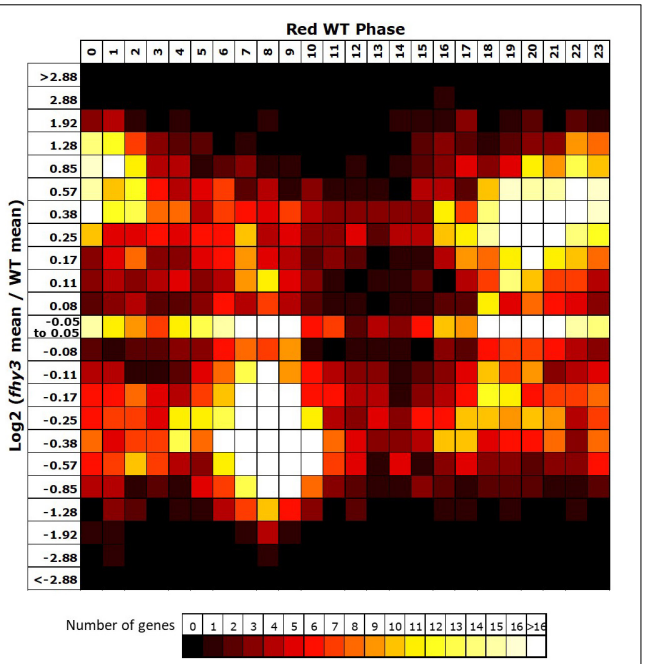

FIGURE 7 | Afternoon-phased genes in wild type show a loss of mean expression in *fhy3* in red light. For all genes identified as rhythmic in wild type in red light, the change in mean expression in *fhy3* was plotted against calculated phase in wild type. Bins for log2 change in mean expression also follow a log2 progression. Each expression change bin covers the range up to the value indicated, starting from the value of the preceding bin.

responses maintained rhythmicity in wild type and *fhy3*, while major carbohydrate degradation, secondary metabolism, and auxin and abscisic acid metabolism, although not significantly enriched among all genes showing rhythmicity in red light (irrespective of white light), did also show rhythmicity in *fhy3* (**Supplementary Figure 6**).

Analysis of Central Clock Gene Expression Indicates Fundamental Circadian Defects in *fhy3*

Analysis of the expression patterns of the central clock genes in *fhy3* in red light revealed the majority remained rhythmic by our definition; though, many showed a dramatic reduction in amplitude (**Figure 4** and **Supplementary Table 6**). The evening genes, *ELF3* and *LUX*, however, experienced such a comprehensive loss of amplitude as to be classed as arrhythmic in *fhy3*. The dawn-phased clock genes, *CCA1*, *LHY*, and *RVE8*, all showed a dramatic loss of peak expression. *PRR9* and *PRR7*, showed both a loss of peak and gain of trough expression levels, damping to an intermediate mean expression level versus wild type levels in red. *PRR5* showed an increase in amplitude, courtesy of higher peak expression levels, whilst *CHE* showed a dramatic loss of peak expression similar to the morning-phased genes. Of the evening phased genes, *TOC1* damped high in *fhy3*, showing higher trough levels, consistent with our analysis of the effect of *fhy3* in red light in *TOC1:LUC* seedlings (**Figure 1**). In becoming arrhythmic, *LUX* also damped high in *fhy3*, whilst *ELF3* damped low. Curiously, *ELF4*, a direct target of FHY3 in its role as a transcription factor, showed little change in expression in *fhy3*. *ELF4*, however, was already damped to extremely low levels in the red light conditions used in this assay (**Figure 4**, **Supplementary Figure 2**, and **Supplementary Table 6**). This lack of impact on *ELF4* expression in red light, though, further supports the proposal that the red-specific loss of rhythmicity in *fhy3* is indicative of a mode of action of FHY3 that is distinct from its role as a transcription factor targeting *ELF4*. qPCR analysis in the same lines used for microarray analysis under identical conditions further confirmed the expression patterns of *CCA1* and *LHY* in wild type and *fhy3* seedlings in constant red light (**Figure 8**). Our qPCR analysis also included the *far1* mutant. In both cases the *far1* mutant showed only a slight reduction in amplitude in contrast to *fhy3*. It is also clear that

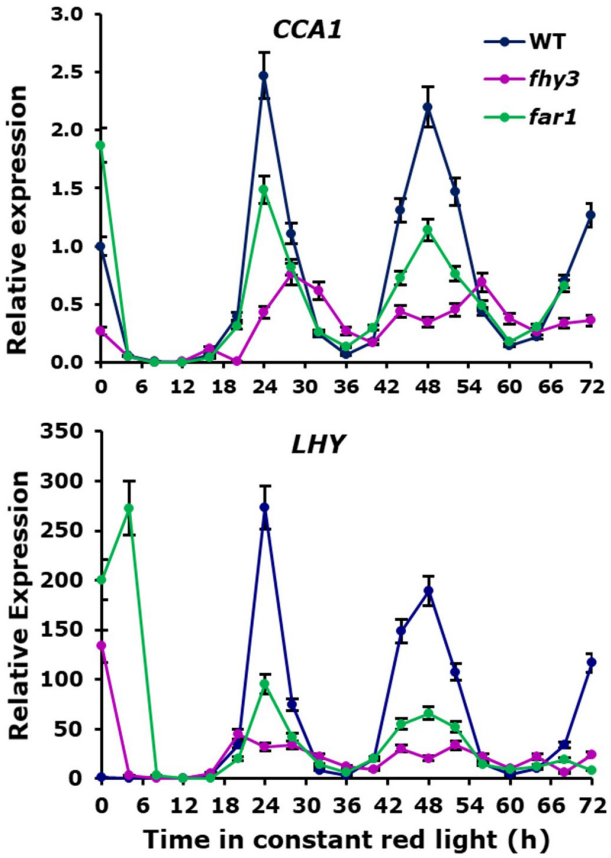

FIGURE 8 | Confirmation of expression patterns of selected central clock genes in constant red light. Wild type, *fhy3* and *far1* mutant seedlings were germinated and entrained in 12 h white light: 12 h dark cycles for 1 week before transfer to constant red light. Expression of *CCA1* and *LHY* was calculated relative to Actin. Data represent the means of three biological replicates ±SE.

the rhythmicity in the *far1* mutant is much more robust than that in *fhy3*. The loss of amplitude is consistent with FAR1 playing a role in the functioning of the FHY3-FAR1 dimer as a positive regulator of *CCA1* gene expression (Li et al., 2011) but the much more dramatic effects of the *fhy3* mutation are, again, consistent with an additional role of FHY3 in maintaining rhythmicity in these conditions.

Analysis of enriched *cis* elements associated with genes showing specific arrhythmicity in *fhy3* revealed only one recognised element, the TBS element, TGGGCC. In contrast, the other two elements that were associated with rhythmicity in red light in wild type seedlings, both variants of the GA motif, were the sole elements enriched in genes which maintained rhythmicity in *fhy3* (**Figure 5** and **Supplementary Figure 3**). The absence of any enrichment of the fbs is also significant in that regard, further supporting the distinction from the mode of action of FHY3 as a transcription factor regulating gene expression *via* the fbs. Appropriately, an analysis of the *cis* elements enriched in genes that are rhythmic in wild type but which show a change in mean expression in *fhy3* revealed the enrichment of the fbs in genes showing at least 1.5-fold decrease in mean expression in *fhy3* (**Figure 5** and **Supplementary Figure 3**). The TGGGCC motif is a CCA1 target (Kamioka et al., 2016). Together with the fact that CCA1 is a specific interactor with FHY3 but not FAR1 (Li et al., 2011), this supports our proposal that the red-specific defect in rhythmicity in *fhy3* may be a result of disrupted CCA1 transcriptional regulation activity. Indeed, we previously showed that FHY3 interaction normally represses the transcriptional activity of CCA1 (Li et al., 2011). Disrupted CCA1 action is also consistent with complete loss of rhythmicity in *fhy3* of two key CCA1 targets, *ELF3* and *LUX* (**Figure 4**).

DISCUSSION

FHY3 Plays an Additional Role in Maintenance of Circadian Rhythmicity, Independent of FAR1

We previously demonstrated that the *fhy3* mutant showed a red light-specific arrhythmicity for several circadian clock-regulated processes. Growth in red or white light results in disrupted rhythmicity for leaf movement and for *CAB2* gene expression (Allen et al., 2006). Subsequent discoveries revealed FHY3 to be a transcription factor which dimerises with its close homologue, FAR1, to activate expression of genes possessing an fbs promoter element, including the *ELF4* central clock gene (Li et al., 2011; Liu et al., 2020). Loss of either FHY3 or FAR1 was shown to result in arrhythmic expression of *ELF4* in constant white light due to an extreme loss of *ELF4* expression (Li et al., 2011). However, the same study demonstrated that the wider loss of rhythmicity in white light, which was originally observed in the *fhy3* mutant (Allen et al., 2006), was only seen in the absence of FHY3 and not in the absence of FAR1 (Li et al., 2011). Here, we have expanded upon this by examining the *fhy3* and *far1* single mutants and the *fhy3 far1* double mutant in red, white and blue light. Both the *fhy3* mutant and the *fhy3 far1* double mutant displayed severely disrupted rhythmicity for expression of *CAT3*, *TOC1*, and *CAB2* expression in red and in white light but showed normal rhythmicity in blue. Conversely, *far1* mutants showed normal rhythmicity in red, blue, and white light, confirming that the role for FHY3 in maintaining rhythmicity in red or white light does not involve FAR1 and likely represents an additional mode of action for FHY3 beyond its role in the FHY3-FAR1 transactivating dimer. In this study we have gathered evidence from microarray analysis supporting a possible explanation for this phenomenon. One key distinction between FHY3 and FAR1 in their involvement in the circadian clock is their differential interaction with the central clock protein, CCA1 (Li et al., 2011). Only FHY3 but not FAR1 interacts with CCA1, and this interaction reduces the transcriptional repressive action of CCA1 (Li et al., 2011). We, therefore, speculated that the additional role for FHY3 in maintenance of circadian rhythmicity in red or white light may relate to this CCA1 interaction. In addition, a recent observation that HY5 acts as an integrator information on the ratio of red and blue light in the regulation of the clock

offered a possible explanation for the occurrence of arrhythmicity in red and in white light but not in blue. HY5 protein is more stable in blue than in red and HY5 binds more strongly to the promoters of a number of central clock genes in blue than in red. Furthermore, *hy5* shows a mutant phenotype intermediate between that in red and blue light (Hajdu et al., 2018) and, thus HY5 action in wild type plants would create a potentially quite different circadian backdrop in these conditions against which FHY3 would be acting. HY5 is another interactor with CCA1 and, indeed, HY5 is another protein which interacts with FHY3 but not FAR1 (Li et al., 2011) suggesting all three may form a complex. Coupled with our earlier finding that FHY3 protein is stabilised in red light (Siddiqui et al., 2016), we, therefore, speculated that, perhaps FHY3 and HY5 together mediate a wavelength-specific regulatory effect on the clock which covers both red and blue input. Such an interaction would likely show a conditional redundancy whereby, in conditions with a high ratio of red to blue wavelengths (red or white light), FHY3 protein would be stable but HY5 protein would be destabilised. Conversely, in blue light, HY5 would be the dominant player. Thus, the impact of the loss of FHY3 would only be observed in red or white light. Consistent with this, our observations show that loss of FHY3 impacts clock gene expression much more in red and white light while Hajdu et al. (2018) have shown that the loss of HY5 much more strongly impacts on clock gene expression in blue light.

Global Circadian Gene Expression Patterns Differ in Red Light

As an initial step in seeking support for these proposals, we sought to examine the impact of loss of FHY3 in red light on the wider transcriptome in the hope of better understanding this distinct FHY3 action. This analysis also afforded the opportunity to compare white light and red light circadian transcriptomes for the first time. We chose a correlation-based curve fitting approach for this as it forms a very convenient method to overall global comparisons of the whole circadian transcriptome, while still assigning circadian rhythmicity and phase to individual genes with statistical certainty. Such an approach also lends itself to analysis of low-resolution, short time course data. Our data indicated that approximately half of the genes that were observed to show circadian oscillation in constant white light showed a loss of rhythmicity in constant red light. In most cases this loss of rhythmicity resulted from a decrease in amplitude in red light. Genes which maintained rhythmicity in red light also preserved the same phase relationships as in white light; though, they showed a slightly later phase across the board. Our data also indicate a loss of mean expression level in red versus white light in many genes which peak during the subjective night. This implies that blue light may be particularly important at this time of day, possibly suggesting that it may be especially important in responding to light beyond the time of expected dusk or prior to the time of expected dawn as days lengthen toward summer. Central clock genes all maintained rhythmicity in red light; however, while many clock genes showed dramatic differences in amplitude in red versus white light, others maintained amplitude or even showed increased amplitude. Amplitude was reduced in *CCA1*, *RVE8*, *PRR9*, *CHE*, *LUX*, and *ELF4* as a result of loss of peak expression level. *ELF4*, particularly, showed a dramatic decrease in both amplitude and mean expression. These configurations point to a specific circadian role for blue light in determining the final patterns of expression of the central clock components observed in white light. The overall effect of the patterns of expression of the central clock components, however, does not appear to be related to simple loss of a positive effect of blue light input as light-induced genes, *LHY* and *TOC1* (Martinez-Garcia et al., 2000; Hsu et al., 2013) are among those that showed no loss of amplitude. A loss of amplitude in the light-responsive *PRR5* also belies this explanation as this is the result of an increase in trough levels, while the light-responsive *ELF3* shows no change in amplitude but dramatically increased mean expression.

Of the daytime and evening-phased clock genes, the triplet of *PRR5*, *LUX*, and *ELF4*, which showed a reduction in amplitude, have all been shown to be regulated by HY5 *via* differential binding of HY5 to the G-box in red versus blue light (Hajdu et al., 2018). The loss of the G-box among elements enriched among rhythmic genes in red light also points to HY5 potentially being a key factor behind the change in expression patterns among central clock genes in red versus white light. Furthermore, the simultaneous enrichment of the G-box among genes showing a decrease in mean expression level in red light also supports this proposal. This is consistent with the observation that HY5 input to the clock is known to change with the ratio of red to blue light. HY5 is stabilised and provides a strong input to the clock in blue, less so in white and less so still in red (Hajdu et al., 2018). On top of this, genes showing the greatest loss of mean expression in red versus white light in our study showed a strong tendency to peak between phase 18 and 21, which coincides with the exact range of peak expression observed by Hajdu et al. (2018) for *HY5* expression. At the same time, the CCA1 target element, the GA motif, became statistically enriched among genes found to be rhythmic in red light, while, the evening element, another CCA1 target element, became less important among rhythmic genes in red light, perhaps implying that changes in CCA1 activity may be an important difference between red and white light. Interestingly, the HY5 protein is also a specific interactor of CCA1 and so it is possible that differences in HY5 stability in white versus red may possibly also have an impact on CCA1 activity to alter the balance of clock coordination in red versus white light.

Our findings also suggest that there are some key differences in overt rhythms in white versus red. While rhythmicity within primary metabolism and stress responses appear to remain unchanged in white versus red light, there appears to be a loss of rhythmicity in raffinose and trehalose metabolism, amino acid synthesis and several secondary metabolic processes in red light. The impact of light wavelength on levels of secondary metabolism is well established and is an important aspect of the design of artificial lighting for horticulture (Darko et al., 2014) but the suggestion that that levels of blue light are also important in maintaining normal circadian regulation of such

secondary metabolic processes and may form an additional factor for consideration by growers.

These findings represent the first comparison of the circadian transcriptomes in red and white light and, overall, reveal subtle differences in overt rhythms but, more importantly, a switch in emphasis within the central mechanism of the clock in red versus white light, although the maintenance of rhythmicity in all clock genes suggests that the components of the mechanism remain the same even if their relative importance or activity changes.

Global Patterns in *fhy3* Indicate Potential Point of Action for FHY3

Our primary aim in examining global gene expression patterns in red light, however, was to examine the impact of the *fhy3* mutation on the functioning of the circadian clock. A comparison of rhythmicity in wild type versus *fhy3* revealed a dramatic decrease in the proportion of rhythmic genes in red light consistent with our earlier analysis of individual output genes. The importance of FHY3 in maintaining rhythmicity in red light is also emphasised by the fact that photosynthesis related processes are no longer overrepresented among rhythmic genes in *fhy3*. Of particular interest, though, was the impact of the mutation on the genes of the central clock. The majority of the clock genes maintained rhythmicity in *fhy3* in red light, including the two well-documented direct target genes of the FHY3/FAR1 transcriptional activating complex, *CCA1* and *ELF4*. *CCA1* did show a reduction in amplitude as has been observed previously (Liu et al., 2020); however, surprisingly, the evening complex gene, *ELF4*, showed no loss of amplitude in *fhy3* in these red light conditions, contrary to the dramatic loss of *ELF4* amplitude observed in *fhy3* in white light (Li et al., 2011). As noted above, *ELF4* expression is already extremely reduced in red light compared to white light in wild type seedlings and it is possible that the lack of impact of the *fhy3* mutation on *ELF4* in red is a result of *ELF4* expression already being effectively minimal. In contrast, there was a much greater impact of *fhy3* elsewhere in the central clock. The two other evening complex genes, *ELF3* and *LUX*, become arrhythmic in *fhy3*, with *ELF3* damping low level and *LUX* damping high. This points to the mis-regulation of these genes perhaps being key to the severe disruption of overt rhythmicity in the *fhy3* mutant. These genes are direct targets of CCA1, supporting our proposal that the interaction of FHY3 with CCA1 and the modulation of CCA1 transcriptional regulator function by FHY3 may be the key to the phenotype. Analysis of the *cis* elements enriched among genes that lose rhythmicity in the *fhy3* mutant, also supports this proposal. Genes becoming arrhythmic show enrichment of the TBS element, TGGGCC, bound by CCA1 (Kamioka et al., 2016). It may also be that the loss of this moderation of CCA1 activity also contributes to the gating defect in *fhy3*. *CCA1* expression is strongly promoted by light. It may be that FHY3 protein which is, itself, stabilised in light, is essential to shepherd the clock through the day, preventing excessive clock resetting by light.

The loss of *LUX* and *ELF3* rhythmicity and the already low levels of *ELF4* expression suggest that the evening complex would be likely to show an overall inability to fulfil its normal function as a cog in the clock in *fhy3*. Mutations in *LUX* and in *ELF3* have both been shown to result in extremely low *CCA1* and *LHY* expression, while *TOC1* expression damps high in *lux* and *elf3* mutants (Hazen et al., 2005; Dixon et al., 2011) exactly as was observed in *fhy3* in red. Again, *cis* element analysis is consistent with clock gene expression, with genes remaining rhythmic in *fhy3* showing enrichment of the GA motif associated with high TOC1 levels (Gendron et al., 2012). Similarly, loss of *ELF3* rhythmicity in *fhy3* in red light could also help to explain the previously observed loss of gating of light input to the clock in the *fhy3* mutant (Allen et al., 2006). The *elf3* mutant also shows a loss of gating of light input (McWatters et al., 2000; Covington et al., 2001).

Further evidence that the circadian defect in the *fhy3* mutant does not relate to its action as a transcription factor in the FHY3-FAR1 transcriptional activation complex comes from the fact that the target fbs *cis* element was not found to be enriched among genes becoming arrhythmic in *fhy3*. However, it was found among genes showing a loss of mean expression in *fhy3*. Thus, this second role of FHY3 is also disrupted in the mutant as would be expected but it appears to result in a more general decrease in target gene expression. Nevertheless, *CCA1* is one of the target genes of the FHY3-FAR1 transcriptional activation complex *via* the fbs element in its promoter and this may also contribute to the low levels of *CCA1* observed in *fhy3*. It is also of interest that, among rhythmic genes, there was a particular grouping of genes with peak phases 7–9 that showed a loss of mean expression in *fhy3*, suggesting that this may be the time at which the FHY3-FAR1 transcriptional activation complex normally acts most strongly. Consistent with this, FHY3 protein is strongly daytime expressed in light dark cycles (Li et al., 2011).

In addition to changes in amplitude among the central clock genes, the morning genes, *CCA1*, *LHY*, and *RVE*, along with the daytime gene, *PRR5*, all show a considerable delay in phase of between 5 and 7 h compared to wild type in *fhy3* in red light (**Supplementary Table 6**). The change in phase in genes which remain rhythmic in *fhy3* is reminiscent of the *cca1 lhy* double mutant phenotype which also shows a change in phase in constant light (Alabadi et al., 2002). The *cca1 lhy* double mutant assumes an earlier phase rather than a later phase (Alabadi et al., 2002); however, this provides a precedent for the fact that dramatically altered levels of all of the central clock components can cause a change in phase angle versus the preceding entraining stimuli. The fact that not all central clock genes in *fhy3* show this phase delay, indicates that there is also a change in the phase angle between the components of the clock loop. It is possible that this change in the relative phases of the clock genes may underlie the strong grouping among those clock output genes which remain rhythmic in *fhy3* into to phase groups, centred on phases 4 and 16. Output pathways from the clock are formed by the direct action of the transcription factors that make up the central clock loop and many output genes are targetted by more than one clock component due to combinations of *cis* elements in their promoters, with the ultimate phase of the target genes being regulated by additive effects. In this way a wide range of phases for output genes can be conferred by a relatively small number of central clock genes. Changes in the relative levels as well as the

relative phases of the central clock gene expression may together cause a narrowing of the range of phases possible. In addition, it is possible that the differences in relative phase between the central clock components and also phase grouping among the output genes could, at least partly, be a result of the gating defect in *fhy3*, whereby improperly regulated light input causes clock resetting at inappropriate times of day. Indeed the strong shift in phase seen in *fhy3* among genes peaking in the subjective afternoon in wild type is consistent with the timing of the defect in gating previously observed in *fhy3* (Allen et al., 2006).

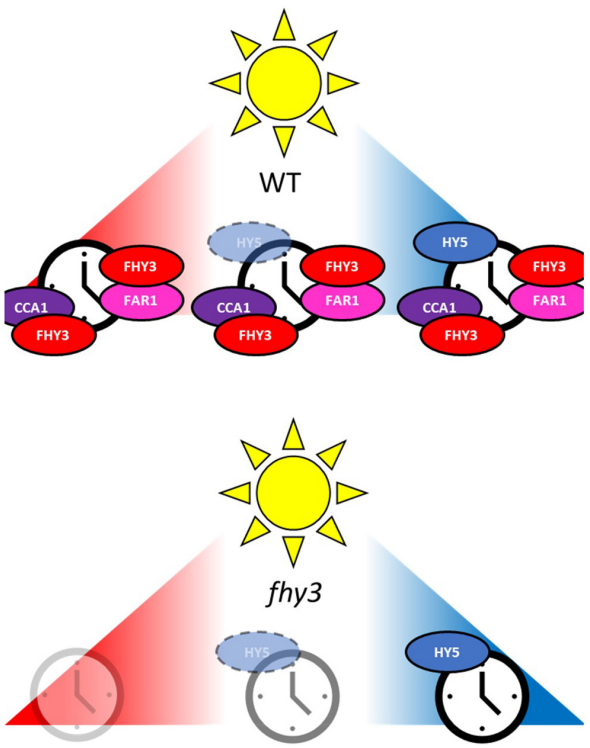

FIGURE 9 | Proposed model for the integration of red and blue light into to the plant clock *via* FHY3 and HY5. FHY3 plays a dual role in light input to the clock. Firstly, FHY3 acts in conjunction with FAR1 to form a transactivating complex targeting the fbs element in the promoter of *CCA1* and *ELF4* genes and is required for high amplitude of their expression (Li et al., 2011; Liu et al., 2020). Secondly, FHY3 but not FAR1 is required for the maintenance of wider overt rhythms in constant white and, particularly, red light, where loss of FHY3 causes severely disrupted rhythmicity. Our evidence suggests that this involves moderation of CCA1 activity. FHY3 but not FAR1 interacts with CCA1 and moderates it transcriptional activity in the clock (Li et al., 2011) and we show here that loss of FHY3 particularly disrupts CCA1 target genes. Our findings further suggest that the wavelength specificity of the *fhy3* mutant phenotype in the maintenance of wider overt rhythms in constant light may reflect a conditional redundancy between FHY3 and HY5 in light input to the clock. We show here that genes most severely impacted in red light compared to white light are HY5 target genes. Levels and activity of HY5 decrease with decreasing ratio of blue to red light resulting in blue light-specific HY5 activity in light input to the clock (Hajdu et al., 2018). We propose that, in the absence of FHY3, HY5 compensates for FHY3 in maintaining rhythmicity in constant blue light. However, we propose that decreasing HY5 activity means that rhythmicity is disrupted in the *fhy3* mutant in constant white and severely disrupted in constant red light.

HY5 and FHY3 Offer a Potential Mechanism for Plasticity in Red and Blue Light Input to the Clock

Our findings point to a conditional redundancy in the roles of HY5 and FHY3 in light input to the clock. Given the fact that HY5 protein shows enhanced stability in blue light while FHY3 protein shows enhanced stability in white and red light (Li et al., 2011; Siddiqui et al., 2016; Hajdu et al., 2018), this may offer a mechanism for plasticity in recruitment of photoreceptor input for the maintenance of normal rhythmicity. The complementary phenotypes of the *fhy3* and *hy5* mutants are consistent with such an arrangement. The *hy5* mutant shows a blue-specific phenotype, while *fhy3* shows a white- and red-specific phenotype. It is possible that this wavelength specificity is the result of conditional redundancy with FHY3 compensating for HY5 in red and white light and HY5 compensating for FHY3 in blue (**Figure 9**). However, although the stability of each is enhanced by specific wavelengths, both proteins none-the-less remain present in all light conditions so this conditional redundancy may depend on levels of the compensating protein falling below a certain threshold in each case. The fact that the *fhy3* mutant phenotype is more extreme than that of *hy5*, would then require that this threshold level for the two proteins is asymmetric. It is also likely that there would be some overlap in action of the two proteins in white light as, rather than showing a simple blue regulated stability, HY5 proteins levels actually respond to the ratio of red to blue light. Indeed, the fact that the *fhy3* phenotype is more extreme in red light than white light (**Figure 1**; Allen et al., 2006) is consistent with a limited amount of HY5 action in this proposed role in white. The fact that FHY3 but not FAR1 interacts with both CCA1 and HY5 leads us to further suggest that this integration may happen as a part of a three-way complex. Our evidence suggests that FHY3 action appears to be *via* moderation of CCA1 activity, something previously demonstrated at a molecular level (Li et al., 2011). However, we also saw some evidence of a change in CCA1 activity in white versus red light alongside evidence of changes in HY5 activity. It is, therefore, tempting to speculate that one point of convergence of red and blue light signals in input to the clock *via* FHY3 and HY5 may be in the moderation of CCA1 action.

CONCLUSION

We have demonstrated that the phytochrome signalling component, FHY3, plays a second role in regulation of the circadian clock that is in addition to its previously described activity within and FHY3-FAR1 dimer as a transcriptional activator of *ELF4* and *CCA1* expression. Loss of only FHY3 and not FAR1 resulted in a red and white light-specific defect in rhythmicity. Our comparison of the transcriptomes of plants grown in red versus white light revealed key differences consistent with the proposal that the previously established role of HY5 as an integrator of the ratio of red to blue light may account for the wavelength specificity of the *fhy3* phenotype. HY5 and FHY3, therefore, appear to redundantly act to integrate red

and blue light input to the clock. Such a plasticity in recruitment of photoreceptor signalling components in input to the clock would allow plants to adapt to a range of light environments. Furthermore, our analysis of the transcriptomes of wild type and *fhy3* mutant seedlings in red light provided strong evidence that FHY3 acts on central clock genes targetted by CCA1, in particular, *ELF3* and *LUX* to maintain rhythmicity. Based on the facts that both HY5 and FHY3 are known interactors with each other and with CCA1, and both moderate the transcriptional activity of CCA1, we propose that the two light signalling proteins, together, may, at least partly carry out this integration of red and blue light input *via* the modulation of CCA1 activity.

DATA AVAILABILITY STATEMENT

The data presented in the study are deposited in the Gene Expression Omnibus (GEO) repository, accession number GSE201929.

AUTHOR CONTRIBUTIONS

BR, HS, and PD contributed to project design. HS and SK prepared RNA for microarray analysis, carried out the bioluminescence analyses of the LUC reporter lines and the qRT-PCR assays. BR analysed the microarray data. BR and PD wrote the manuscript. All authors discussed the results and commented on the manuscript.

FUNDING

This work was supported by a grant from the Biotechnology and Biological Sciences Research Council (BBF02116X1) to PD.

SUPPLEMENTARY MATERIAL

The Supplementary Material for this article can be found online at: https://www.frontiersin.org/articles/10.3389/fpls.2022.862387/full#supplementary-material

REFERENCES

Alabadi, D., Yanovsky, M. J., Mas, P., Harmer, S. L., and Kay, S. A. (2002). Critical role for CCA1 and LHY in maintaining circadian rhythmicity in Arabidopsis. *Curr. Biol.* 12, 757–761. doi: 10.1016/s0960-9822(02)00815-1

Allen, T., Koustenis, A., Theodorou, G., Somers, D. E., Kay, S. A., Whitelam, G. C., et al. (2006). Arabidopsis FHY3 specifically gates phytochrome signaling to the circadian clock. *Plant Cell* 18, 2506–2516. doi: 10.1105/tpc.105.037358

Bailey, T. (2011). DREME: motif discovery in transcription factor ChIP-seq data. *Bioinformatics* 27, 1653–1659. doi: 10.1093/bioinformatics/btr261

Bailey, T. L., and Elkan, C. (1994). Fitting a mixture model by expectation maximization to discover motifs in biopolymers. *Proc. Int. Conf. Intell. Syst. Mol. Biol.* 2, 28–36.

Covington, M. F., Panda, S., Liu, X. L., Strayer, C. A., Wagner, D. R., and Kay, S. A. (2001). ELF3 modulates resetting of the circadian clock in Arabidopsis. *Plant Cell* 13, 1305–1315. doi: 10.1105/tpc.13.6.1305

Covington, M., and Harmer, S. (2007). The circadian clock regulates auxin signaling and responses in Arabidopsis. *PLoS Biol.* 5:e222. doi: 10.1371/journal.pbio.0050222

Creux, N., and Harmer, S. (2019). Circadian rhythms in plants. *Cold Spring Harb. Perspect. Biol.* 11:a034611.

Darko, E., Heydarizadeh, P., Schoefs, B., and Sabzalian, M. (2014). Photosynthesis under artificial light: the shift in primary and secondary metabolism. *Philos. Trans. R. Soc. B Biol. Sci.* 369:20130243. doi: 10.1098/rstb.2013.0243

Devlin, P. F., and Kay, S. A. (2000). Cryptochromes are required for phytochrome signaling to the circadian clock but not for rhythmicity. *Plant Cell* 12, 2499–2510. doi: 10.1105/tpc.12.12.2499

Devlin, P. F., Yanovsky, M. J., and Kay, S. A. (2003). A genomic analysis of the shade avoidance response in Arabidopsis. *Plant Physiol.* 133, 1617–1629. doi: 10.1104/pp.103.034397

Dixon, L., Knox, K., Kozma-Bognar, L., Southern, M., Pokhilko, A., and Millar, A. (2011). Temporal repression of core circadian genes is mediated through EARLY FLOWERING 3 in Arabidopsis. *Curr. Biol.* 21, 120–125. doi: 10.1016/j.cub.2010.12.013

Dodd, A., Bebin, F., Frank, A., and Webb, A. (2015). Interactions between circadian clocks and photosynthesis for the temporal and spatial coordination of metabolism. *Front. Plant Sci.* 6:245. doi: 10.3389/fpls.2015.00245

Edwards, K. D., Anderson, P. E., Hall, A., Salathia, N. S., Locke, J. C., Lynn, J. R., et al. (2006). FLOWERING LOCUS C mediates natural variation in the high-temperature response of the Arabidopsis circadian clock. *Plant Cell* 18, 639–650. doi: 10.1105/tpc.105.038315

Fraser, D., Panter, P., Sharma, A., Sharma, B., Dodd, A., and Franklin, K. (2021). Phytochrome A elevates plant circadian-clock components to suppress shade avoidance in deep-canopy shade. *Proc. Natl. Acad. Sci. U. S. A.* 118:e2108176118. doi: 10.1073/pnas.2108176118

Gendron, J. M., Pruneda-Paz, J. L., Doherty, C. J., Gross, A. M., Kang, S. E., and Kay, S. A. (2012). Arabidopsis circadian clock protein, TOC1, is a DNA-binding transcription factor. *Proc. Natl. Acad. Sci. U. S. A.* 109, 3167–3172. doi: 10.1073/pnas.1200355109

Gommers, C., and Monte, E. (2018). Seedling establishment: a dimmer switch-regulated process between dark and light signaling. *Plant Physiol.* 176, 1061–1074. doi: 10.1104/pp.17.01460

Graf, A., Schlereth, A., Stitt, M., and Smith, A. (2010). Circadian control of carbohydrate availability for growth in Arabidopsis plants at night. *Proc. Natl. Acad. Sci. U. S. A.* 107, 9458–9463. doi: 10.1073/pnas.0914299107

Grundy, J., Stoker, C., and Carre, I. (2015). Circadian regulation of abiotic stress tolerance in plants. *Front. Plant Sci.* 6:648. doi: 10.3389/fpls.2015.00648

Hajdu, A., Dobos, O., Domijan, M., Balint, B., Nagy, I., Nagy, F., et al. (2018). ELONGATED HYPOCOTYL 5 mediates blue light signalling to the Arabidopsis circadian clock. *Plant J.* 96, 1242–1254. doi: 10.1111/tpj.14106

Harmer, S. L., Hogenesch, J. B., Straume, M., Chang, H. S., Han, B., Zhu, T., et al. (2000). Orchestrated transcription of key pathways in Arabidopsis by the circadian clock. *Science* 290, 2110–2113. doi: 10.1126/science.290.5499.2110

Harmer, S., and Kay, S. (2005). Positive and negative factors confer phase-specific circadian regulation of transcription in Arabidopsis. *Plant Cell* 17, 1926–1940. doi: 10.1105/tpc.105.033035

Hazen, S. P., Schultz, T. F., Pruneda-Paz, J. L., Borevitz, J. O., Ecker, J. R., and Kay, S. A. (2005). LUX ARRHYTHMO encodes a Myb domain protein essential for circadian rhythms. *Proc. Natl. Acad. Sci. U. S. A.* 102, 10387–10392. doi: 10.1073/pnas.0503029102

Hearn, T., Ruiz, M., Abdul-Awal, S., Wimalasekera, R., Stanton, C., Haydon, M., et al. (2018). BIG regulates dynamic adjustment of circadian period in Arabidopsis thaliana. *Plant Physiol.* 178, 358–371. doi: 10.1104/pp.18.00571

Henriques, R., Papdi, C., Ahmad, Z., and Bögre, L. (2018). "Circadian regulation of plant growth," in *Annual Plant Reviews Online*, ed. J. Roberts (Hoboken, NJ: Wiley), 675–704.

Hsu, P. Y., Devisetty, U. K., and Harmer, S. L. (2013). Accurate timekeeping is controlled by a cycling activator in Arabidopsis. *Elife* 2:e00473. doi: 10.7554/eLife.00473

Hsu, P., and Harmer, S. (2014). Wheels within wheels: the plant circadian system. *Trends Plant Sci.* 19, 240–249. doi: 10.1016/j.tplants.2013.11.007

Ibanez, C., Kozarewa, I., Johansson, M., Ogren, E., Rohde, A., and Eriksson, M. (2010). Circadian clock components regulate entry and affect exit of seasonal dormancy as well as winter hardiness in Populus trees. *Plant Physiol.* 153, 1823–1833. doi: 10.1104/pp.110.158220

Kamioka, M., Takao, S., Suzuki, T., Taki, K., Higashiyama, T., Kinoshita, T., et al. (2016). Direct repression of evening genes by CIRCADIAN CLOCK-ASSOCIATED1 in the Arabidopsis circadian clock. *Plant Cell* 28, 696–711. doi: 10.1105/tpc.15.00737

Li, C., and Wong, W. (2001). Model-based analysis of oligonucleotide arrays: expression index computation and outlier detection. *Proc. Natl. Acad. Sci. U. S. A.* 98, 31–36. doi: 10.1073/pnas.98.1.31

Li, G., Siddiqui, H., Teng, Y., Lin, R., Wan, X. Y., Li, J., et al. (2011). Coordinated transcriptional regulation underlying the circadian clock in Arabidopsis. *Nat. Cell Biol.* 13, 616–22. doi: 10.1038/ncb2219

Liu, Y., Ma, M., Li, G., Yuan, L., Xie, Y., Wei, H., et al. (2020). Transcription factors FHY3 and FAR1 regulate light-induced CIRCADIAN CLOCK ASSOCIATED1 gene expression in Arabidopsis. *Plant Cell* 32, 1464–1478. doi: 10.1105/tpc.19.00981

Martinez-Garcia, J. F., Huq, E., and Quail, P. H. (2000). Direct targeting of light signals to a promoter element-bound transcription factor. *Science* 288, 859–863. doi: 10.1126/science.288.5467.859

McWatters, H. G., Bastow, R. M., Hall, A., and Millar, A. J. (2000). The ELF3 zeitnehmer regulates light signalling to the circadian clock. *Nature* 408, 716–720. doi: 10.1038/35047079

Michael, T. P., Mockler, T. C., Breton, G., McEntee, C., Byer, A., Trout, J. D., et al. (2008). Network discovery pipeline elucidates conserved time-of-day-specific cis-regulatory modules. *PLoS Genet.* 4:e14. doi: 10.1371/journal.pgen.0040014

Michael, T. P., Salome, P. A., Yu, H. J., Spencer, T. R., Sharp, E. L., McPeek, M. A., et al. (2003). Enhanced fitness conferred by naturally occurring variation in the circadian clock. *Science* 302, 1049–1053. doi: 10.1126/science.1082971

Millar, A. J., and Kay, S. A. (1996). Integration of circadian and phototransduction pathways in the network controlling CAB gene transcription in Arabidopsis. *Proc. Natl. Acad. Sci. U. S. A.* 93, 15491–15496. doi: 10.1073/pnas.93.26.15491

Oakenfull, R., and Davis, S. (2017). Shining a light on the Arabidopsis circadian clock. *Plant Cell Environ.* 40, 2571–2585. doi: 10.1111/pce.13033

Pruneda-Paz, J., Breton, G., Para, A., and Kay, S. (2009). A functional genomics approach reveals CHE as a component of the Arabidopsis circadian clock. *Science* 323, 1481–1485. doi: 10.1126/science.1167206

Rodriguez-Falcon, M., Bou, J., and Prat, S. (2006). Seasonal control of tuberization in potato: conserved elements with the flowering response. *Ann. Rev. Plant Biol.* 57, 151–180. doi: 10.1146/annurev.arplant.57.032905.105224

Siddiqui, H., Khan, S., Rhodes, B. M., and Devlin, P. F. (2016). FHY3 and FAR1 act downstream of light stable phytochromes. *Front. Plant Sci.* 7:175. doi: 10.3389/fpls.2016.00175

Somers, D. E., Devlin, P. F., and Kay, S. A. (1998). Phytochromes and cryptochromes in the entrainment of the Arabidopsis circadian clock. *Science* 282, 1488–1490. doi: 10.1126/science.282.5393.1488

Song, Y., Shim, J., Kinmonth-Schultz, H., Imaizumi, T., and Merchant, S. (2015). Photoperiodic flowering: time measurement mechanisms in leaves. *Ann. Rev. Plant Biol.* 66, 441–464. doi: 10.1146/annurev-arplant-043014-115555

Toledo-Ortiz, G., Huq, E., and Quail, P. H. (2003). The Arabidopsis basic/helix-loop-helix transcription factor family. *Plant Cell* 15, 1749–1770.

Usadel, B., Nagel, A., Steinhauser, D., Gibon, Y., Blasing, O., Redestig, H., et al. (2006). PageMan: an interactive ontology tool to generate, display, and annotate overview graphs for profiling experiments. *BMC Bioinformatics* 7:535. doi: 10.1186/1471-2105-7-535

Wang, H., and Deng, X. W. (2002). Arabidopsis FHY3 defines a key phytochrome A signaling component directly interacting with its homologous partner FAR1. *EMBO J.* 21, 1339–1349. doi: 10.1093/emboj/21.6.1339

Wang, X., Roig-Villanova, I., Khan, S., Shanahan, H., Quail, P. H., Martinez-Garcia, J. F., et al. (2011). A novel high-throughput in vivo molecular screen for shade avoidance mutants identifies a novel phyA mutation. *J. Exp. Bot.* 62, 2973–2987. doi: 10.1093/jxb/err062

Woodley Of Menie, M., Pawlik, P., Webb, M., Bruce, K., and Devlin, P. (2019). Circadian leaf movements facilitate overtopping of neighbors. *Prog. Biophys. Mol. Biol.* 146, 104–111. doi: 10.1016/j.pbiomolbio.2018.12.012

Yan, J., Kim, Y., and Somers, D. (2021). Post-translational mechanisms of plant circadian regulation. *Genes* 12:325. doi: 10.3390/genes12030325

Conflict of Interest: The authors declare that the research was conducted in the absence of any commercial or financial relationships that could be construed as a potential conflict of interest.

Publisher's Note: All claims expressed in this article are solely those of the authors and do not necessarily represent those of their affiliated organizations, or those of the publisher, the editors and the reviewers. Any product that may be evaluated in this article, or claim that may be made by its manufacturer, is not guaranteed or endorsed by the publisher.

frontiers | Frontiers in Plant Science

ORIGINAL RESEARCH
published: 13 July 2022
doi: 10.3389/fpls.2022.854869

In *Arabidopsis thaliana*, RNA-Induced Silencing Complex-Loading of MicroRNAs Plays a Minor Regulatory Role During Photomorphogenesis Except for miR163

Lóránt Lakatos[1]†, Gergely Groma[2]†, Daniel Silhavy[1] and Ferenc Nagy[1]*

[1] Laboratory of Photo and Chronobiology, Biological Research Centre, Institute of Plant Biology, Eötvös Loránd Research Network, Szeged, Hungary, [2] Dermatological Research Group, University of Szeged, Szeged, Hungary

OPEN ACCESS

Edited by:
Karen Halliday,
University of Edinburgh,
United Kingdom

Reviewed by:
Binglian Zheng,
Fudan University, China
Pablo A. Manavella,
CONICET Santa Fe, Argentina
Julieta L. Mateos,
Instituto de Fisiología, Biología Molecular y Neurociencias (IFIBYNE), CONICET-UBA, Argentina

***Correspondence:**
Lóránt Lakatos
lakatos.lorant@brc.hu

†These authors have contributed equally to this work

Specialty section:
This article was submitted to Plant Physiology, a section of the journal Frontiers in Plant Science

Received: 14 January 2022
Accepted: 14 June 2022
Published: 13 July 2022

Citation:
Lakatos L, Groma G, Silhavy D and Nagy F (2022) In Arabidopsis thaliana, RNA-Induced Silencing Complex-Loading of MicroRNAs Plays a Minor Regulatory Role During Photomorphogenesis Except for miR163. Front. Plant Sci. 13:854869. doi: 10.3389/fpls.2022.854869

The shift of dark-grown seedlings to the light leads to substantial reprogramming of gene expression, which results in dramatic developmental changes (referred to as de-etiolation or photomorphogenesis). MicroRNAs (miRNAs) regulate most steps of plant development, thus miRNAs might play important role in transcriptional reprogramming during de-etiolation. Indeed, miRNA biogenesis mutants show aberrant de-etiolation. Previous works showed that the total miRNA expression pattern (total miRNAome) is only moderately altered during photomorphogenesis. However, a recent study has shown that plant miRNAs are present in two pools, biologically active miRNAs loaded to RISC (RNA-induced silencing complex-loaded) form while inactive miRNAs accumulate in duplex form upon organ formation. To test if RISC-loading efficiency is changed during photomorphogenesis. we compared the total miRNAome and the RISC-loaded miRNAome of dark-grown and de-etiolated *Arabidopsis thaliana* seedlings. miRNA sequencing has revealed that although regulated RISC-loading is involved in the control of active miRNAome formation during de-etiolation, this effect is moderate. The total miRNAomes and the RISC-loaded miRNAomes of dark-grown and de-etiolated plants are similar indicating that most miRNAs are loaded onto RISC with similar efficiency in dark and light. Few miRNAs were loaded onto RISC with different efficiency and one miRNA, miR163, was RISC-loaded much more effectively in light than in dark. Thus, our results suggest that although RISC-loading contributes significantly to the control of the formation of organ-specific active miRNA pools, it plays a limited role in the regulation of active miRNA pool formation during de-etiolation. Regulated RISC-loading strongly modifies the expression of miRNA163, could play a role in the fine-tuning of a few other miRNAs, and do not modify the expression of most miRNAs.

Keywords: *Arabidopsis thaliana*, photomorphogenesis, reprogramming of gene expression, miRNA, efficiency of AGO loading, miRNAome, RISC-loaded miRNAome

INTRODUCTION

Light regulates many steps of plant development including germination, seedling development, shade avoidance, and flowering (Deng and Quail, 1999; Casal, 2012; Łabuz et al., 2012). The shift of dark-grown seedlings into light leads to substantial reprogramming of gene expression manifests in dramatic developmental changes. The molecular mechanisms of light-controlled seedling development (photomorphogenesis) are well studied. Light-sensitive photoreceptor molecules sense the intensity and quality of the light and trigger different signaling pathways leading to rapid transcriptional reprogramming and changes in protein stabilities (Legris et al., 2019; Cheng et al., 2021). The function of regulatory RNAs in the control of photomorphogenesis is less understood. MicroRNAs (miRNAs) are single-stranded, ∼21–24 nt long non-coding RNAs that play a critical role in post-transcriptional gene regulation in plants (Naqvi et al., 2012; Wang et al., 2019). miRNAs are produced from long, stem-loop structured RNA Polymerase II transcripts called primary miRNAs (pri-miRNAs) by the microprocessor complex (Chen, 2005; Yu et al., 2017). The core components of the microprocessor are the DICER-LIKE1 (DCL1) RNase III enzyme, the zinc finger protein SERRATE (SE), and the double-stranded RNA binding protein HYPONASTIC LEAVES 1 (HYL1) (Kurihara and Watanabe, 2004; Kurihara et al., 2006; Yang et al., 2006). DCL1, the key factor of the microprocessor, first produces precursor-miRNAs (pre-miRNAs) from the pri-miRNAs and then cleaves the pre-miRNAs at sites determined by structural features, thereby producing miRNA-miRNA* duplexes (Iwata et al., 2013). The duplexes are methylated at their 3′ termini by the HUA ENHANCER1 (HEN1) methyltransferase (Yu et al., 2005). The methylated miRNAs are loaded in a single-stranded form onto the ARGONAUTE 1 (AGO1) protein (or less frequently onto one of the many other AGO proteins) (Carbonell and Carrington, 2015) and form presumably with other proteins the functional RNA-Induced Silencing Complex (RISC) (Azevedo et al., 2010; Giner et al., 2010; Dalmadi et al., 2019). The miRNAs can be transported into the cytoplasm in the miRNA-AGO complex or the miRNA-miRNA* duplex (Yu et al., 2017; Bologna et al., 2018; Wang et al., 2019). In the cytoplasm, miRNA guides AGO1 to the mRNAs that show sequence complementarity with the small RNA to silence the target transcript via mRNA cleavage or translational repression. miRNA expression is strictly regulated, transcription of miRNA genes, processing of pri-miRNAs, selection of AGO protein, and stability of miRNAs are precisely controlled (Xie et al., 2010; Naqvi et al., 2012; Li and Yu, 2021). Moreover, a recent study has shown that in *Arabidopsis thaliana* production of a biologically active miRNA pool can be controlled at the AGO-loading step (Dalmadi et al., 2019). Small RNA-sequencing from the crude extract and gel-filtrated fractions of the crude extract revealed that miRNAs accumulate in two major pools, one that co-fractionates with AGO1 at the high molecular (mol.) weight fractions and a second pool that is present at the low mol. weight fractions. It is proposed that the miRNAs, which co-fractionate with AGO1 are present in the potentially active RISC-loaded form (but see section "Discussion"), while the miRNAs that accumulate at the low mol. weight fractions are present in inactive, miRNA duplex form (Dalmadi et al., 2019). Certain miRNAs mainly accumulate in the active RISC-loaded form, while other miRNAs are predominantly present as duplexes in low mol. weight fractions. The difference between the total miRNA pool (miRNAome) and the RISC-loaded miRNA pool (RISC-loaded miRNAome) is defined as RISC-loading efficiency. A comparison of RISC-loaded fractions of *Arabidopsis* leaves and flowers demonstrated that the RISC-loading efficiency of many miRNAs is organ specifically regulated (Dalmadi et al., 2019).

MicroRNAs regulate many steps of plant development, thus it is expected that miRNAs are also involved in the control of photomorphogenesis. Indeed, *Arabidopsis* mutants affected in miRNA expression show aberrant photomorphogenesis responses. Photomorphogenesis is altered in certain miRNA mutants, for example, miR167b and miR848 act as negative, whereas miR319b and miR160b as positive regulators of photomorphogenesis (Sun et al., 2018). Moreover, the *dcl1-9* and *hyl1-2* miRNA biogenesis mutants were hypersensitive to red light in the hypocotyl elongation assay (Sun et al., 2018). Furthermore, if dark-grown *Arabidopsis* seedlings are de-etiolated (shifted to light), the DCL1, HYL1, and SE microprocessor proteins accumulate to high levels and the pri-miRNA levels of most miRNAs are enhanced (Choi et al., 2020; Bhagat et al., 2022; Jung et al., 2022). The expression of microprocessor components is under complex regulation, for instance, altered transcription, phosphorylation, and protein stability all contribute to the increased HYL1 level during de-etiolation (Choi et al., 2020; Sacnun et al., 2020; Bhagat et al., 2022; Jung et al., 2022). However, high throughput miRNA sequencing (miRNA-seq) revealed that although pri-miRNA levels and microprocessor concentrations are increased during photomorphogenesis, the total miRNAome is only moderately altered (Choi et al., 2020). The total miRNA level remains stable during photomorphogenesis because light stabilizes the FORKHEAD-ASSOCIATED DOMAIN 2 (FHA2) microprocessor suppressor protein, thus miRNA processing is slow despite the enhanced microprocessor concentration (Park et al., 2021). The miRNA composition has also changed moderately during photomorphogenesis. Although many miRNAs accumulate significantly different in the dark-grown and de-etiolated plants, the changes are modest and not consistent between studies (Shikata et al., 2014; Chung et al., 2016; Choi et al., 2020; Li and Yu, 2021). The exception is miR163, which is a light-inducible miRNA that accumulates dramatically during photomorphogenesis (Chung et al., 2016; Choi et al., 2020; Li and Yu, 2021). Upregulation of miR163 is physiologically relevant, and the miR163-mediated silencing of 1,7-PARAXANTHINE METHYLTRANSFERASE (PMXT1) is required for normal primary root elongation during photomorphogenesis (Chung et al., 2016; Li and Yu, 2021).

It is controversial that miRNA biogenesis factors are important for normal photomorphogenesis (Cho et al., 2014; Sun et al., 2018), while total miRNAome is only moderately altered during de-etiolation (Choi et al., 2020). It was also reported that although in de-etiolated plants the total miRNAome changed

only slightly, miRNA activity might be enhanced. During de-etiolation, the expression of certain miRNA target transcripts was declined, while their 3′ cleavage products accumulated (Lin et al., 2017). If the RISC-loading is more efficient in de-etiolated than in dark-grown plants, the biologically active, RISC-loaded miRNAomes would be more different than the total miRNAomes and could explain how light can enhance the target cleavage activity of miRNAs. To test this assumption, we wanted to comparatively study the changes of total miRNAome and RISC-loaded miRNAome during photomorphogenesis. Crude extracts were prepared from dark-grown and de-etiolated *Arabidopsis* seedlings and these extracts were gel-filtrated to separate the RISC-loaded and non-loaded miRNAs. Then miRNA-seq assays were conducted from the crude extracts and from the AGO containing gel-filtrated fractions to analyze the changes of total miRNAomes and the RISC-loaded miRNAomes during photomorphogenesis. We found that both total miRNAome and RISC-loaded miRNAome differed moderately between dark-grown and de-etiolated seedlings. Our results suggest that most miRNAs are loaded with similar efficiency in both dark-grown and de-etiolated samples, few miRNAs are selectively loaded but the differences are modest. The exception was miR163 was much more efficiently loaded onto RISC in de-etiolated plants than in dark-grown seedlings. These data suggest that during photomorphogenesis, regulated RISC-loading plays a critical role in the formation of an active miR163 pool and contributes to the control of the biologically active pool of a few other miRNAs. Thus, we conclude that selective RISC-loading does not substantially control the formation of active miRNAome (except for miR163) during de-etiolation, and instead, it could play a role in the fine-tuning of miRNA expression.

MATERIALS AND METHODS

Plant Material and Growth Conditions

Arabidopsis thaliana Col-0 seeds were put on plates containing 1 × Murashige-Skoog medium supplemented with 1 w/v sucrose and kept in the dark at 4°C for 3 days, and illuminated with white light for 4 h. Then plates were kept in dark at 22°C. On day 5, half of the plates were transferred to white light for 72 h (de-etiolation), while the rest of the plates were kept in dark for 72 h (referred to as light and dark samples, respectively). Finally, 8 days old seedlings were collected and frozen in liquid nitrogen.

Extracts Preparation and Gel-Filtration

Crude extracts used for gel-filtration (and for immunoprecipitation, see later) were prepared in a buffer containing 50 mM Tris pH 7.0, 10 mM NaCl, 5 mM $MgCl_2$, and 4 mM DTT from dark and light samples as described (Dalmadi et al., 2019). Part of the crude extract was stored and used as input. The 400-μl crude extracts were loaded onto a Superdex HR-200 10/30 GL column (Merck Inc., United States). The void volume of the column (7 ml) was released, and then 36 fractions (500 μl) were collected. Even-numbered fractions were used to isolate RNA and odd-numbered fractions were used for protein isolation.

RNA Isolation, Small RNA Northern Hybridization

Inputs and gel-filtrated fractions were extracted with phenol-chloroform-isoamyl alcohol (500:125:1, pH 4.6) and then 1/10th volume of 3M NaOAc was added. RNA was precipitated with 1 vol. of isopropyl alcohol. Resuspended RNAs were used for miRNA-seq and for Northern blot assays. RNA was separated in 8M urea 12% acrylamide (38% acrylamide, 2% bis-acrylamide) 1 × TBE gels and transferred to Hybond + membrane (GE Healthcare, United States). Locked nucleic acid (LNA) (Merck Inc., United States) containing oligonucleotides labeled at the 5′ end with biotin corresponding to the reverse complement of miR163, miR159b, and miR168a were used for miRNA detection. Hybridization and detection were carried out with the North2South^{TM} Chemiluminescent Hybridization and Detection Kit (Thermo Fisher Scientific 17097) according to the instructions of the manufacturer.

Protein Isolation and Western Blotting

Fractions of the gel-filtration experiment were precipitated with four volumes of ethanol, centrifuged with 14,000 × *g* at 4°C for 10 min, and resuspended in 20 μl of 2 × Laemmli buffer. Resuspended fractions and input samples (30 μl of crude extract) were loaded into 10% acrylamide SDS gels, after separation proteins were transferred to PVDF membranes (Bio-Rad, CA, United States; Immun-Blot PVDF Membrane, 1620177). Incubations were carried out with the AGO1 (Agrisera, Sweden AS09 527), actin (Agrisera, Sweden AS13 2640), and histone H3 (Abcam, United States ab1791) antibodies.

Immunoprecipitations

Crude extracts were prepared identically for immunoprecipitation (IP) and gel-filtration. IPs were carried out with the AGO1 antibody (Agrisera Sweden AS09 527) as described (Dalmadi et al., 2019). Samples were taken from inputs (In), supernatant (SN), and the third wash off the resin (W#3). Half of the eluates were diluted in 100 μl IP2 buffer (50 mM TRIS pH 7.5, 150 mM NaCl, 5 mM MgCl2, 4 mM DTT) and then RNA was isolated as described earlier. The second half of the eluate was denatured in 2 × Laemmli buffer. Northern and Western blotting were used to detect miRNAs and proteins as described earlier.

Cell Separation

The separation of nuclei from cytoplasm was performed as described (Dalmadi et al., 2019). One gram of seedling was extracted in 10 ml extraction buffer (10 mM Tris pH 7.5, 1.14 M sucrose, 5 mM MgCl2, 7 mM mercaptoethanol), then the crude extracts were filtered through three layers of Miracloth. After 10 min centrifugation at 4°C at 900 × *g*, samples were taken from the supernatant and hereafter referred to as cytoplasmic extracts. Pellet was washed three times with extraction buffer supplemented with 0.15% Triton X-100 and centrifuged with the same parameters. ˆ100 μl of the supernatants and 200 μl of the third wash were used for RNA and protein extractions. The pelleted washed nuclei were resuspended in a 5 ml solution of

lysis buffer (50 mM Tris pH 7.5, 5 mM $MgCl_2$, and 5 mM KCl), and then 50–50 μl were used for RNA and protein extraction.

High Throughput MicroRNA Sequencing

To characterize total miRNAomes and RISC-loaded miRNAomes from dark-grown and de-etiolated (dark and light, respectively) *Arabidopsis* seedlings, high throughput miRNA sequencing (miRNA-seq) was conducted from crude input extracts of dark and light samples (referred to as D Input and L Input) and from AGO1 containing high mol. weight gel-filtrated fractions of D and L extracts (referred to as D RISC and L RISC for Dark RISC-loaded and Light RISC-loaded samples). AGO1 containing fractions (fraction 3–6) were combined. For each condition, four biological replicas were sequenced. Small RNA libraries have been prepared with QIAseq miRNA Library Kit for Illumina NGS systems according to the manufacturer's protocol (Qiagen, Germany). Sequencing has been performed on Illumina NextSeq 500 platform with 1 × 75 bp SE reads.

Raw sequencing data have been processed first with FastQC to assess the overall quality of sequences, then Unique Molecular Identifiers have been extracted by using UMI_tools (v1.1.1) (Smith et al., 2017). Reads have been filtered using Biopython to include reads that are min. 18 bps and max. 30 bps long. Alignment of reads was performed to NCBI GCA_000001735.1_TAIR10 using Bowtie (v1.2.2) (Langmead et al., 2009). The resulting SAM file has been converted to BAM using the SAMtools view option (v1.10) (Danecek et al., 2021). The BAM file has been deduplicated by grouping reads with the exactly same UMIs together with UMI_tools (v1.1.1). Features have been counted and annotated according to miRbase v22 by feature counts (Liao et al., 2014) (DESeq2 has been used to normalize samples; Love et al., 2014).

Bioinformatical Analysis

The four miRNA sequencing datasets (D Input, L input, D RISC, and L RISC) were uniformly processed. A total of 101 miRNAs were identified (**Supplementary Table 1**), and then miRNAs that were below 10 copies in at least 50% of the four different conditions were excluded from the dataset and were not subjected for comparison. miRNA*s (*refers to the unloaded miRNA strand) were also excluded, thus 34 miRNAs were included in the analysis. The data were normalized to the corresponding total amount of all miRNAs identified in the given experiment. Relative total amounts and RISC-loaded amounts were calculated for all miRNAs in light and dark and were compared. The student's *t*-test was also used to test for differential expression between light and dark conditions of total miRNA amounts as well as for RISC-loaded miRNA amounts. *P*-values lower than 0.05 were considered statistically significant.

RESULTS

Previous results have shown that although miRNA biogenesis mutants show aberrant photomorphogenesis (Cho et al., 2014; Sun et al., 2018), the total miRNAome is only moderately changed (Choi et al., 2020). Here, we wanted to comparatively study the changes of total miRNAome and RISC-loaded miRNAome during photomorphogenesis.

Gel-Filtration Efficiently Separates the RNA-Induced Silencing Complex-Loaded and Unloaded MicroRNAs of the Seedling Extracts

To compare total miRNAomes and RISC-loaded miRNAomes between dark-grown and de-etiolated plants, we should efficiently separate RISC-loaded and unloaded miRNAs. To establish an effective separation system, crude extracts were prepared from *Arabidopsis* seedlings grown for 8 days in the dark or shifted on day 5 from dark to white light for 3 days (referred to as dark and light samples, respectively), and then a part of dark and light samples was subjected to gel-filtration (**Figure 1A**). Fractions were collected and subjected to AGO1, histone H3, actin western blot, and miR163, miR159b, and miR168a small RNA gel blot assays (**Figure 1B**). The studied proteins and miRNAs accumulated similarly in the dark and light samples except that miR163 was detectable only in the light sample. This confirms that miR163 is a light-inducible miRNA. The crude extracts contain both nuclear and cytoplasmic fractions and the nuclear control H3 accumulated in the high mol. weight fractions, while the cytoplasmic control actin was present in the medium mol. weight fractions (**Figure 1B**). As expected, AGO1 was also present in the high mol. weight fractions. miR159b and miR163 RNAs were co-fractionated with AGO1 in the high mol. weight fractions. By contrast, miR168 accumulated to low levels in the AGO1-containing fractions, and it was mainly present in the low mol. weight fractions (**Figure 1B**). These low mol. weight fractions likely correspond to the cytoplasmic free miRNA duplexes (Dalmadi et al., 2019).

To confirm that the miRNAs that co-fractionated with AGO1 could be complex with AGO1, co-immunoprecipitation studies were conducted. AGO1 IP was similarly efficient from dark and light samples. However, a significant amount of AGO1 remained in the supernatant showing that AGO1 IP was partial. As we expected, all three miRNAs can be immunoprecipitated with the AGO1 antibody (**Figure 1C**). MiR159 and miR168 were AGO1 immunoprecipitated with comparable efficiency in dark and light samples (miR163 is not present in the dark samples) suggesting that these two miRNAs are similarly represented in the immunoprecipitated fraction of AGO1 in the dark and light samples.

Taken together, our gel-filtration results indicate that miR159 and miR163 were efficiently loaded onto AGO1 (or less likely to other AGOs that also accumulated in the high mol. weight fractions), while miR168 was inefficiently loaded onto AGOs, and it was mainly present as miRNA duplex. In mature *Arabidopsis* leaves and flowers, AGO1 was also present in the high mol. weight fractions, miR159 and miR163 were efficiently loaded onto AGO1, and miR168 was predominantly present in miRNA duplex form (Dalmadi et al., 2019). Thus, the studied miRNAs show similar AGO loading patterns in the dark-grown and de-etiolated seedlings as well as in the different organs of full-grown plants.

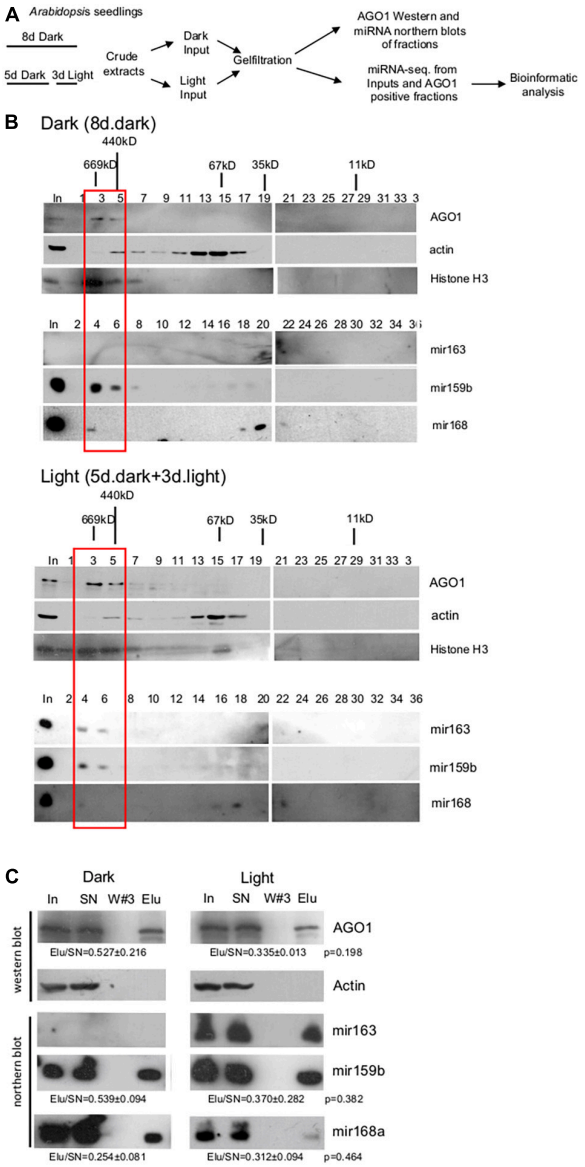

FIGURE 1 | Size-selective separation of miRNAs. **(A)** Schematic representation of the experimental plan. **(B)** Gel-filtration efficiently separates the RISC-loaded and unloaded miRNAs. Crude extracts were prepared from *Arabidopsis* seedlings grown for 8 days at dark (Dark) and from de-etiolated seedlings (Light), which were grown for 5 days at dark and then for 3 days in white light. Gel-filtrated fractions were collected and Western blot assays were conducted with AGO1, histone H3, and actin antibodies or RNAs were isolated from the fractions, and then Northern blot experiments were carried out with biotin-labeled miR163, miR159b, and miR168 LNA oligos. Black sticks represent protein size markers in kilodalton (kDa). The first lanes represent the protein and RNA inputs isolated from the crude extracts (In). The red bracketed fractions (3–6) were combined and used for miRNA-sec. Note that AGO1, miR163, and miR159b accumulate in high mol. Weight fractions, while miR168 is mainly present in low mol. Weight fractions and that miR163 is not detectable in the dark samples. **(C)** miR163, miR159b, and miR168 are associated with AGO1. Crude extracts of dark and light samples were used for immunoprecipitation (IP) using the AGO1 antibody. RNA samples isolated from the input (In), the supernatant (SN), the third wash (W#3), and the pellet (Elu) of the AGO1 IP were used for Northern blot assays. Proteins were isolated from the same sources and subjected to Western blotting to detect AGO1 and the cytoplasmic control actin protein. To estimate the efficiency of AGO1 IP and the ratio of AGO1-loaded fraction of miR168 and miR159, the ratios of Elu and SN signals (Elu/SN) of the light and dark samples were calculated for AGO1 and for the two miRNAs (from three replicas), and then the light and dark Elu/SN values were compared. Elu/Sn mean values and ± standard deviations are shown. The Elu/SN values were not significantly different between dark and light samples (see *p*-values). Note that AGO1 IP was partial, thus it is a semi-quantitative assay.

Total MicroRNA Levels Are Moderately Changed During Photomorphogenesis Except for miRNA163

To comparatively study the changes of total and RISC-loaded miRNAomes during photomorphogenesis (**Figure 1A**), miRNA-seq was conducted from crude input extracts of dark and light samples and the AGO1 containing gel-filtrated fractions of dark and light extracts (referred to as D Input, L Input, D RISC-loaded, and L RISC-loaded samples, respectively). Four biological replicas were studied. Principal component analyses show that the samples are relevantly different (**Supplementary Figure 2**), one component separated the dark and light samples, while the second component separated the input and RISC-loaded samples. The identical samples were grouped closely together. After excluding the miRNA* strands and the miRNAs that were very poorly expressed (see section "Materials and Methods"), we analyzed the expression of 34 miRNAs. First, we compared the miRNAome of D and L inputs. In line with previous studies (Choi et al., 2020; Li et al., 2021), we found that the miRNAomes of D and L inputs were moderately different and 10/34 miRNAs accumulated significantly different (**Figure 2** and **Supplementary Table 2A**). However, the changes are modest, only four miRNAs (miR163, miR319a, miR408, and miR482) showed more than 2-fold differences. Three of them, miR319a, miR408, and miR482, were underrepresented in the L input (0.49, 0.38, and 0.47-fold). miRNA163 was exceptional, it accumulated to low levels in the D input, while it was dramatically increased (∼20.5-fold) in the L input (**Supplementary Table 2A**). These results are consistent with previous results showing that during photomorphogenesis, miRNA163 was dramatically upregulated, while the expression of other miRNAs was changed slightly (Choi et al., 2020; Li et al., 2021).

During Photomorphogenesis, the AGO-Loading Efficiency of miR163 Is Strongly Enhanced While the Loading Efficiency of Other MicroRNAs Is Only Slightly Changed

Next, we compared the RISC-loaded miRNAomes of dark and light samples. The RISC-loaded miRNAomes were also moderately different, 12/34 miRNAs accumulated significantly different and 6-6 miRNAs were overrepresented in the RISC-loaded light and dark samples (**Figure 3** and **Supplementary Table 2B**). However, only four miRNAs show more than 2-fold

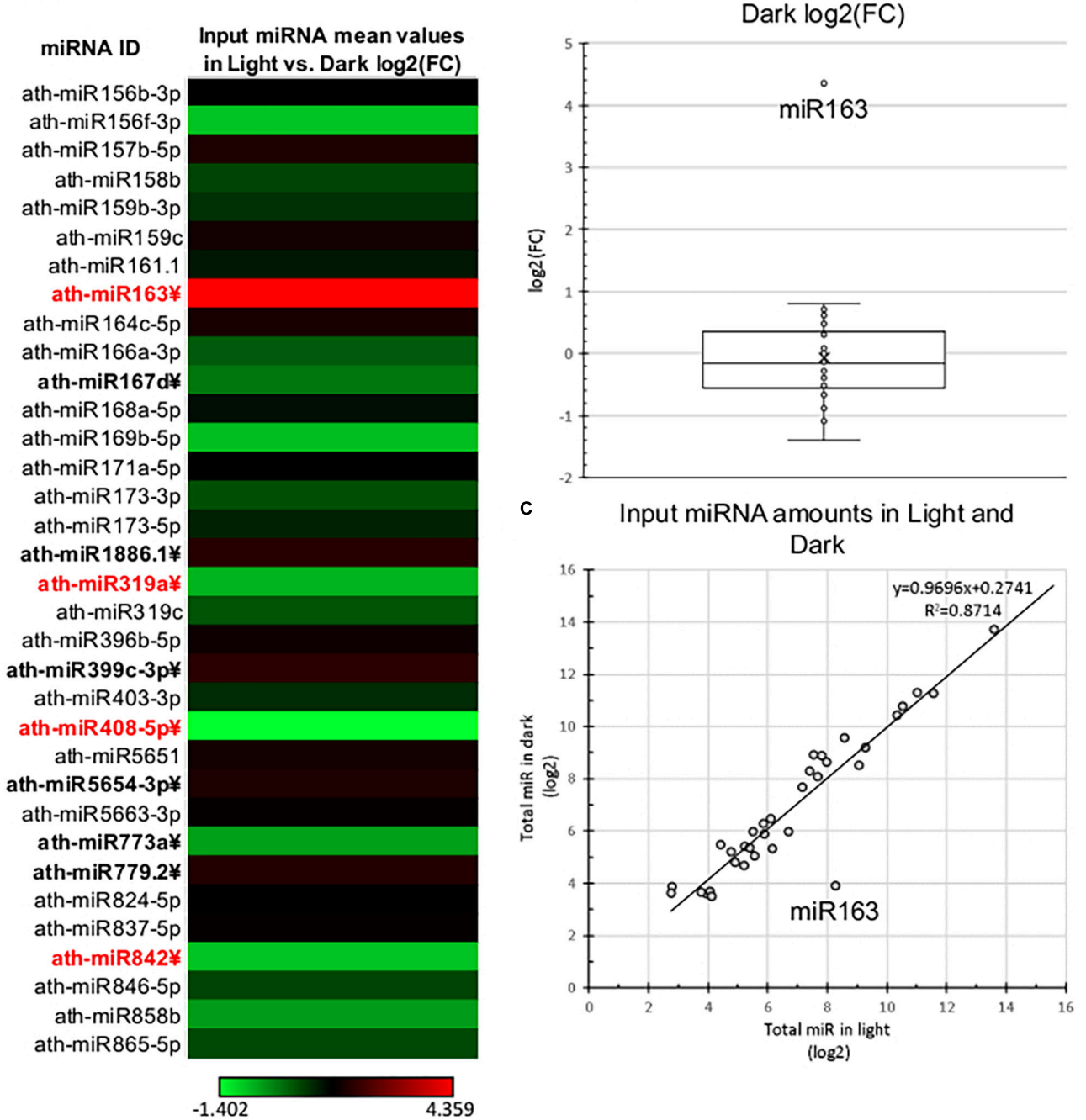

FIGURE 2 | Total miRNA expression of dark-grown and de-etiolated *Arabidopsis* seedlings. **(A)** The heat map of relative expressional differences of miRNAs of dark-grown (Dark) and de-etiolated (Light) seedlings [log2(FC)]. miRNAs that express significantly different are in bold letters, which show at least ±2-fold difference are highlighted in red. **(B,C)** Relative expressional distribution of identified miRNAs in light and dark samples. The salient data point represents miR163 in both **(B,C)**.

differences, miR408 and miR156f-3p were less abundant (0.44 and 0.44-fold), while miR565 (2.2-fold) and miR163 were more abundant in the light RISC-loaded samples. Notably, miR163 was dramatically overrepresented (109.66-fold) in the RISC-loaded de-etiolated sample relative to the dark-grown RISC-loaded sample (**Figure 3** and **Supplementary Table 2B**).

To assess the role of RISC-loading efficiency in the formation of biologically active, RISC-loaded miRNAome during photomorphogenesis, we compared the total miRNAomes and the RISC-loaded miRNAomes. The 10 miRNAs were accumulated differently between light and dark inputs, while 12 miRNAs were between RISC-loaded light and dark samples

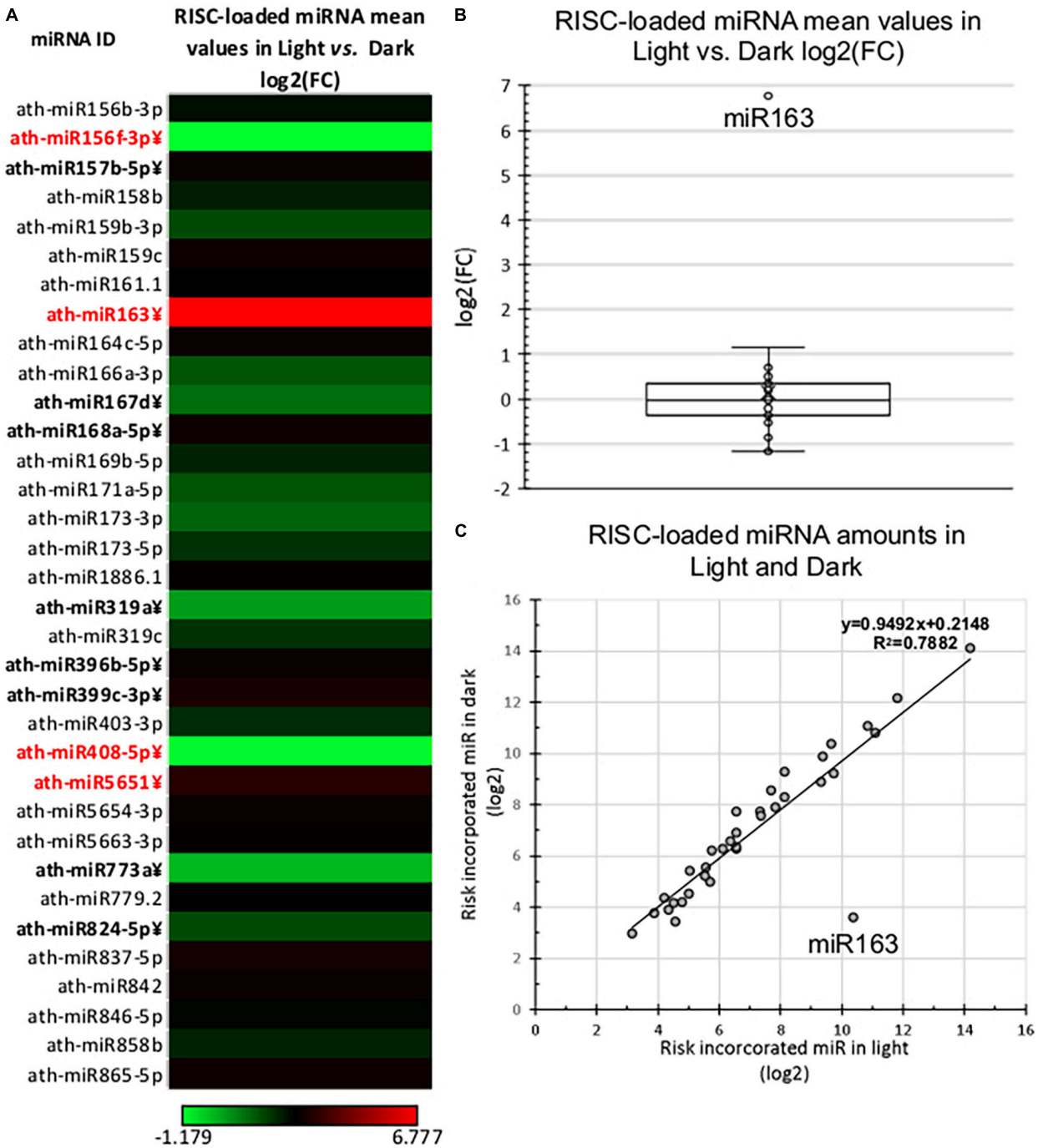

FIGURE 3 | RISC-loaded miRNA expression of dark-grown and de-etiolated *Arabidopsis* seedlings. **(A)** The heat map of the relative expressional ratio of identified RISC-loaded miRNAs in dark-grown (Dark) and de-etiolated (Light) samples [log2(FC)]. miRNAs that express significantly different are in bold letters, which show at least ±2-fold difference are highlighted in red. **(B,C)** Relative RISC-loaded distribution of identified miRNAs in light and dark samples. The salient data point represents miR163 in both **(B,C)**.

(**Figure 4A** and **Supplementary Tables 2A,B**). We did not find any miRNA that showed significant but opposite accumulation in the inputs and the RISC-loaded samples. Four miRNAs (miR842, miR5654-3p, miR1886.1, and miR779.2) were present in significantly different amounts in the inputs but not in the RISC-loaded samples, while six miRNAs (miR824-5p, miR156f-3p, miR5651, miR396b-5p, miR168a-5p, and miR157b-5p) accumulated differently in the RISC-loaded samples but not in the inputs (**Figure 4A**, **Supplementary Figure 3**, and **Supplementary Tables 2A,B**). These data suggest that the

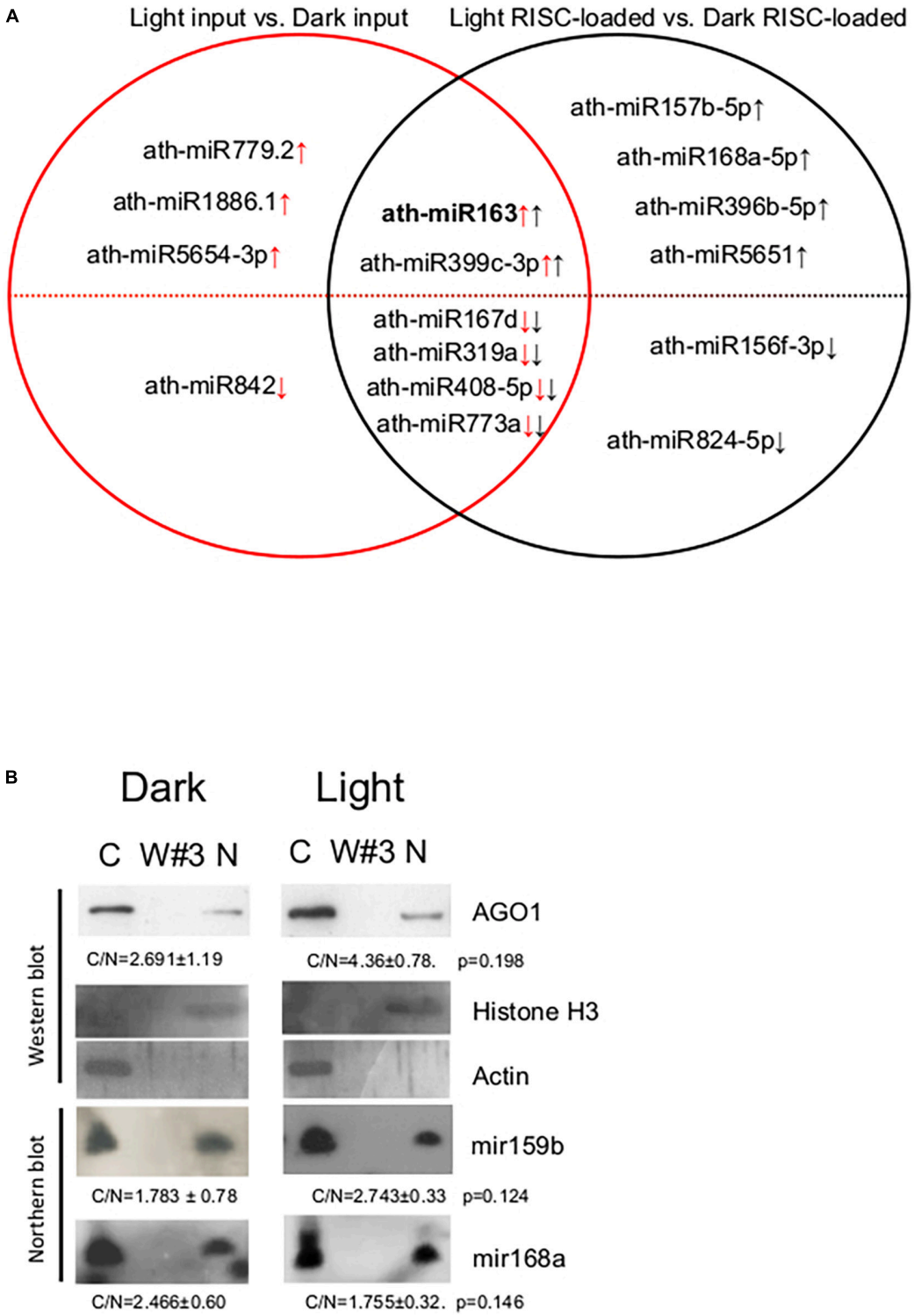

FIGURE 4 | Distribution of AGO1 and miRNAs in the crude extracts of *A. thaliana* seedlings. **(A)** Set diagram of miRNAs that differ between light input and dark input samples, and between light RISC-loaded and dark RISC-loaded samples. Arrows indicate the direction of change in light vs. dark comparison in inputs (red) or RISC-loaded samples (black). **(B)** Nuclear and cytoplasmic fractions were separated from crude extracts of dark-grown (Dark) and de-etiolated (Light) seedlings. RNA and protein samples were isolated from the cytoplasmic fraction (C), the third wash (W#3), and the isolated nuclei (N) and then subjected to Western and Northern analysis. AGO1, nuclear control histone H3, and cytoplasmic control actin proteins were detected. miR168 and miR159b were detected by Northern hybridization. To quantify the distribution, the ratios of cytoplasmic and nuclear signals (C/N) of the light and dark samples were calculated and compared (from three replicas). C/N mean values and ± standard deviations are shown. The C/N values were not significantly different between dark and light samples (see *p*-values).

AGO-loading efficiency of these miRNAs can be different in dark-grown and de-etiolated seedlings. Different AGO loading can compensate for the significantly different accumulation of miRNAs in the inputs and stabilize the active miRNA levels during de-etiolation (miR842, miR5654-3p, miR1886.1, and miR779.2) or could lead to significantly different active miRNA amounts even though that the input levels were similar (miR824-5p, miR156f-3p, miR5651, miR396b-5p, miR168a-5p, and miR157b-5p). Six miRNAs were present in significantly different amounts in both the inputs and RISC-loaded samples (miR773a, miR408-5p, miR319a, miR167d, miR399c-3p, and miR163) (**Figure 4A** and **Supplementary Table 2C**). In five of them (miR773a, miR408-5p, miR319a, miR167d, and miR399c-3p), the differences were similar, thus these miRNAs are loaded onto RISC with similar efficiency in dark-grown and de-etiolated seedlings. By contrast, miR163 was loaded onto RISC much more effectively in light; miR163 was 20-fold more abundant in the light input relative to the dark input, while the difference was increased to 109.6-fold at RISC-loaded samples (**Supplementary Table 2C**). Similar results were obtained when the RISC-loading efficiency was measured by comparing RISC-loaded miRNA values/input miRNA values in dark and light samples (**Supplementary Figure 3**).

Taken together, RISC-loading efficiencies are similar for most miRNAs in both dark-grown and de-etiolate seedlings, moderately changed for certain miRNAs, and considerably increased for miR163.

Argonaute 1 and MicroRNAs Are Similarly Partitioned in Dark-Grown and De-Etiolated Plants

Previous comparative miRNAome, transcriptome, and degradome studies indicated that miRNA cleavage activity is increased in de-etiolated plants (Lin et al., 2017). As our results show that both total and RISC-loaded miRNAomes (except miR163) are similar in dark-grown and de-etiolated seedlings, it is unlikely that more efficient RISC-loading leads to more intense cleavage in light. Light stimulated cleavage could be explained if the nucleocytoplasmic shuttling protein AGO1 and the AGO1-loaded miRNAs are more efficiently exported from the nucleus in de-etiolated plants. To test this assumption, cytoplasmic and nuclear fractions were separated from crude extracts of dark-grown and de-etiolated plants, and then AGO1 protein and miR168 and miR159 levels were studied in the fractions (miR163 was not analyzed as it is not detectable in the dark samples). The fractionation was efficient, and the nuclear and the cytoplasmic control proteins (H3 and actin) were only present in the corresponding fractions (**Figure 4B**). Relevantly, we found that nuclear-cytoplasmic distribution of AGO1 was not significantly different in the dark-grown and de-etiolated plants (although it was slightly overrepresented in the cytoplasm in light). Moreover, miR168 and miR159 were also comparably partitioned (**Figure 4B**). These data do not support the model that different distribution of AGO1 and AGO1-loaded miRNAs would be responsible for the proposed light-enhanced miRNA activity.

DISCUSSION

Previous studies reported conflicting results about the role of miRNAs in the regulation of photomorphogenesis. While findings that miRNA biogenesis factors and certain miRNAs are required for normal photomorphogenesis and that miRNA-guided RISC cleavage activity is increased during de-etiolation indicate that miRNA regulation plays an important role in the control of photomorphogenesis, and the results that the total miRNAome is only slightly changed during de-etiolation suggest that miRNAs do not play a critical regulatory role (Choi et al., 2020; Li et al., 2021). These studies compared total miRNAomes during de-etiolation supposing that it represents the functional miRNAome. However, RISC-loading is regulated in *Arabidopsis*, thus RISC-loaded miRNAome could be different from total miRNAome (Dalmadi et al., 2019). Therefore, we compared the changes in the total miRNAome and the RISC-loaded miRNAome during photomorphogenesis. RISC-loaded miRNAome was selected by isolating miRNAs that co-fractionated with AGO1 (**Figure 1**). The previous study has shown (and our study supports) that miRNAs are present in miRNA duplex form in the low mol. weight fractions or in the AGO1 containing high mol. weight fractions (Dalmadi et al., 2019). This suggests that most miRNAs are loaded onto AGO1 and/or that, all miRNA harboring RISCs accumulate in the high mol. weight fractions even if they contain different AGOs (except AGO4 that contains siRNAs and accumulates in the medium weight fractions). It is proposed (Dalmadi et al., 2019) that AGO1-containing fractions represent the biologically active miRNA pool, thus sequencing of these fractions is an efficient method to characterize the active, RISC-loaded miRNAome (see at the end of the discussion the limitation of the method).

In line with other studies (Choi et al., 2020; Li et al., 2021), we found that total miRNAome altered modestly during de-etiolation, miRNA163 was dramatically upregulated, while few other miRNAs show only moderate changes (**Figure 2**). These subtle expression differences are not easily reproducible, for instance, a recent study reported that only miR163 showed significantly different expression during photomorphogenesis (Li et al., 2021), while we and others found that many miRNAs expressed weakly but significantly different between dark-grown and de-etiolated plants (Choi et al., 2020). The differences in the experimental setup and growing conditions (for instance, we used 8 days dark-grown seedlings while another similar study used 5 days old dark-grown plants) might be responsible for the inconsistencies (Choi et al., 2020). Interestingly, while seedling de-etiolation, which mimics reaching the soil surface, leads to moderate total miRNAome changes, 3 days of dark treatment of long day adapted plant, which simulates reburial, results in a dramatic reduction in miRNA expression (Achkar et al., 2018). While de-etiolation leads to the accumulation of microprocessor components in mainly inhibited complexes, dark shift results in the rapid reduction of HYL1 protein levels (Achkar et al., 2018; Park et al., 2021; Jung et al., 2022).

If RISC-loading is regulated during de-etiolation, the RISC-loaded miRNAomes of dark-grown and de-etiolated

plants should be more different than the total miRNAomes. However, we have found that the RISC-loaded miRNAomes of dark-grown and de-etiolated seedlings are similar (**Figure 3** and **Supplementary Table 2A**), suggesting that RISC-loading efficiency is changed only slightly during photomorphogenesis. miR163 was the exception, it was RISC-loaded much more efficiently in the de-etiolated plant. RISC-loading altered the representation of 10 miRNAs slightly but significantly (**Figure 4A**), four were differentially present in the total miRNAomes but not in the RISC-loaded miRNAome, while six miRNAs were significantly differentially represented only in the RISC-loaded miRNAomes. These data suggest that during de-etiolation, regulated RISC-loading does not fundamentally control the formation of biologically active miRNAome (except miR163, see below) but could contribute to the fine-tuning of miRNA expression. If the export of RISC-loaded miRNAs from the nucleus is more effective in de-etiolated plants, the increased target cleavage activity in the de-etiolated seedlings could be explained even if the RISC-loaded miRNAomes of dark-grown and de-etiolated plants are similar. However, we found that AGO1 and the two studied miRNAs (miR159 and miR168) were present in a comparable amount in the nuclear and cytoplasmic fractions in both the dark-grown and de-etiolated samples (**Figure 4B**). These data suggest that AGO-loaded miRNA export operates similarly during de-etiolation. High-throughput sequencing of nuclear and cytoplasmic fractions during de-etiolation could confirm this conclusion. Taken together, our results indicate that neither regulated RISC-loading nor differences in nuclear export of RISC cannot explain the apparent conflict between the modest miRNAome changes during de-etiolation and the relevant role of miRNA biogenesis factors in normal photomorphogenesis (Sun et al., 2018). Further studies are required to clarify whether miRNA-based regulation is not important for photomorphogenesis or several subtle changes in miRNA expression, loading, and export are physiologically relevant and required for the fine-tuning of gene expression during de-etiolation.

It might be surprising as regulated RISC-loading plays a critical role in forming leaf and flower-specific active miRNAomes (Dalmadi et al., 2019). However, miRNA regulation likely plays a more important role in the control of leaf and flower development than in de-etiolation, thus their biologically active miRNAomes should be more different. Indeed, the total miRNAome was already far different between leaves and flowers and it was further modified by organ-specific regulated RISC-loading (Dalmadi et al., 2019).

MiR163 was an exception, as RISC-loading of miR163 is much more efficient in de-etiolated than in the dark-grown plants. miR163 is a highly specific miRNA; it is an evolutionary young 24 nt long miRNA, whose expression is dramatically enhanced during de-etiolation (Chung et al., 2016; Choi et al., 2020; Li et al., 2021). This increased expression is required for normal photomorphogenesis, and miR163-mediated silencing of PXMT1 methyltransferase promotes primary root growth (Chung et al., 2016; Li et al., 2021). miR163 overexpression during de-etiolation is regulated at different steps including transcriptional activation (Choi et al., 2020) and more efficient RISC-loading (this study). Pri-miR163 is increased to a much higher level (>100-fold) than any other pri-miRNA during de-etiolation (Choi et al., 2020). Its transcription is dramatically activated because the miR163 promoter contains strong binding sites for LONG HYPOCOTYL 5 (HY5) light-activated transcription factor (Li et al., 2021). We found that it was overrepresented >5-fold in the RISC-loaded miRNAome relative to the total miRNAome in the de-etiolated sample (but not in the dark-grown plant) showing that the RISC-loading efficiency of miR163 is much higher in light (**Figure 3**, **Supplementary Figure 3**, and **Supplementary Table 2C**). We propose that a high active miR163 level is required for normal photomorphogenesis and that the enhanced RISC-loading of miRNA163 plays a critical role to reach this high miR163 concentration. RISC-loading efficiency depends on (i) how effectively the miRNA incorporates into RISC and on (ii) the stability of the miRNA in the RISC complex. It was suggested that in light, the degradation of many miRNAs is accelerated, while the stability of miR163 is not altered (Choi et al., 2020). If RISC-loaded miRNA163 is much more stable in light than the other RISC-loaded miRNAs, it could explain the overrepresentation of miRNA163 in the de-etiolated miRNAome. A more likely (but not mutually exclusive) explanation is that RISC incorporation of miR163 is increased in de-etiolated plants. RISC-loading efficiency has been studied only for miR168. It was shown that the secondary structure of precursor RNA defines the efficiency of RISC incorporation (Dalmadi et al., 2021). A light-dependent factor may modify the splicing or secondary structure formation of miR163 precursor, thereby facilitating the incorporation of miRNA163 into RISC in de-etiolated plants. Indeed, the miR163 precursor is unusually long and its splicing is required for efficient miRNA generation (Bielewicz et al., 2013).

Characterization of Active miRNAome

This study is based on the assumption that miRNAs that co-fractionate with AGO1 are present in active RISC complexes. However, a fraction of them may be present in (same-sized) other complexes (Dalmadi et al., 2019). Moreover, as the crude extracts contain both cytoplasmic and nuclear components, part of miRNAs in the high mol. weight gel-filtrated fractions could be present in inactive, nuclear RISC complexes. Although our assays suggest that the export of RISC-loaded miRNA act with similar efficiency in dark-grown and de-etiolated plants, it might be different under other experimental conditions. Thus, separation of cytoplasmic fraction followed by gel-filtration might be a more accurate approach to identify active miRNAome. An alternative way to identify active miRNAome is AGO1 IP and sequencing of co-immunoprecipitated sRNAs (AGO1 RIP-seq) (Trolet et al., 2019). Both methods have advantages and disadvantages, AGO1 RIP-seq is selective but fails to detect miRNAs that are present in other AGOs, while gel-filtration could contain all AGO-bound miRNAs but it is less selective (Dalmadi et al., 2019). As it is not known, which AGOs play important role in de-etiolation, we choose the more general gel-filtration method to select the active miRNAome.

DATA AVAILABILITY STATEMENT

The datasets presented in this study can be found in online repositories. The names of the repository/repositories and accession number(s) can be found below: https://www.ncbi.nlm.nih.gov/, PRJNA795329.

AUTHOR CONTRIBUTIONS

LL and FN designed the study. LL conducted the experiments. GG and LL analyzed the sequencing data. LL, DS, and FN wrote the manuscript. All authors contributed to the article and approved the submitted version.

FUNDING

This work was supported by grants from the Hungarian Scientific Research Fund (K-132633, K-138022, K-136513, and K-139349). GG was supported by the National Research, Development and Innovation Office of Hungary, GINOP-2.2.1-15-2016-00007, and Géza Hetényi (5S 269 A202) research grants.

ACKNOWLEDGMENTS

We would like to thank Lajos Pinter (BRC, Szeged, Hungary) for helping with data analyses and Gabriella Szabo (BRC, Szeged, Hungary) for technical assistance.

SUPPLEMENTARY MATERIAL

The Supplementary Material for this article can be found online at: https://www.frontiersin.org/articles/10.3389/fpls.2022.854869/full#supplementary-material

Supplementary Figure 1 | MiR163, miR159b, and miR168 are associated with AGO1. **(A,B)** Shows the remaining two replicas of **Figure 1C**, therefore the description is as in **Figure 1C**. Statistical analysis of the three replicas is provided in **Figure 1C**.

Supplementary Figure 2 | Principal component analysis (PCA) of total miRNAome and RISC-loaded miRNAome of dark-grown and de-etiolated *Arabidopsis* seedling. PCA shows that the four miRNAomes are well separated. High throughput miRNA sequencing was conducted from crude extracts of dark-grown and de-etiolated seedlings (D. input and L. input, respectively) and from AGO1-containing fractions of gel-filtrated D and L samples (D. RISC-loaded and L. RISC-loaded).

Supplementary Figure 3 | Regulated RISC-loading moderately controls the active miRNAome. **(A,B)** To illustrate the role of regulated RISC-loading in the formation of active, AGO-loaded miRNAome, the RISC-loaded miRNA mean value/Input miRNA mean values of de-etiolated (Light) and dark-grown (Dark) seedlings were compared and the results are presented in **(A)** heat-map and **(B)** relative miRNA distribution forms.

Supplementary Figure 4 | Distribution of AGO1 and miRNAs in the crude extracts of *A. thaliana* seedlings. Nuclear and cytoplasmic fractions were separated from crude extracts of dark-grown (Dark) and de-etiolated (Light) seedlings. RNA and protein samples were isolated from the cytoplasmic fraction (C), the third wash (W#3), and the isolated nuclei (N) and then subjected to Western and Northern analysis. AGO1, nuclear control histone H3, and cytoplasmic control actin proteins were detected. miR168 and miR159b were detected by Northern hybridization. Statistical analysis of the three replicas is provided in **Figure 4B**.

Supplementary Table 1 | (A) Shows miRNAs identified by RNA-seq in all samples. We presented four replicate samples from each condition (RISC light sample replicates 1–4, RISC dark sample replicates 1–4, Input light sample replicates 1–4, and Input dark sample replicates 1–4). **(B)** Contains the list of miRNAs that were applied for analyses in our study. **(C)** Shows miRNA that was excluded from the analyses including miRNA*s. **(D)** Contains duplicated miRNAs. **(E)** displays those miRNAs that were excluded based on low abundance.

Supplementary Table 2 | miRNAs, whose expression is affected by de-etiolation. **(A,B)** List of miRNAs that are differentially present in the **(A)** inputs or **(B)** in the RISC-loaded samples of dark-grown and de-etiolated seedlings (dark and light, respectively). miRNAs with at least ± 2 fold difference are highlighted in red. FC, fold change. **(C)** miR163 is the only miRNA, which is overrepresented in both Input and RISC-loaded light samples **(A,B)**, in which RISC-loading is different in dark and light (FC value of **B**/FC value of **A**).

REFERENCES

Achkar, N. P., Cho, S. K., Poulsen, C., Arce, A. L., Re, D. A., Giudicatti, A. J., et al. (2018). A quick HYL1-dependent reactivation of MicroRNA production is required for a proper developmental response after extended periods of light deprivation. *Dev. Cell* 46, 236–247.e6. doi: 10.1016/j.devcel.2018.06.014

Azevedo, J., Garcia, D., Pontier, D., Ohnesorge, S., Yu, A., Garcia, S., et al. (2010). Argonaute quenching and global changes in dicer homeostasis caused by a pathogen-encoded GW repeat protein. *Genes Dev.* 24, 904–915. doi: 10.1101/gad.1908710

Bhagat, P. K., Verma, D., Singh, K., Badmi, R., Sharma, D., and Sinha, A. K. (2022). Dynamic phosphorylation of miRNA biogenesis factor HYL1 by MPK3 involving nuclear-cytoplasmic shuttling and protein stability in *Arabidopsis*. *Int. J. Mol. Sci.* 23:3787. doi: 10.3390/ijms23073787

Bielewicz, D., Kalak, M., Kalyna, M., Windels, D., Barta, A., Vazquez, F., et al. (2013). Introns of plant pri-miRNAs enhance miRNA biogenesis. *EMBO Rep.* 14, 622–628. doi: 10.1038/embor.2013.62

Bologna, N. G., Iselin, R., Abriata, L. A., Sarazin, A., Pumplin, N., Jay, F., et al. (2018). Nucleo-cytosolic shuttling of ARGONAUTE1 prompts a revised model of the plant MicroRNA pathway. *Mol. Cell* 69, 709–719.e5. doi: 10.1016/j.molcel.2018.01.007

Carbonell, A., and Carrington, J. C. (2015). Antiviral roles of plant ARGONAUTES. *Curr. Opin. Plant Biol.* 27, 111–117. doi: 10.1016/j.pbi.2015.06.013

Casal, J. J. (2012). Shade avoidance. *Arabidopsis Book* 10:e0157. doi: 10.1199/tab.0157

Chen, X. (2005). MicroRNA biogenesis and function in plants. *FEBS Lett.* 579, 5923–5931. doi: 10.1016/j.febslet.2005.07.071

Cheng, M.-C., Kathare, P. K., Paik, I., and Huq, E. (2021). Phytochrome signaling networks. *Annu. Rev. Plant Biol.* 72, 217–244. doi: 10.1146/annurev-arplant-080620-024221

Cho, S. K., Ben Chaabane, S., Shah, P., Poulsen, C. P., and Yang, S. W. (2014). COP1 E3 ligase protects HYL1 to retain microRNA biogenesis. *Nat. Commun.* 5:5867. doi: 10.1038/ncomms6867

Choi, S. W., Ryu, M. Y., Viczián, A., Jung, H. J., Kim, G. M., Arce, A. L., et al. (2020). Light triggers the miRNA-biogenetic inconsistency for de-etiolated seedling survivability in *Arabidopsis thaliana*. *Mol. Plant* 13, 431–445. doi: 10.1016/j.molp.2019.10.011

Chung, P. J., Park, B. S., Wang, H., Liu, J., Jang, I.-C., and Chua, N.-H. (2016). Light-Inducible MiR163 targets PXMT1 transcripts to promote seed germination and primary root elongation in *Arabidopsis*. *Plant Physiol.* 170, 1772–1782. doi: 10.1104/pp.15.01188

Dalmadi, Á., Gyula, P., Bálint, J., Szittya, G., and Havelda, Z. (2019). AGO-unbound cytosolic pool of mature miRNAs in plant cells reveals a novel

regulatory step at AGO1 loading. *Nucleic Acids Res.* 47, 9803–9817. doi: 10.1093/nar/gkz690

Dalmadi, Á., Miloro, F., Bálint, J., Várallyay, É., and Havelda, Z. (2021). Controlled RISC loading efficiency of miR168 defined by miRNA duplex structure adjusts ARGONAUTE1 homeostasis. *Nucleic Acids Res.* 49, 12912–12928. doi: 10.1093/nar/gkab1138

Danecek, P., Bonfield, J. K., Liddle, J., Marshall, J., Ohan, V., Pollard, M. O., et al. (2021). Twelve years of SAMtools and BCFtools. *Gigascience* 10:giab008. doi: 10.1093/gigascience/giab008

Deng, X. W., and Quail, P. H. (1999). Signalling in light-controlled development. *Semin. Cell Dev. Biol.* 10, 121–129. doi: 10.1006/scdb.1999.0287

Giner, A., Lakatos, L., Garcia-Chapa, M., Lopez-Moya, J., and Burgyán, J. (2010). Viral protein inhibits RISC activity by argonaute binding through conserved WG/GW Motifs. *PLoS Pathog.* 6:e1000996. doi: 10.1371/journal.ppat.1000996

Iwata, Y., Takahashi, M., Fedoroff, N. V., and Hamdan, S. M. (2013). Dissecting the interactions of SERRATE with RNA and DICER-LIKE 1 in *Arabidopsis* microRNA precursor processing. *Nucleic Acids Res.* 41, 9129–9140. doi: 10.1093/nar/gkt667

Jung, H. J., Choi, S. W., Boo, K.-H., Kim, J.-E., Oh, Y. K., Han, M. K., et al. (2022). HYL1-CLEAVAGE SUBTILASE 1 (HCS1) suppresses miRNA biogenesis in response to light-to-dark transition. *Proc Natl Acad Sci U S A.* 119:e2116757119. doi: 10.1073/pnas.2116757119

Kurihara, Y., and Watanabe, Y. (2004). *Arabidopsis* micro-RNA biogenesis through dicer-like 1 protein functions. *Proc. Natl. Acad. Sci. U.S.A.* 101, 12753–12758. doi: 10.1073/pnas.0403115101

Kurihara, Y., Takashi, Y., and Watanabe, Y. (2006). The interaction between DCL1 and HYL1 is important for efficient and precise processing of pri-miRNA in plant microRNA biogenesis. *RNA* 12, 206–212. doi: 10.1261/rna.2146906

Łabuz, J., Sztatelman, O., Banaś, A. K., and Gabryś, H. (2012). The expression of phototropins in *Arabidopsis* leaves: developmental and light regulation. *J. Exp. Bot.* 63, 1763–1771. doi: 10.1093/jxb/ers061

Langmead, B., Trapnell, C., Pop, M., and Salzberg, S. L. (2009). Ultrafast and memory-efficient alignment of short DNA sequences to the human genome. *Genome Biol.* 10:R25. doi: 10.1186/gb-2009-10-3-r25

Legris, M., Ince, Y. Ç., and Fankhauser, C. (2019). Molecular mechanisms underlying phytochrome-controlled morphogenesis in plants. *Nat. Commun.* 10:5219. doi: 10.1038/s41467-019-13045-0

Li, M., and Yu, B. (2021). Recent advances in the regulation of plant miRNA biogenesis. *RNA Biol.* 18, 2087–2096. doi: 10.1080/15476286.2021.1899491

Li, T., Lian, H., Li, H., Xu, Y., and Zhang, H. (2021). HY5 regulates light-responsive transcription of microRNA163 to promote primary root elongation in *Arabidopsis* seedlings. *J. Integr. Plant Biol.* 63, 1437–1450. doi: 10.1111/jipb.13099

Liao, Y., Smyth, G. K., and Shi, W. (2014). featureCounts: an efficient general purpose program for assigning sequence reads to genomic features. *Bioinformatics* 30, 923–930. doi: 10.1093/bioinformatics/btt656

Lin, M.-C., Tsai, H.-L., Lim, S.-L., Jeng, S.-T., and Wu, S.-H. (2017). Unraveling multifaceted contributions of small regulatory RNAs to photomorphogenic development in *Arabidopsis*. *BMC Genomics* 18:559. doi: 10.1186/s12864-017-3937-6

Love, M. I., Huber, W., and Anders, S. (2014). Moderated estimation of fold change and dispersion for RNA-seq data with DESeq2. *Genome Biol.* 15:550. doi: 10.1186/s13059-014-0550-8

Naqvi, A. R., Sarwat, M., Hasan, S., and Roychodhury, N. (2012). Biogenesis, functions and fate of plant microRNAs. *J. Cell Physiol.* 227, 3163–3168. doi: 10.1002/jcp.24052

Park, S. J., Choi, S. W., Kim, G. M., Møller, C., Pai, H.-S., and Yang, S. W. (2021). Light-stabilized FHA2 suppresses miRNA biogenesis through interactions with DCL1 and HYL1. *Mol. Plant* 14, 647–663. doi: 10.1016/j.molp.2021.01.020

Sacnun, J. M., Crespo, R., Palatnik, J., Rasia, R., and González-Schain, N. (2020). Dual function of HYPONASTIC LEAVES 1 during early skotomorphogenic growth in *Arabidopsis*. *Plant J.* 102, 977–991. doi: 10.1111/tpj.14681

Shikata, H., Hanada, K., Ushijima, T., Nakashima, M., Suzuki, Y., and Matsushita, T. (2014). Phytochrome controls alternative splicing to mediate light responses in *Arabidopsis*. *Proc. Natl. Acad. Sci. U.S.A.* 111, 18781–18786. doi: 10.1073/pnas.1407147112

Smith, T., Heger, A., and Sudbery, I. (2017). UMI-tools: modeling sequencing errors in unique molecular identifiers to improve quantification accuracy. *Genome Res.* 27, 491–499. doi: 10.1101/gr.209601.116

Sun, Z., Li, M., Zhou, Y., Guo, T., Liu, Y., Zhang, H., et al. (2018). Coordinated regulation of *Arabidopsis* microRNA biogenesis and red light signaling through dicer-like 1 and phytochrome-interacting factor 4. *PLoS Genet.* 14:e1007247. doi: 10.1371/journal.pgen.1007247

Trolet, A., Baldrich, P., Criqui, M.-C., Dubois, M., Clavel, M., Meyers, B. C., et al. (2019). Cell cycle-dependent regulation and function of ARGONAUTE1 in plants. *Plant Cell* 31, 1734–1750. doi: 10.1105/tpc.19.00069

Wang, J., Mei, J., and Ren, G. (2019). Plant microRNAs: biogenesis, homeostasis, and degradation. *Front. Plant Sci.* 10:360. doi: 10.3389/fpls.2019.00360

Xie, Z., Khanna, K., and Ruan, S. (2010). Expression of microRNAs and its regulation in plants. *Semin. Cell Dev. Biol.* 21, 790–797. doi: 10.1016/j.semcdb.2010.03.012

Yang, L., Liu, Z., Lu, F., Dong, A., and Huang, H. (2006). SERRATE is a novel nuclear regulator in primary microRNA processing in *Arabidopsis*. *Plant J.* 47, 841–850. doi: 10.1111/j.1365-313X.2006.02835.x

Yu, B., Yang, Z., Li, J., Minakhina, S., Yang, M., Padgett, R. W., et al. (2005). Methylation as a crucial step in plant microRNA biogenesis. *Science* 307, 932–935. doi: 10.1126/science.1107130

Yu, Y., Jia, T., and Chen, X. (2017). The "how" and "where" of plant microRNAs. *New Phytol.* 216, 1002–10017. doi: 10.1111/nph.14834

Conflict of Interest: The authors declare that the research was conducted in the absence of any commercial or financial relationships that could be construed as a potential conflict of interest.

Publisher's Note: All claims expressed in this article are solely those of the authors and do not necessarily represent those of their affiliated organizations, or those of the publisher, the editors and the reviewers. Any product that may be evaluated in this article, or claim that may be made by its manufacturer, is not guaranteed or endorsed by the publisher.

frontiers | Frontiers in Plant Science

TYPE Original Research
PUBLISHED 23 September 2022
DOI 10.3389/fpls.2022.976449

OPEN ACCESS

EDITED BY
Jordi Moreno-Romero,
Universitat Autònoma de Barcelona,
Spain

REVIEWED BY
Shengguan Cai,
Zhejiang University, China
Feng Xu,
Yangtze University, China

*CORRESPONDENCE
Hongbin Wang
wanghongbing@gzucm.edu.cn
Qi Shen
shenqi@gzucm.edu.cn

SPECIALTY SECTION
This article was submitted to Plant Physiology, a section of the journal Frontiers in Plant Science

RECEIVED 23 June 2022
ACCEPTED 22 August 2022
PUBLISHED 23 September 2022

CITATION
Xie G, Zou X, Liang Z, Wu D, He J, Xie K, Jin H, Wang H and Shen Q (2022) Integrated metabolomic and transcriptomic analyses reveal molecular response of anthocyanins biosynthesis in perilla to light intensity. *Front. Plant Sci.* 13:976449. doi: 10.3389/fpls.2022.976449

Integrated metabolomic and transcriptomic analyses reveal molecular response of anthocyanins biosynthesis in perilla to light intensity

Guanwen Xie, Xiuzai Zou, Zishan Liang, Duan Wu, Jiankuang He, Kaicheng Xie, Honglei Jin, Hongbin Wang* and Qi Shen*

Institute of Medical Plant Physiology and Ecology, School of Pharmaceutical Sciences, Guangzhou University of Chinese Medicine, Guangzhou, China

The perilla anthocyanins have important medicinal and ornamental value, and their contents are significantly affected by light intensity. In view of their molecular mechanisms were not well understood, we integrated the metabolomic and transcriptomic analyses of the light-sensitive perilla variety under different light intensity. The perilla leave color were obviously affected under different treatments. Totally 140 flavonoid metabolites and 2461 genes showed steady change, among which 60 flavonoid metabolites were increased accumulation and 983 genes were upregulated expression under elevated light intensity treatment. Light treatment prominently affected the expression of genes involved in the main anthocyanin metabolites accumulation in perilla leaves. Using WGCNA analysis, we identified 4 key genes in anthocyanin biosynthesis pathway (*CHI*, *DFR,* and *ANS*) and 147 transcription factors (*MYB, bHLH, bZIP, ERF, and NAC*) involved in malonylshisonin biosynthesis. Among them, 6 MYBs and 4 bZIPs were predicted to play important roles in light regulation of malonylshisonin biosynthesis based on phylogenetic construction, correlation analysis, *cis*-acting element identification and qPCR verification. The identified key genes and regulatory factors will help us to understand the potential mechanism of photo-regulated anthocyanin accumulation in perilla.

KEYWORDS

***Perilla frutescens*, metabolomic, transcriptomic, photoinduced, weighted gene co-expression network analysis (WGCNA), transcription factor**

Introduction

Light is essential for plant growth and plays a key environmental factor regulating plant development. The intensity, quality, periodicity, and direction of light directly affect the biosynthesis of metabolites in plants. The influence of light on anthocyanin formation plays an important role in controlling the color of fruits such as grape (Azuma et al., 2012), eggplant (Jiang et al., 2016) and apple (Feng et al., 2013).

Anthocyanins, the largest group of natural water-soluble plant pigments, are widely present in flowers, fruits, leaves, and tubers in the plant kingdom (Chen et al., 2012). Anthocyanins are phenolic compounds containing C6-C3-C6 hydroxyl aromatic rings as a basic skeleton (Kong et al., 2003). The type and final color of anthocyanin are determined by its main backbone and the positions, quantities, and structures of conjugated sugars and covalent modifications (Kocic et al., 2011; Liu Y. et al., 2018). The major anthocyanins include cyanidin, delphinidin, malvidin, pelargonidin, peonidin, and petunidin, as well as their derivatives (Kong et al., 2003; Zhao et al., 2014; Khoo et al., 2017). Anthocyanins are important ingredients of healthy foods, with medicinal value for preventing neurological and cardiovascular diseases, cancer, diabetes, and age-related degenerative diseases (Kong et al., 2003; Zhao et al., 2014; Khoo et al., 2017). Hence, anthocyanins have attracted extensive attention worldwide in recent years.

Perilla frutescens (L.) is an annual herb in the Lamiaceae. Perilla has been widely cultivated in China for more than 2000 years and is currently cultivated in Korea, Japan, and other Asian countries (Nitta et al., 2005a). Perilla is used as traditional herb, oil crops and popular spice. This main medicinal value of perilla is listed in the Chinese Pharmacopeia, including anti-oxidant (Saita et al., 2012), antibacterial (Yamamoto and Ogawa, 2002), anti-inflammatory (Yang et al., 2013; Huang et al., 2014), cough-suppressing (Ahmed, 2019), lipid-lowering, and antitumor properties (Lin et al., 2007). Perilla is divided into red perilla and green perilla according to plant color. Besides its medicinal value, red perilla is also used as an ornamental plant due to its dark red leaves and stems. The red pigment of perilla leaves is also widely used as a food coloring, cosmetic additive, and medicinal compound.

Malonylshisonin [cyanidin 3-*O*-(6”-*O*-(E)-*p*-coumaryl)-β-D-glucopyranoside-5-*O*-(6”’-*O*-malonyl)-β-D-glucopyranoside], an unique and major cyanindin-type anthocyanin, was identified in red perilla (Honda et al., 1994; Saito and Yamazaki, 2002; Fujiwara et al., 2018; Jiang et al., 2020). They possessed antioxidant and anti-allergy properties in previous research (Makino et al., 2003; Meng et al., 2006). The biosynthetic pathway of malonylshisonin was recently elucidated. The basic anthocyanin steps involved in 4-coumaroyl-CoA were catalyzed to form cyanidin. The main steps were catalyzed by chalcone synthase (CHS), chalcone isomerase (CHI), flavanone 3-hydroxylase (F3H), flavonoid 3’-hydroxylase (F3’H), dihydroflavonol 4-reductase (DFR), and anthocyanin synthase (ANS). Whereafter, the cyanidin is converted to malonylshisonin via a process catalyzed by flavonoid 3-glucosyltransferase (3-GT), anthocyanin acyltransferase (ACT), anthocyanin 5-glucosyltransferase (5-GT), and anthocyanin malonyltransferase (MAT) (Saito and Yamazaki, 2002; Jiang et al., 2020; Zhou et al., 2021). As previous research in other plants, anthocyanin biosynthesis is regulated by the MBW ternary transcriptional complex (R2R3-MYB, basic helix-loop-helix [bHLH], and WD40 repeat protein [WDR]) (Holton and Cornish, 1995; Feng et al., 2010; Lloyd et al., 2017), basic leucine zipper (bZIP) (An et al., 2017), and MYC transcription factors.

Light could induce anthocyanin accumulation in perilla leaves. In a previous study of red perilla, anthocyanin accumulation and the expression of anthocyanin biosynthetic genes in leaves were lower under weak vs. strong light conditions (Zheng et al., 2019). However, the molecular mechanisms underlying light-induced anthocyanin biosynthesis in perilla remain unknown. Here, we explored anthocyanin biosynthesis and the mechanism of its photoinduction in red perilla using a light-sensitive cultivated variety. We treated the plants with different light intensities and analyzed the regulatory networks of anthocyanin biosynthesis and accumulation by performing comprehensive metabolomic and transcriptomic analyses. Our findings shed light on the putative molecular regulation of photoinduced anthocyanin accumulation in red perilla.

Materials and methods

Plant materials and treatments

In our previous work, we planted more perilla varieties in light incubator and found that the plant color of ’PF899’ variety was more sensitive to light intensity. The variety is extremely sensitive to changes in light intensity, with green leaves in weak light and dark red leaves in increased light intensity. Hence, the light-sensitive perilla variety was selected in the study. After germination, the plants were grown in a greenhouse at the Guangzhou University of Chinese Medicine in Guangdong province, China (23°3’N, 113°23’E) under a weak light intensity (WL; 15 μmol/m^2) until the three-leaf stage. The plants were transferred to moderate light (ML; 180 μmol/m^2) for 6 days, followed by transfer to weak light (15 μmol/m^2) for 6 days (recovery light conditions, RL). The plants were grown under a 12 h/12 h light/dark photoperiod and fertilized according to standard practices. Each treatment group was treated with three pots, each pot had five plants. Three biological replicates were performed for each treatment group. The leaves from three treatments were collected, immediately frozen in liquid nitrogen, and stored at –80°C for metabolomic and transcriptomic analysis. And in transcriptome analysis,

a group of materials at moderate light (ML; 180 μmol/m2) for 12 h was added.

Measuring total anthocyanin and flavonoid contents

Leaves from different treatment groups were weighed and pulverized. To measure total anthocyanins, each 0.1 g leaf tissue sample was combined with 0.1% hydrochloric acid methanol reagent and incubated at 40°C for 40 min to extract total anthocyanins. The optical densities at 530, 620, and 650 nm were measured with a UV spectrophotometer; 0.1 mol/L hydrochloric acid methanol solution was used as a blank control. Total anthocyanin content was calculated according to Greey's formula (Lee and Ohnishi, 2003; Nitta et al., 2005b). To measure total flavonoids, perilla leaf powder was combined with an equal volume of 70% ethanol, and 1 mL of the extract and 1 mL of 5% sodium nitrite solution were added to a volumetric bottle. After shaking well for 6 min, 1 mL of 10% aluminum nitrate test solution was added to the flask, which was then mixed for 6 min. After adding 10 mL of sodium hydroxide test solution, the sample was mixed. Finally, 70% ethanol was added to bring the volume to 25 ml. After 15 min, the absorbance of the sample at 500 nm was measured by UV-vis spectrophotometry with 70% ethanol as a blank control. The rutin was used as the standard curve to calculate the content of total flavonoids.

Metabolomics sample preparation and detection

The freeze-dried samples were crushed, and 100 mg of powdered tissue was combined with 1.2 mL of 70% methanol. After centrifuging at 12,000 rpm for 10 min, the extracts were filtered (SCAA-104, 0.22 μm pore size), and the metabolites in the extracts were analyzed used an UPLC-ESI-MS/MS system (UPLC, SHIMADZU Nexera X2; MS, Applied Biosystems 4500 Q TRAP). The conditions were as follows: UPLC: column, Agilent SB-C18 (1.8 μm, 2.1 mm * 100 mm). The mobile phase consisted of solvent A (pure water with 0.1% formic acid) and solvent B (acetonitrile with 0.1% formic acid). Sample measurements were performed with a gradient program. The column temperature was set to 40°C and the injection volume was 4 μL. The effluent was alternatively connected to an ESI-triple quadrupole-linear ion trap (QTRAP)-MS. LIT, and triple quadrupole (QQQ) scans were acquired on a triple quadrupole-linear ion trap mass spectrometer (Q TRAP), AB4500 Q TRAP UPLC/MS/MS System, equipped with an ESI Turbo Ion-Spray interface, operating in positive and negative ion mode, and controlled by Analyst 1.6.3 software (AB Sciex). The ESI source operation parameters were as follows: ion source, turbo spray; source temperature 550°C; ion spray voltage (IS) 5500 V (positive ion mode)/–4500 V (negative ion mode); ion source gas I (GSI), gas II (GSII), and curtain gas (CUR) were set at 50, 60, and 25.0 psi, respectively; the collision-activated dissociation (CAD) was high. Instrument tuning and mass calibration were performed with 10 and 100 μmol/L polypropylene glycol solution in QQQ and LIT mode, respectively. QQQ scans were acquired as multiple reaction monitoring (MRM) experiments with collision gas (nitrogen) set to moderate. Positive ion mode optimizes cluster removal voltage (DP) and Collision electric (CE) for individual MRM transitions were performed by further DP and CE optimization. A specific set of MRM transitions was monitored for each period based on the metabolites eluted within that period.

RNA sequencing and annotation

A Tiangen RNA Prep Pure Kit for Plants was used to extract total RNA from *P. frutescens* leaves. A NanoDrop 2000 spectrophotometer (Thermo Scientific, Wilmington, DE, United States) was used to measure total RNA concentration and quality. RNA samples that met the requirements were sent to Wuhan Bena Technology Service Co., Ltd. (Wuhan, China) for transcriptomic sequencing. RNA-seq libraries (*P. frutescens* leaves collected at WL, ML12 h, ML6d, and RL × 3 replicates) were constructed and sequenced using the Illumina HiSeq4000 platform, and clean reads were mapped to the perilla reference genome using HISAT with default parameters.

Identification of differential metabolites and differentially expressed genes

The metabolome data in this study was identified with chemical library MWDB (Metware Database), which were established by Metware Metabolism Company. Materials was quantitative based on secondary spectrum information, and isotope signals were removed during analysis, which contained K + ions and Na + ionsRepeated signals of NH4 + ions and fragments of other substances with larger molecular weight were identified. Metabolites with significantly different levels between groups were determined based on Variable Importance in Projection (VIP) ≥ 1 and absolute log2FC (fold change) ≥ 1. VIP values were extracted from the OPLS-DA results, and score plots and permutation plots were generated using the R package MetaboAnalystR. The data were log transformed (log2) and subjected to mean centering before OPLS-DA. To avoid overfitting, a permutation test (200 permutations) was performed. Gene expression levels were calculated as fragments per kilobase of transcript per million mapped reads (FPKM). Differentially expressed genes (DEGs) were identified from normalized read count data using DESeq2.34. Genes with $|\log2(\text{fold change})| \geq 1$ and $p < 0.01$ were considered to be DEGs.

Hierarchical cluster analysis, Pearson correlation coefficients, and principal component analysis

The HCA (hierarchical cluster analysis) results of samples and metabolites were presented as heatmaps with dendrograms, while PCC (Pearson correlation coefficients) between samples were calculated by the core function in R and were presented only as heatmaps. Both HCA and PCC were carried out with the R package pheatmap. For HCA, normalized signal intensities of metabolites (unit variance scaling) were visualized as a color spectrum. Unsupervised PCA (principal component analysis) was performed using the statistics function prcomp within R[1]. The data were unit variance scaled prior to unsupervised PCA.

Gene ontology enrichment and Kyoto encyclopedia of genes and genomes enrichment analysis

The identified metabolites were annotated using the Kyoto Encyclopedia of Genes and Genomes (KEGG) Compound database[2]. Gene function annotation was performed using four databases: National Center for Biotechnology Information (NCBI[3]), non-redundant protein sequences (NR[4]), the Swiss-Prot protein sequence database, and Gene Ontology (GO[5]). The annotated metabolites and genes were then mapped to the KEGG Pathway database[6]. Pathways with significantly regulated metabolites were subjected to MSEA (metabolite sets enrichment analysis), and their significance was determined based on *p*-values from hypergeometric tests. Finally, the DEGs in the WL, ML12h, ML6d, and RL groups were subjected to GO and KEGG pathway enrichment analysis.

Weighted gene co-expression network analysis of metabolome and transcriptomic data

The weighted gene co-expression network analysis (WGCNA) package was used to generate co-expression network modules between metabolites and genes. Using the automatic network construction function (blockwise Modules) with default parameters, co-expression modules were obtained based on TOM (topological overlap measure). The initial clusters were merged on eigengenes. The eigengene value was calculated for each module and used to search for associations with key anthocyanin substances. The transcriptional regulatory networks were generated by combining the Pearson correlation coefficient (PCC > 0.85) between genes and transcription factors, and the *cis*-element binding sites were predicted in the promoter regions of key anthocyanin genes in the same module. The networks were visualized by CYTOSCAPE (v.3.7.2, United States) (Kohl et al., 2011).

Phylogenetic analysis

The conservative domain of the candidate MYBs and bZIPs from perilla and other plants were used to construct phylogenetic. Accession numbers of MYBs and bZIPs from other plants are shown in **Supplementary Table S8**. The neighbor-joining (NJ) tree was constructed using the poison model with MEGA-X with 1000 bootstrap replicates. The phylogenetic trees were visualized using the iTOL web tool[7].

Quantitative reverse-transcription PCR

Quantitative reverse-transcription PCR was performed as previously described (Livak and Schmittgen, 2001). Total RNA was isolated from the samples using a MAGEN RNA Extraction Kit (MAGEN, United States), and reverse transcription was performed using an Evo M-WLV RT Kit (Accurate, Hunan, China). Primers for each gene (*ANS*, *CHI*, *DFR*, and so on) were designed using Primer 5.0; the primers are listed in **Supplementary Table S9**. The specificity of the primers was verified by agarose gel electrophoresis. PCR amplification was performed using a LightCycler 480 II REAL-TIME PCR system (Roche, Basel, Switzerland). The qPCR cycling conditions were 1 cycle of pre-denaturation at 95°C, 30 s; 40 cycles of 95°C for 5 s and 60°C for 30 s; dissolution at 95°C for 5 s; 60°C for 1 min. All genes were amplified with three replicates, and the perilla *Actin* gene was used as an internal reference gene.

Results

Various anthocyanin content of perilla under different light intensity treatments

To identify the leaves color and major pigment components under different light, we observed and measured the total anthocyanin and total flavonoid contents during different light intensity treatments. The perilla leaves color under different light intensities were obviously affected. The leaves and seedlings

1 www.r-project.org
2 http://www.kegg.jp/kegg/compound/
3 https://www.ncbi.nlm.nih.gov/
4 https://www.ncbi.nlm.nih.gov/refseq/about/nonredundantproteins
5 http://www.geneontology.org/
6 http://www.kegg.jp/kegg/pathway.html
7 http://itol.embl.de/index.shtml

of the light-sensitive red perilla variety were green when cultured under weak light intensity (15 μmol/m^2, WL). After transferring to moderate light intensity (180 μmol/m^2, ML) for 6 days, the leaves and whole plants turned dark red. When returned to weak light intensity for 6 days (15 μmol/m^2, RL), the leaf color gradually returned to partially green (**Figure 1A**). Like the changes of the leaf color, total anthocyanin and total flavone levels significantly increased under ML treatment and then decreased in RL compared with WL (**Figures 1B,C**). These results demonstrate that light intensity significantly affects the leaf color and the accumulation of total anthocyanins and total flavones in leaves of the light-sensitive perilla variety.

Metabolome detection under different light intensity treatments

To assess anthocyanin components under different light treatments, we performed metabolomic analysis using UPLC-ESI-MS/MS. The samples were clearly clustered by PCA (**Supplementary Figure S1**). In total, 293 flavonoid metabolites were identified, including 103 flavonols, 72 flavones, 34 anthocyanins, and 84 other derivatives (**Figure 2A**; **Supplementary Table S1**). There were 90, 55, and 81 differentially expressed metabolites (DEM) in WL vs. ML, ML vs. RL, and WL vs. RL, respectively (**Figure 2B**).

Quantitative analysis showed that approximately 140 (48%) flavonoid metabolites were affected under different light intensity treatments in perilla leaves. Among these, 62 metabolites were significantly induced under increased light intensity, including 23 flavonols, 19 flavones, and 5 anthocyanins (**Supplementary Table S2**). Among them, the contents of malonylshisonin increased 1.7-fold under ML treatment compared with WL and decreased 0.8-fold under RL treatment compared with ML (**Supplementary Table S3**). Naringin chalcone and dihydroquercetin (early intermediates in the anthocyanin biosynthesis pathway), as well as cyanidin-3,5-*O*-diglucoside, cyanidin-3-*O*-(6"-*O*-*p*-coumaryl) glucoside-5-*O*-glucoside, and cyanidin-3-*O*-(6"-*O*-*p*-coumaryl) glucoside (important precursors of malonylshisonin) were all detected in this study. Interestingly, the levels of naringin chalcone, dihydroquercetin, and cyanidin-3-*O*-(6"-*O*-*p*-coumaryl) glucoside increased by 4. 3-, 5. 8-, and 3.2-fold (**Supplementary Table S3**), respectively, under ML treatment compared with WL. By contrast, the cyanidin-3,5-*O*-diglucoside contents decreased by 0.6-fold under ML treatment compared with WL. These results suggest that light intensity affects accumulation of the metabolites in anthocyanin biosynthesis pathway in perilla.

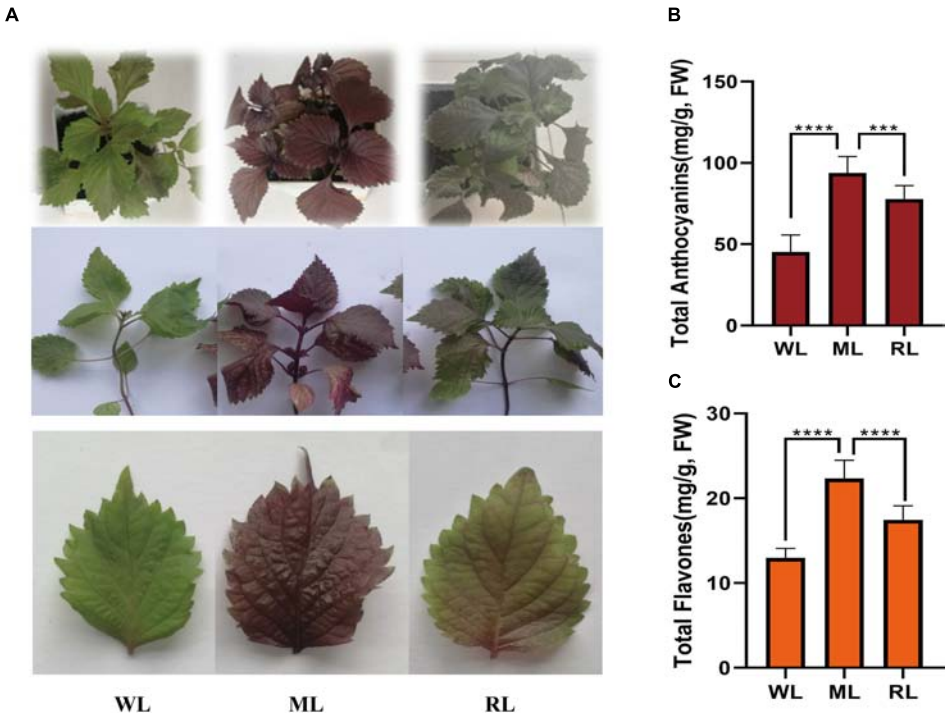

FIGURE 1
Leaf color, anthocyanin, and flavone contents of perilla under different light intensity treatments. **(A)** Phenotypes of perilla. **(B)** Total anthocyanin contents of perilla leaves. **(C)** Total flavone contents of perilla leaves under WL, weak light; ML, moderate light for 6 days; RL, recovered weak light for 6 days. **** Indicates *P* value < 0.0001.

10.3389/fpls.2022.976449

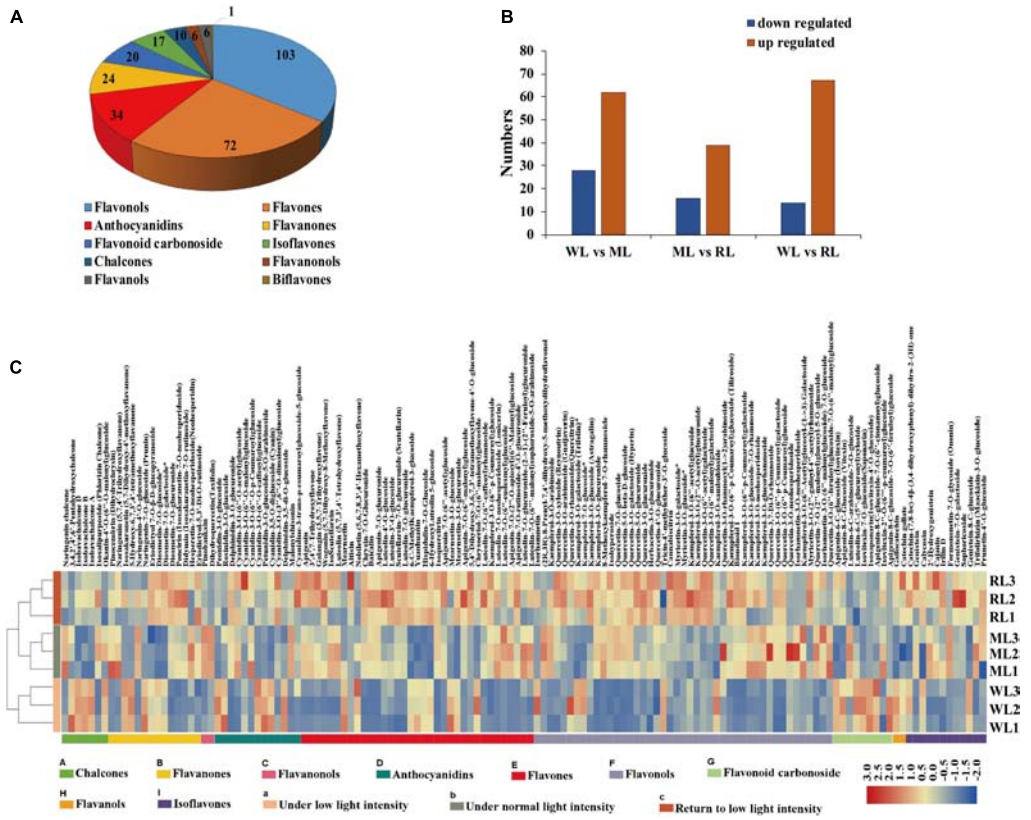

FIGURE 2
The flavonoid metabolites of perilla leaves under different light intensity treatments. **(A)** Types of flavonoid metabolites detected. **(B)** Differentially expressed metabolites (DEMs) in WL vs. ML6d, ML 6d vs. RL, and WL vs. RL. **(C)** Contents of flavonoid metabolites in perilla leaves under different light intensity treatments.

According to the change trends of flavonoid metabolites under different treatments, they were divided into eight categories. The levels of subclass 4 and subclass 7 members initially increased, then decreased, possessed consistent pattern with total anthocyanin contents. Both malonylshisonin and naringin chalcone belong to subclass 7. The levels of subclass 2 and subclass 6 members continuously increased under ML and RL treatment (**Supplementary Figure S2**). The cyanidin-3-*O*-(6''-*O*-*P*-coumaryl) glucoside-5-*O*-glucoside and dihydroquercetin belong to subclass 2 and subclass 4, respectively. The four subclasses attracted our main attention.

Transcriptomic analysis under different light intensity treatments

To explore the molecular regulatory mechanism of the perilla anthocyanin metabolites in response to light intensity, we performed transcriptomic sequence. Considering the rapid response of transcriptomic level to light treatment, we added a short treatment (12 h) under 180 μmol/m^2 of light (ML12h). After RNA sequencing and data filtering, 701.64 million clean reads with 105 Gb clean data were obtained. The Q20 reached 97%, with an average GC content of 48%. When we mapped the sequencing reads to perilla reference genomes, we obtained an average unique mapping ratio of 82.94% and a multiple mapping ratio of 10.19% (**Supplementary Table S4**).

Subsequently, we identified DEGs among all samples. And most of DEGs were responsed to light intensity showing to the results of GO analysis (**Supplementary Figure S3**). Compared to the WL group, 3290 and 3026 genes were upregulated in ML12h and ML6d, respectively. Compared to the RL group, 4043 and 3219 genes were upregulated in ML12h and ML6d, respectively (**Figure 3A**). Among the upregulated genes under ML treatment, 983 genes showed increased expression under short (12 h) and long (6 days) treatments compared with WL (**Figure 3B**). These DEGs are mainly involved in metabolic pathways, phenylalanine and tyrosine tryptophan biosynthesis and phenylalanine metabolism in the KEGG enrichment (**Figure 3C**). By contrast, 1478 genes were downregulated in RL compared with ML (**Figure 3D**). The down-regulated genes were enriched in biosynthesis of secondary metabolites, phenylalanine and tyrosine tryptophan biosynthesis, tyrosine metabolism,

phenylalanine metabolism, and flavonoid biosynthesis in the KEGG enrichments (**Figure 3E**). Based on the expression pattern, we divided all DEGs into 26 categories (**Supplementary Figure S4**). The 983 and 1478 DEGs most belong to Profile 20 (upregulated in ML12h and ML6d compared with WL) and Profile 23 (downregulated in RL compared with ML12h and ML6d), respectively. These photo-response genes attracted our main attention.

The metabolites and key genes in the anthocyanin biosynthesis pathway

We identified metabolites and genes involved in the anthocyanin and flavones biosynthetic pathways (**Figure 4**). Malonylshisonin biosynthesis involves 10 catalytic reactions, containing the initial cyanidin biosynthesis and the latter cyanidin derivatization pathway (Saito and Yamazaki, 2002; Jiang et al., 2020). Naringin chalcone, dihydroquercetin, cyanidin-3,5-*O*-diglucoside, cyanidin-3-*O*-(6"-*O*-*p*-Coumaroyl) glucoside, cyanidin-3-*O*-(6"-*O*-*p*-Coumaroyl) glucoside-5-*O*-diglucoside, and malonylshisonin were identified in the metabolomic analysis. Except for cyanidin 3,5-*O*-glucoside, these metabolites obviously accumulated under increased light intensity. Then, we identified 95 genes encoding the 10 anthocyanin synthases in the malonyshisonin biosynthetic pathway (**Figure 4** and **Supplementary Table S5**). Furthermore, 32 genes were upregulated after light treatment, which encode the key rate-limiting enzymes in the basic anthocyanin biosynthetic pathway. Among these, 18 genes (including *PAL, 4CL, CHS, F3'H, ANS, 5-GT, and MAT*) were more strongly upregulated under 12 h ML treatment, and five genes (including *F3H, 3-GT, ACT, and CHI*) had higher expression levels under 6 days ML treatment. Only one *C4H* gene was expressed at high levels under both 12 h and 6 days ML treatments. These results suggest that light intensity remarkably influences the gene expression and metabolite accumulation involving in anthocyanin biosynthesis in perilla leaves.

Moreover, we identified 14 light-regulated flavones based on analysis of the flavonoid biosynthesis pathway. Most of these compounds accumulated under light treatment. Specifically, the contents of luteolin, apigenin, and baicalin increased by 5. 0-, 5. 4-, and 11.6-fold, respectively, under ML treatment compared with WL. Comparatively, the levels of apigenin-6,8-di-C-glucoside, luteolin-7-*O*-glucoside, and chrysin decreased under ML treatment. Because many genes involved in the accumulation of these substances are unknown, we only detected *FSII*, *F6H*, and *UBGT* in the flavone biosynthetic pathway (**Supplementary Table S5**). Like the malonylshisonin biosynthesis genes, both *FSII* and *UBGT* were upregulated under ML treatment compared with WL. In view of luteolin, apigenin and more flavones possess pharmacological effects (Lei et al., 2020; Liang et al., 2020; Rizzo et al., 2021), the results show that strongly accumulated flavones under elevated light treatment, with provided potential application for further research.

Integrated transcriptomic and metabolomic analysis

To gain further insight into the regulation of anthocyanin biosynthesis in response to light intensity, we performed WGCNA to identify co-expression networks between anthocyanin metabolites and gene expression levels. Ten co-expression modules were identified based on their similar expression patterns (**Figure 5A**). The turquoise module is positively correlated with anthocyanins, malonylshisonin, and other metabolites (**Figure 5B**). We therefore focused on those genes in the turquoise module. We identified anthocyanin biosynthesis and transcription factor genes in this module and used gene pairs with correlation coefficients more than 0.85 to construct a regulatory network (**Figure 5C** and **Supplementary Table S7**). Five important genes involved in anthocyanin biosynthesis were identified in the turquoise module, including *ANS*, *4CL*, *DFR*, and *CHI*, which were positively correlated with total anthocyanin and malonylshisonin contents. The 147 transcription factors were also identified, mainly encoding MYB, bHLH, bZIP, ERF, and NAC in the module. Notably, *MYB5*, *MYB12*, *bZIP2*, *bZIP6, bHLH1*, *bHLH7,* and *bHLH9* had high connectivity with malonylshisonin and five anthocyanin biosynthesis genes. The MYB_related2, MYB_related4 had high positive correlation with malonylshisonin. Moreover, the expression level of most identified MYB and bZIP genes were strongly upregulated under ML treatment compared with WL and downregulated under RL treatment compared with ML (**Figure 5D**). By contrast, *MYB22, bHLH1*, *bHLH7,* and *bHLH9* were negatively correlated with malonylshisonin content. *MYB22* and *bHLH1* were also negatively correlated with total anthocyanin contents (**Supplementary Table S6**). Hence, these transcription factors were speculated to play important roles in regulating malonylshisonin accumulation under different light intensities.

Candidate MYB genes involved in anthocyanin biosynthesis

MYB transcription factors are major members of MBW ternary transcriptional complex, which is an important regulator of anthocyanin metabolism in many plants (Lloyd et al., 2017; Li et al., 2020; Wang et al., 2020; Zhang et al., 2020; Ning et al., 2021). In WGCNA analysis, we identified 38 MYB transcription factors, containing 37 R2R3-MYB subfamily members and one 1R-MYB (MYB10). These MYBs showed high correlation coefficient with malonylshisonin and five

10.3389/fpls.2022.976449

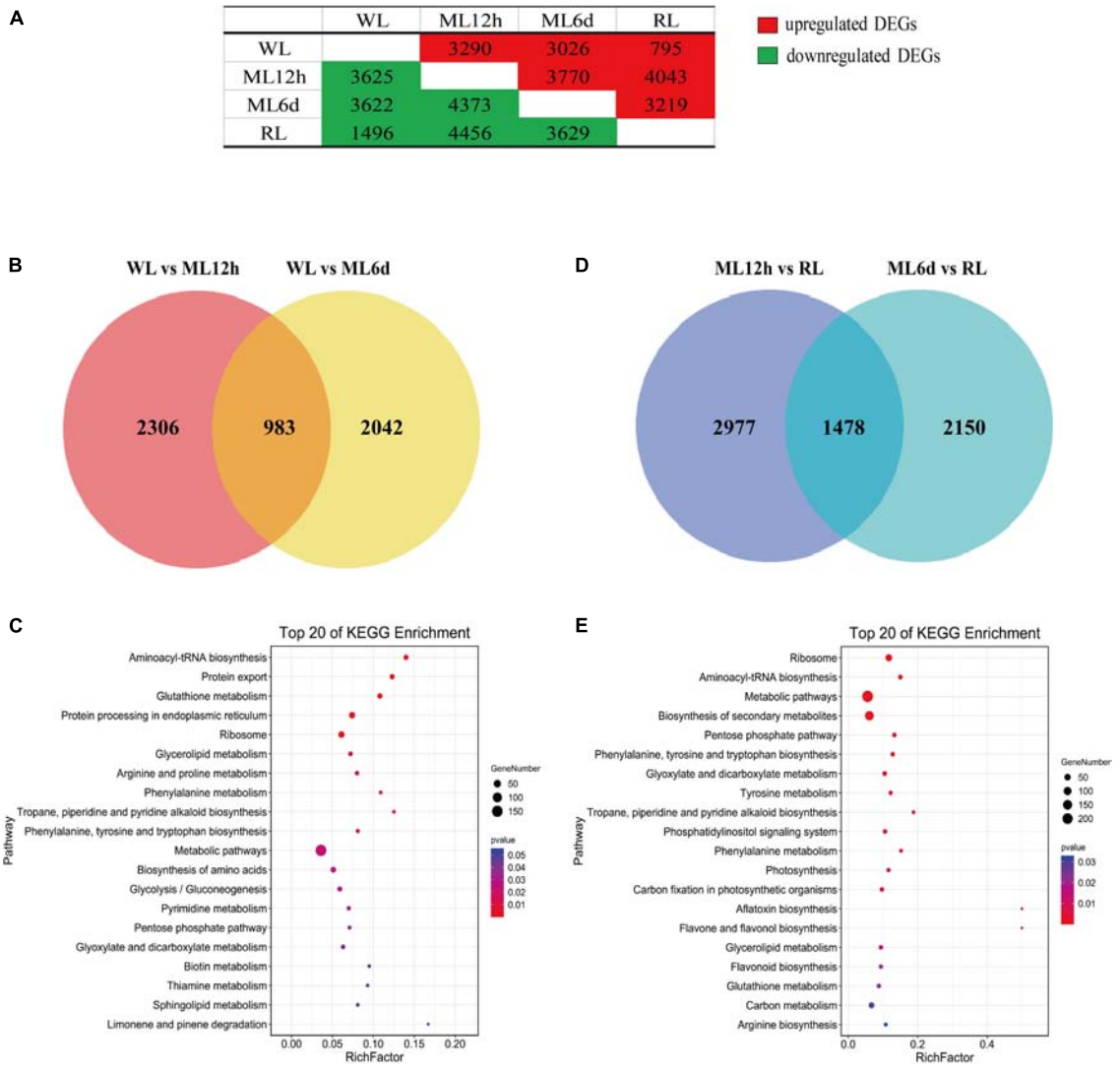

FIGURE 3
Venn diagram and KEGG pathways of the DEGs under different light intensity treatments. **(A)** Number of upregulated and downregulated differentially expressed genes (DEGs) in pair-wise comparisons. **(B)** Venn diagram and **(C)** top 20 KEGG pathways of upregulated genes of the ML12h and ML6d groups compared with WL. **(D)** Venn diagram and **(E)** top 20 KEGG pathways of downregulated genes in the RL group compared with ML12h and ML6d.

anthocyanin biosynthesis genes (Supplementary Figure S5). Among them, 22 R2R3-MYB members were highly induced under ML treatment, while 15 were downregulated in response to light treatment (Figure 5D).

To examine the MYB transcription factors involved in regulating anthocyanin accumulation, we constructed a phylogenetic tree combined the MYBs that we identified in perilla and were previously reported to regulate anthocyanin accumulation in other plants. The phylogenetic tree was divided into three subclasses (Figure 6A). Subclass I contains perilla MYB12, MYB2 and key anthocyanin-regulated MYBs from Arabidopsis and apple. Subclass II includes 11 perilla MYBs and three Arabidopsis R2R3-MYB family members. Among them, *MYB8* and *MYB14* showed peak expression under ML12h treatment. Subclass III includes 25 MYBs from perilla and IbMYB340. Among them, *MYB4* and *MYB37* were expressed at high levels and responded to light treatment.

For further explore the relationships between the MYBs and anthocyanin biosynthesis, we performed correlation analysis of 15 selected MYBs with anthocyanin metabolites and 17 key anthocyanin biosynthesis genes. Among these, 9 MYBs showed positive correlations with anthocyanin metabolites and 6 showed positive correlations with key anthocyanin biosynthesis genes (Figure 6B). Interestingly, *MYB12* and *MYB19* showed significantly positive correlations with most anthocyanin biosynthesis genes (Figure 6C). The *MYB12* had

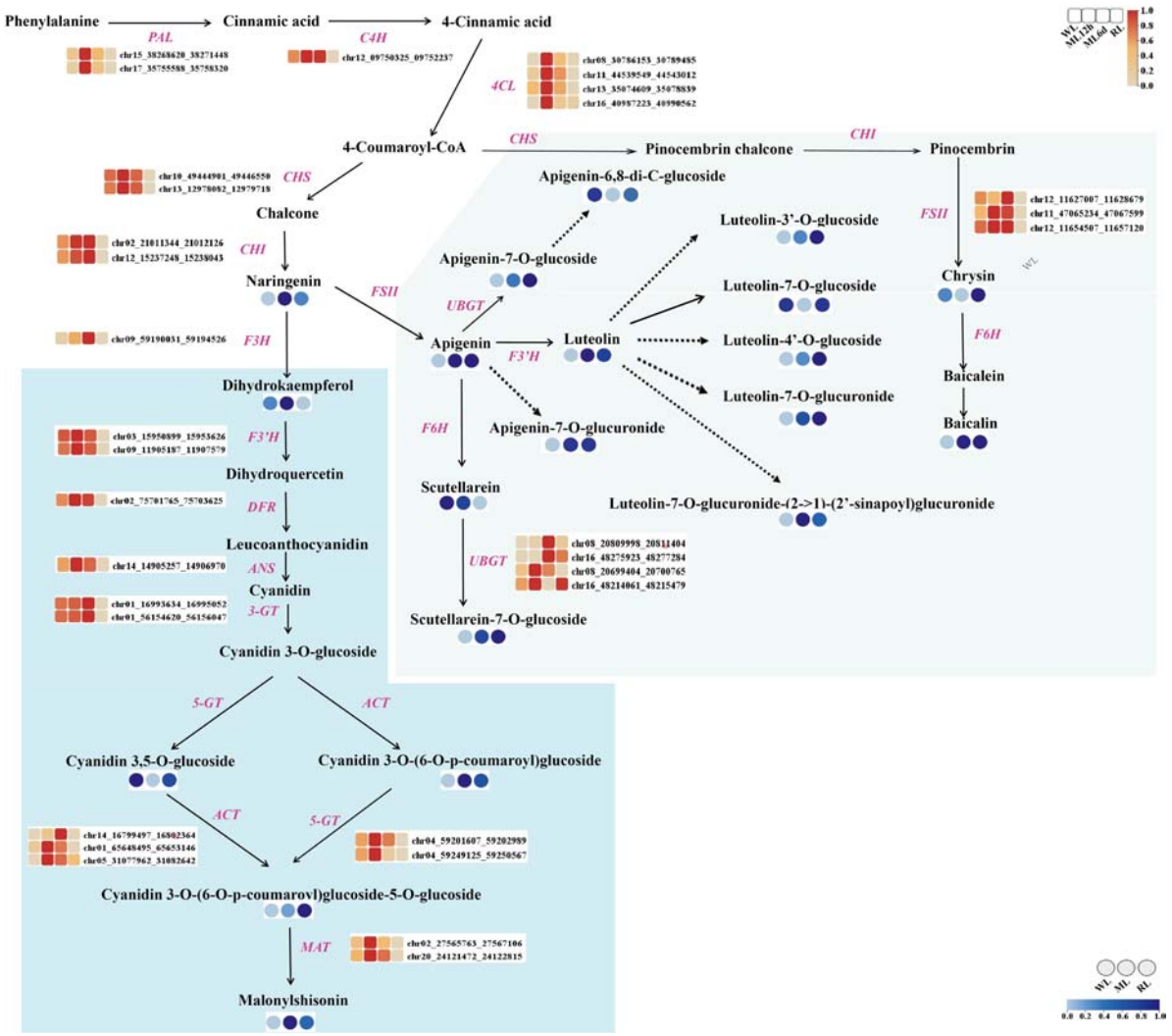

FIGURE 4
The metabolites and genes involving in the anthocyanin biosynthesis pathway under different light intensity treatments in perilla leaves. The blue background indicates the major malonylshisonin biosynthetic pathway. The green background indicates the major flavonoid biosynthetic pathway. The blue color in the circle indicates the level of the metabolite under WL, ML, and RL treatment. The red color in the blocks represents the relative expression levels of genes under WL, ML12h, ML6d, and RL treatments. PAL, phenylalanine ammonia lyase; C4H, cinnamate 4-hydroxylase; 4CL, 4-coumarate-CoA ligase; CHS, chalcone synthase; CHI, chalcone isomerase; F3H, flavanone 3-hydroxylase; F3'H, flavonoid 3'-hydroxylase; DFR, dihydroflavonol reductase; ANS, anthocyanin synthase (leucoanthocyanin dioxgenase); 3-GT, flavonoid 3-glucosyltransferase; ACT, anthocyanin acyltransferase; 5-GT, anthocyanin 5-glucosyltransferase; MAT, anthocyanin malonyltransferase.

been reported in malonylshisonin formation, which was found in responsive to light treatment in the study.

Furthermore, the *cis*-acting elements of four key anthocyanin biosynthesis genes, including *DFR*, *CHI1*, *CHI2*, and *ANS*, were analyzed. Several light-response elements and hormone-response elements were identified in the four anthocyanin genes (**Supplementary Figure S7**). Interestingly, we identified CCAAT-box and MYB-recognition element (MRE) *cis*-acting elements in the promoter regions of perilla *CHI1* and *ANS*, respectively (**Supplementary Figure S7**). Combining WGCNA analysis, phylogenetic analysis, and *cis*-acting element analysis, more MYB transcription factors were predicted to regulate malonylshisonin accumulation under the light treatment in perilla.

Candidate bZIP genes involved in anthocyanin biosynthesis

The bZIP transcription factors were recently reported to regulate anthocyanin biosynthesis (Hu et al., 2019; Liu et al., 2019; Wang et al., 2020). In the turquoise module, we also identified 6 bZIP transcription factors (**Supplementary Figure S6**). These perilla bZIPs were divided into two subclasses

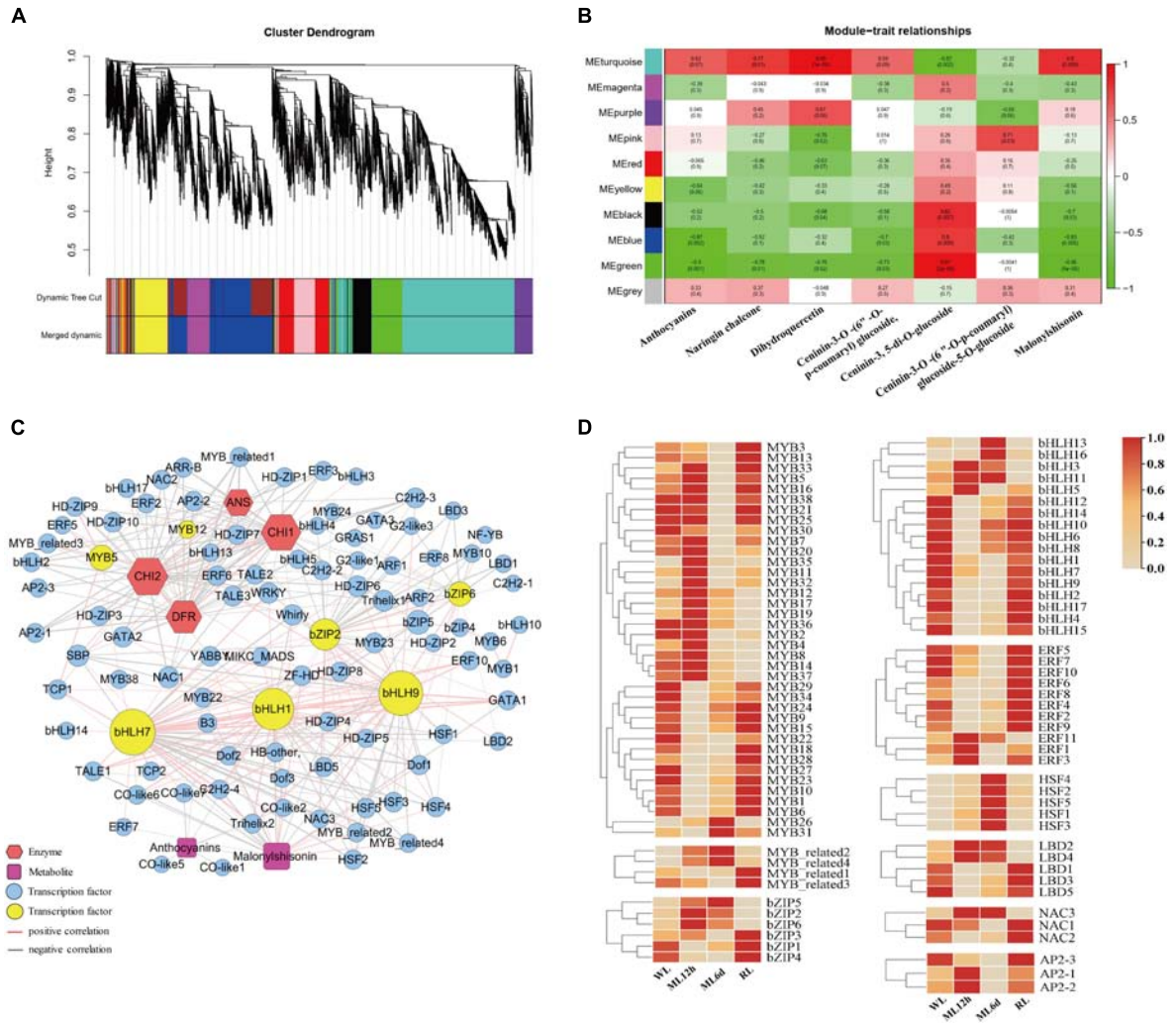

FIGURE 5
Weighted correlation network analysis (WGCNA) of the anthocyanin biosynthetic pathway. **(A)** Dendrogram of the co-expression modules (clusters). The major tree branches constitute 10 modules labeled with different colors. **(B)** Heat map showing the correlations between modules and anthocyanin compounds. Red indicates a positive correlation, and green indicates a negative correlation between the cluster and the sample. **(C)** Co-expression network of the genes and metabolites with correlation coefficients greater than 0.85. **(D)** Heat maps of the expression levels of genes encoding MYBs, MYB-related, bZIPs, bHLHs, ERFs, HSFs, LBDs, NACs, and AP2s based on the transcriptomic data.

in the evolutionary tree (Figure 7A). Subclass I consist of bZIP4 and bZIP3 from perilla, along with HY5 transcription factors from other plants. Subclass II consists of 4 bZIP transcription factors from perilla, along with MdbZIP44, LcABF3, and MdABI5. Co-expression analysis showed that *bZIP2*, *bZIP5*, and *bZIP6* share positive regulatory relationships with key anthocyanin biosynthesis genes (*CHI1*, *CHI2*, *ANS*, and *DFR*), while *bZIP1*, *bZIP3*, and *bZIP4* share negative regulatory relationships with these genes (Figure 7B). Interestingly, *bZIP2*, *bZIP5*, and *bZIP6* showed significant positive correlations with total anthocyanin and malonylshisonin contents and most anthocyanin biosynthesis genes (Figure 7C). The promoter sequences of *CHI1*, *CHI2*, *ANS*, and *DFR* all contain G-boxes, a light-responsive binding site that is recognized by bZIP transcription factors (Supplementary Figure S7). The *bZIP2* and *bZIP6* were identified to encode G-box binding factor 3 in perilla, suggesting that they may play key roles in the light response and the anthocyanin regulation.

Quantitative RT-PCR analysis of the candidate genes involved in anthocyanin biosynthesis in *Perilla frutescens*

We measured the expression levels of anthocyanin biosynthesis genes (*CHI1*, *CHI2*, *ANS*, and *DFR*) and important

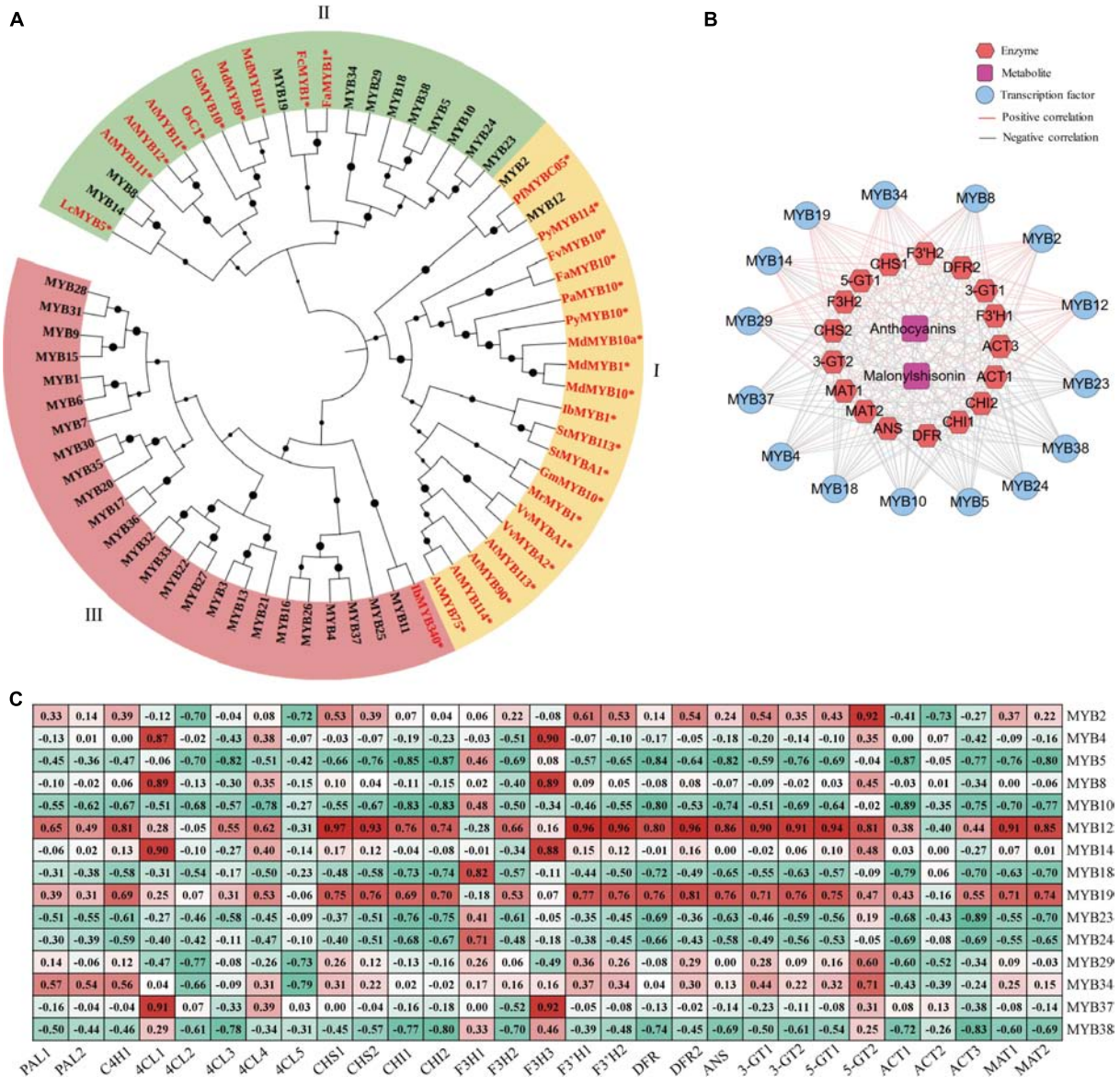

FIGURE 6
The MYB transcription factors involved in anthocyanin biosynthesis in perilla. **(A)** Phylogenetic relationships of MYBs between perilla and other plants. Yellow, green, and pink background indicate three subclasses in the evolutionary tree. The dots next to the nodes represent bootstrap values of 1000 replicates. The red font and symbol * indicate that these objects have been reported. **(B)** Co-expression networks between candidate MYBs. **(C)** Correlation coefficients between candidate MYB transcription factors and key anthocyanin biosynthesis genes. At, *Arabidopsis thaliana*; Vv, *Vitis vinifera*; St, *Solanum tuberosum*; Pb, *Pyrus* x *bretschneideri*; Os, *Oryza sativa* Japonica; Pf, *Perilla frutescens* var. *crispa*; Pa, *Prunus avium*; Py, *Pyrus pyrifolia* var. *culta*; Mr, *Morella rubra*; Md, *Malus domestica*; Lc, *Litchi chinensis*; Ib, *Ipomoea batatas*; Gh, *Gossypium hirsutum*; Gm, *Garcinia mangostana*; Fa, *Fragaria* x *ananassa*; Fv, *Fragaria vesca*; Fc, *Fragaria chiloensis*.

transcription factor genes (*MYB*, *bZIP*, and *bHLH*) involved in anthocyanin regulation by qRT-PCR (Figure 8). Combined the transcriptomic and qRT-PCR data, the candidate genes showed similar expression patterns. The anthocyanin biosynthesis genes (*CHI1*, *CHI2*, *ANS*, and *DFR*), MYB genes, and bZIP genes were upregulated under increased light intensity. These genes were all upregulated after a short (12 h) moderate light intensity treatment and downregulated after a long treatment (6 days), and their expression continued to decline under low light intensity. The response of the anthocyanin biosynthesis genes to light intensity treatment might be the direct cause of accumulation of anthocyanin metabolites. The MYB transcription factor genes were more sensitive to short vs. long light treatment, pointing to their important regulatory functions in anthocyanin metabolite accumulation. The *bZIP2* and *bZIP6* are homologous to the important light-response

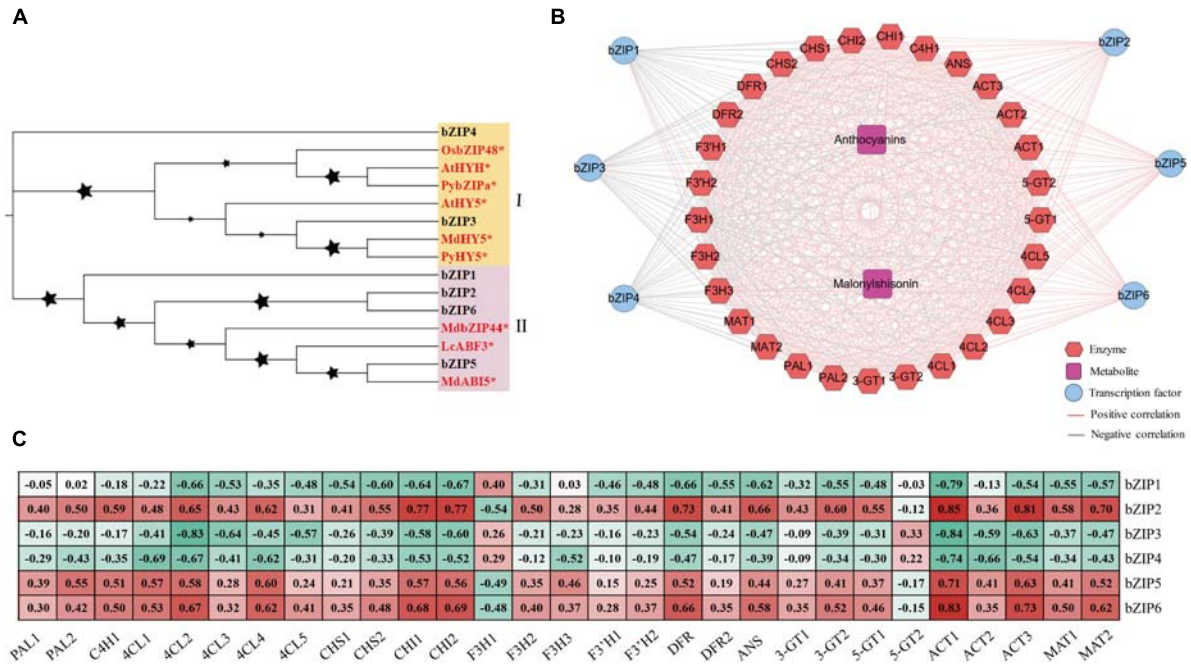

FIGURE 7
The bZIP transcription factors involved in the light response and anthocyanin regulation in perilla. **(A)** Phylogenetic relationships of bZIP transcription factors. Yellow and pink background indicate two subclasses in the evolutionary tree. The stars next to the nodes represent bootstrap values of 1000 replicates. The red font and symbol * indicate that these objects have been reported. **(B)** Co-expression networks between candidate bZIPs. **(C)** Correlation coefficients between candidate bZIP transcription factors and key anthocyanin biosynthesis genes. At, *Arabidopsis thaliana*; Py, *Pyrus pyrifolia*; Os, *Oryza sativa* Japonica; Md, *Malus domestica*; Lc, *Litchi chinensis*.

transcription factor gene *HY5*. Both were upregulated after a short light treatment. We also identified *bHLH1* and *bHLH7* transcription factor genes in perilla. Interestingly, both genes were downregulated under light treatment. The *bHLH1* and *bHLH7* encode PIF3 and PIF7, respectively. The PIFs were negatively regulation factors in response to light in other plants. The downregulated trend of *bHLH1* and *bHLH7* under light treatment is consistent with their functions. The expression patterns of key anthocyanin biosynthesis genes and transcription factors in response to light points to their important roles in regulating anthocyanin biosynthesis.

Discussion

Leaf color and anthocyanin accumulation are important traits for the medicinal and ornamental value of perilla (Ishikura, 1981; Yu et al., 2017). Perilla leaves color is highly sensitive to light conditions, providing an opportunity to study the molecule mechanism of anthocyanin biosynthesis and regulation (Mastropasqua et al., 2020).

In this study, we performed metabolomic and transcriptomic analyses of the light-sensitive perilla variety under different light intensity treatments. The metabolomic analysis identified 293 flavonoid compounds. Focus on malonylshisonin, the major anthocyanin metabolites in perilla, obviously increased in response to increased light treatment. Malonylshisonin biosynthesis involves 10 catalytic reactions, containing the initial cyanidin biosynthesis and the latter cyanidin derivatization pathway. In the latter steps, cyanidin-3-*O*-glucoside is converted to cyanidin-3-*O*-(6"-*O*-*p*-coumaryl) glucoside and cyanidin 3,5-*O*-glucoside (Springob et al., 2003). Under ML treatment, the content of cyanidin 3,5-*O*-glucoside was decreased, whereas the content of cyanidin-3-*O*-(6"-*O*-*P*-coumaryl) glucoside was increased, suggesting that the metabolic flow favored the formation of cyanidin-3-*O*-(6"-*O*-*P*-coumaryl) glucoside under light treatment. Next, we investigated the biosynthesis genes of malonylshisonin accumulation under different light treatments. Previous work found that nearly all the genes encoding the enzymes (except for *CHI*) showed higher expression in red perilla than in green perilla (Jiang et al., 2020). In the current study, the genes encoding CHS, CHI, F3H, DFR, and ANS, the rate-limiting enzymes in the anthocyanin biosynthetic pathway (Takos et al., 2006), were obviously responded to light treatment. These genes may play important roles in malonylshisonin accumulation in perilla leaves under light treatment.

In the WGCNA and correlation analysis, *ANS*, *CHI*, and *DFR* were positively correlated with malonylshisonin

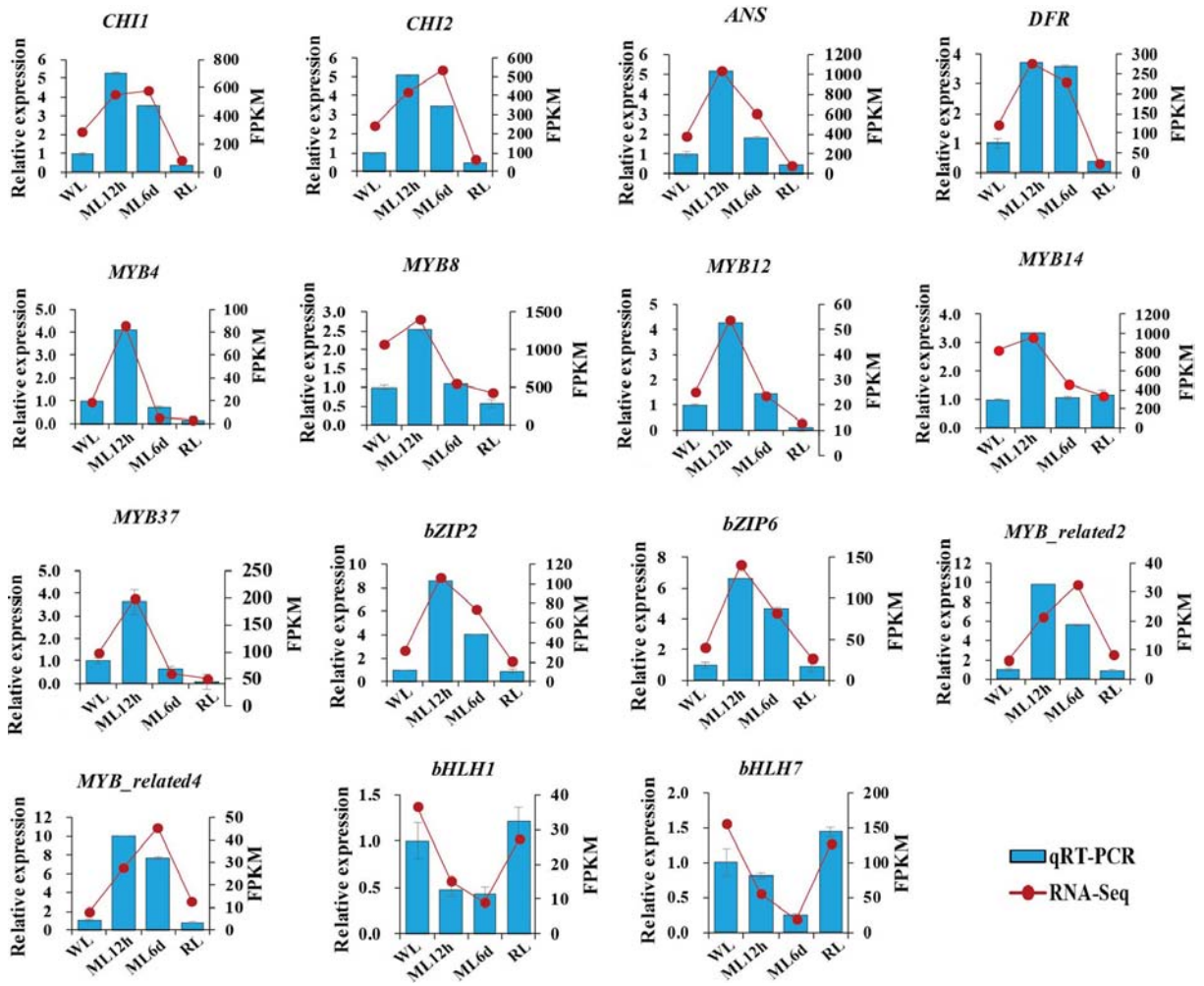

FIGURE 8
Relative expression levels of candidate genes. The histogram indicates gene expression data form qRT-PCR. The line chart indicates FPKM from transcriptomic sequence. Data are presented as means ± standard deviation (n = 3).

content. The homologous proteins of ANS, CHI, and DFR were responded to light treatment in other plants (Britsch, 1990; Menssen et al., 1990; Saito et al., 1999). CHI is the rate-limiting enzyme for flavonoid biosynthesis (Bednar and Hadcock, 1988; McKhann et al., 1998; Shimada et al., 2003). The expression of *CHI* increases in rice in response to high light levels and UV irradiation (Albert et al., 2009; Park et al., 2021). DFR catalyzes the conversion of dihydroquercetin to leucoanthocyanidin, which is recognized as a pivotal step in anthocyanin biosynthesis (Xie et al., 2004; Miyagawa et al., 2015; Ni et al., 2020). The expression of *DFR* is downregulated in the shade in *Brassica oleracea* (Liu et al., 2020). ANS catalyzes the oxidation of leucoanthocyanidin (Turnbull et al., 2000, 2003), and *ANS* is upregulated by high-light treatment in *Arabidopsis thaliana* (Zheng et al., 2019, 2021). In the current study, the expression levels of the perilla genes *CHI1*, *CHI2*, *DFR*, and *ANS* all increased under ML treatment. These results indicate that these genes play a major role in determining malonylshisonin biosynthesis in different light intensities.

Plants respond to light via photoreceptors and employ multiple transcription factors to regulate anthocyanin metabolites formation (Zhang et al., 2021). To further identify the key regulation factors, we used WGCNA method to comprehensively analyze metabolites and key genes in perilla. In this study, the 147 transcription factors were also identified based on WGCNA analysis. Among them, R2R3-MYBs have been widely researched. There are four Arabidopsis thaliana R2R3-MYB family members (AtMYB113, AtMYB90, AtMYB114, and AtMYB75) were reported control anthocyanin biosynthesis in vegetative tissues (Gonzalez et al., 2008). AtMYB75 (also called PAP1) activates the transcription of *CHS*, *DFR*, and *ANS* (Shi and Xie, 2010, 2011) and participates in the regulation of anthocyanin biosynthesis by HY5 via the

transcriptional activation of its promoter (Shin et al., 2013). The MdMYB10 and MdMYB1 are key anthocyanin-related transcription factors in apple (Takos et al., 2006; Espley et al., 2007). In apple, the expression of *MdMYB1* and its allele *MdMYB10* is induced by sunlight (Takos et al., 2006; Feng et al., 2013). The expression of *MdMYB10* is also regulated by HY5, which binds to the G-box in the *MdMYB10* promoter in a light-responsive manner, thereby affecting the expression of downstream structural genes and anthocyanin accumulation in apple (An et al., 2017). Interestingly, PfMYB12 were identified shares complete sequence identity with MYBC05. The MYBC05 was previously reported to promote the production of anthocyanins, which is thought to bind to myC-F3G1 and PFWD to form the MBW complex, which promotes the production of anthocyanins in red perilla (Yamazaki et al., 2003; Yamazaki and Saito, 2011). Hence, the PfMYB12 and PfMYB2 are clustered with above MYBs, which are thought to important function in anthocyanin light-responsive accumulation. Next, The PfMYB8 and PfMYB14 were clustered with three AtMYBs (AtMYB11, AtMYB12, AtMYB111), which targeted several flavonoid biosynthesis genes, including *CHS*, *CHI*, *F3H*, and *FLS1* in Arabidopsis (Stracke et al., 2007). AtMYB12 and AtMYB111 also control flavonol accumulation in roots in a light-dependent manner (Stracke et al., 2017). PfMYB4 and PfMYB37 were clustered with IbMYB340, which interacted with IbERF71 and IbbHLH2 to regulate anthocyanin biosynthesis in sweet potato (Ning et al., 2021). Moreover, MYB-binding sites, including MBS, MRE, and CCAAT-box elements, were identified in the promotors of *CHI1*, *CHI2*, and *ANS*. The CCAAT-box is the binding site of the HvMYB1 transcription factor in barley (Alexander et al., 2019). The MRE cis-acting elements is recognized and bound by BrPAP1 transcription factor, which regulates anthocyanin biosynthesis in *Brassica rapa* (Yang et al., 2021). These findings suggest that these MYBs play important roles in regulating anthocyanin accumulation in perilla in response to different light intensities. To sum up, the six PfMYB (PfMYB2, PfMYB12, PfMYB8, PfMYB14, PfMYB4, and PfMYB37) were predicted to possess important function in photosensitive anthocyanin regulation in perilla.

The bZIP family, one of the largest transcription factor families in plants, is involved in physiological processes such as plant development, environmental signaling, and stress responses (Djamei et al., 2007; Liu C. C. et al., 2018; Xiao et al., 2021). The bZIP transcription factor HY5 is an important transcription factor involved in light signal transduction and plant pigment accumulation in response to light (Holm et al., 2002; Stracke et al., 2010; Shin et al., 2013; Gangappa and Botto, 2016). HY5 also promotes flavonoid accumulation in response to both visible and UV-B light. Using WGCNA, we identified six bZIP transcription factors in the co-expression modules. Perilla bZIP3 and bZIP4 clustered with HY5s from other plants. In the previous research, HY5 could responds to receptors for blue, red/far-red, and ultraviolet light (Oyama et al., 1997; Ang et al., 1998; Chattopadhyay et al., 1998; Brown and Jenkins, 2008) and directly binds to G-box or ACE-box elements in the promoters of MYB genes to promote their expression to promote flavonoid biosynthesis (Holm et al., 2002; Stracke et al., 2010; Shin et al., 2013). Perilla *bZIP3* and *bZIP4* were both induced by light but showed negative regulatory relationships with anthocyanin pathway genes in the current study. By contrast, *bZIP2* and *bZIP6* showed positive regulatory relationships with most anthocyanin biosynthesis genes and possess light-regulated traits in perilla. *bZIP2* and *bZIP6* encode G-box binding protein 3 (GBF3) transcription factors. In Arabidopsis, GBF3 has the same gene expression pattern as HY5, and its binding sites showed a 86.7% overlap with those of HY5 under changing light conditions, suggesting that GBF3 might interfere with the function of HY5 (Kurihara et al., 2020). bZIP2 and bZIP6 also clustered with MdbZIP44 and LcABF3. MdbZIP44 promotes anthocyanin accumulation in response to abscisic acid by enhancing the binding of MdMYB1 to the promoters of downstream target genes in apple (An et al., 2018). LcABF3 activates the promoter region of *LcMYB1* and structural genes such as *LcF3'H* and *LcDFR* to modulate anthocyanin biosynthesis in lychee (Hu et al., 2019). Interestingly, *bZIP2* and *bZIP6* had the highest correlations with *CHI1* and *CHI2* in WGCNA. The *CHI1* and *CHI2* promoters contain G-box *cis*-acting elements, which can be recognized and combined by bZIPs. That means bZIP2 and bZIP6 perhaps together with MYBs, activated the transcription of the key candidate anthocyanin biosynthesis genes and promote the accumulation of malonylshisonin under moderate light intensity. Moreover, the *bHLH1* and *bHLH7* encode PIF3 and PIF7. Phytochrome-interacting factor (PIF) genes are downregulated in the presence of light. These bHLH transcription factors function as primary partners of the red/far-red light receptors phytochromes in light signaling (Nozue et al., 2007). Our results indicate that bHLH1 and bHLH7 negatively regulate anthocyanin biosynthesis in the light, which is consistent with the function of PIFs in the light response.

In the research, we also identified 14 important flavone metabolites in perilla leaves, including luteolin, apigenin, baicalein, scutellarein, and their glycoside derivatives. Luteolin can attenuate allergic nasal inflammation (Jeon et al., 2014; Liang et al., 2020). Apigenin and apigenin-7-diglucuronide can mitigate oxidative stress and possesses anti-inflammatory activity (Bian et al., 2017; Kasiri et al., 2018). Baicalin represses C/EBP beta via redox homeostasis, representing a potentially effective treatment for Parkinson's disease (Lei et al., 2020). They are all possess a certain of pharmacological functions and got more attention. The accumulation of 10 flavones increased in perilla leaves in response to moderate light treatment. This increase in the levels of pharmacologically important flavones indicates that the value of perilla can be

increased under the proper light conditions. The flavonoid biosynthesis and its regulation require further study in perilla.

In summary, the regulation of light intensity signal in plants is a complex process. We mainly focused on the red perilla malonylshisonin synthesis pathway. In addition, the function of each candidate gene needs to be confirmed by different methods. Therefore, further work is required to elucidate the mechanism of light signal in perilla plants.

Conclusion

This study integrated the metabolomic and transcriptomic analyses of the light-sensitive perilla variety under different light intensity. The light intensity significantly affects the color, metabolite accumulation and gene expression involved in the main anthocyanin biosynthesis in perilla leaves. Based on WGCNA analysis, key genes and transcription factors were identified. What's more, 6 MYBs and 4 bZIPs were predicted to play important roles in light-regulated anthocyanin biosynthesis. The identified key genes and regulatory factors will help us to understand the potential mechanism of photo-regulated anthocyanin accumulation in perilla.

Statistical analysis

Statistical analyses were performed by Student's *t*-test and one-way ANOVA using SPSS 23.0 (SPSS Inc., Chicago, IL, United States). Least significant difference (LSD) was used to compare treatment means, and $p = 0.05$ was considered as statistically significant.

Data availability statement

The datasets presented in this study are deposited in the Genome Sequence Archive in National Genomics Data Center, Beijing Institute of Genomics, Chinese Academy of Sciences. The accession number is PRJNA837648.

Author contributions

GX: writing – original draft, conceptualization, methodology, formal analysis, investigation, and data curation. HW: supervision, project administration, and funding acquisition. QS: planned and designed the research, methodology, data curation, and writing – review and editing. XZ and ZL: performed the experiments. HJ: supervision. DW: data analysis. JH and KX: plants cultivation. All authors have read and approved the final version of the manuscript.

Funding

This work was funded by the National Natural Science Foundation for regional fund (31860391), the National Natural Science Foundation of China Grant (31970261), and the Talent Support Project of Guangdong (2019TQ05N182).

Conflict of interest

The authors declare that the research was conducted in the absence of any commercial or financial relationships that could be construed as a potential conflict of interest.

Publisher's note

Supplementary material

The Supplementary Material for this article can be found online at: https://www.frontiersin.org/articles/10.3389/fpls.2022.976449/full#supplementary-material

References

Ahmed, H. M. (2019). Ethnomedicinal, Phytochemical and Pharmacological Investigations of *Perilla frutescens* (L.) Britt. *Molecules* 24:102. doi: 10.3390/molecules24010102

Albert, N. W., Lewis, D. H., Zhang, H., Irving, L. J., Jameson, P. E., and Davies, K. M. (2009). Light-induced vegetative anthocyanin pigmentation in Petunia. *J. Exp. Bot.* 60, 2191–2202.

Alexander, R. D., Wendelboe-Nelson, C., and Morris, P. C. (2019). The barley transcription factor Hv*MYB1* is a positive regulator of drought tolerance. *Plant Physiol. Biochem.* 142, 246–253. doi: 10.1016/j.plaphy.2019.07.014

An, J. P., Qu, F. J., Yao, J. F., Wang, X. N., You, C. X., Wang, X. F., et al. (2017). The *bZIP* transcription factor MdHY5 regulates anthocyanin accumulation and nitrate assimilation in apple. *Hortic. Res.* 4:17023. doi: 10.1038/hortres.2017.56

An, J. P., Yao, J. F., Xu, R. R., You, C. X., Wang, X. F., and Hao, Y. J. (2018). Apple *bZIP* transcription factor MdbZIP44 regulates abscisic acid-promoted anthocyanin accumulation. *Plant Cell Environ.* 41, 2678–2692. doi: 10.1111/pce.13393

Ang, L. H., Chattopadhyay, S., Wei, N., Oyama, T., Okada, K., Batschauer, A., et al. (1998). Molecular interaction between COP1 and *HY5* defines a regulatory switch for light control of *Arabidopsis* development. *Mol. Cell* 1, 213–222. doi: 10.1016/S1097-2765(00)80022-2

Azuma, A., Yakushiji, H., Koshita, Y., and Kobayashi, S. (2012). Flavonoid biosynthesis-related genes in grape skin are differentially regulated by temperature and light conditions. *Planta* 236, 1067–1080. doi: 10.1007/s00425-012-1650-x

Bednar, R. A., and Hadcock, J. R. (1988). Purification and characterization of chalcone isomerase from soybeans. *J. Biol. Chem.* 263, 9582–9588. doi: 10.1016/S0021-9258(19)81556-9

Bian, M., Zhang, Y., Du, X., Xu, J., Cui, J., Gu, J., et al. (2017). Apigenin-7-diglucuronide protects retinas against bright light-induced photoreceptor degeneration through the inhibition of retinal oxidative stress and inflammation. *Brain Res.* 1663, 141–150. doi: 10.1016/j.brainres.2017.03.019

Britsch, L. (1990). Purification and characterization of flavone synthase I, a 2-oxoglutarate-dependent desaturase. *Arch Biochem. Biophys.* 282, 152–160. doi: 10.1016/0003-9861(90)90099-k

Brown, B. A., and Jenkins, G. I. (2008). UV-B signaling pathways with different fluence-rate response profiles are distinguished in mature *Arabidopsis* leaf tissue by requirement for UVR8. *HY5*, and *HYH*. *Plant Physiol.* 146, 576–588. doi: 10.1104/pp.107.108456

Chattopadhyay, S., Ang, L. H., Puente, P., Deng, X. W., and Wei, N. (1998). *Arabidopsis bZIP* protein *HY5* directly interacts with light-responsive promoters in mediating light control of gene expression. *Plant Cell* 10, 673–683. doi: 10.1105/tpc.10.5.673

Chen, X. Q., Nagao, N., Itani, T., and Irifune, K. (2012). Anti-oxidative analysis, and identification and quantification of anthocyanin pigments in different coloured rice. *Food Chem.* 135, 2783–2788. doi: 10.1016/j.foodchem.2012.06.098

Djamei, A., Pitzschke, A., Nakagami, H., Rajh, I., and Hirt, H. (2007). Trojan horse strategy in Agrobacterium transformation: Abusing MAPK defense signaling. *Science* 318, 453–456. doi: 10.1126/science.1148110

Espley, R. V., Hellens, R. P., Putterill, J., Stevenson, D. E., Kutty-Amma, S., and Allan, A. C. (2007). Red colouration in apple fruit is due to the activity of the *MYB* transcription factor *MdMYB10*. *Plant J.* 49, 414–427. doi: 10.1111/j.1365-313X.2006.02964.x

Feng, F., Li, M., Ma, F., and Cheng, L. (2013). Phenylpropanoid metabolites and expression of key genes involved in anthocyanin biosynthesis in the shaded peel of apple fruit in response to sun exposure. *Plant Physiol. Biochem.* 69, 54–61. doi: 10.1016/j.plaphy.2013.04.020

Feng, S., Wang, Y., Yang, S., Xu, Y., and Chen, X. (2010). Anthocyanin biosynthesis in pears is regulated by a R2R3-*MYB* transcription factor Py*MYB10*. *Planta* 232, 245–255. doi: 10.1007/s00425-010-1170-5

Fujiwara, Y., Kono, M., Ito, A., and Ito, M. (2018). Anthocyanins in *perilla* plants and dried leaves. *Phytochemistry* 147, 158–166. doi: 10.1016/j.phytochem.2018.01.003

Gangappa, S. N., and Botto, J. F. (2016). The Multifaceted Roles of *HY5* in Plant Growth and Development. *Mol. Plant* 9, 1353–1365. doi: 10.1016/j.molp.2016.07.002

Gonzalez, A., Zhao, M., Leavitt, J. M., and Lloyd, A. M. (2008). Regulation of the anthocyanin biosynthetic pathway by the *TTG1/bHLH/Myb* transcriptional complex in *Arabidopsis* seedlings. *Plant J.* 53, 814–827. doi: 10.1111/j.1365-313X.2007.03373.x

Holm, M., Ma, L. G., Qu, L. J., and Deng, X. W. (2002). Two interacting bZIP proteins are direct targets of COP1-mediated control of light-dependent gene expression in *Arabidopsis*. *Genes Dev.* 16, 1247–1259. doi: 10.1101/gad.969702

Holton, T. A., and Cornish, E. C. (1995). Genetics and Biochemistry of Anthocyanin Biosynthesis. *Plant Cell* 7, 1071–1083. doi: 10.2307/3870058

Honda, G., Yuba, A., Nishizawa, A., and Tabata, M. (1994). Genetic control of geranial formation in *Perilla frutescens*. *Biochem. Genet.* 32, 155–159. doi: 10.1007/BF00554619

Hu, B., Lai, B., Wang, D., Li, J., Chen, L., Qin, Y., et al. (2019). Three LcABFs are Involved in the Regulation of Chlorophyll Degradation and Anthocyanin Biosynthesis During Fruit Ripening in Litchi chinensis. *Plant Cell Physiol.* 60, 448–461. doi: 10.1093/pcp/pcy219

Huang, B., Lin, C., Chen, Y., and Kao, S. (2014). Anti-inflammatory effects of *Perilla frutescens* leaf extract on lipopolysaccharide-stimulated RAW264.7 cells. *Mol. Med. Rep.* 10, 1077–1083. doi: 10.3892/mmr.2014.2298

Ishikura, N. (1981). Anthocyanins and Flavones in Leaves and Seeds of *Perilla* Plant. *Agric. Biol. Chem.* 45, 1855–1860. doi: 10.1271/bbb1961.45.1855

Jeon, I. H., Kim, H. S., Kang, H. J., Lee, H., Jeong, S. I., Kim, S. J., et al. (2014). Anti-Inflammatory and Antipruritic Effects of Luteolin from *Perilla* (*P. frutescens* L.) Leaves. *Molecules* 19, 6941–6951. doi: 10.3390/molecules19066941

Jiang, M., Ren, L., Lian, H., Liu, Y., and Chen, H. (2016). Novel insight into the mechanism underlying light-controlled anthocyanin accumulation in eggplant (*Solanum melongena* L.). *Plant Sci.* 249, 46–58. doi: 10.1016/j.plantsci.2016.04.001

Jiang, T., Guo, K., Liu, L., Tian, W., Xie, X., Wen, S., et al. (2020). Integrated transcriptomic and metabolomic data reveal the flavonoid biosynthesis metabolic pathway in *Perilla frutescens* (L.) leaves. *Sci. Rep.* 10:16207. doi: 10.1038/s41598-020-73274-y

Kasiri, N., Rahmati, M., Ahmadi, L., and Eskandari, N. (2018). The significant impact of apigenin on different aspects of autoimmune disease. *Inflammopharmacology* 26, 1359–1373. doi: 10.1007/s10787-018-0531-8

Khoo, H. E., Azlan, A., Tang, S. T., and Lim, S. M. (2017). Anthocyanidins and anthocyanins: Colored pigments as food, pharmaceutical ingredients, and the potential health benefits. *Food Nutr. Res.* 61:1361779. doi: 10.1080/16546628.2017.1361779

Kocic, B., Filipovic, S., Nikolic, M., and Petrovic, B. (2011). Effects of anthocyanins and anthocyanin-rich extracts on the risk for cancers of the gastrointestinal tract. *J. Buon.* 16, 602–608.

Kohl, M., Wiese, S., and Warscheid, B. (2011). Cytoscape: Software for visualization and analysis of biological networks. *Methods Mol. Biol.* 696, 291–303.

Kong, J. M., Chia, L. S., Goh, N. K., Chia, T. F., and Brouillard, R. (2003). Analysis and biological activities of anthocyanins. *Phytochemistry* 64, 923–933. doi: 10.1016/S0031-9422(03)00438-2

Kurihara, Y., Makita, Y., Shimohira, H., and Matsui, M. (2020). Time-Course Transcriptomics Study Reveals Mode of bZIP Transcription Factors on Light Exposure in *Arabidopsis*. *Int. J. Mol. Sci.* 21:1993. doi: 10.3390/ijms21061993

Lee, J. K., and Ohnishi, O. (2003). Genetic relationships among cultivated types of *Perilla frutescens* and their weedy types in East Asia revealed by AFLP markers. *Genet. Resour. Crop Evol.* 50, 65–74. doi: 10.1023/A:1022951002271

Lei, K., Shen, Y., He, Y., Zhang, L., Zhang, J., Tong, W., et al. (2020). Baicalin Represses C/EBP beta via Its Antioxidative Effect in Parkinson's Disease. *Oxid. Med. Cell Longev.* 2020:8951907. doi: 10.1155/2020/8951907

Li, C., Wu, J., Hu, K. D., Wei, S. W., Sun, H. Y., Hu, L. Y., et al. (2020). PyWRKY26 and PybHLH3 cotargeted the Py*MYB*114 promoter to regulate anthocyanin biosynthesis and transport in red-skinned pears. *Hortic. Res.* 7:37. doi: 10.1038/s41438-020-0254-z

Liang, K., Yu, S., Huang, W., and Yen, H. (2020). Luteolin Attenuates Allergic Nasal Inflammation via Inhibition of Interleukin-4 in an Allergic Rhinitis Mouse Model and Peripheral Blood from Human Subjects with Allergic Rhinitis. *Front. Pharmacol.* 11:291. doi: 10.3389/fphar.2020.00291

Lin, C., Kuo, C., Wang, J., Cheng, J., Huang, Z., and Chen, C. (2007). Growth inhibitory and apoptosis inducing effect of *Perilla frutescens* extract on human hepatoma HepG2 cells. *J. Ethnopharmacol.* 112, 557–567. doi: 10.1016/j.jep.2007.05.008

Liu, C., Yao, X., Li, G., Huang, L., and Xie, Z. (2020). Transcriptomic profiling of purple broccoli reveals light-induced anthocyanin biosynthetic signaling and structural genes. *PeerJ* 8:e8870. doi: 10.7717/peerj.8870

Liu, C. C., Chi, C., Jin, L. J., Zhu, J., Yu, J. Q., and Zhou, Y. H. (2018). The bZip transcription factor *HY5* mediates CRY1a-induced anthocyanin biosynthesis in tomato. *Plant Cell Environ.* 41, 1762–1775. doi: 10.1111/pce.13171

Liu, H., Su, J., Zhu, Y., Yao, G., Allan, A. C., Ampomah-Dwamena, C., et al. (2019). The involvement of PybZIPa in light-induced anthocyanin accumulation via the activation of PyUFGT through binding to tandem G-boxes in its promoter. *Hortic. Res.* 6:134. doi: 10.1038/s41438-019-0217-4

Liu, Y., Tikunov, Y., Schouten, R. E., Marcelis, L., Visser, R., and Bovy, A. (2018). Anthocyanin Biosynthesis and Degradation Mechanisms in *Solanaceous* Vegetables: A Review. *Front. Chem.* 6:52. doi: 10.3389/fchem.2018.00052

Livak, K. J., and Schmittgen, T. D. (2001). Analysis of relative gene expression data using real-time quantitative PCR and the 2(-Delta Delta C(T)) Method. *Methods* 25, 402–408. doi: 10.1006/meth.2001.1262

Lloyd, A., Brockman, A., Aguirre, L., Campbell, A., Bean, A., Cantero, A., et al. (2017). Advances in the *MYB-bHLH-WD* Repeat (MBW) Pigment Regulatory Model: Addition of a WRKY Factor and Co-option of an Anthocyanin *MYB* for Betalain Regulation. *Plant Cell Physiol.* 58, 1431–1441. doi: 10.1093/pcp/pcx075

Makino, T., Furuta, Y., Wakushima, H., Fujii, H., Saito, K., and Kano, Y. (2003). Anti-allergic effect of *Perilla frutescens* and its active constituents. *Phytother. Res.* 17, 240–243. doi: 10.1002/ptr.1115

Mastropasqua, L., Dipierro, N., and Paciolla, C. (2020). Effects of Darkness and Light Spectra on Nutrients and Pigments in Radish, Soybean, Mung Bean and Pumpkin Sprouts. *Antioxidants* 9:558. doi: 10.3390/antiox9060558

McKhann, H. I., Paiva, N. L., Dixon, R. A., and Hirsch, A. M. (1998). Expression of genes for enzymes of the flavonoid biosynthetic pathway in the early stages of the Rhizobium-legume symbiosis. *Adv. Exp. Med. Biol.* 439, 45–54. doi: 10.1007/978-1-4615-5335-9_4

Meng, L., Lozano, Y., Bombarda, I., Gaydou, E., and Li, B. (2006). Anthocyanin and flavonoid production from *Perilla frutescens*: Pilot plant scale processing including cross-flow microfiltration and reverse osmosis. *J. Agric. Food Chem.* 54, 4297–4303. doi: 10.1021/jf0604079

Menssen, A., Höhmann, S., Martin, W., Schnable, P. S., Peterson, P. A., Saedler, H., et al. (1990). The En/Spm transposable element of *Zea mays* contains splice sites at the termini generating a novel intron from a dSpm element in the A2 gene. *EMBO J.* 9, 3051–3057. doi: 10.1002/j.1460-2075.1990.tb07501.x

Miyagawa, N., Miyahara, T., Okamoto, M., Hirose, Y., Sakaguchi, K., Hatano, S., et al. (2015). Dihydroflavonol 4-reductase activity is associated with the intensity of flower colors in delphinium. *Plant Biotechnol.* 32, 249–255. doi: 10.5511/plantbiotechnology.15.0702b

Ni, J., Ruan, R., Wang, L., Jiang, Z., Gu, X., Chen, L., et al. (2020). Functional and correlation analyses of dihydroflavonol-4-reductase genes indicate their roles in regulating anthocyanin changes in Ginkgo biloba. *Ind. Crop Prod.* 152:112546. doi: 10.1016/j.indcrop.2020.112546

Ning, Z., Hu, K., Zhou, Z., Zhao, D., Tang, J., Wang, H., et al. (2021). *IbERF71*, with *IbMYB340* and *IbbHLH2*, coregulates anthocyanin accumulation by binding to the *IbANS1* promoter in purple-fleshed sweet potato (*Ipomoea* batatas L.). *Plant Cell Rep.* 40, 157–169. doi: 10.1007/s00299-020-02621-0

Nitta, M., Lee, J. K., Kang, C. W., Katsuta, M., Yasumoto, S., Liu, D. J., et al. (2005a). The distribution of *Perilla* species. *Genet. Resour. Crop Evolution* 52, 797–804. doi: 10.1007/s10722-003-6017-5

Nitta, M., Lee, J. K., Kobayashi, H., Liu, D., and Nagamine, T. (2005b). Diversification of Multipurpose Plant *Perilla Frutescens*. *Genet. Resour. Crop Evolution* 52, 663–670. doi: 10.1007/s10722-003-6013-9

Nozue, K., Covington, M. F., Duek, P. D., Lorrain, S., Fankhauser, C., Harmer, S. L., et al. (2007). Rhythmic growth explained by coincidence between internal and external cues. *Nature* 448, 358–361. doi: 10.1038/nature05946

Oyama, T., Shimura, Y., and Okada, K. (1997). The *Arabidopsis HY5* gene encodes a bZIP protein that regulates stimulus-induced development of root and hypocotyl. *Genes. Dev.* 11, 2983–2995. doi: 10.1101/gad.11.22.2983

Park, S. I., Park, H. L., Bhoo, S. H., Lee, S. W., and Cho, M. H. (2021). Biochemical and molecular characterization of the rice chalcone isomerase family. *Plants (Basel)* 10:2064. doi: 10.3390/plants10102064

Rizzo, V., Ferlazzo, N., Curro, M., Isola, G., Matarese, M., Bertuccio, M. P., et al. (2021). Baicalin-Induced Autophagy Preserved LPS-Stimulated Intestin22(5):2315.al Cells from Inflammation and Alterations of Paracellular Permeability. *Int. J. Mol. Sci.* 22:2315. doi: 10.3390/ijms22052315

Saita, E., Kishimoto, Y., Tani, M., Iizuka, M., Toyozaki, M., Sugihara, N., et al. (2012). Antioxidant Activities of *Perilla frutescens* against Low-Density Lipoprotein Oxidation in Vitro and in Human Subjects. *J. Oleo. Sci.* 61, 113–120. doi: 10.5650/jos.61.113

Saito, K., Kobayashi, M., Gong, Z., Tanaka, Y., and Yamazaki, M. (1999). Direct evidence for anthocyanidin synthase as a 2-oxoglutarate-dependent oxygenase: Molecular cloning and functional expression of cDNA from a red forma of *Perilla frutescens*. *Plant J.* 17, 181–189. doi: 10.1046/j.1365-313x.1999.00365.x

Saito, K., and Yamazaki, M. (2002). Biochemistry and molecular biology of the late-stage of biosynthesis of anthocyanin: Lessons from *Perilla frutescens* as a model plant. *New Phytol.* 155, 9–23. doi: 10.1046/j.1469-8137.2002.00440.x

Shi, M. Z., and Xie, D. Y. (2010). Features of anthocyanin biosynthesis in pap1-D and wild-type *Arabidopsis thaliana* plants grown in different light intensity and culture media conditions. *Planta* 231, 1385–1400. doi: 10.1007/s00425-010-1142-9

Shi, M. Z., and Xie, D. Y. (2011). Engineering of red cells of *Arabidopsis thaliana* and comparative genome-wide gene expression analysis of red cells versus wild-type cells. *Planta* 233, 787–805. doi: 10.1007/s00425-010-1335-2

Shimada, N., Aoki, T., Sato, S., Nakamura, Y., Tabata, S., and Ayabe, S. (2003). A cluster of genes encodes the two types of chalcone isomerase involved in the biosynthesis of general flavonoids and legume-specific 5-deoxy(iso)flavonoids in Lotus japonicus. *Plant Physiol.* 131, 941–951. doi: 10.1104/pp.004820

Shin, D. H., Choi, M., Kim, K., Bang, G., Cho, M., Choi, S. B., et al. (2013). *HY5* regulates anthocyanin biosynthesis by inducing the transcriptional activation of the *MYB*75/PAP1 transcription factor in *Arabidopsis*. *Febs. Lett.* 587, 1543–1547. doi: 10.1016/j.febslet.2013.03.037

Springob, K., Nakajima, J., Yamazaki, M., and Saito, K. (2003). Recent advances in the biosynthesis and accumulation of anthocyanins. *Nat. Prod. Rep.* 20, 288–303. doi: 10.1039/b109542k

Stracke, R., Favory, J. J., Gruber, H., Bartelniewoehner, L., Bartels, S., Binkert, M., et al. (2010). The *Arabidopsis bZIP* transcription factor *HY5* regulates expression of the PFG1/*MYB12* gene in response to light and ultraviolet-B radiation. *Plant Cell Environ.* 33, 88–103. doi: 10.1111/j.1365-3040.2009.02061.x

Stracke, R., Ishihara, H., Huep, G., Barsch, A., Mehrtens, F., Niehaus, K., et al. (2007). Differential regulation of closely related R2R3-*MYB* transcription factors controls flavonol accumulation in different parts of the *Arabidopsis thaliana* seedling. *Plant J.* 50, 660–677. doi: 10.1111/j.1365-313X.2007.03078.x

Stracke, R., Turgut-Kara, N., and Weisshaar, B. (2017). The At*MYB12* activation domain maps to a short C-terminal region of the transcription factor. *Z. Naturforsch. C. J. Biosci.* 72, 251–257. doi: 10.1515/znc-2016-0221

Takos, A. M., Jaffé, F. W., Jacob, S. R., Bogs, J., Robinson, S. P., and Walker, A. R. (2006). Light-induced expression of a *MYB* gene regulates anthocyanin biosynthesis in red apples. *Plant Physiol.* 142, 1216–1232. doi: 10.1104/pp.106.088104

Turnbull, J., Sobey, W., Aplin, R., Hassan, A., Schofield, C., Firmin, J., et al. (2000). ChemInform Abstract: Are Anthocyanidins the Immediate Products of Anthocyanidin Synthase? *Chem. Commun.* 32, 2473–2474. doi: 10.1039/b007594i

Turnbull, J. J., Nagle, M. J., Seibel, J. F., Welford, R. W., Grant, G. H., and Schofield, C. J. (2003). The C-4 stereochemistry of leucocyanidin substrates for anthocyanidin synthase affects product selectivity. *Bioorg. Med. Chem. Lett.* 13, 3853–3857. doi: 10.1016/S0960-894X(03)00711-X

Wang, Y., Zhang, X., Zhao, Y., Yang, J., He, Y., Li, G., et al. (2020). Transcription factor *PyHY5* binds to the promoters of *PyWD40* and P*yMYB10* and regulates its expression in red pear 'Yunhongli No. 1'. *Plant Physiol. Biochem.* 154, 665–674. doi: 10.1016/j.plaphy.2020.07.008

Xiao, S., Liu, Y., Wang, A., Liu, Y., Li, X., Liu, Z., et al. (2021). The response of tartary buckwheat and 19 bZIP genes to abscisic acid (ABA). *Mol. Biol. Rep.* 48, 4341–4350. doi: 10.1007/s11033-021-06449-z

Xie, D. Y., Jackson, L. A., Cooper, J. D., Ferreira, D., and Paiva, N. L. (2004). Molecular and biochemical analysis of two cDNA clones encoding dihydroflavonol-4-reductase from Medicago truncatula. *Plant Physiol.* 134, 979–994. doi: 10.1104/pp.103.030221

Yamamoto, H., and Ogawa, T. (2002). Antimicrobial activity of *perilla* seed polyphenols against oral pathogenic bacteria. *Biosci. Biotech. Bioch.* 66, 921–924. doi: 10.1271/bbb.66.921

Yamazaki, M., Makita, Y., Fester, K., and Saito, K. (2003). Regulatory mechanisms for anthocyanin biosynthesis in chemotypes of *Perilla frutescens* var. crispa. *Biochem. Eng. J.* 14, 191–197. doi: 10.1016/S1369-703X(02)00222-X

Yamazaki, M., and Saito, K. (2011). Molecular genetic study on the anthocyanin chemotypes of *Perilla frutescens* var. crispa. *Nat. Prod. Commun.* 6, 423–427. doi: 10.1177/1934578X1100600322

Yang, E., Ku, S., Lee, W., Lee, S., Lee, T., Song, K., et al. (2013). Barrier protective effects of rosmarinic acid on HMGB1-induced inflammatory responses in vitro and in vivo. *J. Cell Physiol.* 228, 975–982. doi: 10.1002/jcp.24243

Yang, J., Song, H. D., Chen, Y., Chen, B., Kim, M., Kim, P., et al. (2021). A single amino acid substitution in the R2R3 conserved domain of the BrPAP1a transcription factor impairs anthocyanin production in turnip (*Brassica rapa subsp. rapa*). *Plant Physiol. Biochem.* 162, 124–136. doi: 10.1016/j.plaphy.2021.02.011

Yu, H., Qiu, J. F., Ma, L. J., Hu, Y. J., Li, P., and Wan, J. B. (2017). Phytochemical and phytopharmacological review of *Perilla frutescens* L. (Labiatae), a traditional edible-medicinal herb in China. *Food Chem. Toxicol.* 108, 375–391. doi: 10.1016/j.fct.2016.11.023

Zhang, S., Zhang, L., Zou, H., Qiu, L., Zheng, Y., Yang, D., et al. (2021). Effects of Light on Secondary Metabolite Biosynthesis in Medicinal Plants. *Front. Plant Sci.* 12:781236. doi: 10.3389/fpls.2021.781236

Zhang, Z., Shi, Y., Ma, Y., Yang, X., Yin, X., Zhang, Y., et al. (2020). The strawberry transcription factor FaRAV1 positively regulates anthocyanin accumulation by activation of Fa*MYB10* and anthocyanin pathway genes. *Plant Biotechnol. J.* 18, 2267–2279. doi: 10.1111/pbi.13382

Zhao, C. L., Chen, Z. J., Bai, X. S., Ding, C., Long, T. J., Wei, F. G., et al. (2014). Structure-activity relationships of anthocyanidin glycosylation. *Mol. Divers* 18, 687–700. doi: 10.1007/s11030-014-9520-z

Zheng, X. T., Chen, Y. L., Zhang, X. H., Cai, M. L., Yu, Z. C., and Peng, C. L. (2019). ANS-deficient *Arabidopsis* is sensitive to high light due to impaired anthocyanin photoprotection. *Funct. Plant Biol.* 46, 756–765. doi: 10.1071/FP19042

Zheng, X. T., Yu, Z. C., Tang, J. W., Cai, M. L., Chen, Y. L., Yang, C. W., et al. (2021). The major photoprotective role of anthocyanins in leaves of Arabidopsis thaliana under long-term high light treatment: Antioxidant or light attenuator? *Photosynth. Res.* 149, 25–40.

Zhou, P., Yin, M., Dai, S., Bao, K., Song, C., Liu, C., et al. (2021). Multi-omics analysis of the bioactive constituents biosynthesis of glandular trichome in *Perilla frutescens*. *BMC Plant Biol.* 21:277. doi: 10.1186/s12870-021-03069-4

frontiers | Frontiers in Plant Science

TYPE Original Research
PUBLISHED 20 August 2024
DOI 10.3389/fpls.2024.964476

OPEN ACCESS

EDITED BY
Anna N. Stepanova,
North Carolina State University, United States

REVIEWED BY
Guadalupe Fernandez Milmanda,
Flemish Institute for Biotechnology, Belgium
Olga V. Voitsekhovskaja,
Komarov Botanical Institute (RAS), Russia

*CORRESPONDENCE
Clarence J. Swanton
cswanton@uoguelph.ca

†These authors have contributed equally to this work

RECEIVED 08 June 2022
ACCEPTED 30 July 2024
PUBLISHED 20 August 2024

CITATION
Berardi N, Amirsadeghi S and Swanton CJ (2024) Plant competition cues activate a singlet oxygen signaling pathway in *Arabidopsis thaliana*. *Front. Plant Sci.* 15:964476. doi: 10.3389/fpls.2024.964476

Plant competition cues activate a singlet oxygen signaling pathway in *Arabidopsis thaliana*

Nicole Berardi[1†], Sasan Amirsadeghi[2†] and Clarence J. Swanton[2*]

[1]Ontario Ministry of Agriculture, Food and Rural Affairs, Guelph, ON, Canada, [2]Department of Plant Agriculture, University of Guelph, Guelph, ON, Canada

Oxidative stress responses of *Arabidopsis* to reflected low red to far-red signals (R:FR ≈ 0.3) generated by neighboring weeds or an artificial source of FR light were compared with a weed-free control (R:FR ≈1.6). In the low R:FR treatments, induction of the shade avoidance responses (SAR) coincided with increased leaf production of singlet oxygen ($^1O_2$). This $^1O_2$ increase was not due to protochlorophyllide accumulation and did not cause cell death. Chemical treatments, however, with 5-aminolevulinic acid (the precursor of tetrapyrrole biosynthesis) and glutathione (a quinone A reductant) enhanced cell death and growth inhibition. RNA sequencing revealed that transcriptome responses to the reflected low R:FR light treatments minimally resembled previously known *Arabidopsis* $^1O_2$ generating systems that rapidly generate $^1O_2$ following a dark to light transfer. The upregulation of only a few early $^1O_2$ responsive genes (6 out of 1931) in the reflected low R:FR treatments suggested specificity of the $^1O_2$ signaling. Moreover, increased expression of two enzyme genes, the *SULFOTRANSFERASE ST2A* (*ST2a*) and the early $^1O_2$-responsive *IAA-LEUCINE RESISTANCE (ILR)-LIKE6* (*ILL6*), which negatively regulate jasmonate level, suggested that repression of bioactive JAs may promote the shade avoidance (versus defense) and $^1O_2$ acclimation (versus cell death) responses to neighboring weeds.

KEYWORDS

acclimation response, *Arabidopsis thaliana*, low red to far-red ratio, plant competition, RNA sequencing, shade avoidance response, singlet oxygen signaling, jasmonate-dependent defenses

Introduction

Singlet oxygen ($^1O_2$) is a potent oxidant that is generated in photosynthetic and non-photosynthetic tissues under multiple stresses (Dmitrieva et al., 2020). Several reports on the lifetime and diffusion distance of $^1O_2$ in cellular environments indicate that $^1O_2$ may diffuse through cell membranes (Dmitrieva et al., 2020; Ogilby, 2010; Hatz et al., 2007; Skovsen et al., 2005). Indeed, in *Chlamydomonas reinhardtii*, the photosystem II (PSII)-

generated $^1O_2$ under high light stress reached cytosol and induced expression of the glutathione reductase homologue GPXH (Fischer et al., 2007). These studies along with the detection of osmotic stress- and drought-induced $^1O_2$ in *Arabidopsis* roots (Chen and Fluhr, 2018; Mor et al., 2014) indicate the possibility of $^1O_2$ generation in cellular compartments other than chloroplast.

Under severe stress conditions, high levels of $^1O_2$ can damage cellular components and impair plant function through photo-inhibition and uncontrollable cell death (Laloi and Havaux, 2015). At sub-lethal levels, however, $^1O_2$ initiates signaling pathways that trigger disparate stress responses including acclimation to excess light and programmed cell death (op den Camp et al., 2003; Ledford et al., 2007; Laloi and Havaux, 2015; Waszczak et al., 2018; Ambastha et al., 2020).

Several plant systems allow for the study of $^1O_2$ signaling. These include the conditional fluorescent (*flu*) mutant of *Arabidopsis* (Meskauskiene et al., 2001; op den Camp et al., 2003), the *tigrina* (*tig-d.12*) mutant of barley (Lee et al., 2003), and the *chlorina1* (*ch1*) mutant of *Arabidopsis* (Ramel et al., 2013a). The *flu* and *tig-d.12* mutants produce $^1O_2$ in the light from dark-accumulated photosensitizer protochlorophyllide (Pchlide), whereas the *ch1* mutant of *Arabidopsis* and the *chlorina-f2* mutant of barley are deficient in chlorophyll b (Kim et al., 2009; Havaux et al., 2007; Havaux and Tardy, 1997; Leverenz et al., 1992). In the *ch1* mutant of *Arabidopsis*, PSII is confined to its reaction center due to the inability of PSII light-harvesting antennae to assemble without chlorophyll b. Without light-harvesting complex II (LHCII), PSII lacks photoprotective mechanisms like nonphotochemical quenching. Consequently, increasing photon flux density can lead to PSII overexcitation and the formation of $^1O_2$ (Ramel et al., 2013a; Dall'Osto et al., 2010). While these mutant systems have provided valuable insight into the $^1O_2$ signaling pathways, few plant systems allow the controlled induction of $^1O_2$ and investigation of $^1O_2$ signaling within wild type plants. Recently, $^1O_2$ generation was detected in wild type *Arabidopsis* leaves following transfer of the FR light-treated seedling to white light (Page et al., 2017). This white light-mediated induction of $^1O_2$ was due to Pchlide accumulation and led to suppression of major chlorophyll synthesis and photosynthetic genes presumably to prevent photo-oxidative damage during de-etiolation (Page et al., 2017).

Despite the detection of $^1O_2$ in wild type *Arabidopsis* leaves following a short-time (two hours) FR light treatment and exposure to white light (Page et al., 2017), it is not clear whether $^1O_2$ can be induced under low R:FR light environments. Such $^1O_2$ induction may provide an opportunity to explore the involvement of $^1O_2$ signaling as an intermediary between low R:FR light-mediated phytochrome inactivation and modulation of growth-defense trade-offs in response to competition cues. Under low R:FR light environments, phytochrome inactivation promotes growth-related hormonal pathways, while attenuating jasmonic acid (JA)-mediated defense responses (Ballaré, 2014; de Wit et al., 2016; Fernández-Milmanda and Ballaré, 2021). Attenuation of JA synthesis is also indispensable for triggering acclimation response to $^1O_2$ and prevention of cell death, while $^1O_2$-mediated photo-damage and cell death correspond with JA accumulation (Ramel et al., 2013a; Ramel et al., 2013b). Recently, a sulfotransferase (*ST2a*) has been shown to be up-regulated as a molecular link between low R:FR light environments and attenuation of JA-mediated defense responses through sulfation of bioactive JAs (Fernández-Milmanda et al., 2020). In addition, to a lesser extent, the low R:FR light upregulated the early $^1O_2$-responsive amidohydrolase *ILL6* (op den Camp et al., 2003), which catalyzes the amido-hydrolysis of JA-isoleucine (Fernández-Milmanda et al., 2020). Given that Pchlide accumulation in the FR light-adapted plants leads to $^1O_2$ production under white light (Page et al., 2017), a possibility arises that *ST2a* up-regulation in the low R:FR environments may be linked to $^1O_2$-mediated signaling. In this work, wild-type *Arabidopsis* was used as a model to distinguish whether increased leaf production of $^1O_2$ in response to competition cues is due to reflected far-red light from neighboring weeds and to gain insights into the $^1O_2$ signaling under low R:FR light environments. Our findings under biological weedy and artificial sources of reflected low R:FR light show that elongation growth responses occur concurrently with $^1O_2$ appearance suggesting its signaling role in response to competition cues. The $^1O_2$ appearance is not a consequence of Pchlide accumulation and not sufficient to cause cell death but chemical treatments that increase Pchlide level or decrease chloroplast electron transport efficiency result in cell death and growth inhibition. The $^1O_2$ signatures under the biological and artificial low R:FR light treatments differ dramatically from those in *Arabidopsis* mutants that rapidly generate $^1O_2$ after dark to light transfer. Finally, the upregulation of *ST2a and ILL6* and the suppression of bioactive JAs may also operate in the acclimation to $^1O_2$ under weed competition.

Materials and methods

Plant material and growth conditions

Wild-type *Arabidopsis thaliana* (ecotype Columbia) plants were raised in controlled environment growth chambers (Model CMP 3244 Conviron, Winnipeg, Canada) with a 12-hour photoperiod, an irradiance of 160 μmol m^{-2} s^{-1}, a temperature of 21/18°C, and a relative humidity of 60%. The weed-free control (R:FR ≈ 1.6), biological low R:FR (R:FR ≈ 0.3), and artificial low R:FR (R:FR ≈ 0.3) light treatments were set up by placing plastic tubes (8 × 18 cm, 1 L) in the center of plastic pots (16 × 15 cm, 3.36 L) (Airlite Plastics Company, Omaha, USA). Drainage holes were drilled in the tubes and pots. For the control and the artificial low R:FR light treatments, the area between the plastic pot and plastic tube was filled with Turface MVP (Profile Products LLC, Buffalo Grove, USA). For the biological low R:FR treatment, the area between the plastic pot and plastic tube was filled with Sunshine Mix #4 (Sungro Horticulture, Agawam, MA) and seeded (≈ 200 g m^{-2}) with a commercial mixture of grass seeds (The Scotts Compnay LLC, Marysville, USA). This mixture of grass seeds consisted of perennial ryegrass (*Lolium perenne* L.), creeping red fescue (*Festuca rubra* L.), Kentucky bluegrass (*Poa pratensis* L.), and chewing fescue (*Festuca rubra* L.) (The Scotts Compnay LLC, Marysville, USA). The grass was watered twice a week and was fertilized every two weeks with a nutrient solution as described previously (Tollenaar, 1989). A dense grass was established within two months and generated a stable

biological source of reflected FR light without direct contact between the grass and experimental plants. A simulated FR light environment (artificial low R:FR; R:FR ≈ 0.3) was generated using 13 W, 162 mA far-red LEDs (Phillips Canada). Seeds of *Arabidopsis* were planted in a mix of PGx (Premier Horticulture LTD, Quebec, Canada) and perlite (Perlite Canada Inc., Quebec, Canada) at a ratio of 3:1 in 355 mL (8×10 cm) plastic cups (Dart Container Corp., Mason, USA). The plastic cups were then placed inside the plastic tubes in each pot in the respective light environments (Figure 1). The central plastic tube acted as a barrier preventing water exchange and nutrient flow between the *Arabidopsis* plants in the cups and the grass. Further, the empty space between the bottom of the cup and bottom of the central tube prevented secretion of grass metabolites to *Arabidopsis* roots. Light interference in the growth chambers was eliminated using a white opaque plastic divider between the weed-free control and biological low R:FR while allowing a free upward air flow (1.55 m^3 min^{-1}) across treatments. *Arabidopsis* plants were grown under weed-free control conditions for 21 days and fertilized weekly with a modified Hoagland's solution (10 mM KNO_3, 10 mM $Ca(NO_3)_2.4H_2O$, and 2.5 mM KH_2PO_4). *Arabidopsis* plants were then exposed to either the biological or artificial low R:FR light treatment for 12 hours a day for seven days or kept under control conditions before plants were sampled. The light spectral composition of the weed-free control, biological low R:FR, and artificial low R:FR light treatments were determined at plant height. The incoming and reflected light quantity and quality were measured at nine locations across each treatment using a LI-COR-180 spectrometer (Li-COR Biosciences; Lincoln, NE, USA). For incoming light measurements, the spectrometer was held level at plant height facing the lights. For reflected light measurements, the spectrometer was held level facing the plants. A summary and detailed information about the light spectral composition in the weed-free control, biological low R:FR and artificial low R:FR light treatments are presented in Supplementary Table 1.

Singlet oxygen imaging

Singlet oxygen formation was detected in 4-week-old *Arabidopsis thaliana* leaves using Singlet Oxygen Sensor Green (SOSG) (ThermoFisher, Waltham, USA). A 500 µM stock solution of SOSG was prepared by dissolving 100 µg of SOSG in 330 µL of methanol and diluted to a working concentration of 10 µM SOSG using 50 mM potassium phosphate buffer (pH 7.5) and 0.01% Tween-20 as a non-ionic surfactant. Plants were manually infiltrated with the 10 µM SOSG solution using a 60 ml needleless syringe and placed back in the treatment for two hours. The SOSG fluorescence (excitation ~450-490 nm; emission ~500-550 nm) was detected using an Axio Zoom V16 fluorescence stereo microscope with a Pan NeoFluor Z 1x/0.25 FWD 56 mm lens and a 38 HE filter set (Zeiss Canada, Toronto, Canada). All leaf images were obtained using the same magnification and an exposure of 500 milliseconds. The SOSG fluorescence signal was quantified using the image analysis application Fiji (Schindelin et al., 2012). Briefly, the fluorescence signal in each leaf image was quantified in five equal (200 × 200) regions of interest (ROIs) and averaged to obtain the mean fluorescence signal. For each treatment, 25 independent images were analyzed.

Pigment analysis

To quantify photosynthetic pigments, leaf discs (nine mm) were taken from the mid-section of fully expanded *Arabidopsis* leaves (4-week-old) and placed in 1.5 mL of 80% acetone. The leaf discs were incubated in the dark at -20°C for 24 hours until total removal of chlorophyll. Absorbance was measured at 470, 626, 645, 646, 647, 663, and 664 nm. The concentration of Pchlide, chlorophyllide a (Chlide a), chlorophyll a (Chl a), chlorophyll b (Chl b), and total carotenoids were calculated using the previously described equations (Brouers and Michel-Wolwertz, 1983; Lichtenthaler and Wellburn, 1983). A more detailed quantification of individual carotenoids including lutein, β-carotene, violaxanthin, and neoxanthin was performed by high performance liquid chromatography (HPLC). Approximately, 20 mg of fresh ground tissue was used for HPLC analysis. To extract prenyl lipids, 250 µL of acetone:ethyl acetate (3:2; v/v) was added to each sample followed by the addition of 100 µL of ethyl acetate and 200 µL of dH_2O. Each sample was then vortexed for five seconds and centrifuged (10 seconds burst) to achieve phase separation. The upper ethyl acetate layer was transferred into a vial and 50 µL of the ethyl acetate layer was separated on a five µm Spherisorb ODS-2 reverse-phase column (250 × 4.6 mm, Supelco) thermostated at 23°C. A linear gradient from 100% acetonitrile:water:trimethylamine (9:1:0.01) to 100% ethyl acetate was used to elute the samples at a flow rate of 1 mL min^{-1} over 45 minutes. Lutein, β-carotene, violaxanthin, and neoxanthin were detected at A_{440} with a detection limit of 0.05 nmol and were quantified based on external calibration standards of high purity. For these HPLC standards, lutein was obtained from Cayman Chemicals (Ann Arbor, MI, USA). β-carotene, violaxanthin, and neoxanthin were obtained from Sigma Aldrich (Oakville, ON, Canada).

Chemical treatments

All chemicals were made up in 10 mM MES buffer (pH 6.5) and 0.01% tween-20 as a surfactant. The final concentrations of chemicals were 10 mM ALA (5-aminolevulinic acid; the precursor of tetrapyrrole biosynthesis), 50 mM, 100 mM, 150 mM, and 200 mM GSH (reduced glutathione; a quinone A reductant), and 50 mM, 100 mM, 150 mM, and 200 mM H_2O_2 (hydrogen peroxide; an oxidizing agent). For the ALA treatment, the upper and lower leaves of 4-week-old *Arabidopsis* plants were sprayed with a two mL solution of ALA. In total, four experiments were performed and ALA was sprayed on three plants per treatment per experiment. For the GSH and H_2O_2 treatments, the rosette leaves of 3-week-old *Arabidopsis* plants were sprayed with a one mL solution of GSH or H_2O_2. After spraying, plants were allowed to dry for one hour before transfer back to the treatments. The extent of cell death by ALA was monitored and imaged every 24 hours for a total of 72 hours. The extent of cell death by GHS and H_2O_2 was monitored every 24 hours and imaged 96 hours after spraying. In total, three independent experiments with a similar time course were performed and each chemical was sprayed on five plants per treatment per experiment. In separate experiments, the extent of

cell death by GSH was quantified in 18 plants per concentration per treatment using the image analysis application Fiji (Schindelin et al., 2012). Dead leaf area was calculated by subtracting the green leaf area from total leaf area and expressed as percentage of leaf cell death.

RNA-sequencing

RNA extraction from 4-week-old *Arabidopsis* rosette leaves and subsequent DNase treatment of RNA samples were performed using a RNeasy PowerPlant kit (Qiagen) and an RNase-Free DNase kit (Qiagen) according to the manufacturer's instructions. In total, nine samples consisting of three treatments (weed-free, biological low R:FR, and artificial low R:FR light) with three replicates, each consisting of a pool of leaves from three individual plants, were analyzed. The RNA quality and quantity were determined using an Agilent 2100 Bioanalyzer (Agilent Technologies). The RNA libraries were constructed using the Illumina TrueSeq RNA kit in three replicates according to the manufacturer's protocol. The RNA libraries were sequenced on an Illumina sequencer (NovaSeq 6000) at the Genome Quebec Innovation Center (McGill University, Canada) to obtain ≈25 M reads per replicate. Differentially expressed gene (DEG) analysis was performed by Harvest Genomics Inc. (Guelph, Canada), where the quality control of raw.fastq files was performed prior to sequence alignment to the reference genome (https://www.ncbi.nlm.nih.gov/assembly/GCF_000001735.4/) using Bowtie 2 v2.4.3. Count data were retrieved using HTSeq (version 0.13.5) and DEGs were determined using DESeq2 (version 1.30.1). The Benjamini-Hochberg false discovery rate (FDR) correction was used within DESeq2 (version 1.30.1) to obtain adjusted *p*-values (*p*adj). Tables of $\log_2$ fold change (lfc) were generated as described previously (Zhu et al., 2019). The RNA-seq raw reads and expression analysis are available in the NCBI gene expression omnibus (GEO) data repository under accession GSE213185 (https://www.ncbi.nlm.nih.gov/gds/?term=GSE213185).

Real-time quantitative reverse transcription PCR assays

Total RNA was extracted from 4-week-old *Arabidopsis* leaves using the TRI Reagent (Sigma Aldrich Canada). In total, 16 samples from two independent experiments were analyzed. In each experiment, eight samples were taken from two treatments (weed-free and biological low R:FR light) each consisting of rosette leaves from four individual plants. The DNAse treatment and sample cleanup were performed using the RNAase-Free DNase Set (Qiagen Inc. Canada) and the RNeasy MinElute Cleanup kit (Qiagen Inc. Canada), respectively. Prior to RT-qPCR assays, RNA quality was determined using an Agilent 4150 TapeStation System (Agilent, CA, USA) according to the manufacturer's instructions. The RNA samples were reverse transcribed using the High Capacity cDNA Reverse Transcription kit following the supplied protocol (Applied Biosystems, Canada). Real-time PCR assays were performed using a QuantaStudio Real Time PCR system (Thermo Fisher Scientific Inc., Canada). Each PCR reaction (20 µl) consisted of 10 µl of 2× SsoAdvanced Universal Inhibitor-Tolerant SYBR supermix (Bio-Rad, Cat No: 172-5017), 0.8 µl of PCR forward and reverse primer mix at 5 µM (final concentration of primer at 200 nM), 4.2 µl of water and 5 µl of 8× diluted cDNA. The thermal cycler conditions were 3 minutes at 98°C polymerase activation step, followed by 40 cycles of a two-step qPCR (10 seconds of 98°C denaturation, 30 seconds of 60°C combined annealing/extension). The amplified PCR products were compared with the *PROFILIN1* (*PRF1*) as a housekeeping gene and relative changes in gene expression were quantified using the $2^{-\Delta\Delta ct}$ equation (Livak and Schmittgen, 2001). Primers were designed using PrimerQuest Tool (Integrated DNA Technologies, Coralville, USA). The primer sequences used for qPCR were: *SULFOTRANSFERASE 2A* (At5G07010) *ST2a* fwd 5'-ACCTCAAGCATGAAGAGCATTC-3' and *ST2a* rev 5'-CCCTTCATCTTCTTCGGCTTTC-3'; *SULFOTRANSFERASE 2B* (At5G07000) *ST2b* fwd 5'-AAGCG AAGGCCAAGAAGAA-3' and *ST2b* rev 5'-GTAACGATT TCTCCGTCCTCTC-3'; *IAA-LEUCINE RESISTANCE (ILR)-LIKE6* (At1g44350) *ILL6* fwd 5'-TCTTGGTGCTGCCCATATTC-3' and *ILL6* rev 5'-AAGCTCCGTCTTCGATCATATTC-3'; *U-BOX E3 UBIQUITIN LIGASE* (At3g19380) *PUB25* fwd 5'-CGACTT CACACTCATCCCTAAC-3' and *PUB25* rev 5'-CAGCTGGTTGT TTAGGAGTAGG-3'; *PRF1* (At2G19760) fwd 5'-GGTGAACAA GGAGCTGTGAT-3' and *PRF1* rev 5'-GGTTCATCGTAGAA GCCAAAGA-3'.

Statistical analysis

Statistical analysis was performed using SAS version 9.4 and PROC GLIMMIX. The experiments were arranged as a randomized complete block design. The light treatment was considered the fixed effect, while replication was considered the random effect. Least-square means were generated, and means were separated with a Tukey's honest significant difference (HSD) test. Unless stated otherwise, each replicate consisted of five *Arabidopsis* samples per treatment and three replications per experiment. A type I error of 0.05 was used for all tests of significance. A power analysis was performed to ensure adequate power was achieved.

Results

The shade avoidance response is accompanied by an increase of $^1O_2$ level in leaves

We exposed 3-week-old *Arabidopsis* plants to the biological and artificial low R:FR light for 12 hours a day for seven days or kept them in the weed-free control condition. This exposure to reflected low R:FR light was under resource-independent competition, where incoming light, water and nutrients were not limiting factors. Further, we prevented direct root contact between the *Arabidopsis* plants and the surrogate weeds by a plastic tube in the center of the

10.3389/fpls.2024.964476

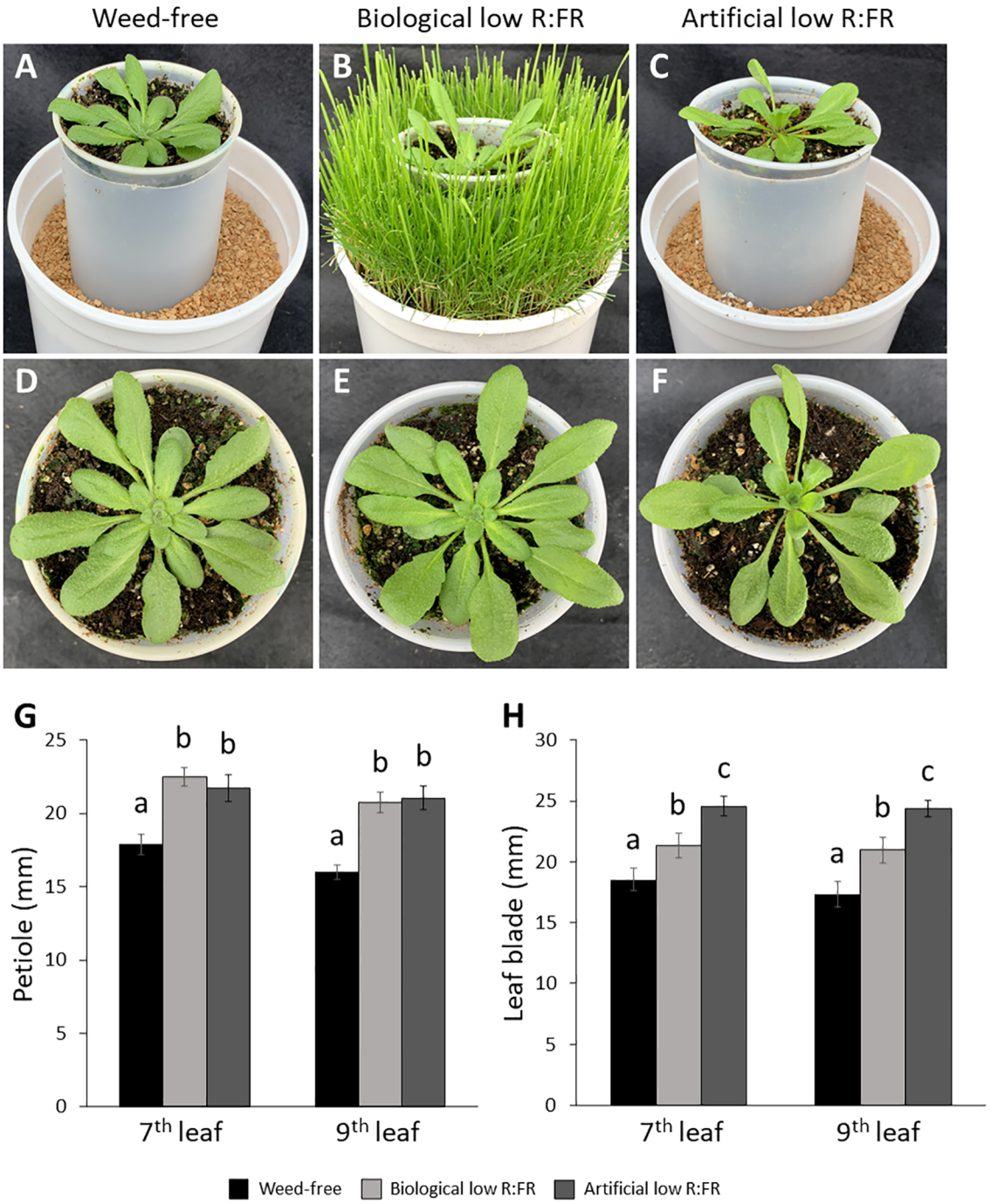

FIGURE 1
Weed-free control **(A)**, biological low R:FR **(B)**, and artificial low R:FR **(C)** treatments with reflected R:FR of ≈1.6, ≈0.3, and ≈0.3, respectively. *Arabidopsis* plants were exposed to the biological and artificial low R:FR light for 12 hours a day for seven days or kept under control (weed-free) condition prior to sampling. Plastic cups containing *Arabidopsis* seedling were placed in a plastic tube in the center of the pots to prevent direct root contact with neighbouring weeds. Note the hyponastic leaf growth in the biological and artificial low R:FR treatments. Normal leaf growth in the control **(D)**, and petiole elongation in the biological low R:FR **(E)**, and artificial low R:FR **(F)** treatments. Increases in petiole **(G)** and leaf blade **(H)** lengths of 7th and 9th leaf (4-week-old) in the low R:FR treatments. Black bars represent the control treatment while light grey and dark grey bars represent the biological low R:FR and artificial low R:FR light treatments, respectively. Note the similar elongation responses of *Arabidopsis* in separate growth chambers with the biological and artificial sources of reflected low R:FR light. Data represent means ± SEM for three independent experiments each consisting of five plants per treatment. Means were separated using Tukey's HSD test (P<0.05). Letters indicate statistical significance of differences across treatments.

pots (Figures 1A–C; Supplementary Table 1). Elongation growth and leaf hyponasty were typical shade avoidance responses (Figures 1A–F). The biological and artificial low R:FR treatments caused similar elongation responses in the petiole lengths (23% and 26%) and leaf blade lengths (14% and 19%) of 4-week-old *Arabidopsis* plants (Figures 1G–H). These shade avoidance responses were accompanied by increases in leaf production of $^1O_2$ in the biological and artificial low R:FR treatments (Figures 2A–C).

Quantification of SOSG fluorescence by the image analysis application Fiji (Schindelin et al., 2012) revealed 2.6× and 3.0× increase in mean fluorescence signal in the biological and artificial low R:FR treatments, respectively, compared with the weed-free control. In addition, mean fluorescence signal in the artificial low R:FR treatments was significantly higher than the biological low R:FR treatment (Figure 2D; Supplementary Table 2). These results not only indicated that the biological low R:FR treatment could elicit the shade avoidance responses in the absence of direct resource competition but also suggested that the $^1O_2$, which was predominantly generated by the reflected FR light from neighboring weeds, might be a molecular component of the shade avoidance response.

Increased leaf production of $^1O_2$ in the low R:FR light environments is not due to the accumulation of chlorophyll precursors

Induction of $^1O_2$ in the *flu* mutant of *Arabidopsis* is the result of photosensitization of accumulated Pchlide following transfer from dark to light (Meskauskiene et al., 2001). To investigate whether a similar mechanism is responsible for increased leaf production of $^1O_2$ in the low R:FR treatments, the levels of Pchlide, Chlide a, Chl a, Chl b, and total Chl were compared with that of control plants using spectrophotometry. The levels of Pchlide were not significantly altered by the biological and artificial low R:FR treatments (Figure 3A), while the Chlide a levels were significantly decreased (9.4% and 25.9%, respectively) compared with the control (Figure 3B). In addition, significant decreases were found in the levels of Chl a (10.3% and 8.2%), Chl b (26.9% and 21.9%), and total Chl (9.6% and 25.3%) in the biological and artificial low R:FR treatments compared with the control (Figures 3C–E). Further, exposure of *Arabidopsis* plants in the biological and artificial low R:FR treatments to dark periods of two, four, and six hours did not affect Pchlide levels (Figure 3A). The Chlide a levels were decreased in the biological and artificial low R:FR treatments (13.9% and 35.7%, respectively) after two hours of dark incubation (Figure 3B). This decrease, however, was significant only in the artificial low R:FR treatment. Further, a significant decrease (34%) was found in the artificial low R:FR treatment after four hours of dark incubation. Although the Chlide a levels in the low R:FR treatments were not significantly different from the weed-free control after six hours of dark incubation, the Chlide a level in the artificial low R:FR treatment was significantly lower (19.3%) than the biological low R:FR treatment (Figure 3B). The Chl a levels were decreased after two hours (13.5% and 39.4%) and four hours (22.1% and 36.1%) of dark incubation compared with the control (Figure 3C). These decreases, however, were significant only in the artificial low R:FR treatment and no significant difference was found between treatments after six hours of dark incubation (Figure 3C). The levels of Chl b were decreased after two hours in the biological and artificial low R:FR treatments

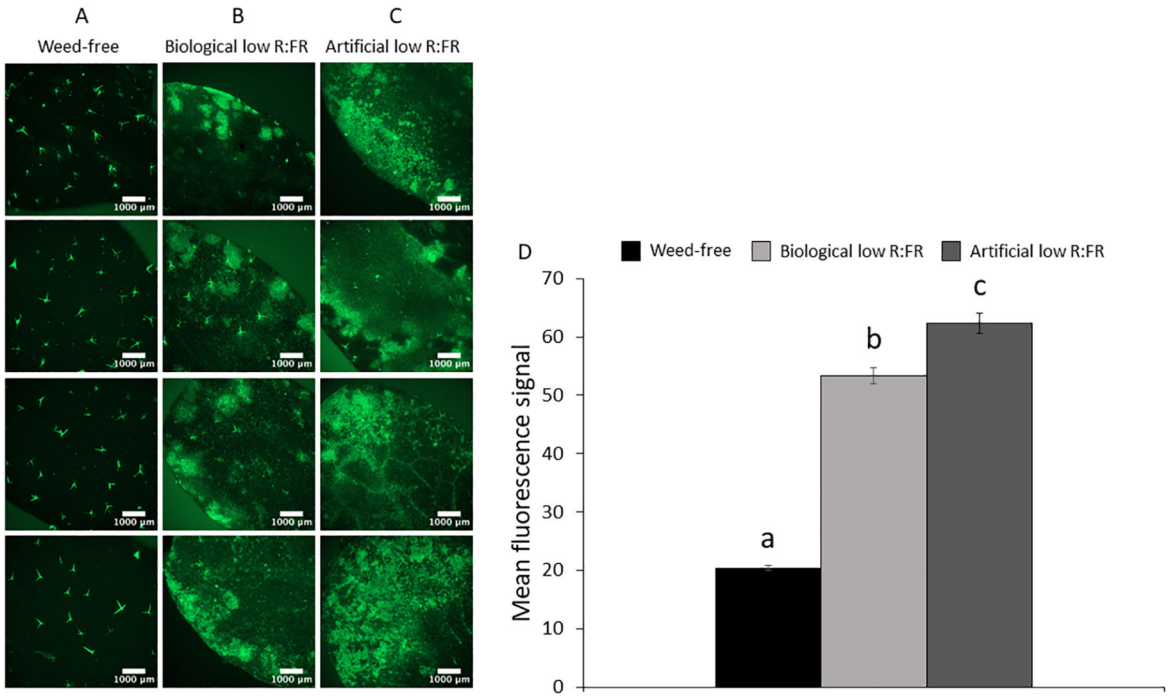

FIGURE 2
Basal level of $^1O_2$ in the weed-free control **(A)** and increases in $^1O_2$ levels in the biological low R:FR **(B)** and artificial low R:FR **(C)** treatments. Each panel shows four representative images of independent leaf samples. Four-week-old *Arabidopsis* plants were infiltrated with 10 µM SOSG and the SOSG fluorescence was imaged two hours after infiltration at an exposure time of 500 milliseconds. Scale bar represents 1000 µm. Significant increases in mean fluorescence signal in the biological and artificial low R:FR treatments **(D)**. The SOSG fluorescence was quantified using the image analysis application Fiji (Schindelin et al., 2012). Data represent means ± SEM for 25 independent leaf samples per treatment (Supplementary Table 2). Means were separated using Tukey's HSD test (P<0.05). Letters indicate statistical significance of differences across treatments.

10.3389/fpls.2024.964476

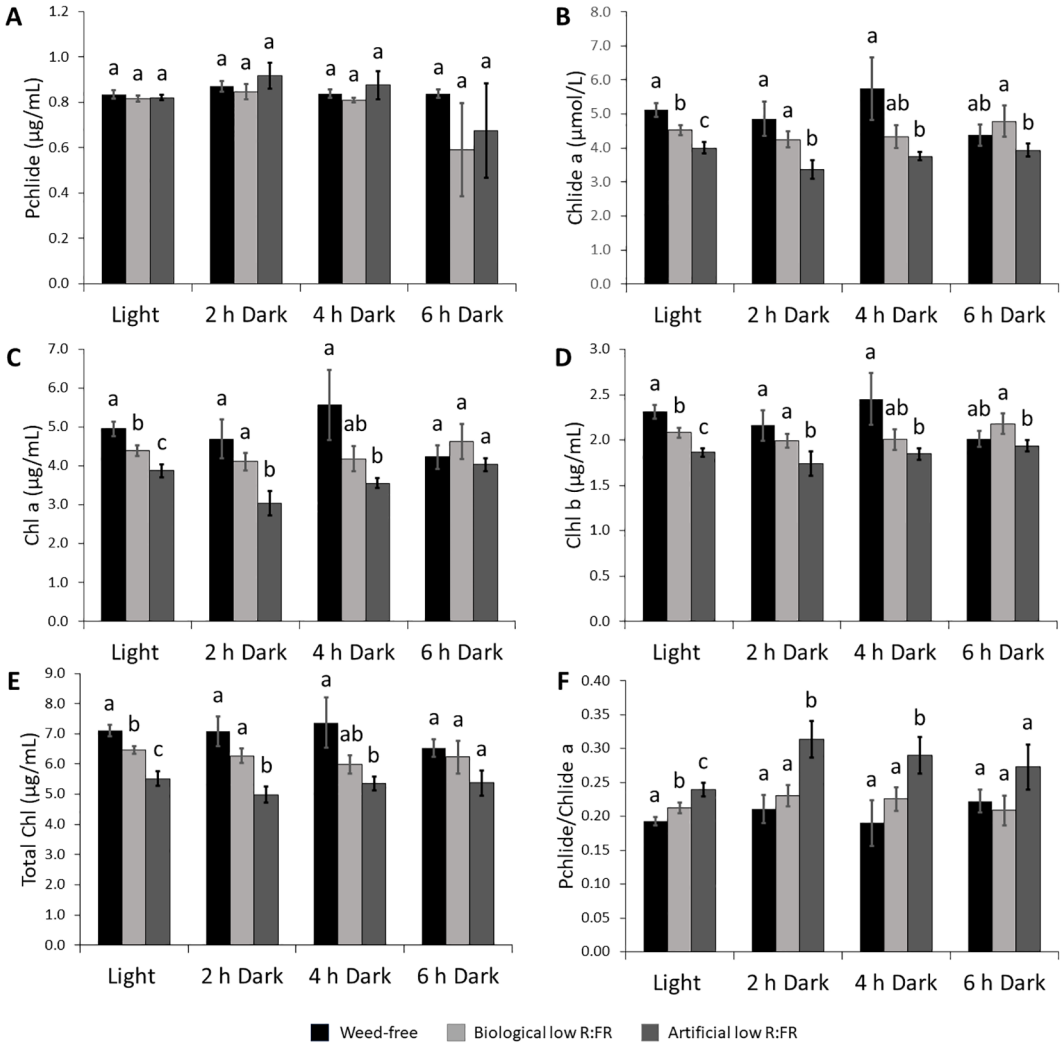

FIGURE 3
Changes in the levels of photosynthetic pigments in the biological and artificial low R:FR treatments in the light and after two, four, and six hours of dark incubation. *Arabidopsis* plants were exposed to the biological and artificial low R:FR light for 12 hours a day for seven days or kept under control (weed-free) condition prior to sampling. Black bars represent the control while light grey and dark grey bars represent the biological and artificial low R:FR treatments, respectively. No significant change in Pchlide levels in the reflected low R:FR treatments and after dark incubation for two, four, and six hours **(A)**. Decreases in Chlide a levels in the reflected low R:FR treatments and after dark incubation for two and four hours **(B)**. Decreases in Chl a **(C)**, Chl b **(D)**, and total Chl **(E)** levels in the reflected low R:FR treatments and after dark incubation for two and four hours. Increases in the ratio of Pchlide to Chlide a in the artificial low R:FR treatment and after dark incubation for two and four hours **(F)**. Data represent means ± SEM for three independent experiments each consisting of three plants per treatment. Means were separated using Tukey's HSD test ($P<0.05$). Letters indicate statistical significance of differences across treatments.

(9.2% and 24.9%, respectively). This decrease, however, was significant only in the artificial low R:FR treatment. Further, a significant decrease (23.2%) was found in the artificial low R:FR treatment after four hours of dark incubation (Figure 3D). Although the levels of Chl b in the biological and artificial low R:FR treatments were not different from the weed-free control after six hours of dark incubation, the level of Chl b in the artificial low R:FR treatment was significantly lower (12.2%) compared with the biological low R:FR treatment (Figure 3D). The levels of total Chl were decreased in the biological and artificial low R:FR treatments only after two hours (12.1% and 34.7%) and four hours (20.6% and 31.8%) of dark incubation (Figure 3E). Again, these decreases were significant only in the artificial low R:FR treatment (Figure 3E). In the biological and artificial low R:FR treatments, *Arabidopsis* plants displayed higher ratios of Pchlide to Chlide a (Pchlide/Chlide a) compared with the control (Figure 3F). The higher Pchlide/Chlide a may be due to decreased conversion of Pchlide to Chlide a. It is not clear whether higher Pchlide/Chlide a may contribute to $^1O_2$ generation. After two and four hours of dark incubation, however, Pchlide/Chlide a were increased in the artificial low R:FR treatment only, whereas six hours of dark incubation did not affect Pchlide/Chlide a (Figure 3F). The lack of accumulation of Pchlide in the dark (Figure 3A), however, suggests that $^1O_2$ generation in the low R:FR treatments occurs via a different mechanism than in the *flu* mutant of *Arabidopsis*.

10.3389/fpls.2024.964476

Low R:FR light environments decrease total carotenoid content and differentially alter levels of xanthophylls

Since carotenoids are the most efficient physical quenchers of $^1O_2$ that primarily protect photosystems from oxidative damage (Triantaphylidès and Havaux, 2009), we investigated whether increased leaf production $^1O_2$ in the low R:FR light treatments was due to decreases in carotenoid levels. We found that total carotenoid levels were decreased by 7.1% and 37.7% in the biological and artificial low R:FR treatments, respectively (Figure 4A). When individual xanthophyll levels were examined by HPLC, however, there appeared to be no difference between the levels of lutein (Figure 4B), β-carotene (Figure 4C), violaxanthin (Figure 4D), and neoxanthin (Figure 4E) in the biological low R:FR treatment compared with the control. In the artificial low R:FR treatment, however, the levels of lutein, β-carotene, and violaxanthin were deceased by 17.6%, 13.1%, and 17.1%, respectively, compared with the control. The neoxanthin level in this treatment was significantly lower than in the biological low R:FR treatment but did not differ from that of the control. Therefore, the observed decrease in total carotenoids in the biological low R:FR treatment does not appear to be due to decreases in the levels of lutein, β-carotene, violaxanthin, and neoxanthin. In contrast, the decreased level of total carotenoids in the artificial low R:FR treatment may be attributable to decreases in the levels of lutein, β-carotene, and violaxanthin. Further, these results suggest that the $^1O_2$ induction by the artificial low R:FR treatment may arise from decreased levels or the suppression of

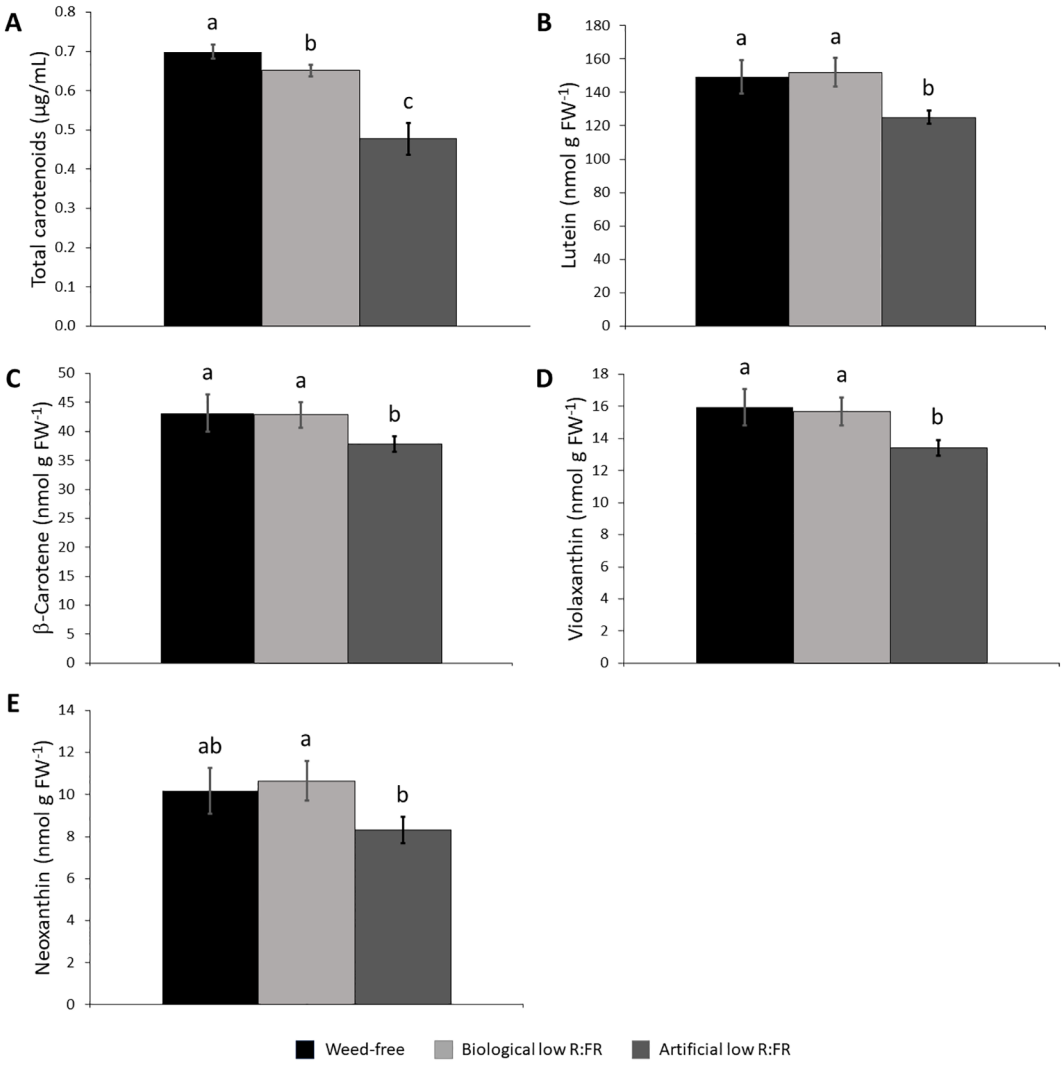

FIGURE 4
Effect of the reflected low R:FR treatments on carotenoid content. *Arabidopsis* plants were exposed to the biological and artificial low R:FR light for 12 hours a day for seven days or kept under control (weed-free) condition prior to sampling. Black bars represent the control while light grey and dark grey bars represent the biological and artificial low R:FR treatments, respectively. Decreases in total carotenoid content in the biological and artificial low R:FR treatments **(A)** and no changes in the levels of lutein **(B)**, β-carotene **(C)**, violaxanthin, **(D)**, and neoxanthin **(E)** in the biological low R:FR treatment. The levels of lutein, β-carotene, and violaxanthin in the artificial low R:FR treatment are lower than that in the control.Total carotenoid data represent means ± SEM for four replicates consisting of three plants per treatment while individual carotenoid data represent means ± SEM for three independent experiments each consisting of three plants per treatment. Means were separated using Tukey's HSD test (P<0.05). Letters indicate statistical significance of differences across treatments.

protective function of these carotenoids. These mechanisms however, do not appear to be behind the $^1O_2$ induction by the biological low R:FR treatment. Unlike the artificial low R:FR treatment, the inability of the biological low R:FR treatment to decrease the levels of the above-mentioned carotenoids may be attributable to the effects associated with the surrogate weed used for the biological low R:FR treatment. We do not, however, rule out the involvement of other carotenoids such as zeaxanthin, which is also a potent physical quencher of $^1O_2$ (Triantaphylidès and Havaux, 2009).

Low R:FR light environments increase susceptibility to cell death by ALA

It is well recognized that both light-dependent and light-independent induction of $^1O_2$ can trigger cell death responses (Wagner et al., 2004; Ramel et al., 2013a; Mor et al., 2014; Chen and Fluhr, 2018). We sprayed *Arabidopsis* plants in the control, biological, and artificial low R:FR treatments with ALA (10 mM) to increase the levels of photodynamic tetrapyrrole intermediates in these plants and compare their susceptibility to cell death. After 24 hours, plants in the biological low R:FR treatment wilted, while the control displayed little sign of cellular damage (Figures 5A, B, E, F). After 48 hours, signs of cellular damage were apparent on all the plants, however, it was more severe in the biological low R:FR treatment (Figures 5A, C, E, G, M, O). After 72 hours, the control plants exhibited minor signs of cell death in small localized patches, while in the biological low R:FR treatment, plants displayed total necrosis with the exception of the growing points (Figures 5A, D, E, H). Plants in the artificial low R:FR treatment exhibited cell death more severe than the control treatment, but less so than the biological low R:FR treatment (Figures 5A, D, M, P). Further, after spraying ALA, plants that were transferred from the low R:FR treatments to the control treatment displayed similar cell death symptoms as the plants that had been replaced into their respective treatments pre-spray (Figures 5I–L, Q–T). These results suggest that further increases in $^1O_2$ levels in the low R:FR treatments may tip the $^1O_2$ balance from an acclimation response towards a cell death response.

Low R:FR environments differentially enhance cell death and growth inhibition responses to GSH

It has been established that GSH can increase and H_2O_2 can decrease photo-oxidative damage through the control of the redox state of the quinone A (Q_A)-quinone B (Q_B)-plastoquinone (PQ) pools (Karpinska et al., 2000). We examined susceptibility of *Arabidopsis* plants to GSH and H_2O_2 in the low R:FR environments. Treatment of *Arabidopsis* plants with increasing concentrations of GSH (50 mM to 200 mM) resulted in more severe cell death and growth inhibition in the low R:FR environments compared with the weed-free control (Figure 6). Quantification of leaf cell death by the image analysis application Fiji (Schindelin et al., 2012) revealed significant increases in leaf cell death (%) in the biological low R:FR (65%, 80%, 73%, and 71%) and artificial low R:FR (110%, 55%, 24%, and 31%) treatments relative to the weed-free treatment at 50, 100, 150, and 200 mM GSH, respectively (Figure 7; Supplementary Table 3). In contrast, treatment of *Arabidopsis* plants with increasing concentrations of H_2O_2 (50 mM to 200 mM) resulted in small and localized patches of cell death in all environments with no distinguishable differences in susceptibility to H_2O_2 between the low R:FR light and control environments (Figure 8). These results suggest that the effects of GSH on reduction of the Q_A-Q_B-PQ pools, efficiency of chloroplast electron transport, and cell death may be exacerbated under low R:FR light environment.

A few early $^1O_2$-responsive genes are induced under low R:FR light environments

RNA-sequencing was performed to compare differentially expressed genes (DEGs) in wild type *Arabidopsis* under 12-hour low R:FR light per day for one week and 1931 previously reported early $^1O_2$-responsive genes in the mutant backgrounds and rose Bengal-treated wild type *Arabidopsis* (op den Camp et al., 2003; Gadjev et al., 2006; Alboresi et al., 2011; Mor et al., 2014). A summary of the number of base pairs sequenced and the number of reads mapped is presented in Table 1, which shows an average percentage of mapped reads of 81.7%. Results revealed that 57 of the 1931 $^1O_2$-responsive genes were differentially expressed in the low R:FR treatments (Table 2; Supplementary Table 4). Moreover, only six of the 57 $^1O_2$-responsive genes were commonly up-regulated in the biological and artificial low R:FR treatments, and four previous studies (Tables 2, 3). The minimal similarity between gene expression profiles in the previous four studies and the present study suggests that disparate modes of $^1O_2$ generation in different genetic backgrounds may elicit unique $^1O_2$ signatures. Further, growth conditions, tissue types and plant age may also affect $^1O_2$ signatures. These results also suggest that the levels of $^1O_2$ in the low R:FR treatments may not be high enough to induce a $^1O_2$ signaling pathway similar to other *Arabidopsis* systems such as the *flu* mutant (op den Camp et al., 2003), Alternatively, a $^1O_2$ signaling might have occurred at an earlier time point after the low R:FR light exposure.

Negative regulators of jasmonate accumulation are induced under low R:FR light environments

Increases in $^1O_2$ levels in the low R:FR treatments were below a threshold to induce a cell death response (Figures 1, 2). The lack of a cell death response suggested induction of a $^1O_2$ acclimation response, which is known to be induced by low levels of JA (Ramel et al., 2013b). Therefore, we sought to determine whether genes involved in regulation of bioactive JA levels were up-regulated by the low R:FR treatments. RNA-seq analysis revealed that the early $^1O_2$-responsive gene *ILL6* (op den Camp et al., 2003), which is involved in negative regulation of bioactive JA levels (Bhosale et al., 2013), was up-regulated (Table 3). We also found that not only the sulfotransferase *ST2a* but also the closely related *ST2b* was up-regulated in the biological and artificial low R:FR treatments (Table 3). Up-regulation of the sulfotransferase *ST2a* that

10.3389/fpls.2024.964476

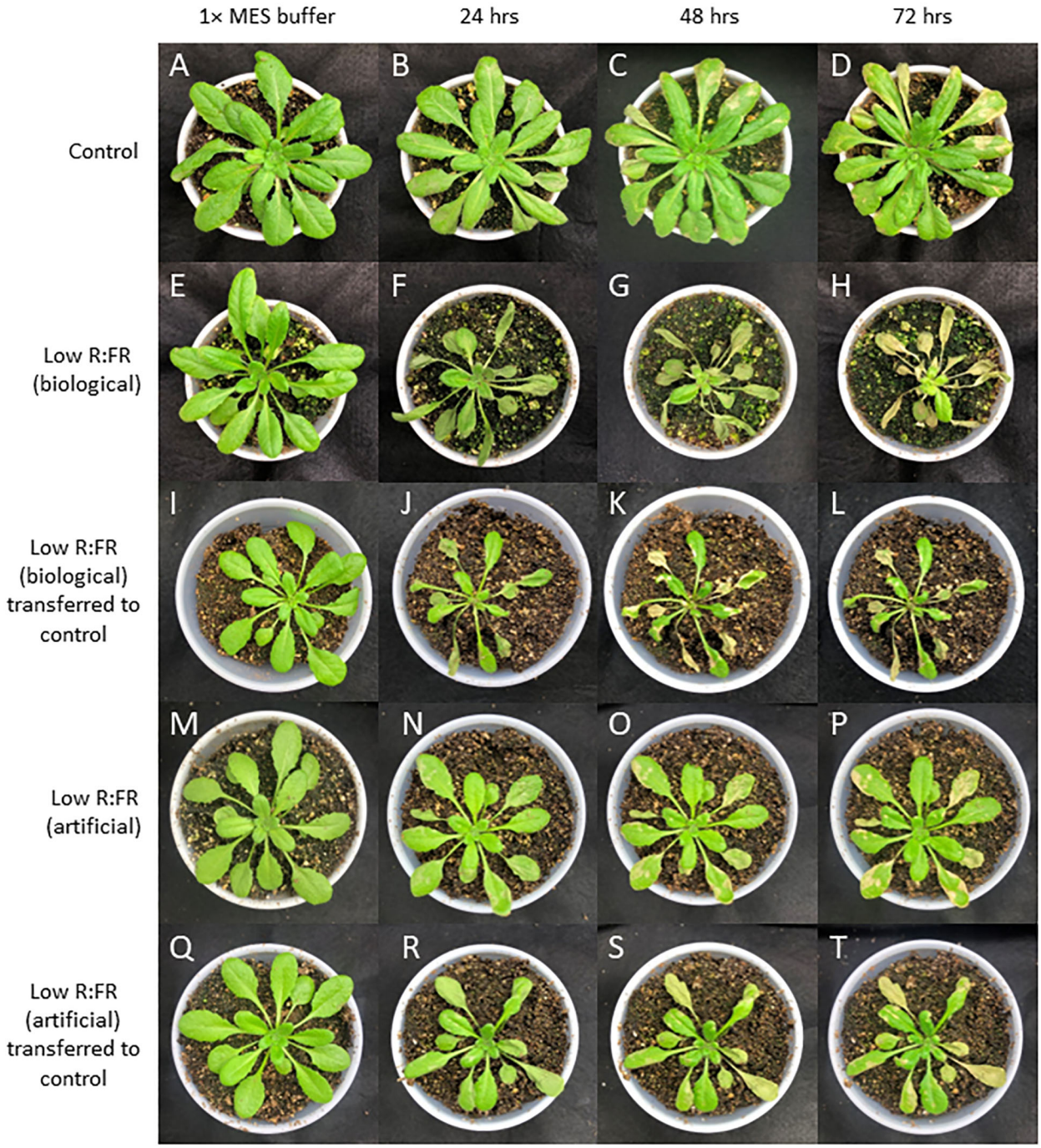

FIGURE 5
The time course (0-72 h) of *Arabidopsis* responses to ALA in the control, biological and artificial low R:FR treatments. *Arabidopsis* plants were exposed to the biological and artificial low R:FR light for 12 hours a day for seven days or kept under control (weed-free) condition prior to sampling. Control plants for each treatment were sprayed with a two mL solution of 1x MES buffer (10 mM; pH 6.5), while treated plants were sprayed with a two mL solution of 10 mM ALA in 1x MES buffer and placed back in their original treatments or transferred from the reflected low R:FR treatments to the control treatment. Experiments were repeated four times and ALA was sprayed on three plants per treatment per experiment. No damage by 1x MES buffer in the control, but minor damage by ALA after 24 h and localized patches of cell death after 48 and 72 hours **(A–D)**. Signs of wilting 24 h after ALA treatment, progression of cellular damage and necrosis after 24 and 48 hours in the biological low R:FR **(E–H)**. A similar trend after transfer of the ALA-treated plants from the biological low R:FR to the control treatment **(I–L)**. Less severe damage by ALA in the artificial low R:FR light **(M–P)** compared with the biological low R:FR treatment. Persistence of sensitivity to cell death after transfer of the ALA-treated plants from the artificial low R:FR to the control treatment **(Q–T)**.

catalyzes the conversion of 12-hydroxy JA (OH-JA) to JA sulfate (HSO_4-JA) (Gidda et al., 2003) is a major mechanism diverting JA precursors from bioactive JA pools thus attenuating JA signaling under low R:FR light (Fernández-Milmanda et al., 2020). Since *ST2b* lacks sulfotransferase activity (Gidda et al., 2003; Fernández-Milmanda et al., 2020), its function under low R:FR treatments is not clear. The relationships between JA accumulation and $^1O_2$-induced cell death (Przybyla et al., 2008), and between suppression

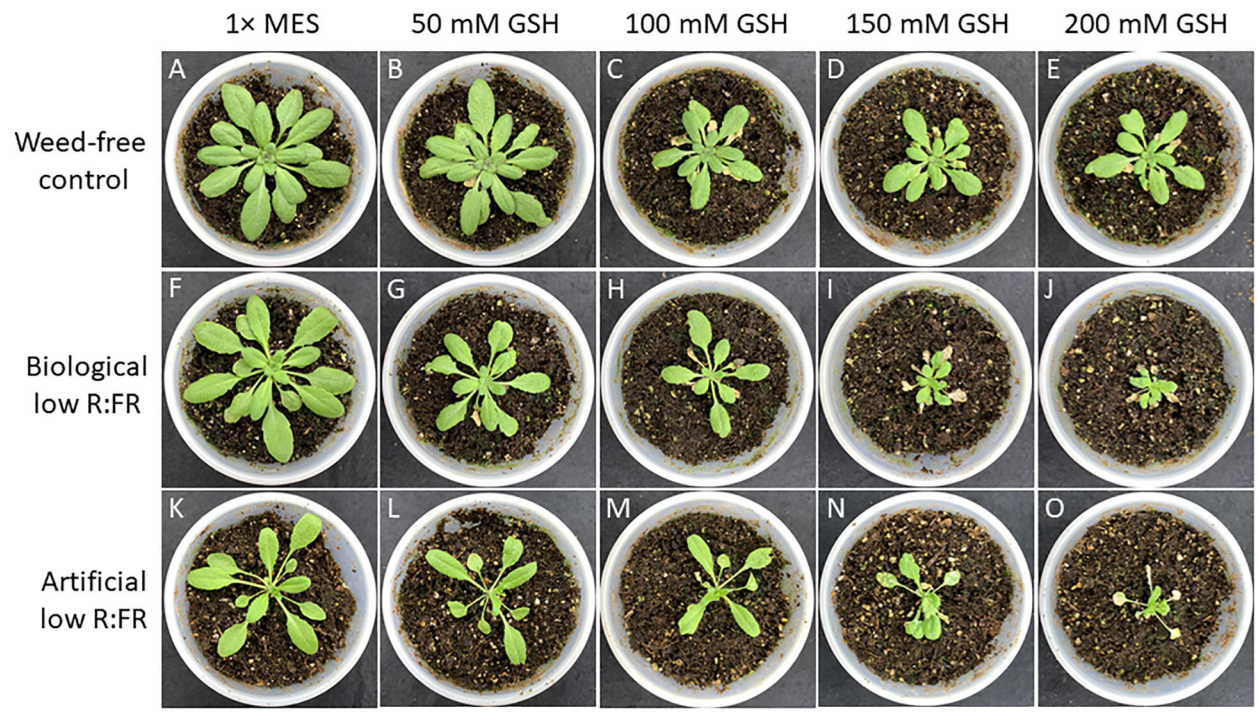

FIGURE 6
Responses of *Arabidopsis* plants to increasing concentrations of reduced glutathione (GSH) from 50 mM to 200 mM in the weed-free control **(A–E)**, biological low R:FR light **(F–J)**, and artificial low R:FR **(K–O)** light treatments. At the 3-week stage, six *Arabidopsis* plants from each treatment were taken from the growth chambers and all rosette leaves of each plant were sprayed with a one mL solution of each GSH concentration containing 0.01% Tween-20 as a wetting agent. Control plants for each treatment were sprayed with a one mL solution of 1x MES buffer (10 mM, pH 6.5) containing the same concentration of Tween-20. After spraying, the plants were kept outside the growth chambers to dry for one hour and transferred back to the respective treatments. Experiments were repeated three times with five plants per treatment and progression of cell death, and growth inhibition were monitored for one week. Note the dramatic differences in cell death and growth inhibition responses to increasing concentrations of GSH between the control and low R:FR light treatments particularly at 150 mM and 200 mM GSH.

of JA synthesis and photo-tolerance (Ramel et al., 2013a, b) have been well established. Therefore, the up-regulation of *ILL6* and *ST2a* in the low R:FR treatments may represent a possible connection between the low R:FR light, attenuation of bioactive JA levels, and $^1O_2$ acclimation response.

Induction of jasmonate repressors connects reflected far-red light cues from neighboring weeds with $^1O_2$ acclimation response

We performed two independent RT-qPCR assays to investigate whether the reflected far-red light from neighboring weeds was indeed responsible for the induction of JA repressors and $^1O_2$ responsive genes. We included in our experiments *ST2a* (a negative regulator of JA) and the closely related *ST2b*, as well as the early $^1O_2$ responsive genes *ILL6*, which is also a negative regulator of JA, and *PUB25*, which encodes a U-box E3 ligase involved in plant organ growth. We found that all of these transcripts in *Arabidopsis* leaves were at higher levels in the biological low R:FR treatment relative to weed-free control (Figure 9) confirming the expression profile of the selected genes in RNA-seq results (Table 3). These results further suggested that hydrolysis of bioactive JA conjugates (JA-isoleucine) by the $^1O_2$ responsive *ILL6* and sulfation of JA metabolites by *ST2a* may act to promote both the shade avoidance response and the $^1O_2$ acclimation response under resource-independent weed competition.

Discussion

Our results indicate that induction of SAR in *Arabidopsis* due to proximity to neighboring weeds coincides with increased leaf production of $^1O_2$ (Figures 1, 2). Some of the elongation responses are modulated by the low R:FR light-mediated elevation of the volatile hormone ethylene in plants or in the canopy environment (Pierik et al., 2004a, b). Other reports have shown the suppression of terpenoids and other green leaf volatiles under low R:FR light (Kegge et al., 2013) and suggested the dominant effect of light signaling over volatile cues during weed-crop interactions (Pierik and de Wit, 2014). We are not, however, aware of any previous work describing $^1O_2$ induction in plants by volatile compounds emanating from neighboring weeds. Moreover, a similar $^1O_2$ increase along with induction of the SAR in the artificial low R:FR treatment (Figures 1, 2) suggests that the low R:FR light emanating from neighboring weeds may be the main signal responsible for increased $^1O_2$ production.

Environmental stress factors elevate reactive oxygen species (ROS) levels in plants (Fryer et al., 2002; Hideg et al., 2002; Xiong et al., 2002; Apel and Hirt, 2004). Disparate ROS such as $^1O_2$ and O_2^-/H_2O_2, which

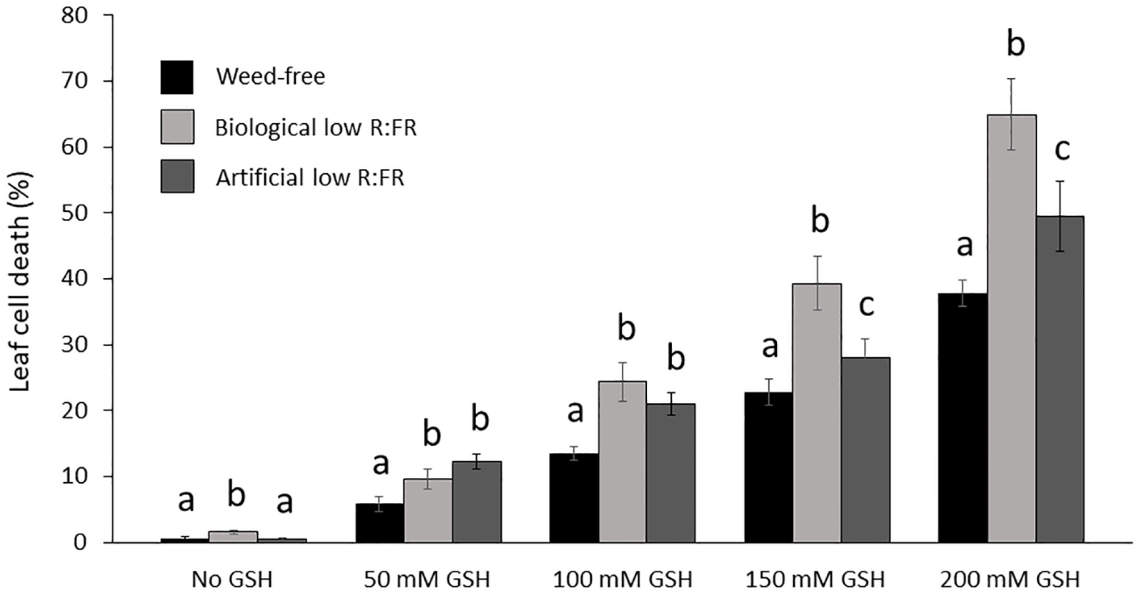

FIGURE 7
Increases in mean leaf cell death (%) by reduced glutathione (50, 100, 150, and 200 mM GSH) in the weed-free control, biological, and artificial low R:FR light treatments. Plants were treated as described in Figure 6. Note the significant increase in mean cell death (%) at each GSH concentration in the low R:FR light treatments relative to the respective weed-free treatment. Data represent means ± SEM for 18 plants per concentration per treatment. Means were separated using Tukey's HSD test ($P<0.05$). Letters indicate statistical significance of differences across treatments. Images of plants were analyzed by the image analysis application Fiji (Schindelin et al., 2012). For each plant, dead leaf area was determined by subtracting green leaf area from total leaf area and expressed as percentage of leaf cell death (Supplementary Table 3).

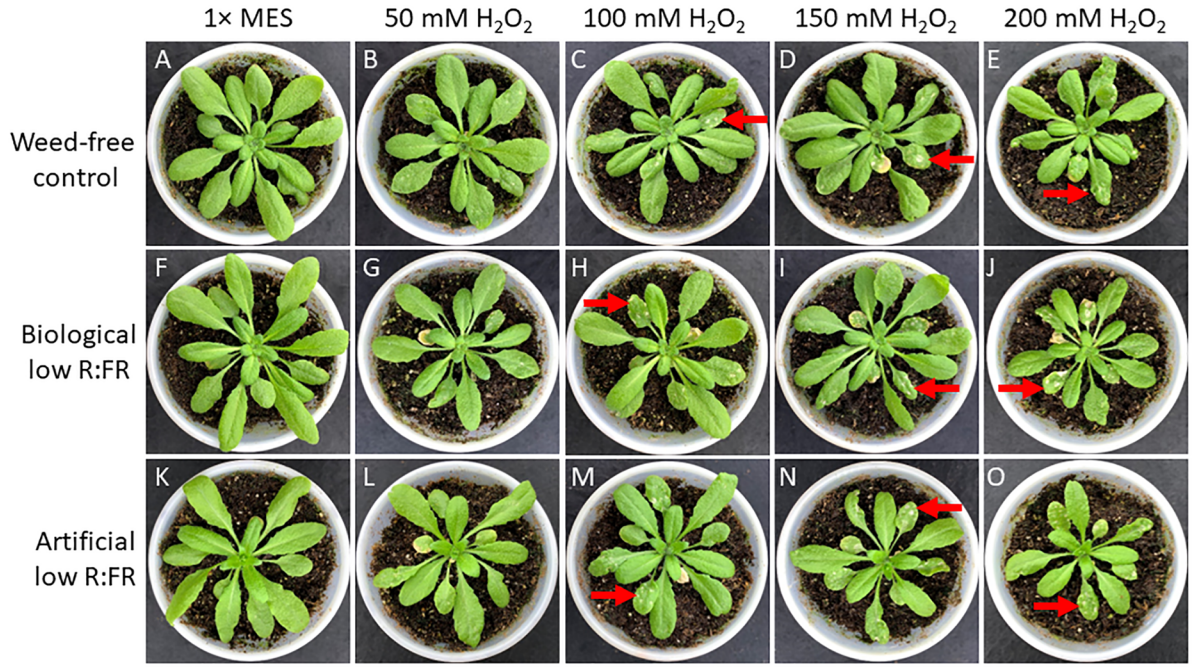

FIGURE 8
Responses of *Arabidopsis* plants to increasing concentrations of H_2O_2 from 50 mM to 200 mM in the weed-free control **(A–E)**, biological low R:FR light **(F–J)**, and artificial low R:FR **(K–O)** light treatments. At the 3-week stage, six *Arabidopsis* plants from each treatment were taken from the growth chambers and all rosette leaves of each plant were sprayed with a one mL solution of each H_2O_2 concentration containing 0.01% Tween-20 as a wetting agent. Control plants for each treatment were sprayed with a one mL solution of 1x MES buffer (10 mM, pH 6.5) containing the same concentration of Tween-20. After spraying, the plants were kept outside the growth chambers to dry for one hour and transferred back to the respective treatments. Experiments were repeated three times with five plants per treatment and progression of cell death was monitored for one week. Note that higher concentrations of H_2O_2, in contrast to GSH, did not result in a differential cell death in the low R:FR light treatments. Arrows indicate a few patches of cell death across all treatments at higher H_2O_2 concentrations.

TABLE 1 Percentages of sequence reads mapped to the *Arabidopsis thaliana* reference genome.

Treatment	Replicate	No. base pairs sequenced	No. mapped reads	Percent mapped
Weed-free Control	1	65519462	53635248	81.9
	2	53780900	43933391	81.7
	3	98252102	79942744	81.4
Biological low R:FR	1	67826222	55934659	82.5
	2	63146232	51830813	82.1
	3	102906614	84638761	82.2
Artificial low R:FR	1	174670054	141719839	81.1
	2	81621146	66435905	81.4
	3	159953262	130315365	81.5
Average		96408444	78709636	81.7

are elevated under disparate physiological conditions (Apel and Hirt, 2004), may also exhibit antagonistic interactions under certain conditions. This antagonistic interaction was exemplified in the *flu* mutant of *Arabidopsis* in which suppression of H_2O_2 by overexpression of a thylakoid-bound ascorbate peroxidase resulted in enhanced $^1O_2$-mediated cell death and growth inhibition (Laloi et al., 2007). Also, the simultaneous induction of $^1O_2$ and reduction of O_2^- in the etiolated *phytochrome interacting factor 3* and *phytochrome interacting factor quadruple* mutants of *Arabidopsis* upon transfer to light has been attributed to the antagonistic effect of $^1O_2$ on O_2^- and H_2O_2 (Chen et al., 2013). Given the established specificity of $^1O_2$- and O_2^-/H_2O_2-dependent signaling in the *flu* mutant of *Arabidopsis* (Laloi et al., 2007), the $^1O_2$ induction in the low R:FR light treatments may give rise to a distinct stress signaling response. A recent study found no increase in the intensity of SOSG fluorescence in *Arabidopsis* leaf discs following a two-hour exposure to supplemental FR light (Dmitrieva et al., 2021). This discrepancy may be due to small size of leaf discs (0.5 × 0.5 cm), lower concentration of SOSG (5 μM), and the short duration of exposure to FR light (two hours). Several lines of evidence indicate that a FR light pre-treatment of *Arabidopsis* results in Pchlide accumulation (Sperling et al., 1997; McCormac and Terry, 2002). Further, photo-excitation of Pchlide following transfer of *Arabidopsis* from FR light to white light resulted in rapid generation of $^1O_2$ (Page et al., 2017). In the absence of FR light, Pchlide accumulation in the dark and photo-excitation following transfer to light is the mechanism behind rapid $^1O_2$ generation in the *flu* mutant (op den Camp et al., 2003). Also, differential effects of several components of the *Arabidopsis* light signaling pathway (PHYTOCHROMES, PHYTOCHROME INTERACTING FACTORS, ELONGATED HYPOCOTYL 5, ELONGATED HYPOCOTYL 5 HOMOLOG, and CONSTITUTIVE PHOTOMORPHOGENIC 1) on $^1O_2$ production and cell death following transfer to light corresponded closely to the Pchlide levels formed during seedling de-etiolation (Chen et al., 2013). Accumulation of Pchlide, however, does not appear to be the main cause of $^1O_2$ generation in the wild-type *Arabidopsis* under the low R:FR light treatments as Pchlide levels were not significantly different from the control, nor did Pchlide levels increase following dark incubations for up to six hours (Figure 3A). Although the mechanism of $^1O_2$ generation under our low R:FR treatments is not clear, decreased levels of Chlide a (Figure 3B), and therefore, increases in Pchlide to Chlide ratios (Figure 3F) may be interpreted as slower conversion rates of Pchlide to Chlide allowing for photo-excitation of a part of free Pchlide and thus $^1O_2$ generation.

TABLE 2 Comparison of early $^1O_2$-responsive DEGs in the reflected low R:FR treatments and four previously studied $^1O_2$ generating systems.

Category		No. of genes
(1) DEGs in four plant $^1O_2$ generating systems[a]		1931
(2) Common DEGs identified in (1) and biological low R:FR		57
(3) Common DEGs identified in (1), (2) and artificial low R:FR		6
Up (+) or down (-) regulated in (1)	Up (+) or down (-) regulated in (2)	No. of genes
+	+	21
-	-	5
+	-	9
-	+	17

[a] op den Camp et al., 2003; Gadjev et al., 2006; Alboresi et al., 2011; Mor et al., 2014.
Arabidopsis plants were exposed to the biological and artificial low R:FR light for 12 hours a day for seven days or kept under control (weed-free) condition prior to sampling. Six $^1O_2$-responsive genes were consistently upregulated in the reflected low R:FR treatments and other four $^1O_2$ generating systems (op den Camp et al., 2003; Gadjev et al., 2006; Alboresi et al., 2011; Mor et al., 2014). Data represent three independent experiments with a total of nine samples from three treatments (weed-free, biological low R:FR, and artificial low R:FR light) with three replicates, each consisting of a pool of leaves from three individual plants.

Carotenoids (car) including lutein, zeaxanthin, and β-carotene are potent physical and chemical quenchers of $^1O_2$ (Trebst, 2003; Triantaphylidès and Havaux, 2009; Dogra and Kim, 2020). The lack of zeaxanthin and lutein in the lycopene-ε-cyclase and violaxanthin de-epoxidase double mutant (*npq1 lut2*) of *Arabidopsis* resulted in $^1O_2$ generation under a combination of low temperature and high light stress (Alboresi et al., 2011). In addition, $^1O_2$ generation in the *npq1 lut2* mutant was accompanied by an increase in Chl a/Chl b and a decrease in Chl/Car reflecting the reduction of PSII/PSI and induction of carotenoid biosynthetic genes as $^1O_2$-mediated acclimation responses (Alboresi et al., 2011). Under the low R:FR treatments, however, $^1O_2$ induction did not coincide with such increases (data not shown), indicating differences in $^1O_2$ acclimation responses between these $^1O_2$ generating systems under two different stresses. In addition, the levels of lutein, β-carotene, violaxanthin, and neoxanthin were not affected by the biological low R:FR treatment, while total carotenoid levels were decreased in the biological and artificial low R:FR treatments (Figure 4). Decreases in chlorophylls and carotenoids are among universal responses to low R:FR light (Meng et al., 2019; Zhen and Bugbee, 2020; Kong and Nemali, 2021; Frosch and Mohr, 1980; Li and Kubota, 2009) and are regulated by phytochrome in a coordinated and co-localized manner (Meier et al., 2011; Rodríguez-Villalón et al., 2009; Welsch et al., 2000; Von Lintig et al., 1997). Although carotenoid deficiency may lead to $^1O_2$ generation (Krieger-Liszkay, 2005), it is not clear whether

TABLE 3 Induction of early $^1O_2$-responsive and sulfotransferase genes by the biological and artificial low R:FR light treatments.

DEGs	Gene name/TAIR description	Log_2FC (biological)	Log_2FC (artificial)	*P*-value
	Early $^1O_2$ responsive genes			
(1) *At3g10720*	*INV*; pectin methylesterase inhibitor	1.18	0.24	3.5×10^{-3}
(2) *At3g19380*	*PUB25*; U-box E3 ubiquitin ligase	0.75	0.34	2.2×10^{-3}
(3) *At4g01870*	*TolB*; tolB protein-like protein	0.73	0.02	1.6×10^{-2}
(4) *At5g57560*	*TCH4*; a cell wall-modifying enzyme	1.64	0.07	1.9×10^{-2}
(5) *At1g44350*	*ILL6*; IAA-leucine resistance (ILR)-like6	3.26	0.09	2.6×10^{-3}
(6) *At5g24810*	*ABC1K11*; ABC1 family protein	0.97	0.09	1.2×10^{-2}
	Sulfotransferases			
(7) *At5g07010*	*ST2a*; sulfotransferase 2a	3.32	10.02	7.7×10^{-9}
(8) *At5g07000*	*ST2b*; sulfotransferase 2b	1.16	2.23	4.9×10^{-3}

Arabidopsis plants were exposed to the biological and artificial low R:FR light for 12 hours a day for seven days or kept under control (weed-free) condition prior to sampling. Data represent three independent experiments with a total of nine samples from three treatments (weed-free, biological low R:FR, and artificial low R:FR light) with three replicates, each consisting of a pool of leaves from three individual plants.

decreases in chlorophylls (Figure 3) and total carotenoids (Figure 4) in the low R:FR treatments contribute to $^1O_2$ generation.

It is known that ALA is the first committed compound in the synthesis of tetrapyrrole pigments (Tanaka and Tanaka, 2007; Beale, 1990). Earlier studies have shown that plants fed with exogenous ALA accumulate tetrapyrrole intermediates including protoporphyrin IX and Pchlide (Gough, 1972; Mascia, 1978). These intermediates are highly photodynamic and generate $^1O_2$ as the major ROS in the light (Becerril and Duke, 1989; op den Camp et al., 2003; Shao et al., 2007; Rebeiz et al., 1988). Similarly,

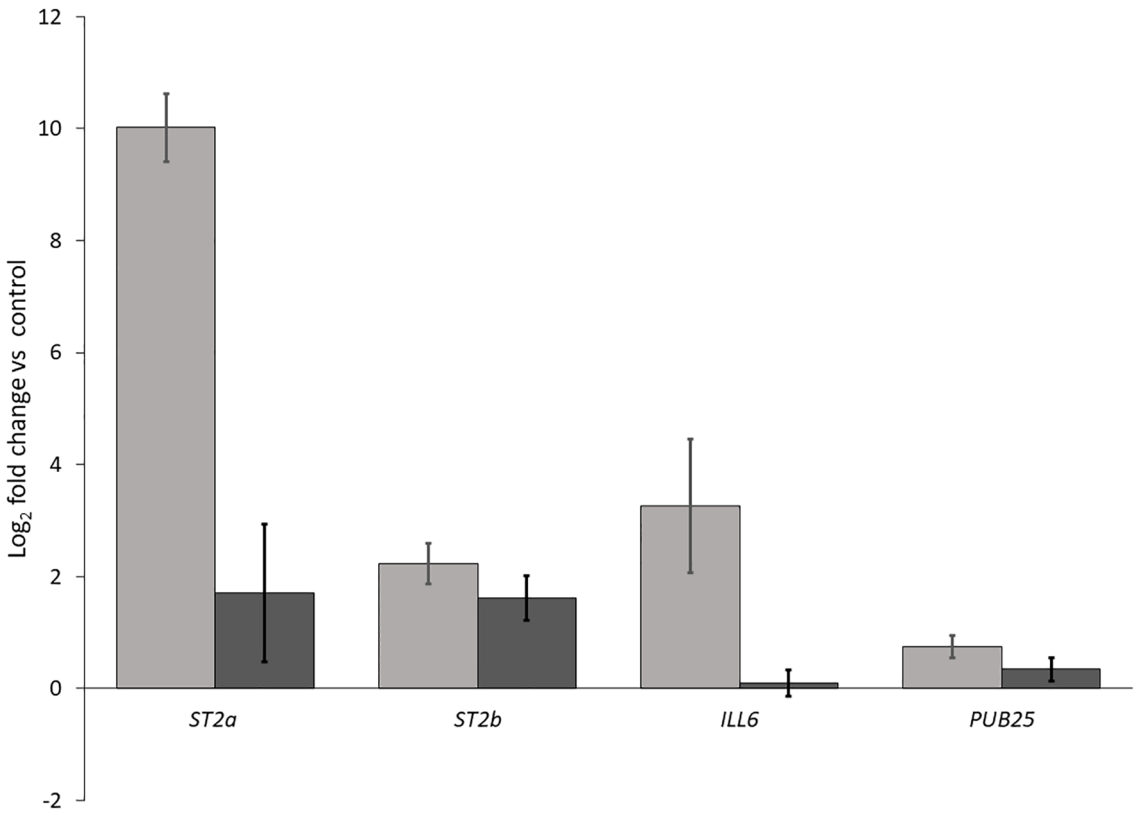

FIGURE 9
Increases in transcript levels of *ST2a*, *ST2b*, *ILL6*, and *PUB25* in the biological low R:FR treatment relative to the weed-free control. Data represents fold change gene expression in the biological low R:FR light relative to the weed-free control treatment ± SEM for two independent experiments each consisting of leaves from four plants per treatment ($P \leq 0.05$).

exogenous treatment of *Arabidopsis* leaves with ALA resulted in a cell death response, which was exaggerated under the low R:FR treatments (Figure 5). This differential response cannot be attributed to higher Pchlide level prior to ALA feeding as Pchlide levels in the low R:FR treatments were not significantly different from the control (Figure 3A). Given the direct relationship between the $^1O_2$ levels and the extent of cell death in *Arabidopsis* leaves (op den Camp et al., 2003; Laloi et al., 2007), the differential cell death response under the low R:FR treatments (Figure 5) may be due to higher $^1O_2$ levels prior to the ALA treatment. This may increase susceptibility to cell death following ALA feeding. Such increased susceptibility to cell death due to higher steady-state cellular levels of ROS has been shown in tobacco plants treated with the signaling molecules salicylic acid and nitric oxide (Amirsadeghi et al., 2006). This $^1O_2$-mediated susceptibility to cell death by ALA may provide an explanation for the differential cell death responses of *Arabidopsis* plants under low R:FR light treated with ALA and transferred to the control (Figures 5I–L, Q–T). This, to some extent, is reminiscent of the increased sensitivity to oxidative stress and cell death due to a salicylic acid-dependent accumulation of O_2^- and H_2O_2 under short days in the *fhy3 far1* double mutant of *Arabidopsis* lacking two light signaling components FAR-RED ELONGATED HYPOCOTYL3 (FHY3) and FAR-RED IMPAIRED RESPONSE1 (FAR1) (Ma et al., 2016). On the other hand, the cell death response in the *AtIPS1* mutant of *Arabidopsis* lacking 1L-myo-inositol-1-phosphate synthase activity under long days did not result in increased ROS sensitivity (Meng et al., 2009). Therefore, we do not exclude the possibility that factors other than higher steady state $^1O_2$ levels in the low R:FR treatments may contribute to increased susceptibility to cell death by ALA.

A recent study indicated that the complexity of leaf tissue including the cuticle layer shielding the upper and lower epidermis could limit SOSG penetration into *Arabidopsis* leaves (Prasad et al., 2018). Force infiltration with a syringe led to nonuniform penetration and distribution of SOSG in the leaf spaces while the resulting mechanical injury induced a strong SOSG fluorescence signal (Prasad et al., 2018). In contrast, pressure infiltration of *Arabidopsis* leaf pieces with a shut syringe resulted in uniform delivery of SOSG to the leaf tissue without $^1O_2$ induction (Prasad et al., 2018). In our experiments, we used pressure infiltration with a 60 mL syringe allowing for complete infiltration of whole plant tissue while avoiding mechanical injury that could trigger $^1O_2$ production. Given the complexity of leaf tissue and the uneven occurrence of SOSG fluorescence signal in the leaf samples (Figures 2B, C), we do not rule out the possibility of nonuniform generation of SOSG in the leaf cell compartments such as chloroplasts in the cells across the leaf tissue. This uneven occurrence of SOSG fluorescence signal is to some extent similar to that in *Arabidopsis* leaves following transfer from FR light to white light (Page et al., 2017). In addition, increases in mean fluorescence signal in the biological low R:FR (2.6×) and artificial low R:FR (3.0×) (Figure 2D) were similar to that reported one hour after the transfer of FR light-treated *Arabidopsis* to white light (Page et al., 2017).

High concentrations of H_2O_2 and GSH in the chloroplast can increase the degree of oxidation and reduction of quinone A (Q_A), respectively. While higher degrees of Q_A oxidation by H_2O_2 enhance the efficiency of electron transport in PS II, higher degrees of Q_A reduction by GSH have the opposite effect. Therefore, the H_2O_2 action can decrease and the GSH action can increase the extent of photo-oxidative stress and photoinhibition (Karpinska et al., 2000). Based on the opposing effects of H_2O_2 and GSH on the redox state of Q_A and efficiency of electron transport in PS II, it was hypothesized that treatment of the *flu* mutant of *Arbabidopsis* with H_2O_2 may reduce and treatment with GSH may increase $^1O_2$ production and growth inhibition (Laloi et al., 2007). Given that our experimental low R:FR environments enhanced $^1O_2$ production, we examined whether GSH treatment could enhance cell death. Although it was not clear to what extent GSH could reach the chloroplasts, our observations indicated that higher concentrations of GSH could result in differential cell death and growth inhibition responses in the low R:FR environments (Figures 6, 7). This was, however, not the case in the H_2O_2-treated plants. Increasing concentrations of H_2O_2 resulted in a few localized patches of cell death in all treatments (Figure 8). The development of these patches of cell death in all treatments may be due to inability of the H_2O_2 detoxifying systems to scavenge excess H_2O_2 at higher concentrations. While in some cases, FR light supplementation has enhanced photosynthetic efficiency of shorter wavelength light (Zhen and van Iersel, 2017), in other cases it has led to overproduction of ROS and damage to PSII and PSI (Tjus et al., 2001). Preferential excitation of PSI over PSII by FR light would enhance electron transfer from the PQ pools to PSI, which would be supplied by GSH. This would mitigate overreduction of PQ pools. Therefore, the observed increases in cell death by GHS in the low R:FR treatments (Figure 6; Supplementary Table 3) may be due to factors other than over-reduction of PQ pools. Alternatively, the damage to PSI and to a greater extent to PSII by FR light-induced ROS (Tjus et al., 2001) would affect the efficiency of electron transport, in which case, addition of excess electron to PQ pools via GSH may exacerbate ROS damage leading to increased cell death.

Our results suggest that under reflected low R:FR light, wild type *Arabidopsis* generates $^1O_2$ via a mechanism different from those reported in four plant $^1O_2$ generating systems (Table 2), allowing the identification of the transcriptomic signature of $^1O_2$ signaling. Differential expression of only 3.2% of the previously reported early $^1O_2$-responsive genes (57 out of 1931) suggests specificity of the $^1O_2$ signaling under reflected low R:FR light stress (Table 2; Supplementary Table 4). This specificity is further highlighted by the up-regulation of only six previously reported $^1O_2$-responsive genes in the biological and artificial low R:FR light treatments (Table 3). Among these, *ILL6*, which is also known to be rapidly induced within two hours following $^1O_2$ release (op den Camp et al., 2003), encodes an amidohydrolase that catalyzes the cleavage of isoleucine (Ile) from JA-Ile thus making JA biologically inactive (Bhosale et al., 2013). Recently, the up-regulation of *ILL6* was reported under low R:FR light as part of a mechanism that attenuates the JA signaling pathway (Fernández-Milmanda et al., 2020). Our results suggest that the up-regulation of *ILL6* in the reflected low R:FR treatments may be an $^1O_2$ response, which raises the intriguing possibility that attenuation of the JA signaling pathway may be partly mediated via a $^1O_2$ signaling pathway. This attenuation

is a major process that generates a trade-off between defense and growth in favor of the SAR under plant competition (Fernández-Milmanda et al., 2020). It has been demonstrated that attenuation of the JA signaling pathway under a 10-hour low R:FR light treatment occurs via the up-regulation of the sulfotransferase *ST2a*. The *ST2a* encoded protein exclusively catalyzes the conversion of JA to sulfated JA (HSO_4-JA), while the closely related *ST2b* fails to respond to the above FR light treatment and is dispensable for the accumulation of HSO_4-JA (Fernández-Milmanda et al., 2020). We found that both *ST2a* and *ST2b* were up-regulated under a 12-hour reflected low R:FR light treatment for seven days (Table 3; Figure 9) and cannot exclude the possibility that *ST2a* and *ST2b* may be $^1O_2$-responsive. The discrepancy in the *ST2b* response may be due to differences in experimental FR light conditions.

Upregulation of *ST2a* and *ST2b* have been shown in a transgenic *Arabidopsis* line with suppressed mitochondrial serine acetyltransferase (SAT3) level (Haas et al., 2008). It is noteworthy that upregulation of *ST2a* and *ST2b* in the SAT3 line coincided with the downregulation of disease or pathogen response genes whose responses are coordinated by methyl jasmonate (Haas et al., 2008). Although the upregulation of *ST2b* (Table 3; Figure 9) suggests that it may play a role under certain low R:FR light conditions, it is not feasible to predict the function of a plant sulfotransferase solely based on its sequence similarity to sulfotransferases with known functions (Hirschmann et al., 2014). So far, there is no evidence for the involvement of *ST2b* in the JA pathway. Initial screens for *ST2b* substrates found no activity against hydroxyjasmonate compounds (Gidda et al., 2003). Further, a recent study found no evidence for the JA sulfation by *ST2b* under low R:FR light (Fernández-Milmanda et al., 2020).

An important question regarding $^1O_2$ induction under reflected low R:FR light is whether $^1O_2$ serves a physiological function under plant competition. Under this condition, generation of high levels of $^1O_2$ can place the rapidly growing plants at a disadvantage as high levels of $^1O_2$ can steer the cell fate towards cell death (Danon et al., 2005; Kim et al., 2012). We envision a possibility that the low R:FR-mediated attenuation of JA accumulation by *ST2a* and *ILL6* may result in an acclimation response to $^1O_2$. This acclimation response, in contrast to a cell death response (Ramel et al., 2013b), may have a growth inhibitory effect similar to that in the *flu* mutant (Laloi et al., 2006, 2007). This growth inhibitory effect of $^1O_2$ may be exploited by plants under competition to modulate elongation growth to avoid excess elongation in anticipation of oncoming competition. The growth inhibitory effect of $^1O_2$ may also be exerted via the action of other $^1O_2$-responsive genes. In this regard, overexpression of the early $^1O_2$-responsive *PUB25*, which encodes a U-box E3 ubiquitin ligase (Table 3), is known to cause growth inhibition in *Arabidopsis* (Li et al., 2021). Interestingly, *PUB25* was among the $^1O_2$-responsive genes that were upregulated under the biological and artificial low R:FR treatments (Table 3), and may play a role in modulation of growth by $^1O_2$.

In closing, our results indicate that $^1O_2$ production is an early response to reflected FR light from neighboring weeds. Our biological low R:FR light treatment allows the investigation of $^1O_2$ acclimation responses under resource-independent competition. Under this condition, $^1O_2$ itself may contribute to the acclimation response by up-regulating genes such as *ILL6*, which acts to reduce the pool of bioactive JAs. Further, the demonstration of up-regulation of *ST2b* under artificial and biological low R:FR light environments allows further investigations into the role of *ST2b* in plant competition.

Data availability statement

The datasets presented in this study can be found in online repositories. The names of the repository/repositories and accession number(s) can be found in the article/Supplementary Material.

Author contributions

NB and SA carried out the experimental work and wrote the manuscript. NB performed data analysis. CS contributed to the experimental design and revised the manuscript. All authors contributed to the article and approved the submitted version.

Funding

The author(s) declare financial support was received for the research, authorship, and/or publication of this article. Financial support for this work was partially provided by the Natural Sciences and Engineering Research Council of Canada, File RGPIN-2022-03454 (CJS). This research was undertaken thanks in part to the University of Guelph's Food from Thought research program, funded by the Canada First Research Excellence Fund.

Acknowledgments

The authors would like to thank Harvest Genomics Inc. for technical guidance and analysis of RNA sequencing data. We extend our sincere thanks to Dr. Michaela Strüder-Kypke (Molecular and Cellular Imaging Facility, University of Guelph) for providing expertise and assistance on fluorescence microscopy. We thank Dr. Tariq Akhtar and Kevin Rea for their technical expertise and assistance on HPLC. We also thank Jing Zhang for her expertise and assistance on RT-qPCR.

Conflict of interest

The authors declare that the research was conducted in the absence of any commercial or financial relationships that could be construed as a potential conflict of interest.

Publisher's note

Supplementary material

The Supplementary Material for this article can be found online at: https://www.frontiersin.org/articles/10.3389/fpls.2024.964476/full#supplementary-material

SUPPLEMENTARY TABLE 1
Incoming and reflected light spectral composition in the weed-free control, biological low R:FR and artificial low R:FR treatments.

SUPPLEMENTARY TABLE 2
Fluorescence intensity in leaf images of SOSG-treated *Arabidopsis* plants in the weed-free control, biological low R:FR and artificial low R:FR treatments.

SUPPLEMENTARY TABLE 3
Image analysis of leaf cell death in GSH-treated *Arabidopsis* plants in the weed-free control, biological low R:FR and artificial low R:FR treatments.

SUPPLEMENTARY TABLE 4
Expression profiles of $^1O_2$-responsive genes in the biological and artificial low R:FR treatments.

References

Alboresi, A., Dall'osto, L., Aprile, A., Carillo, P., Roncaglia, E., Cattivelli, L., et al. (2011). Reactive oxygen species and transcript analysis upon excess light treatment in wild-type *Arabidopsis thaliana* vs a photosensitive mutant lacking zeaxanthin and lutein. *BMC Plant Biol.* 11, 62. doi: 10.1186/1471-2229-11-62

Ambastha, V., Chauhan, G., Tiwari, B. S., and Tripathy, B. C. (2020). Execution of programmed cell death by singlet oxygen generated inside the chloroplasts of *Arabidopsis thaliana*. *Protoplasma* 257, 841–851. doi: 10.1007/s00709-019-01467-y

Amirsadeghi, S., Robson, C. A., McDonald, A. E., and Vanlerberghe, G. C. (2006). Changes in plant mitochondrial electron transport alter cellular levels of reactive oxygen species and susceptibility to cell death signaling molecules. *Plant Cell Physiol.* 47, 1509–1519. doi: 10.1093/pcp/pcl016

Apel, K., and Hirt, H. (2004). Reactive oxygen species: metabolism, oxidative stress, and signal transduction. *Annu. Rev. Plant Biol.* 55, 373–399. doi: 10.1146/annurev.arplant.55.031903.141701

Ballaré, C. L. (2014). Light regulation of plant defense. *Annu. Rev. Plant Biol.* 65, 335–363. doi: 10.1146/annurev-arplant-050213-040145

Beale, S. I. (1990). Biosynthesis of the tetrapyrrole pigment precursor, delta-aminolevulinic acid, from glutamate. *Plant Physiol.* 93, 1273–1279. doi: 10.1104/pp.93.4.1273

Becerril, J. M., and Duke, S. O. (1989). Protoporphyrin IX content correlates with activity of photobleaching herbicides. *Plant Physiol.* 90, 1175–1181. doi: 10.1104/pp.90.3.1175

Bhosale, R., Jewell, J. B., Hollunder, J., Koo, A. J., Vuylsteke, M., Michoel, T., et al. (2013). Predicting gene function from uncontrolled expression variation among individual wild-type *Arabidopsis* plants. *Plant Cell* 25, 2865–2877. doi: 10.1105/tpc.113.112268

Brouers, M., and Michel-Wolwertz, M. R. (1983). Estimation of protochlorophyll (ide) contents in plant extracts; re-evaluation of the molar absorption coefficient of protochlorophyll(ide). *Photosynth. Res.* 4, 265–270. doi: 10.1007/BF00052130

Chen, T., and Fluhr, R. (2018). Singlet Oxygen plays an essential role in the root's response to osmotic stress. *Plant Physiol.* 177, 1717–1727. doi: 10.1104/pp.18.00634

Chen, D., Xu, G., Tang, W., Jing, Y., Ji, Q., Fei, Z., et al. (2013). Antagonistic basic helix-loop-helix/bZIP transcription factors form transcriptional modules that integrate light and reactive oxygen species signaling in *Arabidopsis*. *Plant Cell* 25, 1657–1673. doi: 10.1105/tpc.112.104869

Dall'Osto, L., Cazzaniga, S., Havaux, M., and Bassi, R. (2010). Enhanced photoprotection by protein-bound vs free xanthophyll pools: a comparative analysis of chlorophyll b and xanthophyll biosynthesis mutants. *Mol. Plant* 3, 576–593. doi: 10.1093/mp/ssp117

Danon, A., Miersch, O., Felix, G., op den Camp, R. G., and Apel, K. (2005). Concurrent activation of cell death-regulating signaling pathways by singlet oxygen in *Arabidopsis thaliana*. *Plant J.* 41, 68–80. doi: 10.1111/j.1365-313X.2004.02276.x

de Wit, M., Galvão, V. C., and Fankhauser, C. (2016). Light-mediated hormonal regulation of plant growth and development. *Annu. Rev. Plant Biol.* 67, 513–537. doi: 10.1146/annurev-arplant-043015-112252

Dmitrieva, V. A., Domashkina, V. V., Ivanova, A. N., Sukhov, V. S., Tyutereva, E. V., and Voitsekhovskaja, O. V. (2021). Regulation of plasmodesmata in *Arabidopsis* leaves: ATP, NADPH and chlorophyll b levels matter. *J. Exp. Bot.* 72, 5534–5552. doi: 10.1093/jxb/erab205

Dmitrieva, V. A., Tyutereva, E. V., and Voitsekhovskaja, O. V. (2020). Singlet oxygen in plants: generation, detection, and signaling roles. *Int. J. Mol. Sci.* 21, 3237. doi: 10.3390/ijms21093237

Dogra, V., and Kim, C. (2020). Singlet oxygen metabolism: from genesis to signaling. *Front. Plant Sci.* 10. doi: 10.3389/fpls.2019.01640

Fernández-Milmanda, G. L., and Ballaré, C. L. (2021). Shade avoidance: Expanding the color and hormone palette. *Trends Plant Sci.* 26, 509–523. doi: 10.1016/j.tplants.2020.12.006

Fernández-Milmanda, G. L., Crocco, C. D., Reichelt, M., Mazza, C. A., Köllner, T. G., Zhang, T., et al. (2020). A light-dependent molecular link between competition cues and defense responses in plants. *Nat. Plants* 6, 223–230. doi: 10.1038/s41477-020-0604-8

Fischer, B. B., Krieger-Liszkay, A., Hideg, E., Snyrychová, I., Wiesendanger, M., and Eggen, R. I. (2007). Role of singlet oxygen in chloroplast to nucleus retrograde signaling in *Chlamydomonas reinhardtii*. *FEBS Lett.* 581, 5555–5560. doi: 10.1016/j.febslet.2007.11.003

Frosch, S., and Mohr, H. (1980). Analysis of light-controlled accumulation of carotenoids in mustard (*Sinapis alba* L.) seedlings. *Planta* 148, 279–286. doi: 10.1007/BF00380039

Fryer, M. J., Oxborough, K., Mullineaux, P. M., and Baker, N. R. (2002). Imaging of photo-oxidative stress responses in leaves. *J. Exp. Bot.* 53, 1249–1254. doi: 10.1093/jexbot/53.372.1249

Gadjev, I., Vanderauwera, S., Gechev, T. S., Laloi, C., Minkov, I. N., Shulaev, V., et al. (2006). Transcriptomic footprints disclose specificity of reactive oxygen species signaling in *Arabidopsis*. *Plant Physiol.* 141, 436–445. doi: 10.1104/pp.106.078717

Gidda, S. K., Miersch, O., Levitin, A., Schmidt, J., Wasternack, C., and Varin, L. (2003). Biochemical and molecular characterization of a hydroxyjasmonate sulfotransferase from *Arabidopsis thaliana*. *J. Biol. Chem.* 278, 17895–17900. doi: 10.1074/jbc.M211943200

Gough, S. (1972). Defective synthesis of porphyrins in barley plastids caused by mutation in nuclear genes. *Biochim. Biophys. Acta* 286, 36–54. doi: 10.1016/0304-4165(72)90086-4

Haas, F. H., Heeg, C., Queiroz, R., Bauer, A., Wirtz, M., and Hell, R. (2008). Mitochondrial serine acetyltransferase functions as a pacemaker of cysteine synthesis in plant cells. *Plant Physiol.* 148, 1055–1067. doi: 10.1104/pp.108.125237

Hatz, S., Lambert, J. D. C., and Ogilby, P. R. (2007). Measuring the lifetime of singlet oxygen in a single cell: addressing the issue of cell viability. *Photochem. Photobiol. Sci.* 6, 1106–1116. doi: 10.1039/b707313e

Havaux, M., Dall'Osto, L., and Bassi, R. (2007). Zeaxanthin has enhanced antioxidant capacity with respect to all other xanthophylls in *Arabidopsis* leaves and functions independent of binding to PSII antennae. *Plant Physiol.* 145, 1506–1520. doi: 10.1104/pp.107.108480

Havaux, M., and Tardy, F. (1997). Thermostability and photostability of photosystem II in leaves of the Chlorina-f2 barley mutant deficient in light-harvesting chlorophyll a/b protein complexes. *Plant Physiol.* 113, 913–923. doi: 10.1104/pp.113.3.913

Hideg, E., Barta, C., Kálai, T., Vass, I., Hideg, K., and Asada, K. (2002). Detection of singlet oxygen and superoxide with fluorescent sensors in leaves under stress by photoinhibition or UV radiation. *Plant Cell Physiol.* 43, 1154–1164. doi: 10.1093/pcp/pcf145

Hirschmann, F., Krause, F., and Papenbrock, J. (2014). The multi-protein family of sulfotransferases in plants: composition, occurrence, substrate specificity, and functions. *Front. Plant Sci.* 5. doi: 10.3389/fpls.2014.00556

Karpinska, B., Wingsle, G., and Karpinski, S. (2000). Antagonistic effects of hydrogen peroxide and glutathione on acclimation to excess excitation energy in *Arabidopsis*. *IUBMB Life* 50, 21–26. doi: 10.1080/15216540050176548

Kegge, W., Weldegergis, B. T., Soler, R., Eijk, M. V., Dicke, M., Voesenek, L. A. C. J., et al. (2013). Canopy light cues affect emission of constitutive and methyl jasmonate-induced volatile organic compounds in *Arabidopsis thaliana*. *New Phytol.* 200, 861–874. doi: 10.1111/nph.12407

Kim, E. H., Li, X. P., Razeghifard, R., Anderson, J. M., Niyogi, K. K., Pogson, B. J., et al. (2009). The multiple roles of light-harvesting chlorophyll a/b-protein complexes define structure and optimize function of *Arabidopsis* chloroplasts: a study using two chlorophyll b-less mutants. *Biochim. Biophys. Acta* 1787, 973–984. doi: 10.1016/j.bbabio.2009.04.009

Kim, C., Meskauskiene, R., Zhang, S., Lee, K. P., Ashok, M. L., Blajecka, K., et al. (2012). Chloroplasts of *Arabidopsis* are the source and a primary target of a plant-specific programmed cell death signaling pathway. *Plant Cell* 24, 3026–3039. doi: 10.1105/tpc.112.100479

Kong, Y., and Nemali, K. (2021). Blue and far-red light affect area and number of individual leaves to influence vegetative growth and pigment synthesis in lettuce. *Front. Plant Sci.* 12. doi: 10.3389/fpls.2021.667407

Krieger-Liszkay, A. (2005). Singlet oxygen production in photosynthesis. *J. Exp. Bot.* 56, 337–346. doi: 10.1093/jxb/erh237

Laloi, C., and Havaux, M. (2015). Key players of singlet oxygen-induced cell death in plants. *Front. Plant Sci.* 6. doi: 10.3389/fpls.2015.00039

Laloi, C., Przybyla, D., and Apel, K. (2006). A genetic approach towards elucidating the biological activity of different reactive oxygen species in *Arabidopsis thaliana*. *J. Exp. Bot.* 57, 1719–1724. doi: 10.1093/jxb/erj183

Laloi, C., Stachowiak, M., Pers-Kamczyc, E., Warzych, E., Murgia, I., and Apel, K. (2007). Cross-talk between singlet oxygen- and hydrogen peroxide-dependent signaling of stress responses in *Arabidopsis thaliana*. *Proc. Natl. Acad. Sci. U.S.A.* 104, 672–677. doi: 10.1073/pnas.0609063103

Ledford, H. K., Chin, B. L., and Niyogi, K. K. (2007). Acclimation to singlet oxygen stress in *Chlamydomonas reinhardtii*. *Eukaryot. Cell* 6, 919–930. doi: 10.1128/EC.00207-06

Lee, K. P., Kim, C., Lee, D. W., and Apel, K. (2003). *TIGRINA d*, required for regulating the biosynthesis of tetrapyrroles in barley, is an ortholog of the FLU gene of *Arabidopsis thaliana*. *FEBS Lett.* 553, 119–124. doi: 10.1016/S0014-5793(03)00983-9

Leverenz, J. W., Öquist, G., and Wingsle, G. (1992). Photosynthesis and photoinhibition in leaves of chlorophyll b-less barley in relation to absorbed light. *Physiol. Plant* 85, 495–502. doi: 10.1111/j.1399-3054.1992.tb05817.x

Li, Q., and Kubota, C. (2009). Effects of supplemental light quality on growth and phytochemicals of baby leaf lettuce. *Environ. Exp. Bot.* 67, 59–64. doi: 10.1016/j.envexpbot.2009.06.011

Li, J., Zhang, Y., Gao, Z., Xu, X., Wang, Y., Lin, Y., et al. (2021). Plant U-box E3 ligases *PUB25* and *PUB26* control organ growth in *Arabidopsis*. *New Phytol.* 229, 403–413. doi: 10.1111/nph.16885

Lichtenthaler, H. K., and Wellburn, A. R. (1983). Determinations of total carotenoids and chlorophylls a and b of leaf extracts in different solvents. *Biochem. Soc. Transact.* 11, 591–592. doi: 10.1042/bst0110591

Livak, K. J., and Schmittgen, T. D. (2001). Analysis of relative gene expression data using real-time quantitative PCR and the 2(-Delta Delta C(T)) method. *Methods* 25, 402–408. doi: 10.1006/meth.2001.1262

Ma, L., Tian, T., Lin, R., Deng, X. W., Wang, H., and Li, G. (2016). Arabidopsis FHY3 and FAR1 regulate light-induced myo-Inositol biosynthesis and oxidative stress responses by transcriptional activation of MIPS1. *Mol. Plant* 9, 541–557. doi: 10.1016/j.molp.2015.12.013

Mascia, P. (1978). An analysis of precursors accumulated by several chlorophyll biosynthetic mutants of maize. *Mol. Gen. Genet.* 161, 237–244. doi: 10.1007/BF00330996

McCormac, A. C., and Terry, M. J. (2002). Loss of nuclear gene expression during the phytochrome A-mediated far-red block of greening response. *Plant Physiol.* 130, 402–414. doi: 10.1104/pp.003806

Meier, S., Tzfadia, O., Vallabhaneni, R., Gehring, C., and Wurtzel, E. T. (2011). A transcriptional analysis of carotenoid, chlorophyll and plastidial isoprenoid biosynthesis genes during development and osmotic stress responses in *Arabidopsis thaliana*. *BMC Syst. Biol.* 5, 77. doi: 10.1186/1752-0509-5-77

Meng, Q., Kelly, N., and Runkle, E. S. (2019). Substituting green or far-red radiation for blue radiation induces shade avoidance and promotes growth in lettuce and kale. *Environ. Exp. Bot.* 162, 383–391. doi: 10.1016/j.envexpbot.2019.03.016

Meng, P. H., Raynaud, C., Tcherkez, G., Blanchet, S., Massoud, K., Domenichini, S., et al. (2009). Crosstalks between myo-inositol metabolism, programmed cell death and basal immunity in *Arabidopsis*. *PloS One* 4, e7364. doi: 10.1371/journal.pone.0007364

Meskauskiene, R., Nater, M., Goslings, D., Kessler, F., op den Camp, R., and Apel, K. (2001). FLU: a negative regulator of chlorophyll biosynthesis in *Arabidopsis thaliana*. *Proc. Natl. Acad. Sci. U.S.A.* 98, 12826–12831. doi: 10.1073/pnas.221252798

Mor, A., Koh, E., Weiner, L., Rosenwasser, S., Sibony-Benyamini, H., and Fluhr, R. (2014). Singlet oxygen signatures are detected independent of light or chloroplasts in response to multiple stresses. *Plant Physiol.* 165, 249–261. doi: 10.1104/pp.114.236380

Ogilby, P. R. (2010). Singlet oxygen: there is indeed something new under the sun. *Chem. Soc. Rev.* 39, 3181–3209. doi: 10.1039/b926014p

op den Camp, R. G., Przybyla, D., Ochsenbein, C., Laloi, C., Kim, C., Danon, A., et al. (2003). Rapid induction of distinct stress responses after the release of singlet oxygen in *Arabidopsis*. *Plant Cell* 15, 2320–2332. doi: 10.1105/tpc.014662

Page, M. T., McCormac, A. C., Smith, A. G., and Terry, M. J. (2017). Singlet oxygen initiates a plastid signal controlling photosynthetic gene expression. *New Phytol.* 213, 1168–1180. doi: 10.1111/nph.14223

Pierik, R., Cuppens, M. L., Voesenek, L. A., and Visser, E. J. (2004a). Interactions between ethylene and gibberellins in phytochrome-mediated shade avoidance responses in tobacco. *Plant Physiol.* 136, 2928–2936. doi: 10.1104/pp.104.045120

Pierik, R., and de Wit, M. (2014). Shade avoidance: phytochrome signalling and other aboveground neighbour detection cues. *J. Exp. Bot.* 65, 2815–2824. doi: 10.1093/jxb/ert389

Pierik, R., Whitelam, G. C., Voesenek, L. A., de Kroon, H., and Visser, E. J. (2004b). Canopy studies on ethylene-insensitive tobacco identify ethylene as a novel element in blue light and plant-plant signaling. *Plant J.* 38, 310–319. doi: 10.1111/j.1365-313X.2004.02044.x

Prasad, A., Sedlářová, M., and Pospíšil, P. (2018). Singlet oxygen imaging using fluorescent probe Singlet Oxygen Sensor Green in photosynthetic organisms. *Sci. Rep.* 8, 13685. doi: 10.1038/s41598-018-31638-5

Przybyla, D., Göbel, C., Imboden, A., Hamberg, M., Feussner, I., and Apel, K. (2008). Enzymatic, but not non-enzymatic, 1O2-mediated peroxidation of polyunsaturated fatty acids forms part of the EXECUTER1-dependent stress response program in the *flu* mutant of *Arabidopsis thaliana*. *Plant J.* 54, 236–248. doi: 10.1111/j.1365-313X.2008.03409.x

Ramel, F., Ksas, B., Akkari, E., Mialoundama, A. S., Monnet, F., Krieger-Liszkay, A., et al. (2013a). Light-induced acclimation of the *Arabidopsis* chlorina1 mutant to singlet oxygen. *Plant Cell* 25, 1445–1462. doi: 10.1105/tpc.113.109827

Ramel, F., Ksas, B., and Havaux, M. (2013b). Jasmonate: A decision maker between cell death and acclimation in the response of plants to singlet oxygen. *Plant Signal. Behav.* 8, e26655. doi: 10.4161/psb.26655

Rebeiz, C. A., Montazerzouhoor, A., Mayasich, J. M., Tripathy, B. C., Wu, S. M., Rebeiz, C. C., et al. (1988). Photodynamic herbicides. Recent developments and molecular basis of selectivity. *Crit. Rev. Plant Sci.* 6, 385–436. doi: 10.1080/07352688809382256

Rodríguez-Villalón, A., Gas, E., and Rodríguez-Concepción, M. (2009). Phytoene synthase activity controls the biosynthesis of carotenoids and the supply of their metabolic precursors in dark-grown *Arabidopsis* seedlings. *Plant J.* 60, 424–435. doi: 10.1111/j.1365-313X.2009.03966.x

Schindelin, J., Arganda-Carreras, I., Frise, E., Kaynig, V., Longair, M., Pietzsch, T., et al. (2012). Fiji: an open-source platform for biological-image analysis. *Nat. Methods* 9, 676–682. doi: 10.1038/nmeth.2019

Shao, N., Krieger-Liszkay, A., Schroda, M., and Beck, C. F. (2007). A reporter system for the individual detection of hydrogen peroxide and singlet oxygen: its use for the assay of reactive oxygen species produced in *vivo*. *Plant J.* 50, 475–487. doi: 10.1111/j.1365-313X.2007.03065.x

Skovsen, E., Snyder, J. W., Lambert, J. D. C., and Ogilby, P. R. (2005). Lifetime and diffusion of singlet oxygen in a cell. *J. Phys. Chem. B.* 109, 8570–8573. doi: 10.1021/jp051163i

Sperling, U., van Cleve, B., Frick, G., Apel, K., and Armstrong, G. A. (1997). Overexpression of light-dependent PORA or PORB in plants depleted of endogenous POR by far-red light enhances seedlings survival in white light and protects against photooxidative damage. *Plant J.* 12, 649–658. doi: 10.1046/j.1365-313X.1997.00649.x

Tanaka, R., and Tanaka, A. (2007). Tetrapyrrole biosynthesis in higher plants. *Annu. Rev. Plant Biol.* 58, 321–346. doi: 10.1146/annurev.arplant.57.032905.105448

Tjus, S. E., Scheller, H. V., Andersson, B., and Møller, B. L. (2001). Active oxygen produced during selective excitation of photosystem I is damaging not only to photosystem I, but also to photosystem II. *Plant Physiol.* 125, 2007–2015. doi: 10.1104/pp.125.4.2007

Tollenaar, M. (1989). Response of dry matter accumulation in maize to temperature: I. Dry matter partitioning. *Crop Sci.* 29, 1239–1246. doi: 10.2135/cropsci1989.0011183X002900050030x

Trebst, A. (2003). Function of beta-carotene and tocopherol in photosystem II. *Z Naturforsch. C J. Biosci.* 58, 609–620. doi: 10.1515/znc-2003-9-1001

Triantaphylidès, C., and Havaux, M. (2009). Singlet oxygen in plants: production, detoxification and signaling. *Trends Plant Sci.* 14, 219–228. doi: 10.1016/j.tplants.2009.01.008

Von Lintig, J., Welsch, R., Bonk, M., Giuliano, G., Batschauer, A., and Kleinig, H. (1997). Light-dependent regulation of carotenoid biosynthesis occurs at the level of phytoene synthase expression and is mediated by phytochrome in *Sinapis alba* and *Arabidopsis thaliana* seedlings. *Plant J.* 12, 625–634. doi: 10.1046/j.1365-313X.1997.00625.x

Wagner, D., Przybyla, D., Op den Camp, R., Kim, C., Landgraf, F., Lee, K. P., et al. (2004). The genetic basis of singlet oxygen-induced stress responses of *Arabidopsis thaliana*. *Science* 306, 1183–1185. doi: 10.1126/science.1103178

Waszczak, C., Carmody, M., and Kangasjärvi, J. (2018). Reactive oxygen species in plant signaling. *Annu. Rev. Plant Biol.* 69, 209–236. doi: 10.1146/annurev-arplant-042817-040322

Welsch, R., Beyer, P., Hugueney, P., Kleinig, H., and Von Lintig, J. (2000). Regulation and activation of phytoene synthase, a key enzyme in carotenoid biosynthesis, during photomorphogenesis. *Planta* 211, 846–854. doi: 10.1007/s004250000352

Xiong, L., Schumaker, K. S., and Zhu, J. K. (2002). Cell signaling during cold, drought, and salt stress. *Plant Cell* 14, S165–S183. doi: 10.1105/tpc.000596

Zhen, S., and Bugbee, B. (2020). Substituting far-red for traditionally defined photosynthetic photons results in equal canopy quantum yield for CO2 fixation and increased photon capture during long-term studies: Implications for re-defining PAR. *Front. Plant Sci.* 11. doi: 10.3389/fpls.2020.581156

Zhen, S., and van Iersel, M. W. (2017). Far-red light is needed for efficient photochemistry and photosynthesis. *J. Plant Physiol.* 209, 115–122. doi: 10.1016/j.jplph.2016.12.004

Zhu, A., Ibrahim, J. G., and Love, M. I. (2019). Heavy-tailed prior distributions for sequence count data: removing the noise and preserving large differences. *Bioinformatics* 35, 2084–2092. doi: 10.1093/bioinformatics/bty895

Frontiers in
Plant Science

Cultivates the science of plant biology and its applications

The most cited plant science journal, which advances our understanding of plant biology for sustainable food security, functional ecosystems and human health.

Discover the latest Research Topics

See more →

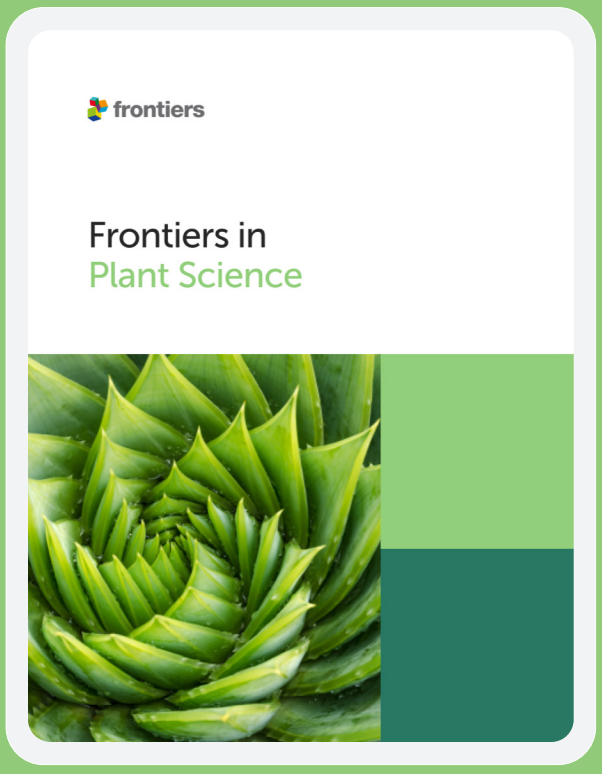

Frontiers

Avenue du Tribunal-Fédéral 34
1005 Lausanne, Switzerland
frontiersin.org

Contact us

+41 (0)21 510 17 00
frontiersin.org/about/contact